Structural inheritance and magmatism during continental breakup in West Greenland and Eastern Canada

ALEXANDER LEWIS PEACE

Structural inheritance and magmatism during continental breakup in West Greenland and Eastern Canada

Alexander Lewis Peace

A thesis submitted to Durham University in fulfilment of the requirements for the degree of Doctor of Philosophy

2016

Declaration

No part of this thesis has previously been submitted for a degree at this or any other university. The work described in this thesis is entirely that of the author, except where reference is made to previously published or unpublished work.

Copyright

'I may not have gone where I intended to go, but I think I have ended up where I needed to be.' – Douglas Adams

Table of Contents

List of Figures

Chapter 1

Chapter 2

Chapter 3

Chapter 4

Chapter 7

List of Tables

Chapter 1

No tables in this chapter.

Chapter 2

No tables in this chapter.

Chapter 3

Chapter 4

Chapter 5

Chapter 6

Chapter 7

Chapter 8

No tables in this chapter.

Abstract

Continental extension causes rifting and thinning of the lithosphere that may result in breakup and eventually the initiation of seafloor spreading and passive continental margin development. Ambiguity exists regarding the roles of magmatism and structural inheritance during rifting and continental breakup during this process. This study focuses on the importance of these controls on the Mesozoic-Cenozoic separation between West Greenland and Eastern Canada. It is important to improve our knowledge of the processes that influenced breakup as the current understanding of these processes is limited and also to reduce hydrocarbon exploration risk in this tectonic setting. During this study passive margin processes were investigated using a variety of methodologies at a range of scales from that of conjugate margin pairs (Chapters 4 and 5), through margin and basin scale studies (Chapter 6) to the smallest scale on individual igneous intrusions (Chapter 7). At the largest scale an assessment of the magmatic and structural asymmetry between the conjugate margins of the Labrador Sea based primarily on field data and subsequent analysis near Makkovik, Labrador, but also other large-scale geophysical datasets demonstrated that early rifting was dominated by simple shear rather than pure shear. In such a scenario Labrador was have been the lower plate margin to the upper plate southwest Greenland margin. Further analysis of field observations indicated that rifting of the Labrador Sea region may have been aided by a favourably orientated basement metamorphic fabric and that observable onshore brittle deformation structures may be related to Mesozoic rifting. Further north in the Davis Strait, seismic interpretation at the margin and basin scale allowed a series of seismic surfaces, isochrons and a new offshore fault map to be produced. The results of this analysis demonstrated that the geometry of rift basins was primarily controlled by pre-existing structures, an assertion supported by observations of reactivation onshore in West Greenland. Finally, at the smallest scale, results of numerical modelling offshore Newfoundland demonstrated that even on non-volcanic passive margins, intrusive magmatism can influence thermal evolution. In addition, the presence of widespread igneous rocks on passive margins may be indicative of regional-scale thermal perturbations that should be considered in source rock maturation studies. Overall, the conclusion of this project is that both magmatism and structural inheritance have profoundly influenced the continental breakup between West Greenland and Eastern Canada, and that interplay between these two complex groups of mechanisms may have also contributed to the geological evolution of this area.

Acknowledgements

Supervisory team

I would like to start by thanking the supervisory team as the quality of the project, this thesis and my own development as a geoscientist would have been significantly poorer if this dedicated group hadn't been so involved, enthusiastic and knowledgeable.

Firstly, I would first like to acknowledge my primary supervisor Ken McCaffrey who has over the last four has provided the support and guidance required to reach this point. Thank you for keeping me on track and for reading the many painful iterations of this thesis, papers, posters, presentations and chapters. I would also like to acknowledge the dedication and optimism that Jonny Imber has provided throughout this project. Thank you for replying to emails, even at obscene times of the day and for all the feedback, advice and jokes that probably shouldn't be repeated (ever!). I would also like to thank Richard Hobbs for always being friendly and willing to dedicate time to students, including hearing out my ideas even when they are little more than speculation. I would like to thank Jeroen van Hunen for providing help with the modelling chapter and for always making the time for his students. Finally, I would like to acknowledge Keith Gerdes as my industrial supervisor who has on many occasions brought a different perspective to problems and situations, input for which I would like to thank him.

Friends and family

I would like to start this section by acknowledging the contribution that my partner Jessie Harris has made towards helping me reach this point. Thanks for all the great times in the UK and on our trips abroad. I am really looking forward to the next stage of our lives together in St. Johns.

Next, I would like to extend my thanks to my family in particular my parents and my brother Joe for their kindness and support. I would also like to thank my Nana, Grandad, Aunty Enid, Aunty Jean and Uncle Dave for the support they have provided before and during this project.

I would like to thank the following past and present members of the Earth Sciences community at Durham University for the friendship and advice they have given me; Adam Robinson, Alex Burton-Johnson, Ben Hedley, Ben Maunder, Bob Jamieson, Cat Hirst,

Chris Harbord, Christian Schiffer, Clayton Grove, Diveena Danaban, Edward Dempsey, Edward Inglis, Elizabeth Atar, Harriet Ridley, Jack Lee, Jing Zhang, Jordan Phethean, Josie Mahony, Kate Horan, Katie Strang, Kevin Burton, Loraine Pastoriza, Mark Brodie, Sam Clark, Simon Mathias, Peter András, Peter Reynolds, Pete Tollan, Sarah Clancy, Tom Jones and Tom Utley.

In no particular order I would also like to thank the following people from outside the Department of Earth Sciences for being great friends before, during (and hopefully after) my PhD; Matthew and Alison Gibbings, Matthew Keeves, Catherine Peake, Kevin Milburn, James Stokes, Caroline Webb, Cat Oldham, Pete Forsyth and Daniel Robinson.

The scientific community

Outside of the supervisory team and I would like to acknowledge the contribution of the following individuals for the many enlightening conversations both in person and by email that have helped develop the ideas contained within this thesis: Tony Dore, Erik Lundin, Gillian Foulger, Geoff Nowell and Nick Schofield.

Supporting companies

I would like to thank Royal Dutch Shell for providing funding for this PhD project in the form of a CeREES studentship, and for the expertise and advice which they have given throughout this project. In addition to my industry supervisor Keith Gerdes individuals at Shell who have helped with this project in no particular order include; Dave Steel, Martin Grecula, Dominic Maloney and Stephanie Wadsworth.

In addition to Royal Dutch Shell there are several other companies that have contributed towards my PhD project and deserve acknowledgement. This research would also not have been possible without the provision of the seismic data by Spectrum Geo Ltd, where Anna Marszalek (formally of Spectrum Geo Ltd) is acknowledged for helping in securing data access and Schlumberger for the provision of the Petrel software.

Technical and administrative staff in the Department of Earth Sciences

The technical staff in the Department of Earth Sciences are thanked wholeheartedly as without them this project would not have been possible, or at least I would have probably had to write it by hand in the dark. I would like to thank Matthew Hepburn, Gary

Wilkinson and Dave Stevenson for keeping my computer in working order. I would also like to thank Ian Chaplin for preparing my thin sections.

I would also like to acknowledge the office staff in the Department of Earth Sciences. In particular I would like to thank Paula Elliot and Karen Atkinson for the work they did during the planning of the Makkovik fieldwork. I would also like to thank Laura Haswell (now of Durham University Business School) for always being friendly and making sure demonstrators got paid correctly, as well as Janice Oakes for being fun, particularly on the Lake District trips.

Other groups at Durham University

I would like to acknowledge the role that the Centre for Doctoral Training (CDT) in Energy at Durham University has played throughout my PhD. In particular I would like to thank Douglas Halliday and Lynn Gibson, as without these people I very much doubt that the CDT at Durham University would exist. I would also like to thank the CDT for contributing towards the costs of the fieldwork. Finally, I would like to thank the CDT members past and present for the many engaging discussion

St. Aidan's College at Durham University are acknowledge firstly for providing a welcoming environment during my undergraduate studies and secondly for contributing to the costs of attending AAPG ACE 2016 in Calgary, Canada through the Russell-Smith travel grant.

The community of Makkovik

The community of Makkovik, Labrador, Canada are thanked for allowing us to conduct research in their territory and for being welcoming to us. I would like to thank Reg Andersen and Mary Ford for their hospitality and local knowledge, without which a significant amount if this work would not have happened.

Chapter 1

Introduction

1.0 Project motivation

Continental extension causes rifting and thinning of the lithosphere that may result in continental breakup, the initiation of seafloor spreading and passive margin formation (e.g. Eldholm and Sundvor, 1979). Hydrocarbons are known to occur at many passive margins (e.g. Skogseid, 2001) and, because many passive margins are associated with widespread magmatism (Franke, 2013; Geoffroy, 2005), it is important to understand: 1) the role of igneous rocks in petroleum systems (e.g. the impact of igneous activity on source rock maturation); 2) the variable manifestations of magmatism on 'volcanic' and 'non-volcanic' passive margins; and 3) the fundamental mechanisms leading to passive margin formation and structural variability between margins, including observations of conjugate margin asymmetry. After a brief overview placing this study within the context of plate tectonics, continental breakup and passive margin formation, the importance of improving our understanding of these topics is detailed and the specific questions addressed in this thesis are outlined.

1.1 This study in the context of plate tectonics

According to Romm, (1994) the earliest dated recognition of the similarity and suggestion of separation between the coastlines of America and of Europe and Africa was likely to have been in the Thesaurus Geographicus by Ortelius (1596). It was, however, not until Taylor (1910) and Wegener (1912) that the theory of continental drift was formulated in a scientific manner. The next major development was the concept of seafloor spreading (Dietz, 1961; Hess, 1962) which was conceived as a result of sufficient data collected in the ocean basins post World War II (Kearey et al., 2009). Plate tectonic theory, which assumes the outer shell of the Earth comprises multiple, rigid bodies capable of moving

with respect to one another, was developed from the theories of continental drift and seafloor spreading (e.g. McKenzie and Parker, 1967; McKenzie, 1970).

Continental extension causes rifting and thinning of the lithosphere that may result in continental breakup and eventually the initiation of seafloor spreading along with passive continental margin formation, a phenomenon expanded upon further in this chapter then in greater detail in Chapter 2. Plate tectonics has been successful in explaining many observations of both the surface and the interior of the Earth (e.g. Dewey and Horsfield, 1970; Sandwell et al., 2005) including the process of continental breakup (e.g. Eldholm and Sundvor, 1979), with significant developments being made with regards to passive margin formation over the last few decades (Boillot and Froitzheim, 2001; Huismans and Beaumont, 2011). However, despite this success several key processes relating to passive margin formation remain unclear, including the fundamental mechanisms governing continental breakup (McKenzie, 1978; Lister et al., 1986) and the causes of the variability in the structures produced by this process, particularly with respect to magmatism (e.g. White, 1992) and structural inheritance (e.g. Wilson, 1966; Morley et al., 2004). This is because plate tectonics is a kinematic model, and as such, it assumes rigid plates (Kearey et al., 2009). Therefore, plate tectonics predicts divergent margins but does not predict the manner in which continental breakup occurs, i.e. it does not predict pre-breakup stretching or magmatism. The study of the processes governing continental breakup and passive margin formation form the focus of this work. The brief introduction to these concepts, presented in this chapter, is followed by a discussion of the key knowledge gaps in Chapter 2 that focuses on the poorly understood roles of magmatism and tectonic inheritance.

Continental breakup (e.g. White, 1992) results in a tectonic plate consisting of both oceanic and continental crust (Geoffroy, 2005), joined via complex and variable zone of transitional crust known as the Ocean-Continent Transition Zone (OCTZ - Eagles et al.,

2015). Defining the location and nature of the OCTZ (Wilson et al., 2001b) at passive margins has, however, proven to be an elusive endeavour (e.g. Gaina et al., 2013) namely due to the non-unique geophysical signatures of the candidate crustal types and morphologies. However, it is well established that understanding the nature of this transition is essential in constraining continental breakup, passive margin formation (e.g. Mutter, 1985; Wilson et al., 2001) and hydrocarbon exploration (Skogseid, 2001; Holford et al., 2014) in and around this setting. The spatial and temporal evolution of rift systems, particularly the interaction between magmatic, crustal and mantle processes are often subjects of debate within the continental margins community (Foulger, 2005; Peron-Pinvidic et al., 2012) and are areas of considerable energy industry interest (Alves et al., 2014). It is for this reason that this thesis aims to provide insights into the roles of magmatism (Chapters 4 and 7), inherited structure (Chapters 5 and 6) and the interaction between these phenomena (Chapter 8) as the variable roles of these factors during continental breakup remain equivocal.

This project was designed to enhance our understanding of the fundamental processes governing continental breakup and the formation of passive margins (Wilson et al., 2001a), one of the first order processes of plate tectonics (e.g. Geoffroy, 2005; Franke, 2013). However, in addition to the purely scientific motivation for expanding our knowledge on passive margins economic factors have also driven this research, as poor understanding of passive margins inhibits aspects of hydrocarbon exploration and production on passive margins (Alves et al., 2014). This is particularly true for passive margins containing high amounts of magmatic rocks (e.g. Skogseid, 2001; Holford et al., 2013), which may have been previously overlooked by exploration teams in favour of more conventional settings with a perceived lower risk level. The nature of magmatism and hydrocarbon exploration on passive margins is expanded upon in Chapter 2.

1.2 Study aims

Overall, the aim of this thesis is to increase the scientific understanding of processes occurring before, during and after continental breakup between Eastern Canada and West Greenland, and in particular the roles of structural inheritance and magmatism. An explanation of West Greenland and Eastern Canada as the choice of study area is provided in section 1.4 of this Chapter.

The specific questions that this thesis addresses are:

- To what extent are structural and magmatic asymmetry expressed at conjugate passive margins, and what are the fundamental causes of asymmetry, and the implications for magmatic distribution and petroleum systems?
- How do pre-existing structures, such as faults, shear zones and paleo-orogenic fronts within the crystalline, continental basement, influence the processes of rifting, continental breakup and passive margin formation?
- How does rift-related magmatism affect the prospectively of sedimentary basins on passive margins, and in particular the maturity of potential hydrocarbon source rocks?

1.3 Thesis Outline

This thesis is presented as a series of 'journal-style' research papers (Chapters 4-7), preceded by three introductory chapters (including this chapter) and followed by a discussion and conclusions chapter, bringing together the findings of the four main data chapters. The main data chapters are organised by scale with Chapters 4 and 5 covering the large-scale processes governing continental breakup, Chapter 6 considers the basin-scale

evolution and Chapter 7 the processes operating on the scale of individual igneous intrusions (prospect scale).

1.3.1 Thesis Structure

This section provides a brief outline of the contents of each chapter which constitute this thesis.

Chapter 1 – *'Introduction'*

An overview of the project including its structure and rationale. This chapter also includes the context of the study locations with respect to one another, and the geological history of the North Atlantic region.

Chapter 2 – *'Passive continental margins: formation, classification and petroleum exploration'*

This chapter provides an overview of the mechanisms documented in the literature controlling the process of continental breakup in the context of plate tectonics from a global perspective. Passive margin nomenclature, classification, formation, structure and petroleum exploration is then considered with a particular focus on volcanic or magma-rich passive margins.

Chapter 3 – *'Data and methodologies'*

This chapter summarises the variety of methodologies used to investigate passive margins globally and also provides detailed descriptions of the methods and techniques used for the analysis of the data presented in this thesis.

Chapter 4 – *'An evaluation of Mesozoic rift-related magmatism on the margins of the Labrador Sea: implications for rifting and passive margin asymmetry'*

This chapter integrates data obtained during fieldwork in Labrador in summer 2015 with large-scale geophysical datasets to study various aspects of asymmetry between the margins of Southwest Greenland and Labrador. Our findings allow us to propose that the Labrador Sea rifted under a simple shear dominated regime. The contents of this chapter have been published in its current form as:

> **Peace, A.,** McCaffrey, K., Imber, J., Phethean, J., Nowell, G., and Gerdes, K., Dempsey, E., (*2016*). An evaluation of Mesozoic rift-related magmatism on the margins of the Labrador Sea: implications for rifting and passive margin asymmetry. *Geosphere* Vol.12 No.6 doi: http://dx.doi.org/10.1130/GES01341.1

As first author of this publication my contribution to this work included organising and undertaking the fieldwork, sample preparation, data analysis, concept development and manuscript preparation. The content of this chapter were also presented at the AAPG ACE in June 2016 in Calgary, Canada.

Chapter 5 – '*The onshore expression of brittle deformation associated with the opening of the Labrador Sea and its relationship with the regional metamorphic fabric near Makkovik, Labrador, Canada*'

This chapter presents preliminary results from the analysis of structural data obtained during the Labrador fieldwork, including; 1) an analysis of the regional metamorphic fabric in the study area and its potential relationship to rift propagation in the Labrador Sea and 2) a stress inversion depicting a potential onshore expression of deformation related to the opening of the Labrador Sea.

Chapter 6 – *'The role of pre-existing structures during continental breakup between West Greenland and North Eastern Canada'*

This chapter integrates several geophysical and geological datasets to investigate the role of pre-existing structure on the process of continental breakup between Greenland and Eastern Canada. The contents of this chapter have been presented at the following conferences:

- American Association of Petroleum Geologists (AAPG) Annual Convention and Expedition (ACE) 2014 in Houston, USA and now available in Search and Discover as:

  Peace, A., McCaffrey, K., Imber, J., Hobbs, R., van Hunen, J., and Gerdes, K., (2014). Formation of the volcanic margins of West Greenland and North- Eastern Canada. AAPG ACE Houston, AAPG Search and Discovery, doi: http://dx.doi.org/10.13140/RG.2.1.1545.1128

- The 4th Conjugate Margins conference 2014, St. Johns, Newfoundland as:

  Peace, A., McCaffrey, K., Imber, J., Hobbs, R., van Hunen, J., Foulger, G. and Gerdes, K., (2014). Formation of the West Greenland Volcanic margin: Exploring alternatives to the plume hypothesis. 4th Atlantic Conjugate Margins Conference, p161-162, doi: http://dx.doi.org/10.13140/RG.2.1.4727.1925

- The research collaboration showcase at PETEX 2014 as:

Peace, A., Gerdes, K., McCaffrey, K., Imber, J., Hobbs, R., van Hunen, J., (2014). Formation of the West Greenland Volcanic Margin. PETEX Research Collaboration showcase.

- The Arthur Holmes Meeting 2016, London, UK as:

  Wilson, R., McCaffrey, K., Holdsworth, R., **Peace, A.,** Imber, J and GEUS., (2016). Tectonic inheritance during extension in rifts and passive margins: A Greenland Case Study. Arthur Holmes Meeting 2016. The Wilson Cycle: plate tectonics and structural inheritance during continental deformation.

This work has also received the following awards:

- 1st place student poster at the 4th Conjugate Margins conference, 2014
- 2nd place in the research collaboration showcase at PETEX, 2014

The intention is to submit part of this work to a Geological Society of London Special Publication on the theme of the Wilson Cycle, which is a collection of the contributions presented at the Arthur Holmes meeting 2016.

Chapter 7 –*'Quantifying the influence of sill intrusion on the thermal evolution of non-volcanic passive margins: an example from ODP 210-1276, offshore Newfoundland, Canada'*

This chapter investigates through numerical modelling the thermal influence of intrusive magmatism upon source rock maturation on the Newfoundland margin. The contents of this chapter have now been published as:

Peace, A., McCaffrey, K., Imber, J., Hobbs, R., van Hunen, J. & Gerdes, K., (*2015*). Quantifying the influence of sill intrusion on the thermal evolution of organic-rich sedimentary rocks in non-volcanic passive margins: an

example from ODP 210-1276, offshore Newfoundland, Canada. *Basin Research* http://dx.doi.org/10.1111/bre.12131

As first author of this publication my contribution was to provide the original concept, design and write the MATLAB numerical models and prepare the manuscript. The content of this chapter was also presented at VMSG 2014 in Edinburgh, UK and EGU 2013 in Vienna, Austria.

Chapter 8 – *'Discussion and Conclusions'*

This chapter integrates the findings of the previous chapters to provide an overview of the various factors influencing the formation of the West Greenland and Eastern Canadian passive margins at different observational scales. Consideration is also given to possibilities for future work on this area based on the findings of this study. Finally, this chapter provides a complete list of the conclusions made in Chapters 4-7.

References

A complete list of references cited in this thesis.

Appendices

A compilation of additional material amassed during the preparation of this thesis organised by chapter.

1.4 The context of this study within the North Atlantic

The North Atlantic is an ocean basin located in the northern hemisphere between North America and Europe (Fig. 1.1). It lies adjacent to the Central Atlantic to the south and the Arctic Ocean to the north, although there is no physical boundary between these ocean basins.

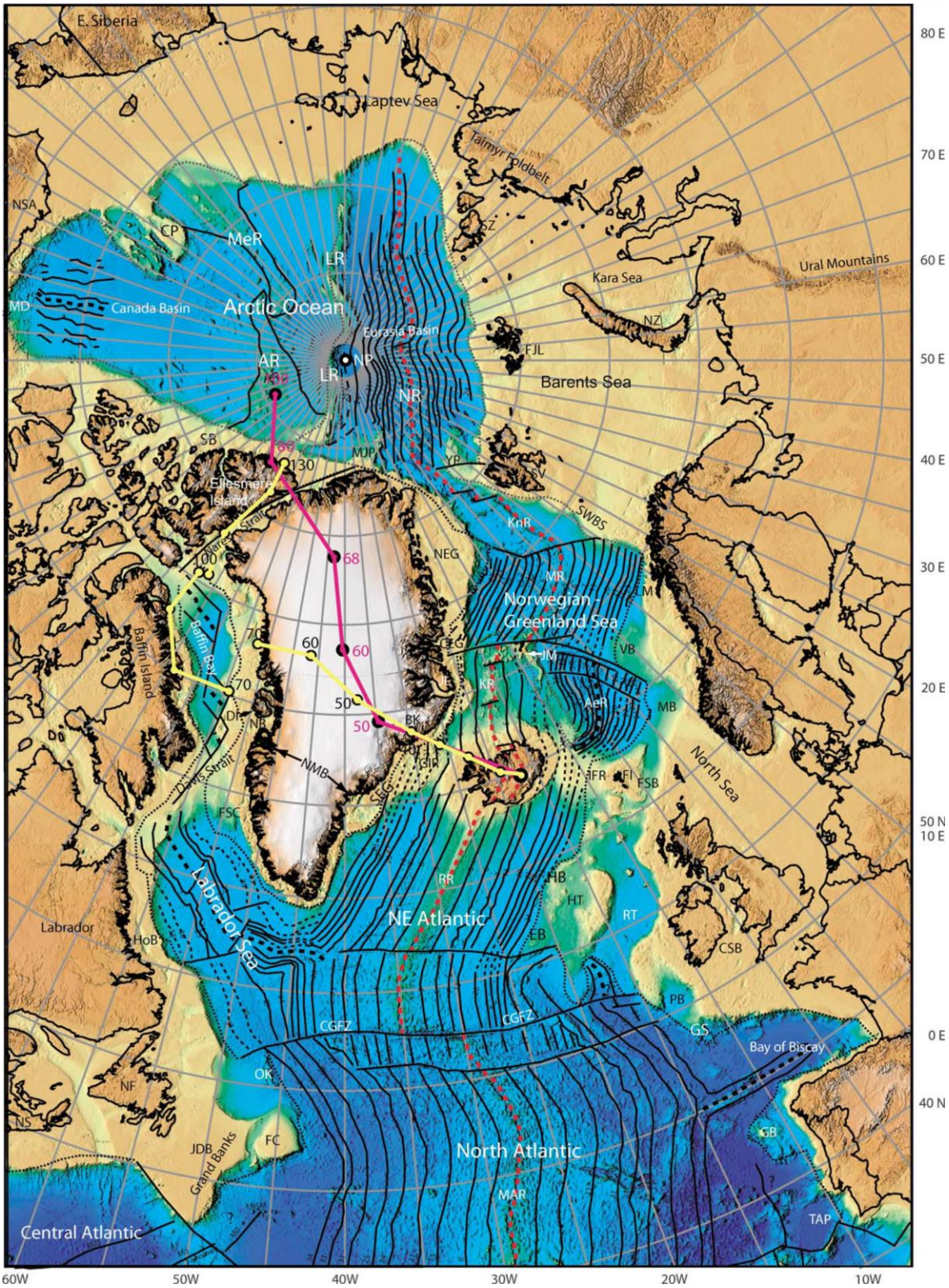
E. Siberia
Laptev Sea
Taimyr Foldbelt
NSA
CP
MeR
LR
SZ
Ural Mountains
Kara Sea
MD
Canada Basin
Arctic Ocean
Eurasia Basin
NZ
FJL
AR
NP
LR
Barents Sea
NR
SB
MJP
YP
Ellesmere Island
Nares Strait
SWBS
KnR
NEG
MR
Norwegian Greenland Sea
LM
Baffin Bay
Baffin Island
VB
JM
KR
AeR
MB
Davis Strait
BK
NMB
IFR
FI
FSB
North Sea
FSC
SEG
Labrador Sea
RR
HB
HT
NE Atlantic
RT
Labrador
HoB
EB
CSB
PB
CGFZ
GS
Bay of Biscay
OK
NF
NS
JDB
FC
Grand Banks
North Atlantic
GB
MAR
TAP
Central Atlantic
80 E
70 E
60 E
50 E
40 E
30 E
20 E
50 N
10 E
0 E
40 N
60W
50W
40W
30W
20W
10W

Figure 1.1

Geography and bathymetry of the Arctic, North and Central Atlantic oceans (Smith and Sandwell, 1997; Jakobsson et al., 2000) and magnetic anomalies (Lundin and Doré, 2005) plotted using a polar stereographic projection. Also included are the proposed hotspot tracks of Forsyth et al. (1986) (magenta), Lawver and Muller, (1994) (yellow), and Lawver et al. (2002) (red). AR = Alpha ridge; AeR = Aegir ridge; BK = Blosseville Kyst; CEG = central east Greenland; CGFZ = Charlie Gibbs Fracture Zone; CP = Chukchi Plateau; CSB = Celtic Sea Basins; DI = Disco Island; EB = Edoras Bank; FC = Flemish Cap; FSC = Fylla Structural Complex; FI = Faroe Islands; FJL = Franz Josef Land; FSB = Færoe Shetland Basin; JDB = Jeanne D'Arc Basin; GIR = Greenland-Iceland ridge; GB = Galicia Bank; GS = Goban Spur; HB = Hatton Bank; HoB = Hopedale Basin; HT = Hatton Trough; IFR = Iceland-Faeroe ridge; JL = Jameson Land; JM = Jan Mayen microcontinent; K = Kangerlussuaq; KnR = Knipovich ridge; KR = Kolbeinsey ridge; LM = Lofoten Margin; LR = Lomonosov ridge; MAR = Mid-Atlantic Ridge; MD = McKenzie Delta; MB = Møre Basin; MeR = Mendelev ridge; MJP = Morris Jesup Plateau; MR = Mohns ridge; NB = Nuussuaq Basin; NEG = northeast Greenland; NL = Newfoundland; NP = North Pole; NR = Nansen ridge; NS = Nova Scotia; NSA = north slope of Alaska; NZ = Novaya Zemlya; OB = Orphan Basin; OK = Orphan Knoll; PB = Porcupine Basin; RR = Reykjanes ridge; RT = Rockall Trough; SB = Sverdrup Basin; SEG = southeast Greenland; SV = Svalbard; SWBS = southwest Barents Sea margin; SZ = Severnaya Zemlya; TAP = Tagus abyssal plain; VB = Vøring Basin; YP = Yermak Plateau. Reproduced from Lundin and Doré, (2005).

This thesis is comprised of studies conducted at three key North Atlantic locations in Eastern Canada and West Greenland (Fig. 1.2). These locations are: 1) the Labrador Sea (Chapters 4 and 5), 2) the Davis Strait (Chapter 6) and 3) offshore Newfoundland (Chapter 7). The study locations were each selected for their potential to address the key questions identified in section 1.0, using new and existing datasets outlined in Chapter 3. Each of the locations provides observations and interpretations at a different scale, allowing us to examine how different processes manifest in the discussion section of this thesis in Chapter 8. Although it may have been possible to conduct similar analysis at multiple geographically separated locations globally, this study sought to work on different aspects

of margin formation in Eastern Canada and West Greenland to provide a well constrained geographical remit to the study of passive margins. The other reason for choosing the West Greenland and Eastern Canadian conjugate margins is that compared to other conjugate pairs there has been limited oceanic crust production (e.g. Srivastava, 1978) and no subduction of oceanic lithosphere, making conjugate margin studies much easier. Wilson et al. (2001a) recognised that to fully understand the large-scale evolution of passive margins the study of conjugate pairs must be undertaken, an approach which is carried through much of this thesis in particular in Chapter 4, whereby a conjugate margin study is conducted in the Labrador Sea region.

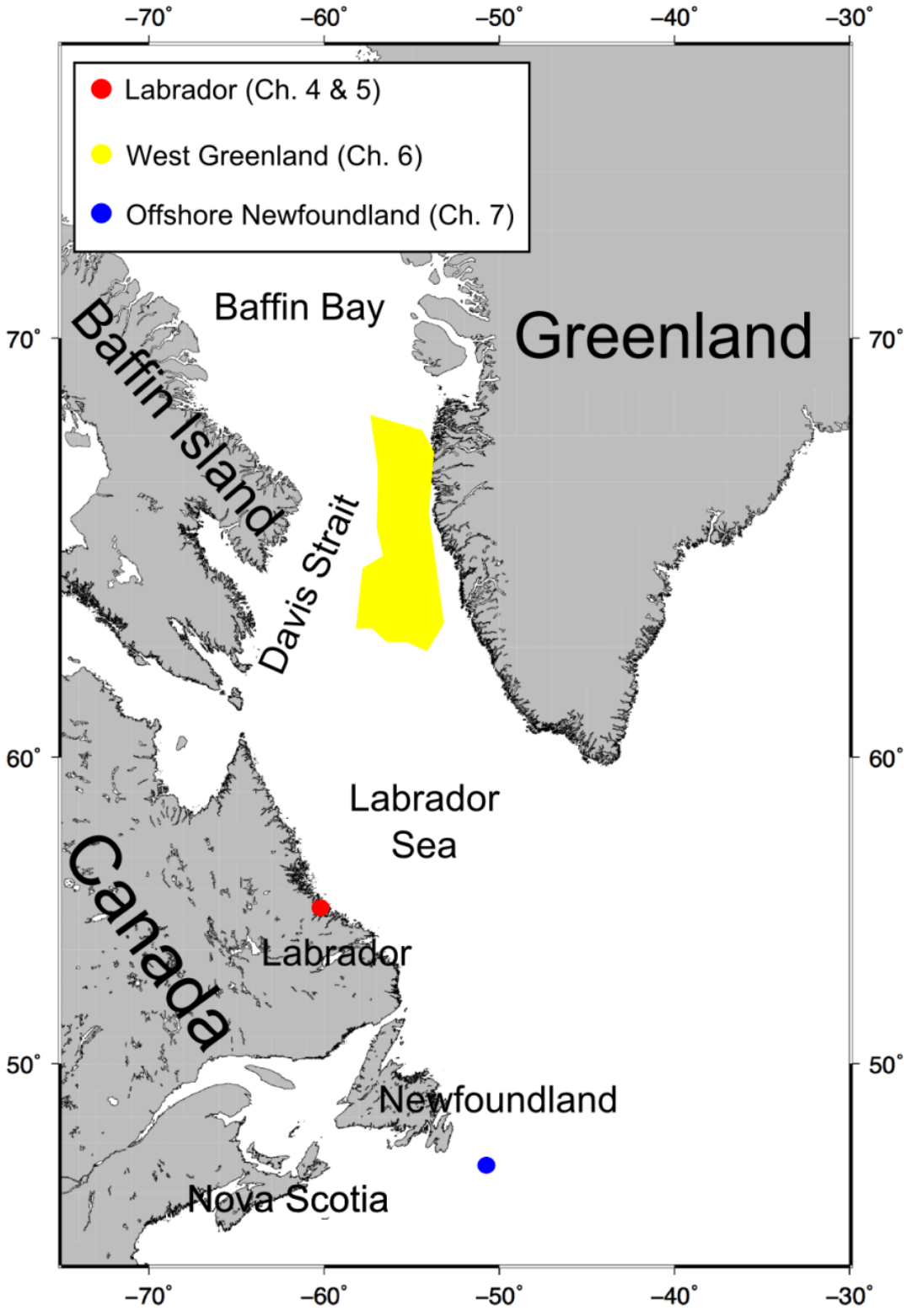

Figure 1.2

A map of the northwest Atlantic region showing the locations of the three main study areas analysed in this study. Plotted using a Mercator projection in GMT.

The location of the fieldwork (Chapters 4 and 5) was primarily selected because the region in proximity to the town of Makkovik, Labrador, Canada was claimed to be the only onshore exposure of Mesozoic rift-related magmatism on the Labrador margin (Tappe et al., 2007). The study enabled us to compare rift-related magmatism onshore Labrador to studies of the widespread equivalent magmatism exposed onshore on the conjugate southwest Greenland margin (Larsen et al., 2009) and offshore on the Labrador Shelf (Umpleby, 1979). An assessment of the degree of symmetry in the rift-related magmatism, and other attributes (e.g. sediment thickness and bathymetry) emerged from this work with implications for whether in this case rifting occurred under simple (Lister et al., 1986) or pure shear (McKenzie, 1978). The reason an assessment of conjugate margin symmetry was required is because the mode by which rifting occurs remains unclear (e.g. Wilson et al., 2001a). Another reason for selecting Makkovik as a study location was to collect data to compare the geometry and kinematics of Mesozoic-aged deformation structures associated with the opening of the Labrador Sea with observations made elsewhere on the margins of this ocean basin (West Greenland - Abdelmalak et al., 2012).

The Davis Strait was chosen as the location of the seismic interpretation detailed in Chapter 6 for a number of reasons. Firstly, onshore field-based studies made a testable prediction for the offshore geology that rifting, basin geometry and transform development was primarily controlled by the reactivation of pre-existing structures (Wilson et al., 2006; Japsen et al., 2006) and secondly, studies of the onshore geology show that continental breakup occurred through multiple basement terrains (e.g. St-Onge et al., 2009). Thus, the Davis Strait provided the ideal natural laboratory to evaluate the role of structural inheritance during continental breakup. The other reason that the Davis Strait was chosen was because adequate seismic, exploration well and onshore structural data was made

available to the project at or adjacent to this location. The nature of these datasets are described fully in Chapter 3 of this thesis.

The numerical modelling work detailed in Chapter 7 was conducted on the Ocean Drilling Program well ODP 210-1276 (Tucholke et al., 2004a) on the Newfoundland margin, offshore Eastern Canada (Chapter 7). This was chosen as the location to conduct the numerical modelling of the thermal influences of an igneous intrusion on organic rich sediments because of the abundance of previous work (e.g. Deemer et al., 2010; Shillington et al., 2004; Tucholke et al., 2004b) that has provided excellent constraints for the numerical models which would not have been possible at many other locations, particularly in proximity to the other study locations detailed in this thesis (Fig. 1.2).

1.5 Geological Setting of the North Atlantic

This section is intended to provide an overview of the large-scale geological setting of the North Atlantic region (Fig. 1.1) to supplement the more detailed, local geological settings described in the concise 'journal-style' data chapters, and to show that although the study areas (Fig 1.2) are geographically separated from one another they are linked through a shared geological history of Mesozoic breakup of the North Atlantic. Additionally, the large-scale datasets (e.g. sediment thickness, oceanic magnetic data, gravity and bathymetry detailed in Chapter 3), allowed observations and interpretations to be linked between the locations.

To understand the development of the Atlantic Ocean it is important to understand the sequence of events prior to continental breakup in order to determine the role, if any, played by pre-existing structures on subsequent breakup related processes (e.g. Holdsworth et al., 2001; Jackson, 1980). In particular, previous orogenic activity must be understood (Krabbendam, 2001) as this represents the most important mechanism of lithospheric

rejuvenation within continental regions (Houseman and Molnar, 2001). Orogenic activity comprises a number of processes which may cause weakening or strengthening (Krabbendam, 2001) of the crust including: crustal thickening (e.g. Houseman and England, 1993) resulting in gravitational instabilities (Houseman and Molnar, 2001) and weakening due to metamorphism of the thickened crust (Ryan, 2001) and the development/reactivation of deep faults and shear zones (Jackson, 1980). The process of tectonic inheritance is expanded upon in Chapter 2, with a particular focus on the role of pre-existing structures during rifting and continental breakup. The complex sequence of Archean, Proterozoic and Paleozoic deformation events prior to Mesozoic rifting in the North Atlantic are likely to have created significant heterogeneities into the crust and lithosphere of the region. The role of such structures for the Mesozoic evolution of the North Atlantic region is an understudied topic that this study (Chapters 5 and 6) aims to address.

The tectonic history of the North Atlantic is intricate and includes several deformation events (e.g. Peron-Pinvidic et al., 2012). The oldest recorded deformation in the North Atlantic region is Archean in age, and includes terrains across the region (Fig. 1.3) such as the North Atlantic Craton of Greenland and the Nain Province of Eastern Canada (Nutman and Collerson, 1991; Bridgwater et al., 1973).

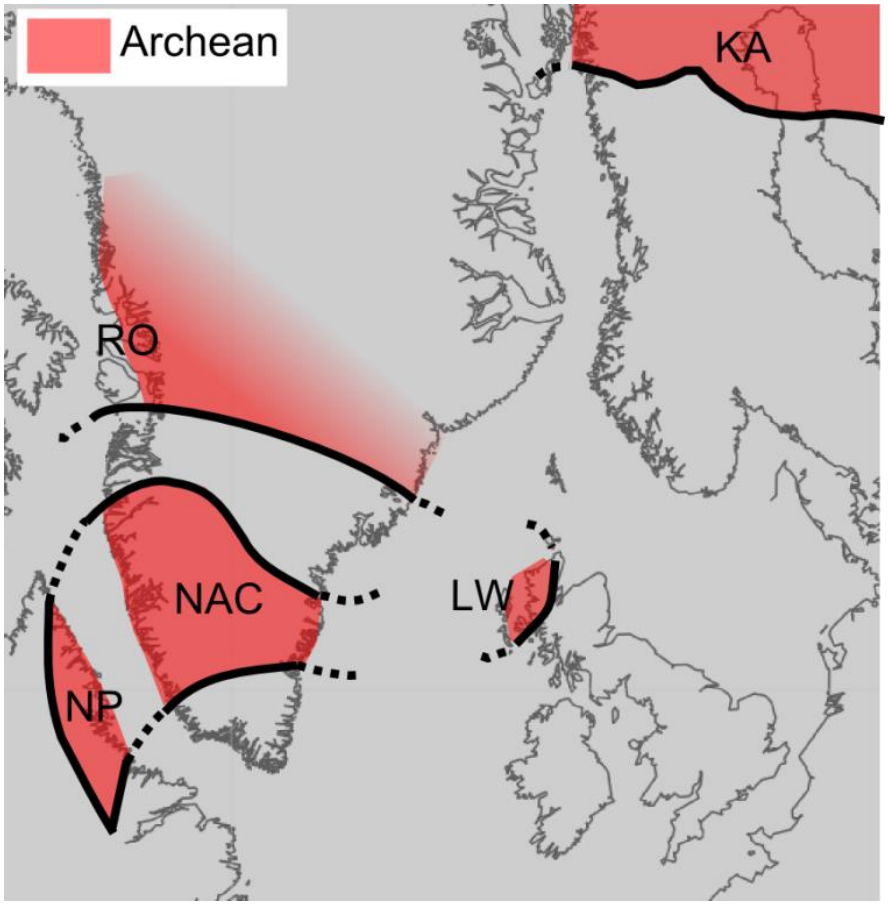

Figure 1.3

An overview of Archean terrains of the North Atlantic region compiled from St-Onge et al. (2009) and Connelly and Mengel, (2000) at 200 Ma plotted prior to continental breakup in GPlates using the reconstruction of Seton et al. (2012). Abbreviations: NP = Nain Province, NAC = North Atlantic Craton, RO = Rinkian Orogen, LW = Lewisian and KA = Karelian.

During the Paleoproterozoic the North Atlantic region was again subjected to multiple deformation events (St-Onge et al., 2009). Accretionary terrains of Paleoproterozoic age are documented across the region (St-Onge et al., 2009; Connelly and Mengel, 2000) (Fig. 1.4) but of particular interest to this study are the Makkovik (e.g. Ketchum et al., 2002), Ketilidian (e.g. Garde et al., 2002), Nagssugtoqidian (e.g. Kolb, 2014) and Torngat (Centreville and Scott, 1998) orogens as they occurred adjacent to the primary study area to the West of Greenland.

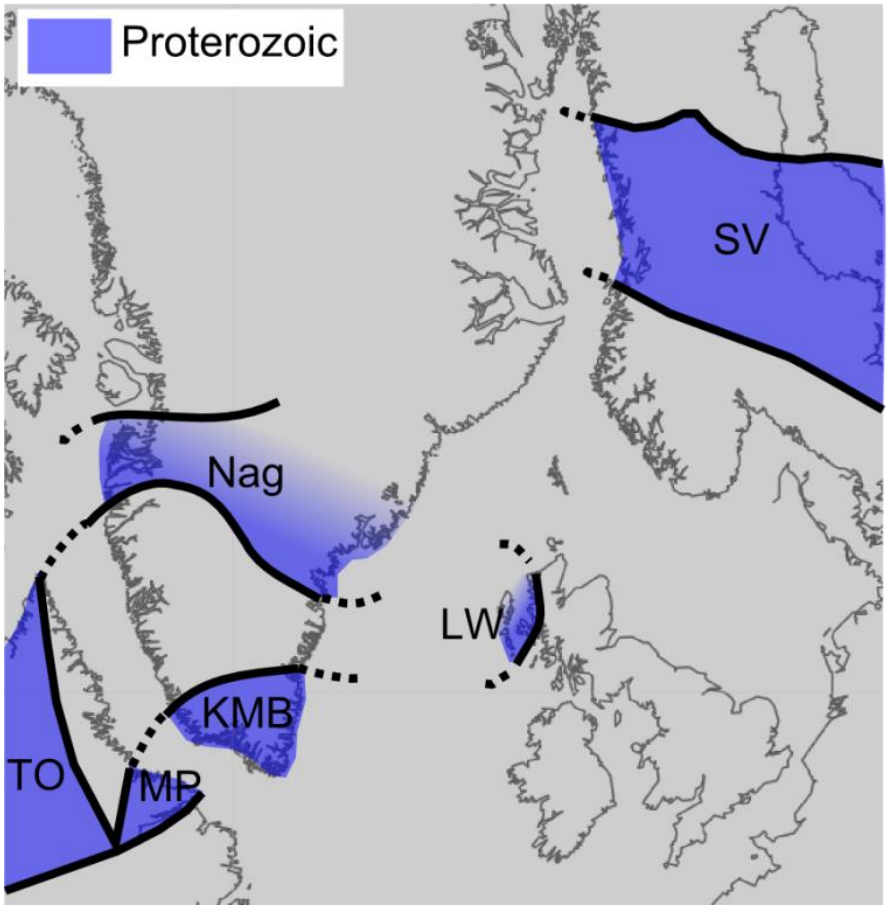

Figure 1.4

The locations of Proterozoic deformation across the North Atlantic region. Modified from St-Onge et al. (2009) and Connelly and Mengel (2000) at 200 Ma plotted prior to continental breakup in GPlates using the reconstruction of Seton et al. (2012). TO = Torngat Orogen, MP = Makkovik Province, KMB = Ketilidian Mobile Belt, Nag = Nagssugtoqidian Orogen, LW = Lewisian and SV = Svecofennian Orogen.

For more than 400 Ma (Rivers, 1997) between the late Mesoproterozoic to early Neoproterozoic parts of the study area were deformed by the Grenvillian orogeny (Rivers, 2008). The Grenville Province was formed during thrusting and modified by later extension (Rivers, 2008).

The last significant widespread deformation event prior to the development of the Atlantic Ocean was the Caledonian Orogeny (McKerrow et al., 2000). It was the general parallelism between this orogeny and location of the North Atlantic margins that led

previous workers to propose the idea that continental breakup may have occurred along old orogenic fronts (Wilson, 1966). The Caledonian Orogeny (Fig. 1.5) as defined by McKerrow et al. (2000) to include all the Cambrian, Ordovician, Silurian and Devonian tectonic events associated with the development and subsequent closure of the Iapetus Ocean, occupying a time interval of around 200 Ma (McKerrow et al., 2000). The main mountain building events occurred in the Ordovician and Silurian (Woodcock and Strachen, 2000) and subsequent gravitational collapse of the Caledonian orogeny occurred by Devonian times (Fossen and Dunlap, 1998; Roberts, 2003). Geographically the Caledonian Orogeny includes parts of the British Isles, Ireland, Scandinavia and East Greenland (McKerrow et al., 2000), and its continuation in the south, the Appalachian Orogen in eastern North America (Hatcher, 2010; Haworth et al., 1988) (Fig. 1.5).

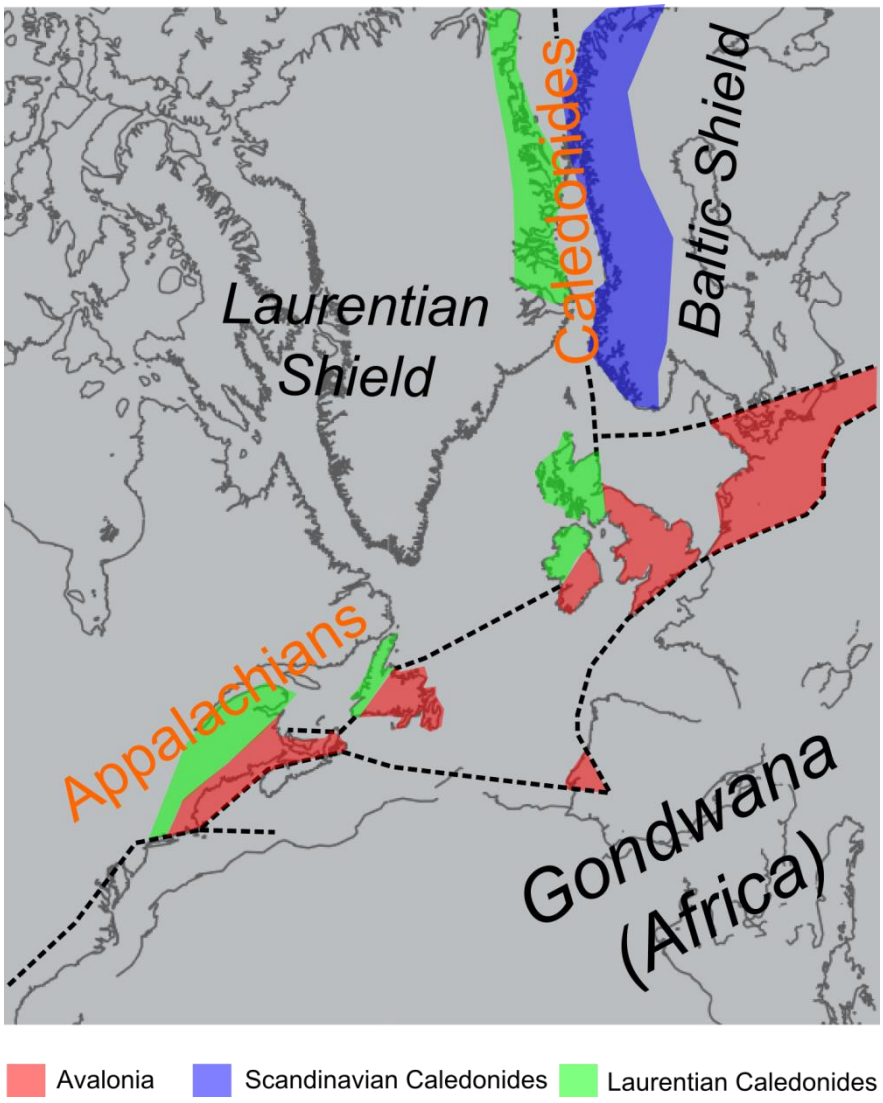

Figure 1.5

An overview of the Caledonian-Appalachian orogen (Haworth et al., 1988) as summarised by (McKerrow et al., 2000) plotted at 200 Ma prior to continental breakup in GPlates using the reconstruction of Seton et al. (2012).

After the Caledonian orogeny several rifting episodes occurred in the region culminating in continental breakup in the Early Paleocene (Labrador Sea) and Early Eocene (NE Atlantic) (e.g. Mjelde et al., 2008). The chronology of the Mesozoic to Tertiary rifting and breakup in the North Atlantic region is well studied and thus it is reasonably well constrained due to the abundance of previous work (e.g. Oakey and Chalmers, 2012; Gaina et al., 2009; Torsvik et al., 2001; Chalmers and Laursen, 1995; Srivastava, 1978). The earliest evidence

of rifting is interpreted to be around the Triassic time or possibly earlier according to the age of coast-parallel dykes onshore in West Greenland (Larsen et al., 2009). However, it was in the Cretaceous when the extensional stress regime is inferred to have been particularly intense (Larsen et al., 2009), with widespread evidence for rifting having been documented across the North Atlantic region. This tectono-stratigraphic and structural evidence (e.g. Gregersen and Skaarup, 2007) includes syn-rift volcanic rocks (e.g. Alexis Formation - Umpleby, 1979), faulting (e.g. Abdelmalak et al., 2012) and a notable change in the composition of rift-related magmatism (Larsen et al., 2009).

Reconstructions of the onset of seafloor spreading in the North Atlantic show that it propagated northwards from the Central Atlantic in the Jurassic (ca. 175-180) (e.g. Lundin, 2002) (Fig. 1.6). Thus, the oldest oceanic crust in the region is found adjacent to the continental margins closest to the Central Atlantic (e.g. Lundin, 2002), a spatial relationship that is evident in the Müller et al. (2008) seafloor age model based on magnetic lineation analysis (Fig. 1.6). By the Late Aptian seafloor spreading had reached the Galacia Bank (Srivastava and Tapscott, 1986) and, by Middle to Late Aptian time, it had propagated as far as the Goban Spur (Tate, 1993). By the Santonian, the spreading axis had reached the Charlie Gibbs Fracture Zone (CGFZ – Figs. 1.1 and 1.6) (Lundin, 2002). Seafloor spreading was then initiated in the Labrador Sea in the Early Paleocene (Chalmers and Laursen, 1995) and in the NE Atlantic by the Early Eocene (e.g. Mjelde et al., 2008). Seafloor spreading is generally accepted to have reached Baffin Bay by the Latest Maastrichtian or Earliest Paleocene (Chalmers and Pulvertaft, 2001). Then in the Oligocene seafloor spreading in the Labrador Sea and Baffin Bay ceased, driven by a change in the direction of movement of Greenland (Srivastava and Roest, 1999).

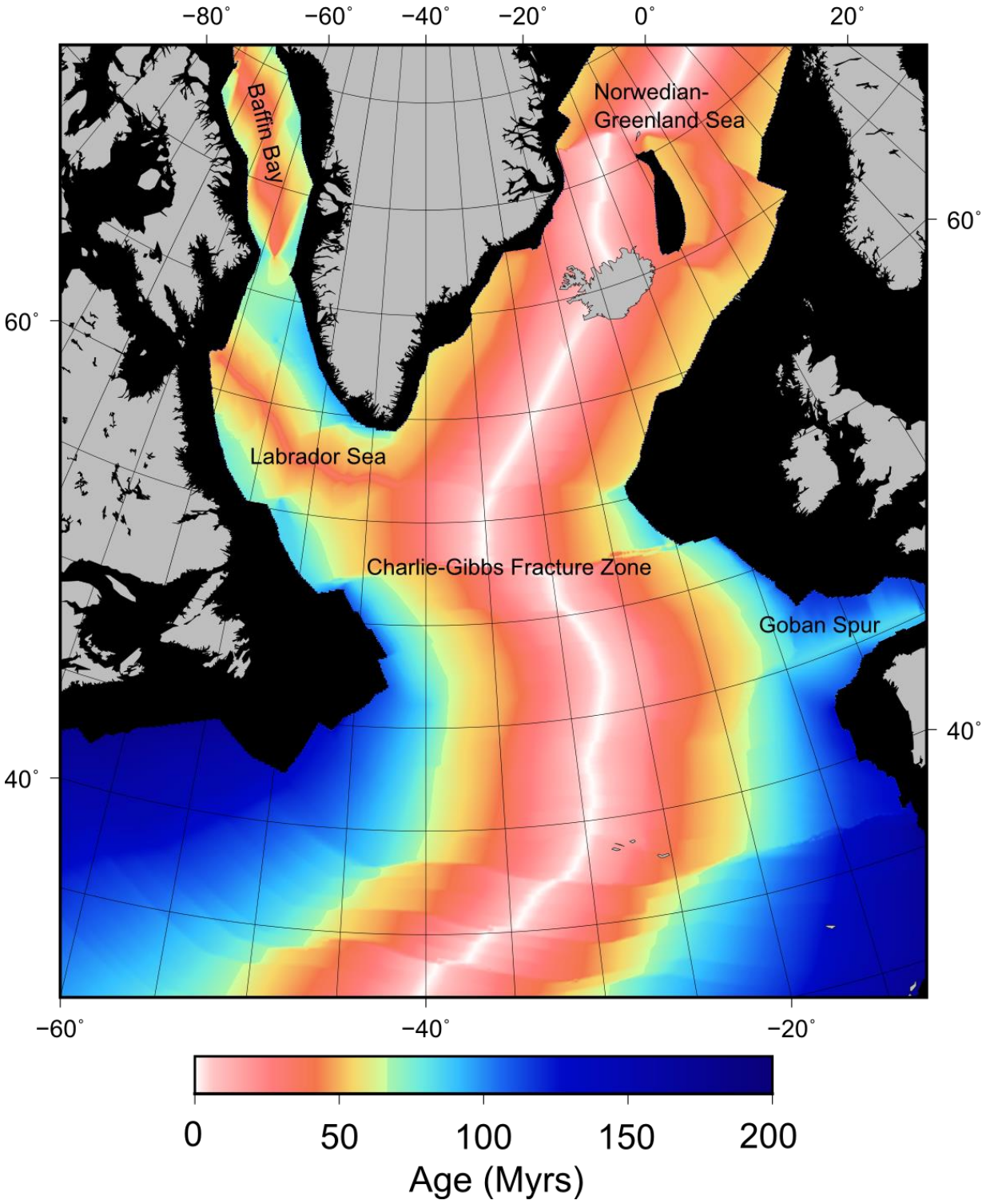

Figure 1.6

Age of the oceanic crust in the North Atlantic ocean according to the compilation of Müller et al. (2008). This compilation is based on oceanic magnetic and gravity data (Smith and Sandwell, 1997) at a resolution of 2 arc minutes. Plotted using a polar stereographic projection in GMT.

The complex propagation of seafloor spreading in the North Atlantic as described above is summarised by Oakey and Chalmers, (2012) into three key stages: 1) the Paleocene (onset to ca. 55 Ma) separation between North America and Greenland; 2) the Eocene (ca. 55 Ma – ca. 35 Ma) continued separation between Greenland and North America with Greenland moving as an independent plate from Eurasia; and 3) since the Oligocene (ca. 35 Ma – present) the continued separation of Eurasia and Greenland with the latter now being attached to North America (end of seafloor spreading west of Greenland). This is depicted in Figure 1.7 using the reconstruction of Seton et al. (2012).

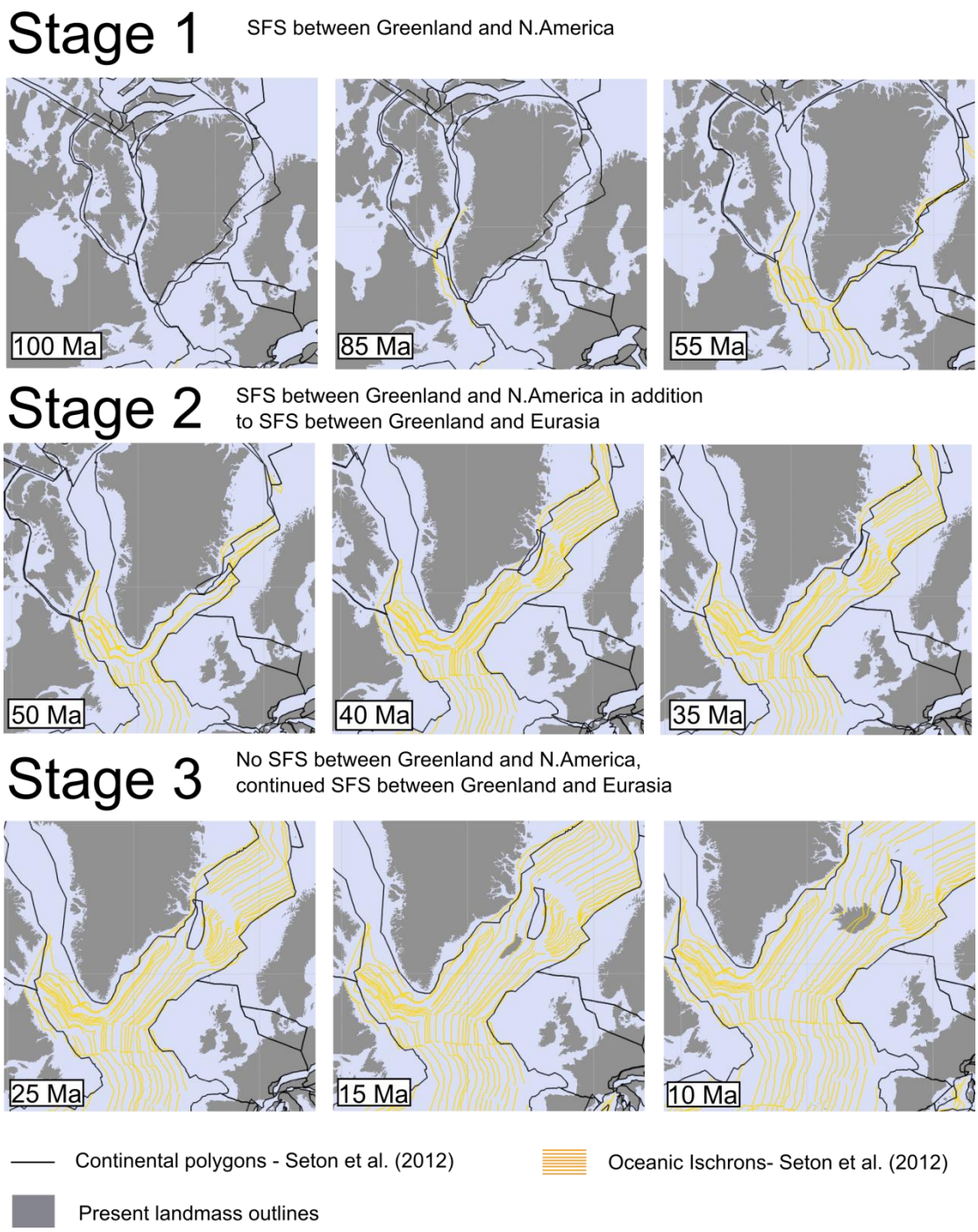

Figure 1.7

The three stages of breakup of the North Atlantic (Oakey and Chalmers, 2012) shown using the reconstruction of Seton et al. (2012) displayed using a Mercator projection in GPlates. SFS = Seafloor spreading.

The second of the stages identified by Oakey and Chalmers, (2012) begins at ca. 55 Ma and represents one of the most complex times during the evolution of the North Atlantic

region as several key events occurred in very close temporal proximity. These events include: 1) the onset of seafloor spreading to the east of Greenland (Srivastava, 1978); and 2) widespread volcanism across the North Atlantic region (White, 1988). Thus, determining the chronology of events ca. 55 Ma in the North Atlantic is crucial to understanding the fundamental mechanisms operating during continental breakup in the region. Several hypotheses have been proposed to explain the events at ca. 55 Ma in the North Atlantic including arrival of the proto-Icelandic plume (White, 1988) and intraplate deformation in Europe (Nielsen et al., 2007).

Contemporaneous with the breakup of the North Atlantic, widespread voluminous magmatism was produced (e.g. White, 1988) mostly as a large igneous province known as the North Atlantic Igneous Province (NAIP - Fig. 1.8) (e.g. Hansen et al., 2009) but also as earlier rift-related melts such as the margin parallel dykes of West Greenland (ca. 142 Ma - Larsen et al., 2009) and the post-breakup U-reflector of Newfoundland (Ca. 96 - 106 Ma - Hart and Blusztajn, 2006). The NAIP (Fig. 1.8) is typically considered to comprise all the Paleogene intrusive rocks from Scandanavia, Britain and Ireland, both East and West Greenland, and Baffin Island (e.g. Upton, 1988) including the widespread seaward dipping reflectors (SDRs) (Eldholm et al., 1986). The extrusive rocks of the NAIP cover an area of at least ~1.3 x 10^6 km^2, whilst the total volume of both the extrusive and intrusive rocks is estimated to be ~6.6 x 10^6 km^3 (Eldholm and Grue, 1994). The NAIP is interpreted to have experienced two main periods of melt emplacement: 1) ca. 62- 58 Ma and 2) ca. 57-53 Ma, with distinct peaks of greater abundance within these emplacement intervals at ca. 60 Ma and ca. 55 Ma respectively, implying a greater amount of melt generation (Hansen et al., 2009).

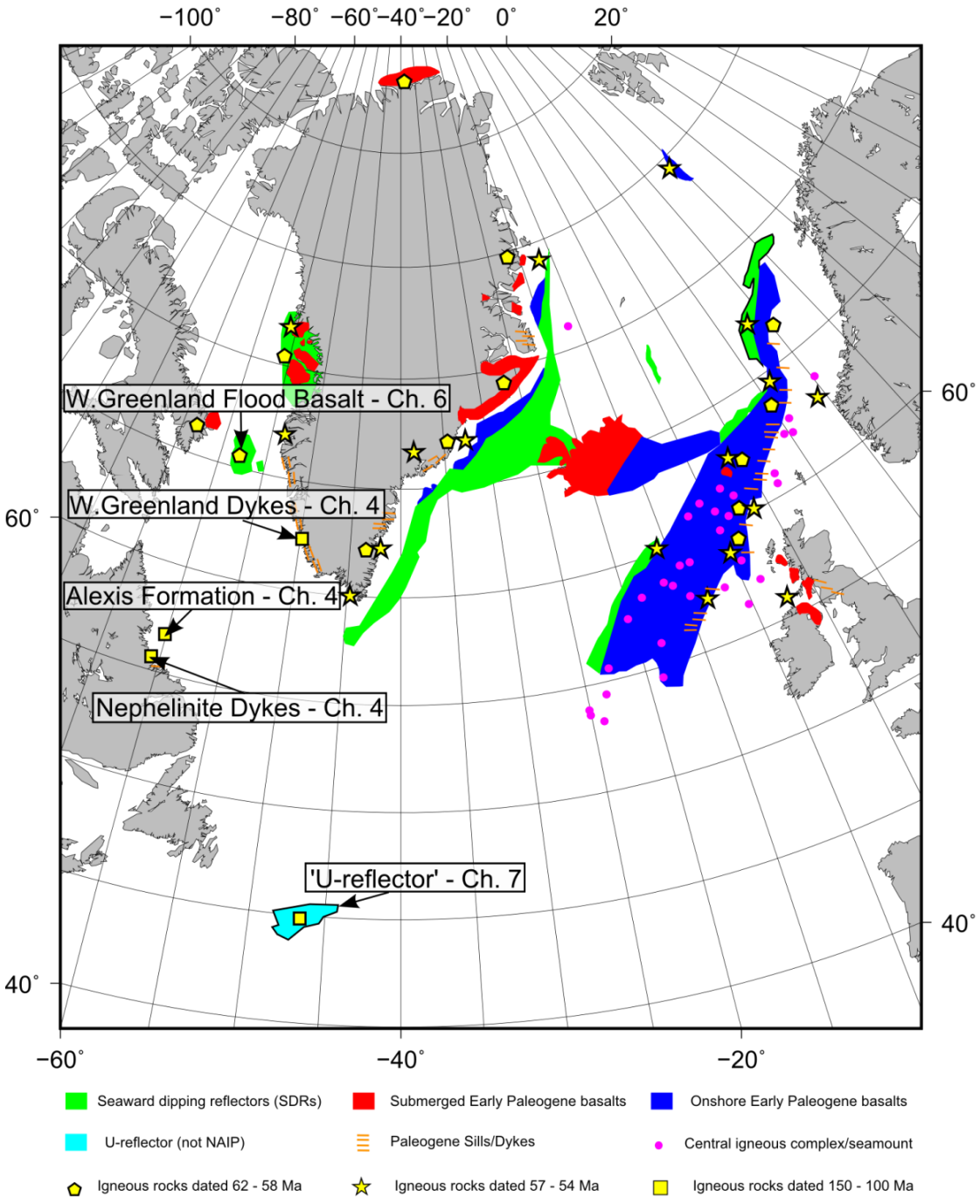

Figure 1.8

An overview of the NAIP modified from Hansen et al. (2009) and other earlier breakup related igneous rocks in particular those studied in detail in this study including; the Cretaceous dykes of West Greenland (Larsen et al., 2009) (Chapter 4), the Alexis Formation offshore Labrador (Umpleby, 1979) (Chapter 4), the Nephelinite dykes onshore Labrador (Tappe et al., 2007) (Chapter 4) and the U-reflector, offshore Newfoundland (e.g. Deemer et al., 2010) (Chapter 7).

The mechanisms controlling the causes, consequences, variability and distribution both spatially and temporally of the breakup related magmatism both in the North Atlantic and for continental breakup generally are relatively poorly understood (White, 1992; Foulger, 2005). The debate essentially focuses on whether a thermal anomaly in the mantle is required to produce such large quantities of melt in such a short period of time (e.g. Foulger et al., 2005). The dominant school of thought in the literature is that the arrival of the proto-Icelandic plume, which is the precursor to the alleged plume now located under Iceland, was the primary cause of the widespread volcanism. However, the presence and role of mantle plumes during rifting and opening of the North Atlantic remains equivocal (e.g. Foulger, 2001; Lundin and Doré, 2005) and there are numerous aspects of the North Atlantic breakup that are claimed to be incompatible with the mantle plume hypothesis (Lundin and Doré, 2005). The term 'plume' in this thesis is defined as a convective upwelling of lower mantle material due to thermal instability near the core–mantle boundary (Morgan 1971), although some ambiguity is associated with this term in the scientific literature.

Whether a mantle plume is required to produce the breakup related igneous rocks is not the only aspect of breakup related magmatism that requires further research. Another understudied area includes understanding why early rift-related magmatism is often unevenly distributed between conjugate margins (Red Sea - Dixon et al., 1989). Understanding the asymmetric magmatic distributions observed between conjugate margin pairs could lead to an increase in our understanding of the mechanisms governing early rift development (Chapter 4). In addition to studying the melt generation and distribution processes this study aims to understand how breakup related magmatism in the North Atlantic has interacted with the surrounding material, in particular the way in which magmatism could have influenced petroleum systems (Chapter 7).

Chapter 2

Passive continental margins: formation, classification and petroleum exploration

2.0 Introduction

The term passive margin is a synonym of Atlantic-type margin, rifted margin, trailing-edge margin, or divergent margin (Bradley, 2008). Passive margins are among the most common of the Earth's first order tectonic features, with a present day aggregate length of 105,000 km, which is greater than either the oceanic spreading ridges (65,000 km) or convergent plate boundaries (Bradley, 2008). Most of the major oceanic basins on Earth contain passive margins, but it is the North and South Atlantic where the abundance of the research has taken place on several margins which are considered to be typical of all passive margins (e.g. Iberia-Newfoundland – Peron-Pinvidic et al., 2007; Brazil-Angola – Contrucci et al., 2004; Davison, 1997) (Fig. 2.1). Such a geographical bias in the coverage of research and data towards certain Atlantic margins, has led to challenges when models developed from studies of these specific margins have been applied globally (e.g. Wilson et al., 2001). This is one of the reasons that this study was conducted primarily in the Labrador Sea-Baffin Bay rift system, as compared to other parts of the Atlantic this area has received less attention from the research community.

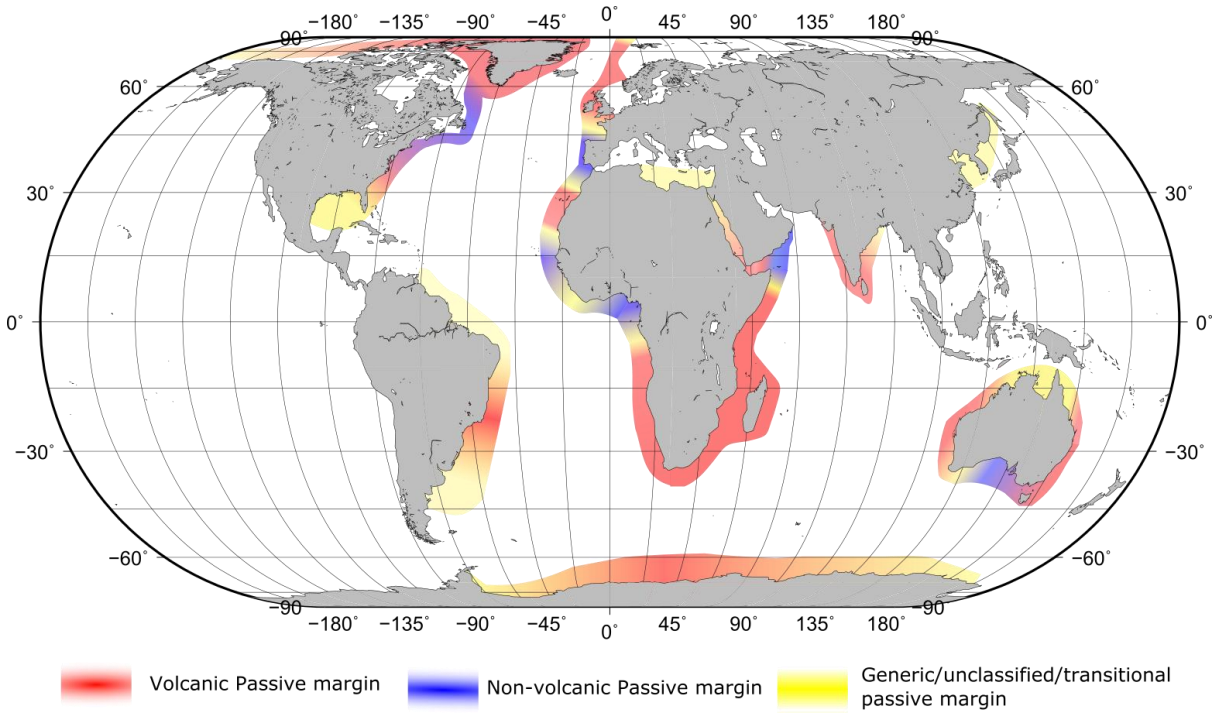

Figure 2.1

Global map depicting the distribution of passive margin types, modified from Magee et al. (2016) originally from

The aims of this chapter are to: 1) review and summarise the classification and formation of passive margins, based on the previous literature; and 2) to discuss the characteristics of petroleum systems on passive margins, with a particular focus on the magma-rich (or volcanic) end-member variety. Significant knowledge gaps in our understanding of passive margins are also identified in this chapter to expand upon the rationale and aims outlined in Chapter 1.

2.1 The classification and structure of passive margins

Although magmatism invariably accompanies all continental breakup (White, 1992) passive margins are traditionally classified as one of two end-member types, either: 1) volcanic passive margins (VPM), or 2) non-volcanic passive margins (NVPM), in

reference to the relative abundance or scarcity of igneous rocks produced during rifting and breakup (e.g. Geoffroy et al., 2015; Franke, 2013; Geoffroy, 2005; White, 1992).

Both VPMs and NVPMs occur globally (Fig 2.1) (Geoffroy, 2005; Magee et al., 2016). White et al. (2003) state that NVPMs are the more abundant variety of passive margin, whereas Menzies et al. (2002) and Skogseid (2001) claim that most margins are VPMs. This ambiguity suggests that the distinction between VPMs and NVPMs is not always as clear as this binary classification scheme implies, and that a spectrum of margin types between the two end-members is probable (Franke, 2013). NVPM may in fact be an inappropriate term as there are no passive margins entirely devoid of igneous rocks (Franke, 2013), because melt generation, to a greater or lesser extent is an integral part of all continental breakup (White, 1992). Indeed previous studies have been devoted to studying occurrences of magmatism at margins classified as NVPMs (e.g. Newfoundland - Deemer et al., 2010; South Australia - Meeuws et al., 2016; West Iberia - Whitmarsh et al., 2001b). For this reason some studies use the terms ‘magma-rich’ and ‘magma-poor’ to describe volcanic and non-volcanic margins respectively (e.g. Franke, 2013). The distinction between VPMs and NVPMs forms the basis of many models of VPM genesis, whereby NVPMs provide a reference margin type and VPMs are claimed to require a thermal anomaly in the mantle (White, 1992). This school of thought is, however, not universally accepted as it inevitably leads to models requiring a thermal anomaly in the mantle to produce the excess magmatism (e.g. Lundin and Doré, 2005), a concept explored later in this chapter, then revisited in Chapter 8. Despite the possible ambiguity in the distinction between VPMs and NVPMs there are several key structural components that are claimed to be unique to each end-member variety of passive margin (Fig. 2.2). The features that are unique to the different margin types are discussed in the subsequent sections of this chapter.

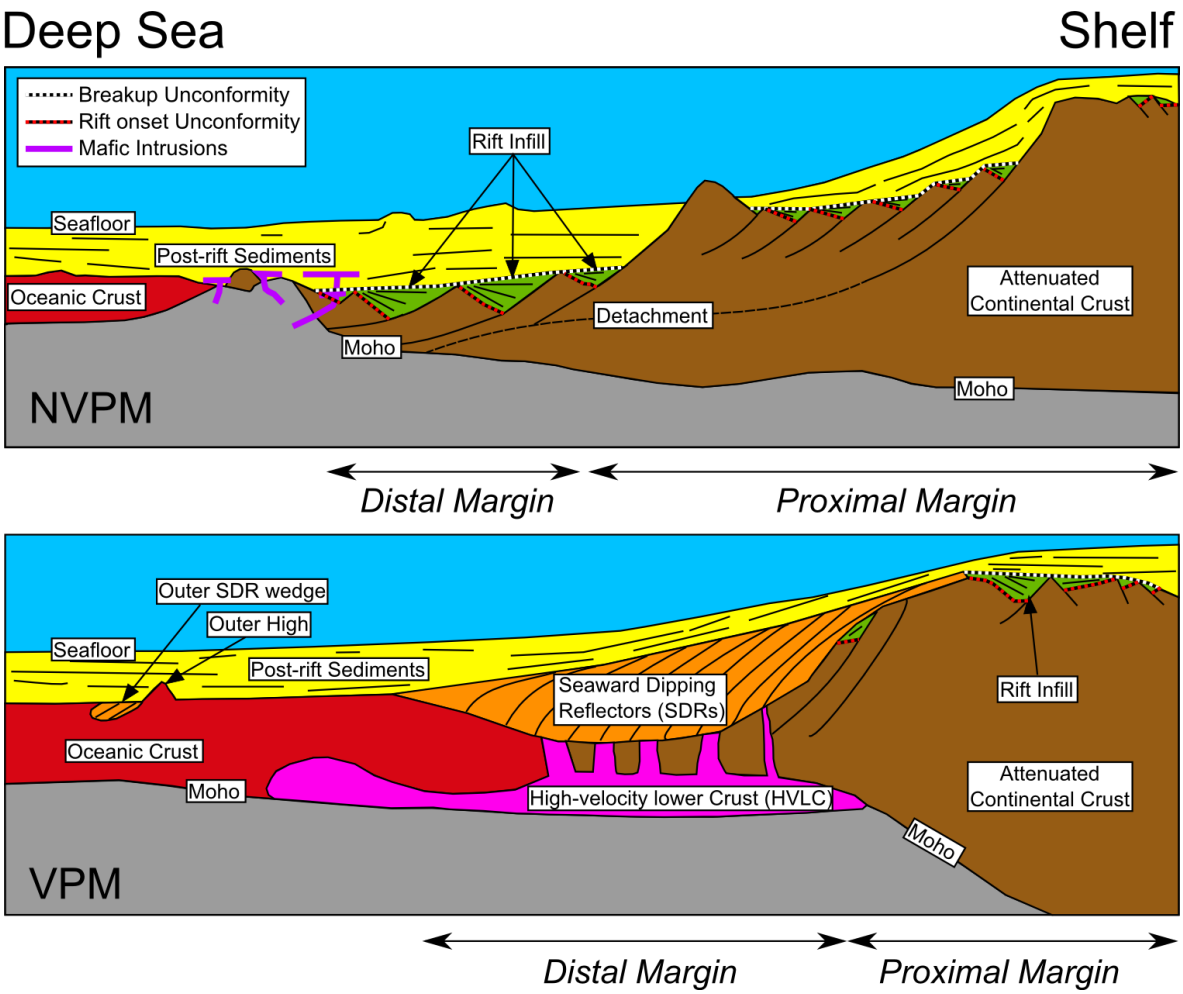

Figure 2.2

A schematic comparison of the structure of non-volcanic and volcanic passive margins in cross section view, modified from Franke (2013).

The tectonostratigraphic development of both volcanic and non-volcanic passive margins is very similar in the broadest sense, and can be divided into pre-, syn- and post-rift stages (Williams, 1993). The pre- and syn-rift are separated from one another by the 'rift onset unconformity' (ROU), whilst the syn-rift is separated from the post-rift by the 'break-up unconformity' (BU) (Franke, 2013). Both the ROU and the BU usually give rise to prominent seismic reflections due to the significant impedance contrasts generated by the period of no deposition or erosion.

2.1.1 Volcanic passive margins

VPMs are located globally (Fig. 2.1). Examples of well-studied VPMs are mostly located in the Atlantic including; the Norwegian (e.g. Fernandez et al., 2005) and East Greenland (e.g. Brooks, 2011) margins. However, non-Atlantic VPMs which are relatively well studied include the northwest shelf of Australia (e.g. Frey et al., 1998) and West Indian margin (e.g. Ajay et al., 2010).

Compared to NVPMs, VPM's display an abrupt ocean-continent transition (White, 1992), whilst other unique features of VPMs include: voluminous thick flood basalts usually as part of a large igneous province (LIP); volcanic rocks imaged on seismic reflection profiles as seaward dipping reflectors (SDRs); and high-velocity lower crust with Vp (seismic velocity) in excess of 7 km/h (Franke, 2013).

SDRs (Fig. 2.2) are imaged on seismic reflection profiles as a package of reflectors in close proximity to the OCT (Mutter, 1985; Eldholm et al., 1986; Chalmers, 1997), which are interpreted to represent thick sequences of volcanic rocks erupted prior to continental breakup (Eldholm et al., 1986). Several SDR packages have been drilled, including the western margin of the Rockall Plateau (DSDP leg 81; Roberts et al., 1984), the Norwegian margin (ODP leg 104; Eldholm et al., 1986) and the SE Greenland margin (ODP legs 152 (Larsen and Saunders, 1998) and 163 (Duncan et al., 1996)). These drilling results concluded that SDRs represent volcanic flows which occurred in a sub-aerial setting. At VPMs the OCT is typically quite abrupt (50-100 km) with the transition occurring in the vicinity of the SDRs (Franke, 2013).

In normal continental crust, the P-wave velocity (Vp) usually only exceeds 7.0 km/h in cratons or shields (Holbrook et al., 1992). However, crustal velocity studies of VPMs (e.g. Chian et al., 1995a) have shown that high velocity lower crust (HVLC) with Vp in excess of 7.3 km/h is a common feature (Franke, 2013). HVLC has not been directly sampled due

to its significant depth (e.g. 25-30 km on the Vøring Margin - Mjelde et al., 2015). Interpretation of HVLC on VPMs include; massive intrusions, mafic underplating, serpentinised mantle and/or inherited metamorphic rocks (Franke, 2013). Some margin-parallel magnetic anomalies, such as the East Coast Magnetic Anomaly (ECMA) (Behn and Lin, 2000), have also been attributed to the presence of magnetically susceptible lower crustal bodies that potentially correspond to HVLC. The volume of igneous material attributed to crustal underplating could be around 70% of the total magmatism observed at VPMs (White, 1992); it is therefore important that the nature of the HVLC is studied if the development of VPMs is to be better understood. The existence of magmatic underplating and the implications for rifting of the Labrador Sea are discussed in Chapter 4.

Voluminous flood basalts are a common contribution to the total magmatic budget of VPMs (e.g. White, 1992). Surface flows may extend hundreds of kilometres from the source if the supply of magma is sufficient and the flow is not impeded by topographic features (White, 1992). Flood Basalts can often be observed on seismic reflection lines as a high amplitude reflector (Fig. 2.3), which in some cases, can cause issues with imaging sub-basalt geology (e.g. Ziolkowski et al., 2003; Christie and White, 2008; Jegen et al., 2009).

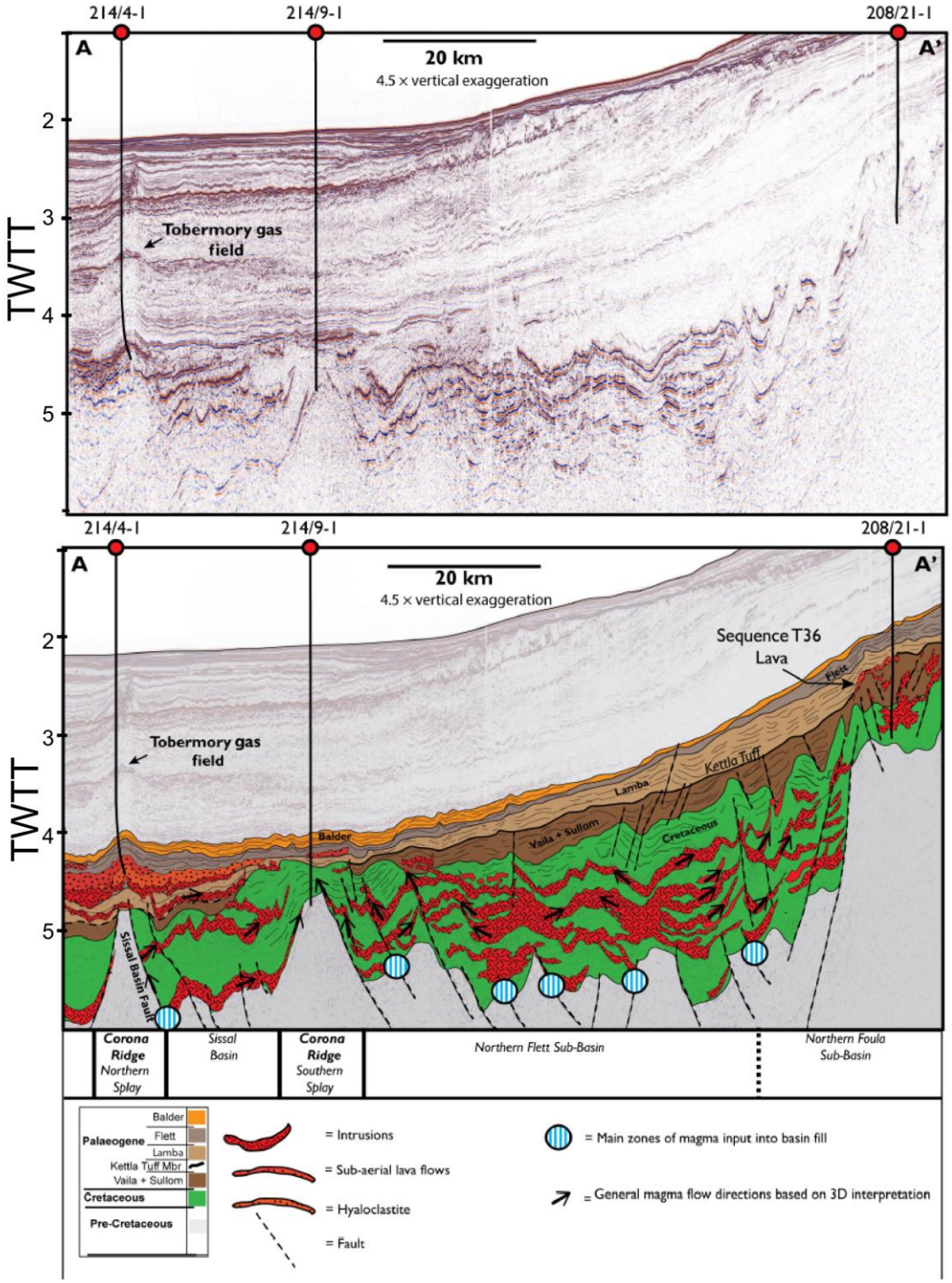

Figure 2.3

A NW-SE trending seismic reflection profile from the PGS FSB MagaSurveyPlus in the Faero-Shetland basin going through the Flett and the Sissal sub-basins and intersecting key wells in the area. This seismic section demonstrates the seismic characteristics of both intrusive igneous rocks and sub-aerial lava flows, types of magmatism that are abundant on the seismic data analysed in this study in Chapter 6. Reproduced from Schofield et al. (2015).

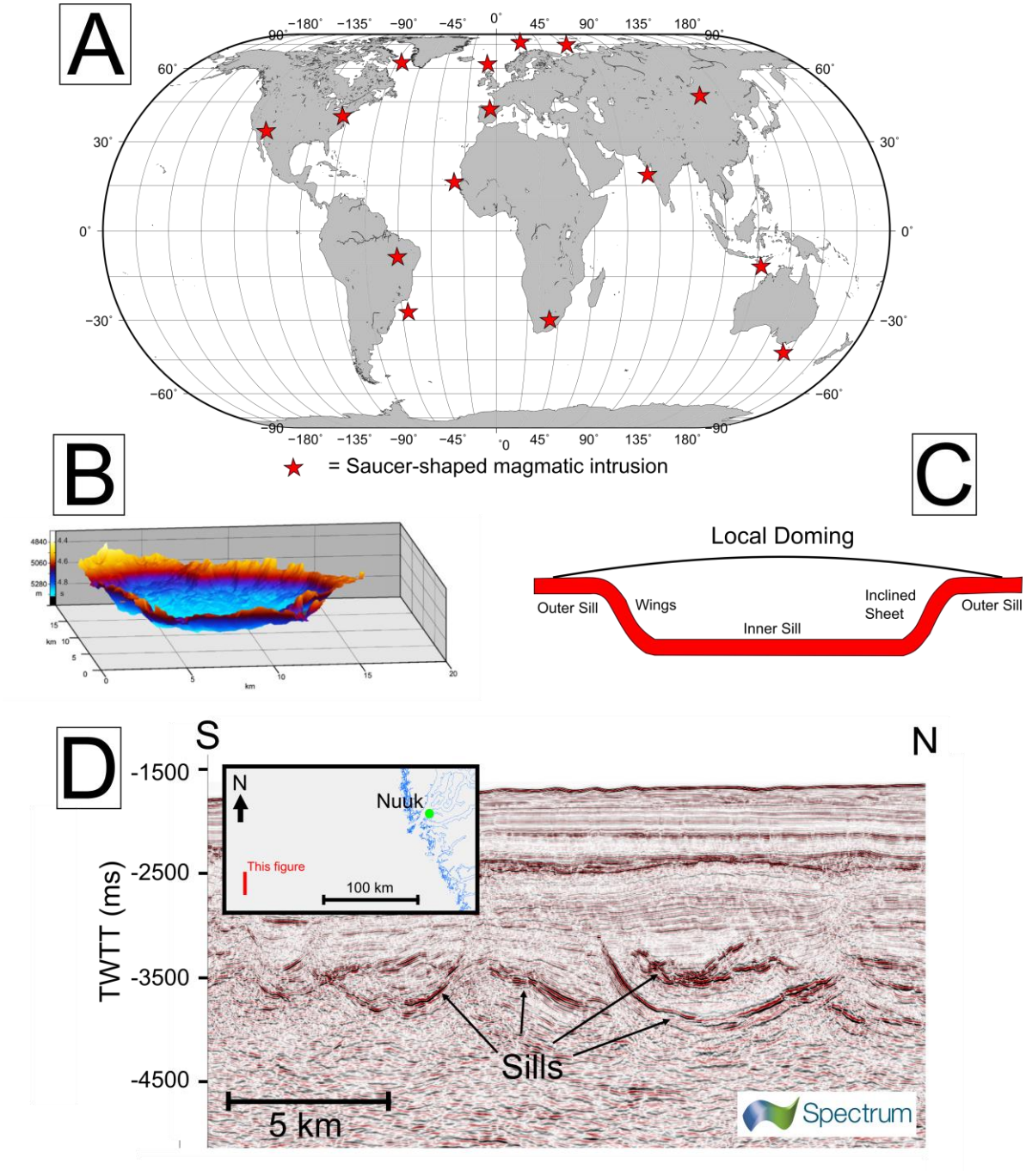

Figure 2.4

A) The global distribution of saucer-shaped sill, B) 3D visualisation of a saucer-shaped sill, C) schematic depiction of the doming or 'forced folds' (e.g. Magee et al., 2014) above a saucer-shaped sill and D) an example of saucer-shaped sills within Cretaceous-Paleocene sediments offshore West Greenland. Parts A), B) and C) of this figure are modified from Polteau et al. (2008).

Many VPMs also display evidence for abundant intrusive magmatism (Hansen and Cartwright, 2006; White, 1992). Intrusive magmatism related to continental breakup can

manifest as both dykes (e.g. southwest Greenland - Larsen et al., 2009) and sills (e.g. the Faroe-Shetland sill complex - Schofield et al., 2015). Intrusive igneous rocks at passive margins often manifest as large stacked complexes of 'saucer-shaped' sills (Fig. 2.4) (Magee et al., 2016; Duraiswami and Shaikh, 2013; Polteau et al., 2008) which can sometimes force the sediments above into an antiformal structure known as a 'forced fold' (Hansen and Cartwright, 2006; Magee et al., 2014). The typical saucer shaped geometry of these sill complexes imaged on seismic data at VPMs has been confirmed using field analogues including the Karoo volcanic province in South Africa (e.g. Galerne et al., 2011).

2.1.2 Non-volcanic passive margins

NVPMs are defined as much by the absence of structures observable at VPMs as having distinct features of their own (Franke, 2013) as SDRs, HVLC and widespread igneous rocks are absent at NVPM (Franke, 2013; White, 1992). However, a unique feature of NVPMs is the wide OCTZ which typically comprises a region of highly attenuated crust that is much wider than the comparable region found at most VPMs (Peron-Pinvidic et al., 2007; Tucholke et al., 2007; Franke, 2013) (Fig. 2.2).

An abundance of work has shown that there is an intimate association between NVPMs, hyperextended lithosphere and exhumed serpentinised upper mantle, with some of the most well studied hyperextended NVPMs being the Iberian-Newfoundland conjugate margins (Tucholke et al., 2007; Peron-Pinvidic et al., 2007) but other examples also include the margins of the Labrador Sea (Chalmers and Pulvertaft, 2001; Chian et al., 1995a) and the South China Sea (Pichot et al., 2014; Franke et al., 2014; Li et al., 2014). In Chapter 4 of this thesis analysis of the transitional zone of the non-volcanic margins of the

Labrador Sea which according to some workers (Chian et al., 1995b) contain a hyperextended, serpentinised zone is presented.

As with their more volcanic counterparts NVPMs are found globally (Fig. 2.1). Some of the most well-studied examples of NVPMs are as with VPMs found in the Atlantic and include; the Brazil-Angola conjugate margins (e.g. Contrucci et al., 2004; Aslanian et al., 2009) and the Iberia-Newfoundland conjugate margins (e.g. Tucholke et al., 2007; Peron-Pinvidic et al., 2007; Whitmarsh et al., 2001b). However, other relatively well studied NVPMs from outside the Atlantic include the South China Sea (e.g. Barckhausen et al., 2014; McIntosh et al., 2014) and South Australian margin (e.g. Sayers et al., 2001).

2.2 The formation and development of passive margins

This section first describes the processes that are considered to be generic to the formation of all passive margins. The possibility of whether unique processes are required for the formation of VPMs and NVPMs are then discussed.

The events which are integral to the formation of all passive margins are: 1) continental rifting; 2) breakup (oceanic crust production); and 3) thermal subsidence (e.g. Franke, 2013; Geoffroy, 2005). However, not all rifts progress through all these stages to become passive margins, instead many rifts fail to reach complete breakup e.g. the North Sea (Rattey and Hayward, 1993).

Continental rifting represents the initial stages of continental breakup (Allen and Allen, 2005; Franke, 2013). For a rift to initiate a sufficient horizontal deviatoric stress is required to stretch the lithosphere (McKenzie, 1978; Allen and Allen, 2005). The tension required to initiate a rift can be caused by several phenomenon including: 1) plate motions; 2) thermal buoyancy due to asthenospheric upwellings; 3) traction at the base of the

lithosphere caused by convecting asthenosphere and 4) gravitational forces caused by variations in crustal thickness (Huismans et al., 2001). The causes of the horizontal deviatoric stress is expanded upon later in this section.

The next key stage in the formation of passive margins is continental breakup (Peron-Pinvidic, 2016; Franke, 2013). Breakup is commonly attributed to the end of rifting and the onset of seafloor spreading, which is facilitated by the final rupture of the continental lithosphere (Peron-Pinvidic, 2016). Seafloor spreading is defined by Whitmarsh et al. (2001b) as an 'essentially axisymmetric process active at an accretionary plate boundary that leads, within the resolution of current magnetochronological time scales, to the continuous formation of new oceanic crust'.

Post-breakup (formation of new oceanic crust) the margins of the rift usually isostatically subside (e.g. Orange Basin, South Africa - Hirsch et al., 2010). The subsidence which occurs after rifting on passive margins is driven by the mechanical effects of rifting and a relaxation of the thermal anomaly associated with rifting (Allen and Allen, 2005). Nevertheless, some passive margins do display evidence for uplift (North Atlantic - Japsen et al., 2010) sometimes resulting in reactivation of syn-rift faults in the post-rift interval (Cloetingh et al., 2008).

NVPMs are crucial to our understanding of passive margins as they demonstrate that significant stretching of the lithosphere is not necessarily accompanied by large-scale melting (White, 1992; Whitmarsh et al., 2001b). This observation has been taken by previous workers to imply that an additional thermal anomaly is required to produce the voluminous melts that constitute VPMs (e.g. White, 1992). As a result much of the research into passive margin formation focuses on the causal mechanisms leading to the distinction between VPMs (e.g. Callot et al., 2001) and NVPMs (e.g. Whitmarsh et al.,

2001). This has led previous work to typically consider continental rifting to occur either as a result of 'active' upwelling asthenosphere at the location of the rift or as a result of 'passive' lithospheric extension driven by far field forces (Sengör and Burke, 1978) (Fig. 2.5). Whether the formation of VPMs as opposed to NVPMs actually requires a fundamentally different mechanism has however been the subject of debate (Bowling and Harry, 2001), with many previous workers invoking mantle plumes to explain the widespread igneous rocks present at VPMs (e.g. Gerlings et al., 2009; Larsen and Saunders, 1998; Starkey et al., 2009). Some previous studies have however highlighted the questionable role of thermal anomalies in the mantle (i.e. mantle plumes - Morgan, 1971) during continental breakup and volcanic margin formation (e.g. Lundin and Doré, 2005; Franke, 2013). It is, however, well recognised that VPMs develop from volcanic rifts and NVPMs develop from relatively magma-poor rifts but the mechanism leading to volcanic and non-volcanic rifts is not universally agreed upon (Geoffroy, 2005). Some numerical modelling work has suggested that a thermal anomaly in the mantle is not required to account for the difference between volcanic and non-volcanic margins (e.g. Bowling and Harry, 2001) whereas in other numerical modelling work a thermal anomaly is required (e.g. Farnetani and Richards, 1994).

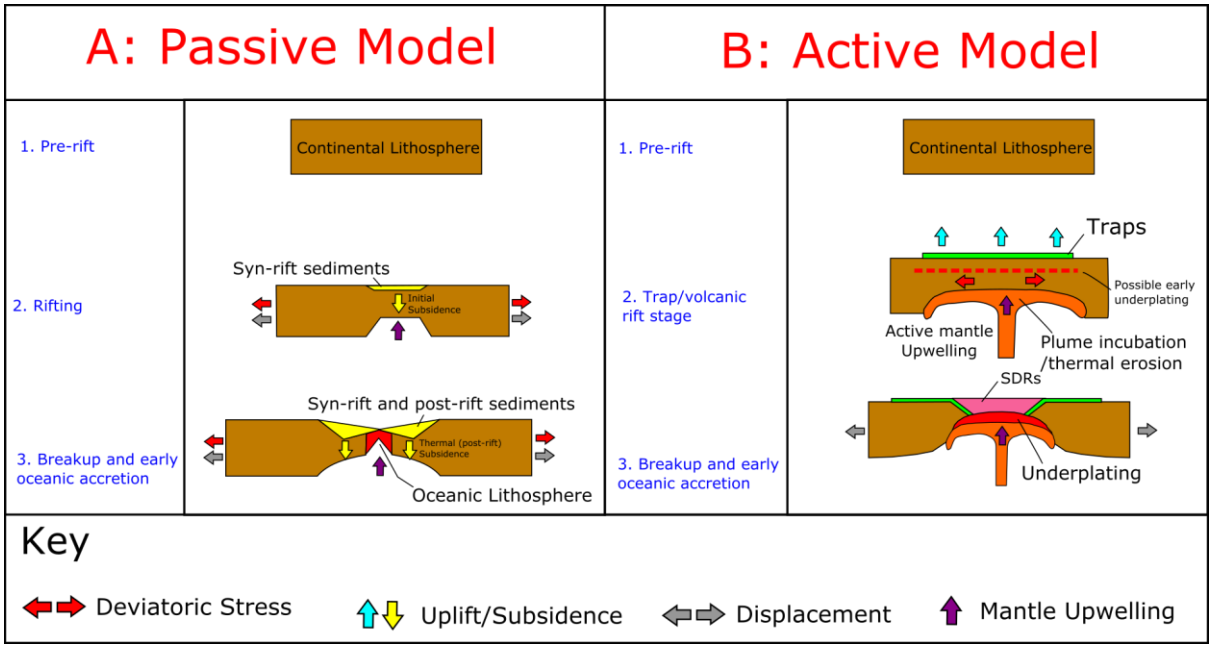

Figure 2.5

Comparison of A) the passive and B) the active models of rifting and margin formation. Modified from Geoffroy (2005) based on the concepts of Sengör and Burke (1978).

In the active model of rifting a thermal anomaly in the mantle (for example a mantle plume e.g. Morgan, 1971) thermally thins the bottom of the lithosphere (Saunders et al., 1992). This causes adiabatic melting, at a rate that increases with time due to a decrease in the mantle pressure through time as a result of thinning of the lithosphere (Saunders et al., 1992). The passive model on the other hand extension is purely driven by plate tectonic processes, resulting in the passive upwelling of the buoyant sub-lithospheric mantle beneath the rift (Sengör and Burke, 1978).

2.2.1 Asymmetry in conjugate passive margins

Many passive margins, of both the volcanic and non-volcanic variety (Fig. 2.2), display considerable asymmetry in a number of observable phenomena (e.g. the South Atlantic - Becker et al., 2016; Flament et al., 2014). The question of whether rifts are fundamentally asymmetric and, if so, what controls the asymmetry has been the focus of considerable

research (e.g. Huismans and Beaumont, 2002). However, the causes of such asymmetry remain unclear. An abundance of work relates rift and subsequent conjugate passive margin asymmetry to the mode by which rifting occurred, i.e. whether the rifting was dominated by a pure (McKenzie, 1978) or a simple shear (Wernicke, 1981; Wernicke, 1985; Lister et al., 1986) rifting regime (Fig. 2.6). The simple shear model predicts that extension occurs along lithosphere-scale normal faults and/or ductile shear zones (e.g. Lister et al., 1986; Etheridge et al., 1989) resulting in highly asymmetric conjugate margins, whereas rifting under a pure shear dominated regime occurs by symmetrical, brittle extension of an upper layer, and ductile stretching of a lower layer (McKenzie, 1978) resulting in more symmetrical rift and conjugate passive margin geometry.

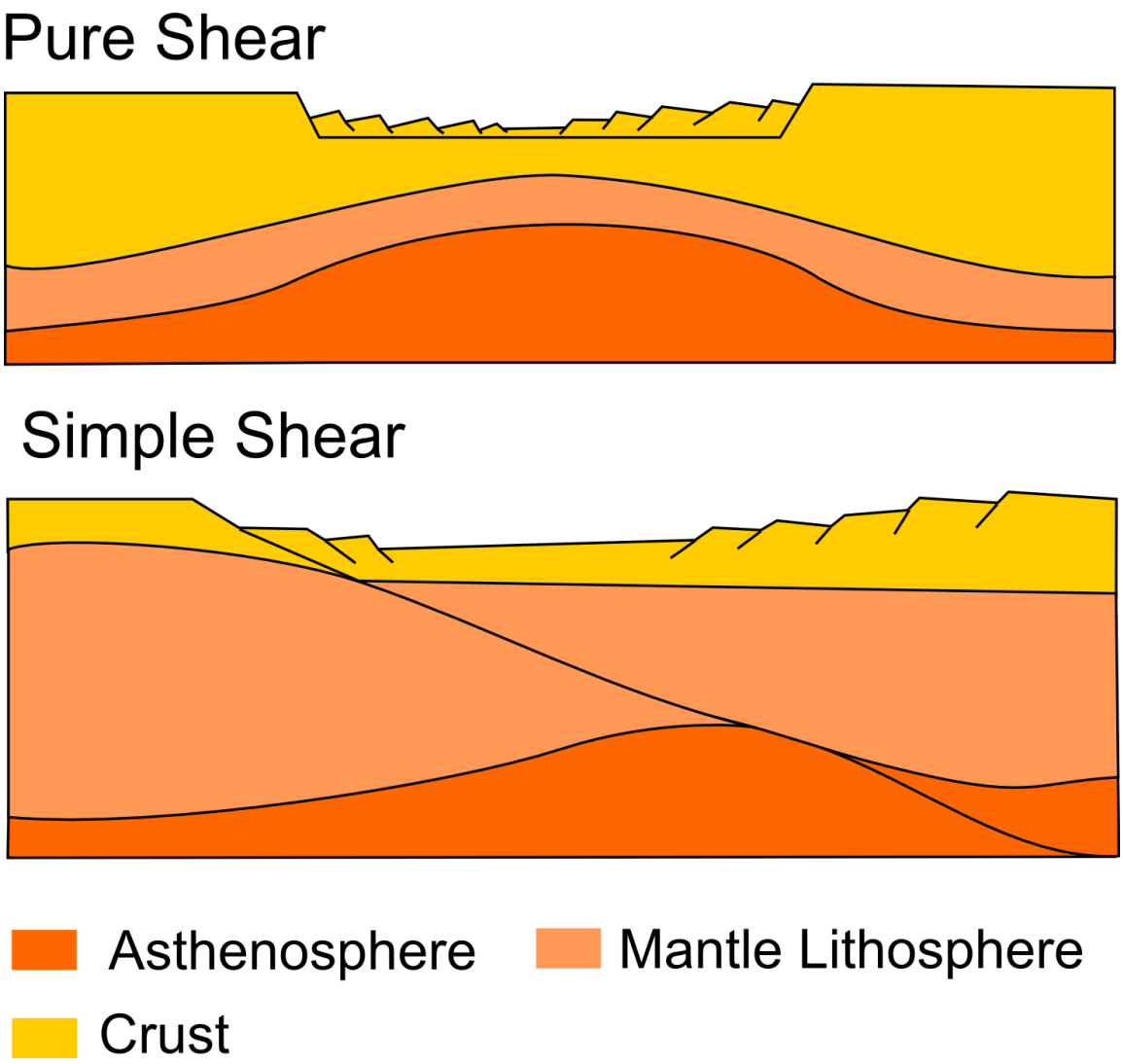

Figure 2.6

A comparison of the end-member pure shear (McKenzie, 1978) and simple shear (Lister et al., 1986; Etheridge et al., 1989) models of rifting (e.g. Allen and Allen, 2005).

However, the extent to which simple shear and pure shear models can explain the degree of asymmetry between conjugate margins has led to debate (e.g. Gillard et al., 2015), with some work suggesting that asymmetry could also be induced by other processes such as initial asymmetric conditions (Corti and Manetti, 2006). As such one area that this work intends to address is how asymmetry in conjugate margins is manifest, what processes could have led to the observed asymmetry and what are the implications of the observed asymmetry (Chapter 4).

2.2.2 The role of structural inheritance in the formation of passive margins

Unlike oceanic crust, the crystalline basement of the continental crust contains evidence of past deformation events and can be considered to be heterogeneous in nature (Holdsworth et al., 2001a; Hand and Buick, 2001). These heterogeneities lead to spatial variations in the mechanical strength and rheological behaviour of rocks (e.g. Anderson, 2012). Thus, the geological development of the continents is significantly influenced by the way in which the existing lithosphere responds to new tectonic events (Sutton and Watson, 1986). Pre-existing structures are defined as mechanical anisotropies in the pre-rift rocks which can occur on a variety of scales from metamorphic mineral fabrics to major tectonic boundaries (Chattopadhyay and Chakra, 2013). Peacock and Sanderson, (1992) recognise three types of directional heterogeneity (anisotropy): 1) layering-alternations of materials with differing mechanical properties (e.g. bedding); 2) continuous anisotropy from pervasive fabrics (e.g. foliation and shear zones); and 3) discrete planes of weakness with reduced cohesion and coefficients of sliding friction (e.g. faults and cleavage planes).

Tectonic inheritance is the process by which such pre-existing structures may influence a subsequent geological event (e.g. Holdsworth et al., 2001a; Mora and Huismans, 2016; Armitage et al., 2010). Pre-existing geological structures are well accepted to be capable of exerting a considerable influence upon a range of tectonic settings including: 1) rifting and subsequent continental breakup (e.g. Ravelo et al., 2006; Gibson et al., 2013; Manatschal et al., 2015; Chenin et al., 2015; Dore et al., 1997); 2) orogenic and collisional zones (e.g. Ryan, 2001; Lister et al., 2001); 3) strike-slip systems (e.g. Holdsworth et al., 2001b; Rogers et al., 1989); 4) and magmatic systems (e.g. Valentine and Krogh, 2006; Ashby, 2013; Hutton, 1988). Previous work has documented the influence of pre-existing structures at plate scales (e.g. Krabbendam, 2001; Houseman and Molnar, 2001); regional scales (e.g. Wu et al., 2016; Roberts and Houseman, 2001; Paech, 2001); outcrop scales

(e.g. Japsen et al., 2006; Wilson et al., 2006) and grain scales (e.g. Hippler and Knipe, 1990). Aspects of the rifting and continental breakup process that pre-existing structures can influence include, but are not limited to: magmatism (e.g. Bureau et al., 2013; Ashby, 2013); sedimentary basin geometry (e.g. Morley et al., 2004); fault locations, geometry and timing (e.g. Korme et al., 2004; Wu et al., 2016).

There is a wealth of both geological and geophysical knowledge to suggest that rejuvenation often occurs in preference to the formation of new structures during deformation (Butler et al.,1997). The rejuvenation of pre-existing crustal and lithospheric features essentially occurs via two related processes; reactivation and reworking (Holdsworth et al., 2001a). Reactivation involves the rejuvenation of discrete structures such as faults (e.g. McCaffrey, 1997), whereas reworking involves repeated focusing of metamorphism, deformation or magmatism on the same crustal or lithospheric volume (e.g. craton reactivation - Tappe et al., 2007; repeated metamorphism - Manhica et al., 2001). Both reactivation and reworking however may represent the same processes operating at different scales, and thus some ambiguity exists in distinguishing between the these two processes in the literature (Holdsworth et al., 2001a). In this study we consider the roles of both reactivation and reworking as endmember processes both of which could have influenced the incomplete breakup of Greenland and North America.

Although it has long been recognised that pre-existing geological structures are capable of influencing later geological events (e.g. Wilson, 1966) the way in which such structures have directly and indirectly influenced continental breakup remains an area of active research due to the variable manifestations of pre-existing structures within the rifting cycle. It is for this reason that, as outlined in Chapter 1, investigating the role of pre-existing structures during continental breakup is one of the primary aims of this study (Chapters 5 and 6). It is the wide range of scales in which the rejuvenation of pre-existing

structures may occur (Holdsworth et al., 2001a) that is one of the reasons this study has been conducted using different methodologies at different scales. Understanding the role of tectonic inheritance during rifting and continental breakup is particularly important as heterogeneities in the continental crust are widespread and likely to be long lived as continental crust is not normally subducted during convergence and collision (Holdsworth et al., 2001b).

At the largest scale (reworking), it has long been recognised that continental breakup often occurs along older orogenic fronts (Wilson, 1966), as evidenced by the presence of passive margins to older orogenic belts (e.g. Chenin et al., 2015). Thus, a major control on the large-scale location of passive margins is considered to be older orogenic belts (Audet and Bürgmann, 2011). However, not all orogenic belts are likely to be susceptible to facilitating continental breakup, as only the orogenic belts currently located in proximity to passive margins are claimed to be likely to be reworked during continental breakup such as the North Atlantic Caledonides, whereas orogenic belts located far from passive margins such as the Central Asian Urals are claimed to be unlikely to be reworked (Fig. 2.7 - Krabbendam, 2001). Older orogenic belts may be susceptible to becoming the location of future breakup due to the abundance of structures that they contain upon which deformation may be focused. Thus, reworking may actually represent a large-scale manifestation of widespread, yet focused, reactivation (Holdsworth et al., 2001a). Orogenic belts are also susceptible to rejuvenation due to their relative gravitational instability (e.g. Houseman and Molnar, 2001).

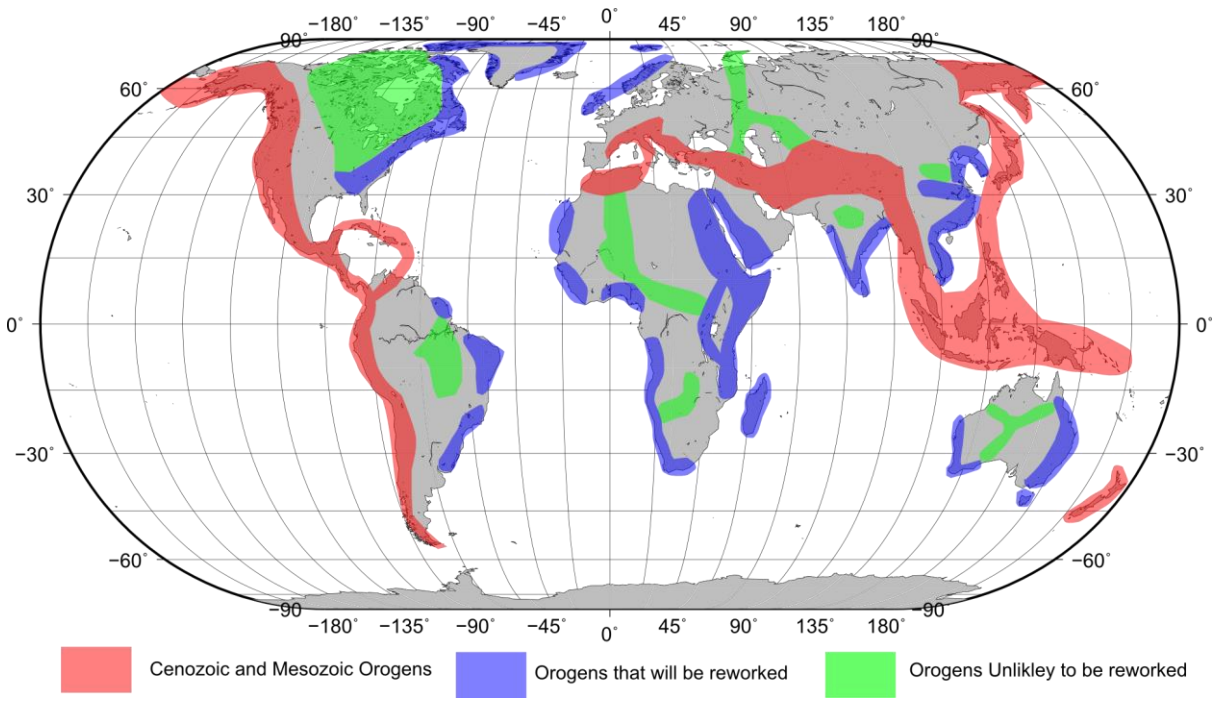

Figure 2.7

The present day global distribution of orogenic belts and their likelihood of being reworked. Modified from Krabbendam, (2001)

The smaller scale process of reactivation (Holdsworth et al., 2001a) is another aspect of tectonic inheritance investigated by this study (Chapter 6). Reactivation is defined by Holdsworth et al. (1997) as 'the accommodation of geologically separable displacement events (at intervals > 1 Ma) along pre-existing structures. The time scale recognised by Holdsworth et al. (1997) is important because this distinguishes multiple phases of movement from within the same seismic cycle (Wallace, 1984). Holdsworth et al. (1997) chose an interval of >1 Ma as this was considered to represent the limit of the resolvable time interval in most ancient settings. However, in some locations where more precise geochronological work is possible (e.g. Re-Os dating - Dichiarante et al., 2016) a shorter timescale for reactivation may be possible (Holdsworth et al., 1997). Two types of reactivation have been identified by Holdsworth et al. (1997): 1) 'geometric reactivation' that is where reactivated structures display different senses of relative displacement for

successive events; and 2) ‘kinematic reactivation’ that is where reactivated structures display similar senses of displacement for successive events. Identification of reactivation can include stratigraphic, structural, kinematic geochronological and neotectonic criteria (Holdsworth et al., 1997).

Reactivation of discrete structures such as faults occurs due to their relative weakness in comparison to the surrounding material (Morley et al., 2004; Morley, 1995), with previous work showing that pre-existing fabrics lying up to 45-60° to the regional extension direction are commonly followed by extensional faults (Morley, 1995), demonstrating the importance of understanding the relationship between pre-existing structures and rift propagation. Many examples of discrete rejuvenation of geological structures have been documented including; the Gulf of Aden margin (Bellahsen et al., 2006), onshore West Greenland (Japsen et al., 2006; Wilson et al., 2006), the Ethiopian rift (Korme et al., 2004) and Caledonian faults in Ireland (McCaffrey, 1997).

Overall, the role of pre-existing structure in rift and passive margin development is important yet extremely variable and very specific to a particular location dependent on the nature of pre-existing structures and their interaction with subsequent deformation. Thus, despite considerable research effort the interaction between pre-existing structures and rift development is an area of research in which the analysis presented in this thesis aims to contribute further, as understanding how previous geological events influence the process of continental breakup is critical in constraining the processes controlling passive margin formation. Here, we consider the role of pre-existing structures at a range of scales from orogenic belts to discrete individual faults in the initiation and evolution of continental breakup between West Greenland and Eastern Canada (Chapters 5, 6 and 8).

2.3 Hydrocarbon exploration and production on passive margins

It is well recognised that rifts and passive margins offer significant hydrocarbon exploration and production opportunities (Skogseid, 2001; Ziegler, 1992; Morley, 1995), with five out of the six tectonic settings identified by Mann et al. (2003) as containing giant oil and gas fields being types of rift, passive and transform margins. Passive margins represent a significant host for both current (e.g. offshore Newfoundland – DeSilva, 1999) and future hydrocarbon provinces (e.g. the Arctic – Spencer et al., 2011), a trend that is likely to continue as global demand for hydrocarbons increases (White et al., 2003). Sedimentary basins on passive margins contain a significant proportion of the worlds hydrocarbon resources (Mann et al., 2003), and despite a considerable research effort there remains vast underexplored regions on the continental margins (Alves et al., 2014) for example the margins of the Arctic region (Spencer et al., 2011) including Baffin Bay (Haggart, 2014) and the Barents Sea (Henriksen et al., 2011). The huge economic potential of this tectonic setting has motivated the hydrocarbon industry to continue exploration of passive margins in increasingly deep-water (> 500 m) settings (White et al., 2003; Alves et al., 2014). Through time improvements in drilling and seismic technologies have allowed exploration and production to be undertaken in greater depths of water (Alves et al., 2014). However, hydrocarbon exploration of passive margins presents multiple challenges of both an engineering and geological nature. Despite the challenges posed to operating in this setting (Alves et al., 2014) economic factors have and will continue to push exploration into more remote locations.

There are a number of reasons that passive margins and their precursory rifts provide an attractive tectonic setting in which to explore for hydrocarbons (Ziegler, 1992; Skogseid, 2001). Firstly, stretching and rifting of the continental lithosphere results in thinning and after an initial period of uplift (e.g. Esedo et al., 2012) long-term subsidence occurs (McKenzie, 1978). This subsidence produces accommodation space in which thick syn-rift

and post-rift sedimentary successions may be deposited (Allen and Allen, 2005), as demonstrated by the NOAA total sediment thickness dataset (Divins, 2003) (Fig. 2.8). The thick sedimentary successions found on passive margins allow for source rocks to be sufficiently buried to achieve maturation, as well as providing later intervals which may act as a reservoir or seal in the petroleum system (Ziegler, 1992). Passive margins are also conducive to trapping hydrocarbons that have migrated (Ziegler, 1992) due to numerous opportunities for the creation of such trapping structures often occurring including; margin inversion (Japsen et al., 2010).

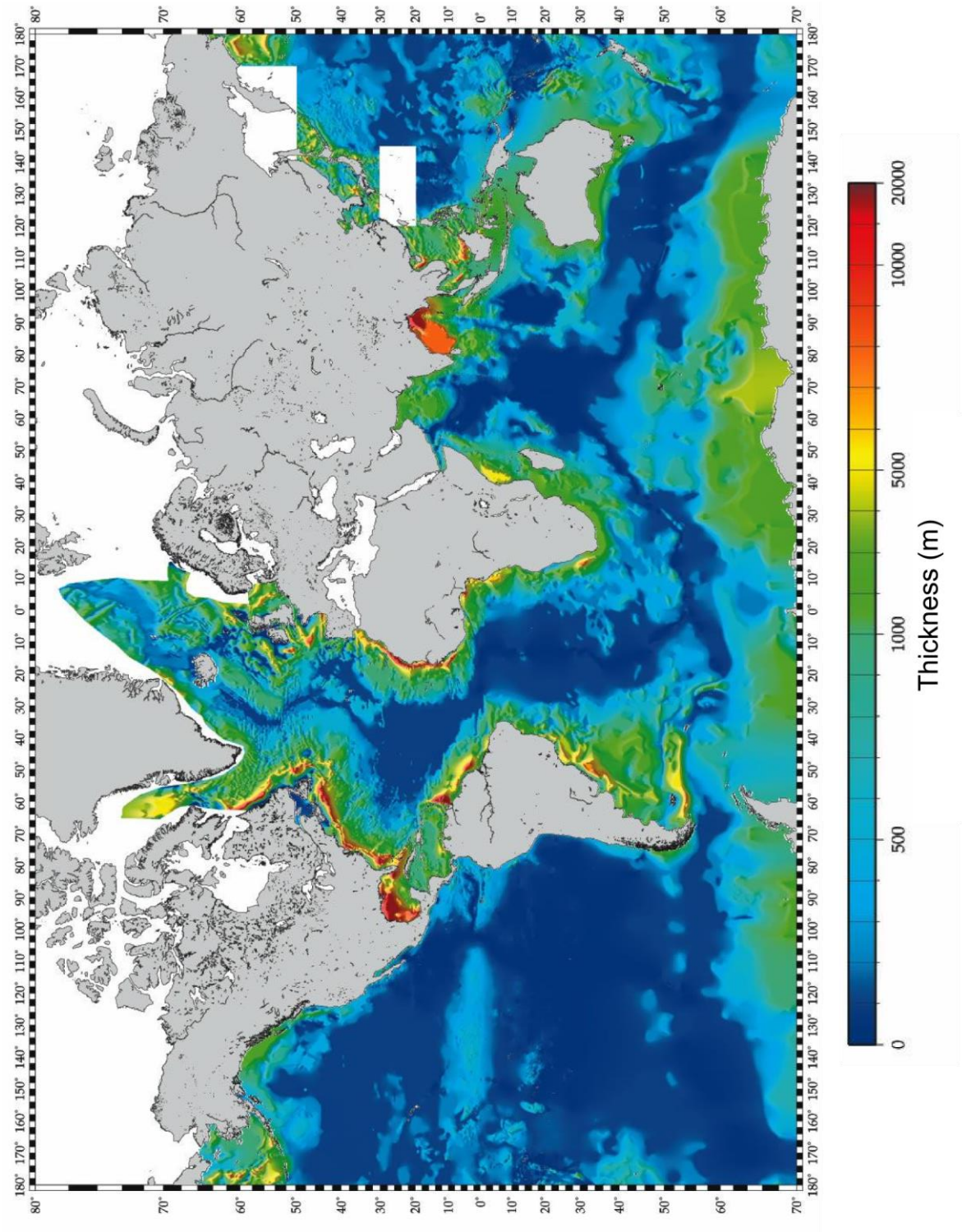

Figure 2.8

Global map of the NOAA total sediment thickness dataset version 2 (https://www.ngdc.noaa.gov/mgg/sedthick/sedthick.html) (Divins, 2003) demonstrating the thick sedimentary cover found on many of the world's passive margins (Fig. 2.1).

2.3.1 Petroleum systems on volcanic passive margins

Despite the wealth of economic opportunity offered by passive margins for hydrocarbon exploration and production (e.g. Alves et al., 2014) unique challenges and opportunities are presented to such activities on VPMs (e.g. Skogseid, 2001; Schutter, 2003). Hydrocarbon exploration has typically in the past attempted to avoid basins containing significant quantities of igneous rocks due to the perceived detrimental influence of igneous rocks on petroleum systems (Rohrman, 2007), with most hydrocarbon discoveries in crystalline rocks being found unintentionally (Petford and McCaffrey, 2003). However, as petroleum exploration has been required to consider new regions to acquire hydrocarbons many frontier regions that were originally overlooked containing abundant igneous rocks are now considered as potential exploration targets (Western Australia - Holford et al., 2012; West of Sheltland - Rateau et al., 2013).

Challenges to petroleum exploration and production at VPM's include: 1) increased heat flow (Fjeldskaar et al., 2008); 2) imaging beneath igneous rocks (Maresh et al., 2006); 3) significant compartmentalisation from sills, dykes and hydrothermal activity (Holford et al., 2013); 4) reduced subsidence due to the additional support provided by magmatic underplating (Skogseid, 2001) and 5) drilling through thick basalt sequences (Karner and Shillington, 2005). Despite the aforementioned challenges of hydrocarbon exploration and production this tectonic setting also offers unique opportunities for example: 1) the use of flood basalts as seismic markers (e.g. Schutter, 2003); 2) the 'additional' maturation effects of burial and heating in proximity to igneous rocks (e.g. Schutter, 2003; Fjeldskaar et al., 2003; Hurter and Pollack, 1995); 3) formation of 'forced folds' above sills potentially forming trapping structures (Hansen and Cartwright, 2006; Magee et al., 2012); Thus, constraining the timing, nature, distribution and mechanisms associated with igneous activity at VPMs is crucial in reducing exploration risk at this setting (e.g. Holford et al.,

2013). This is particularly paramount when we recall that despite the vast resource potential of deep water passive margins (Alves et al., 2014) it is possible that the majority of margins VPMs (Menzies et al., 2002) and even NVPMs actually contain some igneous rocks (e.g. Newfoundland Margin - Deemer et al., 2010).

Quantifying heat flow through the development of a passive margin is crucial for constraining source rock maturity (Fjeldskaar et al., 2003; Fjeldskaar et al., 2008; Wang et al., 2012). This is particularly relevant on VPMs due to the higher heat flow at this setting (Geoffroy, 2005). The effects of heat flow on maturation of organic matter on VPMs can be considered to have two contributors; 1) the background or regional heat flow and 2) the localised effects of individual igneous rocks (Holford et al., 2012) (Fig. 2.9). An example of heat flow from magmatism influencing maturation occurs in the Vøring Basin on the Norwegian margin, where modelling suggests that the maturity effects of the underplated body are significant with both oil and gas generation occurring 5 – 10 Myrs earlier than in models without the additional heat from and underplated magmatic body (Fjeldskaar et al., 2003). Overall, additional heat from igneous rocks at VPMs may influence source rock maturation and therefore must be quantified to reduce exploration risk at these settings (Schutter, 2003). Any additional heat flow at VPMs does not necessarily negatively influence petroleum systems as the extra heat could potentially allow organic material to become mature at shallower depths and in some cases place otherwise immature source rocks within the oil window (Holford et al., 2013). It is for this reason that the maturation effects of igneous intrusions on the Newfoundland NVPM form the focus of Chapter 7.

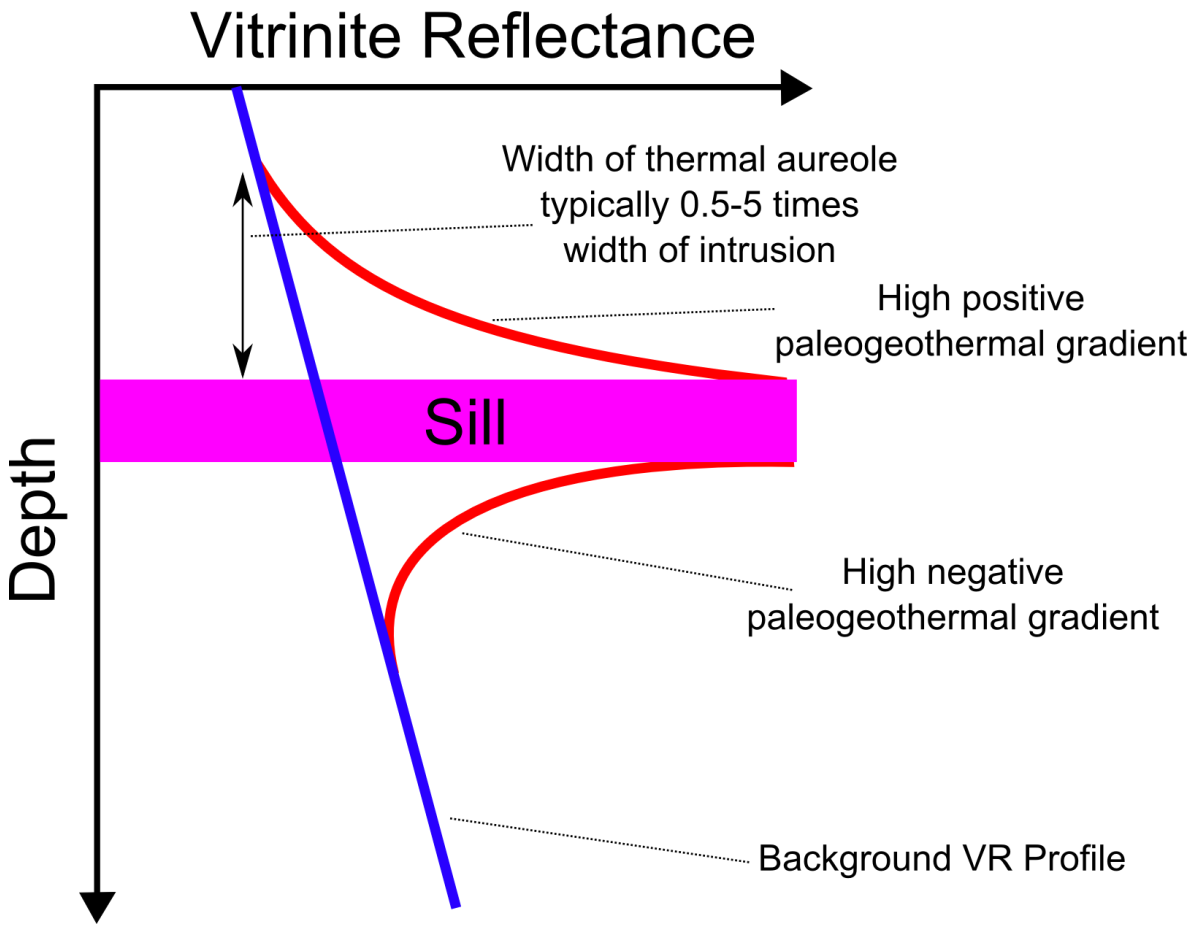

Figure 2.9

Schematic depiction of a typical vitrinite reflectance profile (e.g. Pross et al., 2007) in immediate proximity to a sill. Modified from Holford et al. (2013).

Compartmentalisation of reservoirs by igneous intrusions can be a major challenge to hydrocarbon exploration on VPMs (e.g. Holford et al., 2013), particularly as many of these effects are beneath the scale of the seismic imaging resolution, a restriction expanded upon in Chapter 3. Igneous intrusions occur as both sills and dykes (Galerne et al., 2011) and often form interconnected networks (Fig. 2.10) which can crosscut basin stratigraphy (Holford et al., 2013). The way in which intrusions influence reservoirs is highly variable and dependent on many individual, specific local factors as a result of the basin stratigraphy and the nature of the magmatism (Holford et al., 2013). Thus, several possible scenarios for the interaction between intrusions and reservoirs have been proposed by

Holford et al. (2013) ranging from an unaffected reservoir right through to igneous intrusions being capable of directly reducing hydrocarbon charge of reservoir sands (Fig. 2.10), demonstrating that further work is required to fully understand the influence of igneous rocks upon hydrocarbon reservoirs. In addition to compartmentalisation of reservoirs by sills and dykes (Holford et al., 2013) degradation or improvement of reservoirs associated with hydrothermal fluids due to igneous rocks could influence the viability of a petroleum system (Schutter, 2003), as it is well known that hydrothermal activity often accompanies the igneous rocks in sedimentary basins at VPMs (e.g. The Faroe-Shetland Basin - Grove, 2013).

In addition to igneous rocks influencing sedimentary reservoir rocks it is possible for igneous rocks to actually be the hydrocarbon bearing reservoir unit as is the case in Rosebank (Schofield and Jolley, 2013). At the Rosebank Field in the Faroe-Shetland Basin volcanic rocks are not just a seal to the petroleum system they are in fact an integral part of the petroleum system (e.g. Schofield and Jolley, 2013). Given that this type of hydrocarbon play is relatively new further research is required to understand whether it has the potential to operate elsewhere, particularly on passive margins with abundant volcanic rocks. Igneous rocks also form reservoirs for hydrocarbon accumulations in a limited number of other settings such e.g. the documented granite reservoir intervals in Western Indonesia (Koning, 2003).

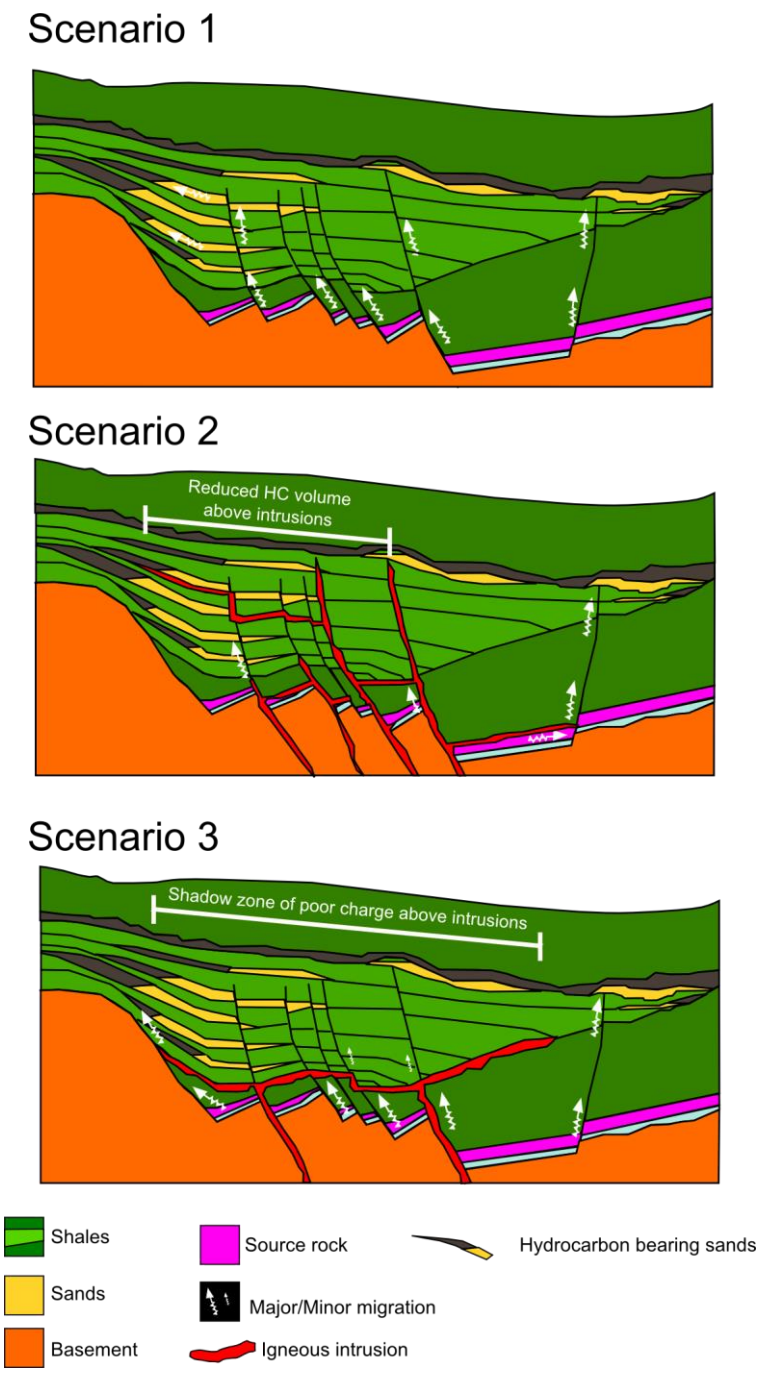

Figure 2.10

Schematic depictions of the end-member impacts of igneous intrusions upon a conventional sandstone play. Modified from Holford et al. (2013) and Rateau et al. (2013). Scenario 1 – No intrusions. Petroleum system unaffected. Scenario 2 – Compartmentalisation of source rock intervals. Hydrocarbons trapped close to source, unable to migrate to reservoirs leading to reduced charge. Scenario 3 – Compartmentalisation of basin fill. Intrusions act as barriers to hydrocarbon migration, resulting in shadow zones of under filled reservoir units overlying the intrusions.

The key challenge associated with hydrocarbon exploration of VPMs is seismic imaging beneath igneous rocks (Roberts et al., 2005; Christie and White, 2008; Gallagher and Dromgoole, 2007), typically flood basalts or sill complexes which can cover very large areas at passive margins (White, 1992) often at shallow depths in the sedimentary section thereby masking the sub-basalt geology (e.g. Ziolkowski et al., 2003; Jegen et al., 2009). However, as these units often produce as a high amplitude or 'bright' reflector on seismic data they can be used as a regional marker (Fig. 2.3) (Schutter, 2003), particularly if occurrences of the igneous rock have been dated using methods such as $^{40}Ar/^{39}Ar$ (Larsen et al., 2009).

Despite all the aforementioned challenges to exploration and production at VPMs there are some notable opportunities also present at this tectonic setting as a direct result of the abundant igneous rocks (e.g. Skogseid, 2001; Petford and McCaffrey, 2003). Firstly, it has been proposed that if sufficient organic material was deposited during the formation of SDRs then a petroleum system could be present here (Franke, 2013). In such a system the thick basalt flows have been proposed as a seal, whilst burial beneath these flows could contribute to the maturation of organic matter. It has also been proposed that intrusive igneous rocks could actually provide a conduit for hydrocarbon migration through an otherwise impermeable reservoir (e.g. the Northern South Yellow Sea Basin - Lee et al., 2006).

Despite the abundance of knowledge outlined above and considerable research effort the nature of petroleum systems on passive margins, and in particular VPMs, is an area that requires further work and as such this thesis aims to contribute. This is particularly paramount as petroleum exploration is pushed further into unexplored regions where operating costs may be higher (Alves et al., 2014). Here, I aim to increase the

understanding of petroleum systems on the West Greenland and Eastern Canadian margins in order to reduce certain aspects of the exploration risk.

Chapter 3

The study of passive margins: datasets and methodologies

3.0 Introduction

As detailed in the in Chapters 1 and 2, passive margin processes operate at a complete range of scales and dependent on the aspect being investigated different methodologies are required. It is for this reason that in this work a wide variety of methodologies were utilised to study the range of phenomena at this tectonic setting. The majority of information regarding passive margin formation, structure, processes and hydrocarbon potential (Chapter 2) has been derived through large-scale geophysical studies (e.g. Srivastava and Keen, 1995; Shillington et al., 2004) often supplemented by exploration wells (e.g. Gouiza et al., 2016; McWhae et al., 1980). However, numerous other types of data and studies have also contributed to our knowledge including but not limited to: field-based studies (e.g. Manatschal, 2004; Wilson et al., 2006); numerical (e.g. Fjeldskaar et al., 2008; Simon et al., 2009; Bowling and Harry, 2001) and analogue modelling (e.g. Morley et al., 2004; Corti et al., 2007; McClay and White, 1995); remote sensing (e.g. Japsen et al., 2006; Casu and Manconi, 2016); and geochemistry (e.g. Holm et al., 1993; Larsen et al., 2009; Tappe et al., 2007).

This section supplements, where necessary, the more concise details of the methods and datasets provided in chapters 4-7 as these chapters were written as succinct journal-style research papers. The sections within this chapter begin with descriptions of the methods and types of data that have contributed to the knowledge of passive margins globally, followed by detailed descriptions of the methodologies utilised during the analysis of the data presented in chapters 4-7 thesis.

3.1 Seismic data

Of all the methods described in this chapter and utilised in this study seismic methods (reflection and refraction) have probably provided the greatest contribution to the

collective understanding of passive margins (e.g. Shillington et al., 2004; Dalhoff et al., 2003; Lonergan et al., 2013; Wu et al., 2016; Keen et al., 1994). The acquisition of seismic data involves propagating seismic waves through the subsurface and recording the return times generated by reflection or refraction of the seismic wave at geological boundaries which mark a change in the physical properties of the subsurface (e.g. Lonergan and White, 1999). Seismic waves are parcels of elastic strain energy that propagate outwards from a seismic source, which can either be controlled, such as an explosion or air gun, or naturally occurring seismic waves from earthquakes in passive seismic acquisition (e.g. Schiffer et al., 2014).

There are two types of seismic wave, namely body waves and surface waves (Fig. 3.1). Body waves propagate through the body of an elastic solid whereas surface waves propagate along the surface of the solid. Two types of body wave are recognised, P-waves (compressional) and S-waves (shear). P-waves are longitudinal waves that propagate by compressional and dilatational uniaxial strains in the direction of wave travel. S-waves propagate by simple shear strain in a direction perpendicular to the direction of wave travel. The velocity of seismic wave propagation is determined by the physical properties (density and seismic velocity, and thus seismic impedance) of the medium in which the wave is traveling through (Bacon et al., 2003).

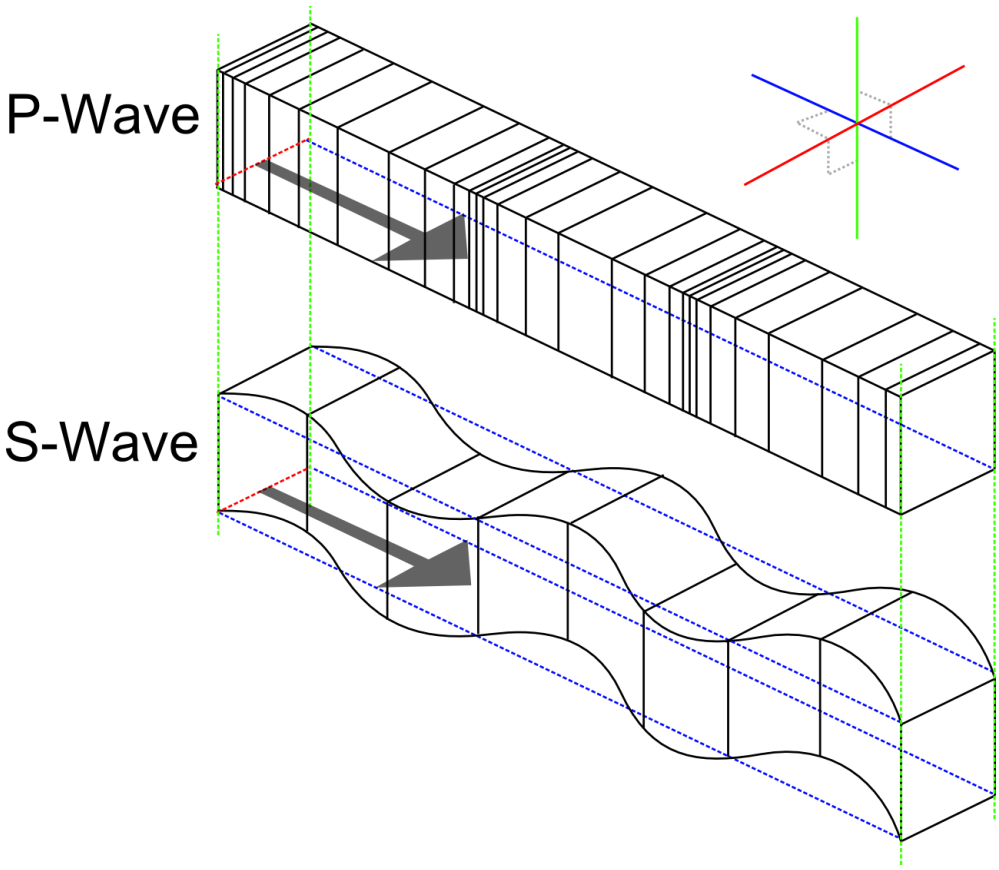

Figure 3.1

Schematic comparison of the differing propagation style of P-waves and S-waves, the two types of body seismic wave (Kearey and Brooks, 1991). The grey arrows indicate the direction of wave propagation, whilst the blue, green and red axes represent the x, y and z directions respectively. Modified from Kearey and Brooks, (1991).

3.1.1 Seismic reflection data

One of the most useful types of data for the study of passive margins is seismic reflection data, which have a vertical scale in two-way travel time (TWTT). Seismic reflection methods are particularly well suited to mapping stratigraphic successions due to the near-horizontal nature of stratigraphic discontinuities, which are imaged as reflections (Vail and Mitchum, 1977). As seismic reflection data are particularly suited to studying sedimentary basins there is an abundance of seismic reflection data on many passive margins due to the

hydrocarbon potential of this tectonic setting (Chapter 2). The reason that seismic reflection data are particularly useful for imaging stratigraphic successions is as a result of physical rock properties varying more as a function of depth due to the differing physical properties of layers in the sedimentary sequence rather than horizontally for example due to facies changes (Vail and Mitchum, 1977).

2D and increasingly 3D seismic reflection data have been progressively collected on many of the worlds passive margins primarily driven by the hydrocarbon potential of this tectonic setting (e.g. the Brazilian margin - Contreras et al., 2010). Typically sparse 2D seismic data is obtained in relatively unexplored and understudied areas. Then following interpretation of the sparse 2D data if an area looks to show the potential to be economically prospective a denser 2D grid or even 3D seismic data is collected on focused areas that have been identified as potential hydrocarbon exploration targets.

Not all seismic data acquisition is however acquired by the hydrocarbon industry as many academic groups have also obtained seismic data on passive margins for purely scientific reasons for example the SCREECH (Studies of Continental Rifting and Extension on the Eastern Canadian sHelf) work offshore Newfoundland, Canada (Shillington et al., 2004). Such scientific studies have provided invaluable knowledge on aspects of passive margins beyond the economically prospective sedimentary basins that form the focus of the hydrocarbon industry acquisition of offshore seismic data. Academic studies have in particular provided vital knowledge regarding the nature of the ocean-continent transition (e.g. Shillington et al., 2004), a part of the margin which is not usually considered to be a hydrocarbon exploration target but does contain crucial information regarding the nature of continental rifting, breakup and subsequent passive margin formation.

The seismic reflection data collection and analysis method can essentially be broken down

into three stages; 1) acquisition, 2) processing and 3) geological interpretation (Kearey and Brooks, 1991). These three stages are discussed in detail in the preceding sections.

3.1.2 Acquisition of offshore seismic reflection data

The simplest form of seismic reflection data would be a 1D point measurement with the source and receiver located at exactly the same point (Bacon et al., 2003). In such a setup the resulting data could be displayed as a 'seismic trace' or seismograph, that is a graph of the amplitude of the signal received against time with time on the vertical axis. On a 1D seismic trace reflectors are displayed as excursions from the ambient signal level (Bacon et al., 2003). To understand the nature of the subsurface geology however the collection of 2D and 3D seismic data is much more useful than a simple 1D experiment as spatial variation and extent of subsurface horizons can be imaged. Thus, almost all modern seismic reflection data collected is 2 or 3D.

An interface between two different subsurface lithologies may correspond to a change in the bulk rock density (Brown, 2011). Such a change in bulk rock density can induce a change the seismic velocity of a propagating seismic P-wave which in turn creates a change in acoustic impedance (Z) across the interface between the two lithologies. The acoustic impedance (Z) of a contact between two lithologies is a product of rock density (ρ) and the velocity (v) of the propagating seismic P-wave such that:

$$Z = \rho v \qquad \text{Equation 3.1}$$

Many attributes of the subsurface affect the velocity of the propagating seismic wave including; composition, porosity, fluid content, texture and elastic modulus (Kearey and Brooks, 1991). To determine the amplitude of a recoded wavelet the amplitude of the incoming wave is multiplied by the reflection coefficient (R), which can be calculated

from the acoustic impedance of the two interfaces with differing physical properties such that:

$$R = \frac{\left(\frac{V_2}{\rho_2} - \frac{V_1}{\rho_1}\right)}{\left(\frac{V_1}{\rho_1} - \frac{V_2}{\rho_2}\right)} \qquad \text{Equation 3.2}$$

Where: v_1 and ρ_1 are the seismic wave velocity and bulk rock density of an overlying unit (lithology 1 – Fig. 3.2) and v_2 and ρ_2 are the seismic wave velocity and bulk rock density of an underlying unit (lithology 2 - Fig. 3.2). The implication of this is that should a particular stratigraphic interval be homogeneous (or near homogenous) in terms of the aforementioned physical properties it will display little or no reflectivity in TWTT. The variation in the magnitude of the acoustic impedance boundary determines the amplitude of the recorded wavelet, thus a large difference in acoustic impedance results in a high amplitude, or 'bright' reflector.

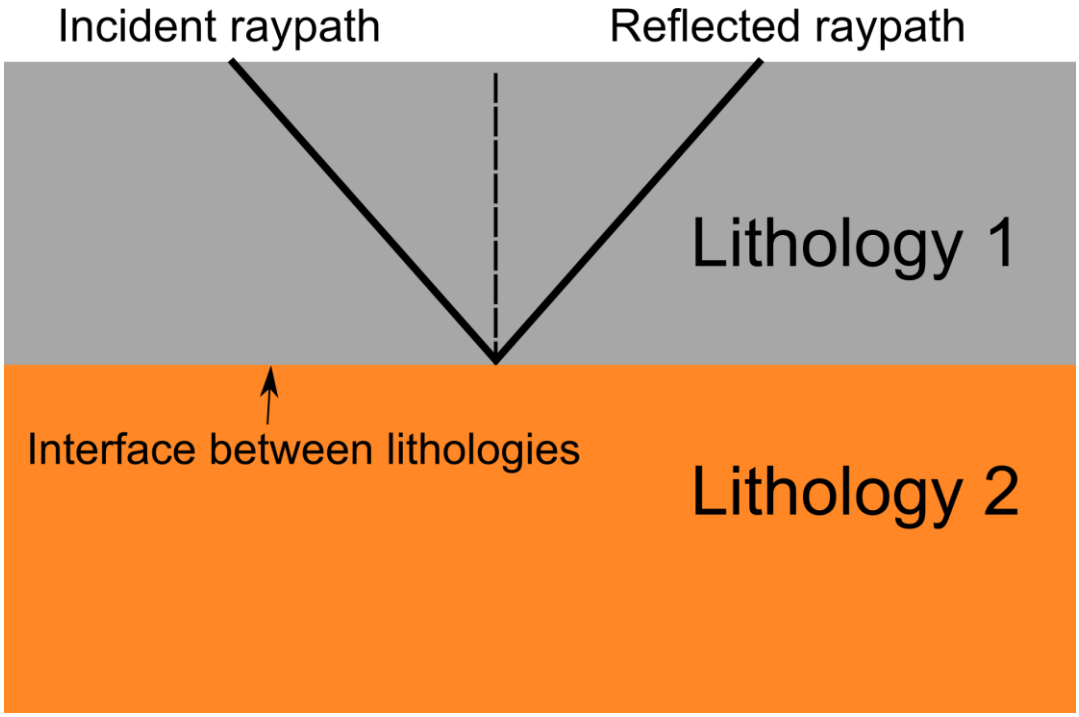

Figure 3.2

Schematic dipication of the incident and reflected P-wave associated with a change in acoustic impedance at the interface between two lithologies of differing bulk rock density. Modified from Kearey and Brooks (1991).

The resolution of seismic data is primarily a product of the acquisition method. Understanding both the horizontal and vertical spatial resolution of seismic data are crucial to conducting a valid interpretation, particularly through intervals of minimal reflectivity on seismic profiles. The vertical resolution of seismic reflection data is a measure of the capability to recognise individual reflections from a closely space package that is measured with respect to the wavelength (λ) of the reflected wavelet (Kearey and Brooks, 1991). The vertical resolution is equal to a quarter of the wavelength (λ/4) (Brown, 2011), where the wavelength (λ) is defined as:

$$\lambda = \frac{v}{f}$$ Equation 3.3

Where: v = the seismic velocity and f = the dominant frequency. Equation 3.3 demonstrates that the shorter the wavelength the higher the frequency, which in turn provides a higher seismic resolution. Vertical resolution of seismic reflection data is also dependant on the depth of the interface being imaged as rocks usually become more compact at depth, thus density and therefore seismic velocity usually increase with depth. Conversely, the frequency of a propagating seismic wave decreases with depth as higher frequencies become attenuated, resulting in a decrease in seismic resolution with depth (Kearey and Brooks, 1991). The horizontal resolution is controlled by two main factors: 1) the detector spacing; and 2) the physical limit imposed by the actual process of seismic wave reflection (Kearey and Brooks, 1991). The Fresnel Zone represents (Fig. 3.3) the absolute physical limits of the horizontal resolution of seismic reflection, as reflections which are not separated by a distance of at least this amount cannot be individually resolved. The width (w) of the Fresnel Zone is related to the wavelength (λ) and the reflector depth (z) (Kearey and Brooks, 1991) such that:

$$w \approx (2z\lambda)^{0.5} \qquad \text{for } z >> \lambda \qquad \text{Equation 3.4}$$

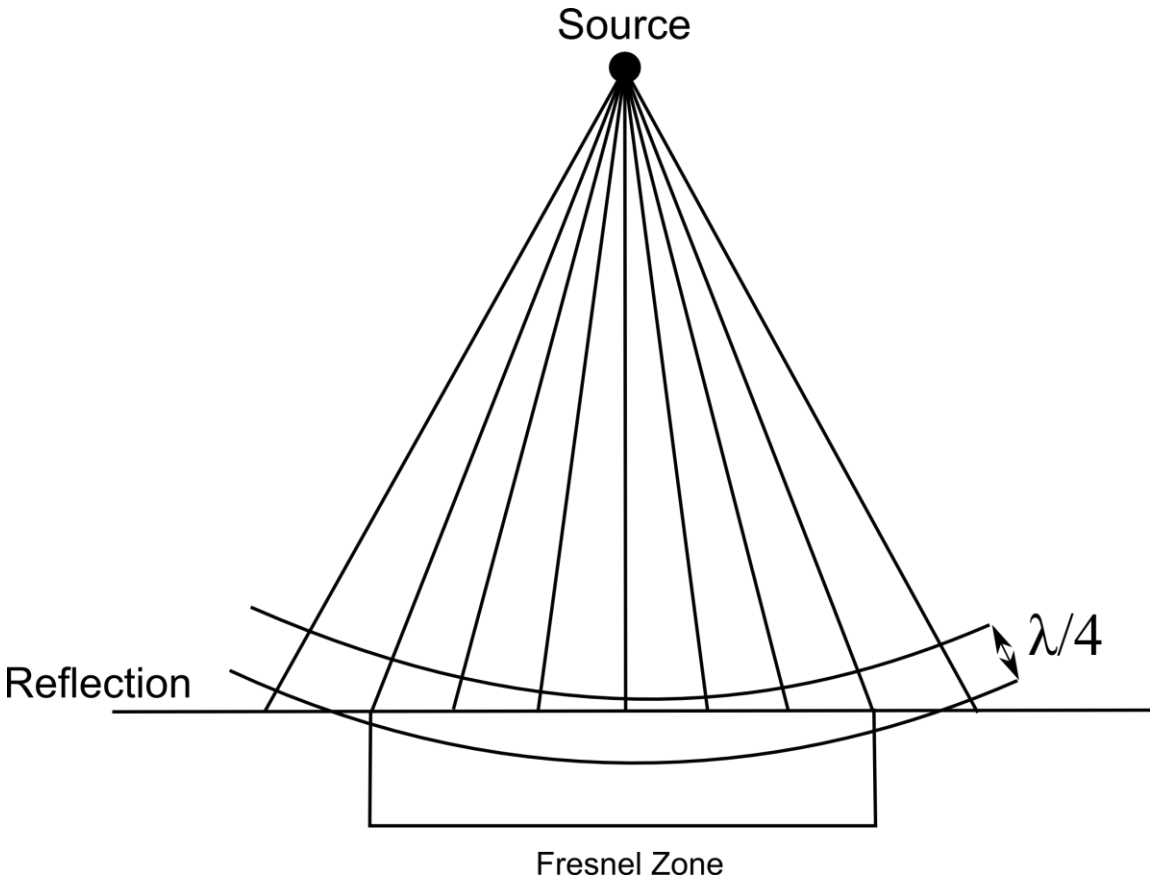

Figure 3.3

A schematic depiction of the Fresnel Zone, that is the part of a reflector from which energy is returned within half a wavelength of the initial reflected arrival. Modified from Kearey and Brooks (1991).

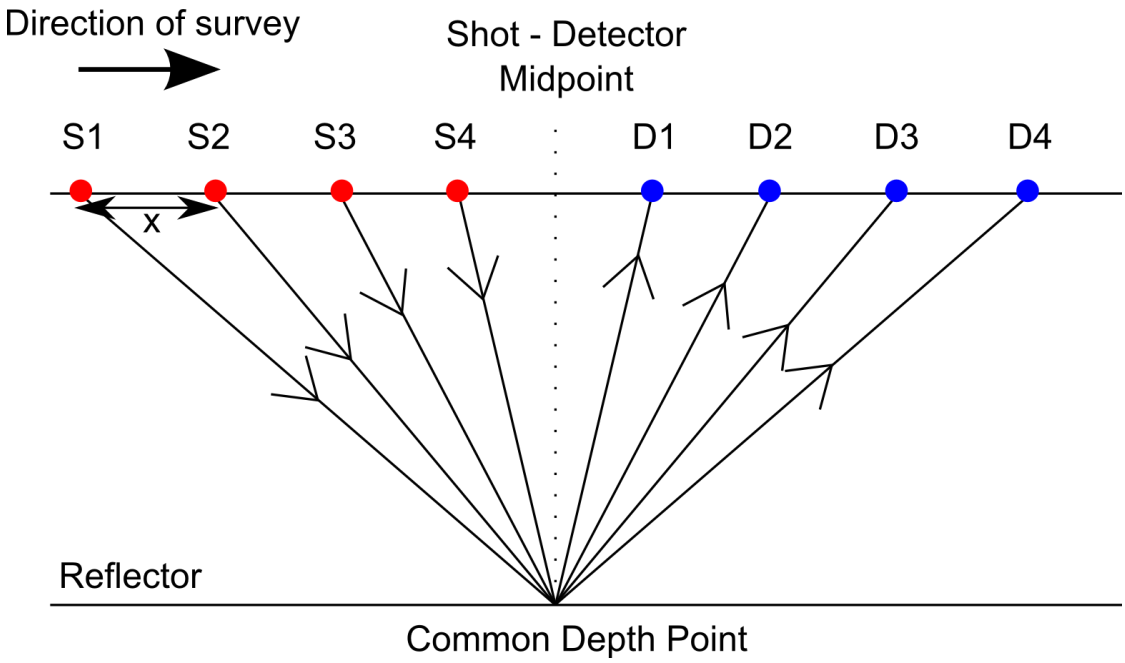

Figure 3.4

Schematic depiction of common depth-point (CDP) seismic reflection profiling modified from Kearey and Brooks (1991) and Bacon et al. (2003) for a 4 fold survey for shot spacing x. S1-4 indicate shot points, whilst D1-4 indicate detector points.

Figure 3.4 demonstrates schematically how as a seismic reflection survey proceeds traces recorded at different source receiver offsets can be combined ('stacked') to enhance the signal to noise ratio (Bacon et al., 2003). The number of individual source-receiver pairs that contribute to the stack is called the fold of the data (Bacon et al., 2003). Multi-fold 2D seismic reflection data is standard procedure and results in an improvement in the signal to noise ratio. If the detectors in a multi-channel seismic reflection survey are moved forwards such that no two reflected ray paths sample the same point on a subsurface reflector, the survey is said to be 'single-fold'. In such a single-fold scenario each seismic trace represents a unique sampling point on a reflector. In common depth point (CDP) profiling, the standard method of 2D seismic reflection acquisition, the survey is arranged

so that a set of traces that have been recorded at different offsets contains reflections from a CDP on the reflector (Fig. 3.4). The locations of the shot points and detectors for such a set of traces are known as CDP gather and have a common midpoint (CMP) below which the CPD is assumed to lie (Kearey and Brooks, 1991). In a 2D seismic reflection survey the common depth points are all assumed to lie within the vertical section of the survey line.

The acquisition of seismic data on passive margins inevitably involves working offshore collecting data from a boat due to the submerged nature of passive margins (e.g. Contreras et al., 2010). There are some advantages of collecting seismic data offshore as opposed to onshore including fewer obstacles to navigate (Bacon et al., 2003) but this environment can also produce challenges for acquisition such as the presence of objects such as other boats and icebergs as well as environmental regulations such as those protecting marine mammals (e.g. Parsons et al., 2009; Parsons et al., 2008). For the acquisition of offshore seismic data a purpose-built boat designed specifically for seismic acquisition is used to tow at least one energy source and one or more cables containing receivers to record the reflected data (Bacon et al., 2003). The seismic source is usually an array of air guns which are designed to produce a short energy pulse vertically downwards. Seismic reflection surveys are normally designed for a certain depth of penetration at a specific horizontal and vertical resolution (Bacon et al., 2003).

One of the greatest challenges in acquiring good quality seismic data at passive margins is imaging beneath structures such as volcanic rocks (e.g. Maresh et al., 2006) or salt (e.g. Rowan, 2014). Imaging beneath volcanic rocks such as flood basalts and sill complexes (e.g. Ziolkowski et al., 2003) is particularly paramount given that these are integral components of VPMs (e.g. Magee et al., 2016; White, 1992). The reason that volcanic

rocks are difficult to image beneath is due to their high seismic impedance contrast with the surrounding sedimentary lithologies and the scattering of high frequency energy that they cause. However, work continues to be done on improving the quality and depth of sub-basalt seismic imagery (e.g. Maresh et al., 2006; Ziolkowski et al., 2003; Christie and White, 2008). This is particularly relevant to this study as the seismic data analysed in Chapter 6 images numerous igneous rocks (e.g. Chapter 2 – Fig. 2.3D).

3.1.3 Migration and processing of seismic reflection data

Seismic reflection profiles must be transformed to allow for the fact that the reflection points are laterally shifted relative to the source/receiver locations in a process known as migration (Bacon et al., 2003). For migration of seismic data to be unnecessary (a zero-offset case) the reflected ray must exactly follow the path of the incidence ray, therefore the angle of incidence at the reflecting surface must be 90°. This zero-offset case is unlikely given that; 1) reflection points are unlikely to be located directly below the surface point, 2) subsurface horizons are likely to be dipping and 3) there may be several reflections from the same horizon (Bacon et al., 2003). The width of the Fresnel Zone (Fig. 3.3) determines the horizontal resolution, which can be improved by migration (Kearey and Brooks, 1991).

In addition to migration other processing techniques are usually applied to seismic data to improve the quality of the imagery prior to geological interpretation. One such common aspect of the processing of seismic reflection data is the removal of undesirable features created during acquisition that are not a feature of the subsurface geology known as artefacts. One such common type of artefact is a multiple (Fig. 3.5). Multiples are produced when an incident seismic wave is reflected multiple times before arriving at the receiver. Figure 3.5 demonstrates how a seabed multiple forms and how this could

interfere with interpretation of geological structures located at the same time interval. Multiples are a particular problem when surveying in shallow water depths due to the multiple time interval being only shortly after the primary event arrival. Artefacts including multiples do not greatly affect the data analysed in this thesis.

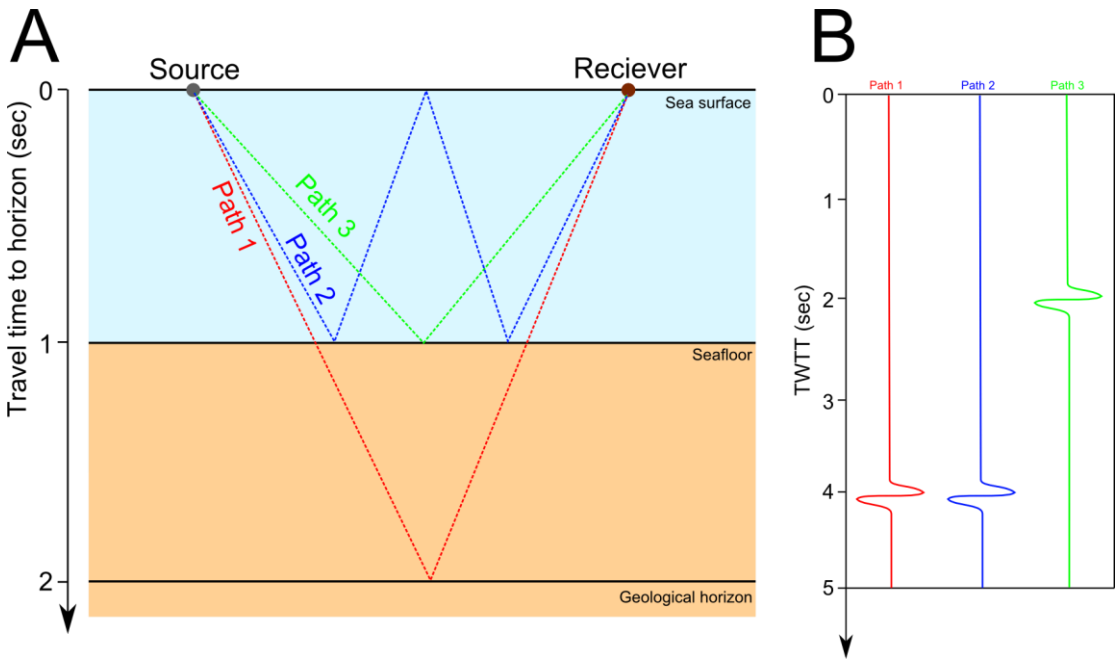

Fig. 3.5

A) A schematic depiction of the generation of seafloor multiples and B) hypothetical seismic traces for seismic waves that have followed paths 1, 2 and 3 in part A of this figure. This figure demonstrates how multiples could result in ambiguity in interpreting subsurface geological horizons during a seismic reflection study. Paths 1 and 3 are primary reflections, whereas path 2 is a seafloor multiple.

3.1.4 Interpretation of seismic reflection data

The final stage in the seismic reflection method is geological interpretation of the processed data. There are essentially two approaches to seismic interpretation; structural analysis and sequence stratigraphy (Vail and Mitchum, 1977) but in reality both complement each other and thus they are usually applied simultaneously (Kearey and Brooks, 1991). Seismic interpretation relies heavily on human perception, so it is not

surprising to find different workers often interpret the same seismic dataset differently (e.g. Hansen and Cartwright, 2007; Thomson, 2007). Recent work has sought to increase the rigorousness of the seismic interpretation methodology by recognition that often non-unique interpretations are possible and that these should be recognised and considered in the presentation of seismic interpretation results (Macrae et al., 2016).

The main principle of seismic stratigraphy is that within the resolution of the seismic data reflections approximate gross bedding and thus can be assumed to approximate time lines (Vail and Mitchum, 1977). This relies on the fact that reflectors are produced at distinct impedance contrasts resulting from bedding interfaces and not from lateral facies changes within the sedimentary system.

3.1.5 Seismic reflection data in this study

Although seismic reflection data are used to some extent in all of the data chapters (Chapters 4, 5, 6 and 7) the main chapter which utilises seismic interpretation is the work in the Davis Strait in Chapter 6. All seismic reflection data in this thesis were interpreted as stacked, processed and migrated lines as no seismic processing was undertaken as part of this project. All seismic interpretation presented in this thesis was primarily carried out using Schlumberger's Petrel interpretation software (2014 version). Additional analysis of the interpreted data utilised the Generic Mapping Tools (GMT) 5 package, ArcGIS 10.3 and MATLAB 2015b software packages.

Four seismic data sets are used in this study: 1) the Spectrum West Greenland Reprocessed 2012 survey; 2) the BGR-77 Survey; 3) the 901, 902 and 903 lines (Labrador Sea); and 4) the SCREECH survey (Grand Banks, Offshore Newfoundland) (Fig. 3.6).

The Spectrum West Greenland Reprocessed 2012 survey (Fig. 3.6A) accounts for most of

the seismic data used in this study (Chapter 6). This survey is actually a compilation of multiple surveys collected by different operators at different times using different acquisition techniques and parameters (Fig 3.6A and Table 3.1). Although the quality of the seismic data is generally quite good for a regional study such as this there was some variation within the quality of these sub-surveys as a result of the differing acquisition and processing parameters used. The lowest quality data belonged to the BUR71 sub-survey as this was acquired using older, lower frequency equipment. This survey was nominally 24 fold and was acquired in 1971 with a shotpoint interval of 50 m and a relatively short 2.4 km streamer (Table 3.1).

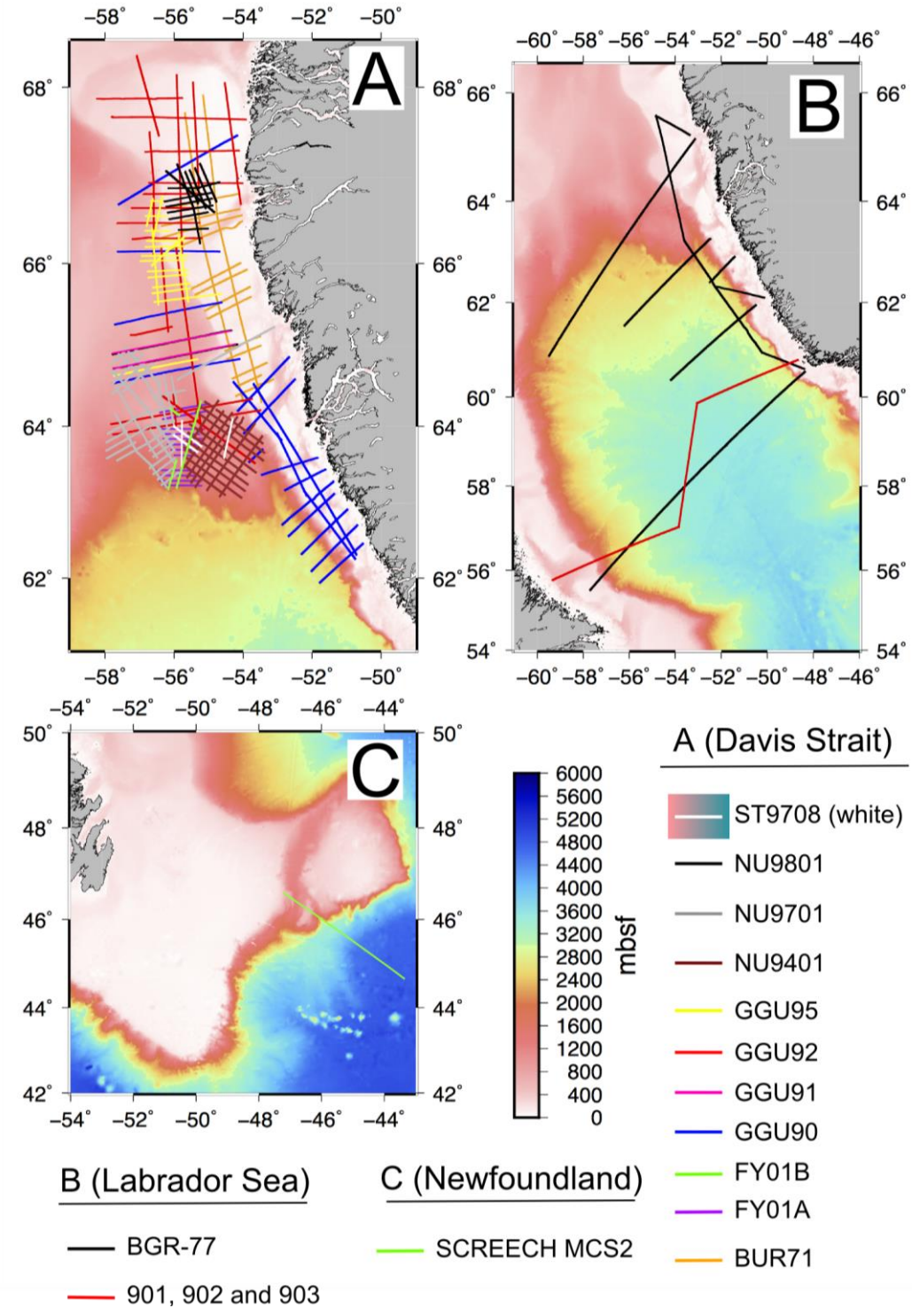

Figure 3.6

The locations of the seismic surveys utilised in this study shown plotted on the global bathymetry map (Smith and Sandwell, 1997) in A) the Davis Strait (Chapter 6), B) the Labrador Sea (Chapters 4 and 5) and C) the Grand Banks (Chapter 7).

Survey Name	Date Acquired	Acquired by	Data Supplied	Available (Km)	Processed (Km)	SP Interval (m)	Group Interval (m)	Cable Length (m)	Number Channels	Nominal Fold	Record Length (s)
BUR71	1971	Burmah Oil	GEUS	3247	1884	50	100	2400	24	24	6
FY01A/B	2001	Statoil	GEUS	948	895	25	12.5	6000	480	120	8
GGU90	1990	GGU	GEUS	3288	2114	25	25	3000	120	60	8
GGU91	1991	GGU	GEUS	339	336	25	25	3000	120	60	8
GGU92	1992	GGU	GEUS	3031	2636	25	25	3000	120	60	8
GGU95	1995	GEUS	GEUS	3769	1060	25	12.5	3000	240	60	8
ST9708	1997	Statoil	GEUS	2293	212	25	12.5	3600	288	72	8
NU9401	1994	Nunaoil	Nunaoil	1708	1708	25	12.5	3000	240	60	8
NU9701	1997	Nunaoil	Nunaoil	2115	2006	25	12.5	3000/3600	240/288	60/72	8
NU9801	1998	Nunaoil	Nunaoil	709	710	25	12.5	4500	360	90	8

Table 3.1

Acquisition parameters for the Spectrum West Greenland Repro 2012 seismic reflection surveys shown in Figure 3.6. The data in this table was provided by Spectrum (processing and acquisition report in Appendix).

This study also had access to the West Greenland side of the survey of the BGR-77 survey (Fig. 3.6B). This data was acquired by BGR (Bundesanstalt für Geowissenschaften und Rohstoffe) in 1977. Extracts from the processing and acquisition report are provided in

German in the Appendix.

The seismic line used to constrain the sills modelling work (Chapter 7) was collected as part of the SCREECH survey, a seismic survey designed to provide insights into the basin stratigraphy and crustal structure in proximity to Ocean Drilling program ODP sites 1276 and 1277 (Shillington et al., 2004; Tucholke et al., 2004). Multi-channel Seismic (MCS) data were acquired using a 480 channel, 6 km streamer configuration on the Maurice Ewing vessel. The MCS data have a sampling interval of 4 ms^{-1}, a shot-spacing of 50 m, a fold of 60, a recording length of ~16 s, and a common midpoint (CMP) spacing of 6.25 m (Shillington et al., 2004).

3.1.6 Seismic refraction data

In addition to seismic reflection data, seismic refraction studies have provided insights into the velocity structure of passive margins, allowing geophysicists to interpret the composition and geometry of passive margins at depth. Many of the same challenges which must be overcome during the acquisition of seismic reflection data are shared by the acquisition of seismic refraction data, including those associated with working offshore.

In this study published seismic refraction data are used in Chapter 4 to compare the crustal structure of the conjugate margins of the Labrador Sea. The seismic refraction profiles in the Labrador Sea (Chian et al., 1995a; Chian et al., 1995b) were collected to supplement the deep seismic reflection lines (Keen et al., 1994) in the area. The refraction profiles used to constrain crustal structure in Chapter 4 were shot in 1990 during the CSS Hudson cruise 90-013, with shots fired every 60 s to give a shot interval of c. 120 m (Chian et al., 1995b). The data were collected using 21 ocean bottom seismometers (OBS) and stored on cassette tapes (Chian et al., 1995b). Processing of the refraction data included; band-pass filtering

of 4-8 Hz, clipping of high amplitudes gain increasing linearly with horizontal range and coherency mixing (Chian et al., 1995b).

3.2 Other (non-seismic) geophysical datasets

In addition to seismic reflection and refraction profiles other large-scale geophysical datasets were used in this study to provide areal continuity between the geographically separated locations of the study sites (Chapter 1). Datasets of this type that have contributed to our understanding of passive margins include; bathymetry (Smith and Sandwell, 1997), potential field (gravity – e.g. Sandwell et al., 2014 and magnetics – e.g. Maus et al., 2009), total sediment thickness (Divins, 2003) and age of the ocean crust (Müller et al., 2008).

3.2.1 Bathymetric Data

In this study bathymetric data are used in all four of the data chapters (Chapter 4-7) to provide the areal context to the geological setting of the study areas. The bathymetric dataset used is version 17.1 of the Smith and Sandwell global compilation (http://topex.ucsd.edu/WWW_html/mar_topo.html) (Smith and Sandwell, 1997) which was last updated in November 2014. This dataset has a horizontal resolution of 1 – 12 km and was derived by combining available depth soundings with high-resolution marine gravity information from the Geosat and ERS-1 satellite datasets (Smith and Sandwell, 1997).

3.2.2 Potential field data

Potential field data includes both gravity and magnetic data (Kearey and Brooks, 1991). High-resolution gravity and magnetic surveys have contributed significantly to the current

understanding of the structure of the Earth by allowing scattered geological observations to be integrated into regional interpretations (Gunn, 1997).

3.2.2.1 Gravity anomaly data

Gravity data are used throughout this study to both provide background context to the study locations and also directly in the analysis, particularly in Chapter 6 to aid with the location of faults that offset the pre-rift basement. The gravity data used in this study was version 23.1 of the Smith and Sandwell global compilation (http://topex.ucsd.edu/WWW_html/mar_grav.html) (Sandwell et al., 2014). Both the free air anomaly (FAA) and a calculated Bouguer anomaly were used in this study. The calculation of the Bouguer anomaly was performed in the Generic Mapping Tools (GMT) software using and an average crustal density of 2.7 gcm^{-3}.

3.2.2.2 Magnetic data

The aim of a magnetic survey is to investigate the subsurface geology on the basis of anomalies in the Earth's magnetic field that arise from the magnetic properties of the underlying rocks (Kearey and Brooks, 1991). Magnetic surveying of the ocean basins has made vast contributions to the collective understanding of many aspects of continental breakup, oceanic crust production and passive margin formation (e.g. Maus et al., 2009). Early magnetic surveying of the ocean floor revealed that oceanic crust is characterised by a pattern of linear magnetic anomalies that is attributed to stripes of oceanic crust that are alternatively magnetised in a normal and reverse direction (Mason and Raff, 1961). This led to theory of seafloor spreading and the establishment of a timescale for the polarity transitions (Heirtzler and Hayes, 1967; Heirtzler et al., 1968). Magnetic data were not interpreted during this study. However, previous interpretations of oceanic magnetic data do contribute to geological setting of this project by providing information regarding the

age and extent of oceanic crust (e.g. the Labardor Sea - Srivastava and Roest, 1999). The EMAG (Earth Magnetic Anomaly Grid) Version 2 (Maus et al., 2009) global compilation of oceanic magnetic data was also referred to during this research, to again provide regional context.

3.2.3 Total sediment thickness data

Total sediment thickness data were used in this study mostly in Chapter 4 to compare sediment distribution between the conjugate margins of the Labrador Sea and to also provide the regional geological context in the other data chapters. In this study we have used the NOAA Total Sediment Thickness of the World's Ocean's and Marginal Seas version 2 (https://www.ngdc.noaa.gov/mgg/sedthick/sedthick.html) (Divins, 2003). The NOAA Total Sediment Thickness data has a resolution of 5 x 5 arc-minutes and was compiled from three principle sources: 1) previously published isopach maps; 2) oceanic drilling results; and 3) seismic reflection profiles (Divins, 2003).

3.3 Offshore exploration well data

Offshore exploration well data are one of the main data types in many studies of passive margins, as this type of data can provide a key geological tie to the seismic data and other geophysical datasets, this is particularly true for seismic reflection data. Offshore well data are utilised in three of the four data chapters (Chapters 4, 6 and 7), but the main areas that this type of data are included is in the Davis Strait study (Chapter 6) and in the thermal maturity modelling work offshore Newfoundland (Chapter 7).

3.3.1 Seismic-well ties

The seismic study in the Davis Strait (Chapter 6) utilised data from six exploration wells that are for the most part not located near one another (Rasmussen et al., 2003) in a study

area that is c. 600 km by c. 250 km. The six exploration wells (Fig. 3.7) were tied to the nearest seismic lines using the checkshots collected at the wellsite to convert well depth in metres to depth in TWTT. The wells are located relatively close to the 2D seismic profiles with a maximum offset of c. 150 m between the well and the nearest 2D seismic reflection profile (Fig. 3.7).

Having established a time-depth relationship the seismic-well ties were then checked against the same ties made between the seismic data and the wells by the previous work (e.g. Døssing, 2011; Dalhoff et al., 2003). It was deemed unnecessary to undertake detailed seismic-well ties using sonic velocity and density logs to produce synthetic seismic profiles given that the data utilised in this study is essentially analogous to that of a regional exploration survey that identifies megasequences (Vail and Mitchum, 1977) rather than individual reflections. As such producing better constrained seismic-well ties would not address the larger ambiguities in the study caused by the spatial resolution of the data (Fig. 3.6 and 3.7), particularly as many of the small basins identified in Chapter 6 which constitute the study area do not have any well control.

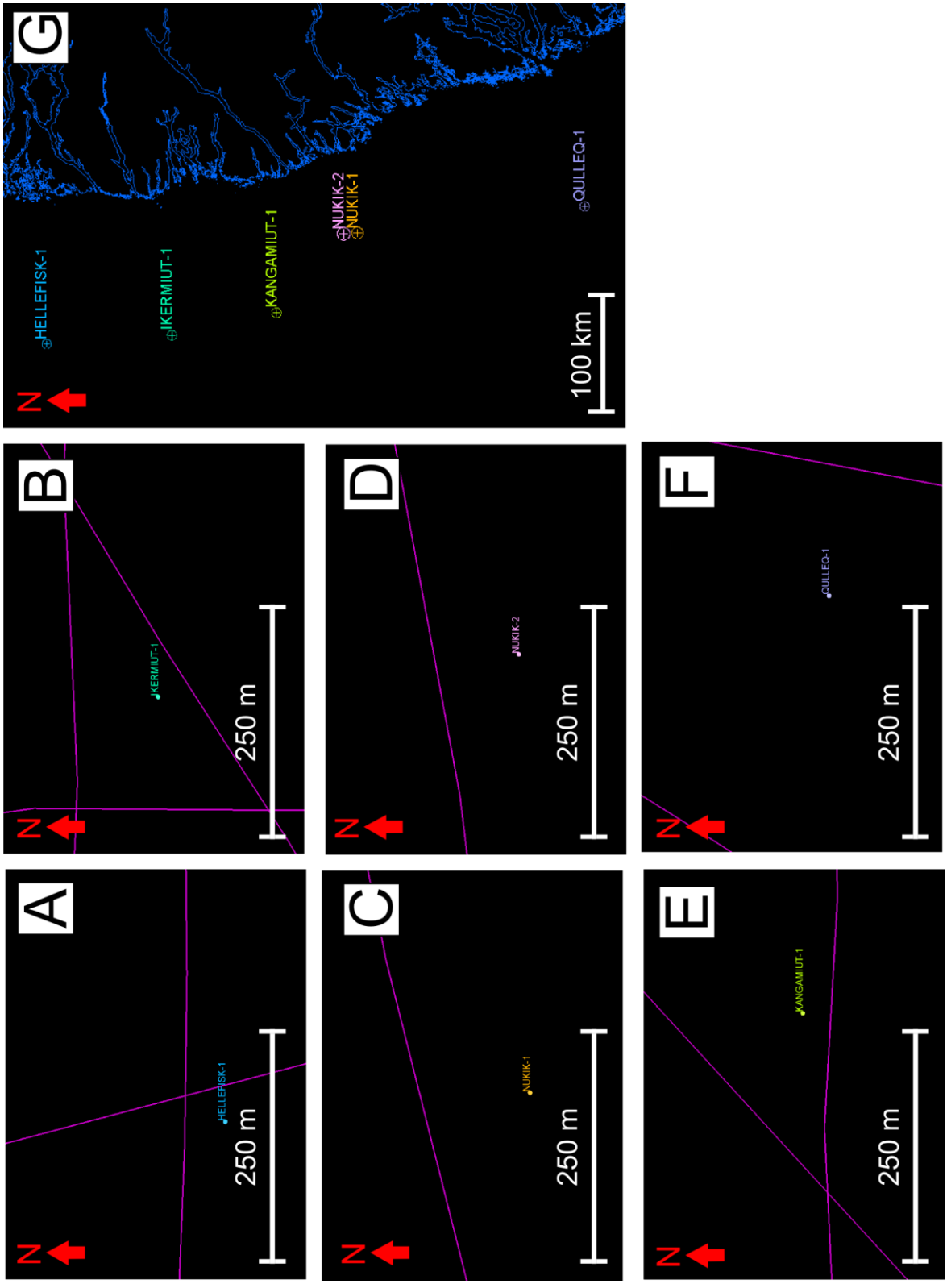

Figure 3.7

Proximity to the nearest 2D seismic profile for the exploration wells used in Chapter 6. Including: A) Hellefisk-1; B) Ikermiut-1; C) Nukik-1; D) Nukik-2; E) Kangamiut-1 and F) Quelleq-1.

3.4 Field based studies of passive margins

Field-based studies of passive margins can be considered to fall into four categories: 1) studies of ancient, uplifted passive margins (e.g. The Chenaillet Ophiolite - Manatschal et al., 2011); 2) studies of modern, exposed coastlines adjacent to present-day passive margins (e.g. West Greenland - Wilson et al., 2006; Japsen et al., 2006; Larsen et al., 2009); 3) studies of active rifts that may represent a precursor to eventual continental break-up (e.g. Ethiopian Rift - Corti, 2009); and 4) analogue studies on other tectonic settings with comparable structures (e.g. the Moab Fault - Berg and Skar, 2005), lithologies (e.g. saucer-shaped sills, Karoo Basin - Aarnes et al., 2011) or processes (e.g. mantle dynamics at Yellowstone - Pierce and Morgan, 2009) to passive margins.

The study of ancient uplifted passive margins have been instrumental in developing our understanding of passive margins because analogues of many of the structures observable on seismic data can be observed at outcrops (e.g. Manatschal, 2004). The study of ancient passive margins is however inhibited by later tectonic and metamorphic events usually related to ocean closure and subsequent uplift of the margin during orogeny, for example the 'Alpine overprint' in the European Alps (Padovano et al., 2015). The Tethyan margin now preserved in the European Alps is interpreted to represent an uplifted ancient passive margin (e.g. Decarlis et al., 2015). One such part of the ancient Tethyan margin which can be used as an analogue for the distal oceanic portion of a passive margin is the Chenaillet Ophiolite in the French/Italian Alps (Manatschal et al., 2011). At the Chenaillet Ophiolite (Fig. 3.8), a well exposed ocean floor sequence can be observed which was only weakly overprinted by later Alpine tectonics during its incorporation into the Alpine nappe stack (Manatschal et al., 2011). A concern regarding this type of analogue study however, is to attempt to find generic models for all passive margins from the limited number of uplifted

ancient passive margins (Wilson et al., 2001b). Many of the aspects observed at these limited field examples of exposed margins may be caused by locality specific processes and not be representative of passive margin development in general.

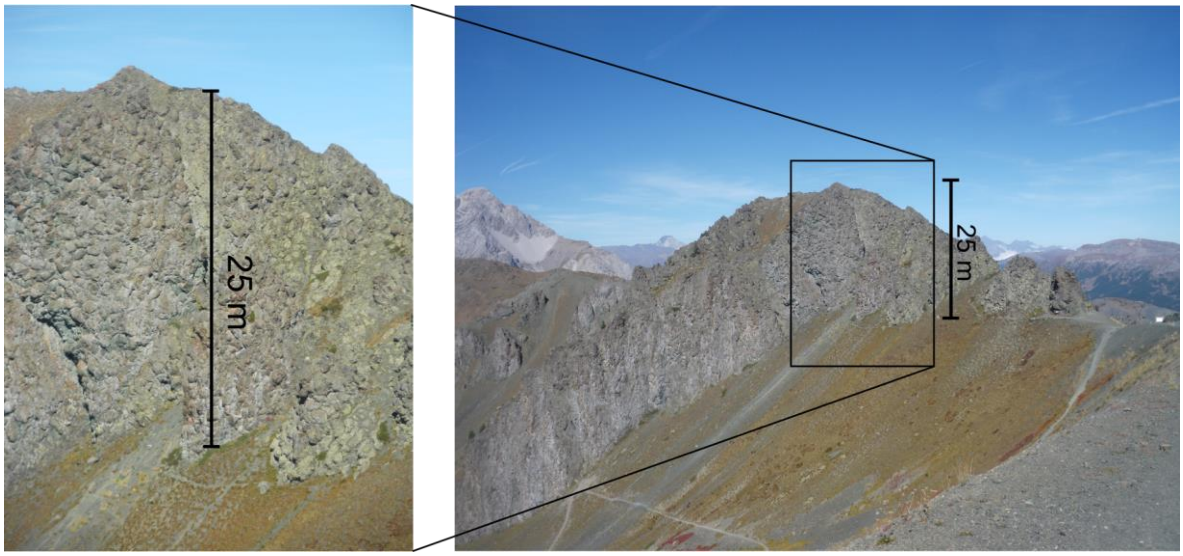

Figure 3.8

Pillow basalts forming part of the oceanic crustal sequence of within the Chenaillet Ophiolite in the French/Italian Alps observed during fieldwork in September 2013. Photos taken looking south towards the outcrop.

Studies on the modern coastlines adjacent to passive margins have been instrumental in providing knowledge of the offshore portions of passive margins (Japsen et al., 2006; Ashby, 2013; Wilson et al., 2006). These types of field-based studies have in particular contributed knowledge to our understanding of the roles of pre-existing structures (Wilson et al., 2006), magmatism (Larsen et al., 2009), uplift and subsidence (Dam et al., 1998). It is this type of field-based study conducted adjacent to a modern passive margin that forms the basis of the analysis detailed in chapters 4 and 5 on the Labrador Sea, where we evaluate the extent of rift-related magmatism in Labrador (Chapter 4) and consider the onshore expression of rifting and its relationship to pre-existing structures (Chapter 5).

The study of active rifts (e.g. Dead Sea Rift - Garfunkel et al., 1981) has also provided insights into many aspects of the early stages of continental breakup and thus passive margin formation including: 1) demonstrating the variability of rift systems prior to continental breakup (Ruppel, 1995); 2) the processes of strain localisation within syn-rift fault systems (e.g. Suez rift, East Africa - Gawthorpe et al., 2003) and 3) the role of magmatism in rift development (e.g. East Africa - Bosworth, 1987; Stab et al., 2015).

Finally, the use of field data and observations from non-passive margin tectonic settings to understand aspects of passive margin development such as faulting, sedimentation and magmatism has also contributed to the study of passive margins. These studies are particularly useful when considering processes that are beyond the seismic resolution, as described in the previous section. One such study of this type was conducted by Hutton, (2009) in the Theron Mountains of Antarctica where features of igneous intrusions such as bridge structures can be observed, which may be comparable to certain aspects of magmatism present on VPMs (Magee et al., 2016).

Overall, it can be seen that field-based research has and will continue to contribute towards the understanding of passive margins. This is particularly relevant where the resolution of geophysical data is insufficient to providing images with a unique interpretation.

3.4.1 Makkovik fieldwork

Between June and July in 2015 one month was spent conducting fieldwork around the small town of Makkovik in Labrador, Canada. The primary aim of the fieldwork was to identify and characterise the extent and field relationships of the previously studied Mesozoic igneous rocks interpreted to be related to rifting prior to the opening of the Labrador Sea (Tappe et al., 2007). The intended purposes of characterising the rift-related magmatism near Makkovik were: 1) to quantify the variability and extent of the Mesozoic

rift-related magmatism, allowing us to understand certain aspects of the nature of early rift development; and 2) to characterise both the pre- and syn-rift structures to understand the process of reactivation and the nature of syn-rift deformation related to the opening of the Labrador Sea. The results of the work addressing these two fieldwork aims are detailed in Chapters 4 and 5, respectively.

3.4.2 Structural analysis of field data

During the Makkovik field campaign an abundance of structural data was collected including orientation data for all dykes sampled, basement fractures, veins and metamorphic mineral fabric (Chapter 5). These data were analysed in the MyFault software version 1.05 by Pangea Scientific (Michael, 1984) to estimate the orientation of the principle stress axes during the deformation events leading to the formation of these structures.

Stress inversion uses fault plane orientations and slip vectors to reconstruct past stress configurations (Angelier, 1990). The underlying assumption of stress inversion is that the slip on a plane occurs in the direction of the maximum resolved shear stress (Bott, 1959). Our stress inversion was performed using the minimised shear stress variation method, a standard inversion method (e.g. Dempsey et al., 2014; Abdunaser and McCaffrey, 2015) that allows all faults to fail simultaneously, enabling us to calculate the orientation and relative magnitudes (stress ratios) during deformation of the fault set. The minimized shear stress variation method is an improvement over simpler calculations such as simple shear tensor average (Michael, 1984). The purpose of the stress inversion in this study was to determine if the observed onshore deformation events are related to previous interpretations of the Mesozoic rifting direction prior to the opening of the Labrador Sea (e.g. Abdelmalak et al., 2012). The results of the stress inversion in proximity to Makkovik

were then compared to similar studies elsewhere on the margins of the Labrador Sea-Baffin Bay rift system, in particular the work of Abdelmalak et al. (2012) in West Greenland.

3.4.3 Geochemical (XRF) and petrological analysis of field data

A total of twenty-four thin sections were produced in the thin section laboratory at Durham University to characterise the petrology of the samples collected during fieldwork. The aim of this was to further development concepts based on the observations made in the field.

The first stage of the thin section preparation was to cut the rock samples obtained during fieldwork to appropriate sizes for the production of thin sections (approximately 4 x 2 x 1 cm). The samples were then smoothed down on a series of lapping plates starting with a 40 μm diamond disk, then progressing to a 20 μm diamond disk, and finally by hand on a 9.5 μm lapping plate. The purpose of the smoothing process was to minimise unwanted abrasions on the surface of the sample. The next stage of the thin section preparation process was to make sure that the glass slides which the sample were mounted to were the correct thickness. This process was undertaken on a Logitec lapping machine. On this machine the thickness can be set, with a diameter of 1300 μm used as a slide thickness during the preparation of the samples analysed in this study. The slides of a known thickness were then dried on a hot plate set at 60° for 30 minutes. The smoothed rock samples were then glued to the prepared glass slide using Epotek 301. The samples and the slides were then placed in a vertical clamp on another hot plate at 60° for 1 hour 30 minutes to ensure that the Epotek 301 epoxy was set. Once the Epotek 301 was set the samples were thinned using a Petrothin thin sectioning machine, which includes both a cutting and a grinding disk. The cutting disk was used first to reduce the sample to 500 μm, the samples were then reduced further using the disk on the thin sectioning machine. After

thinning using the disk on the Petrothin the samples were then either thinned by hand to the required thickness or by using the automatic Logitec lathe. Finally, the samples were cleaned, dried and labelled. Some thin sections in this study were covered using a cover slip but most were left open to allow for analysis using a scanning electron microscope (SEM).

Petrographic descriptions were made on the thin sections at Durham University to supplement the petrographic descriptions made both in the field and on hand specimens. Analysis of the thin sections was primarily undertaken using a Leica DM2500 petrographic microscope.

Some of the samples obtained during fieldwork were examined using a SEM. The SEM used for this analysis was the Hitachi TM-1000. Examination using an SEM was undertaken on both uncovered thin sections and on rock chips. In both cases the sample was fixed to an aluminium platform with carbon tape. Carbon tape was then wrapped over the sample and back to the aluminium base plate to further reduce the builds up of charge whilst inside the SEM vacuum chamber.

In addition to the petrological analysis the field observations were supplemented by whole rock geochemistry (X-ray Fluorescence - XRF) of igneous lithology samples. The XRF major element analysis was undertaken at the University of Leicester (UK) to determine the weight percent of major elements as oxides (raw data including values for standards are available in the Appendix). The XRF laboratory at the University of Leicester operates a PANalytical Axios Advanced X-Ray Fluoresence spectrometer which runs a 4Kw Rhodium (Rh) anode end window super sharp ceramic technology X-Ray tube. The major element analysis was performed on fused beads to eliminate mineralogical effects and reduce inter-element effects.

Re-Os (Rhenium-Osmium) geochronological analysis was conducted at Durham University on pyrite samples from two fieldwork locations in an attempt to establish a better constrained age estimates. The methodology used in the Re-Os analysis followed the same procedure as Dichiarante et al. (2016). The Re-Os analysis however produced ages >3 Ga, a value well in excess of the age of the oldest basement units in the area (LaFlamme et al., 2013) and thus could not be used to provide a better constrained age for the deformation event analysed in Chapter 5. The results of the Re-Os analysis are available in the Appendix.

3.5 Numerical and analogue modelling of rifting and passive margin formation

Numerical and analogue modelling of extensional tectonic systems is another research area that has contributed greatly to our understanding of the processes of continental breakup and passive margin formation. Models are essential to this study area as they allow observations to be made on processes that either occur either on extremely long time scales or are unobservable by direct means such as mantle processes including; mantle plumes (Redmond and King, 2004) and small-scale convetion (SSC- Simon et al., 2009; Ballmer et al., 2007). A complete range of both temporal and spatial scales can be modelled depending on the process being studied extending from models on the scale of individual igneous intrusions (e.g. Fjeldskaar et al., 2008; Wang et al., 2010) to mantle convection models (e.g. van Hunen and Čadek, 2009). The numerical modelling conducted during this study in Chapter 7 is of the former type. Although no analogue modelling was undertaken as part of this study concepts developed from analogue models such as the oblique rifting models of Morley et al. (2004) and the structural inheritance work of Autin et al. (2013) have contributed towards the interpretation of the results in the Davis Strait analysis (Chapter 6).

3.5.1 Numerical modelling in this study

Numerical modelling was used in Chapter 7 of this thesis to quantify the thermal influence of intrusive magmatism on organic-rich sediments on the Newfoundland margin. This was chosen as the location to conduct the numerical modelling due to the abundance of previous work providing numerous geological constraints (e.g. Hart and Blusztajn, 2006; Deemer et al., 2010; Pross et al., 2007) for the numerical modelling which would not have been possible at many other locations.

In the models presented in Chapter 7 a finite differences method was used to solve the heat diffusion equation in MATLAB for spatially variable physical parameters using the method described in Fjeldskaar et al. (2008). The outputs of our thermal models are then used as an input into the EASY%R_o vitrinite reflectance model (Sweeney and Burnham, 1990; Burnham and Sweeney, 1989). The method used is described fully in the methodology section in Chapter 7 and in Appendix B of Fjeldskaar et al. (2008).

Chapter 4

An evaluation of Mesozoic rift-related magmatism on the margins of the Labrador Sea: implications for rifting and passive margin asymmetry

This chapter has been published as:

Peace, A., McCaffrey, K., Imber, J., Phethean, J., Nowell, G., and Gerdes, K., Dempsey, E., (*2016*). An evaluation of Mesozoic rift-related magmatism on the margins of the Labrador Sea: implications for rifting and passive margin asymmetry. *Geosphere* V.12 No.6

4.0 Summary

The Labrador Sea is a small (~900 km wide) ocean basin separating southwest Greenland from Labrador, Canada. It opened following a series of rifting events that began as early as the Late Triassic or Jurassic, culminating in a brief period of seafloor spreading commencing by polarity chron 27 (C27; Danian) and ending by C13 (Eocene-Oligocene boundary). Rift-related magmatism has been documented on both conjugate margins of the Labrador Sea. In southwest Greenland this magmatism formed a major coast-parallel dyke swarm as well as other smaller dykes and intrusions. Evidence for rift-related magmatism on the conjugate Labrador margin is limited to igneous lithologies found in deep offshore exploration wells, mostly belonging to the Alexis Formation, along with a postulated Early Cretaceous nephelinite dyke swarm (ca. 142 Ma) that crops out onshore, near Makkovik, Labrador. Our field observations of this Early Cretaceous nephelinite suite lead us to conclude that the early rift-related magmatism exposed around Makkovik is volumetrically and spatially limited compared to the contemporaneous magmatism on the conjugate southwest Greenland margin. This asymmetry in the spatial extent of the exposed onshore magmatism is consistent with other observations of asymmetry between the conjugate margins of the Labrador Sea, including the total sediment thickness in offshore basins, the crustal structure, and the bathymetric profile of the shelf width. We propose that the magmatic and structural asymmetry observed between these two conjugate margins is consistent with an early rifting phase dominated by simple shear rather than pure shear deformation. In such a setting Labrador would be the lower plate margin to the southwest Greenland upper plate.

4.1 Introduction

Stretching of the continental lithosphere results in rifting and may lead to continental breakup accompanied by seafloor spreading (Eldholm and Sundvor, 1979). The production of pairs of conjugate continental passive margins is the inevitable result of the continental

breakup process (Geoffroy, 2005). Although conjugate margins may inherit similar geological and structural components, many aspects of these conjugate pairs often display significant asymmetry.

The degree of symmetry displayed between conjugate passive margins has traditionally been linked to the mode by which the preceding rifting occurred (Lister et al., 1986), with models of continental rifting being described as either pure shear (McKenzie, 1978), simple shear (Wernicke, 1985), or combinations of these (Lister et al., 1986). Rifting under a pure shear–dominated regime occurs by symmetrical, brittle extension of an upper layer and ductile stretching of a lower layer. The simple shear model of rifting predicts that extension occurs along lithosphere-scale normal faults and/or ductile shear zones usually resulting in an asymmetric rift in cross section (e.g. Lister et al., 1986; Etheridge et al., 1989). The large detachment faults required by simple shear models are claimed to be mechanically problematic (Ranero and Pérez-Gussinyé, 2010); it has also been claimed that both conjugate margins often display characteristics of being the upper plate to the detachment fault (Lavier and Manatschal, 2006). It has also been argued that it is difficult to generate melt under simple shear rifting (Latin and White, 1990). Despite these problems, the simple shear model or derivatives of it are often used to explain various aspects of asymmetry on conjugate margin systems, for example, the South Atlantic margins (Becker et al., 2016). Testable predictions of the detachment model of passive margin formation (Lister et al., 1986) include a wide continental shelf, and deep sag basins overlying the sedimentary synrift fill on the lower plate margin. In contrast, the upper plate margin remains relatively unfaulted with an induced continental drainage divide caused by uplift due to magmatic underplating.

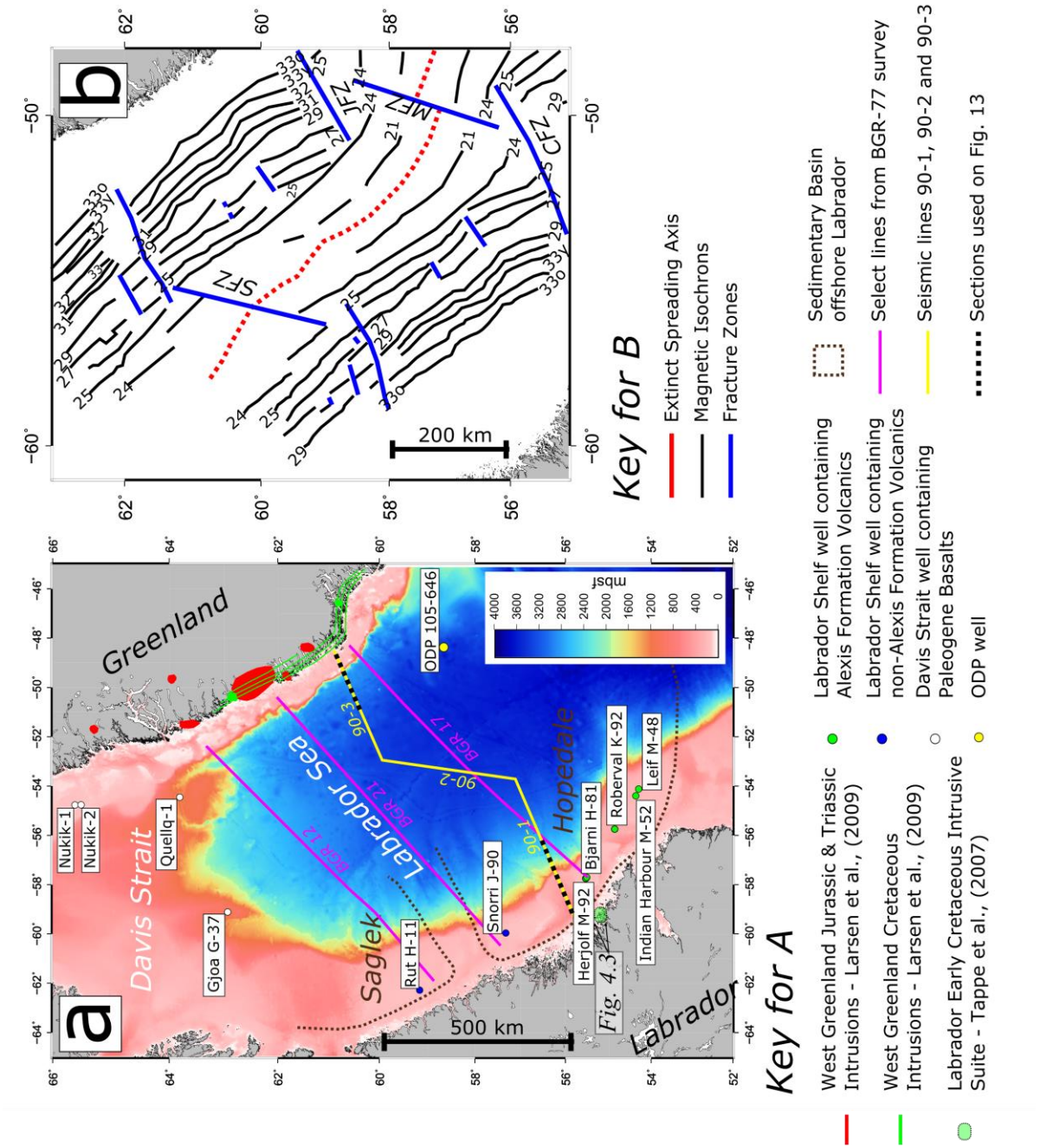

Figure 4.1

A) Summary of documented occurrences of early rift-related (Triassic–Cretaceous) magmatism on the margins of the Labrador Sea, both onshore and in offshore wells. ODP—Ocean Drilling Program. B) Interpretation of the age and structure of oceanic crust in the Labrador Sea (modified from Srivastava and Roest, 1999). Abbreviations: SFZ—Snorri fracture zone; CFZ—Cartwright fracture zone; JFZ—Julinhaab fracture zone; MFZ—Minna fracture zone. The bathymetry data are from Smith and Sandwell, (1997; global topography and bathymetry).

In this contribution we assess the degree of asymmetry displayed by the conjugate margins of the Labrador Sea (Fig. 4.1A) to determine if rifting prior to the formation of these margins is likely to have taken place under a pure or a simple shear–dominated regime. This assessment was achieved through observations made during four weeks of field work between June and July 2015 near the town of Makkovik, Labrador, Canada. The primary aim of the field work was to identify and characterise the spatial extent and field relationships of previously described Mesozoic igneous rocks, which Tappe et al. (2007) related to rifting prior to the opening of the Labrador Sea. Field observations were supplemented by whole-rock geochemistry (X-ray fluorescence, XRF) of igneous rock samples. Our field data are then considered in the context of observations from elsewhere on the margins of the Labrador Sea. We integrate these observations with analysis of large-scale geophysical data sets including that of the National Oceanic and Atmospheric Administration (NOAA; Divins, 2003), seismic reflection profiles, and the Smith and Sandwell (1997) global topography data set to further test our interpretation of margin asymmetry.

4.2 Geological setting

The Labrador Sea separates Labrador in eastern Canada from southwest Greenland (Fig. 4.1A) and is floored by a small (~900 km wide) oceanic basin that provides an ideal place to study conjugate passive margin pairs where the production of oceanic crust was relatively limited (Chalmers and Laursen, 1995). Rifting of the Labrador Sea has previously been attributed to either a pure shear–type model, based on seismic and other geophysical data indicating that faulting is confined to the upper crust (Keen et al., 1994), or a simple shear–type model, based on observations of the asymmetry of the transition zones (Chian et al., 1995a).

Rifting prior to the opening of the Labrador Sea started as early as the Late Triassic to Jurassic, based on ages obtained from dyke swarms in West Greenland that are interpreted to be related to early rifting (Larsen et al., 2009) (Fig. 4.1A). The early seafloor spreading

history of the Labrador Sea is poorly constrained, with the oldest undisputed magnetic anomaly interpretation in the Labrador Sea being from polarity chron 27 (C27; Danian; Chalmers and Laursen, 1995). However, seafloor spreading may have initiated earlier, at C32 (Campanian) in the southern Labrador Sea and C28 (Maastrichtian) in the northern Labrador Sea (Srivastava, 1978). Seafloor spreading in the Labrador Sea underwent a major reorganisation and change in spreading direction at C24–C25N (Thanetian–Ypresian) (Fig. 4.1B), coincident with the onset of North Atlantic spreading (Srivastava, 1978). After the reorganisation of the North Atlantic and Labrador Sea between C24 and C25N there was a reduction in the rate of seafloor spreading before it eventually ceased at C13N (Eocene-Oligocene boundary) (Geoffroy, 2001).

The sedimentary basins offshore Labrador record the progressive opening of the Labrador Sea from south to north (DeSilva, 1999) during the Mesozoic. Two major sedimentary basins are present off the coast of Labrador (DeSilva, 1999): the Hopedale Basin in the south and the Saglek Basin to the north (Fig. 4.1A). Both the Saglek and Hopedale Basins contain synrift and postrift, clastic-dominated sequences of Cretaceous to Pleistocene age (Jauer et al., 2014). Exposures of Mesozoic and Cenozoic sediments onshore along the Labrador coast are extremely rare (Haggart, 2014).

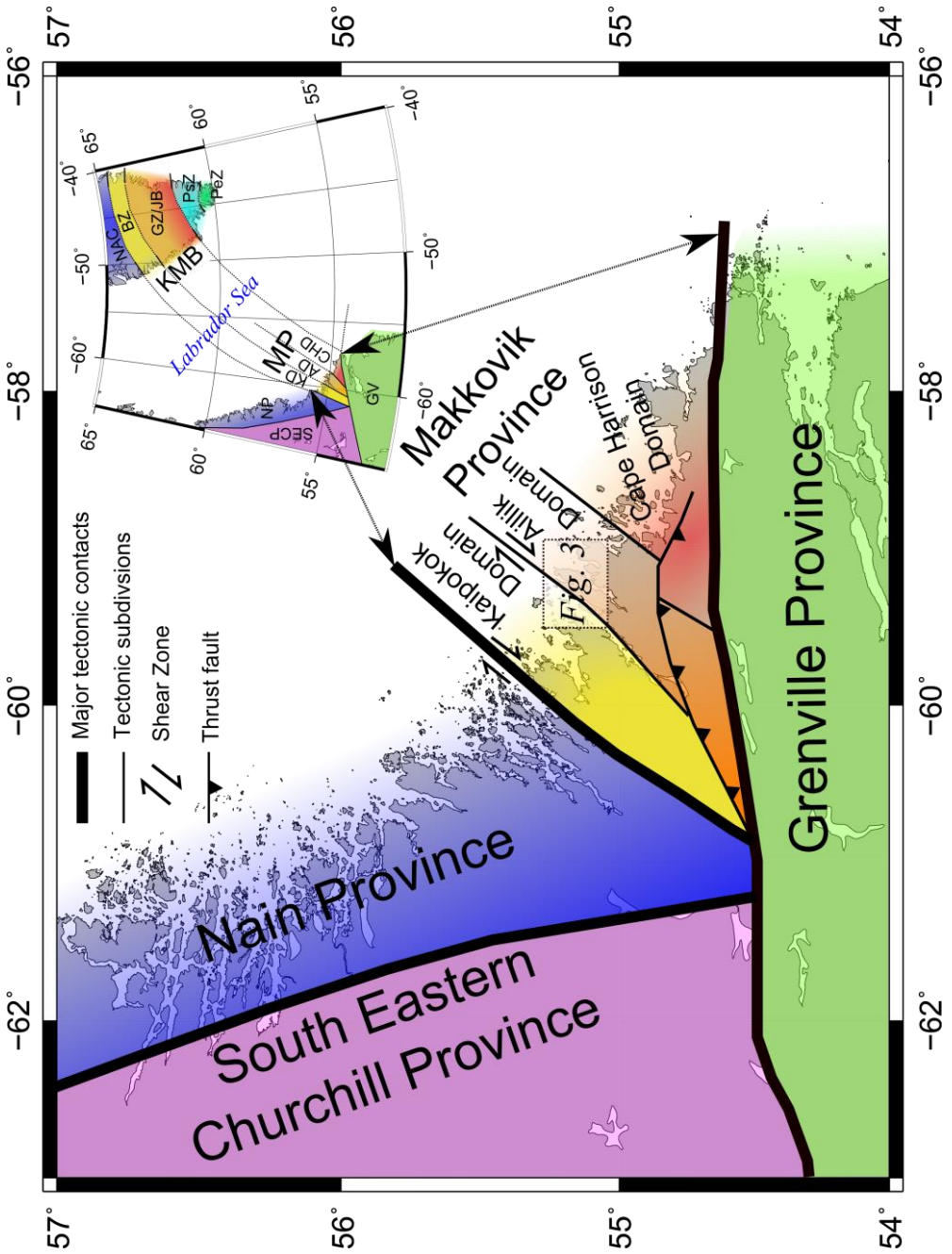

Figure 4.2

Simplified tectonic framework of central Labrador modified from LaFlamme et al. (2013), including the location of Figure 4.3 within the Makkovik Province. Abbreviations: NAC—North Atlantic Craton; BZ—Border Zone; GZ/JB—Granite Zone/Julianehåb Batholith; NP—Nain Province; MP—Makkovik Province; PsZ—Psammite Zone; PeZ—Pelite Zone; SECP—southeastern Churchill Province; KD—Kaipokok Domain; AD—Aillik Domain; GV—Grenville Province; KMB—Ketilidian Mobile Belt. Inset: The correlation of the Makkovik and Ketilidian orogenic belts modified from (Kerr et al., 1997).

From north to south the basement tectonic units exposed at surface on the coast of Labrador are the Archean Nain Province, the Paleoproterozoic Makkovik Province, and the Mesoproterozoic Grenville Province (LaFlamme et al., 2013; Fig. 4.2). The Makkovik Province is separated from the Nain Province by the Kanairiktok shear zone (Culshaw et al., 2000) and from the Grenville Province by the Grenville Front, which marks the northern limit of widespread Grenvillian deformation (Funck et al., 2001). The Makkovik Province is characterised as a Paleoproterozoic accretionary belt and is the smallest defined tectonic component of the Canadian shield (Ketchum et al., 2002). Prior to the opening of the Labrador Sea the Makkovik Province was adjacent to the Ketilidian mobile belt (KMB; Fig. 4.2), which currently forms part of southwest Greenland (e.g. Garde et al., 2002; Wardle et al., 2002; Kerr et al., 1997). The Makkovik Province can be separated into three distinct zones with distinctive geological characteristics (Kerr et al., 1996); from northwest to southeast, they are the Kaipokok, Aillik, and Cape Harrison domains (Fig. 4.2) (Kerr et al., 1997).

4.2.1 Onshore rift-related magmatism on the margins of the Labrador Sea

Our field work was carried out in the Aillik domain of the Makkovik Province. Here, the Early Cretaceous nephelinite suite (ca. 142 Ma) located near Makkovik (Fig. 4.3; Table 4.1) is the most recent of three magmatic events identified by Tappe et al. (2007). The older two magmatic events formed a Neoproterozoic ultramafic lamprophyres and carbonatite dyke suite (ca. 590–555 Ma) and a Mesoproterozoic olivine lamproite dyke suite (ca. 1374 Ma) (Tappe et al., 2006). These two older events are not considered to be directly related to the rifting that culminated in the Mesozoic opening of the Labrador Sea (Tappe et al., 2007).

Tappe et al. (2007) Sample number	ST100	ST102	ST241b	L59	ST217	ST103	ST253	ST245	ST254
Composition (Tappe et al., 2007)	Nephelinite	Basanite	Nephelinite	Nephelinite	Basanite	Melilitite	Nephelinite	Basanite	Nephelinite
Samples collected by this work	No *in situ* outcrop at location.	No *in situ* outcrop at location.	AP1-S1 AP1-S2 AP1-S3	Not visited by this study	Not visited by this study	AP2-S1 AP2-S2	AP3-S1	AP4-S1 AP4-S2	Area of basement exposure but no dykes of any age anywhere in proximity to location.
Coordinates of samples collected by this work (WGS84)	N/a	N/a	55.09927 N 59.18356 W	N/a	N/a	55.07389N 59.09430W	55.14959 N 59.01542 W	55.16138N 59.14338W	N/a

Table 4.1

Summary of the relationship between the Early Cretaceous nephelinite suite samples of Tappe et al., (2007) and the samples collected by this work.

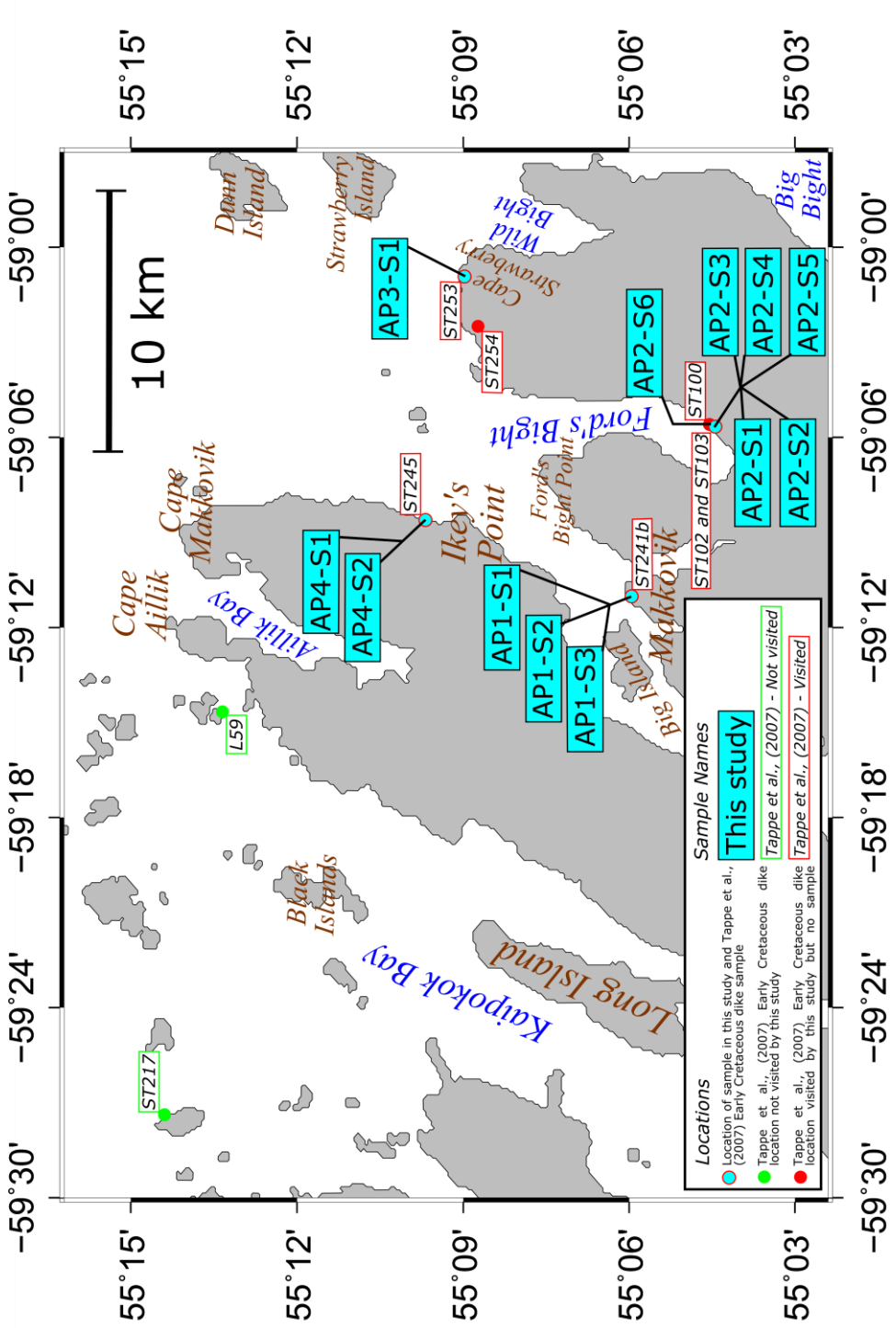

Figure 4.3

Map of the area surrounding Makkovik. Blue filled boxes depict the samples collected and analysed in this study. The Tappe et al. (2007) samples are depicted as smaller red and green boxes, for sites visited and not visited by this study, respectively.

The Tappe et al. (2007) nephelinite suite (Fig. 4.3; Table 4.1) comprises fine-grained olivine melilitite, nephelinite, and basanite dykes and sills as much as 2 m thick with a preferential east-west orientation, and has been characterised as a type of rift-related magmatism. This intrusive suite was claimed by Tappe et al. (2007) to be analogous to the coast-parallel alkaline basaltic dykes observed between 60° and 63°N in West Greenland (Larsen, 2006). The samples categorised by Tappe et al. (2007) as belonging to the nephelinite suite are summarised in Table 4.1, along with their relationship to the samples collected and our analyses (described herein). Here we use the definition of Le Bas (1989) of a nephelinite as containing >20% normative nepheline.

Locality	Character	Rock Type	Method	Age (Ma)	Reference
Uummannaq Fjord	Few small dykes	Ailikite	Rb-Sr	186	Larsen et al. (2009)
Ubekendt Ejland	Small dyke swarm	Camptonite, monchiquite	$^{40}Ar/^{39}Ar$	34 ± 0.2	Storey et al. (1998)
SE Nuussuaq	Dykes and sill, some large	Tholeiitic basalt	$^{40}Ar/^{39}Ar$	56.8 ± 0.2	Larsen et al. (2009)
West of Disko	Volcanic neck	Alkali basalt	$^{40}Ar/^{39}Ar$	27.8 ± 0.6	Storey et al. (1998)
Western Disko	Regional Dyke swarm	Tholeiitic basalt	$^{40}Ar/^{39}Ar$	54.3 ± 0.3	Storey et al. (1998)
Aasiaat district	Three large dykes, one sill	Tholeiitic basalt	$^{40}Ar/^{39}Ar$	56, 61	Larsen et al. (2009)
Itilleq	One dyke	Tholeiitic basalt	$^{40}Ar/^{39}Ar$	64 ± 1.3	Larsen et al. (2009)
Qaqqarsuk	Central complex and dykes	Carbonatite, aillikite	Rb-Sr	Ca. 165	Secher et al. (2009)
			U-Pb*		
Fossilik	One explosion Breccia	Ailikite	Rb-Sr	164.2 ± 1.8	Secher et al. (2009)
Søndre Isortoq	Small dyke swarm	Camptonite, one alkali basalt	$^{40}Ar/^{39}Ar$	56, 58	Larsen et al. (2009)
Godthåbsfjord	Scattered dykes	Camptonite	$^{40}Ar/^{39}Ar$	51.8 ± 0.9	Larsen et al. (2009)
Tikiusaaq	Central complex and dykes	Carbonatite and aillikite	Rb-Sr	155-165	Tappe et al. (2009)
			U-Pb*		
Færingehavn	Few dykes	Aillikite	Rb-Sr	159	Larsen et al. (2009)
			U-Pb	223	
Frederikshåb Isblink	One large dyke	Phonolite	$^{40}Ar/^{39}Ar$	106.1 ± 1.5	Larsen et al. (2009)
Frederikshåb Isblink	Loose dyke swarm	Monchiquite, alnöite, carbonatite	Rb-Sr	149-152	Larsen et al. (2009)
			U-Pb*		
Paamiut	Small dyke swarm	Aillikite	K-Ar	166 ± 5	Larsen and Møller (1968)
Pyramidefjeld	Small dykes and sills, including a thick sheet on Midternæs (16 km NNE)	Aillikite	U-Pb	150 – 152	Frei et al. (2009)
					Larsen et al. (2009)
SW Greenland	Large regional dyke swarm	Mildly alkaline basalt	$^{40}Ar/^{39}Ar$	133 – 141	Larsen et al. (1999)
					Larsen et al. (2009)
Tuttutooq	One or a few sills	Camptonite	$^{40}Ar/^{39}Ar$	115.4 ± 4.7	Larsen et al. (2009)

Table 4.2

*A summary from north to south of documented intrusive rift-related magmatism in West Greenland as summarised by Larsen et al. (2009). * denotes samples dated by Rb-Sr or U-Pb on phlogopite or perovskite.*

Magmatism in West Greenland has also been attributed to early rifting, prior to the opening of the Labrador Sea. According to Larsen et al. (2009) this magmatism is manifest as Mesozoic–Paleogene intrusive rocks that range in scale and abundance from large, coast-parallel dyke swarms to small, poorly exposed dyke swarms or single intrusions (Fig. 4.1; Table 4.2). The large coast-parallel dykes extend for 380 km along the southwest Greenland coast (Larsen et al., 1999). Chalmers et al. (1995) described the later Paleogene breakup-related flood basalts farther north in and around the Davis Strait, but these are beyond the geographical and temporal scope of this study. The igneous rocks observed onshore southwest Greenland (Table 4.2) demonstrate that multiple magmatic events occurred on this margin during and after the Mesozoic. Although many of these events are likely to be rift related, it is extremely unlikely that all these igneous rocks were produced due to the same event.

4.2.2 Offshore rift-related magmatism on the margins of the Labrador Sea

Mesozoic magmatism has also been observed and documented in exploration wells on the Labrador shelf (Fig. 4.1A; Table 4.3) (Umpleby, 1979). Volcanic rocks that are believed to have been erupted during the early stages of rifting are mostly assigned to the Alexis Formation; the type section is recorded in the Bjarni H-81 well (e.g. Ainsworth et al., 2014; Umpleby, 1979). Here a sequence of basalts interspersed with sandstones and silty clays was recorded, but no pyroclastic rocks were documented (Umpleby, 1979). Two cores from the Alexis Formation in Bjarni H-81 have been dated using K-Ar bulk-rock analysis. The lowermost core came from 2510 m and basaltic rocks have been dated as 139 ± 7 Ma (Valanginian), while those in the upper core at 2260 m were dated as 122 ± 6 Ma (Aptian). The age of the lower core is deemed to be less reliable due to alteration; Umpleby (1979) suggested that the inferred duration of ~17 m.y. for the magmatic event

resulting in the eruption of the Alexis Formation is too long and that the lower core might be younger.

The total thickness and areal extent of the basalts of the Alexis Formation is not well constrained, beyond the occurrence of volcanic rocks in the Leif M-48, Robertval K-92, Bjarni H-81, Indian Harbour M-52, and Herjolf M-92 wells (Fig. 4.1A). The Alexis Formation occurs in the Hopedale Basin (Hamilton and Harrison subbasins) and within the southern part of the Saglek Basin, but has not been recorded in the more northern Nain subbasin within the Hopedale Basin (Ainsworth et al., 2014). The thickest recorded occurrence of the Alexis Formation is 357 m in the Robertval K-92 well (Ainsworth et al., 2014). Note that some igneous rocks intersected by wells on the Labrador Shelf have not been assigned to a formation (Ainsworth et al., 2014). Occurrences of unclassified igneous rocks include the "Tuff" and "Diabase" intervals (Canada-Newfoundland and Labrador Offshore Petroleum Board, 2007) in Rut H-11 and the sediments derived from volcanic material in Snorri J-90 (McWhae et al., 1980).

Although no exploration wells have been drilled on the continental shelf offshore southwest Greenland, Site 646 (Leg 105 of the Ocean Drilling Program, ODP) was drilled on oceanic crust in the southern Labrador Sea (Fig. 4.1A). With the exception of the oceanic crust, Site 646 did not encounter igneous rocks; however, sediments containing clasts of mafic material were described (Shipboard Scientific Party, 1987).

4.3 Field observations of Mesozoic magmatism near Makkovik, Labrador

The aim of the field work was to characterise the nature and extent of Mesozoic magmatism near Makkovik to gain insights into rifting in the region prior to the opening of the Labrador Sea. Our field study of the Mesozoic magmatism near Makkovik was guided by the description of the Early Cretaceous magmatism in Tappe et al. (2007) (Fig. 4.3;

Table 4.1). Of the nine locations where Tappe et al. (2007) documented Early Cretaceous magmatism, we visited seven sample locations (with exception of L59 and ST217). Eight samples of igneous material were obtained at four of the seven locations visited during this study. Where appropriate, samples collected adjacent to the dykes are also described to provide geological context and to emphasise the field relationships observed for the dykes.

Well Name	Depths of igneous rocks	Dating Method	Age	Description and Interpretation of igneous rocks
Bjarni H-81	2255 m– TD	K-Ar	139 ±7 Ma for the lower core (2510 m) 122 ±6 Ma for the upper core (2260 m)	Basalts interspersed with sandstones and silty clays, with no pyroclastic rocks. Bjarni H-81 is the type section of the Alexis Formation.
Leif M-48	1839 m – TD	K-Ar	104 ±5 Ma to 131 ±6 Ma.	The Leif Basalts are deemed to be coeval and lithologically similar to those in Bjarni H-81, and thus can be considered part of the Alexis Formation.
Indian Harbour M-52	3250 – 3484 m	K-Ar	90 ±4 Ma for rock fragments (exact stratigraphic position unknown).	The recovered rock samples are lapilli tuff deposits. The volcanic rocks in this well are noted as being lithologically very different from occurrences of the Alexis Formation elsewhere on the Labrador shelf. The lithological difference along with the younger age suggests that these rocks may not part of the Alexis Formation.
Herjolf M-92	3751 m – 4048 m	K-Ar	The top of the volcanic section has been dated as 122 ±2 Ma, whereas the bottom is dated as 314 ±12 Ma. This bottom section is severely altered and thus the age is likely to be unreliable.	Subaerial weathered basalt flows overlying Precambrian basement. Lithologically similar to the igneous rocks in Bjarni H-81, and thus can be considered part of the Alexis Formation.
Roberval K-92	3188 m – 3544 m	N/a	Undated	This is the thickest recorded section of the Alexis Formation (Ainsworth et al., 2014).
Rut H-11	'Tuff' top at 4432 m and 'Diabase intrusive' 4451 m C-NLOPB (2007).	N/a	Undated	Igneous rocks are noted twice in the C-NLOPB (2007) report: "Tuff" top at 4432 m and "Diabase intrusive" 4451m.
*Snorri J-90	3150 m – 3061 m (Umpleby, 1979)	Palynology	Valanginian to Barremin	A series of greywackes, sands, silts and coal beds interpreted to be derived from volcanic rocks which may be coeval with the Alexis Formation but should not be referred to as part of the Alexis Formation (McWhae et al., 1980).

Table 4.3

*Summary of occurrences of volcanic rocks in offshore wells on the Labrador Shelf well depths are from C-NLOPB (2007), whilst all other data and information is from Umpleby (1979) and references therein, unless otherwise stated. * indicates the presence of sediments potentially derived from igneous rocks.*

At three of the Tappe et al. (2007) sample locations (ST100, ST102, and ST245; Fig. 4.3) we were unable to locate the in situ dykes reported by them. Descriptions including mineralogy, texture, and orientation of all the samples are available in the supplemental data (Appendix).

4.3.1 Sample locations, field relationships, and structural analysis

4.3.1.1 Makkovik Peninsula

The three samples with the prefix AP1 represent the three dykes found on the peninsula north of the town of Makkovik (Fig. 4.3), locally referred to as the Hill. The outcrops from which these samples were obtained are on the southern end of a beach (Fig. 4.4) that marks the intersection between a large linear gully that extends 1 km inland on a bearing of 198°, and the western coast of the peninsula. The dykes that provided samples AP1-S1 and AP1-S2 are well exposed, but the dyke from which AP1-S3 was collected is only fully exposed during low tide.

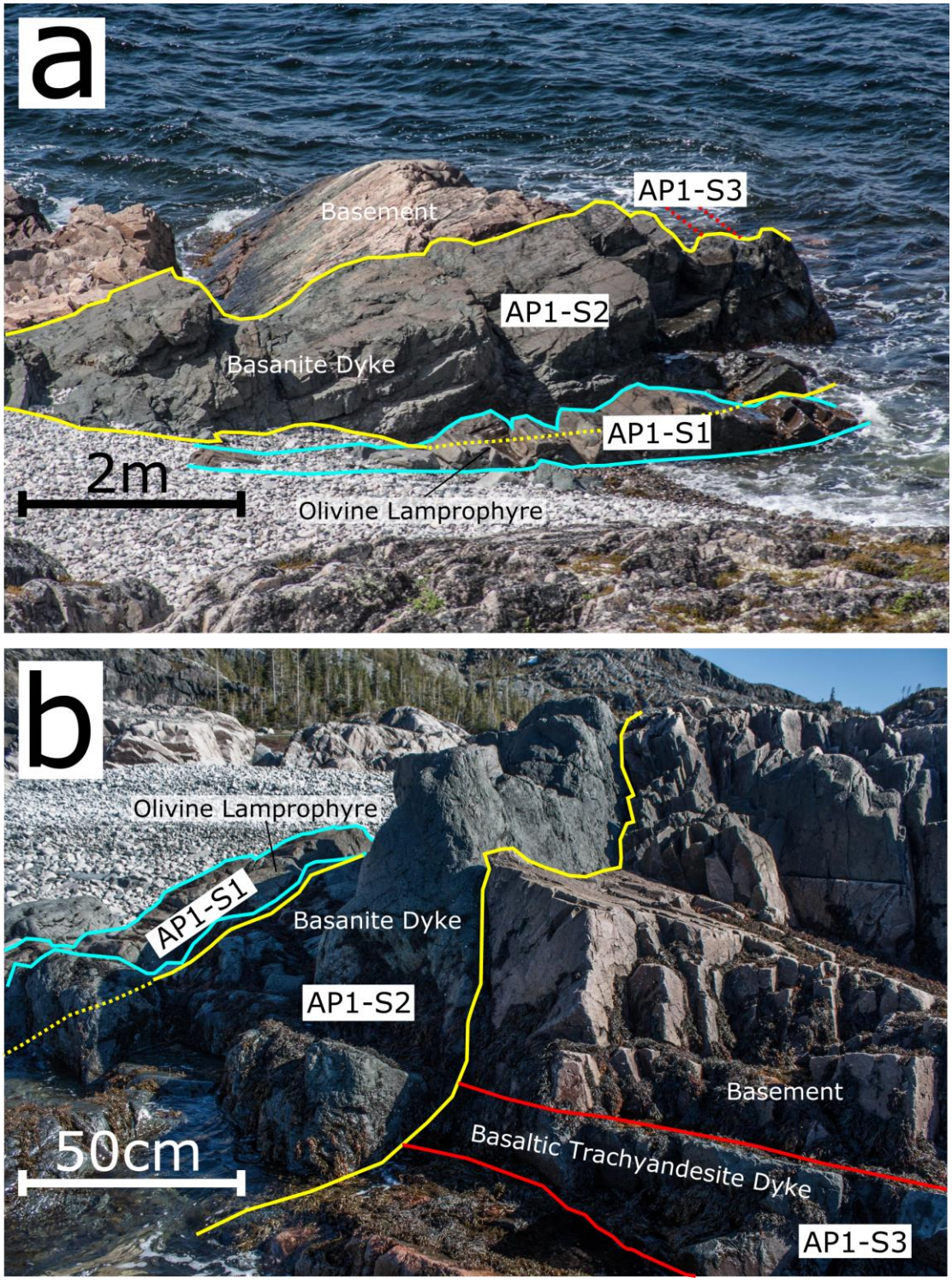

Figure 4.4

A) Looking west onto the location AP1 in which three dyke samples were analysed during the study (AP1-S1, AP1-S2, AP1-S3). B) Looking southeast.

AP1-S1 and AP1-S2 were collected from two different parallel dykes in an approximately north-south orientation (Fig. 4.4), and are ~1 m and ~2 m thick, respectively. The dyke that provided sample AP1-S3 is oriented approximately east-west and is much smaller than the north-south dykes, being only ~30 cm wide. The dyke from which AP1-S3 was obtained is crosscut by the dyke from which AP1-S2 was obtained. The age relationship between AP1-S1 and AP1-S2 could not be determined from field relationships.

4.3.1.2 Ford's Bight

Ford's Bight is the elongate bay between Ford's Bight Point and Cape Strawberry, where three of the nine occurrences of Early Cretaceous magmatism reported by Tappe et al. (2007) are located (Fig. 4.3). Samples in this study with the prefix AP2 were collected at the Tappe et al. (2007) location ST103 on the eastern side of Ford's Bight (Figs. 4.3 and 4.5A), with the exception of AP2-S6, which was collected 45 m away from AP2 on a bearing of 025° (Fig. 4.5B). At the location of AP2 (Fig. 4.5B), a poorly exposed outcrop within the intertidal range (Figs. 5C, 5D) contained two dykes (sites of samples AP2-S1 and AP2-S2), within a diatreme breccia (samples AP2-S5 and AP2-S6) in proximity to exposed metamorphosed basement (samples AP2-S3 and AP2-S4) (Fig. 4.5C). An overview of the spatial relationship between the lithologies at AP2 is provided in Figures 4.5B and 4.5C. Although we visited sites ST100, ST102, and ST103 (Fig. 4.5A) during our field study, no in situ outcrop was found at ST100 and ST102; however, small boulders, as wide as 1 m, of the breccia material similar to that observed in samples AP2-S5 and AP2-S6 were observed at these locations.

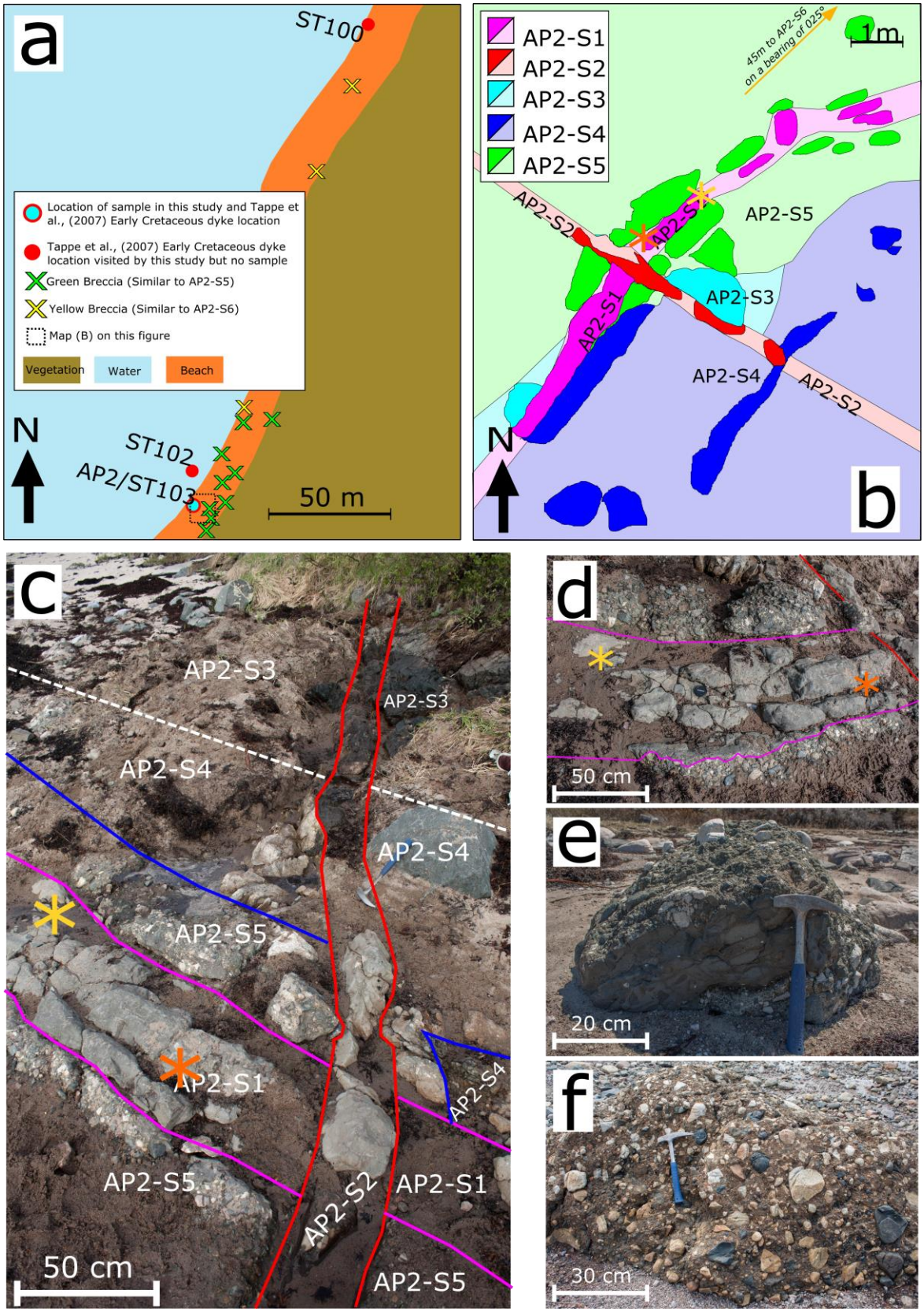
a
ST100
Location of sample in this study and Tappe et al., (2007) Early Cretaceous dyke location
Tappe et al., (2007) Early Cretaceous dyke location visited by this study but no sample
Green Breccia (Similar to AP2-S5)
Yellow Breccia (Similar to AP2-S6)
Map (B) on this figure
Vegetation
Water
Beach
N
ST102
AP2/ST103
50 m
b
AP2-S1
AP2-S2
AP2-S3
AP2-S4
AP2-S5
45m to AP2-S6 on a bearing of 025°
1m
N
c
AP2-S3
AP2-S4
AP2-S5
AP2-S1
AP2-S2
50 cm
d
50 cm
e
20 cm
f
30 cm

Figure 4.5

A) An overview of occurrences of diatreme breccia in Ford's Bight along with the locations of samples collected during this study and Tappe et al. (2007). For the location of the samples on this inset within Ford's Bight, see Figure 4.3. Differentiation is made between a green diatreme breccia that resembles AP2-S5 (green cross) and one that is more yellow in colour, similar to AP2-S6 (yellow cross). Many of the occurrences shown are not in situ. B) The spatial relationship between the different lithologies described at AP2. C) Looking southeast onto the two small (<50 cm) crosscutting melilitite dykes (samples AP2-S1 and AP2-S2) within the Ford's Bight diatreme. D) The contact between dyke 1 (sample AP1-S1) and the surrounding diatreme breccia (sample AP2-S5) looking toward the south. E) Boulder on the beach in Ford's Bight looking west comprising green diatreme breccia (similar to AP2-S5) but with an exceptionally large inclusion of mafic igneous material. (F) Possible in situ outcrop similar to sample AP2-S6 in Ford's Bight looking west. In C and D, purple and red outlines are used to denote the contacts of the dykes from which the samples AP2-S1 and AP2-S2, respectively, were obtained with the breccia and the metamorphosed basement. The blue line in C and D is the contact between the breccia and the basement, whereas the dashed white line represents the boundary between the quartzite basement and an amphibolite dyke also forming part of the basement. The orange and yellow stars in B, C, and D are located at the same point for reference between these subfigures.

The dyke from which sample AP2-S1 (Fig. 4.5) was collected (dyke 1) is oriented approximately north-south, whereas the dyke from which sample AP2-S2 was obtained (dyke 2) is oriented approximately east-west. Both dykes vary in thickness along their observable length; dyke 1 varies in thickness from 25 to 40 cm and dyke 2 varies from 20 to 30 cm. At the AP2 location it was observed that dyke 2 crosscuts dyke 1, and thus the east-west–oriented dyke 2 is younger.

4.3.1.3 Cape Strawberry

Cape Strawberry is a large headland between Ford's Bight and Big Bight to the northeast of Makkovik. Tappe et al. (2007) described Early Cretaceous magmatism on Cape

Strawberry at two locations (ST254 and ST253; Fig. 4.3). We collected sample AP3-S1 in proximity to ST253 (Fig. 4.6). ST254 is the location of the only sample in the Early Cretaceous suite that was been dated by $^{40}Ar/^{39}Ar$ methods (141.6 ± 1.0 Ma) by Tappe et al. (2007), and it is also the only location situated inland (Fig. 4.3). While it is an area of relatively good exposure (Fig. 4.7) of the 1720 Ma Cape Strawberry Granite (Hinchey, 2013), no nephelinite dykes were observed at this location or anywhere in the vicinity. Thus we were unable to establish field relationships or acquire an equivalent sample for further analysis.

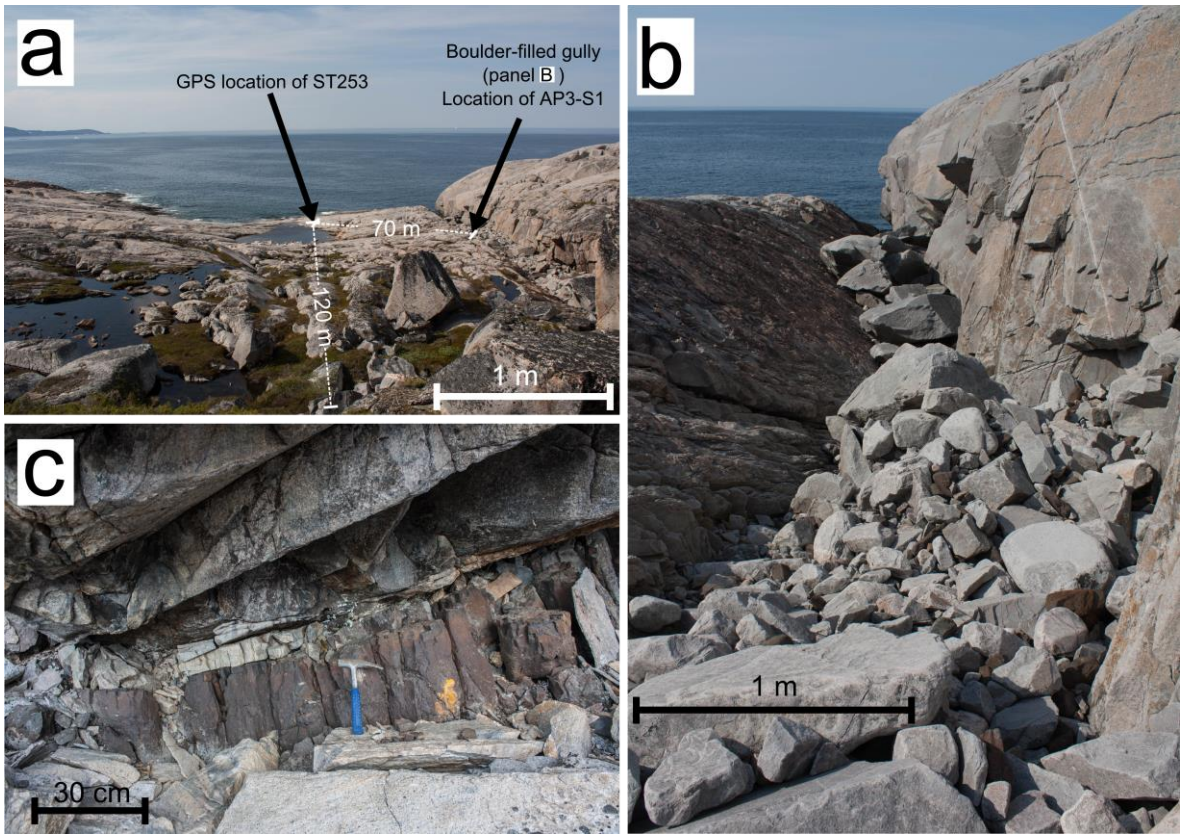

Figure 4.6

A) An overview looking north of the area surrounding the global positioning system (GPS) location of ST253 in Tappe et al. (2007) taken from the location of the in situ dyke shown in C. B) Looking north onto out of situ boulders in the gully 70 m away from ST253. Two rock types of boulders were present in this gully: 1) granite and 2) olivine clinopyroxenite. Our sample AP3-S1 is olivine clinopyroxenite. C) A relatively good

exposure of in situ dyke 120 m away on a bearing of 170° from AP2-ST253, which may have been part of the dyke contributing to the boulders in the gully.

Figure.4.7

Looking northwest from the location of sample ST254. A good exposure of the Cape Strawberry Granite was observed at ST254, but no nephelinite dykes were observed at this location. This is the location of the only sample 40Ar/39Ar dated by Tappe et al. (2007), to which the rest of the Early Cretaceous nephelinite suite is tied.

4.3.1.4 Ikey's Point

Ikey's Point is located on the southeastern side of the large peninsula north of Makkovik (Fig. 4.3). Two dyke samples were collected from the area north of Ikey's Point, at the site of previously reported Mesozoic magmatism, and are denoted with the prefix AP4 (Fig. 4.8). Sample AP4-S1 was collected ~15 m south of ST245, and sample AP4-S2 was collected on a separate dyke a further 5 m south of AP4-S1.

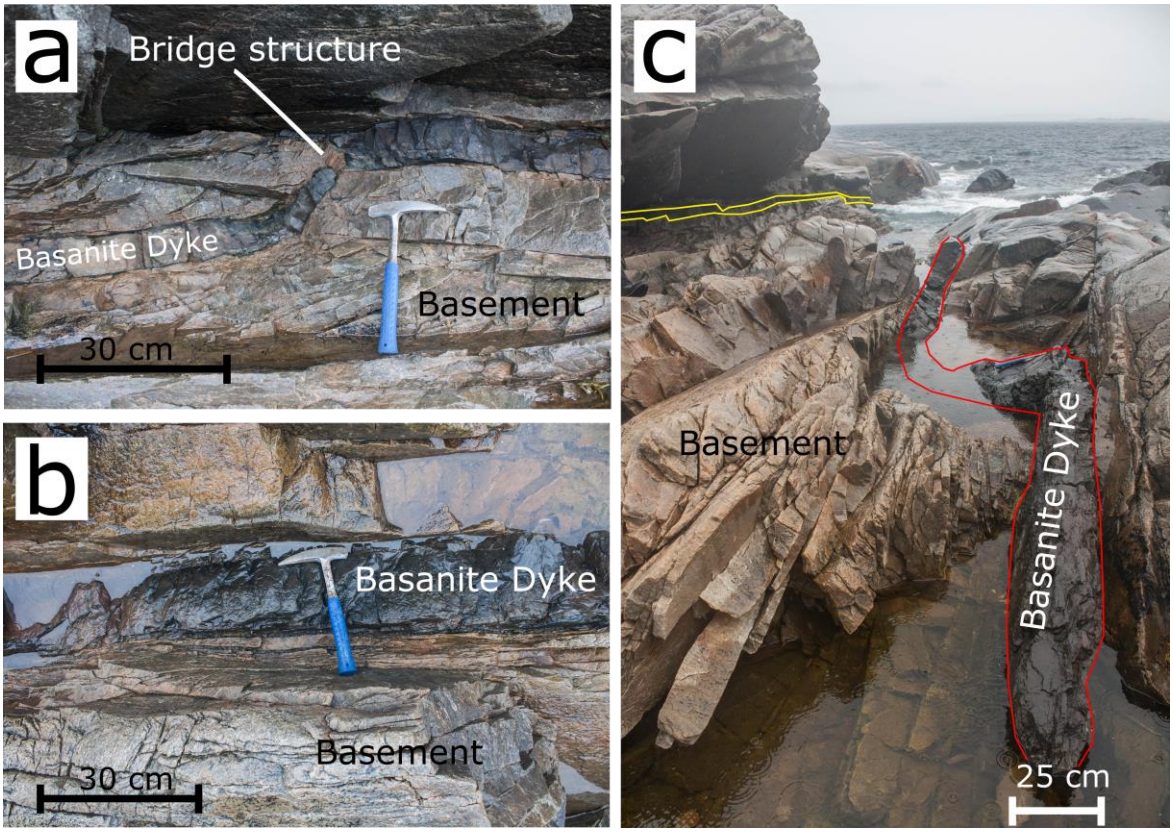

Figure 4.8

A) Looking north toward a bridge structure in a small dyke (sample AP4-S1) observed 15 m south of the global positioning system location of ST245. B) 17 m away from ST245 looking down (north up) onto the other dyke observed at this location (sample AP4-S2). C) Looking east onto location AP4 depicting dykes from which samples AP4-S1 (yellow outline) and AP4-S2 (red outline) were obtained. The dyke from which sample AP4-S2 was obtained also contains a bridge structure.

Samples AP4-S1 and AP4-S2 are both oriented approximately east-west and display multiple bridge structures (Fig. 4.8C). The dykes are <13 cm and 25 cm thick for AP4-S1 and AP4-S2, respectively. No crosscutting relationships were observed between AP4-S1 and AP4-S2, thus relative ages could not be determined for the AP4 dykes.

4.3.2 Structural Analysis

An overview of the orientations of the dykes sampled during this study is provided in Figure 4.9. AP3-S1 is not included in Figure 4.9 because this sample was obtained from a boulder (Fig. 4.6B). Figure 4.9A demonstrates that the dykes sampled by this study do not appear to be part of a singular, systematic dyke swarm. Figure 4.9B demonstrates that none of the dykes analysed during our study at locations where Mesozoic magmatism has been documented previously are margin parallel, i.e., striking 130°–150°. Margin-parallel orientations might be the predominant trend expected for dykes intruded during rifting, unless a stress reorientation occurred at the rift margin (e.g. Philippon et al., 2015).

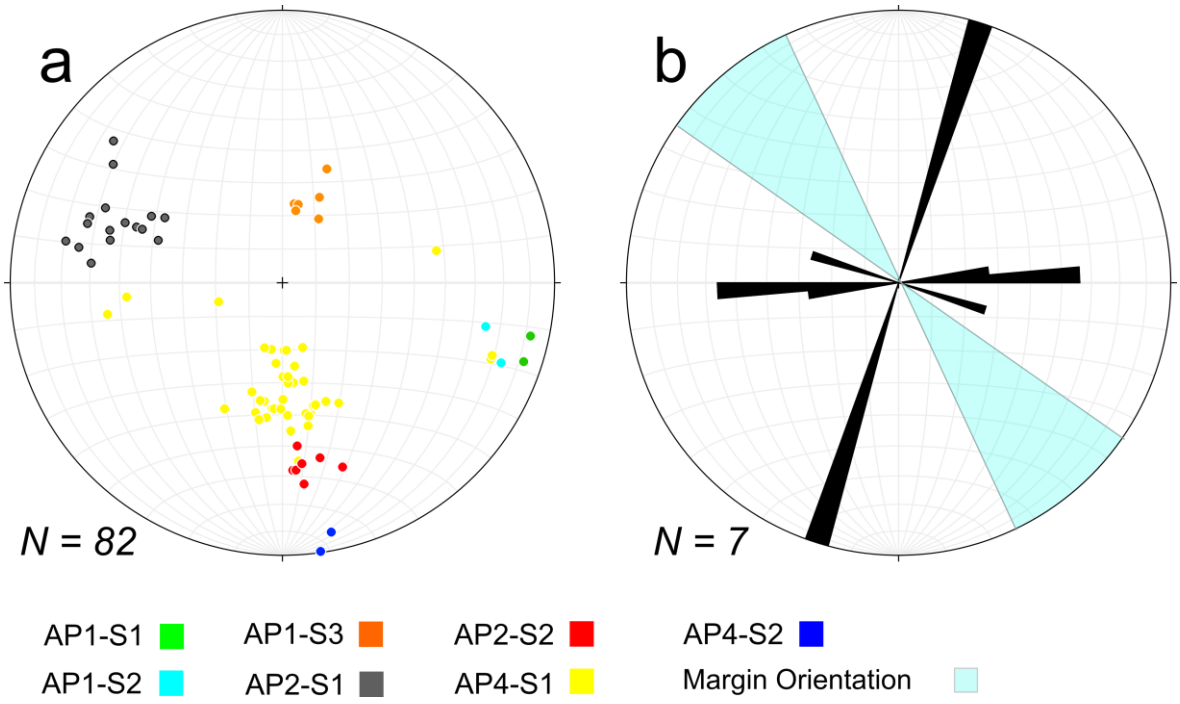

Figure 4.9

A) Stereonet of poles to planes for the dyke contacts at the sample localities. B) Rose diagram using 5° bins of the dyke contacts using the mean value of each dyke contact data set plotted alongside the margin orientation (130° and 150°) derived using the modern coastline on satellite imagery.

4.3.3 Lithological descriptions and XRF analysis

In the following lithologies are described and the results of XRF analysis on the samples obtained by this study are presented. Thin sections in both plane and cross-polarised light are presented in Figure 4.10; full descriptions to complement those given in this section are provided in the Appendix.

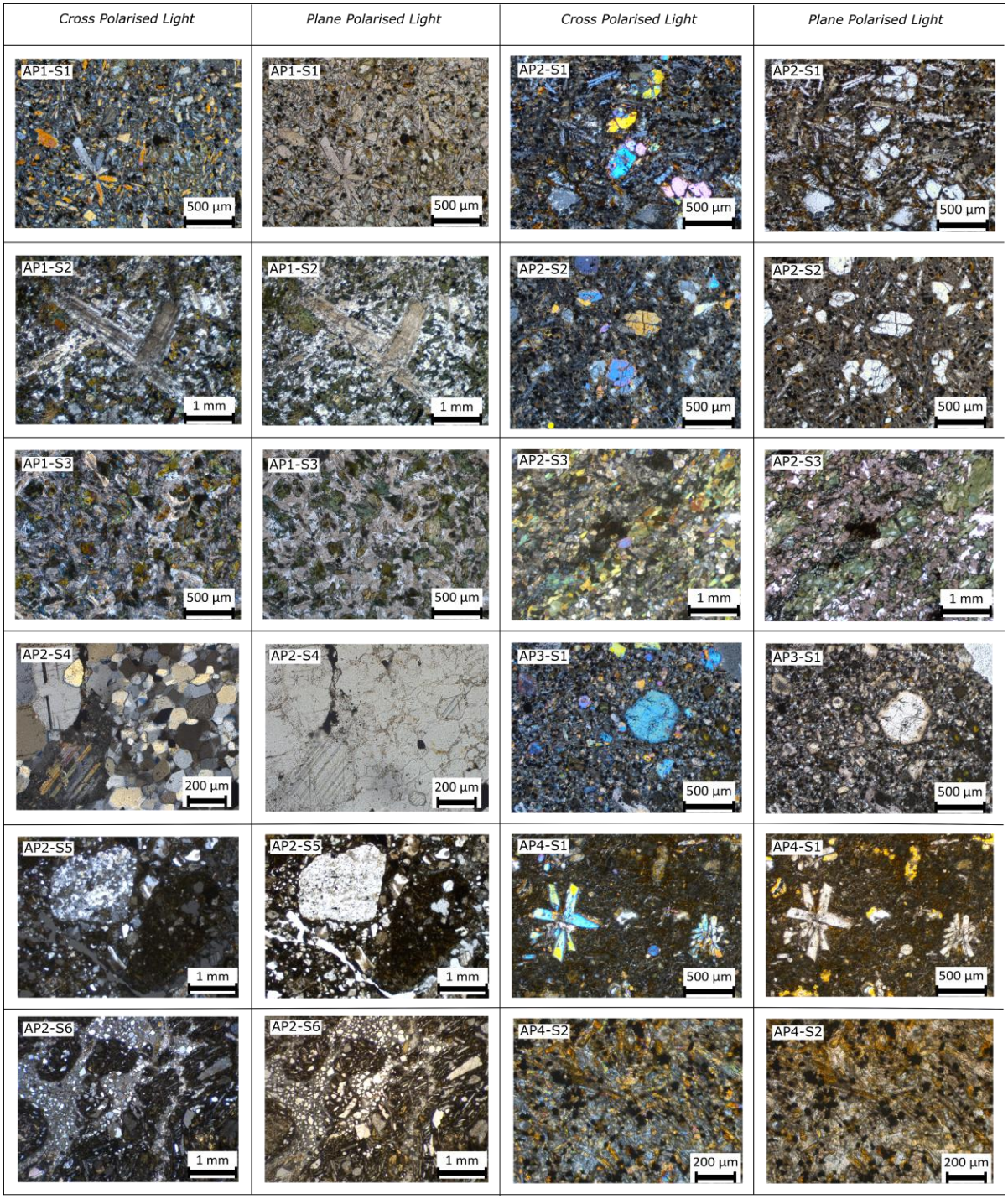

Figure 4.10

Thin section micrographs in both plane and cross-polarised light for all the 1004 samples described herein.

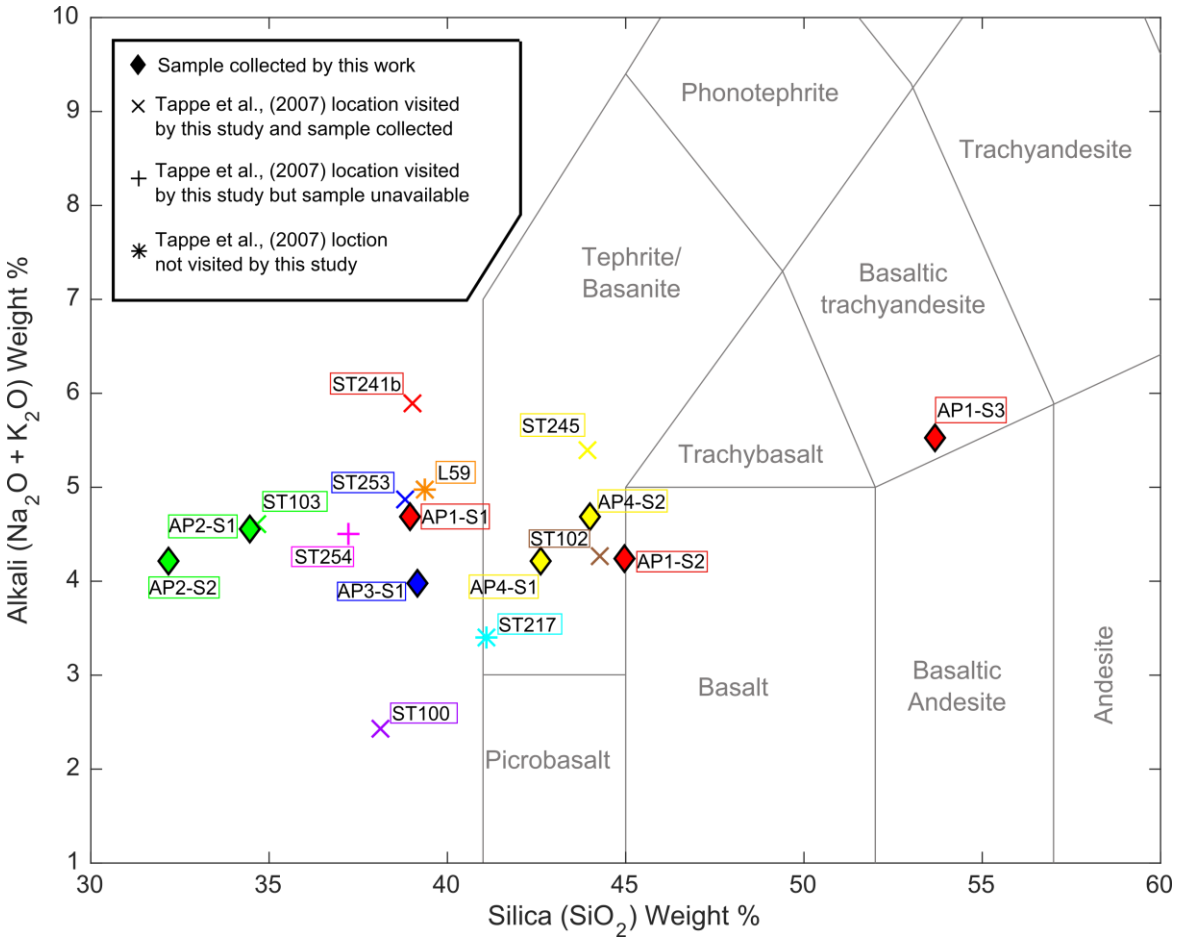

Figure 4.11

Total alkalies versus silica plot (Le Bas et al., 1986) depicting the dyke samples collected and analysed by this study along with the Early Cretaceous nephelinite suite of Tappe et al. (2007). Samples of the same colour represent the same location.

	AP1-S1	AP1-S2	AP1-S3	AP2-S1	AP2-S2	AP3-S1	AP4-S1	AP4-S2
SiO_2	38.93	44.96	53.66	34.43	32.17	39.19	42.62	43.98
TiO_2	2.63	3.31	0.74	2.10	2.15	2.44	1.92	1.90
Al_2O_3	12.93	13.42	17.15	10.79	10.18	12.34	14.33	14.68
Fe_2O_3	13.77	16.91	9.45	11.43	12.04	12.43	12.03	11.87
MnO	0.23	0.33	0.21	0.23	0.24	0.21	0.21	0.18
MgO	8.09	5.36	4.85	10.66	10.96	9.07	6.93	8.45
CaO	11.25	6.94	5.97	16.00	14.52	13.55	10.19	9.99
Na_2O	2.78	3.25	3.14	2.00	2.22	2.26	2.67	2.93
K_2O	1.91	1.00	2.39	2.57	1.99	1.73	1.54	1.75
P_2O_5	1.02	1.86	0.18	2.31	2.58	0.86	0.65	0.66
SO3	0.33	0.01	<0.002	0.82	1.04	0.20	0.15	0.16
CrO3	0.02	0.00	<0.001	0.02	0.02	0.04	0.03	0.03
NiO	0.01	0.00	0.00	0.02	0.02	0.02	0.02	0.02
LOI	5.61	2.27	1.88	5.29	8.40	5.18	6.15	2.73
Total	99.51	99.63	99.62	98.67	98.52	99.51	99.44	99.34

Table 4.4

The results of X-ray fluorescence (XRF) analysis for major element oxides in the dyke samples collected during this study.

4.3.3.1 Makkovik Peninsula

The grey dyke from which sample AP1-S1 was obtained has an extremely fine-grained groundmass that surrounds a main phenocryst phase of clinopyroxene (60%), which is generally arranged into star-shaped clusters of two or more crystals. Highly altered olivine (15%) is also present, along with apatite (<5%), amphibole (<5%), and biotite (<5%). Some vesicles infilled with calcite were as much as 6 mm wide, but most were ~2 mm wide. There is no observable metamorphic mineral fabric in AP1-S1. The SiO2 content of sample AP1-S1 is too low to use the total alkalies versus silica (TAS) classification (Le Bas et al., 1986), but it can be classified as a lamprophyre (Woolley et al., 1996; Rock,

1986) due to the mineral assemblage and composition. Lamprophyre dykes are well studied and known to be extensive in the area (Foley, 1989).

Sample AP1-S2 was collected from a dark green dyke. The most abundant mineral phase is chlorite (50%), which occurs as clusters of multiple crystals in the groundmass. This sample also contains altered plagioclase (30%), amphibole (10%), and apatite (<2%). No metamorphic mineral fabric was observed in sample AP1-S2. Sample AP1-S2 was classified as a basanite according to the TAS classification (Le Bas et al., 1986).

The dyke from which sample AP1-S3 was obtained has a red-brown weathered surface and a blue-grey clean surface. The most abundant mineral phase in AP1-S3 is plagioclase (60%) occurring as highly altered interlocking crystals. Chlorite (25%) is the next most abundant mineral phase and occurs as both individual crystals and clusters. Other minerals present with abundances <5% in sample AP1-S3 include: amphibole, titanite, apatite, and pyrite. As with the other two samples collected at AP1, no mineral fabric is present in AP1-S3. Sample AP1-S3 was classified as a basaltic trachyandesite according to the TAS classification (Le Bas et al., 1986).

In addition to the different mineral assemblages, all the samples analysed from the AP1 location have notably different compositions according to the XRF data (Table 4.4) with the alkali (Na2O + K2O) content of the AP1 samples not being as variable as the SiO2 content (Fig. 4.11). The XRF data from the Makkovik Peninsula shows that SiO2 content is lowest in AP1-S1 and highest in AP1-S3, which is the most felsic of all the samples analysed. The sample with the composition most similar to the data collected by Tappe et al. (2007) is AP1-S1. In summary, the AP1 samples (AP1-S1, AP1-S2 and AP1-S3) have been classified as olivine lamprophyre, basanite, and basaltic trachyandesite, respectively.

Of particular note however, was the absence of the mineral phase nepheline in all the samples collected at this location.

4.3.3.2 Ford's Bight

Samples AP2-S1 and AP2-S2 were obtained from two separate dykes but are virtually indistinguishable from one another in thin section (Fig. 4.10), both texturally and mineralogically. The main mineral phases in both AP2-S1 and AP2-S2 are melilitite (70%) and olivine (20%), resulting in our classification of these dykes as olivine melilitite according to the classification of Woolley et al. (1996). Olivine melilitite is the expected composition at this location according to previous work by Tappe et al. (2007). No metamorphic mineral fabric was observed in either AP2-S1 or AP2-S2.

The XRF major element analysis of AP2-S1 and AP2-S2 demonstrates that these samples have very similar compositions (Fig. 4.11; Table 4.4). There are, however, several small, but notable compositional differences between these two dykes in that sample AP2-S1 has slightly higher SiO2 and total alkali values than sample AP2-S2 (Fig. 4.11). Comparison of the major element XRF data obtained from our AP2 dyke samples (AP2-S1 and AP2-S2) with the major element composition of sample ST103 (Fig. 4.11) obtained by Tappe et al. (2007) demonstrates that all three of these samples have very similar compositions and may represent samples collected from the same dyke.

The two types of metamorphosed basement observed at the AP2 sample sites are an amphibolite (sample AP2-S3) and quartzite (sample AP2-S4) (Figs. 4.5B, 4.5C). Sample AP2-S3 contains amphibole (45%), highly altered plagioclase (35%), epidote (10%), and chlorite (10%). Sample AP2-S4 contains quartz (80%), garnet (7%), calcite (7%), plagioclase (4%), and opaque minerals (2%). Both samples AP2-S3 and AP2-S4 display a distinct metamorphic mineral fabric (Appendix). The exposure of these lithologies is

limited to a few square meters. However, both dykes (samples AP2-S1 and AP2-S2) were observed to continue into these metamorphosed units (Figs. 4.5B, 4.5C). The extent of the continuation of the younger dykes into the metamorphic basement could not be quantified due to lack of exposure.

The final lithology present at the AP2 sample site is a diatreme breccia that hosts the two dykes (samples AP2-S1 and AP2-S2). The diatreme breccia was observed as two distinct varieties, as characterised in samples AP2-S5 and AP2-S6. Sample AP2-S5 was taken from the breccia located at AP2 (Figs. 4.5C, 4.5D) but is also representative of the nearby boulders on the beach (Figs. 4.5A, 4.5E), whereas sample AP2-S6 was taken from a large boulder 45 m away from the rest of the AP2 samples on a bearing of 025° (Fig. 4.5E). AP2-S5 is green in outcrop, whereas AP2-S6 is dark yellow. This colour variation is a reflection of AP2-S5 having a higher ratio of clasts to matrix compared to AP2-S6. The clast types found in both the breccia samples are very similar, mostly consisting of highly variable amounts of quartzite basement, amphibolite dyke, olivine melilitite dyke, and fragments of individual crystals primarily including but not limited to quartz, olivine, microcline feldspar, and plagioclase. Most clasts are angular, except the melilitite inclusions, which are typically rounded with an undulose texture at their perimeters. Clast size in both AP2-S5 and AP2-S6 is extremely variable, ranging from <0.1 mm to >10 cm. The matrix in both the AP2-S5 and AP2-S6 samples is predominantly carbonate.

4.3.3.3 Cape Strawberry

The eastern tip of Cape Strawberry (AP3, Fig. 4.3) is an area of exceptionally well exposed basement rocks (Fig. 4.6A) that were not observed to be intruded by dykes of any type. However, a distinct gully (Fig. 4.6B) filled with two types of boulders (granite and a mafic igneous material) was noted. The mafic igneous material in this gully provided sample

AP3-S1. The boulder from which AP3-S1 was obtained has a red-brown weathered surface and a dark grey clean surface. In hand specimen, calcite-infilled vesicles (to 7 mm) and olivine phenocrysts are visible. The dominant mineral phases in this sample are olivine, both fresh (20%) and serpentinized (15%), along with clinopyroxene in the groundmass (25%) and as a larger crystal phase (15%). The SiO2 content of sample AP1-S1 is too low to use the TAS classification (Le Bas et al., 1986), but it can be classified as a lamprophyre (Woolley et al., 1996; Rock, 1986) due to the mineral assemblage and composition.

The XRF major element analysis of AP3-S1 (Fig. 4.11; Table 4.4) demonstrates that it is compositionally very similar to the igneous rocks sampled by Tappe et al. (2007) near this location, having a nearly identical SiO2 value but slightly lower alkali content. However, given that AP3-S1 does not contain the mineral phase nepheline, as expected the dyke from which AP3-S1 was collected does not belong to the nephelinite suite. The nearest in situ outcrop of the olivine lamprophyre composing the boulders in the gully was 120 m away from the location of ST253 (Fig. 4.6C).

4.3.3.4 North of Ikey's Point

In outcrop the weathered surface of the dyke from which sample AP4-S1 was obtained varies from dark grey through to reddish-brown. The dominant mineral phase in sample AP4-S1 is clinopyroxene, occurring in both the groundmass (40%) and as larger crystals (20%). Olivine also occurs in AP4-S1 as a serpentinized (10%) and unaltered variety (5%). Vesicles with a calcite infill are common in AP4-S1. The XRF data obtained from AP4-S1 (Fig. 4.11; Table 4.4) indicate that this sample is a basanite according to the TAS classification of Le Bas et al. (1986).

Sample AP4-S2 was obtained from a separate dyke 5 m south of the dyke from which sample AP4-S1 was collected (Fig. 4.8). This second dyke is slightly wider, 25 cm; in

outcrop it is brown and more fractured and weathered than the previous dyke. Sample AP4-S2 contains clinopyroxene (50%), plagioclase (20%), and olivine. Some minor opaque minerals are also present in AP4-S2 along with numerous calcite-infilled vesicles. AP4-S2 was classified as a basanite based on the major element composition derived using XRF and plotted on a TAS diagram (Fig. 4.11).

Although both AP4-S1 and AP4-S2 were classified as basanites, slight compositional differences between the two samples are apparent in the XRF major element data (Fig. 4.11; Table 4.4). These results show that AP4-S2 has a slightly higher SiO2 and alkali content than AP4-S1. Given this slight compositional variation between these two dykes, it is very likely that these two dykes represent the same magmatic event, particularly given the similar orientations (Fig. 4.9). Overall our observations and analysis of the data collected at the AP4 location in the area north of Ikey's Point indicate that Early Cretaceous magmatism north of Ikey's Point may comprise two small (13 and 25 cm wide) basanite dykes.

4.4 Bathymetry, sediment thickness and crustal structure

An analysis of the degree of symmetry displayed in the bathymetry, sediment thickness, and crustal structure of the conjugate margins of the Labrador Sea is presented here to complement the asymmetry shown in the magmatic distribution in the preceding discussion (Fig. 4.12). To assess the margin symmetry displayed in the NOAA total sediment thickness (Whittaker et al., 2013) data and the global bathymetry data set (Smith and Sandwell, 1997), profiles approximating the traces of seismic lines BGR77–17, BGR77–21, and BGR77–12 (Fig. 4.1A) were created (Fig. 4.12). These profiles were then extended along the same trajectory as their corresponding seismic line until they reached

the modern coastline, thus allowing us to study the full width of the continental shelf. Our observations of conjugate margin asymmetry are summarised in Table 4.5.

	Labrador	Southwest Greenland
Continental shelf width (Fig. 4.12a- b)	Wide (c. 150 km)	Narrow (c. 50 km)
Maximum offshore sedimentary cover (syn and post rift) (Fig. 4.12c-d)	c. 12,000 m	c. 3,700 m
Onshore intrusive magmatism	Minor nephelinite suite proposed by (Tappe *et al.*, 2007) but disputed by this study	Summarised in Table 4.2
Offshore magmatism	Alexis formation and other volcanics in offshore wells (Table 4.3)	Unknown due to absence of offshore wells, although SDRs are observed on seismic reflection data (Chalmers, 1997)
Crustal scale detachment faults	Possibly – Inferred by the presence of distinct basin (Welford and Hall, 2013)	No

Table 4.5

Summary of major structural and magmatic components of the Labrador and southwest Greenland Margins.

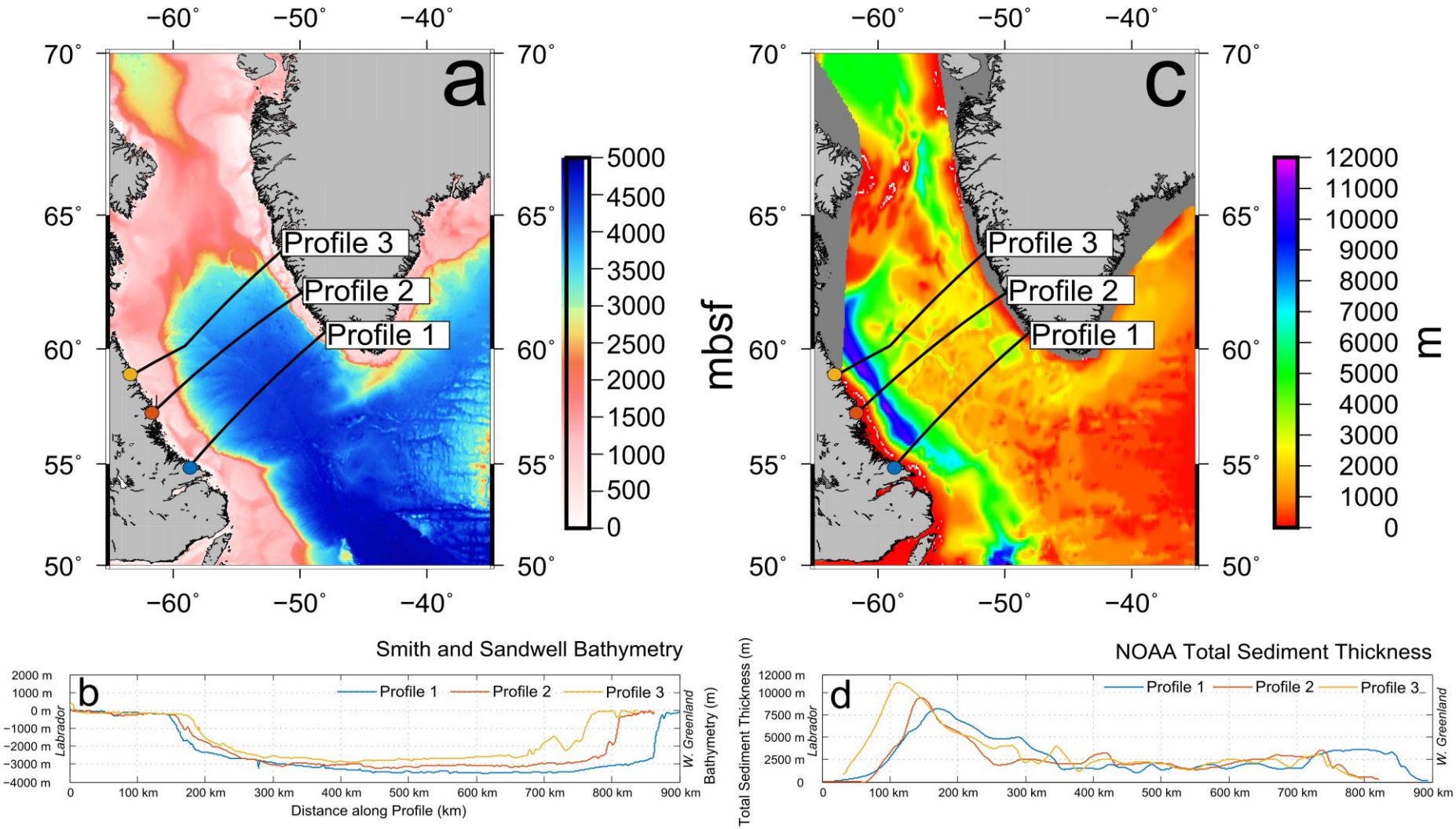
a
c
Profile 3
Profile 2
Profile 1
−60°
−50°
−40°
70°
65°
60°
55°
50°
5000
4500
4000
3500
3000
2500
2000
1500
1000
500
0
mbsf
12000
11000
10000
9000
8000
7000
6000
5000
4000
3000
2000
1000
0
m
Smith and Sandwell Bathymetry
b
2000 m
1000 m
0 m
−1000 m
−2000 m
−3000 m
−4000 m
Labrador
W. Greenland
Bathymetry (m)
0
100 km
200 km
300 km
400 km
500 km
600 km
700 km
800 km
900 km
Distance along Profile (km)
NOAA Total Sediment Thickness
d
Total Sediment Thickness (m)
12000 m
10000 m
7500 m
5000 m
2500 m
0

Figure 4.12

A) Bathymetry of the Labrador Sea from Smith and Sandwell (1997) data; mbsf—meters below seafloor. B) Bathymetric transects along profiles 1, 2, and 3. C) Total sedimentary thickness in the Labrador Sea from the National Oceanic and Atmospheric Administration world's oceans and marginal seas total sedimentary thickness (version 2; Whittaker et al., 2013). D) Total sedimentary thickness transects along profiles 1, 2, and 3. For C and D, the Labrador end of the transect is at the left (0 km) and the West Greenland end is on the right. Profiles 1, 2, and 3 approximately correspond to the seismic reflection lines BGR77–17, BGR77–21, and BGR77–12, respectively. The profiles used in this study have been extended along the same trajectory as their corresponding seismic line to the present coastline, thus allowing us to study the full width of the continental shelf.

Figure 4.12A displays the Smith and Sandwell (1997) global bathymetry data set for the Labrador Sea. The Labrador Sea has a maximum depth of ~3500 m, with water depths mostly <200 m on both continental shelves (Fig. 4.12B). The continental shelf is ~150 km wide offshore Labrador compared to southwest Greenland, where it is mostly <50 km wide. The profiles (Fig. 4.12B) show that the continental shelf remains relatively consistent in width along the southwest Greenland margin, whereas on the Labrador margin it increases to the north.

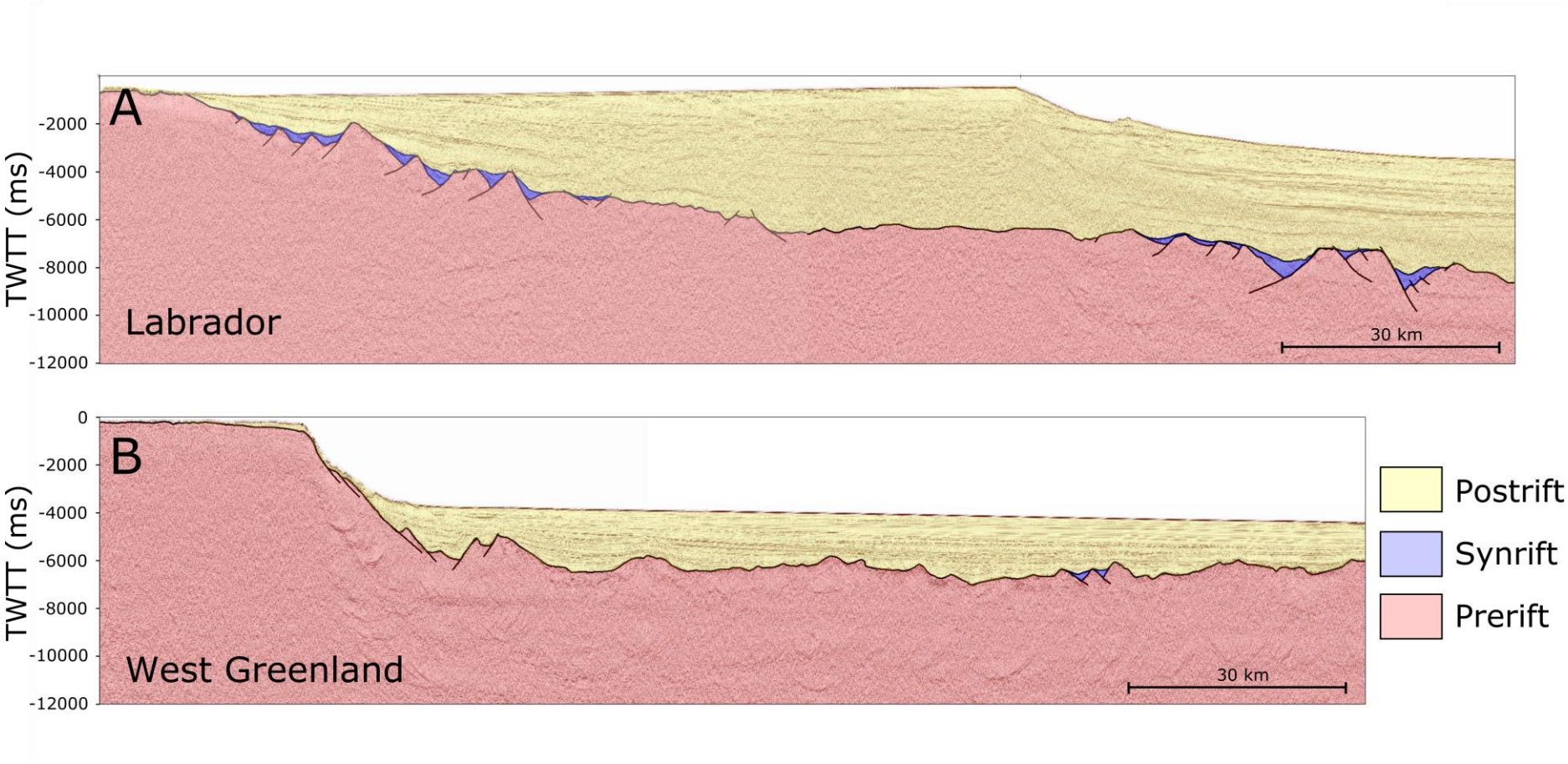

Figure 4.13A+B

Segments of the two-dimensional seismic reflection profiles 90-R1 and 90-R3 for the Labrador (A) and southwest Greenland (B) margins, respectively, with interpretations of the base postrift and base synrift. The location of

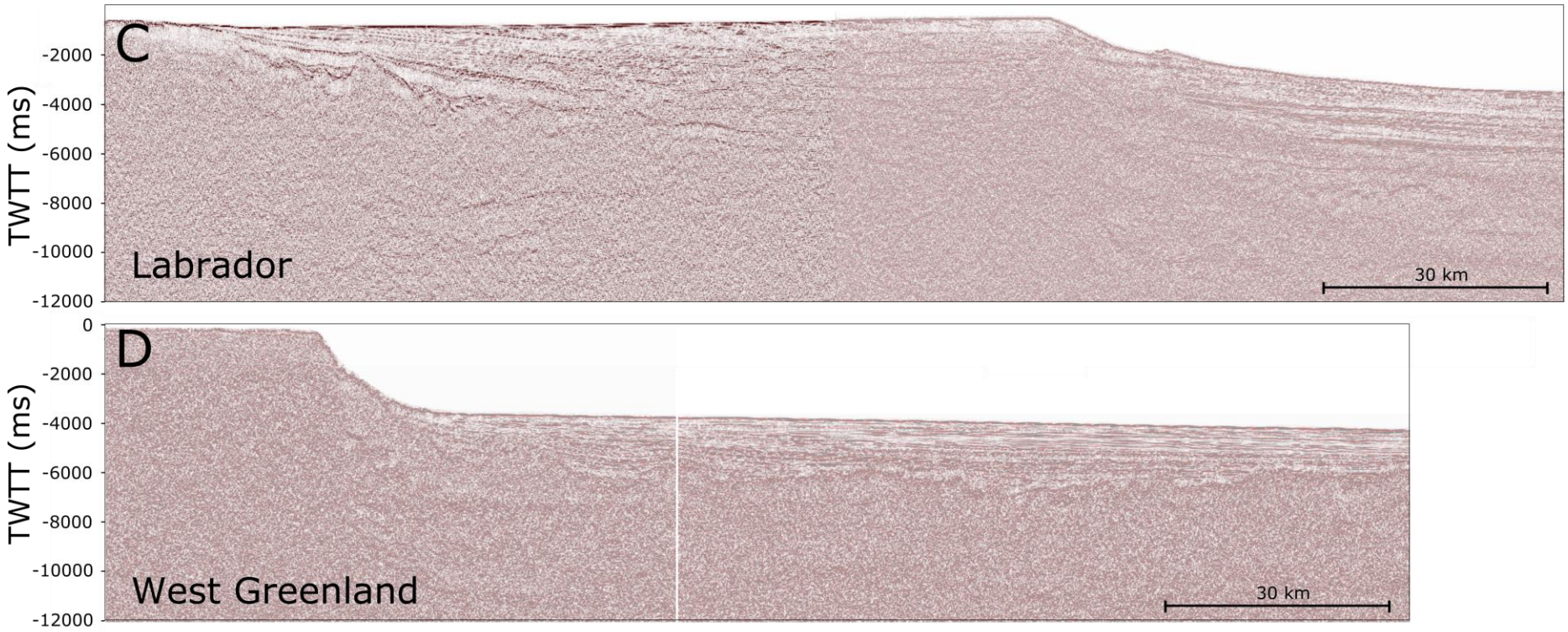

Figure 4.13A+B

Segments of the two-dimensional seismic reflection profiles 90-R1 and 90-R3 for the Labrador (C) and southwest Greenland (D) margins, respectively. The location of these segments is depicted in Figure 4.1.

The distribution of sediments between the margins of the Labrador Sea is highly asymmetric (Welford and Hall, 2013). The Labrador margin displays considerably thicker and more extensive synrift and postrift sedimentary sequences compared to the southwest Greenland margin (Figs. 4.12C, 4.12D, and 4.13). The Labrador margin is dominated by a large margin-parallel basin containing in excess of ~8000 m of sediments for much of its length (Fig. 4.12C). This basin is particularly prominent in the central and northern segments of the margin, where isolated areas contain more than ~11,000 m of sediment infill. Even outside this main basin it can be seen that for a large region extending from ~50 km to ~300 km offshore, a more diffuse area containing ~3000–6000 m of sediment infill is present. This region is much wider at the northern end of the margin compared to the south. In contrast, sediment infill on the southwest Greenland margin is significantly thinner and less spatially extensive than its Labrador conjugate. On the southwest Greenland margin sedimentary basins with thicknesses in excess of 4000 m are absent, with most areas containing <2000 m of sedimentary infill. Thus, comparison of sediment thickness along profiles 1, 2, and 3 (Fig. 4.12D) supports the observation of significantly more sediment deposition on the Labrador margin consistently along the length of the margin. It is interesting that the distance between the start of the profile (modern coastline) and the point of greatest sedimentary thickness appears to decrease from profile 1 in the south to profile 3 in the north. Profiles 1–3 in Figure 4.12D also demonstrate the differing basin geometry between these conjugate margins. On the Labrador margin the main margin-parallel basin appears to represent a distinct feature compared to the southwest Greenland margin where the sedimentary basins, if present, appear to have a less well defined, more diffuse appearance.

The crustal velocity model depicted in Chian, Louden, et al. (1995) that incorporates the data from Chian and Louden (1994) was used to assess asymmetry displayed in the crustal

structure between the Labrador and southwest Greenland margins (Fig. 4.14). Previously workers (e.g. Keen et al., 1994; Chian and Louden, 1994; Chian et al., 1995a) considered the velocity structure of both the southwest Greenland and Labrador margins to be divided into three distinct zones (Fig. 4.14).

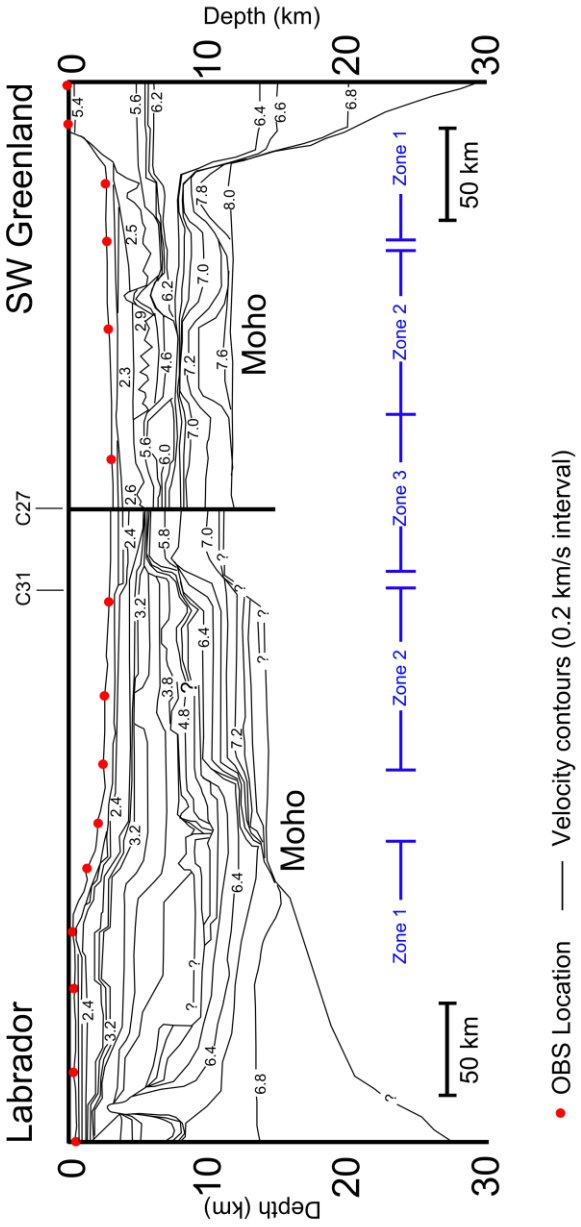

Figure 4.14

Velocity structure of the margins of the Labrador Sea reconstructed to polarity chron C27 (Danian) reproduced from Chian et al. (1995b). OBS—ocean bottom seismograph.

Zone 1 is characterised as a region that has a typical continental crustal velocity structure. On the Labrador margin zone 1 is ~140 km wide and is characterised by highly extended continental crust that has undergone considerable subsidence. However, on the southwest Greenland margin zone 1 is only ~70 km wide and has undergone considerably less subsidence (Chian, et al., 1995a). Zone 2 represents a region of transitional crust located oceanward of zone 1 on both margins (Chian, et al., 1995a). Compared to zone 1, zone 2 displays similar velocity characteristics, and is ~70–80 km wide on both margins. Zone 2 is characterised by a 5-km-thick region with a high velocity (6.4–7.7 km/s) overlain by a thin (<2 km) low-velocity region (4–5 km km/s). Zone 3 is characterised by typical oceanic crustal velocities and is oceanward of zone 2 on both margins.

4.5 Discussion

4.5.1 Comparison of the composition of the Makkovik magmatism with other rift-related magmatism

The XRF results obtained during this study have been compared to other selected occurrences of rift-related magmatism globally (Fig. 4.15). The Yarmony Mountain lavas of the Rio Grande Rift (Leat et al., 1990) were selected for comparison because they are interpreted to represent small-volume, early rift-related melts, and therefore may have been produced in a geological setting similar to that of the proposed Early Cretaceous magmatism near Makkovik (Tappe et al., 2007). The Suez Rift magmatism (Shallaly et al., 2013) was selected because it contains a wide array of rift-related manifestations of magmatism, including sills, dykes, and extrusives. Two magmatic suites attributed to the Central Atlantic Magmatic Province (CAMP) are also included for comparison: Algarve in southern Portugal (Martins et al., 2008) along with the magmatism in Guyana and Guinea

(Deckart et al., 2005). The CAMP magmatism was selected because it enables comparison with a widespread rift-related magmatic event that resulted in continental breakup.

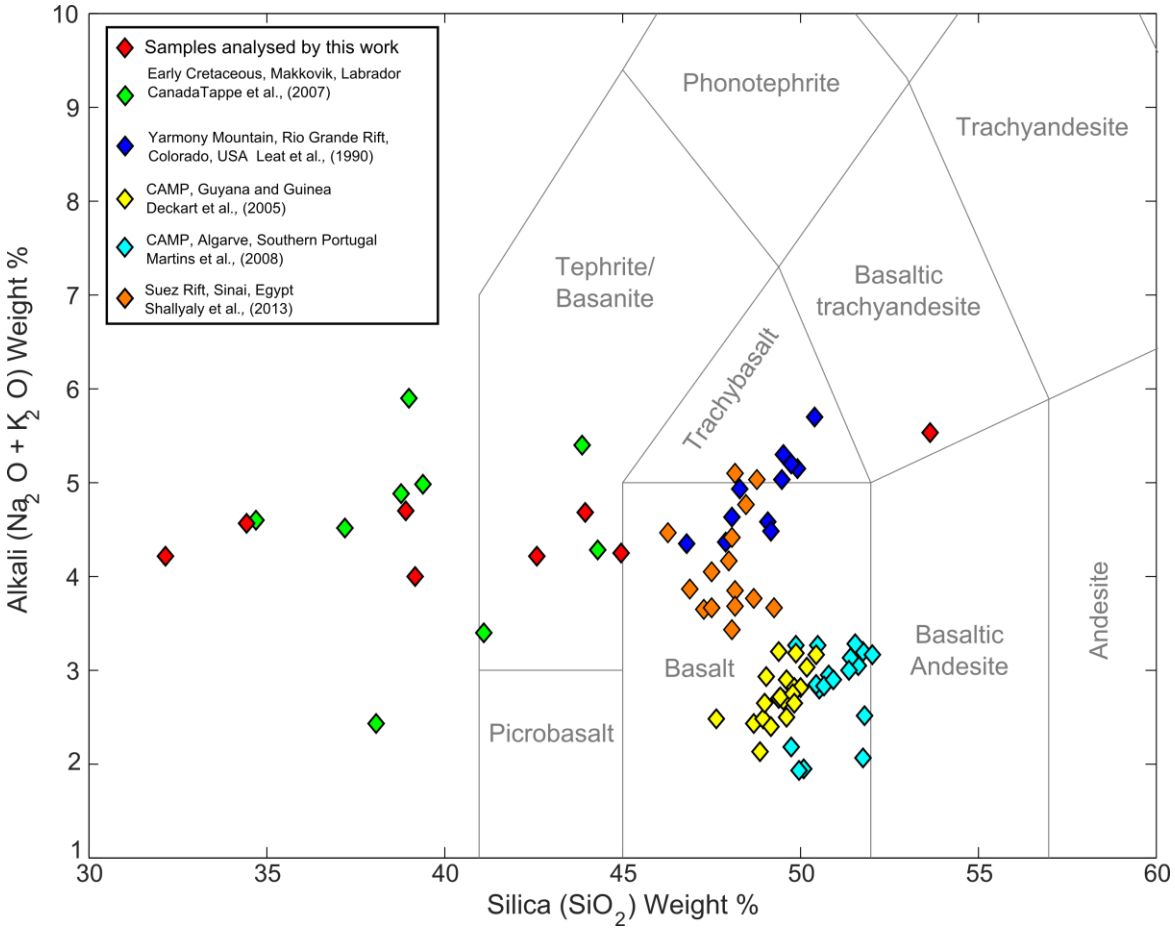

Figure 4.15

Total alkalies versus silica plot Le Bas et al. (1986) depicting the dyke samples collected and analysed by this study along with the Early Cretaceous magmatic suite near Makkovik Tappe et al. (2007)), the Rio Grande Rift, Yarmony Mountain lavas (Leat et al., 1990), the Suez Rift (Shallaly et al., 2013), and the Central Atlantic Magmatic Province (CAMP) in Algarve, southern Portugal (Martins et al., 2008) along with Guyana and Guinea (Deckart et al., 2005).

Comparing the composition of the Makkovik Early Cretaceous nephelinite suite (Tappe et al., 2007) with other selected occurrences of rift-related magmatism shows that it is compositionally more diverse than any of the other magmatic suites considered (Fig. 4.15), displaying greater variation in both the alkali and silica values than any of these systems.

Although it is extremely unlikely that all of the AP samples belong to the Early Cretaceous nephelinite suite (particularly sample AP1-S3), the more mafic AP samples depict a similar range of silica values to the Early Cretaceous nephelinite suite. The Tappe et al. (2007) samples show considerably higher variation in total alkali values than the AP samples or any of the other data sets included for comparison. The wide range of compositions found in the Early Cretaceous nephelinite suite (Tappe et al., 2007) may imply that not all of the dykes analysed by the previous work are part of the same event.

4.5.2 Extent of Mesozoic magmatism around Makkovik

Given the relatively close proximity of Makkovik to observations of Early Cretaceous magmatism in offshore wells (Fig. 4.1; Table 4.2), it would not be unreasonable to observe evidence of contemporaneous early rift-related magmatism cropping out onshore. Our field observations, however, indicate that the Early Cretaceous magmatism around Makkovik is volumetrically and spatially extremely minor compared to the numerous stages of extensive, readily observable intrusive magmatism that preceded it (e.g. Foley, 1989) and the well-documented magmatism on the conjugate southwest Greenland margin (Larsen et al., 2009). Although the field study area around Makkovik (Fig. 4.3) is significantly smaller than the extent of the dykes observed in southwest Greenland, no other evidence for Mesozoic magmatism has been recorded elsewhere onshore Labrador.

Of the seven sample locations in Tappe et al. (2007) visited during this study none provided clear, undisputable evidence for belonging to a contiguous Early Cretaceous magmatic event. We think it is also exceptionally unlikely that the outcrops were removed by subsequent erosion between this study and the work of Tappe et al. (2007). Our observations on the peninsula north of the town of Makkovik (AP1) and on Cape Strawberry (AP3) did not provide sufficient evidence for the Early Cretaceous magmatism

previously described at these locations. The most reliable evidence confirmed by this study for the magmatism characterised by Tappe et al. (2007) as Early Cretaceous was found in Ford's Bight (AP2, Fig. 4.5) and north of Ikey's Point (AP4, Fig. 4.8).

Our AP2 sample location in Ford's Bight is in very close proximity to the diatreme originally described as a sedimentary breccia by King and McMillan (1975) and later as a diatreme by Wilton et al. (2002). Our field observations concur with that of Wilton et al. (2002) that the AP2 sample location is part of the previously documented Ford's Bight diatreme. This confirms that of the nine samples stated as belonging to the Mesozoic dyke suite in Tappe et al. (2007) (Table 4.1), three are part of a diatreme, not a dyke swarm as previously claimed, with two of the Ford's Bight samples locations not containing in situ outcrop. Within the diatreme there are dykes present, but it is misleading to imply that they are part of a singular geographically widespread intrusive event that can be described as the nephelinite suite. The diatreme was mentioned in Tappe et al. (2007, p. 438) as "poorly described mafic dykes cutting a breccia bed"; however, it is not made clear that this area is either 1) the location of three of their samples or 2) a diatreme rather than a dyke swarm. Furthermore, confirming that ST103 is, as expected, an olivine melilitite demonstrates that there is unlikely to be a problem associated with the original acquisition or our use of the coordinates provided by Tappe et al. (2007) and the original characterisation of the mineralogy at ST103. The geological context of the dykes needs clarifying, because the observed dykes in Ford's Bight are intrinsically associated with the diatreme (Wilton et al., 2002) and do not appear to be associated with a regional-scale intrusive event such as that described in Tappe et al. (2007). However, if the biostratigraphic age provided by King and McMillan (1975) of 197–145 Ma is correct, then this is currently the most reliable evidence in the area for Mesozoic magmatism, with the fossils possibly being derived from the maar above the diatreme (White and Ross, 2011).

Our analysis also indicates that one of the dykes north of Ikey's Point at AP4 is likely to be that described and sampled by Tappe et al. (2007), the other basanite dyke at this location being part of the same event. However, even if one or both of the dykes at AP4 is the dyke analysed by Tappe et al. (2007), they are extremely small (13 cm and 25 cm wide) and localised.

Comparison of the XRF data with other suites of rift-related magmatism globally has demonstrated that the nephelinite suite (Tappe et al., 2007) is compositionally much more diverse than the other events considered (Fig. 4.15). This observation provides further evidence that the samples collected by Tappe et al. (2007) might not form part of the same magmatic event.

Overall, our comparison of the field relationships, orientation, mineralogy, and composition of the samples collected at the locations of the samples prefixed with AP2 and AP4, where some evidence for the Early Cretaceous magmatism described by Tappe et al. (2007) was found, suggests that there is no reason to attribute the exceptionally different style of magmatism at in Ford's Bight (AP2) and north of Ikey's Point (AP4) to the same event.

Furthermore, given that the one location in this dyke suite that was dated by $^{40}Ar/^{39}Ar$ methods by Tappe et al. (2007) (sample ST254) was found to not contain any exposed comparable dykes, the coherence of the proposed Early Cretaceous nephelinite suite as being as a result of a singular magmatic event should be reconsidered. In terms of the age of the nephelinite suite characterised by Tappe et al. (2007), the plateau age from the $^{40}Ar/^{39}Ar$ dating is not defined by a continuous outgassing plateau and the two segments used in each are considerably less than the 50% gas release generally accepted as the hallmark of a reliable step-heating age. Even when the two segments in Tappe et al. (2007)

are combined, it seems that the total gas fraction plateau used is only 52%, i.e., only just above 50%. In addition, the problem with the $^{40}Ar/^{39}Ar$ date of Tappe et al. (2007) is the fact that the inverse isochron age is well outside of error and the plateau age is far from the atmospheric value. Thus the $^{40}Ar/^{39}Ar$ age of 142 Ma for sample ST254 is of marginal reliability.

Another aspect of the Early Cretaceous magmatism on the Labrador margin that remains unclear is why the orientations of the dykes observed by Tappe et al. (2007) are described as predominantly east-west. If these dykes are rift related, then they would be expected to have been intruded under the influence of the extensional stress field parallel to the rift axis i.e., coast parallel as they are in southwest Greenland (Larsen et al., 2009). Although the only compositionally appropriate east-west dykes observed by this study were at Ikey's Point (AP4), should a larger suite exist with this orientation it would not be compatible with simple northeast-southwest–trending Mesozoic rifting, culminating in the opening of the Labrador Sea (Abdelmalak et al., 2012).

4.5.3 Implications for early rifting of the Labrador Sea region

The results of this study have demonstrated that considerable asymmetry exists in many aspects of the conjugate margins of the Labrador Sea, including the distribution of rift-related magmatic rocks, the bathymetric expression, the sediment distribution, and the crustal structure. These observations of asymmetry may support a simple shear mode of rifting (Fig. 4.16). Here we systematically evaluate our observations of asymmetry against the predictions of the Lister et al. (1986) simple shear model of passive margin formation that has been previously applied to explain the observed asymmetry in many conjugate margin pairs and rift systems including the Greenland-Norway conjugate margins (Torske and Prestvik, 1991) and the south Atlantic (Becker et al., 2016). Of particular importance when evaluating the simple shear model (Lister et al., 1986) is

whether the polarity of the different aspects of asymmetry all agree with the predictions of the model.

A full comparison of the extent of rift-related magmatism on the margins of the Labrador Sea is inhibited by the absence of well data offshore southwest Greenland (Fig. 4.1A). The nearest offshore well on the Greenland side of the Labrador Sea is Qulleq-1, which is much farther north in the Davis Strait (Fig. 4.1A), and is influenced more by transform margin tectonics rather than the rifted margin regime in the Labrador Sea (Wilson et al., 2006).

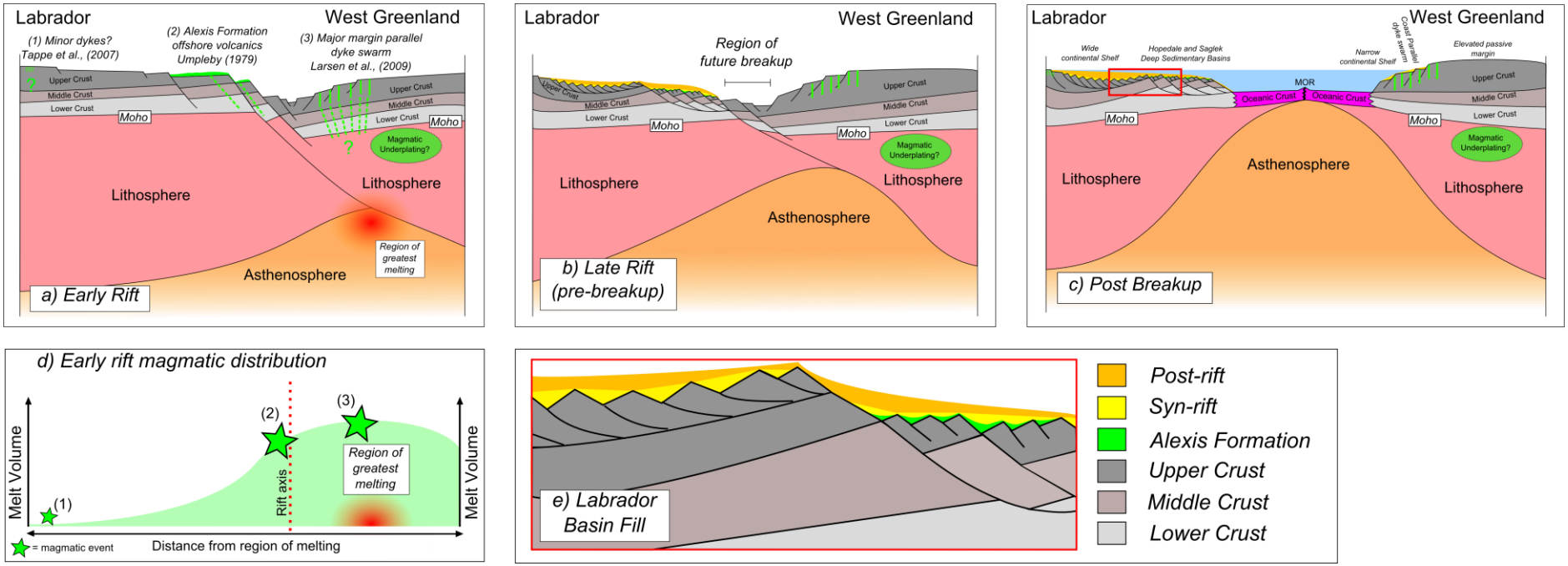

Figure 4.16

A) Conceptual model of early continental rifting prior to the opening of the Labrador Sea under a simple shear rifting regime. B) Conceptual model of late continental rifting. C) Schematic depiction of the post-breakup (present) architecture of the conjugate passive margins of the Labrador Sea showing the preserved architecture from the early simple shear rifting modified from Lister et al. (1986), including the wide and narrow continental shelves for the Labrador and Greenland margins, respectively, the deep sedimentary basins offshore Labrador, and the minimal offshore sedimentary cover and elevated passive margin on the Greenland side of the rift. D) The theoretical distribution of melt volumes against proximity to the rift axis where the region of melting is offset from the rift axis due to the simple shear–type early rifting. The three documented rift-related magmatic events included in green in A and D are: 1) Early Cretaceous nephelinite dykes near Makkovik (Tappe et al., 2007); 2) the offshore Labrador volcanics (Umpleby, 1979); and 3) the coast-parallel dykes onshore southwest Greenland (Larsen et al., 2009). E) Enlarged section off inset C in this figure showing the theoretical basin geometries on the upper plate Labrador margin.

Although the absence of well data offshore southwest Greenland prevents us from making a full comparison of the volume of rift-related magmatism, this study has shown that the Early Cretaceous magmatism identified onshore in Labrador by Tappe et al. (2007) is considerably less extensive than that observed on the coast parallel dykes onshore in southwest Greenland (Larsen et al., 2009). This allows us to state that there is an asymmetric distribution in the extent of the exposed onshore Mesozoic magmatism between the Labrador margin and the southwest Greenland margin. This asymmetric distribution of rift-related magmatism supports the predictions of the simple shear model of passive margin formation, whereby the center of the melt generation may have been offset from the central rift axis (Fig. 4.16A), resulting in a greater amount of melt on the upper plate southwest Greenland margin (Fig. 4.16A). That is, the greater extent of coast-parallel dykes in southwest Greenland suggests that the southwest Greenland margin may represent the upper plate margin in a simple shear system.

Magmatic underplating on the upper plate margin is another prediction of the Lister et al. (1986) simple shear model. High-velocity zones have been observed in seismic studies on these conjugate margins, but whether they represent serpentinized peridotite (Reid and Keen, 1990) or magmatic underplating (Keen et al., 1994) is debatable (Chian et al., 1995b). Chian et al. (1995b) determined that serpentinized peridotite is more consistent with the observations than magmatic underplating. Due to the inconclusive nature of these observations, we have chosen not to use them as evidence in our analysis of the applicability of the simple shear model (Lister et al., 1986) to the margins of the Labrador Sea. However, magmatic underplating might help to explain the absence of significant postrift sedimentary basins offshore southwest Greenland (Figs. 4.12C, 4.12D), as magmatic underplating could provide the additional buoyancy required to prevent significant postrift subsidence from occurring. Alternatively, the lack of postrift sedimentation offshore southwest Greenland could be due to a deficiency of sediment supply to the offshore basins; however, if this was the case we would still expect to observe deeper water depths.

Despite the obvious disparity in the extent of onshore rift-related intrusive magmatism between southwest Greenland and that near Makkovik, quantifying the melt volumes associated with rifting

on each margin even approximately is problematic for a number of reasons. First, offshore magmatism cannot be accurately quantified on both margins given the sparse seismic and well data coverage. Second, it is difficult to estimate the contributions of magmatic underplating and other intrusives in the lower crust; these contributions were estimated by White (1992) to potentially represent three times the volumes of other intrusive and extrusive magmatic rocks on passive margins. However, it seems more likely that significant magmatic underplating is present in southwest Greenland due to the potential additional support this margin has received.

A wider continental shelf on the lower plate margin is another prediction of the simple shear model of passive margin formation (Lister et al., 1986). The asymmetric nature of the bathymetric profiles across the Labrador Sea depicted in this study (Figs. 4.12A, 4.12B) using the Smith and Sandwell (1997) bathymetric data is consistent with a model in which the Labrador margin would be the lower plate margin.

An asymmetric distribution of sedimentation as described in this study is also a prediction of the simple shear model of passive margin formation (Lister et al., 1986), the greater amount of sedimentary deposition occurring on the lower plate margin. The NOAA total sediment thickness data show that the Labrador margin has considerably deeper sedimentary basins (Figs. 4.12C, 4.12D), and thus would represent the lower plate margin in a simple shear system.

Another aspect of the sediment distribution on the margins of the Labrador Sea that supports the simple shear model is the geometry of the marginal basins. In the marginal basin on the Labrador margin the total sediment thickness data profile depicts an abrupt increase in sediment thickness, as opposed to the southwest Greenland margin, where a much less apparent peak in sediment thickness is present. This abrupt increase in sediment thickness may imply a fault-controlled basin as opposed to the marginal basins offshore southwest Greenland, in which the NOAA data record more diffuse sedimentation.

The simple shear model implies a much greater degree of synrift structuring on the lower plate margin. Our analysis has demonstrated that the Labrador margin displays considerably greater

synrift deformation and sedimentation than the southwest Greenland margin. The more significant synrift deformation and sedimentation on the Labrador margin supports a simple shear–dominated mode of early rifting with Labrador being the lower plate margin.

Welford and Hall (2013) calculated sediment difference (excess and deficiency), also using the NOAA sediment thickness data for the Labrador Sea. The work of Welford and Hall (2013) showed that most of the Labrador Sea appears from isostatic calculations to be deficient in sediments, whereas the Hopedale Basin is near balanced and the Saglek Basin has an excess of sediments. Welford and Hall (2007) showed that high gradients in the sediment excess and deficiency could indicate the presence of steep listric faults, a key component of a simple shear–dominated rifting regime, supporting a simple shear model of margin formation in the Labrador Sea.

The velocity structure of the margins of the Labrador Sea (Fig. 4.14; Chian et al., 1995b) also displays asymmetry consistent with a simple shear–dominated phase of early rifting. This is evident in zone 1 (stretched continental crust, Fig. 4.14), where this region is ~140 km wide on the Labrador margin compared to the southwest Greenland margin, where this zone occupies ~70 km. In the simple shear model of passive margin formation the greater amount of stretching, faulting, and subsequent subsidence occurs on the lower plate margin, which, as with the other observations made by this study, would be the Labrador margin. Using their velocity structure, Chian et al. (1995a) proposed a model of continental breakup whereby breakup occurred closer to the southwest Greenland margin. Breakup occurring closer to the southwest Greenland margin is consistent with the other observations implying that southwest Greenland may have constituted the upper plate margin.

Overall, the high degree of magmatic, sedimentary, and structural asymmetry observed between these two conjugate margins allows us to suggest a simple shear mechanism of early rifting, as opposed to rifting under a pure shear–dominated regime. Under a simple shear rifting regime the upper plate margin would be southwest Greenland and the lower plate margin would be Labrador,

according to the distinction between the margin types in the original model by Lister et al. (1986). The asymmetry documented between these margins may have implications for petroleum exploration in the Labrador Sea (e.g. Jauer et al., 2014; Jauer and Budkewitsch, 2010). Such implications include the deeper, potentially more prospective basins on the Labrador margin and the inevitable asymmetry in the heat flow due to the asymmetric magmatic distribution, which may potentially influence the maturation of source material (Peace et al., 2015).

4.6 Conclusions

This study used the previous descriptions of Mesozoic rift-related magmatism (Tappe et al., 2007) to guide field work with the aim of understanding the controls on rifting in the region prior to the opening of the Labrador Sea. Through the field work and subsequent analysis of the data we have further characterised this event, demonstrating that certain aspects differ from the descriptions provided in the previous work. Our conclusions on the characteristics and extent of Early Cretaceous magmatism in proximity to the town of Makkovik are as follows:

1) Early Cretaceous magmatism around Makkovik, Labrador, is volumetrically and spatially extremely minor compared to the numerous other phases of extensive, readily observable intrusive magmatism exposed in the area.

2) Of the nine Early Cretaceous magmatism sample locations described by Tappe et al. (2007), we visited seven for this study. Only two of these seven localities provided any evidence for the magmatism described in the previous work.

3) Mesozoic magmatism is not sufficiently simple and consistent to consider this event as a single coherent intrusive suite of Early Cretaceous nephelinite dykes, as the outcrops are too sparse, variable, and unreliable. At least three of the Tappe et al. (2007) samples are actually from a diatreme, and the rest are either unobservable or ambiguous in nature.

4) The most reliable evidence for Mesozoic magmatism around Makkovik is the diatreme in Ford's Bight dated using fossil evidence by King and McMillan (1975). The diatreme

was not observed to be part of a dyke swarm as implied by the sample locations in Tappe et al. (2007).

Our conclusions on margin asymmetry, rifting mechanisms and the relationship between Mesozoic magmatism in West Greenland and Labrador are the following:

1) The magmatic distribution across these two conjugate margins is extremely asymmetric, with the Mesozoic magmatism exposed at surface in the area around Makkovik being minor compared to observations of rift-related dyking exposed at surface on the conjugate southwest Greenland margin.

2) This asymmetric magmatic distribution complements other observations of asymmetry, including deeper sedimentary basins and a wider continental shelf on the Labrador margin compared to southwest Greenland allowing us to propose a simple shear model for early rifting prior to the opening of the Labrador Sea, as opposed to a pure shear rifting model.

3) In a simple shear rifting model the southwest Greenland margin would be the upper plate margin and the Labrador margin would be the lower plate margin.

Chapter 5

The onshore expression of brittle deformation associated with the opening of the Labrador Sea and its relationship to the metamorphic basement fabric near Makkovik, Labrador, Canada

5.0 The context of this section

In addition to the analysis of rift related magmatism presented in the Chapter 4 of this thesis structural data were also obtained during the Makkovik fieldwork. Besides providing context to the main study presented in Chapter 4 the aim of collecting the structural data presented in this chapter was to: 1) characterise structures which predate Mesozoic rifting; 2) understand the relationship of such structures to rifting; and 3) identify any onshore deformation associated with the opening of the Labrador Sea. The importance of understanding the role of pre-existing structures during rifting and breakup was outlined in Chapters 1 and 2. Studies on the role of pre-existing structures in Labrador are required to compliment studies documenting reactivation on the conjugate West Greenland margin (Wilson et al., 2006; Japsen et al., 2006) to determine if both margins display similar onshore expressions of rifting, including structural rejuvenation (e.g. Holdsworth et al., 2001a).

The data and analysis in this chapter are presented as preliminary results intended to guide future work and show that the region has the potential to facilitate further analysis that could expand knowledge on the nature of early rifting prior to the opening of the Labrador Sea (Roest and Srivastava, 1989; Chalmers and Pulvertaft, 2001). The reason these results are presented as preliminary is because the number and distribution of the measurements is relatively restricted compared to previous similar studies (e.g. Abdelmalak et al., 2012; Dempsey et al., 2014). However, the analysis presented herein suggests that the data is sufficient to provide some insights and guide future work of this kind in the area.

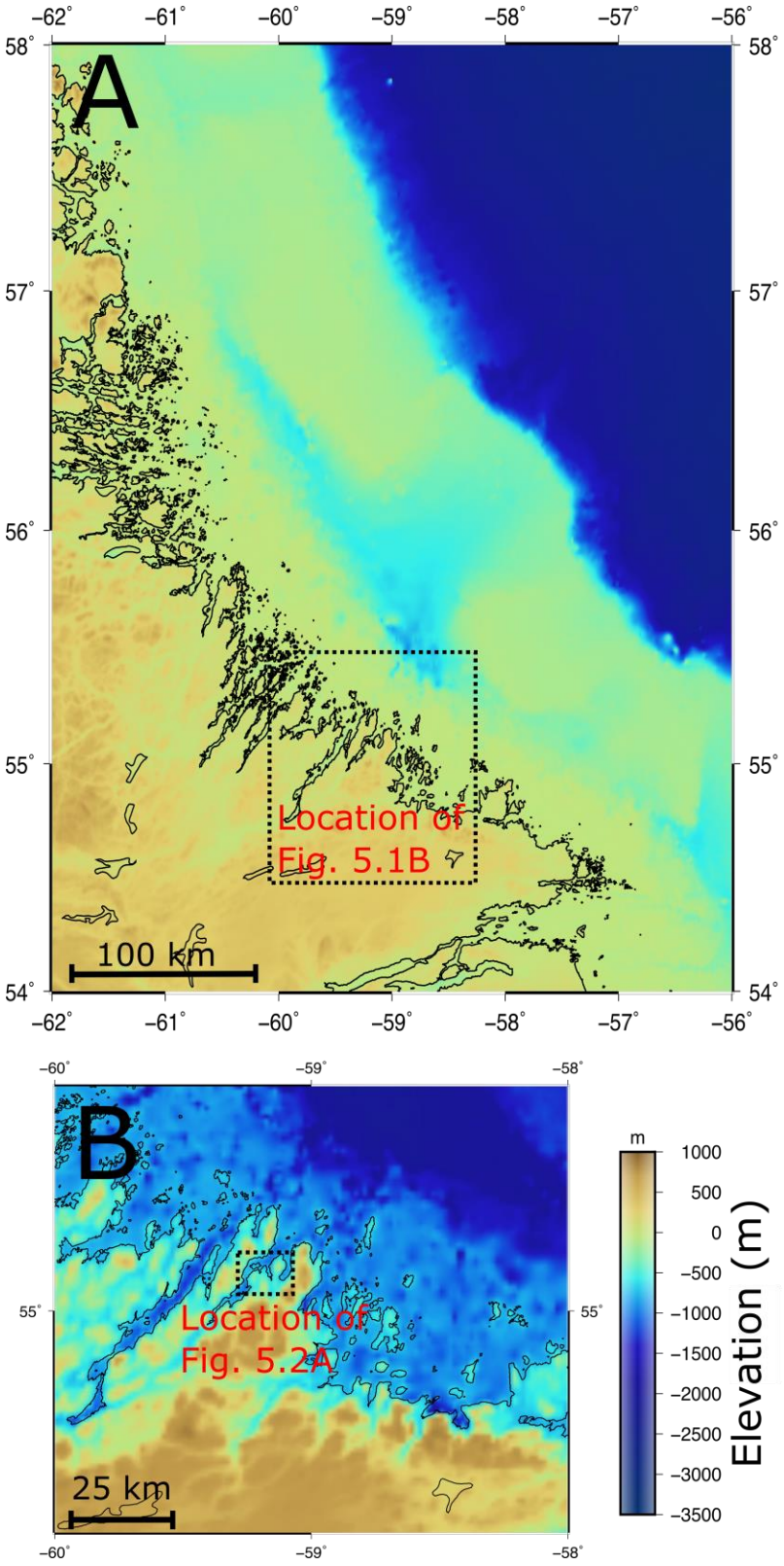

Figure 5.1

The location of the study area in this Chapter.

All data presented in this chapter (Fig. 5.2) were collected in the same geographical study area as the primary study in Chapter 4, within the Aillik Domain of the Makkovik Province, Labrador, Canada (Chapter 4 - Fig. 4.2). Figure 5.2 shows the locations where the data analysed in this section were obtained.

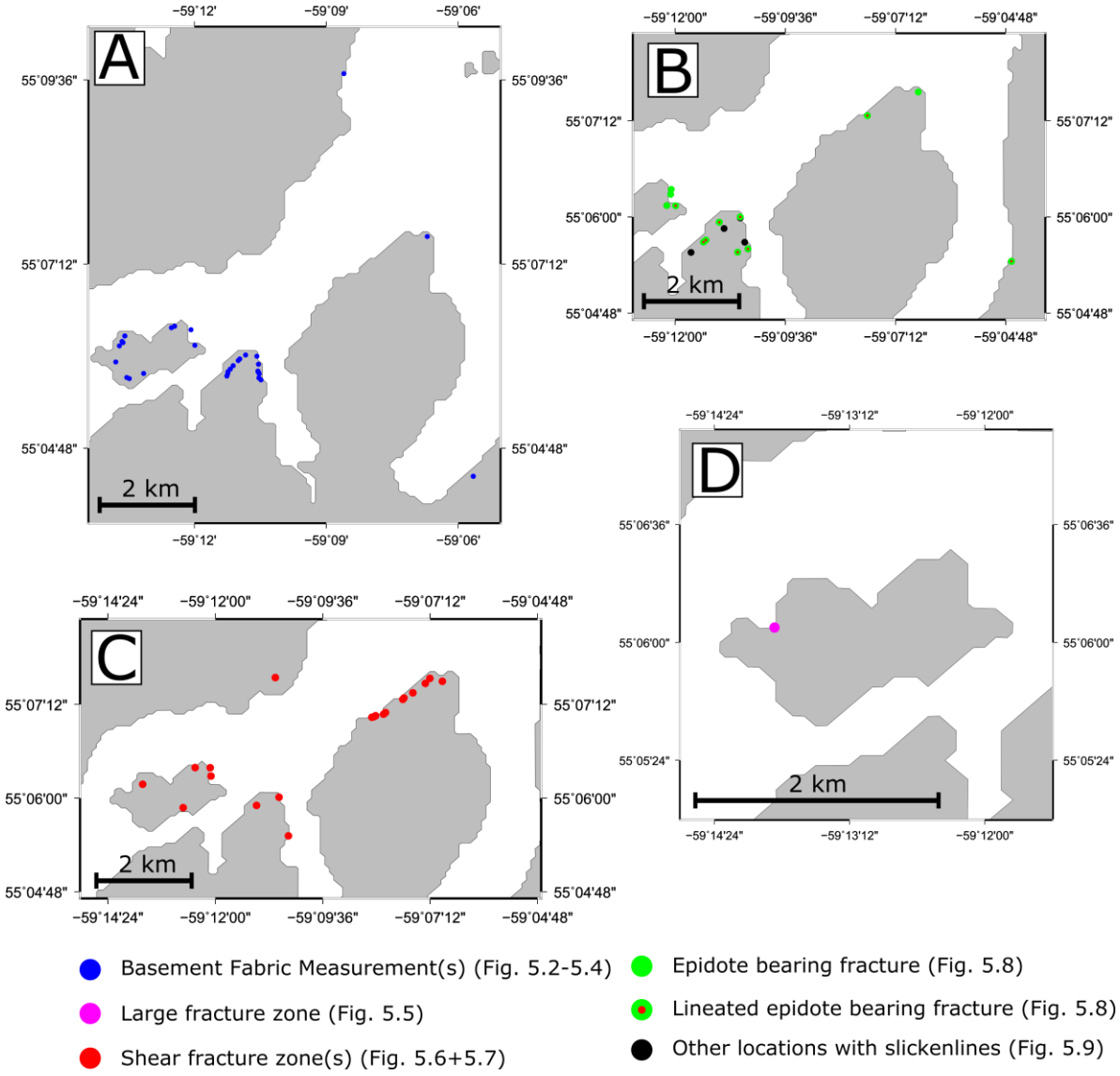

Figure 5.2

The location of the data analysed in this chapter including: A) the locations where basement fabric orientation was measured , B) the locations of the data used in the stress inversion calculations, C) the locations where zones of shear fractures were recorded and D) the large fracture zone on Big Island

described in section 5.3 of this chapter. For location names and a larger scale map see figures 4.1 and 4.3 in Chapter 4 of this thesis.

5.1 Onshore deformation on passive margins

The coastal exposures adjacent to modern, offshore passive margins may preserve evidence for deformation associated with rifting (e.g. Wilson et al., 2006; Abdelmalak et al., 2012) culminating in continental breakup and passive margin formation (Eldholm and Sundvor, 1979; Geoffroy, 2005). However, distinguishing which structures are related to rifting can be particularly difficult as most margins have experienced multiple stages of deformation both prior to rifting (e.g. Wilson, 1966) and in some cases after rifting such as fault reactivation during margin inversion (e.g. Holford et al., 2014). This can make identifying the structures associated with rifting particularly problematic, especially if a rifting episode contained multiple events such as the Labrador Sea region (Oakey and Chalmers, 2012; Abdelmalak et al., 2012). Passive margin settings may also provide the opportunity to characterise the relationship between rift-related deformation and pre-rift structures (e.g. Chenin et al., 2015), concepts which are useful when undertaking offshore studies where such observations are not possible.

5.2 Basement metamorphic fabric

Analysis of the orientation of the metamorphic mineral foliation in the basement was conducted with the aim of characterising the basement fabric to examine the relationship, if any, with rifting direction as inferred by previous work (e.g. Abdelmalak et al., 2012; Oakey and Chalmers, 2012) and the stress inversions as detailed later in this chapter.

Figure 5.3

An example of the metamorphic fabric observed in the basement units on Big Island, NW of Makkovik. Viewing angle is looking down on the exposure with north to the right.

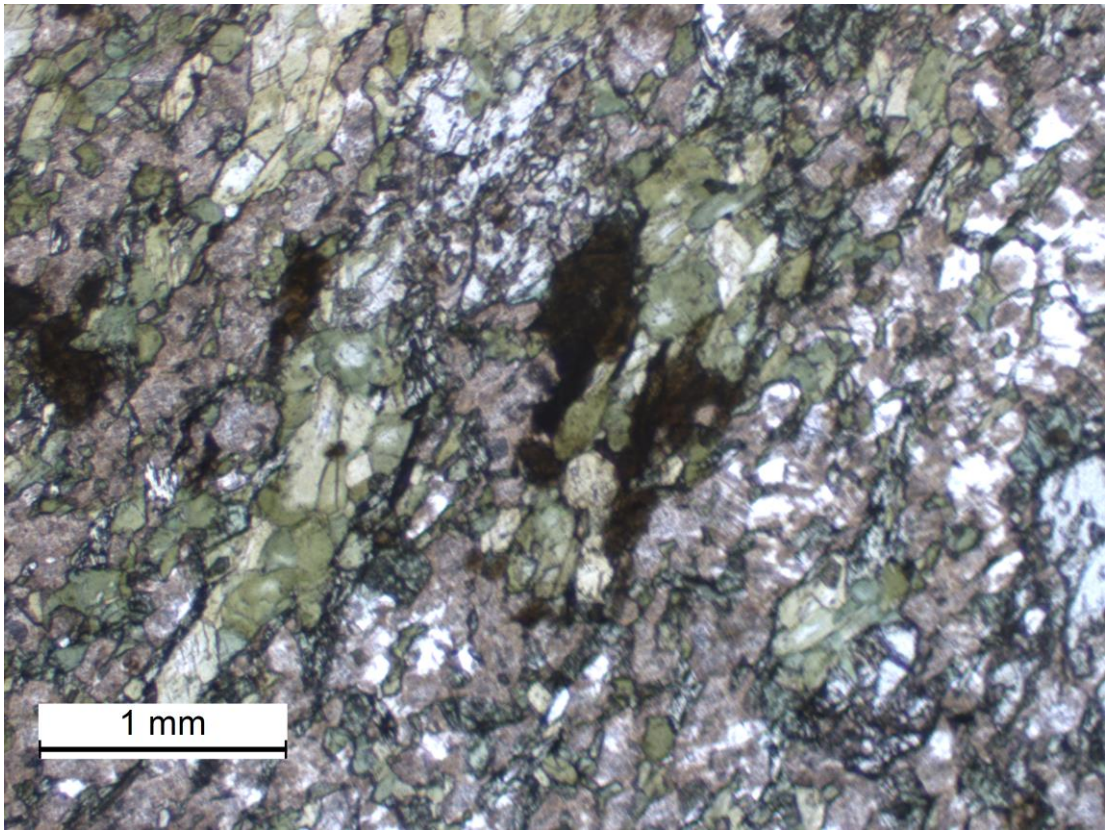

Figure 5.4

Thin section micrograph in plane polarised light depicting the metamorphic mineral foliation in an amphibolite dyke collected in proximity to the AP2 location in Ford's Bight (Chapter 4 – Fig. 4.3). The basement fabric can be seen to have manifest as an alignment of amphibole, plagioclase, epidote and chlorite minerals.

A metamorphic mineral foliation was readily observable in many units in the field (Fig. 5.3) and on thin sections analysed using a petrographic microscope (Fig. 5.4). The orientation data obtained on the basement rocks shows that the metamorphic fabric is consistently striking north-south (dipping east or west) across the study area (Fig. 5.5). The limited data collected suggests that the folding might be asymmetric with the eastern fold limbs being steeper. The fabric was observed to be predominantly planar, although at some localities this aspect of the basement fabric was indistinguishable and thus no measurements were recorded.

It is intriguing that these results show that the basement fabric is orientated approximately perpendicular to the minimum principal stress direction during rifting according to some previous work (Abdelmalak et al., 2012). This allows us tentatively hypothesise that brittle rift-related structures may have formed parallel to the basement metamorphic fabric, a concept considered further later in this chapter and one that should be explored by future work in this area.

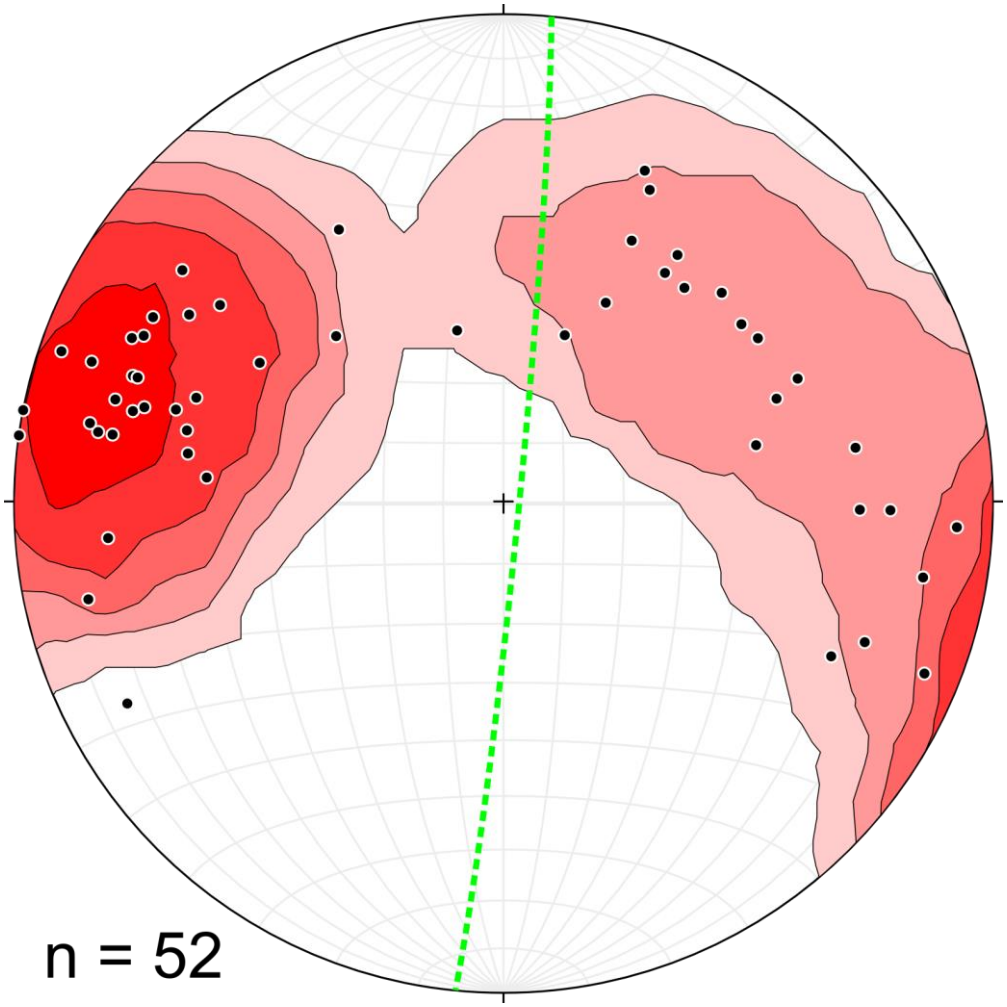

Figure 5.5

Stereonet showing planes to poles for all basement foliation measurements collected during the Makkovik fieldwork. Kamb contouring was used with the results displayed using a 'red ramp' colourbar. Contour interval is 2σ, the counting area is 14.8 % of the Stereonet. Folding is shown by this dataset, with the dominant structural trend of the limbs dipping to the east and west. The axial plane is shown with a dashed green line (005/87 E) was calculated in the Stereonet software for OXS (Cardozo and Allmendinger, 2013).

5.3 Characterisation of brittle deformation

Evidence for brittle deformation was observed across the study area, in all lithological units encountered during the fieldwork. Faults were observed ranging in size from a few cm's to damage zones that are several hundred metres wide (Fig. 5.6A-C) that can potentially be traced inland using satellite data (Fig. 5.6D-E). Establishing relative chronologies for the brittle deformation events was challenging due to a lack of distinguishing characteristics making it difficult to decide which structures belonged to the same deformation event and the manifestation of fracture systems varying between lithologies. Also remarkably few crosscutting relationships enabled observations to be correlated between localities.

Observations of brittle deformation of particular note include: 1) those associated with kinematic indicators on individual structures that were measured in situ and are described and modelled in the subsequent sections; 2) large (> 10 m) deformation zones e.g. north coast of Big Island (Fig. 5.6); and 3) widespread fracture zones in the basement possibly indicating shear deformation (Figs. 5.7 and 5.8).

Wide zones (> 10 m) of intense brittle deformation were observed at several locations, for example on Big Island (Fig. 5.6) but also on Makkovik Peninsula, Cape Strawberry and north of Ikey's Point. The wide zone of intense deformation on the north coast of Big Island is shown on Figure 5.6. Here, a zone of mineralised fault breccia within the felsic basement rocks was observed at a coastal exposure to be around 100 m wide, with a possible continuation inland before lack of exposure prohibited further observations. Within the mineralised breccia some proto-cataclasite regions were observed as bands typically from 10 - 30 cm but in some cases up to 1 m. These fault rocks were classified used the system of (Woodcock and Mort, 2008). A relative age and the possible relationship between the wide zones of deformation (e.g. north coats of Big Island – Fig. 5.6) and the other structures described in this chapter was not established.

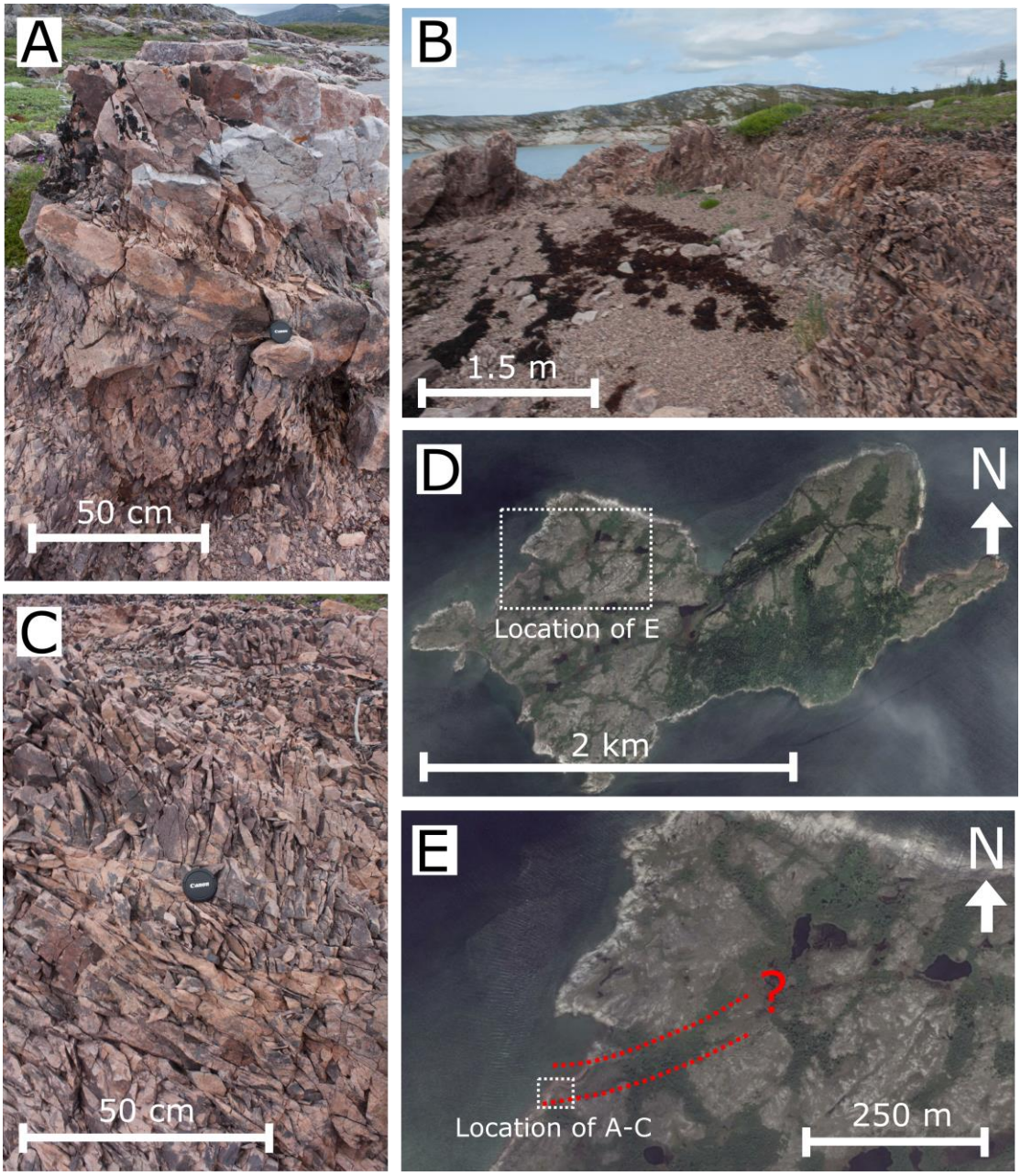

Figure 5.6

Field (A-C) and Google Earth images (D-E) of a zone of extensive intense brittle deformation on Big Island north of Makkovik. Subfigure (E) shows the possible continuation of this zone inland. (A) and (C) are looking southwest whereas (B) is looking northeast.

In addition to the wide zones of brittle deformation (Fig. 5.6) smaller, abundant fracture zones in the basement that potentially represent shear deformation (Fig. 5.6) were also recorded. These display both a sinistral (Fig. 5.7B) and dextral (Fig. 5.7A) shear sense. In total 61 of these fracture

zones were observed across the area studied of which 43 were characterised as dextral and 18 were characterised as sinistral (Fig. 5.8). As with the aforementioned wide zones (> 10 m) of brittle deformation a chronology of the sinistral and dextral deformation events (Fig. 5.7 and 5.8) was not satisfactorily established, as surprisingly few localities were observed with cross cutting relationships between these fracture zones.

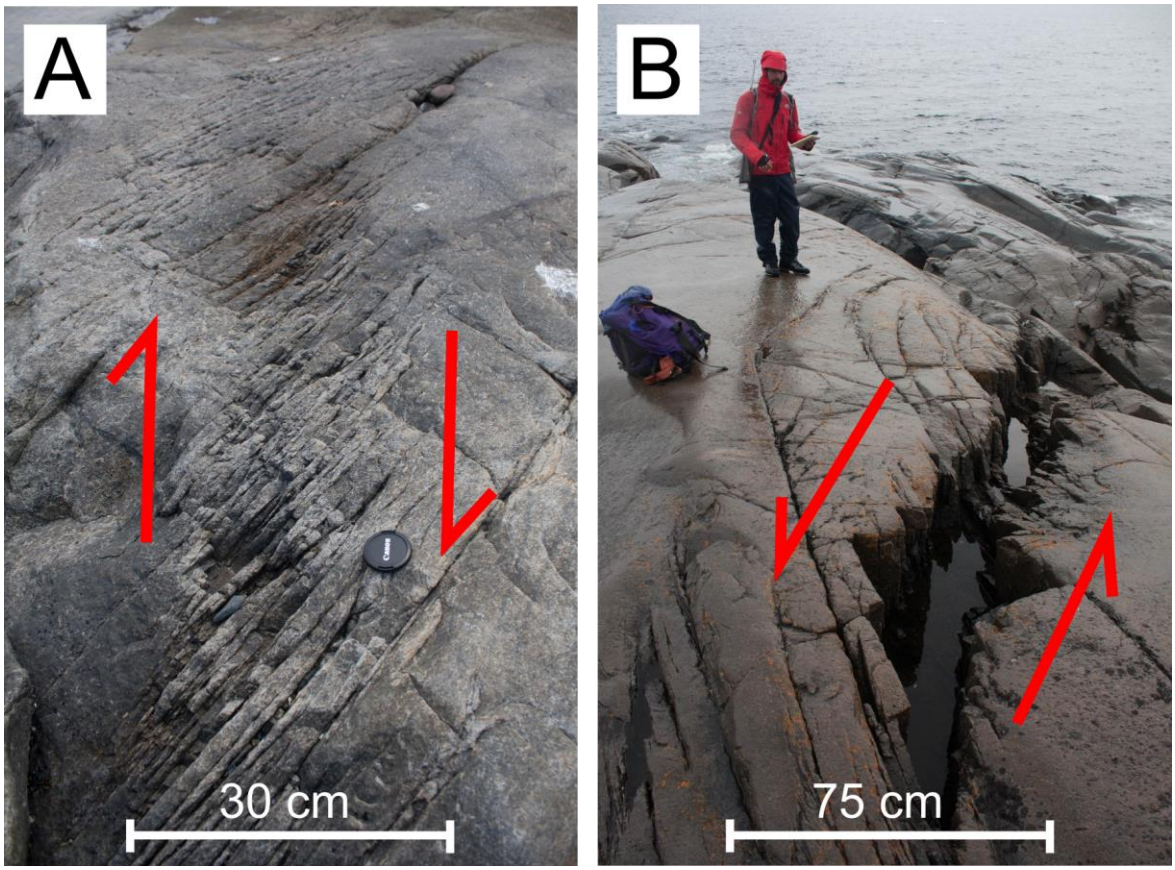

Figure 5.7

Examples of the abundant fracture zones in the basement that potentially indicate shear deformation on A) the north coast of Big Island and B) the coastline north of Ikey's point (Chapter 4 – Fig. 4.3).

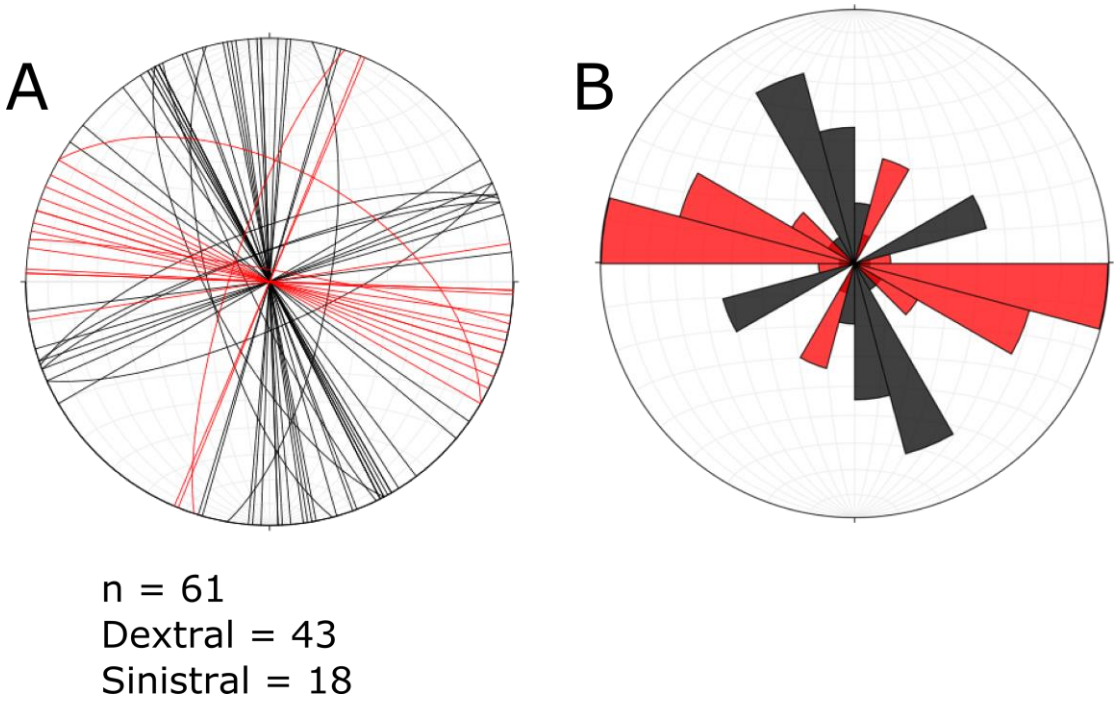

Figure 5.8

A) Stereonet showing the orientations of fracture zones such as those in Figure 5.7 categorised as either sinistral (red) or dextral (black). Most fracture zones are plotted as vertical as their dip could not be discerned from the field observations. B) the data from A) plotted on a rose diagram using 15° bins (total bins = 24) and divided into two dextral and two sinistral sets of structures. The data presented in this figure was plotted in the Stereonet software for OXS (Cardozo and Allmendinger, 2013).

Although brittle deformation was observed to be widespread and readily observable (Figures 5.6 and 5.7), reliable kinematic indicators, such as slickenlines, were not observed in conjunction with much of this deformation. However, some faults and fractures were observed with kinematic indictors. The following section describes the nature of these faults and fractures from which the data modelled in this chapter was obtained.

5.3.1 Characterisation of modelled fracture sets

Some of the brittle deformation observed with slickenlines was associated with significant epidote dominated mineralisation, whilst at other locations little to no mineralisation was observed associated with the deformation. In this chapter stress inversions are performed using the data

obtained on these faults and fractures. In the first model ('inversion A') we model all data irrespective of the presence or absence of mineralisation, whereas in the second model ('inversion B') we only model the data obtained on faults and fractures associated with abundant mineralisation.

The widespread brittle deformation event modelled in inversion B was characterised by the occurrence of abundant mineralisation dominated by epidote but also including pyrite and chalcopyrite on the mineralised surfaces (Fig. 5.9). Preservation of this event is particularly prevalent within various occurrences of the abundant mafic dykes (Chapter 4 and Foley, 1989). The close association of this event with the mafic dykes perhaps indicates that the composition of the mineralisation was strongly influenced by the dykes.

Thus, it is possible that the epidote event is actually part of the same deformation event as that which produced the other kinematic indicators (inversion A); a possibility explored in the discussion of this chapter based on the stress inversion results. Nonetheless, we modelled this event as it represents the only deformation event that could be confidently identified across the study area. The dykes that house the epidote mineralisation are classified as alkaline lamprophyre, ultramafic lamprophyre and carbonatite (Foley, 1989), and they are claimed to belong to the ~590 - 555 Ma intrusive event (Tappe et al., 2006; Tappe et al., 2007). Thus, ~590-555 Ma is taken to provide an upper age limit for the syn-mineralisation deformation event in this study (Fig. 5.9).

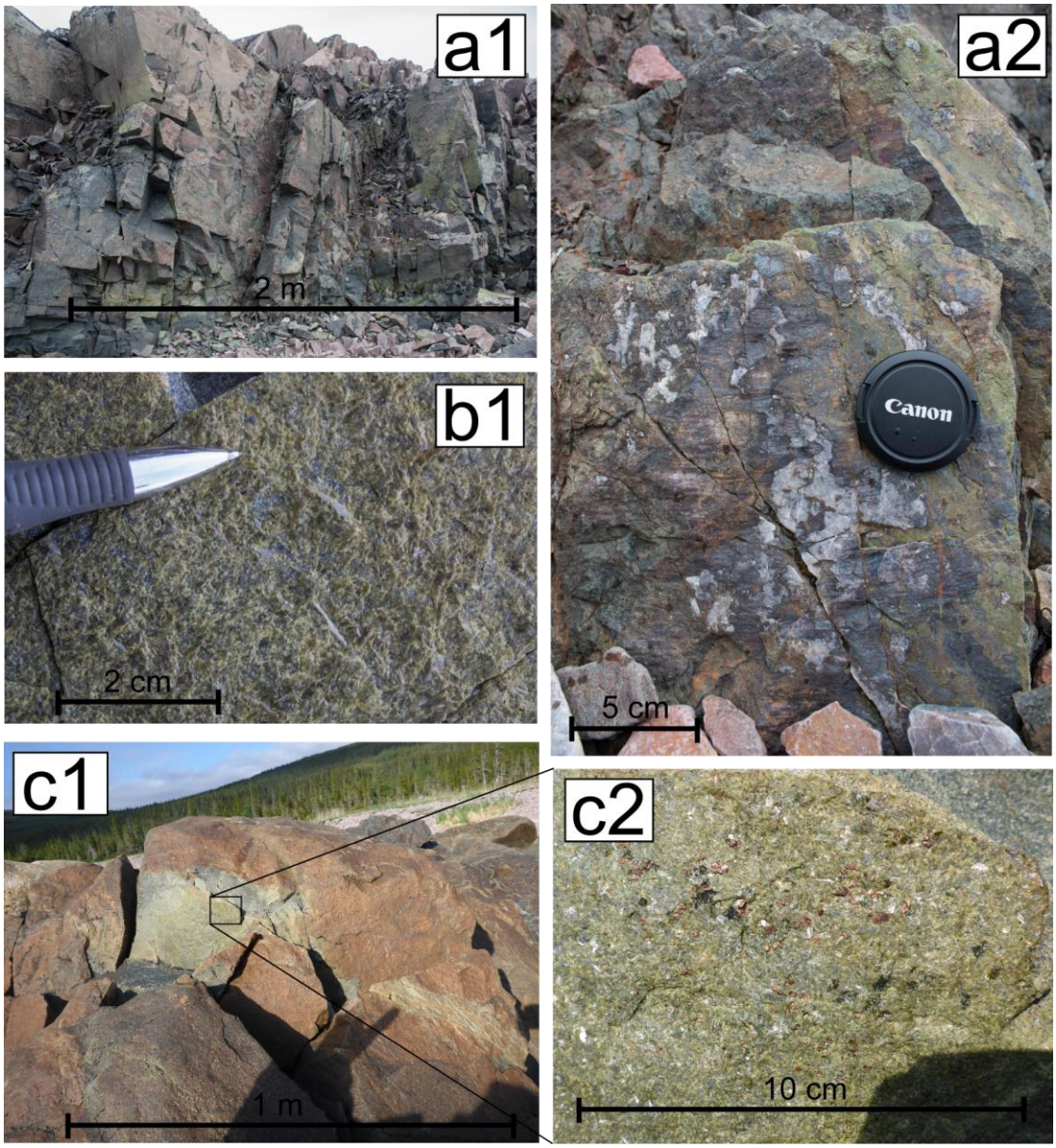

Figure 5.9

Examples of the variability in occurrences of the widespread brittle deformation event associated with epidote mineralisation modelled in this study as inversion B. Subfigure a1) is located on Big Island (Fig. 5.2) where abundant epidote mineralisation often associated with slickenlines such as those in (a2) was observed to be widespread. (b1) was observed on Makkovik Peninsula and shows an example of a mineralised surface in which no kinematic indicators are present, with surfaces such as this potentially representing mode I fractures. Subfigure (c1) shows the outcrop of mafic dyke in Fords Bight from which the pyrite sample (c2) was obtained in which the Re-Os (Rhenium-Osmium) geochronological analysis was conducted (Appendix).

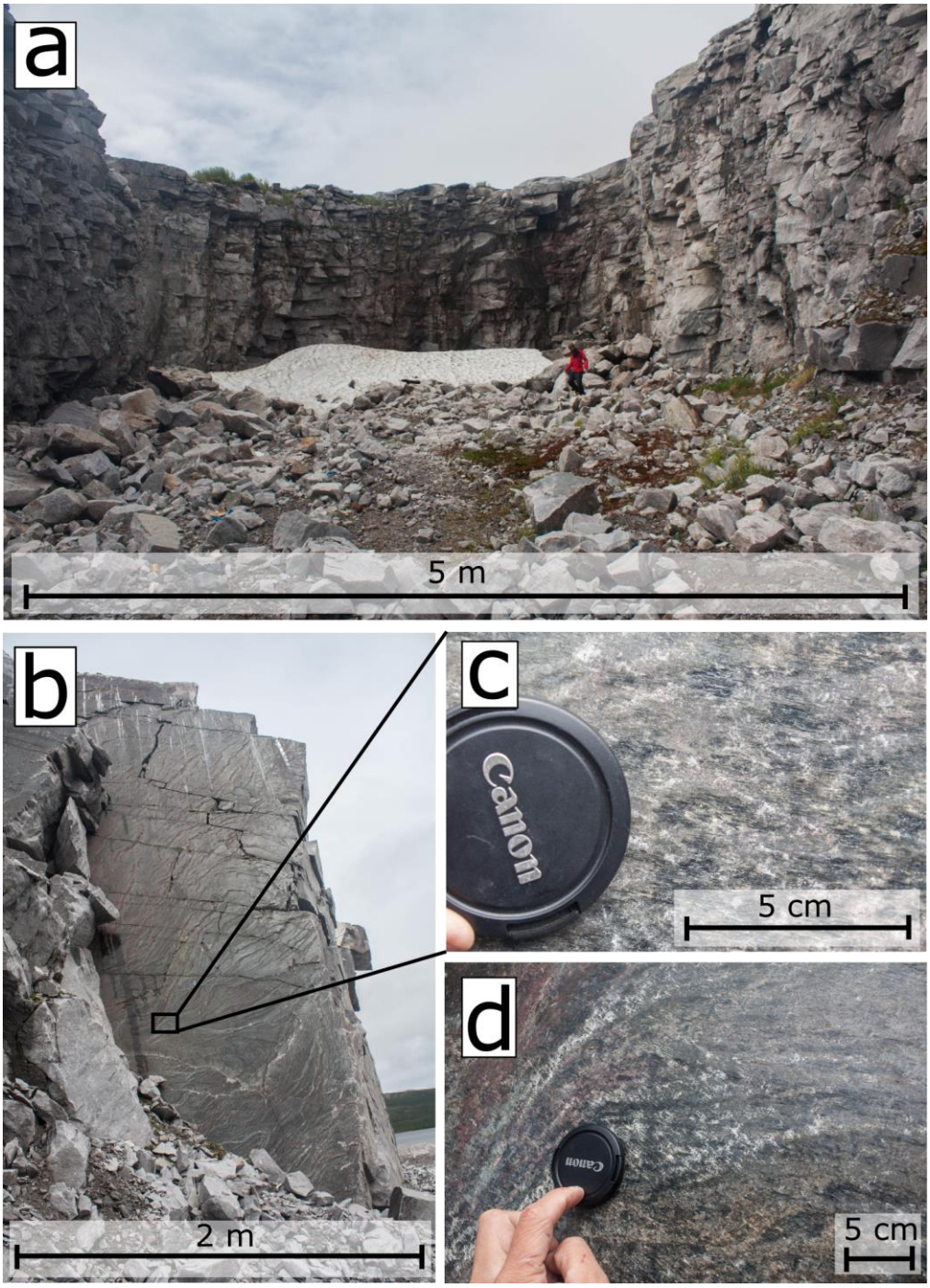

Figure 5.10

An example of brittle deformation not associated with the epidote mineralisation that contributed to the data used in inversion A. The quarry near Makkovik (a) located at 55.0756N/59.169299W contained multiple surfaces similar to (b) with readily observable slickenlines (c and d).

5.4 Stress inversion methodology

Stress inversion uses fault geometry and kinematic data to reconstruct past stress configurations (Angelier, 1990). The main principle of stress inversion is that the slip on a plane occurs in the direction of the maximum resolved shear stress (Bott, 1959). Our stress inversion was performed using the MyFault software version 1.05 by Pangea Scientific Ltd (e.g. Michael, 1984), using the minimised shear stress variation method. The minimized shear stress variation calculation is a standard inversion method (e.g. Dempsey et al., 2014; Abdunaser and McCaffrey, 2015) that allows all faults to fail simultaneously, enabling us to calculate the orientation and relative magnitudes (stress ratios) during deformation of the fault set analysed. The minimised shear stress variation method provides a more robust solution than simpler calculations such as simple shear tensor average (Michael, 1984). The purpose of the stress inversion in this study was to determine if the observed onshore deformation events are compatible with previous interpretations of the Mesozoic rifting direction prior to the opening of the Labrador Sea (e.g. Abdelmalak et al., 2012).

The key assumption of stress inversion is that the magnitude of the slip stress on a fault is similar for all faults in the set at the time of slip (e.g. Michael, 1984) i.e. all deformation is assumed to occur simultaneously within a fault set. For this reason it is particularly important to confidently identify that all the faults analysed belong to the same deformation event. Thus, previous work devotes considerable effort to separating data into separate fault sets (e.g. Abdunaser and McCaffrey, 2015). To deal with this aspect in this study the stress inversion is performed twice, 'inversion A' and 'inversion B'. Inversion A was performed on all kinematic data (slickenlines) collected during the fieldwork (e.g. those collected in the quarry - Fig. 5.10) i.e. no age constraint, whilst inversion B was only performed on deformation characterised by abundant epidote mineralization (Fig. 5.9) as this represents the only brittledeformation that could be age constrained relatively using dated dykes (Tappe et al., 2006; Tappe et al., 2007).

In an attempt to establish a better age constraint, Re-Os (Rhenium-Osmium) geochronological analysis was conducted at Durham University on pyrite samples from two locations 4.7 km apart in

which the epidote mineralisation event was documented. The methodology used in the Re-Os analysis followed the same procedure as Dichiarante et al. (2016). The locations of the pyrite samples which were analysed are; 55.12107°N/59.13016°W (Ford's Bight Point) and 55.091419°N/ 59.077683°W (Ford's Bight – Fig. 5.4(c1-2)). The Re-Os analysis however produced ages (>3 Ga), a value well in excess of the age basement in the area (LaFlamme et al., 2013) and thus could not be used to provide a more constrained age on the deformation event analysed in this section. Thus, at present the most reliable age constraint on the paleostress analysis is that it is penecontemporaneous with the ~590-555 Ma dykes (Tappe et al., 2006; Tappe et al., 2007).

Quality checking the data was conducted firstly in the field by not recording any ambiguous kinematic indicators, and secondly during analysis by ensuring that none of the angles between the fault planes and the kinematic indicators (misfit angle) exceeded the 25°. Our misfit angle tolerance of 25° is far in excess of the misfit angle used in some previous studies e.g. >40 (Abdunaser and McCaffrey, 2015). When using a misfit angle of 25° none of our fault planes required omission from the dataset.

In addition to displaying the calculated principal stress fields the right dihedral graphical representation method (Angelier and Mechler, 1977) has been used to demonstrate the orientations of tension and compression according to the results of the inversion. The right dihedral method is a graphical representation of the range of possible orientations of σ1 and σ3 (Delvaux and Sperner, 2003) which commonly used for evaluating the reliability of the stress inversion (e.g. Zamani et al., 2008).

5.5 Stress inversion results

The results of both stress inversion A and B are shown on Figure 5.11, Table 5.1a and Table 5.1b. 84 measurements were used in stress inversion A, whilst in stress inversion B although 110 fault and fracture planes were recorded (Fig. 5.2 and appendix) only 39 were observed to contain measurable kinematic indicators. Thus, the second stress inversion on just the epidote deformation

event contains 39 data points. The absence of kinematic indicators does not imply that movement did not occur on the other 71 planes (110-39 = 71) with epidote mineralisation but that it has not been preserved. The analysed fault data in both stress inversions A and B includes tensile, normal, reverse and strike slip deformation.

The results of the stress inversion A (all kinematic data) show that if this deformation all occurred during the same event it would likely represent an extensional regime, as σ1 (maximum principal stress) is oriented at 051°/78°, whilst σ3 (maximum principal stress) is orientated 276°/08°. This stress field configuration indicates a near E-W extension direction, as depicted by the red arrows on Figure 5.11A1. The right dihedral method shows a setup consistent with approximately E-W extension. Using the right dihedral method it can be seen that in inversion A σ1 is well constrained, however σ3 and thus σ2 is less well constrained. The validity of associating all the brittle deformation with one event is discussed at the end of the chapter.

The results of the stress inversion on just the epidote bearing faults (inversion B) again indicate that this deformation event occurred during an extensional regime as σ1 (maximum principal stress) is oriented near vertical at 056°/84°, whilst σ3 (minimum stress) is orientated 254°/6°. This stress field configuration indicates an extension direction of approximately ENE-WSW, as depicted by the red arrows on Figure 5.11. Projection of the results of inversion B using the right dihedral method show that both σ1 and σ3 are relatively well constrained, although σ1 is slightly less well constrained than in inversion A. It is however notable how well σ3 is constrained in inversion B.

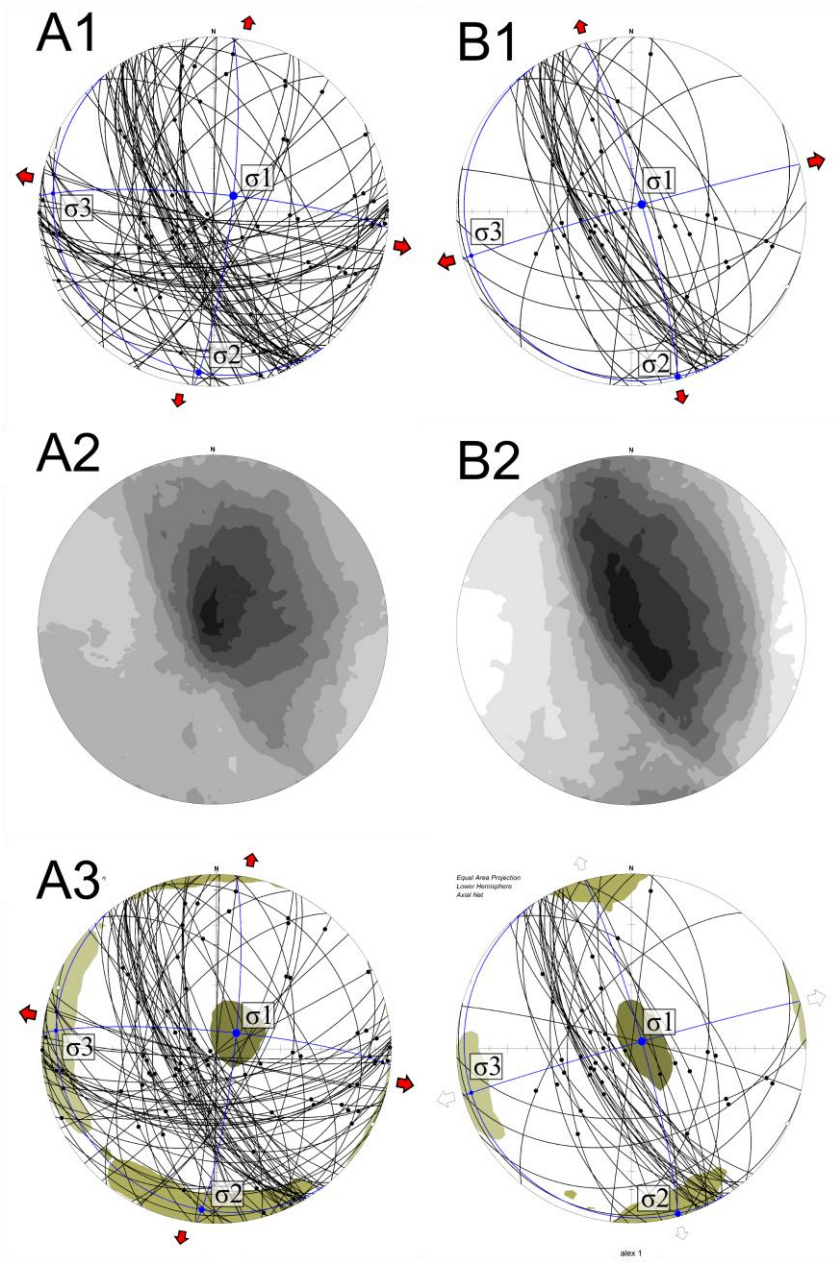

Figure 5.11

Stress inversion results for both inversion A and inversion B, with all subfigures denoted with 'A' related to inversion A and all subfigures denoted with 'B' related to inversion B. Subfigures A1 and B1 display the calculated three principal stress orientations (σ1>σ2>σ3), along with measured fault planes, associated slickenlines and the dominant stretching direction (red arrows). The A2 and B2 subfigures display the stress inversion results using the right dihedral method (Angelier and Mechler, 1977), with a greyscale colourbar from compression (black) to extension (white). Subfigures A3 and B3 show the error calculations associated with the stress inversions. All plots in this figure were produced in MyFault version 1.05.

Principal stress axis	Azimuth	Plunge
σ1	051°	78°
σ2	185°	8°
σ3	276°	8°

Table 5.1a

Calculated principal stress directions from the stress inversion on all modelled data (inversion A).

Principal stress axis	Azimuth	Plunge
σ1	056°	84°
σ2	164°	2°
σ3	254°	6°

Table 5.1b Calculated principal stress directions from the stress inversion on the epidote data (inversion B).

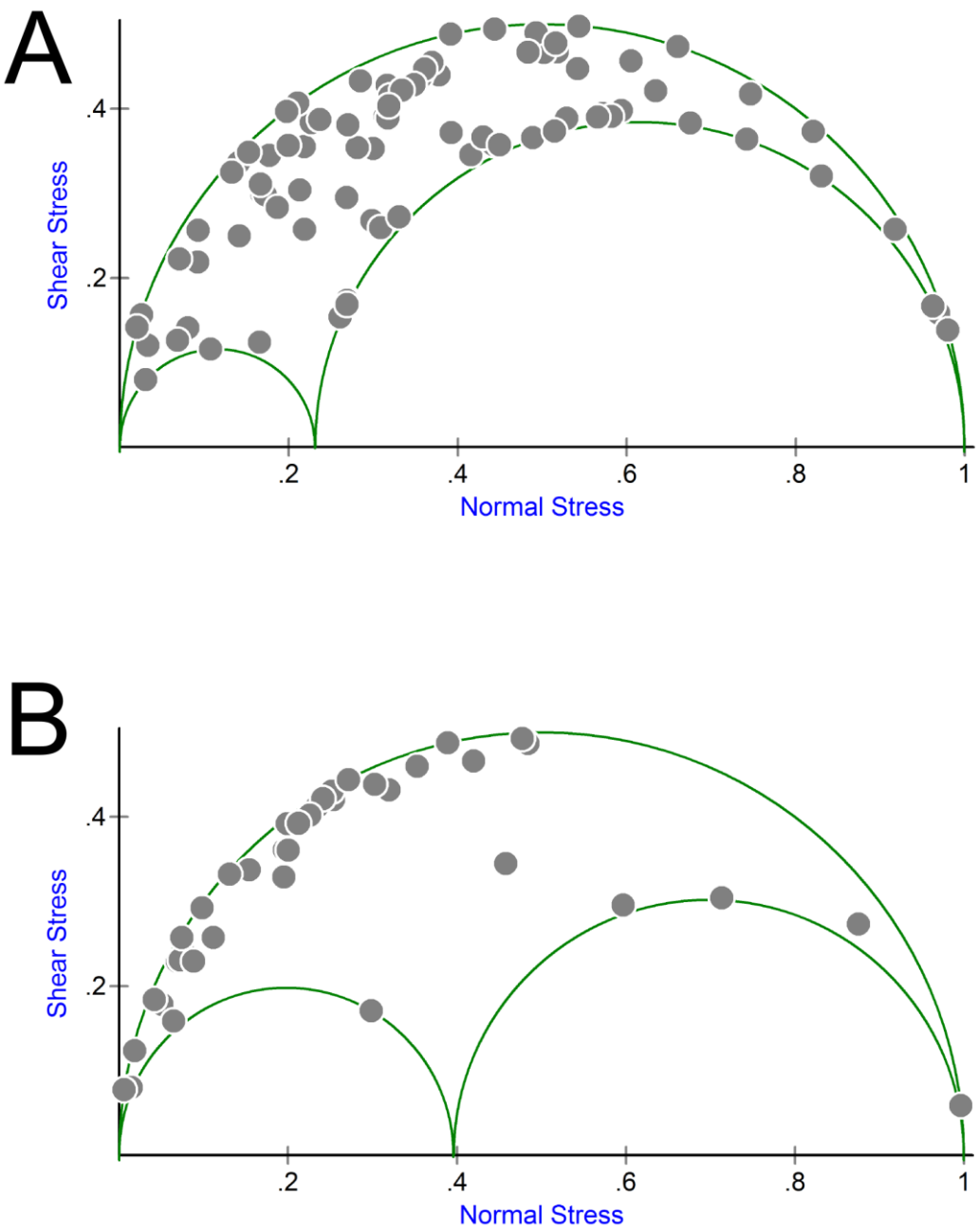

Figure 5.12

Mohr circles for inversions A and B with the maximum resolved stresses in the fault plane shown in grey. This figure demonstrates that inversion B is a better orientated data set to perform a stress inversion on.

Plotting the resolved stresses in the slip direction in both stress inversions A and B on mohr circles (Fig. 5.12) shows that the principal stress orientations in inversion B are better constrained than those of inversion A. A similar situation is displayed when the maximum resolved stresses in the fault plane are plotted.

5.6 Discussion

5.6.1 A potential onshore expression of Mesozoic rifting

Given that a similar extension direction was derived in both inversions (A = ~E-W and B = ~ENE-WSW) it is possible that all modelled deformation (inversion A) was associated with a singular event in which the epidote mineralisation (inversion B) is a localised mineralogical effect related to the abundant mafic dykes (Foley, 1989; Tappe et al., 2006). However, it should be noted that when the entire dataset is modelled the error associated with σ2 and σ3 and the spread of data on the Mohr circle (Fig. 5.12) is much greater, possibly implying that inversion A includes deformation related to multiple geological events. To further test whether all deformation modelled in inversion A is related to a singular Mesozoic event a significantly larger dataset is required from elsewhere on the Labrador margin, initially from outside the Aillik Domain within the Makkovik Province but desirably from outside the Makkovik Province to ensure that this is not a localised stress effect.

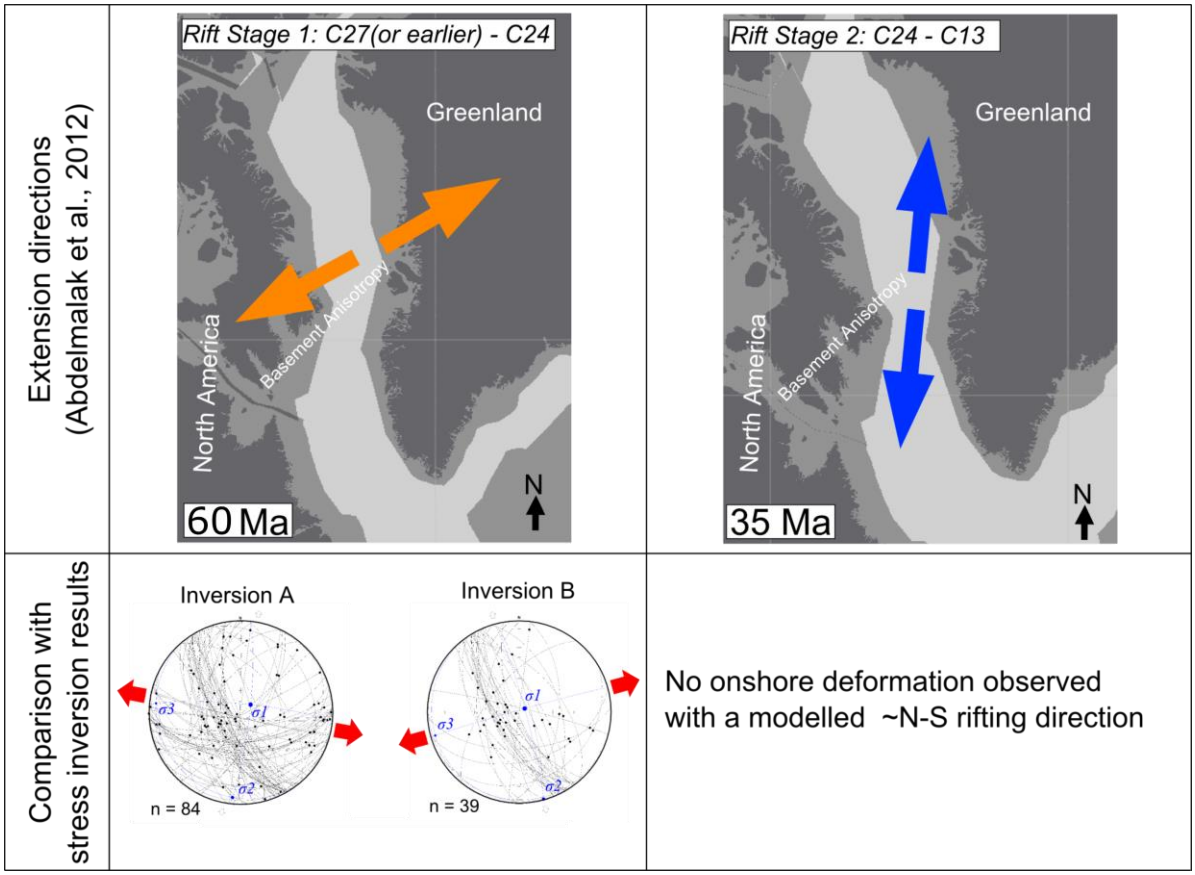

Figure 5.13

Comparison between the stretching directions in Abdelmalak et al., (2012) and the stretching direction (σ3) produced by the inversions in this study.

Abdelmalak et al. (2012) performed stress inversions based on onshore field data obtained on the conjugate West Greenland margin demonstrating that two key stages of rifting can be identified, a conclusion that is concordant with much of the previous work in this area (e.g. Oakey and Chalmers, 2012; Wilson et al., 2006). Comparison between the results of the stress inversions in this study and those of Abdelmalak et al. (2012) show that a similar extension direction has been calculated here as in their rift stage 1 (Ch27 or earlier - Ch24) (Fig. 5.13). Rifting during the second stage identified by Abdelmalak et al. (2012) (~N-S) is inconsistent with the calculated extensional direction in this study. Thus, it is possible that the deformation analysed by Abdelmalak et al., (2012) was produced in the same event as the deformation analysed in the stress inversions in this study. However, the data that constitutes inversion A shows a series of approximately E-W normal

faults that would be consistent with deformation during the latter N-S phase of deformation identified by Abdelmalak et al. (2012). This implies that inversion A might include brittle deformation from both stage 1 and 2.

5.6.2 Stress inversion reliability and errors

Another issue is that it is possible that movement could have occurred on many of the planes where kinematic indicators were not observed but evidence of the movement was not preserved. This however is a limitation that is not unique to this study and effects all stress inversion studies (e.g. Dempsey et al., 2014).

Overall both inversions display minimal errors in the values of the principal stress orientations (Fig. 5.11). This is due in part to the dataset containing a sufficient distribution of orientations to constrain the principal stress orientations and the minimal measuring error between the fault planes and kinematic indicators, as demonstrated by the use of a relatively low misfit angle compared to previous work (e.g. Abdunaser and McCaffrey, 2015). The near vertical nature of σ1 in both inversion A and B again indicates that the results are realistic for extensional deformation. Error analysis of the results of the stress inversion (Fig. 5.11) demonstrates that there is minimal ambiguity associated with σ1 in both inversions A and B. However, σ3 (and thus σ2) is much better constrained in inversion B than in inversion A. This may imply that when modeling the whole dataset (inversion A) multiple deformation events could have been incorporated, an interpretation also backed up by the distribution on the Mohr circle (Fig. 5.12).

Given the minimal error associated with the stress inversions the main caveat is that the only dated age constraint is the ~590-555 Ma dykes (Tappe et al., 2006; Tappe et al., 2007), as the Re-Os analysis conducted during this study provided inconclusive results on both the dated samples (Fig. 5.9).

5.6.3 Basement fabric and Mesozoic rifting

Analysis of the basement fabric data has showed that this structure is striking north-south (dipping east-west) consistently across the study area. When this orientation of basement fabric is considered in the context of both the rifting directions inferred from previous studies (e.g. Abdelmalak et al., 2012) and through the stress inversions performed in this work (Fig. 5.11) it is possible that this basement fabric orientation made the area particularly susceptible to a propagating rift with an east-west extension direction (Fig. 5.14).

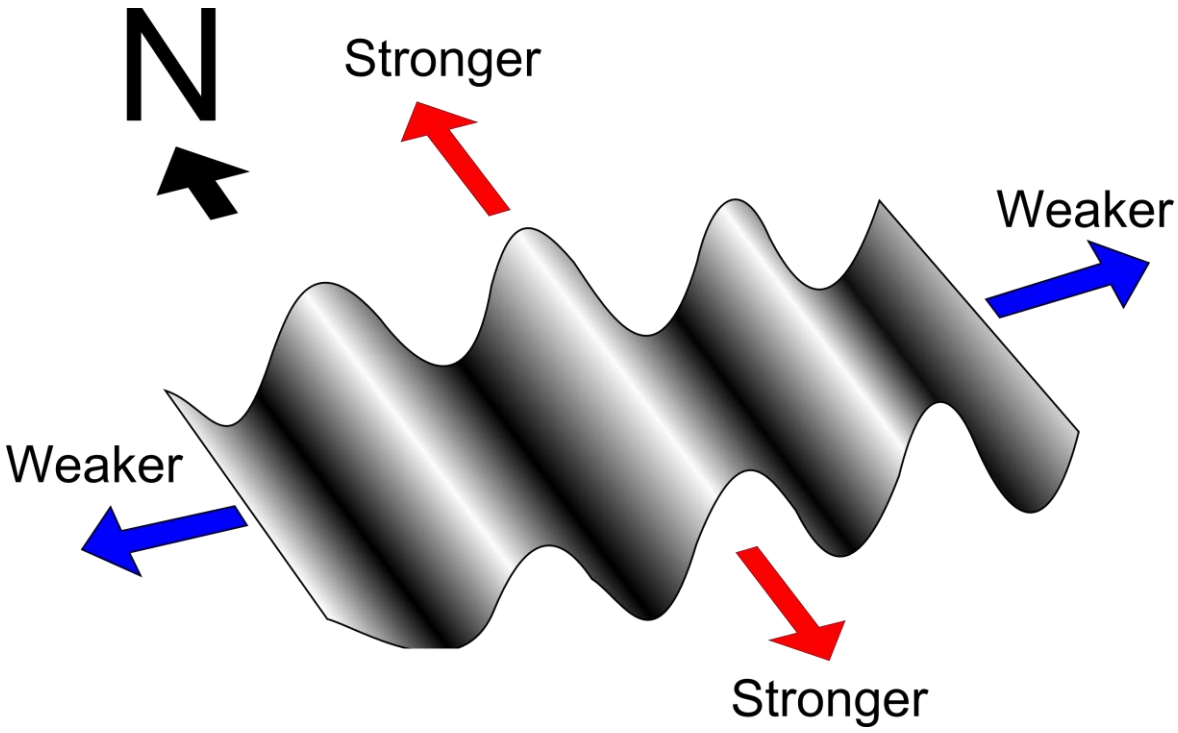

Figure 5.14

Theoretical relative strengths of the crust under different rifting directions with respect to a preexisting metamorphic mineral fabric as observed in proximity to Makkovik (Fig. 5.3, 5.4 and 5.5).

5.7 Conclusions

The conclusions of this preliminary structural study in the Aillik Domain of the Makkovik Province, Labrador are that:

1) The deformation event characterised by abundant epidote mineralisation is likely to have been produced during an ENE-WSW extensional event. This ENE-WSW extensional event is younger than ~590-555 Ma based on the age of mafic dykes containing most of the deformation.

2) It is possible that the post ~590-555 Ma extensional event is the cause of all brittle deformation analysed in the stress inversions in this section, with the epidote mineralisation representing a localized effect due to proximity to mafic dykes. However, to test this hypothesis further considerably more data is required from elsewhere on the Labrador margin.

3) Given the extension directions interpreted by previous work it is possible that the deformation event(s) analysed in this study represent an onshore expression of rifting prior to the opening of the Labrador Sea, that is approximately ENE-WSW during the Cretaceous.

4) The regional metamorphic mineral fabric within the studied part of the Aillik Domain of the Makkovik Province is orientated parallel to the rifting direction inferred by previous studies on the conjugate West Greenland margin and by the stress inversion performed by this work.

5) Such an orientation of the basement fabric with respect to rifting would have potentially made this the Aillik Domain particularly susceptible to ~E-W Mesozoic rifting. Thus, the metamorphic basement fabric is likely to have exerted a considerable effect on rift development by allowing rifting to easily propagate through the proto-Labrador Sea region.

5.8 Future Work

Our fieldwork and subsequent analysis uncovered evidence for multiple brittle deformation events in the Aillik Domain of the Makkovik Province. Establishing a complete chronology of these onshore deformation events should be a priority of future structural work in this region. This

should include attempting to gain an absolute date for the deformation event which was used for the stress inversion in this study. Future studies should also aim to collect data and conduct similar analysis elsewhere on the Labrador margin. The possibility for future studies in light of the preliminary results detailed in this chapter is expanded upon in Chapter 8.

Chapter 6

The role of pre-existing structures during continental breakup and transform system development in the Davis Strait, offshore West Greenland

The contents of this chapter have been presented at the following conferences:

- American Association of Petroleum Geologists (AAPG) Annual Convention and Expedition (ACE) 2014 in Houston, USA and now available in Search and Discover as:

  Peace, A., McCaffrey, K., Imber, J., Hobbs, R., van Hunen, J., and Gerdes, K., (2014). Formation of the volcanic margins of West Greenland and North- Eastern Canada. AAPG ACE Houston, AAPG Search and Discovery, doi:10.13140/RG.2.1.1545.1128

- The 4th Conjugate Margins conference 2014, St. Johns, Newfoundland as:

  Peace, A., McCaffrey, K., Imber, J., Hobbs, R., van Hunen, J., Foulger, G. and Gerdes, K., (2014). Formation of the West Greenland Volcanic margin: Exploring alternatives to the plume hypothesis. 4th Atlantic Conjugate Margins Conference, p161-162, doi: 10.13140/RG.2.1.4727.1925

- The research collaboration showcase at PETEX 2014 as:

  Peace, A., Gerdes, K., McCaffrey, K., Imber, J., Hobbs, R., van Hunen, J., (2014). Formation of the West Greenland Volcanic Margin. PETEX Research Collaboration showcase.

- The Arthur Holmes Meeting 2016, London, UK

  Wilson, R., McCaffrey, K., Holdsworth, R., **Peace, A.,** Imber, J and GEUS., (2016). Tectonic inheritance during extension in rifts and passive margins: A Greenland Case Study. Arthur Holmes Meeting 2016. The Wilson Cycle: plate tectonics and structural inheritance during continental deformation.

This work has also received the following awards:

- 1st place student poster at the 4th Conjugate Margins conference, 2014
- 2nd place in the research collaboration showcase at PETEX, 2014

6.0 Summary

Continental breakup between West Greenland and North Eastern Canada produced the small oceanic basins of the Labrador Sea and Baffin Bay. These are separated by the Davis Strait bathymetric high located offshore West Greenland which represents a transform fault system located mostly on continental crust. Here we interpret 2D seismic reflection data from the Davis Strait constrained using exploration wells, gravity and crustal thickness data to produce a series of seismic surfaces, isochrons and a new offshore fault map. The results have been integrated with plate reconstructions and onshore structural data to build a two stage conceptual model for the offshore fault evolution in which early rift basin formation was controlled primarily by reactivation of pre-existing basement structures. While, this control diminished into the postrift, the location of synrift basins still exerted some control on the location of sedimentation probably due to differential sediment compaction.

6.1 Introduction

Understanding the mechanisms controlling the process of continental breakup (e.g. McKenzie, 1978; Lister et al., 1991) is crucial to further our understanding of the behaviour of the crust under extension (e.g. Autin et al., 2013) as well as reducing the exploration risk at rifted continental margins (e.g. Skogseid, 2001). One such group of interrelated mechanisms that may exert considerable control on the various aspects of continental breakup is the influence that pre-existing geological structures may exert upon rifting and subsequent breakup (e.g. Ravelo et al., 2006; Gibson et al., 2013; Manatschal et al., 2015; Chenin et al., 2015). Here, we consider the role that pre-existing structures potentially played in the initiation and evolution of continental breakup between West Greenland and Eastern Canada.

Pre-existing structures are defined as mechanical anisotropies in the prerift rocks which occur on a variety of scales from metamorphic mineral fabrics to major tectonic boundaries at the largest scale (Chattopadhyay and Chakra, 2013). Tectonic inheritance is the process by which such pre-existing structures may influence a subsequent geological event (Holdsworth et al., 2001a), a phenomenon that has been attributed to observations at both convergent (Ryan, 2001) and divergent tectonic settings (Ravelo et al., 2006). A complete geological cycle of tectonic inheritance has been proposed in which continental breakup occurs along the major weaknesses formed by older orogenic belts (Wilson, 1966), although this is considered to be an over simplification by some work as orogenic activity may actually produce stronger lithosphere that is in fact harder to rift (Krabbendam, 2001).

Understanding the role of tectonic inheritance is key to understanding many aspects of lithospheric deformation, including rifting (e.g. Autin et al., 2013) and passive margin formation (Ravelo et al., 2006). An abundance of previous work has shown that pre-existing structures can profoundly influence numerous aspects of the rifting process including; magmatism (e.g. Bureau et al., 2013), sedimentary basin geometry (e.g. Morley et al., 2004), fault locations and timing (e.g. Korme et al., 2004). The extent to which pre-existing structures influence rift development has been researched using a variety of methods including; natural examples (Morley et al., 2004), numerical models (Cloetingh et al., 1995), analogue experiments (Chattopadhyay and Chakra, 2013) and combinations of these (Corti et al., 2007).

The rejuvenation of pre-existing crustal and lithospheric features essentially occurs via two related processes; reactivation and reworking (Holdsworth et al., 2001a). Reactivation involves the rejuvenation of discrete structures (e.g. Bellahsen et al., 2006), whereas reworking involves repeated focusing of metamorphism, deformation or magmatism on the same crustal or lithospheric volume (e.g. craton reactivation - Tappe et al., 2007; repeated

metamorphism - Manhica et al., 2001). However, both reactivation and reworking may represent the same processes operating at different scales and thus some ambiguity exists in distinguishing between the these two processes in the literature (Holdsworth et al., 2001a). In this study we consider the roles of both reactivation and reworking as endmember processes both of which could have influenced the incomplete breakup of Greenland and North America. Of particular relevance to this study however is the reactivation of discrete pre-existing structures as a possible mechanism to produce normal faults that are not perpendicular to the regional extension direction (e.g. Morley et al., 2004; De Paola et al., 2005) and the role of large-scale basement terrains during rifting (e.g. Krabbendam, 2001).

6.2 Rifting between Greenland and Canada

The Labrador Sea and Baffin Bay (Fig. 6.1) formed due to divergent plate motion between Greenland and North America (e.g. Chalmers and Pulvertaft, 2001). Several phases of rifting between Greenland and North America prior to continental breakup are recognised (Fig. 6.2). According to Oakey and Chalmers (2012) rifting in this region can be summarised into three stages: 1) the Palaeocene separation between North America and Greenland whilst still attached to Eurasia, 2) the Eocene continued separation between Greenland and North America including separation between Eurasia and Greenland (Greenland moving as a separate plate) and 3) since the Oligocene continued separation between Eurasia and Greenland with Greenland being attached to North America i.e. the cessation of seafloor spreading to the west of Greenland (Fig. 6.2).

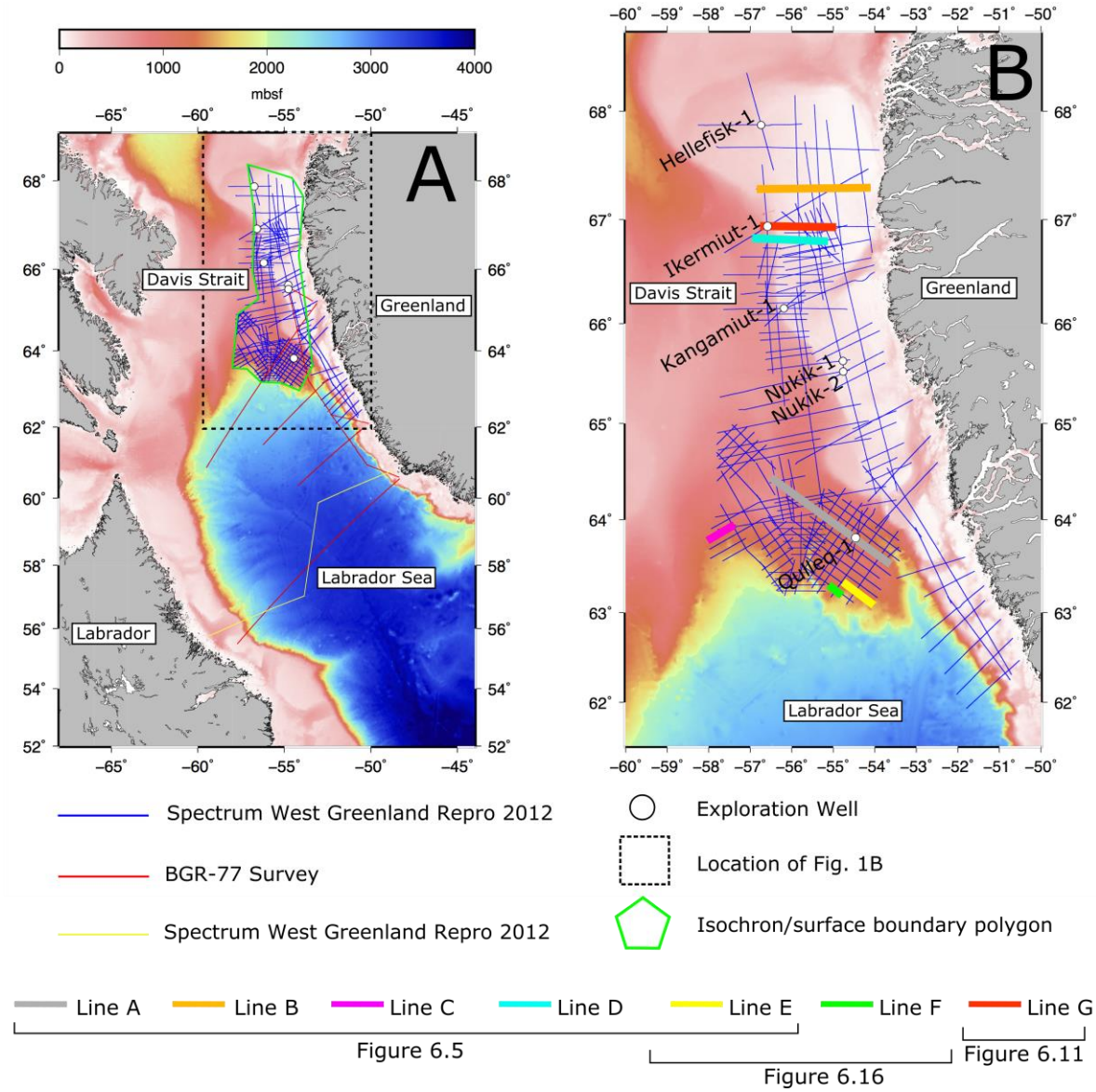

Figure 6.1

A) An overview of the study area in the Davis Strait depicted using the bathymetry data from Smith and Sandwell V17.1. The navigation data from the three seismic datasets are plotted along with the polygon used for surface generation in this study, the locations of the 6 exploration wells in the Davis Strait and selected seismic reflection lines profiles depicted in this chapter. B) The location of the study area in the context of the northwest Atlantic again plotted using the bathymetry data from Smith and Sandwell V17.1.

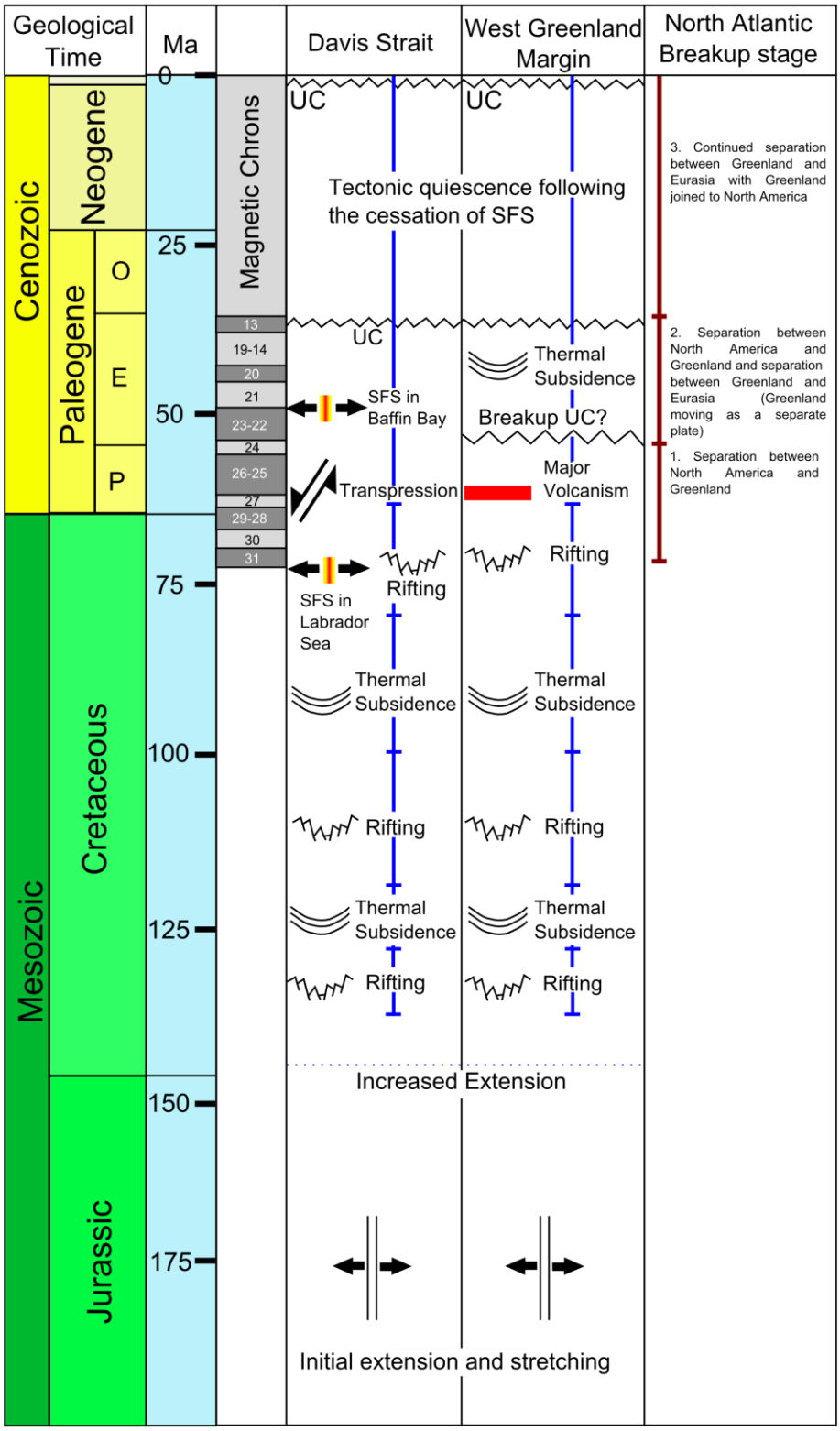

Figure 6.2

Summary of tectonic events in the Davis Strait and West Greenland. modified from McGregor et al. (2012) and Schenk (2011). The North Atlantic breakup stages refer to Oakey and Chalmers (2012).

Continental breakup between West Greenland and Eastern Canada resulted in oceanic spreading in the Labrador Sea and Baffin Bay but not the Davis Strait (Figs. 6.2 and 6.3) prior to the cessation of extension in the region and the opening of the North Atlantic to the east of Greenland (Roest and Srivastava, 1989). The earliest rifting and thus the oldest and most extensive oceanic crust in the Labrador Sea – Baffin Bay system is found in the Southern Labrador Sea (e.g. Srivastava, 1978). Lithospheric stretching in Baffin Bay is also believed to have been sufficient to initiate seafloor spreading (Suckro et al., 2012), although the extent both spatially and temporally of oceanic crust in Baffin Bay is certainly less than that of the Labrador Sea (e.g. Srivastava, 1978). The Davis Strait is a bathymetric high (Fig. 6.1), primarily consisting of continental crust (Dalhoff et al., 2006) which links the small oceanic basins of the Labrador Sea and Baffin Bay via the Ungava transform fault system (Suckro et al., 2013). The Ungava Fault System may represent a 'leaky transform' type setting (Funck et al., 2012) where small amounts of oceanic crust may have been produced at pull-apart basin type settings during rifting but full oceanic spreading has not been initiated as it certainly was in the Labrador Sea and most likely in Baffin Bay (Srivastava, 1978).

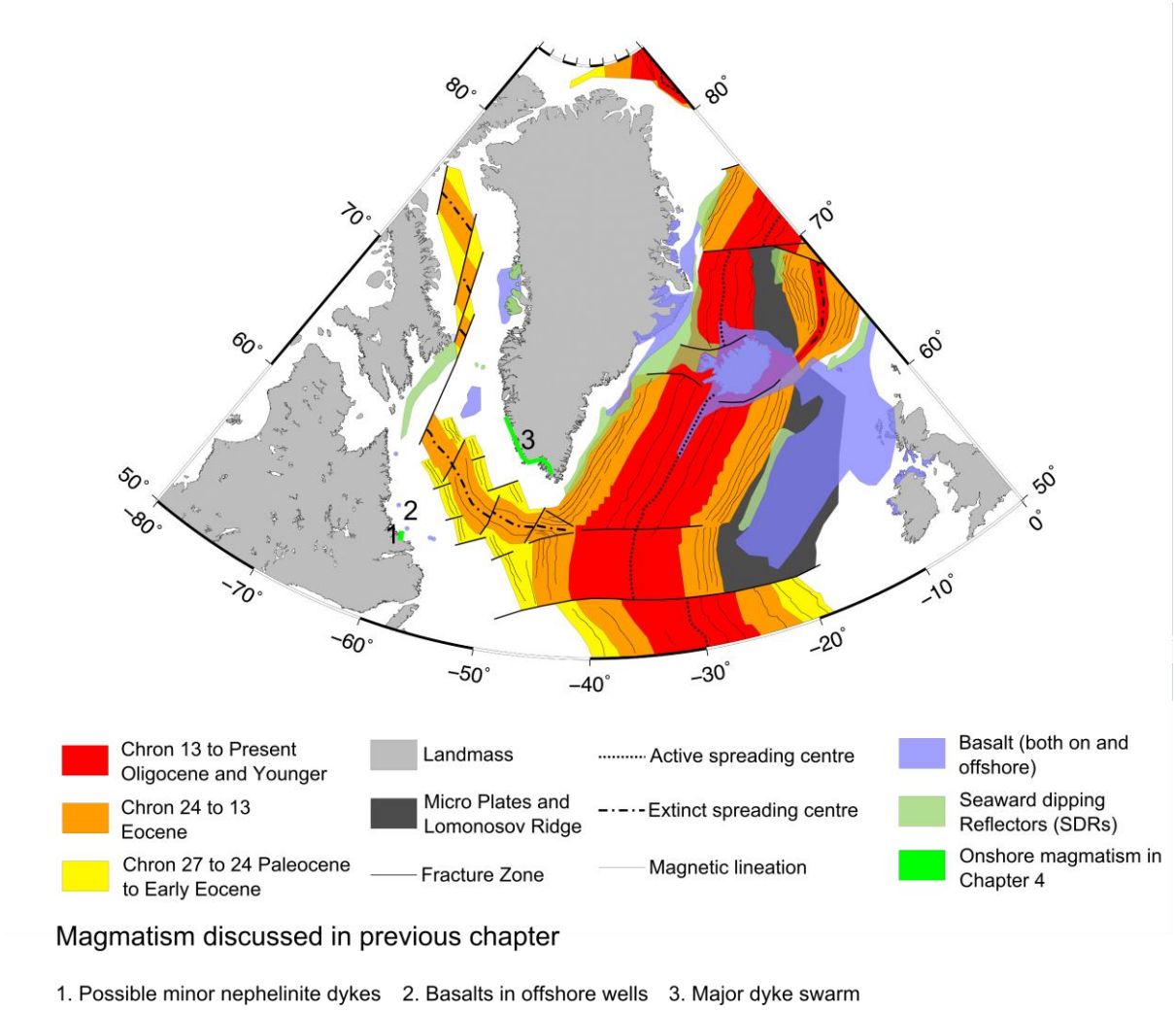

Figure 6.3

An overview of the North Atlantic oceanic spreading systems, including: the age of oceanic crust; major active and extinct spreading axes; major oceanic fracture zones; proposed microplates; and magnetic lineations (Oakey and Chalmers, 2012). The spatial distribution of on and offshore flood basalts and seaward dipping reflectors (SDRs) are overlain (Larsen and Saunders, 1998) in addition to the magmatism discussed in the previous chapter.

In addition to the along margin variability in the manifestation and extent of continental breakup, the abundance and type of igneous rocks (Fig. 6.3) produced during rifting and breakup also varies considerably along the West Greenland Margin (e.g. Keen et al., 2012). The margins of the southern Labrador Sea are classified as typical non-volcanic

margins (Chian et al., 1995a) which become increasingly volcanic in the northern Labrador Sea, Davis Strait (Keen et al., 2012), and Baffin Bay to the north (Suckro et al., 2012). The Davis Strait is classified as a volcanic passive margin (VPM) (Chalmers, 1997) due to the presence of multiple phases of volumetrically extensive igneous rocks (Storey et al., 1998) and a 4-8 km thick high velocity underplated layer (Funck et al., 2007). However, 'volcanic transform margin' may provide a better description for the tectonic setting of the Davis Strait as there is no true oceanic crust (Suckro et al., 2013) and thus no clear ocean-continent transition as would be required for the Davis Strait to be classified as a typical VPM.

6.3 Basement terrains of West Greenland and North Eastern Canada

In order to determine the relationship, if any, between pre-existing geological structures and their influence upon the manifestation of rifting and margin forming processes it is crucial to understand: 1) the sequence of events prior to rifting; 2) the nature of the structural heterogeneities produced by previous events; and 3) the orientation of subsequent rifting with respect to these pre-existing structures. Here we consider the main tectonic units that form the basement of West Greenland and North Eastern Canada and the pre-existing structures they contain. The orogenic events which formed the basement units of this region can be broadly considered to be of three ages (Fig. 6.4). Although the study area (Fig. 6.1) is only comprised of two of these tectonic units (the Nassugtoqidian and the North Atlantic Craton) it is important to understand the crustal makeup of the surrounding units as these may have also influenced the rifting and breakup process.

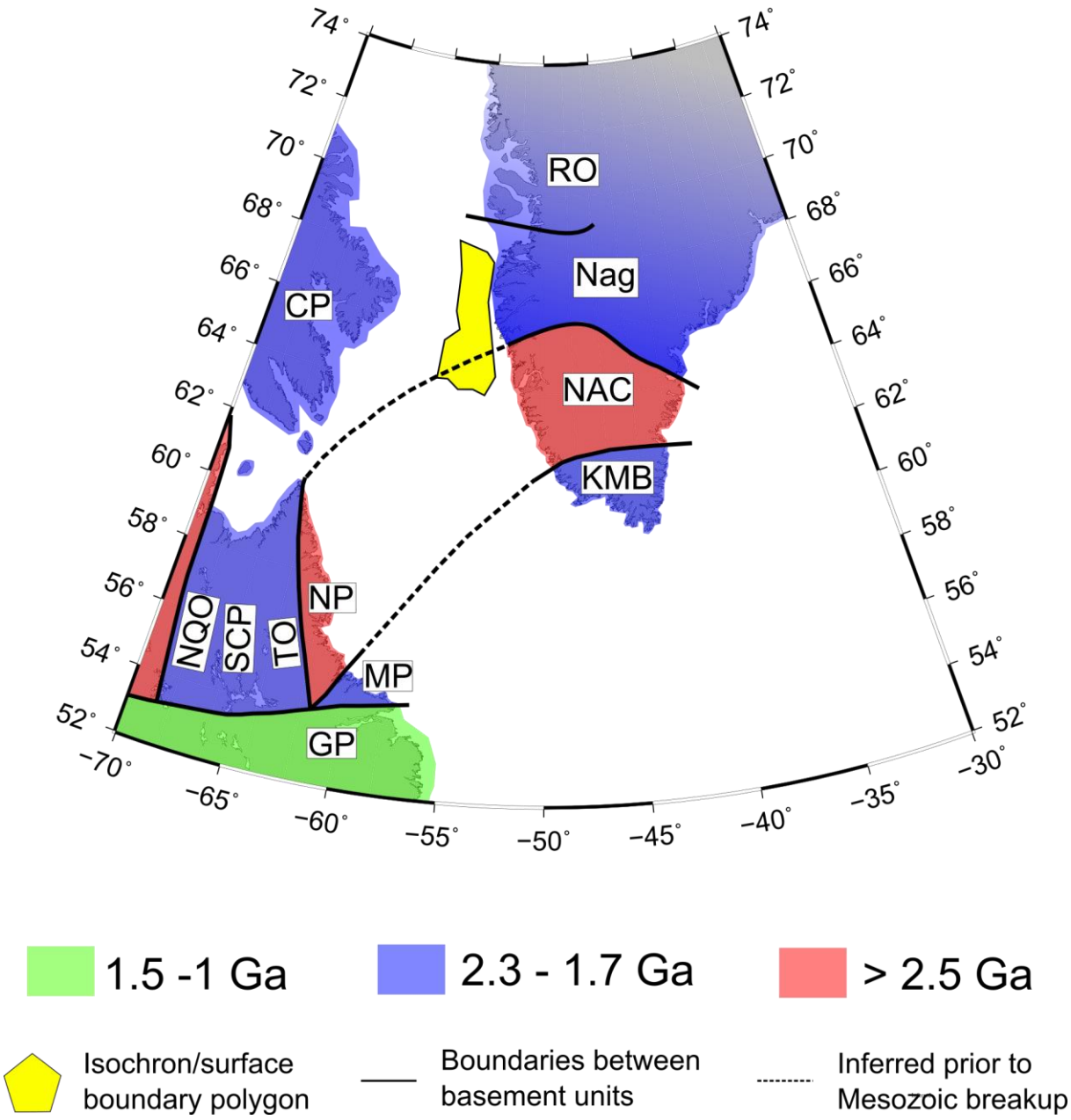

Figure 6.4

The primary study area (yellow polygon) within a simplified overview of basement units in north eastern Canada and Greenland modified from Kerr et al. (1997) and Van Gool et al. (2002), including the location of the boundary polygon used in this study. RO = Rinkian Orogen, Nag = Nagssugtoqidian, CP = Churchill Province, NQO = New Quebec Orogen, SCP = Southern Churchill Province, TO = Torngat Orogen, NP = Nain Province, MP = Makkovik Province, GP = Grenville Province, NAC = North Atlantic Craton and KMB = Ketilidian Mobile Belt.

6.3.1 Nagssugtoqidian and Torngat Orogens

The Nagssugtoqidian Orogen is a belt of Paleoproterozoic deformation and metamorphism in West Greenland (Van Gool et al., 2002) that is bordered to the south by the North Atlantic Craton (NAC) and to the north by the less well-studied Rinkian Orogen and Rae craton (Pulvertaft, 1986). Together, the Nagssugtoqidian and Rinkian orogenic belts may represent a c. 1100 km wide zone of Paleoproterozoic reworking and crustal accretion (Van Gool et al., 2002). The Nagssugtoqidian Orogen is proposed to continue under the ice through central Greenland before reoccurring in East Greenland. The Nagssugtoqidian Orogen is considered to have developed simultaneously with the Torngat Orogen (Fig. 6.4) of Northern Labrador, where both the Torngat and Nagssugtoqidian orogenic belts are interpreted to have formed part of the same passive margin prior to ocean closure and continental collision (Van Gool et al., 2002). This continental collision model of formation is preferred over earlier interpretations of an intra-continental strike-slip setting due to the presence of Paleoproterozoic calc-alkaline dykes which have been attributed to a subduction zone type tectonic setting (Korstgård et al., 1987). Reworked Archean gneisses form a large majority of the Nagssugtoqidian (Van Gool et al., 2002).

6.3.2 The North Atlantic Craton and Nain Province

The North Atlantic Craton is the Archean terrain immediately south of the Nagssugtoqidian and the north of the Ketilidian Mobile Belt (Nutman and Collerson, 1991) (Fig. 6.4). It consists of very early Archean supracrustal rocks, orthogenesis and massive ultramafic rocks. The Archean rocks of West Greenland span the interval 3850 – 2550 Ma (Polat et al., 2014) and are the result of a complex sequence of magmatic, structural and metamorphic events. The Nain Province, Labrador is considered to be the North American continuation of the North Atlantic Craton (St-Onge et al., 2009) (Fig. 6.4).

6.3.3 The Ketilidian Mobile Belt and the Makkovikian Orogen

Paleoproterozoic accretion of crust is recorded in both the Makkovik Province of Labrador (Ketchum et al., 2002) and the Ketilidian Mobile Belt of West Greenland (Garde et al., 2002) (Fig. 6.4). This accretion is likely to have occurred in a convergent arc-continent type active margin (Ketchum et al., 2002). Both the Makkovik Province and the Ketilidian Mobile Belt were largely assembled by 1.71 Ga, after which orogenesis related plutonism and deformation had essentially ceased (Ketchum et al., 2002). Ketchum et al. (2002) thus consider orogenesis to have spanned the interval of 1.9-1.7 Ga, with the original width of the orogenic belt being a minimum of 350 km as preserved in the Ketilidian of southern Greenland.

6.3.4 Onshore structural studies in West Greenland

Investigation of the onshore structural systems in West Greenland has been conducted in the Ketilidian Mobile Belt and North Atlantic Craton domains by Japsen et al. (2006) and in the Nagssugtoquidian orogen by Wilson et al. (2006). Both of these studies analysed Landsat data at both 1:500,000 and 1:100,000 scales, aerial photography and field based studies to ground truth the remote methods. The results of Japsen et al. (2006) and Wilson et al. (2006) are summarized in Table 6.1.

System No.	**Ketilidian Mobile Belt** (Japsen et al., 2006)			**North Atlantic Craton** (Japsen et al., 2006)				**Nagssugtoqidian** (Wilson et al., 2006)
	Landsat		*Field*	*Landsat*		*Aerial*	*Field*	*Landsat, Aerial, Field*
	1:500,000	*1:100,000*		*1:500,000*	*1:100,000*			
1	NE-SW	No Dominant system. A range from NE-SW through to SE-NW.	N-S	N-S	N-S		N-S	ENE-WSW
2	N-S		NE-SW/ ENE-WSW	NE-SW	NE-SW	NE-SW	NE-SW	N-S
3	NNW-SSE		E-W	ENE-WSW	ENE-WSW	ENE-WSW	ENE-WSW	NNW-SSE
4	NNE-SSW		ESE-WNW/ SE-NW	ESE-WNW	ESE-WNW		SE-NW	NNE-SSW
5	E-W to ESE-WNW							E-W to ESE-WNW

Table 6.1

Summary of the onshore structural systems identified using different methodologies in the Ketilidian Mobile Belt, the North Atlantic Craton (Japsen et al., 2006) and the Nagssugtoqidian by Wilson et al. (2006) and Japsen et al. (2006). Orientations quoted in this table represent the strike of the feature, whilst the observed kinematics associated with these structures are discussed later in this chapter in conjunction with the results of our analysis.

6.4 Methodology and datasets

This work integrates both geological and geophysical data from multiple sources. Two 2D seismic surveys were used; the Spectrum West Greenland 2012 Repro and the BGR-77 survey. Lines from further south in the Labrador Sea contributed to the regional context of this study (90-1, 90-2 and 90-3 - Chian et al., 1995). The spatially discrete seismic and exploration well datasets (Fig. 6.1) are complimented by the continuous bathymetry and free air anomaly (FAA) data (Smith and Sandwell, 1997; Sandwell et al., 2014). Crustal thickness data (Welford and Hall, 2013) were also used in this study to provide regional context.

Interpretation of the seismic data, including the integration with the exploration wells and other geophysical datasets was primarily carried out in Schlumberger's Petrel, however some of the analysis utilised ArcGIS, MATLAB and Generic Mapping Tools (GMT). As in previous work on these datasets, all interpretation and analysis was carried out and is presented in two way travel time (TWTT) (e.g. Døssing, 2011; McGregor et al., 2012; Gregersen and Skaarup, 2007; Dalhoff et al., 2003; Sørensen, 2006), an approach that is common in many other seismic interpretation projects (e.g. Wu et al., 2016).

6.4.1 Isochron reconstruction

Isochrons were produced for the total sediment thickness (TST - seafloor to basement) and for eleven interpreted horizons between the seafloor and the basement (Fig. 6.5). The isochron maps enable us to reconstruct where sedimentary depocentres were located during defined geological intervals, particularly when the location and nature of erosional surfaces is also included. In conjunction with interpretation of erosional surfaces between the dated horizons, this this mapping enables us to place constraints on the depositional and erosional history of the study area. The primary study area for the isochron reconstruction

is defined by a c. 610 km long and c. 230 km wide polygon shown in Figure 6.1. The northerly limit of the study area is 68.3°N/-57.1°W, whilst the most southerly point is 62.9°N/54.1°W.

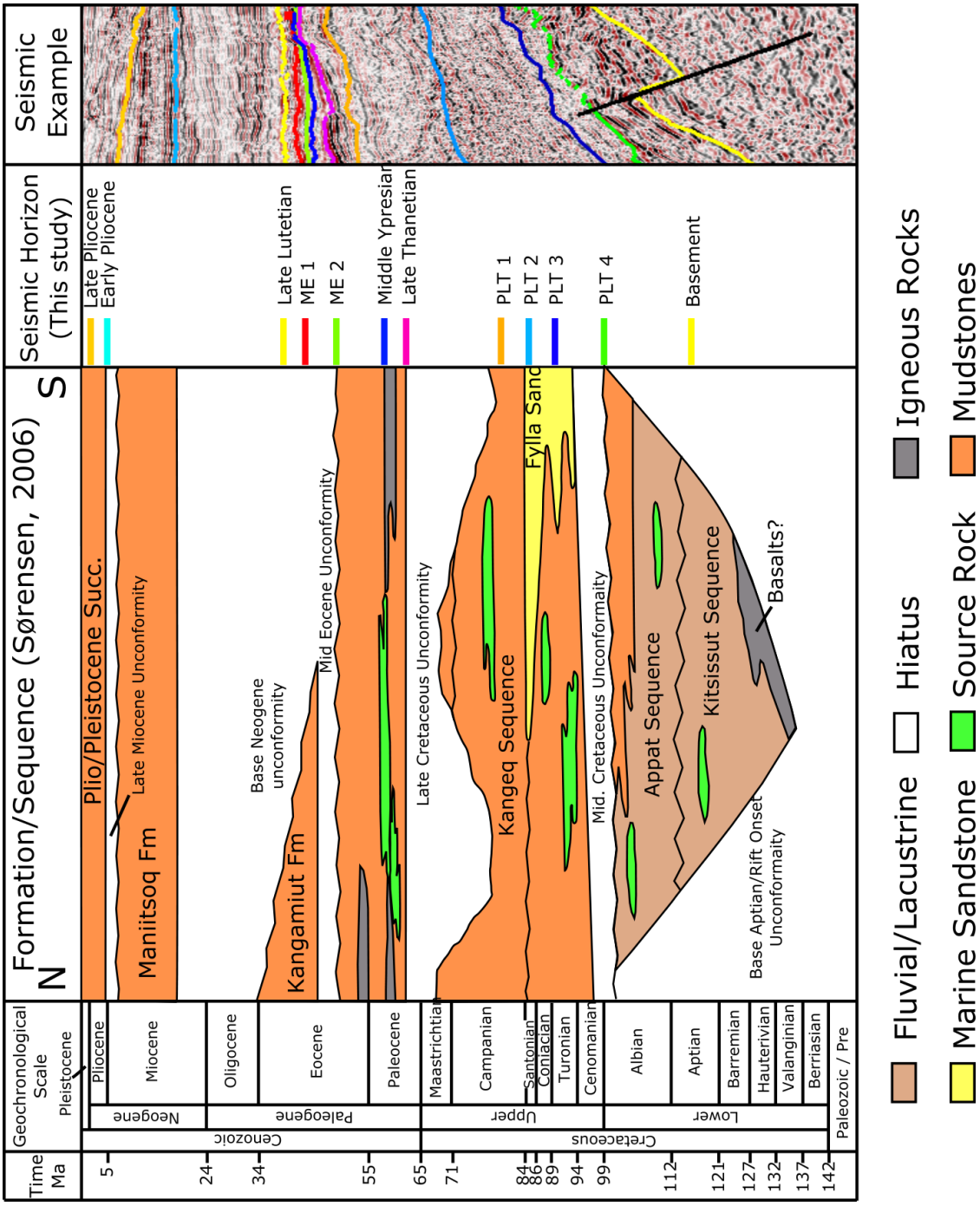

Figure 6.5

Stratigraphic framework for the study area offshore West Greenland (Fig. 6.1) modified from Sørensen (2006) to include the stratigraphic locations of the horizons interpreted in this study.

The first stage of the isochron reconstruction was to identify key surfaces that were capable of being traced across the seismic data in the study region. These surfaces are typically unconformities or high amplitude reflectors (Fig. 6.6). Figure 6.6 shows representative seismic reflection profiles from across the study area. The approximate locations of these lines is shown on Figure 6.1 in addition to other seismic reflection lines described later in this chapter. All profiles included on this figure are extracts from Spectrum's West Greenland repro 2012 survey. The fundamental principle in seismic stratigraphy is that within the resolution of the seismic data, the reflected horizons approximately follow chronostratigraphic surfaces and thus seismic horizons can be considered to approximate time lines that represent discrete events in geological time (Vail and Mitchum, 1977). Due to the sparse nature of the seismic grid horizons were picked on all lines and no auto tracking was used.

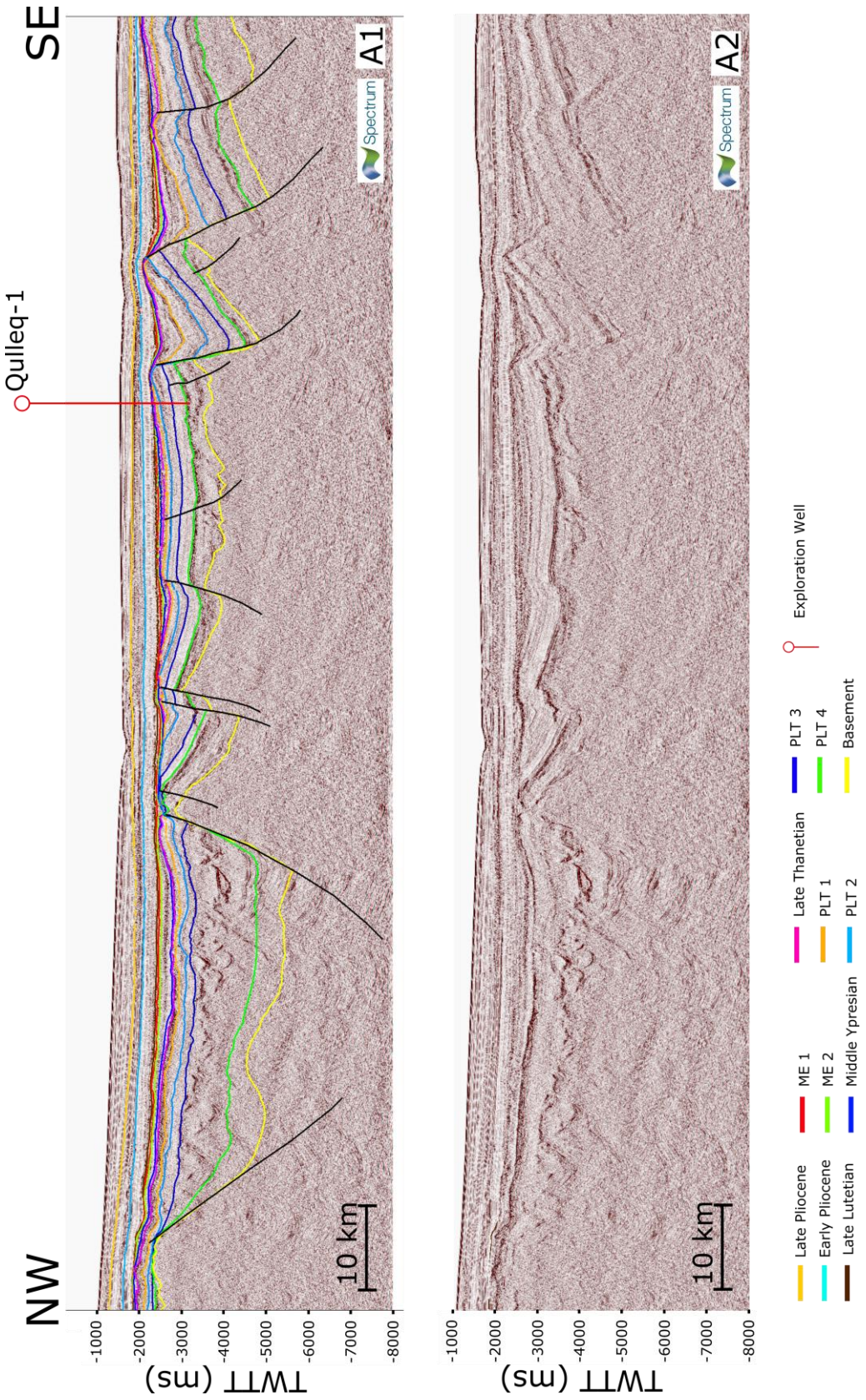

Figure 6.6A

NW-SE orientated seismic line from the southeast of the study area.

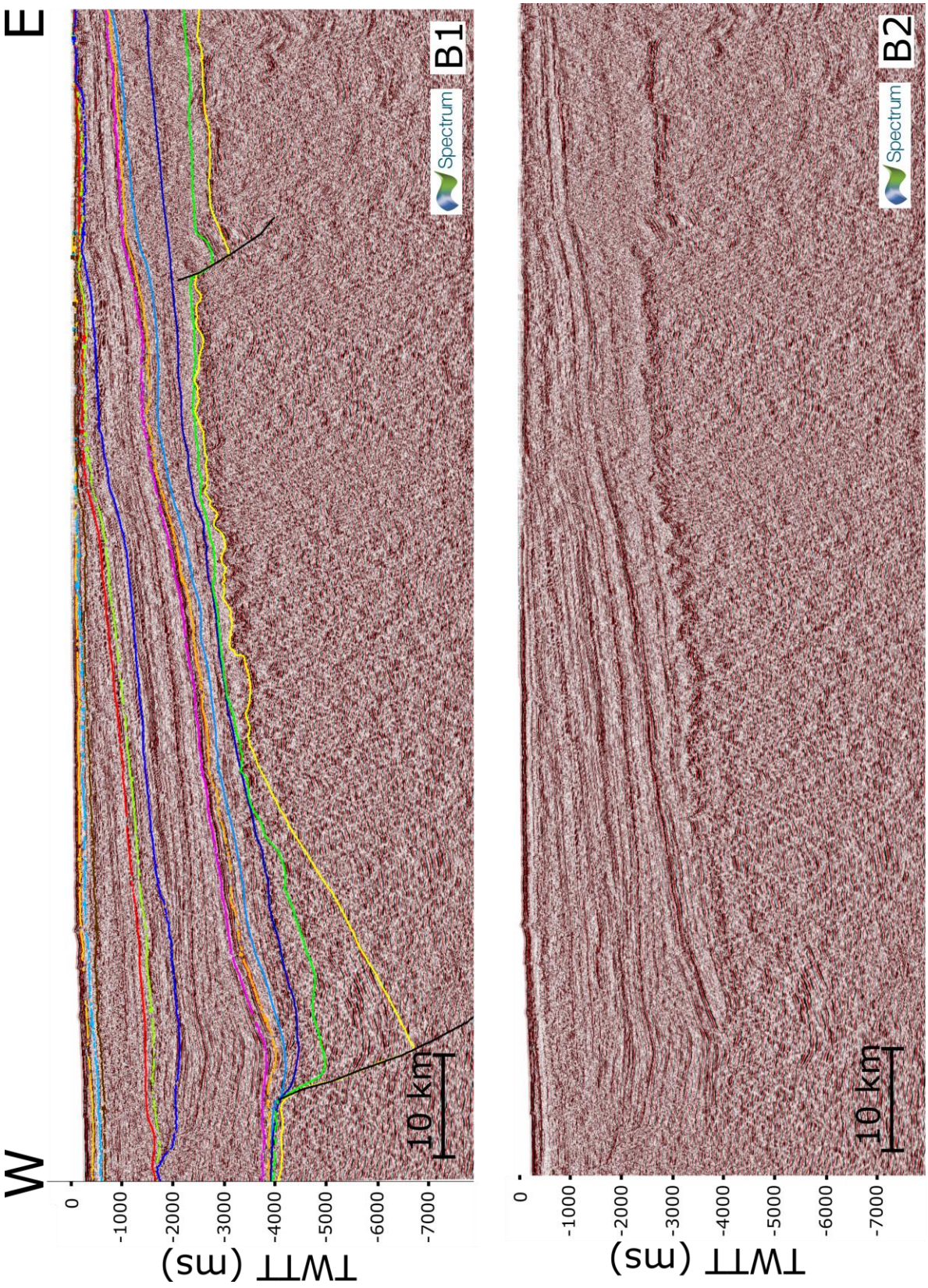

Figure 6.6B

W-E trending seismic line from the north of the study area.

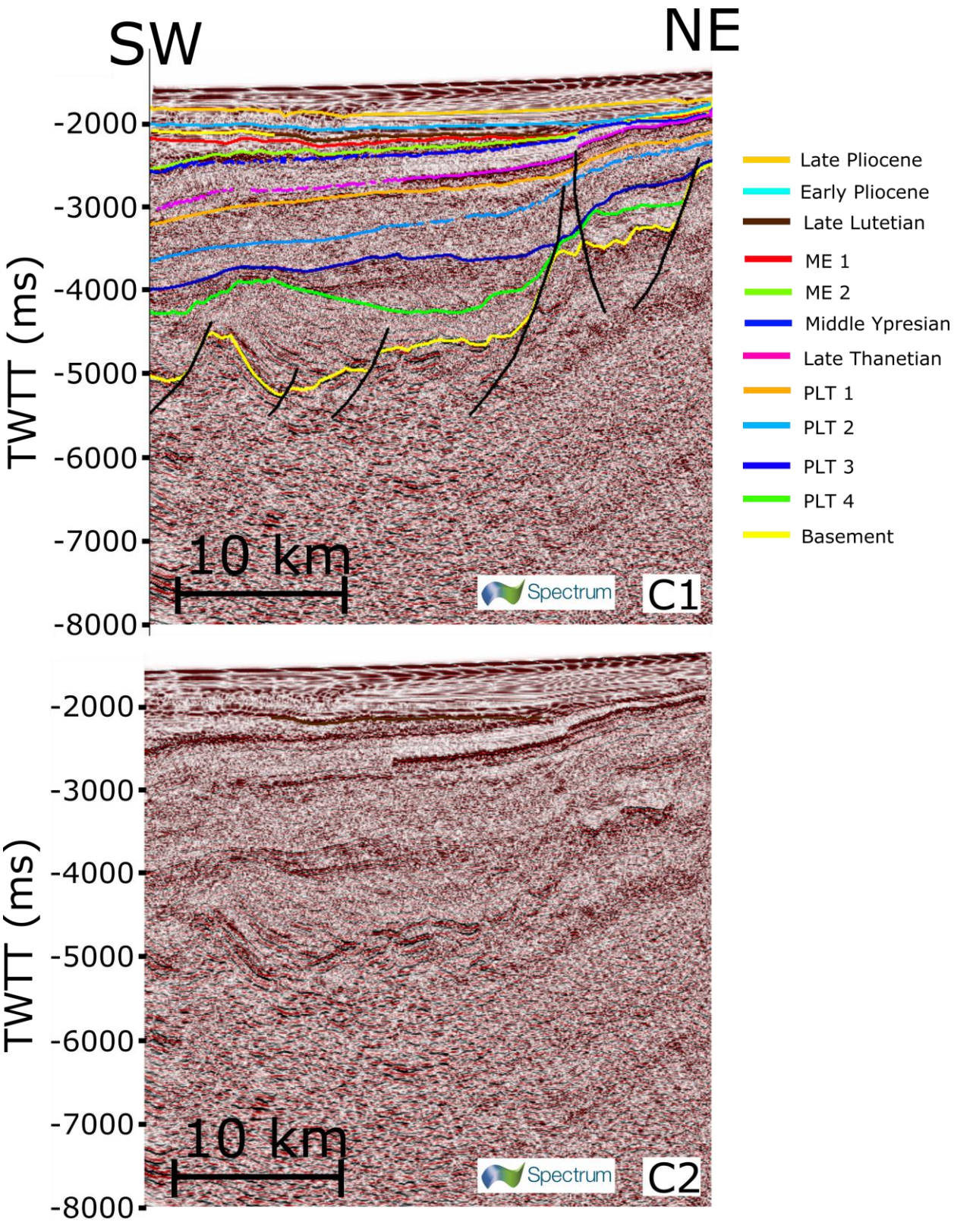

Figure 6.6C

NE-SW orientated seismic line from the southwest of study area.

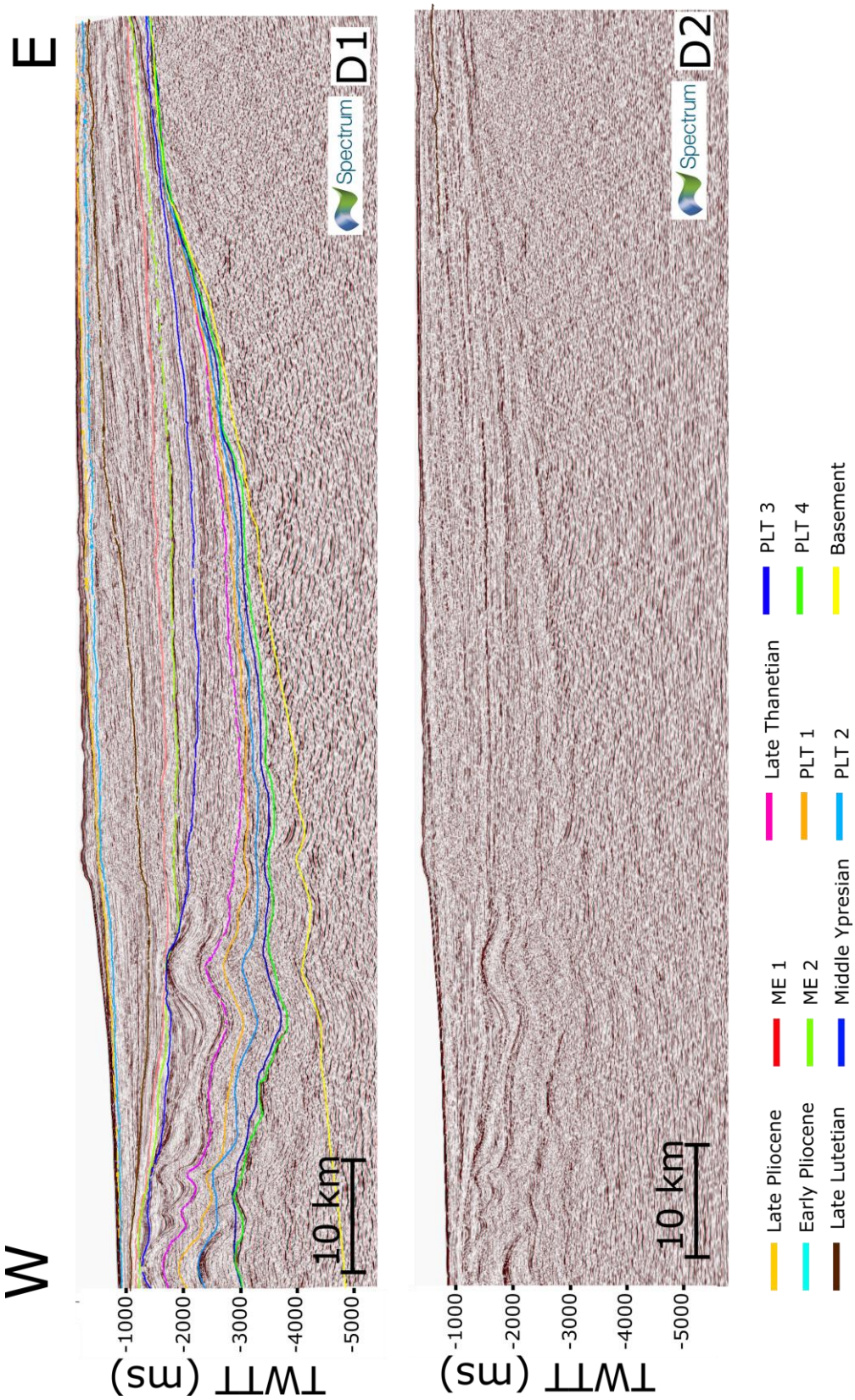

Figure 6.6D

W-E trending seismic line from the north of the study area.

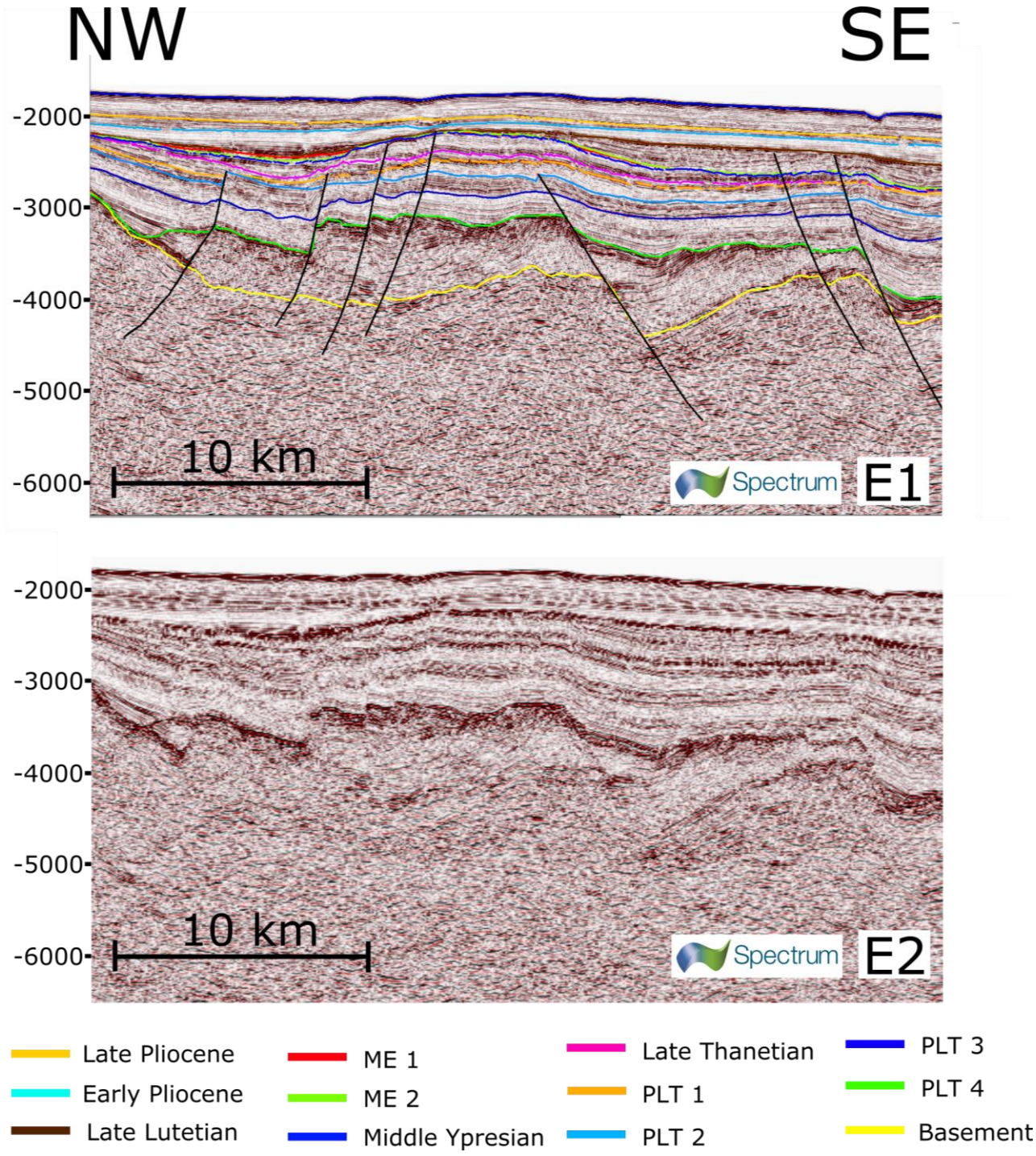

Figure 6.6E

NW-SE orientated seismic line from the south of the study area.

This study utilises data from six exploration wells (Table 6.2) that are with the exception of the two Nukik wells not located near one another (Rasmussen et al., 2003). The six exploration wells were tied to the nearest seismic lines using the checkshots collected at

the wellsite to convert well depth in metres to depth in TWTT. The seismic-well ties were then checked against the same ties made between the seismic data and the wells by the previous work (e.g. Døssing, 2011; Dalhoff et al., 2003). Having tied the exploration wells to the 2D seismic surveys, the horizons were dated using the nearest dated samples in the wells. This temporal constraint provided by the biostratigraphic analysis (Rasmussen et al., 2003; Nøhr-Hansen, 2003; Piasecki, 2003; Rolle, 1985) allows us to relate events depicted in the horizons and isochrons to observations made elsewhere, particularly the onshore geology of West Greenland and Eastern Canada (e.g. St-Onge et al., 2009).

Well Name	Latitude	Longitude	Date	TD	TD Lithology/Formation
Hellefisk-1	67.877944	-56.739161	21/06/1977	3201.2	Basalt (Paleocene?)
Ikermiut-1	66.936572	-56.590681	12/07/1977	3619	Campanian shales
Kangamiut-1	66.150256	-56.190078	02/06/1976	3874	Precambrian basement
Nukik-1	65.526719	-54.760497	02/07/1977	2363.4	Precambrian basement
Nukik-2	65.631775	-54.766831	08/08/1977	2693.8	Masstrichtian Basalt
Qulleq-1	63.813342	-54.451836	10/07/2000	2973	Near base Santonian

Table 6.2

Summary of exploration wells in the Davis Strait with the terminal depth in metres from the RT (rotary table - m) used in this study. Lithology at TD (terminal depth) from Nøhr-Hansen (2003) and (Rolle, 1985).

Using dinoflagellate cysts, twenty one intervals are defined by Nøhr-Hansen (2003) from the late Eocene to the late Early Paleocene, which have been correlated with a new microfossil zonation and previously established North Sea zonations (Bujak and Mudge, 1994). The work of Piasecki (2003) also used dinoflagellate cysts but only on the Qulleq-1 well (Fig. 6.1). The stratigraphy and well correlation is based upon the last appearance datum and abundance of stratigraphically significant species (Nøhr-Hansen, 2003). Where

no material in the well has been identified for a desired interval the position in the well was estimated by tracking seismic horizons that have been tied to surrounding wells and using the next oldest and youngest defined intervals as guidance. In our study this scenario applied to the youngest horizons (Late Lutetian, Early Pliocene and Late Pliocene), at the lower limit of the geological time interval. Some horizons were traced across the study area that could not be exactly tied to dated horizons in any well, thus these surfaces are only age constrained by the dated horizons in proximity to them and interpretations by previous work. This applied to six horizons in this study, two of which occur between the Late Lutetian and Middle Ypresian (the Middle Eocene 1 and 2 horizons), whilst the other four are between the basement horizon and the Late Thanetian (the Pre-Late Thanetian horizons 1 to 4), which is the oldest horizon tied to well data with a biostratigraphic age.

Quality control of the surfaces generated was undertaken to consider the effects of variation in the density of the seismic grid (Fig. 6.7) by progressively removing lines from the basement and the seafloor horizons prior to surface and isochron generation. These tests demonstrated that even with over 50% of the lines removed the approximate locations and geometries of the major depocentres remained unchanged.

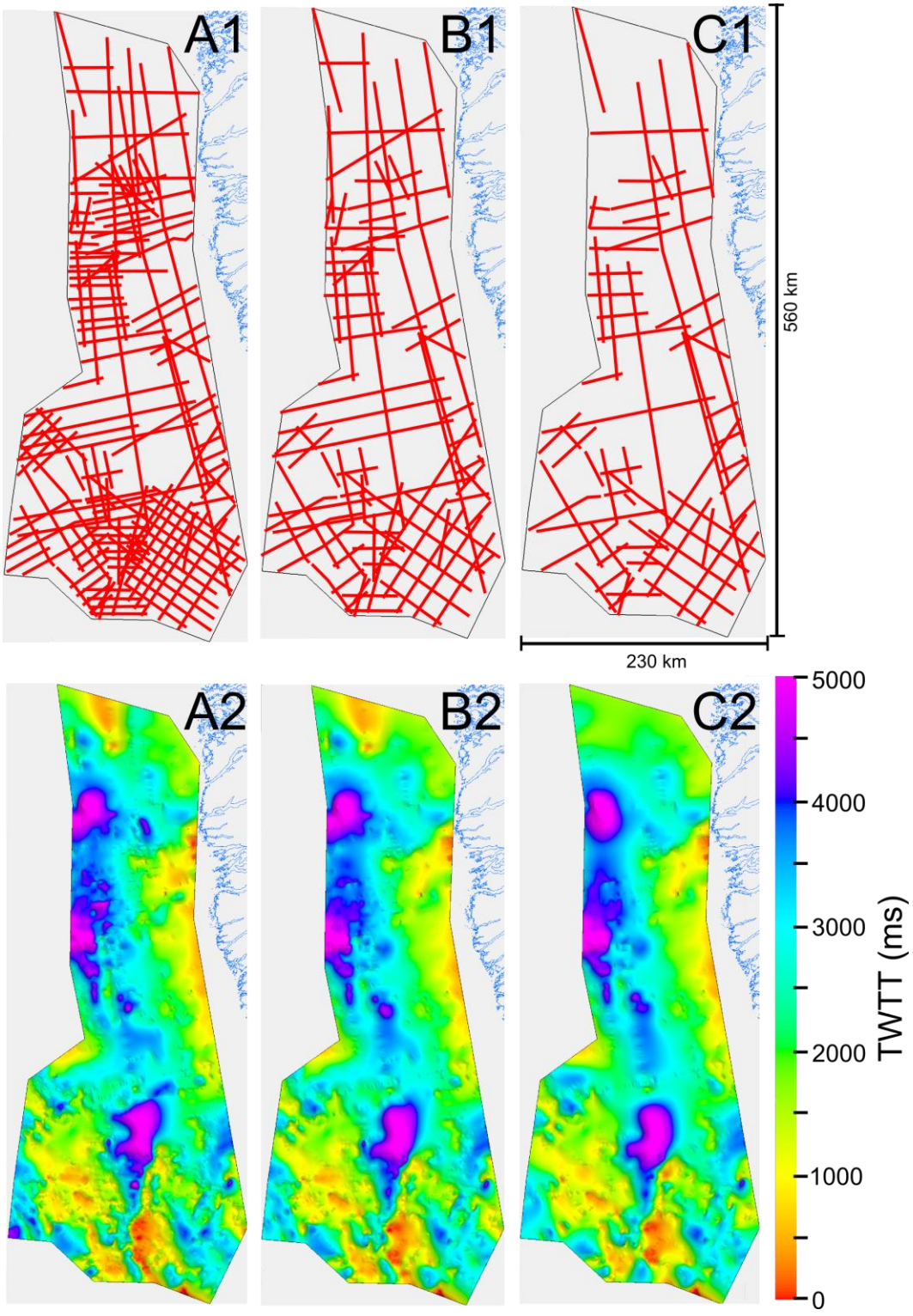

Figure 6.7

Total sediment thickness (top basement horizon to seabed) maps produced after thinning the seismic grid to assess the effects of seismic grid density on surface and subsequent isochron generation. The seismic grid above each isochron depicts the lines used to produce the isochron below.

Our analysis used the gravity data of Smith and Sandwell V23.1 (Sandwell et al., 2014). Both the original free air anomaly (FAA) and a calculated Bouguer anomaly (using an average crustal density of 2.7 gcm^{-3}) were used during the interpretation. Analysis of gravity data was primarily undertaken using the Generic Mapping Tools (GMT) software and in ArcGIS.

6.4.2 Fault mapping and analysis

The aim of the fault mapping was to characterise variations in rift-related deformation that might reveal any potential influence of pre-existing basement structures upon fault location, geometry, orientation and timing.

The first stage of the offshore fault mapping was to interpret faults that offset the basement horizon on the individual 2D seismic lines. These faults were then, where possible, linked between 2D seismic lines primarily based on their orientation, size (both length and offset), style (i.e. normal, strike-slip or thrust) and proximity to one another. Presented herein are the faults that were significant enough to tie between at least two 2D seismic lines and offset the basement horizon. If basin-bounding faults offset the basement horizon and the sediment packages widen towards the footwall they can be considered to be most likely to be related to the Mesozoic rifting and breakup events of interest to this work. 66 faults were deemed capable of being confidently tied between at least two 2D seismic lines. Due to the sparse nature of the seismic grid the free air gravity anomaly (FAA - Sandwell et al., 2014) was used to guide fault linkage between seismic lines, whereby faults were deemed to be likely to follow distinct changes (high horizontal gravity gradient) in the gravity anomaly due to the changes in basement elevation. Previous work has conducted similar offshore fault analysis using seismic reflection data (e.g. Vulcan Sub-Basin, NW Australia - Wu et al., 2016)

We acknowledge that our method has inevitably led to a sampling bias towards larger faults, which may not be representative of the entire fault population as some deformation may have occurred on a scale that is beyond the resolution of the seismic data. Problems with seismic resolution are however intrinsic to the interpretation of seismic data and are not unique to this study.

After interpretation of the fault planes on the seismic data to produce fault plane polygons, polyline shapefiles were created in ArcGIS in order to allow orientation analysis to be conducted. Tracing 2D polylines in map view was again undertaken with the aid of the basement horizon interpretation and free air gravity anomaly V23.1 (Smith and Sandwell, 1997). Analysis of the fault population orientations was conducted using two methodologies. In the first instance fault azimuth was calculated for the entire fault and in the second method faults were split at the polyline vertices prior to azimuth calculation for each individual segment. The second method provides a more realistic representation of fault orientation as many of the faults in the study area change azimuth along strike.

6.4.3 Study limitations

One of the major unavoidable limitations of this work is the spatial distribution of the data (Fig. 6.1). This is particularly apparent in the distribution of the exploration wells with only six wells located in the study area but also in the variability of line density in the 2D seismic grid. The problem of gaps in the data is somewhat overcome by integration of the discrete 2D seismic and well data with the continuous free air gravity and bathymetric data. The effects of the distribution of the 2D seismic grid upon interpreted depocentre geometries have been tested by the grid thinning quality control experiments (Fig. 6.7).

Another potential issue with our methodology of utilising the biostratigraphic ages from the exploration wells (Nøhr-Hansen, 2003) to date horizons is that none of the wells

penetrate particularly deep into the synrift (Table 6.2), as the deepest well in our study area is Kangamiut-1 which has a total depth of 3874 m. Also tracking seismic horizons between discrete basins over basement highs into proximal basins is problematic and does leave some ambiguities in basins without wells, a problem that can only be overcome by acquiring further well data in the area.

The method of interpreting faults, then only using faults capable of being tied between seismic lines could have induced spatial aliasing into our analysis. This is particularly relevant if the large faults follow a different trend to the smaller faults that could not be mapped between 2D seismic lines.

Although our understanding of the regional geology is continually being improved, gaps remain in our knowledge, particularly in the geology beneath the Greenland Ice Sheet and to the north of our study area. For example although the Nagssugtoqidian orogenic belt is observed in both East (Kolb, 2014) and West Greenland (Connelly and Mengel, 2000) its geometry and structure beneath the Greenland Ice Sheet is at present unknown. As such an increase in our understanding of the structure of pre-existing units will help to determine their roles, if any, during rifting and subsequent breakup.

6.5 Results

Representative interpreted seismic lines from across the study area are shown on Figure 6.6 with the locations of these sections shown geographically on Figure 6.1. The interpreted horizons are shown in their stratigraphic positions on Fig. 6.5, whilst the surfaces generated from the interpreted horizons are presented in Figure 6.8 and the isochrons generated from these surfaces are displayed on Figures 6.9 and 6.10. The results of the fault interpretation and mapping are shown on Figures 6.11, 6.12 and 6.13 with the offshore structural map of Chalmers and Pulvertaft (2001) included for comparison on

Figure 6.14. The results of orientation analysis on the fault populations are displayed on Figure 6.15.

6.5.1 Seismic horizon interpretations

This section provides detailed descriptions of the interpreted seismic horizons which were used to generate the surfaces and isochrons in this study. The stratigraphic locations of the interpreted horizons are displayed within the stratigraphic framework provided by Sørensen (2006) based on McWhae et al. (1980) and Balkwill (1987) (Fig. 6.5).

6.5.1.1 Basement horizon

The basement horizon is interpreted as the unconformity (rift onset unconformity – Chapter 2) between the pre-rift and the younger rocks. The distinct unconformable contact representing the basement often, but not always manifests as a high amplitude reflector between reflectors that display minimal organisation and the overlying reflections that in most of the study area are characterised by conformable packages of sediments, some of which contain relatively high amplitude reflectors. This is often one of the most high relief horizons on the seismic profiles. In much of the study area the basement horizon displays a rugose texture. The lack of coherent horizons beneath the interpreted basement can be seen on profiles A-E on Figure 6.6. Although very little organisation is displayed in the reflectors beneath this horizon some high amplitude reflectors are present beneath it which may represent intrusive rocks for example on the south-west end of line C on Figure 6.6.

6.5.1.2 Pre-Late Thanetian Marker 4

Some variation exists in the characteristics of this horizon across the study area, although for the most part its characteristics are consistent, allowing it to be distinguished during interpretation. PLT 4 is usually represented by a high amplitude reflector or reflectors that

are in some cases immediately underlain by a series of further relatively high amplitude reflectors whilst in other cases it is represented by a singular high amplitude reflector. PLT 4 is an unconformity, probably equivalent to the Middle Cretaceous Unconformity in Sørensen (2006). Although the unconformable nature of PLT 4 is displayed on all the seismic reflection profiles in Fig. 6.6 it is particularly apparent in Fig. 6.6E. The reflectors that comprise PLT 4 are usually discontinuous in nature but the horizon as a whole is easily recognised on most seismic lines in the study area as the first high amplitude reflector above the basement horizon. The reflectors below are sometimes chaotic with individual horizons sometimes being difficult to distinguish and trace laterally, however where they can be distinguished they can be seen to be often truncated by PLT 4. The packages of sediments beneath PLT 4 can be seen to expand towards the footwalls of the faults that cut through PLT4. The PLT 4 horizon onlaps onto the basement highs across the study area.

6.5.1.3 Pre-Late Thanetian Marker 3

PLT 3 is characterised by a horizon that is slightly higher amplitude than the horizons above and below which are represented by relatively transparent sediment packages. PLT 3 lies conformably within the sedimentary sequence (Fig. 6.5). The sequences between PLT 3 and 4 can been seen in some areas to expand away from basin bounding faults into the hanging wall sediments. The sequences between PLT 3 and 4 can also be seen in many locations to be crosscut by discontinuous concave upwards high amplitude reflectors which most likely represent igneous intrusions, probably saucer shaped sills (Fig. 6.7A). Above the sills a doming of the horizons is also common (forced folds - Magee et al., 2016). This horizon downlaps onto the PLT 4 and basement horizons across the study area, a phenomena that is particularly apparent in the south of the study area (Fig. 6.6A and E).

6.5.1.4 Pre-Late Thanetian Marker 2

The PLT 2 horizon is similar to PLT 3 in that it lies conformably within the seismic sequence. The reflectivity of the surrounding sequences is variable from transparent in some areas to higher amplitudes elsewhere but PLT 2 always represents a slightly higher amplitude horizon than the surrounding sequences allowing it to be traced.

6.5.1.5 Pre-Late Thanetian Marker 1

As with PLT 2, PLT 1 represents a slightly higher amplitude horizon within a relatively seismically transparent sediment package. The package of reflections between PLT 2 and 1 thins from the centre of the study area to the north and south. On some profiles this horizon can be difficult to distinguish from within the seismically transparent units that bound it. PLT 1 is conformable with the surrounding sequences across the study area.

6.5.1.6 Late Thanetian

The Late Thanetian horizon is one of the most key horizons interpreted as it is easily recognisable across a wide area and in the south of the area it represents a clear unconformable contact which probably extends to the north although this is not clear on the available data. Previous work has recognised a Late Cretaceous unconformity (Sørensen, 2006) which we interpret to represent the eroded stratigraphy prior to this horizon (Fig. 6.6). The Late Thanetian horizon is in many areas represented by a very high amplitude reflector which we interpret to be a reflector from the buried Paleogene flood basalts (e.g. Larsen et al., 1999). The packages from the four PLT horizons can be seen to be clearly truncated by the Late Thanetian horizon (Fig. 6.6A).

6.5.1.7 Middle Ypresian

This high amplitude horizon lies immediately above the unconformity at the top of a seismically low amplitude package of conformable sequences. Although the reflectors comprising this horizon are generally continuous (Fig. 6.6B, C and D) they do occur as less continuous reflectors (e.g. Fig. 6.6A), that typically occur when this horizon is relatively close in TWTT to the Late Thanetian horizon.

6.5.1.8 Middle Eocene Marker 2

The nature of the reflectors constituting the ME 2 horizon vary across the study area, although for the most part its characteristics are consistent enough to allow it to be confidently distinguished during interpretation. On the seismic reflection profiles ME2 usually marks the distinction between a chaotic sediment package in which individual horizons are difficult to determine and the continuous sub-parallel overlying horizons. This horizon can be seen to represent an unconformity over much of the study area. However, where the surrounding packages are thinner in TWTT it is difficult to establish the precise nature of this horizon with the surrounding sequences, a phenomenon particularly paramount in the south of the study area. We interpret the ME 2 horizon to be equivalent to the Middle Eocene unconformity identified by Sorensen (2006) (Fig. 6.5).

6.5.1.9 Middle Eocene Marker 1

ME 1 is a slightly higher amplitude horizon within a generally low amplitude package. The reflectors that comprise this horizon (Fig. 6.6B and D) are usually discontinuous and where the horizon is located close to the other horizons in the south of the study it is difficult to interpret stratigraphic relationships. We interpret the ME 1 horizon to be conformable within the stratigraphic succession across the study area.

6.5.1.10 Late Lutetian

The late Lutetian horizon is a relatively high amplitude reflector at the top of a low amplitude package that can be traced across the study area. The reflectors which comprise this horizon are generally sub-parallel, although in some areas the horizon becomes locally chaotic and indistinct making it more problematic to interpret. The package of horizons between the Late Lutetian and the ME 1 expand northwards and contains many horizons which could be traced locally but not across the study area, these may belong to the Kangamiut formation which is present in the north but not the south (Sørensen, 2006) (Fig. 6.5).

6.5.1.11 Early Pliocene

The Early Pliocene horizon is mostly characterised by medium to high amplitude reflectors that represent a widespread unconformity within the stratigraphic succession, with the sequences above downlapping onto this horizon (Fig. 6.6D). We interpret this unconformity to be equivalent to the Late Miocene unconformity interpreted by Sørensen (2006) (Fig. 6.5). The stratigraphic successions above this horizon are typically sub-parallel, although sigmoidal packages are also present in proximity to this horizon in the centre of the study area. The sequences above and below the Early Pliocene horizon are discontinuous in nature in the centre of the study area, particularly above basement highs in the south where this horizon is located very close in TWTT to those above and below.

6.5.1.12 Late Pliocene

The Late Pliocene horizon is represented by medium amplitude reflectors that lie conformably within the stratigraphic succession (Fig. 6.5). The horizons immediately above and below are mostly sub-parallel, although in the central and southern parts of the study area the packages beneath the Late Pliocene horizon can be seen to be sigmoidal and

discontinuous. Small diverts in this horizon can be seen to coincide with bathymetric lows, possibly representing disruption to the sedimentary sequence by fluid movements.

6.5.2 Seismic surfaces

Although the seismic surfaces (Fig. 6.8) were primarily produced from interpreted seismic horizons (Fig. 6.6) for the generation of the isochrons (Figs. 6.9 and 6.10) key observations have been made by comparing these surfaces with one another and the geometry of features on the individual surfaces.

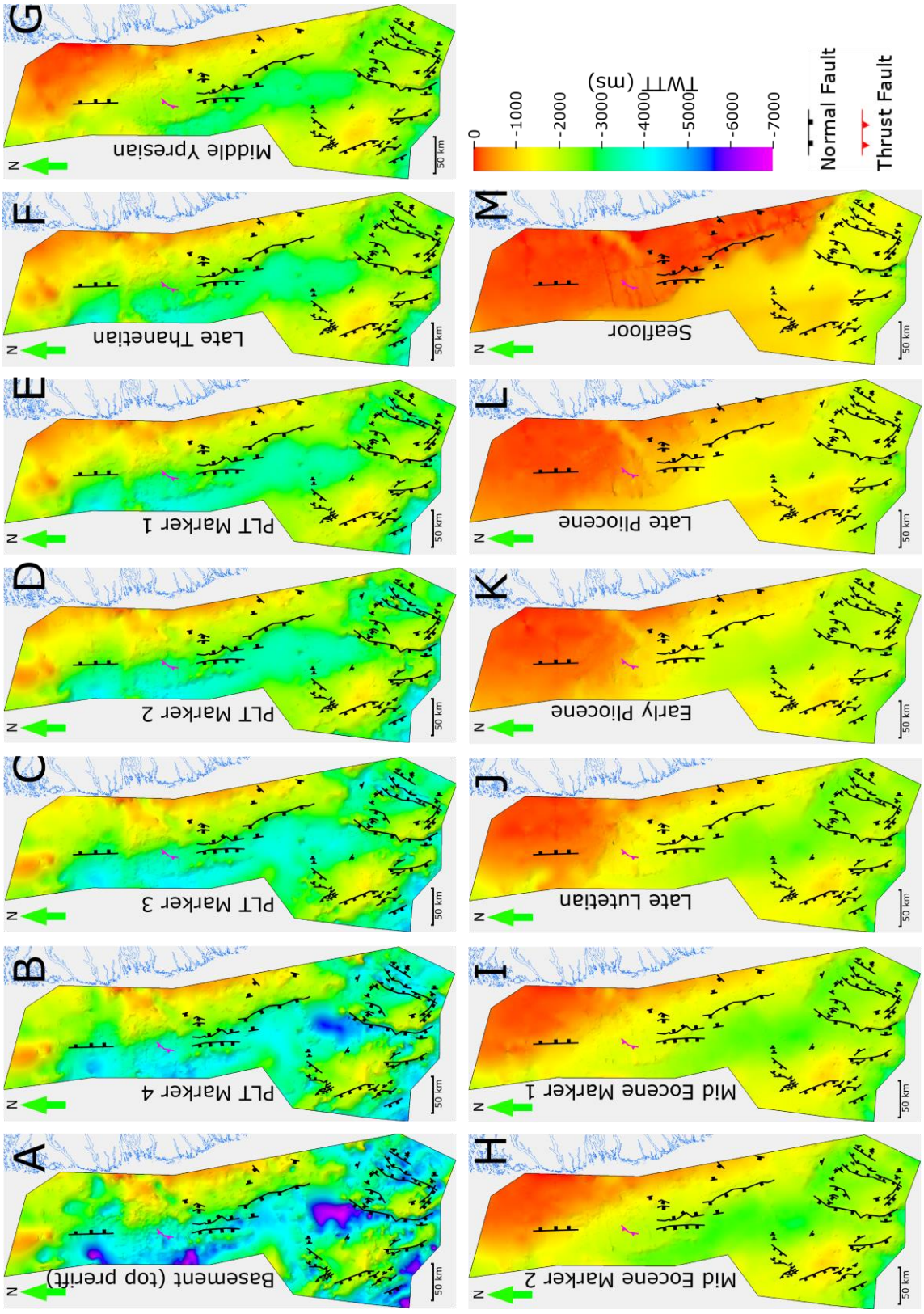

Figure 6.8

Surfaces (TWTT) generated from each horizon interpreted on the seismic lines that lie inside the polygon that defines the study area (Fig. 6.1). PLT = Pre-Late Thanetian (1-4).

The surface of greatest interest to this study is the basement topography surface (Fig. 6.8A) as this contributed to the fault mapping and allowed us to relate basement topography to numerous aspects of the rifting and transform development. The basement topography represents a high relief surface with basement lows located below 7000 ms TWTT whilst in other areas basement highs can be seen to be at or near the seafloor, particularly in the north and east of the study area but also in some parts of the south.

The present bathymetry surface or seabed (Fig. 6.8M) is a low relief surface with essentially three key features: 1) a shallow water platform in the north and east; 2) a deeper area occupying the area southwest and; 3) a channel incised on the southern margin of the polygon. The shallow shelf along the east of the study area has several key features including some low relief incisions that represent a sediment fan, possibly associated with a delta.

Similarities can be observed between the basement horizon (Fig. 6.8A) and the present day bathymetry (Fig. 6.8M). These similarities include but are not limited to: 1) the elongate margin parallel basement high along the eastern edge of the polygon which can be seen to approximate a notable bathymetric high; 2) some basement highs in the south are expressed as bathymetric highs and; 3) the elongate north-south basement low in the south coincides with an incised channel on the modern bathymetry. However, as expected the modern bathymetry most closely resembles the horizons interpreted within the postrift (e.g. Fig. 6.8F-M), with the degree of similarity increasing as the postrift progresses. Overall, Figure 6.8 shows that as the study area has developed through time the amount of relief (horizon topography in TWTT) on the interpreted surfaces can be seen to progressively decrease, i.e. that most relief is displayed by the basement horizon and the least relief is displayed by the modern bathymetry.

6.5.3 Seismic isochrons: Overview

The results of the isochron analysis are shown in Figures 6.9 and 6.10. In conjunction with interpretation of erosional surfaces and geometric relationships with the horizons above and below this allows us to reconstruct the tectonostratigraphic record of margin evolution, and thus study the mechanisms influencing margin evolution.

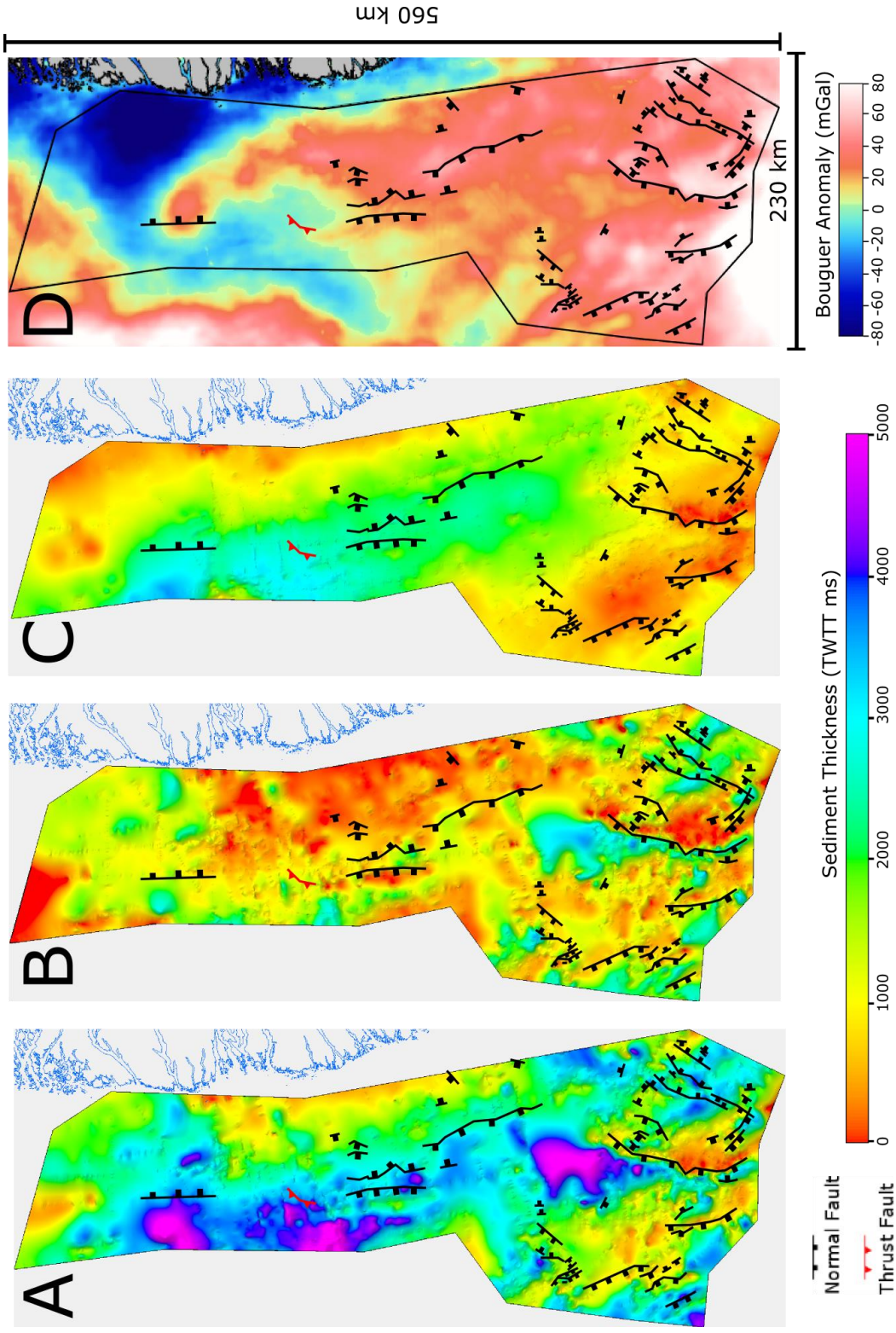

Figure 6.9

Sediment thickness isochrons for: A) Total sediment thickness, B) Basement to Late Thanetian and C) Late Thanetian to Seafloor (all in TWTT ms). D) The Bouguer gravity anomaly calculated using Sandwell and Smith V23 free air anomaly.

6.5.3.1 Total sediment thickness

Total sedimentary thickness (Fig. 6.9A) was calculated between the seafloor and the interpreted basement horizon, representing the top pre-rift, i.e. the total sediment thickness is the sum of the synrift and the postrift contributions. The deepest basins in the study area contain over 5000 ms TWTT of sedimentary and volcanic rocks. Basins of this depth occur in the southern, central and northern parts of the study area. These deep basins essentially form a NNE-SSW trending, margin parallel chain with the major depocentres connected by areas of slightly thinner cover of around 3000 ms TWTT. Sedimentary basins do occur outside of this chain but do not exceed 5000 ms TWTT and are spatially much less extensive.

Comparison between the total sediment thickness isochron and the Bouguer Gravity anomaly (Fig. 6.9D) generated from V23 of the global free air anomaly (Sandwell et al., 2014) has allowed us to examine where the observed anomaly can be explained by the distribution of sediments (i.e. total sedimentary thickness) and where another explanation is required. If the sole contribution to the gravity anomaly were the location of sedimentary basins it would be expected that gravity lows would coincide with deep basins and gravity highs with basement highs, due to the lower density of sedimentary infill compared to the crystalline basement. Thus, if this relationship is not observed deeper structures must provide the variation required to explain the anomalies.

Overall, comparison of the total sedimentary thickness isochron and the Bouguer gravity anomaly shows that the distribution of sedimentary basins alone does not explain the Bouguer gravity anomaly, with areas of deep basins (e.g. in the north of the study area) coinciding with gravity highs. However, it can be seen that the aforementioned deep NNE-

SSW trending basin in the south of the study area has a slightly lower gravity anomaly of c. 15-40 mGal compared to the surrounding area of c. 40-80 mGal (Fig. 6.9D).

6.5.3.2 Large-scale temporal evolution: Basement to Late Thanetian and Late Thanetian to seafloor

Isochrons have not been produced for intervals defined as synrift and postrift, as it is extremely unlikely that rifting ceased simultaneously, particularly given that multiple rifting events have been interpreted (e.g. Abdelmalak et al., 2012; McGregor et al., 2012). However, by comparing the distribution of deposition prior to the Late Thanetian surface with the deposition after this horizon we can gain insights into the long-term differences between the early and late evolution of the study area. The Late Thanetian has been chosen for this analysis as it represents our first dated horizon and significantly different styles of deposition operate before and after this horizon (Fig. 6.10).

The time thickness between the basement horizon and the Late Thanetian in many areas represents the period of thickest sedimentary infill with over c. 3000 ms TWTT preserved in some basins, particularly in the south (Fig. 6.10B). The largest depocentre is the NNE-SSW chain of basins in the south, but other significant depocentres outside this chain are also present. During this interval a distinct north-south disparity in basin aspect ratio can be observed, with the basins in the south tending to be more elongate than their counterparts in the north.

The interval between the Late Thanetian and the modern seafloor is dominated by one area of significantly greater time thickness infill (Fig. 6.10B). This is a singular, elongate, margin parallel basin that for large parts contains up to 4000 ms TWTT of infill towards the north. The margins of this basin are not fault bound and as a result are less abrupt than during the earlier interval, however the transition into areas of lower time thickness is more

abrupt in the north than in the south. Outside of the dominant basin preserved time thickness rarely exceeds c. 1500 ms TWTT.

Comparison between the pre and post Late Thanetian isochrons (Fig. 6.10B and C) shows that the large basins in the south of the study area received a greater amount of their time thickness infill during the earlier interval, whereas the large basin in the north received more during the later interval. Significant basins are located in the north of the study area during the latter interval but no significant time thickness infill is recorded in the south of the study area during the latter interval.

In summary, during the earlier interval (basement to Late Thanetian) the recorded infill in time thickness dominates the south of the study area in small discrete basins, whereas the later interval is dominated by greater time thickness infill in the north of the study area with a more diffuse appearance i.e. not confined to discrete basins. However, despite the large scale difference observed between recorded infill in the pre and post Late Thanetian intervals many of the areas that record lower time thickness infill during the earlier interval continue to display lower amounts of time thickness infill during the later interval. This is particularly apparent in the south, extreme north and eastern edge of the study area. Another similarity between these two intervals is that the areas occupied by major basins during the earlier interval, particularly in the south, continue to record slightly higher time thickness infill than their surroundings in the later interval. The notable exception to this observation is in the southeast of the polygon, where significant time thickness infill characterises the earlier interval whereas minimal infill is record in the later interval.

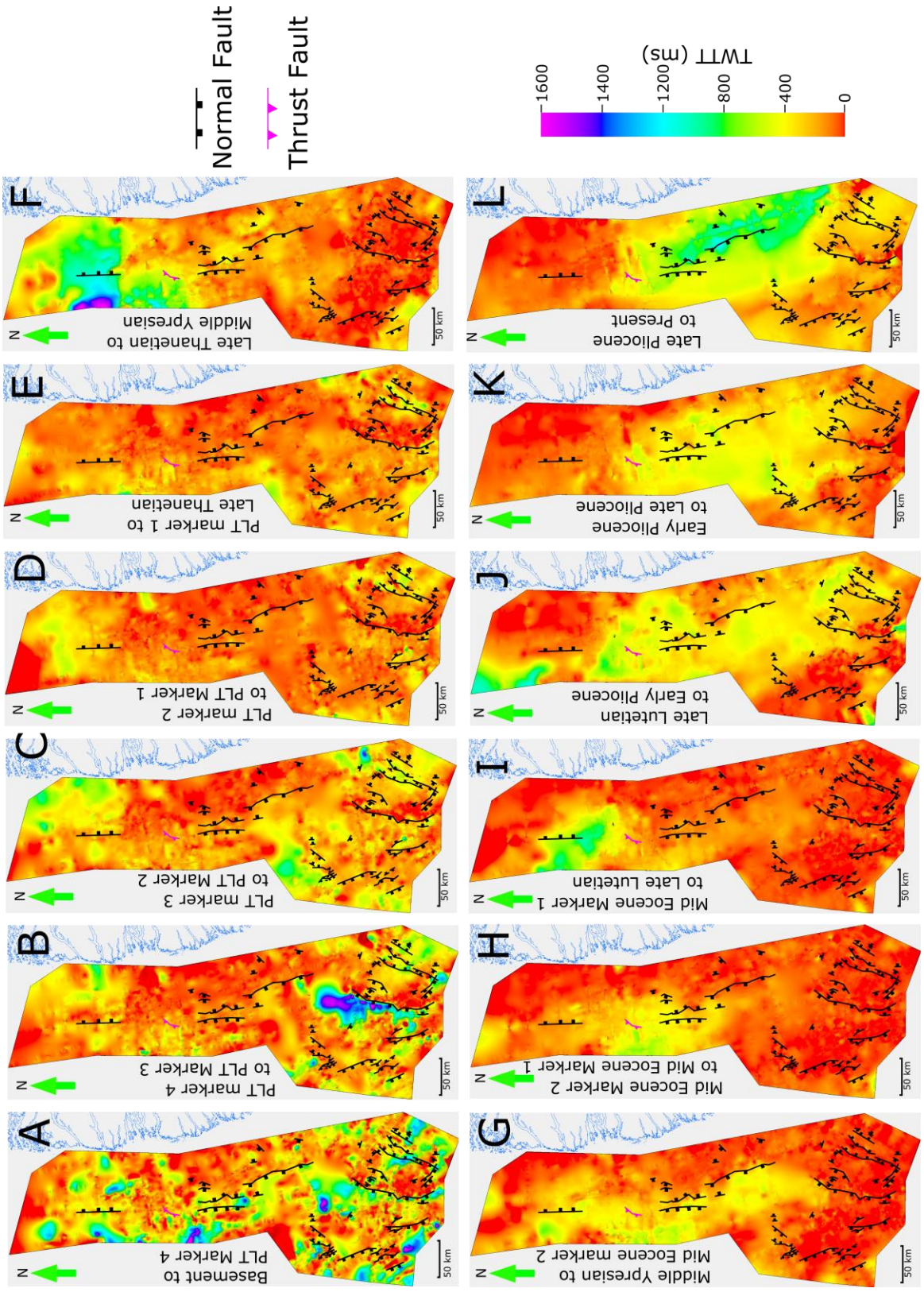

Figure 6.10

Isochrons for the defined geological intervals used in this study. The isochrons A-C (basement horizon to PLT 2) approximate the synrift phase, details of which are provided in the subsequent section.

6.5.3.3 Onset of rifting to Late Thanetian

This is the interval between the basement horizon and our first dated horizon (Late Thanetian) (Fig. 6.10A-E). Between the basement horizon and the Late Thanetian four additional horizons were interpreted on the seismic data, referred to herein as Pre-Late Thanetian (PLT) markers 1-4, with PLT 1 being the youngest and PLT 4 being the oldest. Having considered the interval as a whole in the last section, here we focus on the detail shown by the four markers, starting with the oldest and working towards the youngest.

Between the basement horizon and the PLT marker 4 (Fig. 6.10A) many small depocentres are present across most of the study area, with the exception in the central eastern edge of the polygon. During this interval some deposition occurred along the location of the major elongate basin in the south of the study area where subsequent intervals also show significant time thickness infill.

The spatial distribution of depocentres between the PLT marker 4 and PLT marker 3 (Fig. 6.10B) varies from the previous interval in that the major north-south basin in the south of the study area dominates deposition and the small depocentres which characterised the previous interval are less abundant. Some of the large depocentres from the previous interval, particularly in the central and northern parts of the study area, are now characterised by areas of lower time thickness infill.

Between PLT Markers 2 and 3 (Fig. 6.10C) time thickness infill in the north-south elongate basin in the south of the study area is lower than the previous two intervals. This interval is characterised by diffuse deposition particularly in the northeast and southwest of the study area.

The interval between PLT Marker 2 and 1 (Fig. 6.10D) records a low time thickness infill compared to previous and subsequent intervals. The distribution of depocentres during this interval is relatively similar to the last interval, albeit with generally less deposition. The largest depocentre in this interval is the area of diffuse sedimentation in the north where up to c. 500 ms TWTT of sediments are present. Some infill is recorded in the south at locations where infill was also recorded in previous intervals, particularly at the location of the major southern basin that was identified during previous intervals.

Between PLT Marker 1 and the Late Thanetian horizon (Fig. 6.10E) the area in the north that recorded the diffuse infill during the last interval is now an area of minimal time thickness infill. Although some time thickness infill does continue to occur in small basins in the south of the study area. Interestingly, although this interval is characterised by lower time thickness infill in the south slightly thicker infill is record at the location of the major southern basin which was identified during previous intervals.

6.5.3.4 Late Thanetian to Middle Ypresian

This interval (Fig. 6.10F) contains a very different spatial distribution of depocentres compared to all previous intervals. However, distinct differences between time thickness infill in the north and south of the study area are also present. The area of greatest time thickness infill is in the north where a poorly defined basin is present, with lobes of greater time thickness trending to the east and south away from the greatest thickness on the north western margin of the study area. This depocentre appears to extend beyond our polygon with the area of greatest time thickness infill to the west of the polygon. The southern part of the study area during this interval is characterised by lower time thickness infill not exceeding c. 1000 ms and mostly less than c. 250 ms. Despite the south of the study area

recording lower infill than the north slightly more infill is record at the location of the major southern basin that was identified during previous intervals.

6.5.3.5 Middle Ypresian to Late Lutetian

Between the Middle Ypresian horizon and the Late Lutetian horizon two additional horizons were interpreted on the seismic data, as described in the previous section these are the Mid Eocene Marker 1 (Fig. 6.8H) and 2 (Fig. 6.8I), with the latter being the oldest and the former being the youngest.

For the interval between the Middle Ypresian and Mid Eocene Marker 2 (Fig. 6.10G) the dominant basin is a coast parallel area displaying diffuse sedimentation in map view of c. 400 ms TWTT thick, with a step to the east in the south of the study area. The area of greatest time thickness infill occurs at the northern end of this large basin.

Between Mid Eocene marker 2 and Mid Eocene marker 1, (Fig. 6.10H) the time thickness differs from the previous interval in that the elongate basin that was established during the last interval now has a considerably reduced aspect ratio. The greatest time thickness infill is now located in the centre of the study area.

From the Mid Eocene marker 1 to the Late Lutetian (Fig. 6.10I) a significant depocentre was present in the central northern part of the study area. This basin contains c. 800 ms (TWTT) of sediments. Outside of this major basin minimal time thickness infill was deposited during this interval, of particular note is the area in the south where very little deposition is recorded.

6.5.3.6 Late Lutetian to Early Pliocene

The spatial distribution of time thickness infill during this interval (Fig. 6.10J) varies considerably from the subsequent intervals. Firstly, as with the previous interval, a

significant depocentre is present in the north, its position however has changed from the last interval in that it has shifted to the northwest, with the basin location during the last interval now an area recording minimal time thickness infill. The next major difference between this interval and the previous interval is that the central and southern areas record diffuse infill, compared to previously where these areas record minimal time thickness infill. Finally, two small depocentres on the southern margin of the polygon can be seen during this interval. The eastern most of these two depocentres can be seen to coincide with the major elongate basin which dominated the southern part of the study area during the earliest two intervals.

6.5.3.7 Early Pliocene to Late Pliocene

Between the Early Pliocene and the Late Pliocene (Fig. 6.10K) the greatest time thickness infill manifests as a large basin in the centre of the study area, where c. 400-800 ms (TWTT) of time thickness infill is present. The significant basins in the north during the last interval are no longer present during this interval, with the north now recording reduced amounts of time thickness infill than the previous interval.

6.5.3.8 Late Pliocene to Present

This final interval between the Late Pliocene and the present (Fig. 6.10L) represents a period of significant time thickness infill, particularly in the central and eastern parts of the study area. During this interval up to c. 1200 ms TWTT of infill is recorded in the centre of the main basin. The main basin is again coast parallel, as in previous intervals from the Late Lutetian to the present.

6.5.3.9 North-south disparity

A north-south division can be observed in the isochrons at numerous times and in the Bouguer gravity anomaly. Such a spatial division is apparent between the Late Thanetian and the Middle Ypresian (Fig. 6.10F) and from the Middle Eocene Marker 1 to the Late Lutetian (Fig. 6.10I), where in both of these intervals much greater amount of time thickness infill is recorded in the north than in the south of the study area. A distinct difference between the deposition in the north and the south is also observable in the earliest isochrons where basins in the south have a much greater aspect ratio than their northern counterparts. Another north-south division can be observed in the Bouguer gravity data whereby a strong positive anomaly across the south of the area and a strong negative anomaly is apparent across much of the north of the study area (Fig. 6.9D).

6.5.4 Fault interpretation and mapping results

This section describes the nature of faults that have been mapped on seismic reflection profiles and on the subsequent fault map produced from the interpretation.

6.5.4.1 Fault interpretation on seismic profiles

Normal faults are extremely common across the study area and can be readily observed on nearly all the available seismic reflection profiles. All of the interpreted horizons (Fig. 6.6) have been observed to be offset by normal faults although fault offsets are larger and normal faulting is more widespread within the lower (pre- PLT 2) successions. However, even within these lowermost packages we do not interpret all sequences to be synrift, a concept detailed further in the next section (6.5.5). The offset of normal faults is highly variable across the study area, although no particular area is dominated by much larger faults than elsewhere. Offsets of the basement horizon of c. 1000 ms by normal faults is common across the study area with offsets as much as c. 4000 ms also being observed for example the westward dipping normal fault that bounds the large elongate basin in the

south of the study area. On nearly all of the large (> 1000 ms) normal faults that offset the basement fault dip decreases with depth. Localisation of normal faults with depth was observed in places although this does not appear to be the case for most of the normal faults in the study area. However, localisation may occur at a depth beyond the depth limits of the available seismic reflection data.

Reverse faulting is observed on the seismic data but it is not widespread geographically or stratigraphically (Fig. 6.11) compared to normal faulting. Reverse faulting is confined to the area in proximity to the Ikermiut-1 well (Fig. 6.1), known as the Ikermiut Fault Zone (e.g. Gregersen and Skaarup, 2007; Chalmers and Pulvertaft, 2001). In the Ikermiut Fault Zone reverse faulting was observed in close association with folding affecting the successions prior to the Middle Ypressian Horizon (Fig 6.6 – Line D and Fig. 6.11 – Line G), thus the age of this deformation is post-Middle Ypresian and pre-Middle Eocene 2. Folding was observed in absence of reverse faulting but it most commonly occurs alongside reverse faults (e.g. Fig. 11). Although several reverse faults were interpreted it was only possible to tie one of these across multiple (three) seismic lines (reverse fault 2 – Fig. 6.11). Reverse faults have been observed to offset the basement horizon (reverse fault 2 – Fig. 6.11) and end in proximity to basin bounding normal faults (reverse fault 1 and normal fault on Fig. 6.11), although it was not always possible to determine the nature of the intersection between the reverse faults and the basement on the available data (Fig. 6.11).

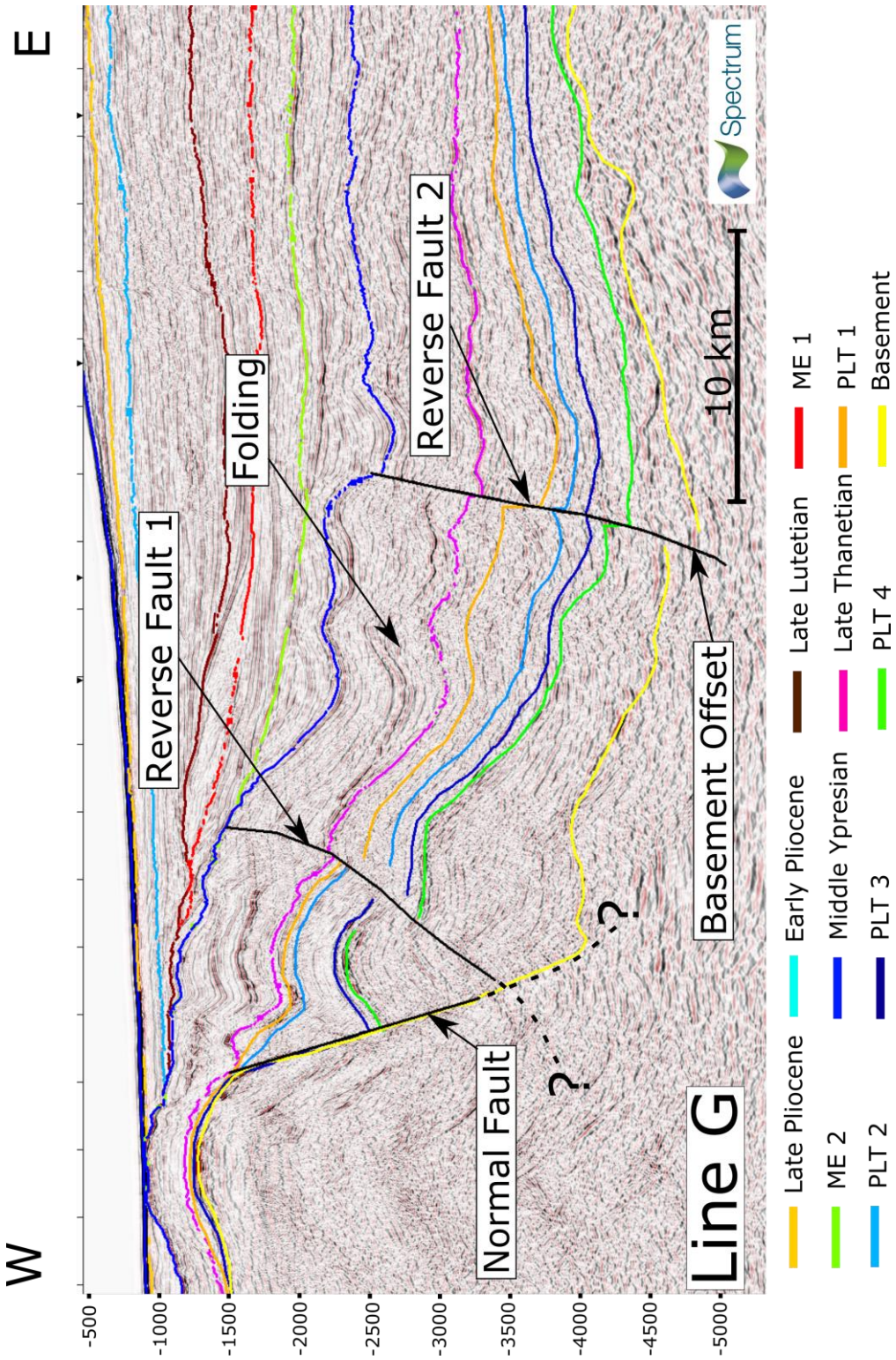

Figure 6.11

Seismic reflection profile G (location shown on Fig. 6.1B) through part of the Ikermiut Fault Zone and associated folding predating the Middle Ypresian horizon (Figs. 6.6).

6.5.4.2 Fault Mapping

The results of the fault mapping are shown on Figures 6.12 and 6.13, with the Chalmers and Pulvertaft (2001) fault map included for comparison on Figure 6.14. Fault mapping was conducted mostly within the polygon used for the surfaces and isochrons (Fig. 6.8, 6.9 and 6.10), but with the addition of faults interpreted to the south of this area on lines that were sufficient for fault interpretation but not for the isochron reconstruction due to the absence of well data. All faults included in this analysis offset the basement horizon and are thus younger than this horizon. The onset of rifting has been dated as early as the Late Triassic but with an intensified stress regime interpreted to have been present in the Early Cretaceous due to a change in composition of the rift-related dykes in West Greenland indicating a much larger degree of melting than the preceding ultramafic dykes (Larsen et al., 2009). Thus, the faults are at least as old as the Early Cretaceous but they may potentially be older.

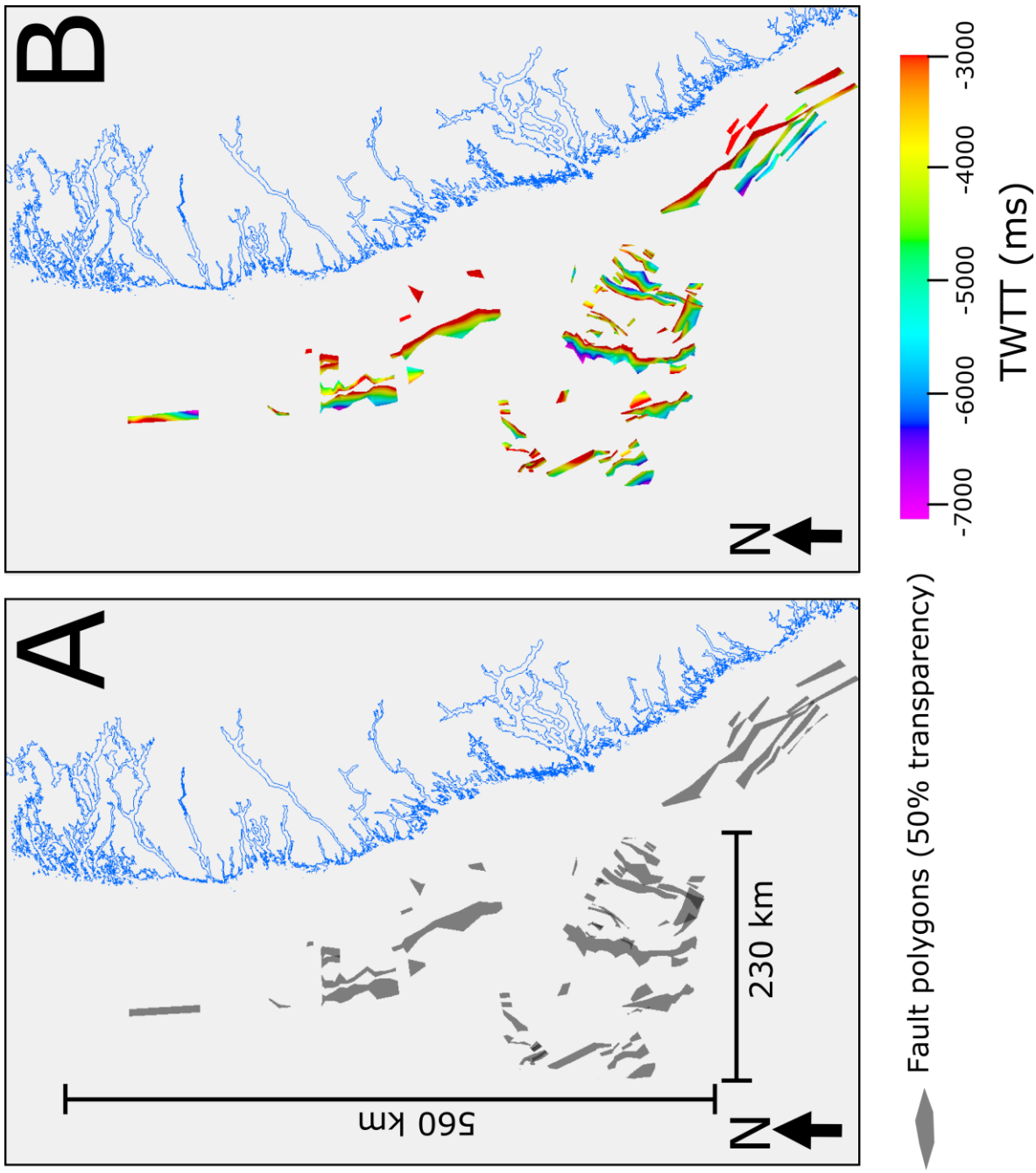

Figure 6.12

Offshore fault mapping results show as: A) fault plane polygons at 50% transparency to allow for the observation of multiple planes under each other in map view; B) fault plane depths in TWTT ms; C)

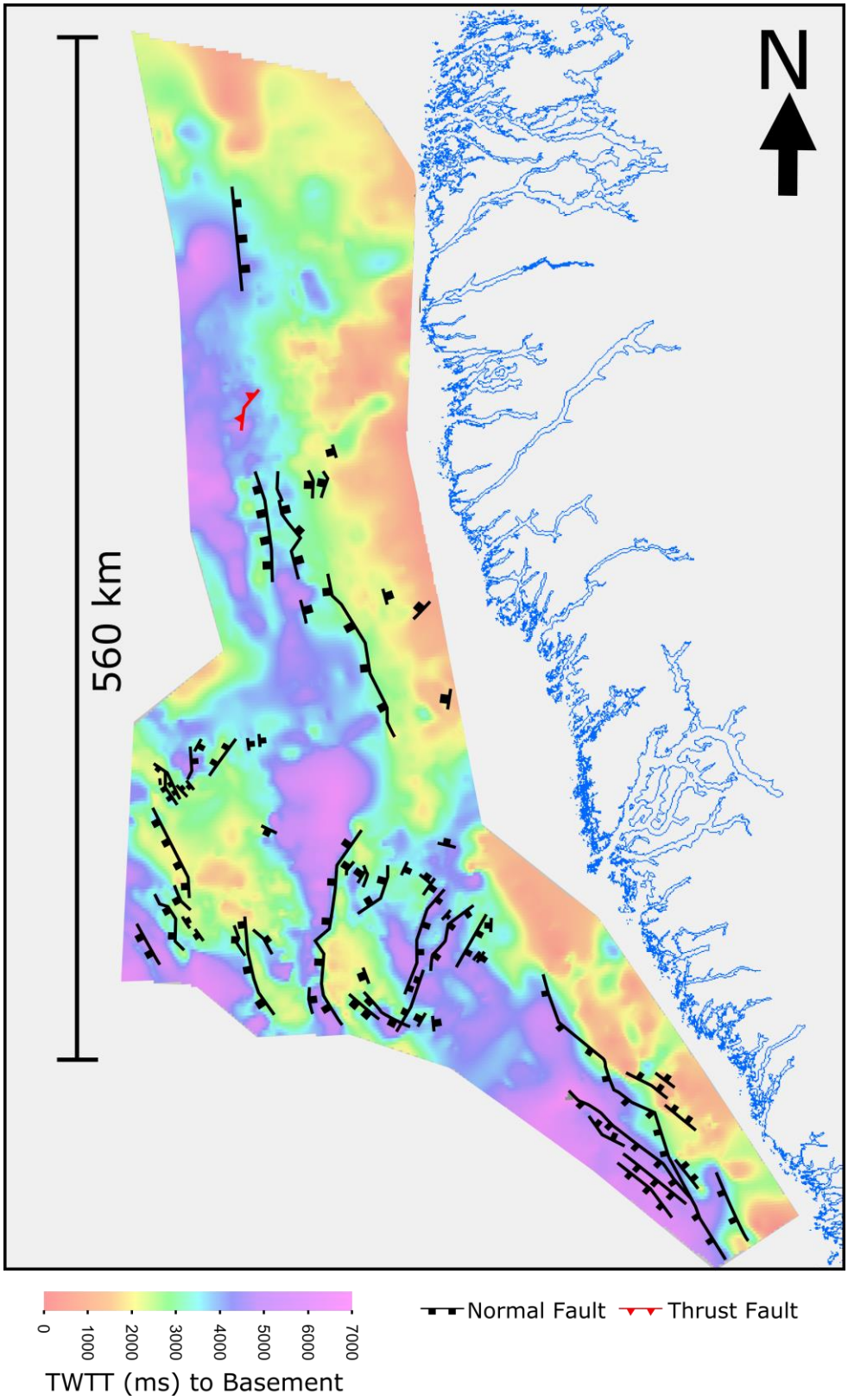

Figure 6.13

Offshore fault map produced by this study overlain on the basement horizon including an extension to the southeast of the primary study area.

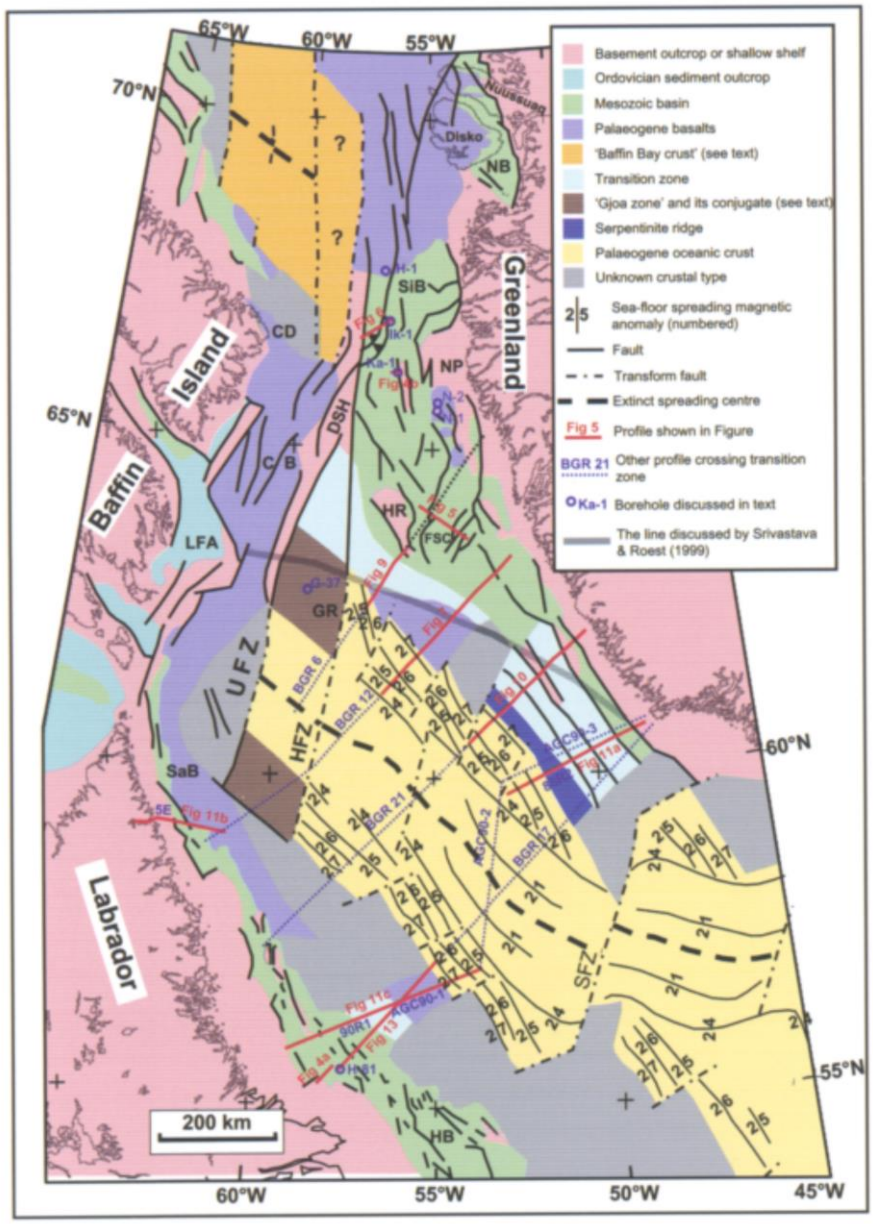

Figure 6.14

Structural map of the Labrador Sea and Davis Strait reproduced from Chalmers and Pulvertaft (2001) based on Chalmers (1991) and Chalmers and Laursen (1995). CB = Cumberland Basin; CD = Cape Dyer; DSH = Davis Strait High; FSC = Fylla Structural Complex; GR = Gjoa Rise; G-37 = Gjoa G-37 borehole; HB = Hopedale Basin; HFZ = Hudson Fracture Zone = HR = Hecla Rise; H-I = Hellefisk-1 borehole; Ik-1 = Ikermiut-1 borehole; Ka-1 = Kangamiut-1 borehole; N-1 and N-2 = Nukik-1 and Nukik-2 boreholes; LFA = Lady Franklin Arch; NP = Nukik Platform; NB = Nuussuaq Basin; SaB = Saglek Basin; SFZ = Snorri Fracture Zone; SiB = Sisimiut Basin; UFZ = Ungava Fault Zone. Figure references on this figure refer to original in Chalmers and Pulvertaft (2001).

Figure 6.12A shows the fault plane polygons at 50% transparency to allow multiple faults occurring above one another to be viewed on the same figure, a feature that only occurs in the southern part of the study area. Fault depths are shown on Figure 6.12B. It can be seen that most faults occur at depths of between 3000 and 6000 ms TWTT but that it is not uncommon for some of the larger faults to reach depths of 7000 ms TWTT. The centre of the study area contains the highest density of shallow basement offsetting faults, which in some cases do not exceed depths of 4000 ms TWTT.

Overall, it can be seen that the southern and central parts of the study area contain a considerably greater density of normal faults than elsewhere. The higher density of normal faults in the central and southern parts of the study area could be in part due to sampling bias as a result of the denser seismic grid in the south (Fig. 6.1). The only place in the study area where reverse faults have been observed is in the northwest of the study area, in proximity to the Ikermiut-1 exploration well (Figs. 6.1 and 6.11).

The geographical distribution of faults mapped by our work in the Davis Strait is very similar to the previous interpretation of Chalmers and Pulvertaft (2001), particularly where both interpretations show the major faults to be approximately north-south trending. The largest faults in our study generally correspond with the majority of the faults mapped by Chalmers and Pulvertaft (2001). The principal difference between this interpretation and the previous work is apparent in the south of the study area where the faults have now been mapped in much greater detail due to the availability of more recent seismic data. Several areas where no faults are shown on the Chalmers and Pulvertaft (2001) map (Fig. 6.14) have been shown using our more recent seismic data to have observable normal faults, this is particularly apparent in the southwest part of the polygon (Fig. 6.13).

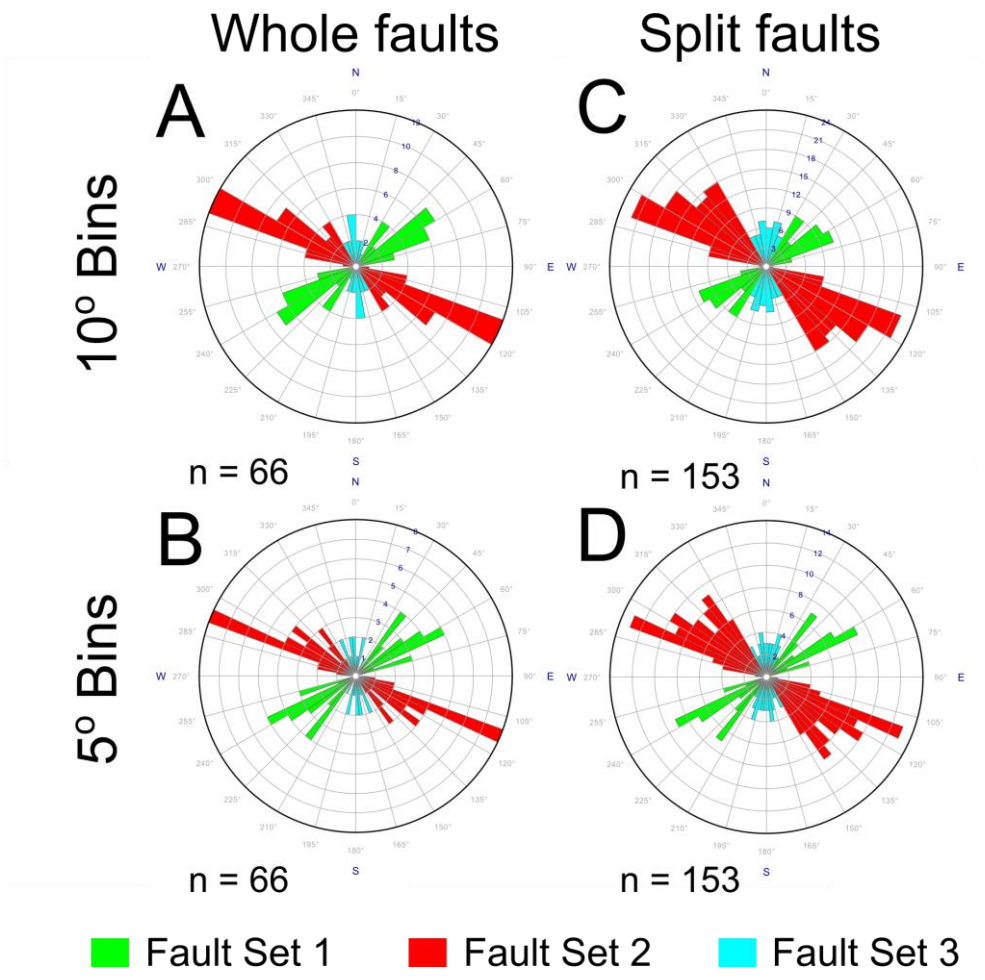

Figure 6.15

A) Rose diagram for whole faults with 10° bins. B) Rose diagram for whole faults with 5° bins. C) Rose diagram for faults split at vertices with 10° bins. D) Rose diagram for faults split at vertices 5° bins.

Analysis of fault strike is shown on rose diagrams in Figure 6.15, with each fault analysed as a single polyline (Fig. 6.15 A & B, n=66) and divided up at its vertices (Fig. 6.15C & D, n=153). This analysis allows us to identify three sets of normal faults based on orientation in addition to the Ikermiut reverse faults (Fig. 6.11). The identified fault systems are NE-SW (Fault Set 1), NW-SE (Fault Set 2) and a N-S (Fault Set 3). The N-S orientated Fault Set 3 is more prominent when analysing the faults as segments divided on their vertices (Fig. 6.15C and 6.15D).

The longest faults and the faults with the largest (< 3000 ms TWTT) offsets belong to fault sets 2 and 3. However, some large faults do also exist in fault sets 1. The longest fault in the study area is the c. 220 km long fault to the south of the main interpretation polygon that belongs to fault set 2. The largest fault in fault set 1 occurs in the southeast of the main interpretation polygon and is c. 60 km long, whilst the longest fault in fault set 3 is the c. 120 km long fault in the south central part of the main interpretation polygon. It is however problematic to further characterise any relationship between orientation, length and offset as orientation changes along the length of most of the faults which is why the orientation of the faults was analysed after dividing them up at their vertices.

6.5.5 The synrift to postrift transition

The interpretation of the horizons (Fig. 6.6), surfaces, (Fig. 6.8), isochons (Fig. 6.9 and 6.10) and faults (Fig. 6.11-6.14) previously described in this section enables us to characterise the nature of the synrift to postrift transition across the study area. However, as recognised by previous work and confirmed by our interpretation herein several rifting phases have affected the study area (Fig. 6.2) and it is unlikely that these events initiated and ceased simultaneously across this large geographical area which intersects several geological terrains (Fig. 6.4). Thus, determining the precise timing of the synrift to postrift transition is problematic, a phenomena recognised by previous work attempting to identify this transition on passive margins (e.g. western Iberian margin - Wilson et al., 2001). When determining whether sediments represent syn or postrift deposition the geometries of the sediment packages were considered, that is whether the package widens towards the footwall of the fault as observed in similar previous work studying the synrift to postrift transition (e.g. Kyrkjebø et al., 2004).

The initial stretching in the Davis Strait is claimed to have occurred in the Jurassic or possibly the Triassic (Larsen et al., 2009) and the most recent rifting event is said to have ended by the Early Paleocene coincident with the onset of seafloor spreading in the Labrador Sea (e.g. McGregor et al., 2012). As our earliest dated horizon is the Late Thanetian (Late Paleocene) we are unable to provide absolute timings on these earlier events. Our interpretation does however allow us to comment on the spatial manifestation of rifting and relative timings of events.

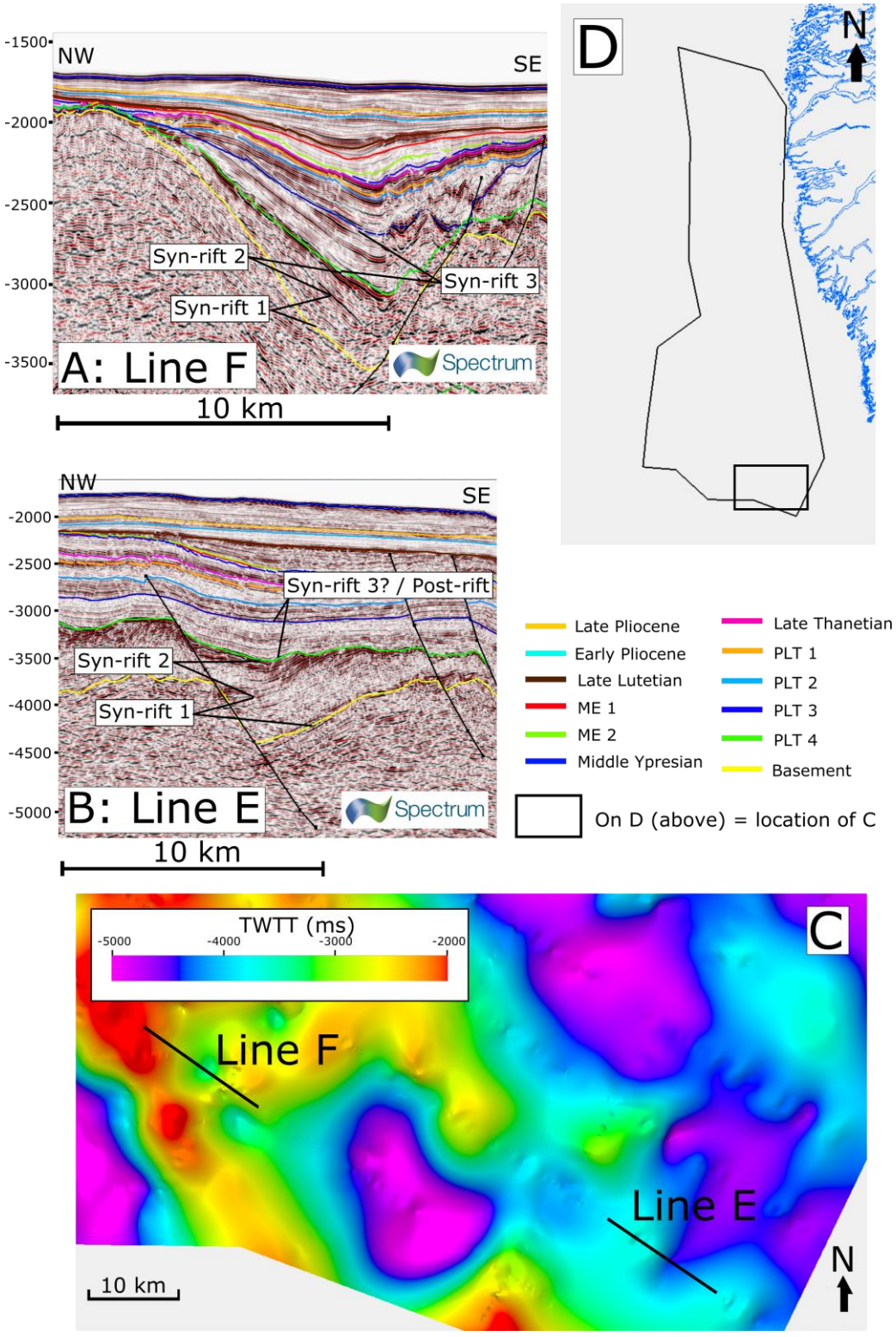

Figure 6.16

(A and B) Extracts from seismic profiles (located on Figure 6.1) demonstrating the variability in the nature of the synrift to postrift transition across a relatively short distance (c. 40 km). C) Locations of line's E and F on depth to basement map.

The earliest evidence for synrift sedimentation was interpreted between the basement and the PLT 4 horizon (Fig. 6.16). Synrift deposition during this interval can be observed across the whole of the study area, but it is particularly evident in the south (e.g. Lines A and E on Figure 6.6) where the data shows the synrift rotation of basement blocks in conjunction with small fault-bound basins in a region known as the Fylla structural complex (Døssing, 2011). Evidence of synrift deposition prior to PLT 4 can also be observed in the north of the study area, although between PLT 4 and the basement horizon in the north it is more difficult to ascertain multiple rifting events and there is less evidence for widespread fault block rotation. Most of the deposition prior to the PLT 4 horizon appears to be synrift but whether it represents a singular phase of rifting or several phases varies across the study area and is probably a product of sediment supply and accommodation space determining whether multiple rift phases are preserved and are observable on the data (Fig. 6.16).

Between the PLT 4 and PLT 3 horizons some areas are characterised by synrift style sedimentation whereas others appear to record postrift sedimentation (Lines E and F - Fig. 6.16). This variability in the nature of this sediment package is shown in Figure 6.16 where observations on two small basins in the south of the study area show that even across a relatively short distance (c. 40 km) the tectonic regime during the deposition of this package is variable. However, for much of the study area the package between PLT 4 and PLT 3 appears to be a postrift package.

The package of sediments between the PLT 3 and PLT 2 horizons is similar to the previously described package (between PLT 4 and PLT 3) in that the syn to postrift characteristics of this package vary across the study area, even over very short distances. However, this package represents postrift deposition over even more of the study area than in the last interval. Although widespread postrift deposition occurs prior to the PLT 2

horizon no synrift deposition occurs after this horizon. Above PLT 2 faulting postdates deposition and thus it represents postrift, subsidence dominated sedimentation. However, this is not to say that everything prior to the PLT 2 horizon is synrift as in many areas the most recent synrift faulting was observed to be much further down in the sedimentary sequence.

Overall, we interpret at least two, possibly three rifting events on the seismic reflection data, an observation concurrent with previous interpretations (e.g. McGregor et al., 2012). These rifting events are all confined to the sequences prior to PLT 2. Thus, the syn to postrift transition can be approximated across the study area by the PLT 2 horizon. Given the dating of the cessation of the latest rifting event by the previous work is the Early Paleocene (e.g. McGregor et al., 2012) it is seems reasonable to consider the PLT 2 horizon to approximate the Early Paleocene in age.

6.6 Discussion

Analysis of the Spectrum and BGR seismic data in the Davis Strait (Fig. 6.1) has demonstrated that through time the location and nature of the thickest infill in the area has changed considerably (Fig. 6.9 and 6.10). Our results have shown that through time the location of infill changes from occurring in discrete fault bound basins, often arranged into elongate chains, to more diffuse time thickness infill (Fig. 6.9). In this section we discuss whether this changing pattern of sediment distribution through time reflects a diminishing role of faulting in controlling the location of sedimentation as the synrift progresses into the postrift, and whether or not the location and orientation of the basin bounding faults is primarily controlled by pre-existing structures. We also examine the relationship between the on and offshore observations and consider the results in the context of the two stage

breakup model proposed by previous workers for this region (e.g. Oakey and Chalmers, 2012; Wilson et al., 2006).

6.6.1 Comparison of on and offshore structures

The study area lies adjacent to both the Nagssugtoquidian Orogen and the North Atlantic Craton (Fig. 6.4). As the offshore continuation of the boundary between these terrains cannot be precisely located we consider structures in both these units as candidates for rejuvenation during Mesozoic rifting. It is however thought provoking that a north-south division is displayed in many of the results of this study (e.g. Figs. 6.10F and 6.10I). This recurring geographical division in the manifestation of rifting and other geological features may be linked to the location of the boundary between the Archean rocks of the North Atlantic Craton in the south and the Nagssugtoquidian to the north. Alternatively, the north south division may be an artefact of the uneven distribution of the seismic data across the study area (Fig. 6.1A), although the grid thinning experiments suggest that the influence of line density is minimal (Fig. 6.7), possibly implying a geological explanation for this observation.

All three major fault sets identified in this work (Fig. 6.15) correspond to structural systems identified onshore by Wilson et al. (2006) in the Nagssugtoquidian (Table 6.1). Purely based on orientation, without implying a causative link, the orientation of fault set 1 in this study corresponds to the dominant system 1, fault set 2 is of a similar orientation to system 2 and fault set 3 in this study is the same orientation as system 3 in Wilson et al. (2006). System 1 is a structural system with a similar trend to the dominant basement fabric in the Nagssugtoqidian, system 2 represents closely spaced faults often showing both sinistral and normal offset, whilst system 3 is a closely spaced set showing a net dextral and normal offset of 20-40 m (Wilson et al., 2006).

The three major fault trends identified in this work (Fig. 6.15) also correspond to structural systems observed onshore in the rocks of Archean North Atlantic Craton (Japsen et al., 2006). Correlation based on orientation between the fault sets identified in this work and the outcrop analysis of Japsen et al. (2006), again without implying a causative link shows that: fault set 1 corresponds with the NE-SW trending deep gullies observed onshore; fault set 2 is the same orientation as the SE-NW trending joints and fractures which dip NE; and fault set 3 is the same orientation as the N-S trending structure dipping moderately to the east, parallel to basement fabrics in the area.

Comparison between the on and offshore structures demonstrates that there are certainly similarly orientated structures present both on and offshore. However, determining whether the structures both on and offshore are reactivated older structures or whether they represent structures created and deformed during Mesozoic rifting requires detailed examination of observed fault orientations with respect to reconstructed rifting directions (e.g. Abdelmalak et al., 2012). In the following sections fault orientations and the distribution of time thickness infill are considered in the context of the two stage rifting model for the region (e.g. Abdelmalak et al., 2012; Oakey and Chalmers, 2012; Wilson et al., 2006).

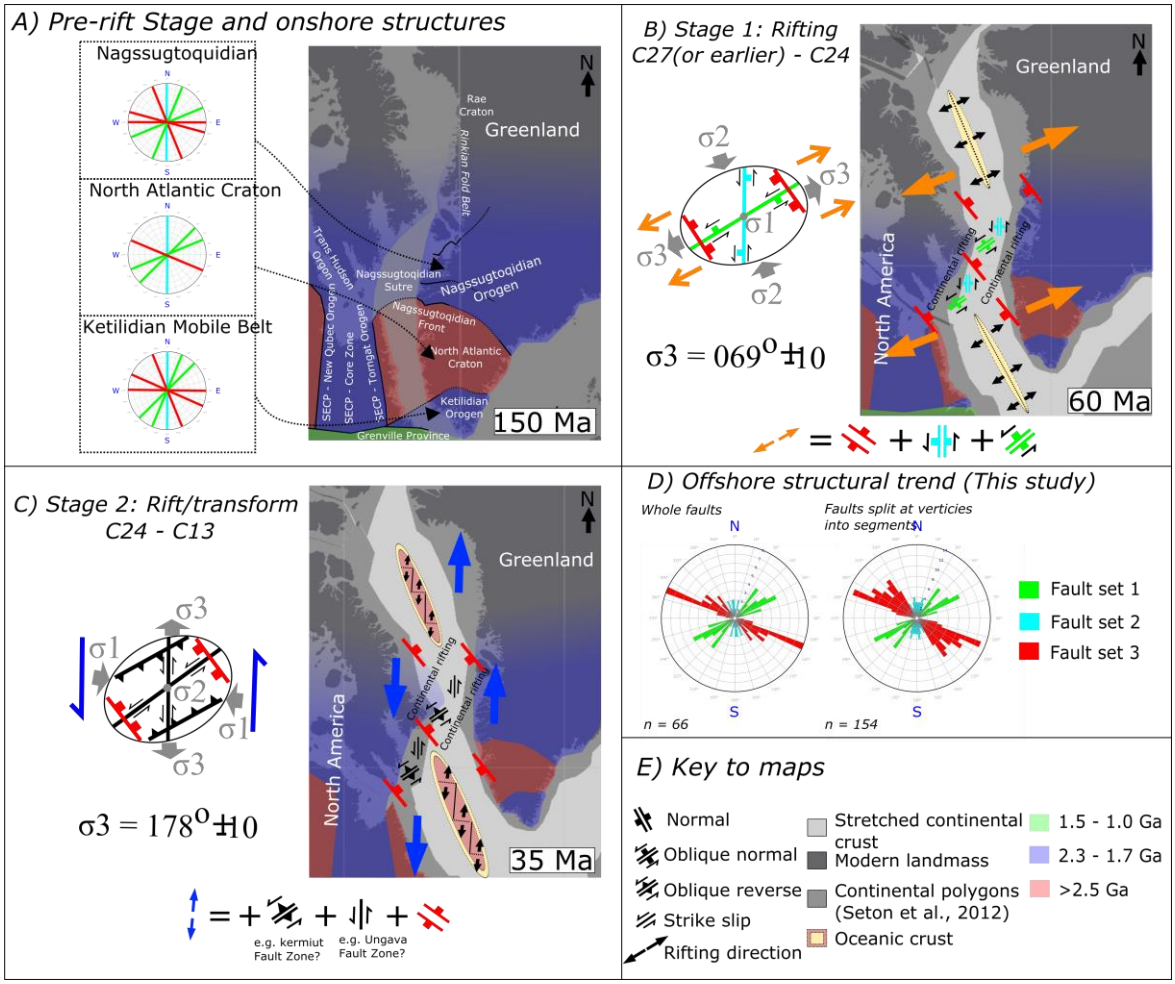

Figure 6.17

A) The pre-rift configuration of North America and Greenland along with graphical representations of the onshore structures in the basement terrains of West Greenland (Japsen et al., 2006; Wilson et al., 2006) coloured using the same colours for similar orientation structure sets as in this study (Fig. 6.15). B) Kinematic model for the 1st rifting stage where stage 1 fault sets 2 and 3 form by exploiting pre-existing trends. C) Kinematic model for the second rifting stage where the Ungava Transform Fault system develops as a result of the lateral offset between Baffin Bay and the Labrador Sea (possibly due to the Nagssugtoqidian and Torngat orogens) and the newly established N-S rifting direction in this interval. D) Summary of the offshore faults as characterised in this study. E) Key to the maps in parts A) B) and C) of this figure.

6.6.1.1 Stage 1: Rifting

The onset of rifting in the Labrador Sea – Baffin Bay system has been dated as early as the Late Triassic but with a particularly intense stress regime in the Early Cretaceous inferred from geochemical analysis of onshore dykes in West Greenland (Larsen et al., 2009). This rifting stage encompasses the oceanic magnetic anomalies from at least C27, possibly earlier, to C24 (Abdelmalak et al., 2012). The earliest dated horizon in our seismic interpretation is the Late Thanetian and thus we cannot contribute a more precise time for the onset of rifting. It is however unlikely that all faults initiated simultaneously at the onset of stretching.

The extension direction during this period was calculated by Abdelmalak et al. (2012) by inversion of onshore kinematic data to be 069° ± 10. The isochrons documenting sediment distribution during this early rift interval are those prior to the Late Thanetian. Sediment deposition in this interval is focused into small isolated, fault bound basins that are in many places organised into approximately N-S orientated chains (Fig. 6.10A and 6.10B), particularly in the south of the study area.

Of the three offshore fault populations identified in the study area (Fig. 6.15) none are perpendicular to a rifting direction of 069° ± 10, as would be expected during orthogonal rifting of a homogeneous medium. The closest to being perpendicular to the reconstructed rifting direction is fault set 2 (~NW-SE). Fault set 2 is the most dominant offshore structural trend documented in this study in terms of the absolute number of faults, some of which are the largest identified structures both by length and maximum offset of the basement horizon. Given the abundance and orientation of fault set 2 with respect to rifting it seems likely that this fault set represents the dominant manifestation of rift-related deformation during this early stage of rifting. This is particularly important as the faults

which constitute fault set 2 appear to be generally large in terms of both length and maximum offset. Onshore in the North Atlantic Craton domain Japsen et al. (2006) were unable to determine any kinematic indicators on their NW-SE system, whilst in the Nagssugtoqidian domain Wilson et al. (2006) showed that the NNW-SSE faults are not the youngest and typically have a dextral strike slip sense. The slightly off-perpendicular orientation with respect to rifting direction could be due to exploitation of a pre-existing structure set such as those identified onshore by Wilson et al. (2006) or Japsen et al. (2006) or it could be due to the error associated with the stress inversion (Abdelmalak et al., 2012) or the fault orientation analysis in this study (Fig. 6.15).

The second most abundant offshore structural trend is fault set 1 (NE-SW). Fault set 1 is approximately parallel to the reconstructed rifting direction, and thus it is difficult to associate these structures with the early rifting without invoking localization onto a pre-existing structure. Our observations on the seismic reflection data show that fault set 1 constitutes normal faults. However, for normal faults to operate under the rifting directions calculated by previous work (Abdelmalak et al., 2012) they are likely to have initiated under the influence of an appropriately orientated pre-existing structure and had a considerable oblique component to their movement. Candidates for such pre-existing structure are present onshore in the North Atlantic Craton domain where Japsen et al. (2006) observed that a NE-SW structural set is characterised by easily distinguishable yet poorly exposed deep wide gullies, whilst in the Nagssugtoqidian domain Wilson et al. (2006) documented a ENE-WSW structure set to be parallel to basement structures, displaying evidence for multiple phases and senses of movement. Overall, fault set 1 would be extremely unfavourable to have produced oblique normal faults without the localization of deformation onto pre-existing structures.

The N-S orientated fault set 3 is the least abundant and extensive of the three fault sets identified offshore in this study. As with the other fault sets identified in this study fault set 3 does not occur perpendicular to the reconstructed rifting direction (Abdelmalak et al., 2012). From the seismic reflection data we interpret fault set 3 to be a set of normal faults, however for N-S normal faults to develop under an extension direction of 069° ± 10 they are likely to have initiated under the influence of an appropriately orientated pre-existing structure and had an oblique component. Onshore in the Nagssugtoqidian domain Wilson et al. (2006) documented a N-S set of faults displaying normal and sinistral senses of movement i.e. the same as inferred for fault set 3 in this study. In the North Atlantic Craton domain, Japsen et al. (2006) document a N-S structural trend as a prominent feature lying parallel to the basement fabric, however they found the N-S orientated faults to have a dextral sense of movement, the opposite as would be required for fault set 3 under the rifting direction of Abdelmalak et al. (2012). However, given that Japsen et al. (2006) find that their N-S structural set is parallel to the basement fabric it is possible that our N-S set is also exploiting the basement fabric. Alternatively, the N-S faults could be related to the second rift stage discussed in the next section.

Our proposed model for the role of pre-existing structures in fault development during rift stage 1 is summarised on Figure 6.17B. Our model for this interval is that fault location and orientation is primarily controlled by pre-existing structures with fault set 1 (NE-SW) representing an oblique normal reactivation; fault set 2 (NW-SE) representing normal faults approximately orthogonal to the rifting direction possibly, but not necessarily always exploiting pre-existing structures and fault set 3 (N-S) representing oblique normal reactivation. Our kinematic model for rift development in this interval is in broad agreement with the previously proposed reactivation model developed onshore that made predictions for the offshore by Wilson et al. (2006). If faulting is primarily controlled by

the pre-existing structures the location of depocentres during this interval, as depicted on the isochrons prior to the Late Thanetian would also be controlled by pre-existing structures.

6.6.1.2 Stage 2: Rifting and transform development

The second stage of extensional deformation offshore West Greenland occured between oceanic magnetic anomalies C24 to C13 (Abdelmalak et al., 2012). This is a period of geological time beginning with the major reorganisation of the North Atlantic and ending with the cessation of seafloor spreading to the west of Greenland (Srivastava and Roest, 1999). Magnetic C24 is in the Ypresian according to the Geological timescale of Gradstein and Ogg (2012) and is within the isochron interval from the Late Thanetian to the Middle Ypresian in this study (Fig. 6.10F). During this interval Greenland moved north with respect to North America (e.g. Suckro et al., 2013) as regional extension occurred in an approximately north-south direction (178° ± 10 - Abdelmalak et al., 2012), a distinctly different orientation from the previous rifting phase (069° ± 10 - Abdelmalak et al., 2012). Deformation during this second rifting phase has been described as a sinistral wrench system (Wilson et al., 2006) based on onshore observations that compressional structures formed in zones of basement anisotropy. Our seismic interpretation depicts sediment deposition during this interval as minimal and chaotic in the south with poorly defined basins, whereas in the north a new relatively deep basin is present. The chaotic nature of deposition during this interval may reflect deposition whilst the large-scale change in stress regime and thus rifting direction was taking place.

The northward movement of Greenland caused the development of a transform fault system in the Davis Strait known as the Ungava Transform (Kerr, 1967) which follows the SE side of a line of positive gravity anomalies (Funck et al., 2012). The Ungava fault

system is associated with sinistral deformation (Wilson et al., 2006) and has areas of transpression along its length such as the Ikermiut fold and fault structures (Fig. 6.6D and 6.11). Although the Ikermiut fault zone lies within our study area (Fig. 6.1) the majority of the deformation associated with the Ungava transform system lies to the west of the seismic data available for this study. Thus, we are unable to comment on the nature of the deformation but are able to make inferences about the causes of the development of this fault system and associated deformation based on the available data.

During this second rifting stage no faults in our study area were documented perpendicular to the proposed north-south extension direction (E-W), as would be expected under extension of a homogenous medium without the influence of pre-existing structures. It is therefore possible that deformation during this interval was influenced by both basement structures and structures formed during the first rifting stage. Although some continued deformation likely occurred on fault set 2 in this rifting stage the primary manifestation of deformation is associated with the initiation and development of the Ungava transform fault system. Our proposed model for the development of the Ungava transform fault system is that it is related to the lateral offset between extension in Baffin Bay and the Labrador Sea, an offset that was likely established in the first rifting stage possibly due to the rift being unable to fully propagate strait through the Nagssugtoqidian and Torngat orogens (Fig. 6.4). When the extension vector changed to ~N-S in the second rift stage (Abdelmalak et al., 2012) deformation was forced to be accommodated through the development of the transform system. Thus, unlike in the first rifting interval where the role of pre-existing structures in rifting was though reactivation of discrete structures the role of pre-existing structures during the second rift stage influences the large-scale manifestation of deformation. Our proposed model for structural development during rift stage 2 is summarized on Figure 6.17C.

6.6.2 The diminishing role of pre-existing structures

As previously detailed we interpret the reduced relief on the seismic surfaces (Fig. 6.8) and the progression of time thickness infill to a more dispersed distribution (Fig. 6.10) through time to represent a reduced influence of basement and rift-related structures as the synrift progressed into the postrift (section 6.5.5) in the Davis Strait. Thus, our 2 stage rift model described in the previous section attributes the primary control on early fault nature and location to be controlled by pre-existing structures. One such mechanical explanation for the diminishing role of basement structures may be the variable lithospheric strength through the rifting sequence.

During rifting the lithosphere would have been thinned resulting in an elevated geothermal gradient caused by bunching of the isotherms resulting in an overall weaker lithosphere. In such a situation the lithosphere may approach an Airy isostasy type situation in which isostatic compensation tends to be extremely local, and may be accommodated by movement of discrete pre-existing structures such as deep-seated faults. As rifting diminishes and eventually ceases, the lithosphere cools through upward heat conduction resulting in an increase in overall lithospheric strength. Isostatic compensation of a stronger lithosphere will favour broad regional flexure rather than localised faulting. Thus, the changing geothermal and strength profiles of the lithosphere through the rift cycle may provide an explanation for the reduced role of discrete pre-existing structures through time.

6.6.3 The influence of prerift and rift-related structures on postrift development

Despite the influence of basement and rift-related structures diminishing through geological time during the postrift interval some expressions of Mesozoic rifting can be identified. For example the highs produced during Mesozoic rifting are often situated in similar locations to distinct bathymetric highs, demonstrating that rift structures have

probably exerted some influence on even the latest evolution of the study area. This phenomenon is particularly apparent on the seismic surface results (Fig. 6.8). The mechanism behind this phenomenon is likely to be differential compaction, whereby less compaction occurs in the areas of minimal cover (Mesozoic highs) due to the presence of the crystalline basement rocks. This mechanism may also explain why areas which were basins in the synrift continue to receive greater amounts of sedimentary infill through the postrift and up to the present day.

6.6.4 Implications for petroleum exploration offshore West Greenland

The results of this study have multiple implications for our understanding of petroleum systems in the Davis Strait region. Firstly, the small isolated basins depicted on the earlier (prior to PLT marker 3) isochrons (Fig. 6.10A-D) would provide a suitable location for the accumulation of organic matter in a spatially restricted environment. Such a restricted environment could lead to anoxic conditions indicative of preservation of source rock material. However, the small basins could make potential source rocks spatially limited and laterally variable, resulting in source rocks being difficult to predict between these small basins. This is particularly important as the time interval where source material offshore West Greenland is believed to have been deposited, primarily within the Cretaceous successions but also in the Palaeocene (Schenk, 2011), corresponds to the isochrons depicting the small isolated basins (Fig. 6.10A-D). Opportunities to form trapping structures occur multiple times; including the major reorganisation at Chron 24 resulting in the strike slip tectonics forming the Ikermiut thrust and fold structures (Fig. 6.11D). A mature source rock is present in the area, as evidenced by recent discoveries (e.g. Schenk, 2011) and is likely to have reached maturity in part due to the deep postrift successions providing sufficient burial for maturation to occur. Another consideration for petroleum exploration in the region is the effects of the abundant breakup related volcanic

rocks in the northern Labrador Sea and Davis Strait will have had on the potential petroleum system in terms of the thermal (e.g. Fjeldskaar et al., 2003) and structural evolution (e.g. Magee et al., 2012).

6.7 Conclusions

Our conclusions on the role of pre-existing structures during Mesozoic rifting between Greenland and Canada are as follows:

1) Three fault systems were identified offshore in the Davis Strait study area. These are 1) NE-SW, 2) NW-SE and 3) N-S. All the fault sets identified offshore correlate with observed structural trends identified onshore by previous work in the North Atlantic Craton and the Nagssugtoqidian orogenic belt. During the first phase of rifting faulting is primarily controlled by pre-existing structures with fault set 1 (NE-SW) representing an oblique normal reactivation; fault set 2 (NW-SE) representing normal faults approximately orthogonal to the rifting direction possibly but not necessarily exploiting pre-existing structures and fault set 3 (N-S) representing oblique normal reactivation. In the second rifting stage, a sinistral transform system developed in the Davis Strait (Ungava Fault Zone) as a result of the lateral offset between the Labrador Sea and Baffin Bay. This lateral offset was established in the first rift stage probably due to the presence of the Nagssugtoqidian-Torngat orogenic belt being unsusceptible to rift propagation. Without the influence of pre-existing structures the manifestation of deformation cannot be easily explained under either the first or second rifting phase.

2) The primary control on the location of rifting has changed through time with basement anisotropy providing the main control on the location and style of early offshore faulting and thus basin development. The dominance of faulting and thus

basement anisotropy as the primary control diminishes throughout the synrift and into the postrift. However, despite the diminishing role of pre-existing structures in the rifting process through time some large structures may continue to remain important even into the postrift. The thermal profile and thus lithospheric strength through the rift cycle may provide an explanation for the diminishing basement influence in that initial rifting may weaken the lithosphere resulting in localised isostatic compensation compared to in the postrift where a stronger lithosphere may result in regional flexure type isostatic compensation.

3) There is a distinct division between the north and south of the study area throughout the studied geological interval, with the synrift being dominated by deposition in the south, whereas the postrift is dominated by deposition in the north. This long-lived division could reflect a significant pre-existing structure that may represent the offshore continuation of the boundary between the Archean North Atlantic Craton and the Palaeoproterozoic Nagssugtoqidian.

Chapter 7

Quantifying the influence of sill intrusion on the thermal evolution of organic-rich sedimentary rocks in non-volcanic passive margins: an example from ODP 210-1276, offshore Newfoundland, Canada

This chapter has been published as:

Peace, A., McCaffrey, K., Imber, J., Hobbs, R., van Hunen, J. & Gerdes, K., (*2015*). Quantifying the influence of sill intrusion on the thermal evolution of organic-rich sedimentary rocks in non-volcanic passive margins: an example from ODP 210-1276, offshore Newfoundland, Canada. *Basin Research* http://dx.doi.org/10.1111/bre.12131

7.0 Summary

Intrusive magmatism is an integral and understudied component in both volcanic and nonvolcanic passive margins. Here, we investigate the thermal effects of widespread (ca. 20,000 km^2) intrusive magmatism on the thermal evolution of organic-rich sedimentary rocks on the nonvolcanic Newfoundland passive margin. ODP 210-1276 (45.41°N, 44.79°W) intersects two sills: an older, upper sill and a younger, lower sill that are believed to correspond to the high amplitude 'U-reflector' observed across the Newfoundland Basin. A compilation of previous work collectively provides; 1) emplacement depth constraints, 2) vitrinite reflectance data and 3) $^{40}Ar/^{39}Ar$ dates. Collectively, these data sets provide a unique opportunity to model the conductive cooling of the sills and how they affect thermal maturity of the sedimentary sequence. A finite differences method was used to model the cooling of the sills, with the model outputs then being entered into the EASY%R_o vitrinite reflectance model. The modelled maturation profile for ODP 210-1276 shows a significant but localised effect on sediment maturity as a result of the intrusions. Our results suggest that even on nonvolcanic margins, intrusive magmatism can significantly influence the thermal evolution in the vicinity of igneous intrusions. In addition, the presence of widespread sills on nonvolcanic passive margins such as offshore Newfoundland may be indicative of regional-scale thermal perturbations that should be considered in source rock maturation studies.

7.1 Introduction

Continental extension causes rifting and thinning of the lithosphere that may result in continental breakup and eventually the initiation of seafloor spreading (Eldholm and Sundvor, 1979). Passive continental margins are a product of this continental breakup and subsequent seafloor spreading (Geoffroy, 2005). Passive margins are traditionally

classified as one of two end-member types: (1) volcanic (VPM) or (2) nonvolcanic (NVPM), in reference to the relative abundance or scarcity of igneous rocks produced during rifting and breakup (e.g. Franke, 2013).

Passive margins globally represent a significant host for both current (e.g. offshore Newfoundland; DeSilva, 1999), and future hydrocarbon exploration targets (e.g. offshore West Africa; Beglinger et al., 2012). Source rock quality, and in particular maturity, is of paramount concern when exploring new areas in deep water passive margins where operating costs may be high. To reduce the exploration risk in these settings, it is thus important to understand and quantify the thermal evolution of NVPMs, and their source rock maturation characteristics. Syn and post-rift magmatism is a common feature on passive margins, with spatially extensive igneous sill complexes being a common feature on both volcanic (e.g. the Western Australian margin; Holford et al., 2013) and nonvolcanic passive margins (e.g. the South Australian Margin; Holford et al., 2012). The heat from these intrusions may contribute to the thermal evolution (Hurter and Pollack, 1995) of a margin, and thus the maturation of potential source rock material. It is for this reason that the additional heat introduced by igneous intrusions into prospective sedimentary basins on passive margins needs to be quantified.

ODP 210-1276 intersects two sills which provide an opportunity to model potential changes in the maturity of the encasing organic-rich sedimentary host rocks instigated by post-rift magmatism in a NVPM. Here, we report the results of 1D conductive modelling of the influence of sill intrusion and compare the model predictions with the measured vitrinite reflectance data of Pross et al. (2007) to estimate the maturation state of the encasing sedimentary rocks. Experiments were also undertaken to understand the roles of timing, hydrothermalism and the duration in which sills acted as magmatic conduits.

The aim of this work was to show that despite all the variables present in a complex intrusive system such as this, a simple model can be used to account for the majority of thermal effects. This allows us to discount less important processes, resulting in insights into the major controls on the thermal maturation of organic-rich sedimentary rocks in proximity to igneous intrusions. We conclude that the sills intersected at ODP 210-1276 have influenced the localised thermal evolution of the sedimentary rocks, which may be indicative of a broader, more regional thermal perturbation in the region covered by the 'U-reflector'. Although, given that ODP 210-1276 essentially represents a 1D profile through a spatially extensive, complex, igneous system, it is likely that the results presented herein are not representative of the situation in other parts of the Newfoundland Basin.

7.2 Geological Setting

The Newfoundland margin was formed during the opening of the North Atlantic and in conjunction with its conjugate, the Iberian margin, it is considered to be a typical NVPM (e.g. Melankholina, 2011; Peron-Pinvidic et al., 2013). ODP site 210-1276 (45.41°N, 44.79°W) was drilled into transitional crust offshore Newfoundland, Canada (Fig. 7.1). The aim of this ODP leg was to provide a greater understanding of the syn and post-rift stratigraphy and magmatic history of the conjugate Newfoundland-Iberia nonvolcanic passive margins (Tucholke et al., 2004a), with the specific aim of targeting what was believed from seismic reflection data to be the breakup unconformity, which ultimately turned out to be igneous intrusions. The drill site is located near the edge of the thinned continental crust (Van Avendonk et al., 2006), with the well encountering two intervals of igneous rocks which are modelled herein. These two intervals; are the only igneous rocks recorded at ODP 210-1276, consisting of an upper, singular sill which is 10.3 m thick and

a lower sill complex where the main body is at least 17.9 m thick (Table 7.1). Drilling ceased 17.9 m after penetrating the main body of the lower sill, thus modelling a sill of this thickness represents a minimum and the thermal influence is likely to be greater. The first sill was emplaced after the onset of seafloor spreading (Peron-Pinvidic et al., 2010), which was initiated by Barremian to Aptian time (anomaly M3 to M0, or 127–112 Ma) (Hopper et al., 2004).

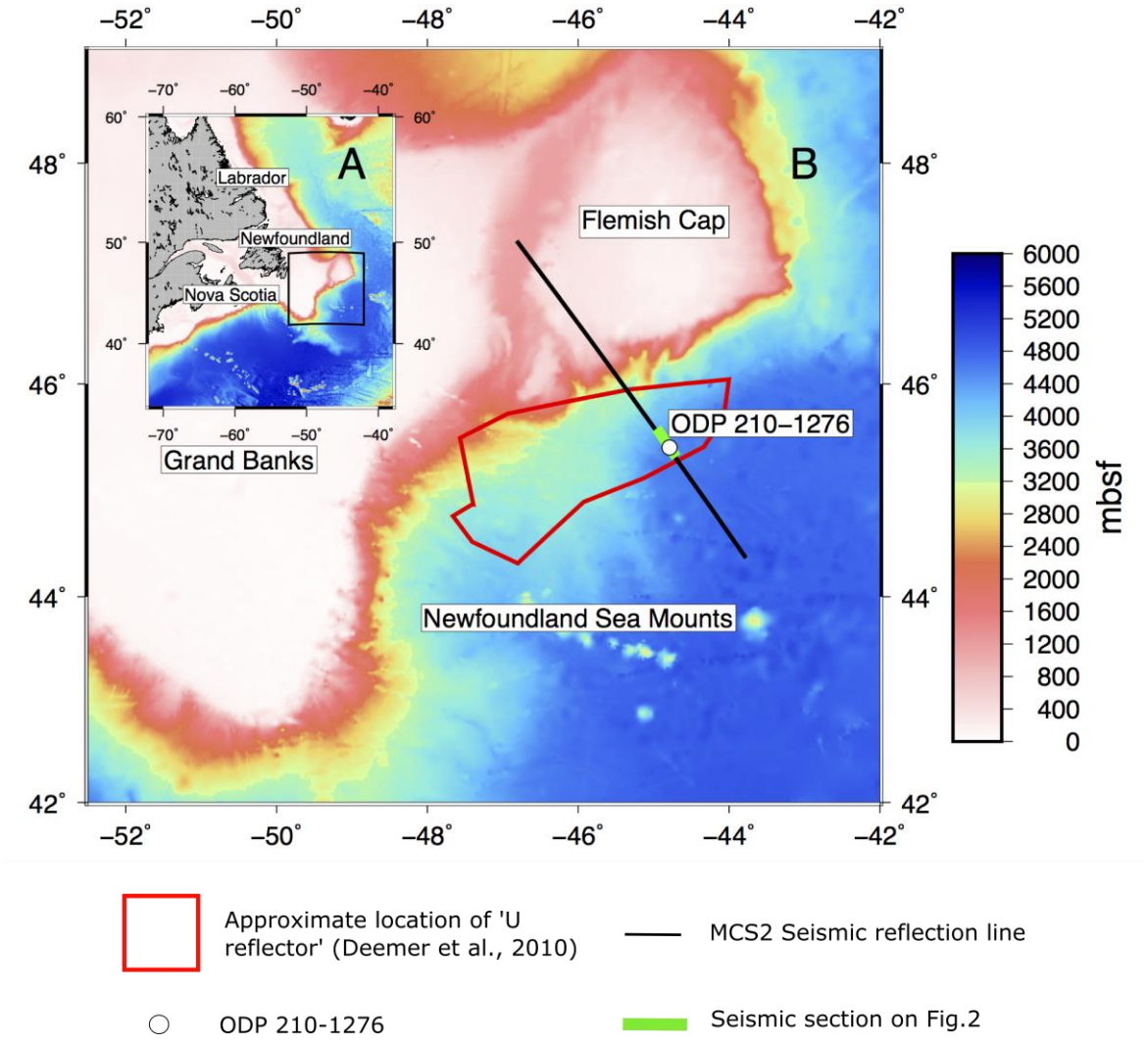

Figure 7.1

(a) An overview of the Eastern Canadian continental margin. (b) The study area showing the location of ODP site 210-1276, along with seismic line MCS2 (section shown in Fig. 7.2 in green) and the approximate location of the 'U-reflector' (Deemer et al., 2010). Bathymetry data produced from satellite altimetry by Smith and Sandwell (1997).

Name	Current top of unit (mbsf)	Current bottom (mbsf)	Thickness (m)	Depth when intruded (mbsf)	Youngest $^{40}Ar/^{39}Ar$ age (ma)	Oldest $^{40}Ar/^{39}Ar$ age (ma)
Upper sill	1612.7	1623	10.30	~260	104.7+/-1.7	105.9+/-1.8
Lower sill	1719	>1736.9	17.90	~590	95.9+/-2	99.7+/-1.8

Table 7.1

Intrusion parameters of the sills at ODP 210-1276. Current positions in well (Tucholke et al., 2004a), depth when intruded (Tucholke et al., 2007b) *and $^{40}Ar/^{39}Ar$ ages (Hart and Blusztajn, 2006).*

Previous work has associated the sills at this site with the widespread 'U-reflector' observed in 2D seismic reflection profiles (e.g. Fig. 7.2) across the Newfoundland basin (e.g. Shillington et al., 2004; Deemer et al., 2010). The U-reflector is considered to represent a suite of post- breakup magmatic intrusions covering an area of ca. 20,000 km^2 Deemer et al. (2010) in an otherwise nonvolcanic margin. It is observable on seismic reflection data as one or two high amplitude reflectors, at a depth corresponding to the igneous intrusions at ODP 210-1276. Within the resolution of the seismic reflection profile it is not possible to determine if the high amplitude reflectors correspond to singular or multiple igneous intrusions, but given the observed situation intersected by ODP 210- 1276 it is likely that the high amplitude reflectors at this depth across the Newfoundland Basin represent at least one igneous intrusion.

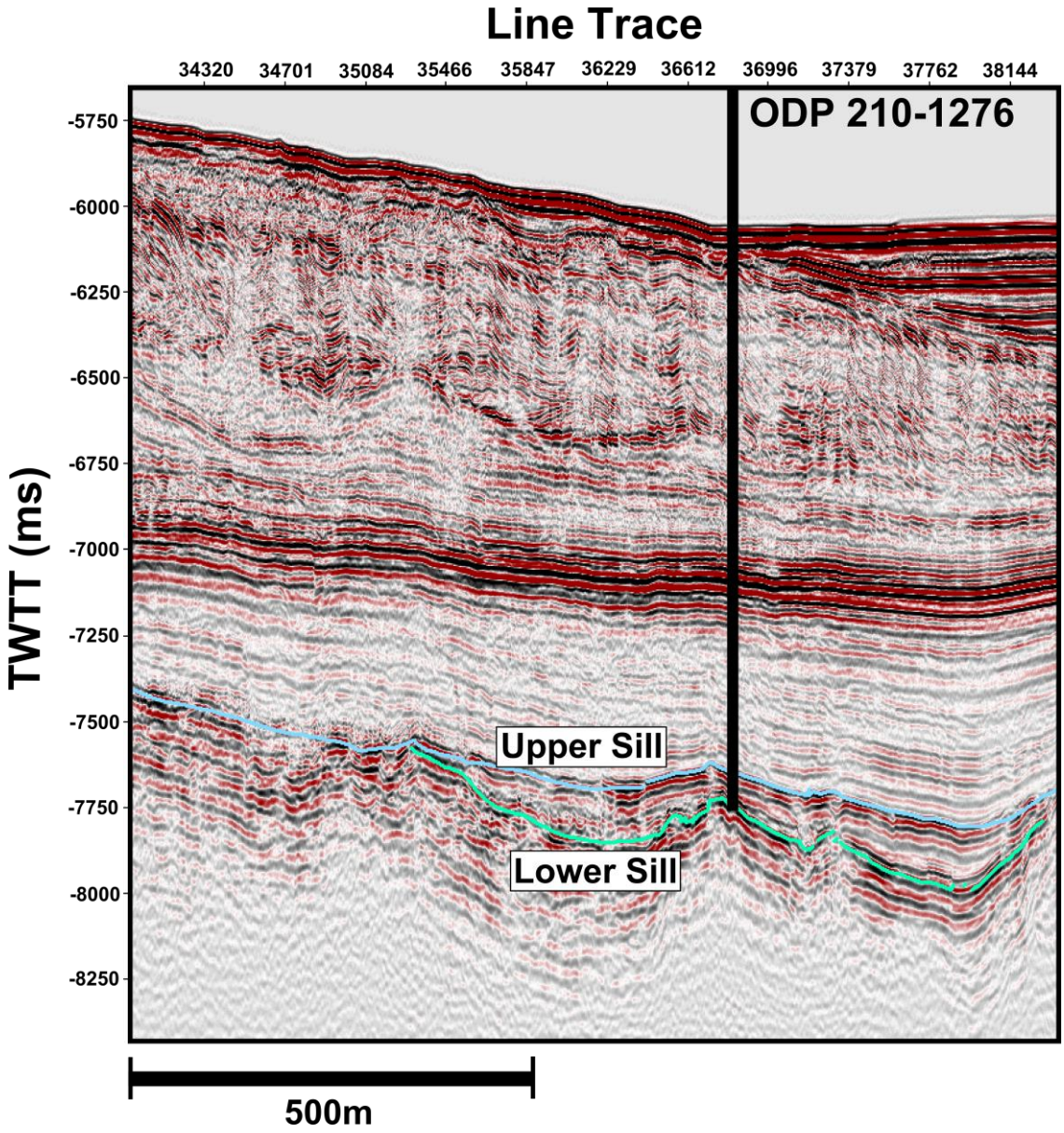

Figure 7.2

Segment of MCS (multichannel seismic) reflection profile SCREECH 2 (Studies of Continental Rifting and Extension on the Eastern Canadian Shelf) by Shillington et al. (2004) where it intersects ODP site 210-1276. The location of this seismic line segment is shown on the study area overview map (Fig. 7.1b). Interpretation of the U-reflector (green/blue lines) from Peron-Pinvidic et al. (2010).

The widespread nature of the sills on the Newfoundland margin (Deemer et al., 2010) implies that this igneous activity represents a significant margin-scale event. In contrast, no significant post-rift intrusive activity is known on the conjugate Iberian margin, implying an asymmetric post-breakup magmatic history (Peron-Pinvidic et al., 2010). The sills of the U-reflector are of interest due to their close proximity to the offshore Newfoundland petroleum systems. Karner and Shillington, (2005) qualitatively suggested that these sills could have implications for the thermal history of the region.

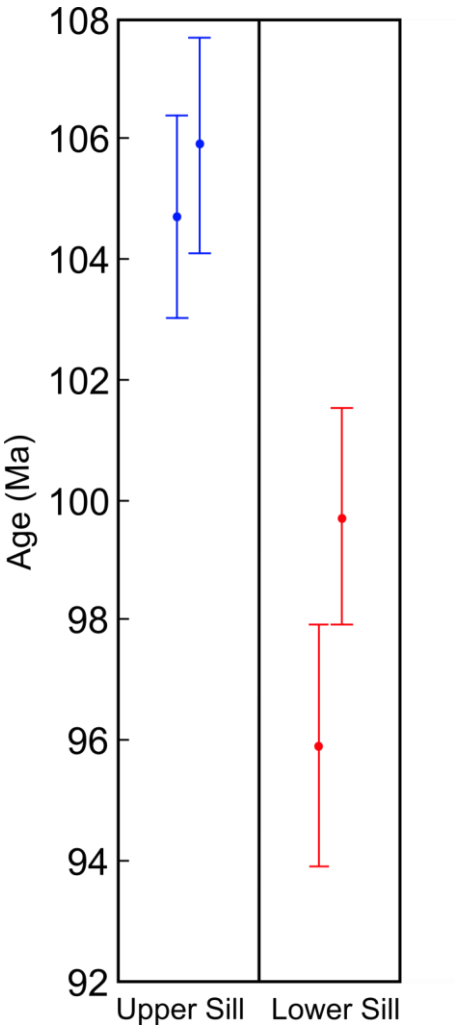

Figure 7.3

$^{40}Ar/^{39}Ar$ dates, and associated 2σ errors for the upper and lower sills from Hart and Blusztajn, 2006.

Chronological analysis by Hart and Blusztajn, (2006) of the sills at ODP 210-1276 provided $^{40}Ar/^{39}Ar$ dates of 104.7 ± 1.7 Ma and 105.9 ± 1.8 Ma for the upper sill, and 95.9 ± 2 Ma and 99.7 ± 1.8 Ma for the lower sill (Table 7.1 and Fig. 7.3). The $^{40}Ar/^{39}Ar$ dates demonstrate that there was a time interval of ca. 5–10 Myrs between the intrusions cooling to their closing temperatures. Compositionally, both sills are classified as alkali basalt – hawaiite (Hart and Blusztajn, 2006).

The sills are located within uppermost Aptian to lowermost Albian syn-rift sequences at ca. 90–160 m and ca. 200–270 m above basement for the upper and lower sills respectively. This is based on the interpretation of seismic reflection profiles, including the SCREECH MCS2 line which crosses ODP 210-1276 (Fig. 7.2), and calculated vertical seismic velocities which are; 4738–5030 ms^{-1}, 5527–6193 ms^{-1} and 1650–3200 ms^{-1} for the upper sill, lower sill and sediments between the sills, respectively, according to Tucholke et al. (2004b).

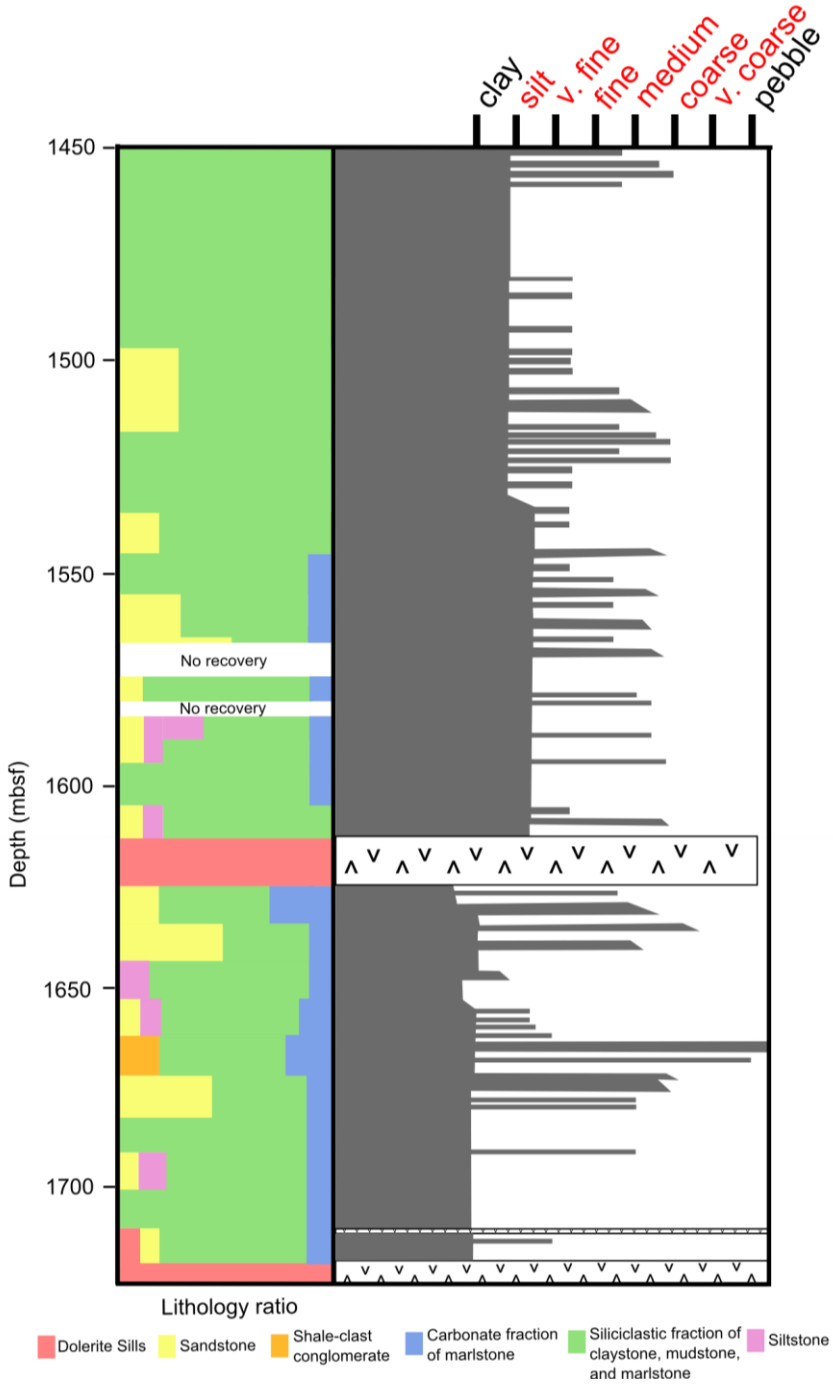

Figure 6.4

Lithostratigraphic column and grain size reproduced from Tucholke et al. (2004a) for the interval of ODP 210-1276 in proximity to the sills, with depth in mbsf (metres below sea- floor). The organic-rich sedimentary rocks of interest to this study can be found in several intervals and are depicted in pink.

The sills were intruded at shallow depths of ca. 260 m and ca. 590 m into relatively unconsolidated, and not overpressured sedimentary rocks, particularly in the lower 30 m of the section (Tucholke et al., 2007b). This suggests that at the drill site the upper sill had considerable mechanical support probably provided by nearby dykes, protecting the underlying sedimentary rocks from compaction due to the load of the later sedimentary over-burden (Peron-Pinvidic et al., 2010). The emplacement depths were calculated by consideration of the $^{40}Ar/^{39}Ar$ dates in the context of the nano-fossil based age vs depth curve provided by Tucholke et al. (2004a). This age depth relationship was established using zonal boundary ages of microfossils at ODP 210-1276. Karner and Shillington, (2005) used a reconstruction of porosity–depth relationships to estimate an intrusion depth of 0–556 m below sea floor. These two independent estimates do not account for any subsequent burial and compaction (Tucholke et al., 2007b).

The sedimentary rocks present at ODP 210-1276 include siltstones, sandstones, carbonates and shale-clast conglomerates (Fig. 7.4). Of most interest to this study are the organic-rich rocks found in several intervals in ODP 210-1276 (Fig. 7.4), as these could provide potential source material. Total Organic Carbon (TOC wt% – the amount of carbon bound in an organic compound) was collected between 801 and 1713 m below seafloor by Tucholke et al. (2004a). TOC values are recorded between 0 and 9.7 wt% at ODP 210-1276, with values in proximity to the intrusions <2 wt%. Pross et al. (2007) conducted a maturation study on the rocks in proximity to the upper sill describing them as predominantly dark grey mud- rocks, with minor sand to silt-based turbidites and black shales (Fig. 7.4).

7.3 Methodology

7.3.1 Model Setup

We performed numerical calculations to investigate the thermal influence of the igneous intrusions intersected at ODP 210-1276 on the surrounding sedimentary rocks. The temperatures obtained from one- dimensional finite difference MATLAB models were entered into the EASY%R_o model of Sweeney and Burnham, (1990) to produce theoretical vitrinite reflectance values.

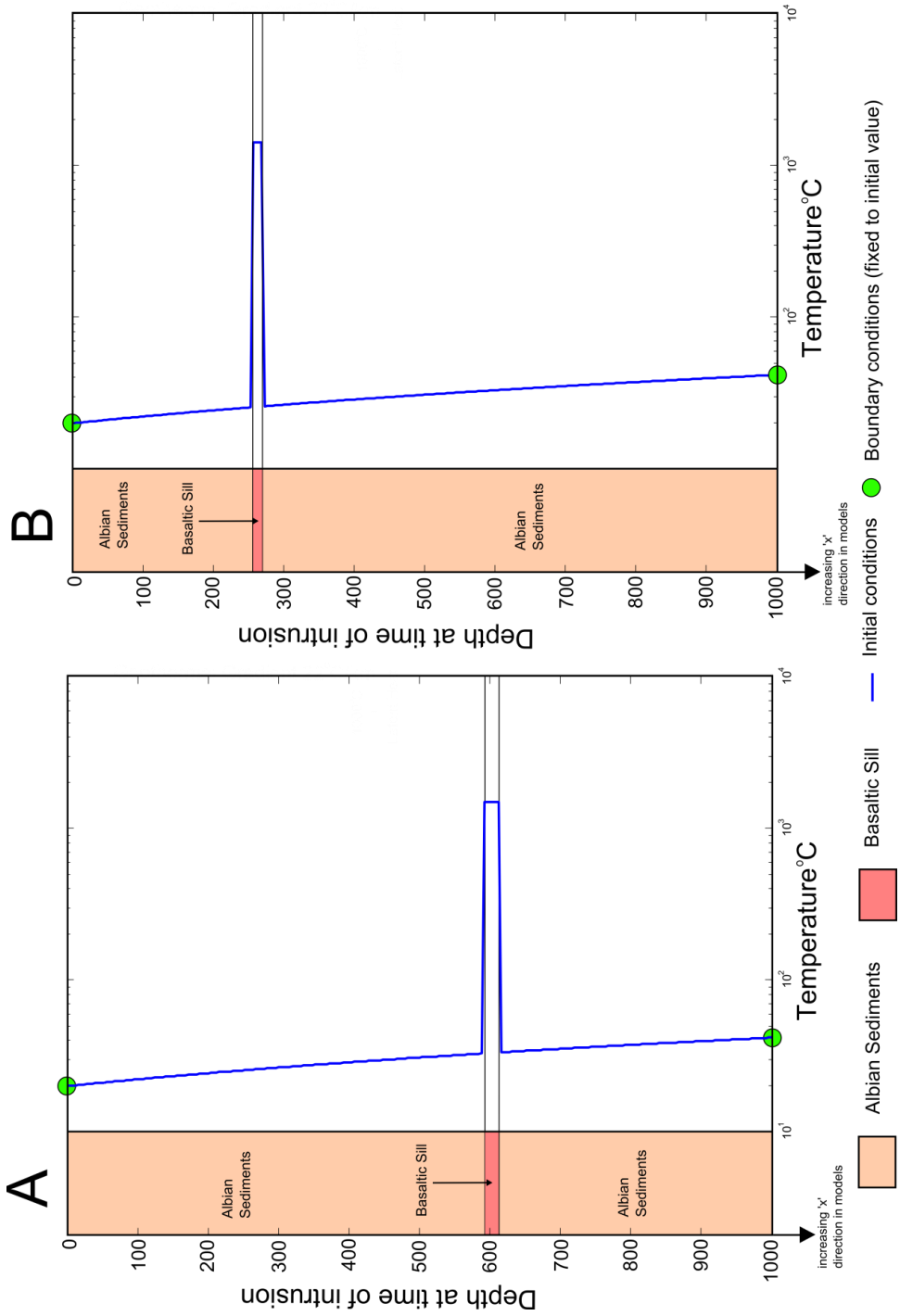

Figure 7.5

Schematic depiction of the model setup for (a) the lower sill and (b) the upper sill. The initial temperature profile is depicted in blue for both (a) and (b). The boundaries are fixed and are shown in green. The relative positions of the two lithologies in (a) and (b) are shown. The parameters applicable to these lithologies can be found in Table 7.2. Model resolution (dx) is 2 m and the time step (dt) is 0.1 years. The X direction in the model is down hole.

Thermal heat diffusion was considered to be the dominant process affecting thermal evolution, and is described in the models by:

$$\frac{\partial T}{\partial t} = D\frac{\partial^2 T}{\partial x^2} \qquad \textit{Equation 7.1}$$

where T is the Temperature, t is time, x is distance and D = the thermal diffusion coefficient:

$$D = \frac{k}{\rho C_p} \qquad \textit{Equation 7.2}$$

where k = thermal conductivity, ρ= density and C_p = specific heat capacity.

The simplifications and assumptions made in our model include: 1) the only form of heat transfer is considered to be conduction; 2) latent heat released from crystallisation of the sills is accounted for by the inclusion of a calculated higher starting temperature equivalent to an extra 488°C; 3) emplacement of the sills was instantaneous; 4) thermal parameters are not temperature dependent; 5) stratigraphical units are considered to be internally homogeneous; and 6) the regional geothermal gradient (Table 7.2) remained constant during margin evolution. The validity of these assumptions is discussed below.

Parameter	Symbol	Value	Units	Reference
Density of country rock	ρ_{host}	2400	kg m^{-3}	Wang et al. (2012)
Density of intrusion	$\rho_{intrusion}$	2960	kg m^{-3}	Wang et al. (2007)
Specific heat capacity of host	C_{p_host}	1090	J kg^{-1} °C^{-1}	Wang et al. (2012)
Specific heat capacity of intrusion	$C_{p\_intrusion}$	820	J kg^{-1} °C^{-1}	Barker et al. (1998)
Conductivity of organic rich host	K_{host}	2.1	W m^{-1} °C^{-1}	Wang et al. (2012)
Conductivity of intrusion	$K_{intrusion}$	2.5	W m^{-1} °C^{-1}	Wang et al. (2012)
Heat release from latent heat of crystalisation	ΔT_{latent}	488	°C	Calculated from $L_{intrusion}$ and $C_{p\_intrusion}$ Equation 3
Diffusion coefficient	D	Varies spatially	m s^{-2}	This work using Equation 2
Latent heat of crystalisation	$L_{intrusion}$	400	kJ kg^{-1}	Spear and Peacock (1989)
Geothermal gradient	G	21.75	°C km^{-1}	Keen (1979)
Starting temperature of intrusion	$T_{initial}$	1000	°C	Barker et al. (1998)
Temperature at surface	T_{surf}	20	°C	This work
Spatial discretisation step	dx	2	m	This work
Timestep	dt	0.1	years	This work
Distance between sills at time of intrusion	H_{past}	330	m	(Tucholke et al. 2004a)
Current distance between sills	$H_{current}$	96	m	(Tucholke et al. 2004a)
Current depth of upper sill top	$S_{current}$	260	m (below sea floor)	(Tucholke et al. 2004a)
Upper sill top at time of intrusion	S_{past}	1612.7	m (below sea floor)	(Tucholke et al. 2004a)
Compaction factor	C	29.09%	%	Calculated from $H_{current}$ and H_{past}
Burial	B	1353	m	Calculated from $S_{current}$ and S_{past}

Table 7.2

Parameters utilised in the thermal modelling and symbols used in equations, excluding the EASY%R_o parameters which are defined alongside the equations and in Table 7.3.

1) Our models assume that heat transfer was by conduction only (e.g. Fjeldskaar et al., 2008; Aarnes et al., 2010; Wang et al., 2010, 2007). Advective heat trans- port by hydrothermal activity is negligible in low permeability materials such as shales (Aarnes et al., 2010), although the stratigraphic sequence encountered in ODP 210-1276 (Fig. 7.4) is dominated by sandstones (Tucholke et al., 2004a) with a higher permeability than shale. Therefore, additional heat advection due to heating and circulation of pore waters may lead to more rapid cooling than conduction alone, and our results may represent a minimum estimate of the cooling rate.

2) We approximate the latent heat effect of magma crystallisation in our model by applying a starting temperature of the sill that is increased with the released heat during magma crystallisation (Equation 7.3):

$$\Delta T_{latent} = \frac{L_{intrusion}}{C_{p\ intrusion}} \qquad \textit{Equation 7.3}$$

where ΔT_{latent} is the additional heat from latent heat of crystallisation, $L_{intrusion}$ is the latent heat of crystallisation (Spear and Peacock, 1989) and C_p intrusion is the specific heat capacity of mafic intrusions (Barker et al., 1998).

The sills are compositionally alkali basalt-hawaiite according to Hart and Blusztajn, (2006). The initial temperature of the intrusion is therefore taken to be 1000°C; the same temperature as previous work modelling intrusions of similar composition (e.g. Barker et al., 1998). Inclusion of latent heat of crystallisation gives a modelled starting temperature

of 1488°C, this includes 488°C additional heat from the latent heat of crystallisation, on top of the initial temperature value of 1000°C for the sills as in Barker et al. (1998).

Latent heat has been omitted by some previous workers in this area of study (e.g. Barker et al., 1998; Fjeldskaar et al., 2008), whereas in others it has been included (e.g. Wang et al., 2012). We choose to include latent heat in our models as it is a physical phenomenon, which could have a significant effect on the results. Although it has been noted by Galushkin, (1997) that models accounting for latent heat could potentially over estimate its effects, as all the additional heat is added instantaneously rather than over the duration in which cooling occurs.

3) The main models presented herein assume instantaneous intrusion. This is a reasonable assumption because the periods of emplacement were probably very short, as multiple samples from the sills gave statistically similar $^{40}Ar/^{39}Ar$ ages (Hart and Blusztajn, 2006). Noninstantaneous intrusion will reduce the thermal effects of the intrusion as multiple smaller bodies will cool faster, than a singular large body. Previous authors modelling the influence of sills on organic matter have also assumed intrusion to be instantaneous (e.g. Aarnes et al., 2010). Considering emplacement to be instantaneous increases the thermal effects of the intrusions in the modelling, and thus may lead to an overestimate of the maturation of organic-rich sedimentary rocks.

4) Keeping the thermal parameters (specific heat capacity and thermal conductivity – Table 7.2) constant over a temperature range simplifies the modelling and is an assumption made by most previous work (e.g. Fjeldskaar et al., 2008). It should also be considered that reducing the variables allows us to study the main controls on maturation, particularly as this study has observed vitrinite reflectance data available to provide a constraint.

6) Our model incorporates spatial variability in the thermal parameters between the units, but the units are internally assumed to be homogeneous, with the host having the thermal properties of dry organic-rich shale. It is assumed to be dry so that heat transfer occurs through conduction only. Two units are recognised in our model; (1) 'host rock' and (2) 'sills' (Table 7.2, Fig. 7.5). This is a simplification also made by previous work (e.g. Wang et al., 2012) which utilised separate values of thermal conductivity, density and specific heat capacity for 'wall rock' and 'magma').

6) The background geothermal gradient used in the model is based upon calculations by Keen, (1979) for the current geothermal gradient on other parts of the Eastern Canadian Margin (17.5°Ckm^{-1} for the Scotian Margin and 26 °Ckm^{-1} for the Labrador Shelf). Our model utilises an average of these values of 21.75 °Ckm^{-1} (Table 7.2) as the study area is located between the Scotian Margin and the Labrador Shelf. Goutorbe et al. (2007) produced a detailed analysis of heat flow along the Eastern Canadian margin from offshore Labrador to Nova Scotia finding, there was no significant variation between the different sub areas on the margin and that the nature of the continental basement and the age of the ocean floor had little influence. The geothermal gradient can justifiably remain constant for the modelled period as it only represents 60, 000 years, and these sills were both emplaced post margin breakup.

The heat diffusion equation is solved in MATLAB with a finite differences method. Initial temperature conditions are shown in Fig. 7.5, and prescribed temperature boundary conditions equal the initial conditions. We model sills of 10 and 18 m thickness for which a vertical resolution of 2 m proved sufficient. Our discretisation allows for spatial variation in thermal parameters.

The $^{40}Ar/^{39}Ar$ ages provided by the previous work of Hart and Blusztajn, (2006) record the closing temperatures, implying that these two cooling events were at least 1.5 Myrs apart (Fig. 7.3 and Table 7.1), a timescale that will be shown below to be much larger than the thermal equilibrium timescales of the sills. In our primary models we therefore consider the sills as individual thermal events rather than having occurred simultaneously. This is an improvement over previous models that consider multiple intrusions occur simultaneously (e.g. Fjeldskaar et al., 2008), potentially overestimating the total heating event. The 40Ar/39Ar dates provided by Hart and Blusztajn, (2006) are highly statistically significant, with a ca. 7.5 Myrs difference using 2σ uncertainties in measured age between the two sills. Comparison between the maximum temperatures achieved (and resulting maturation effects) when simultaneous intrusion is assumed was also modelled, and compared to the results of modelling the sills separately (Fig. 7.6).

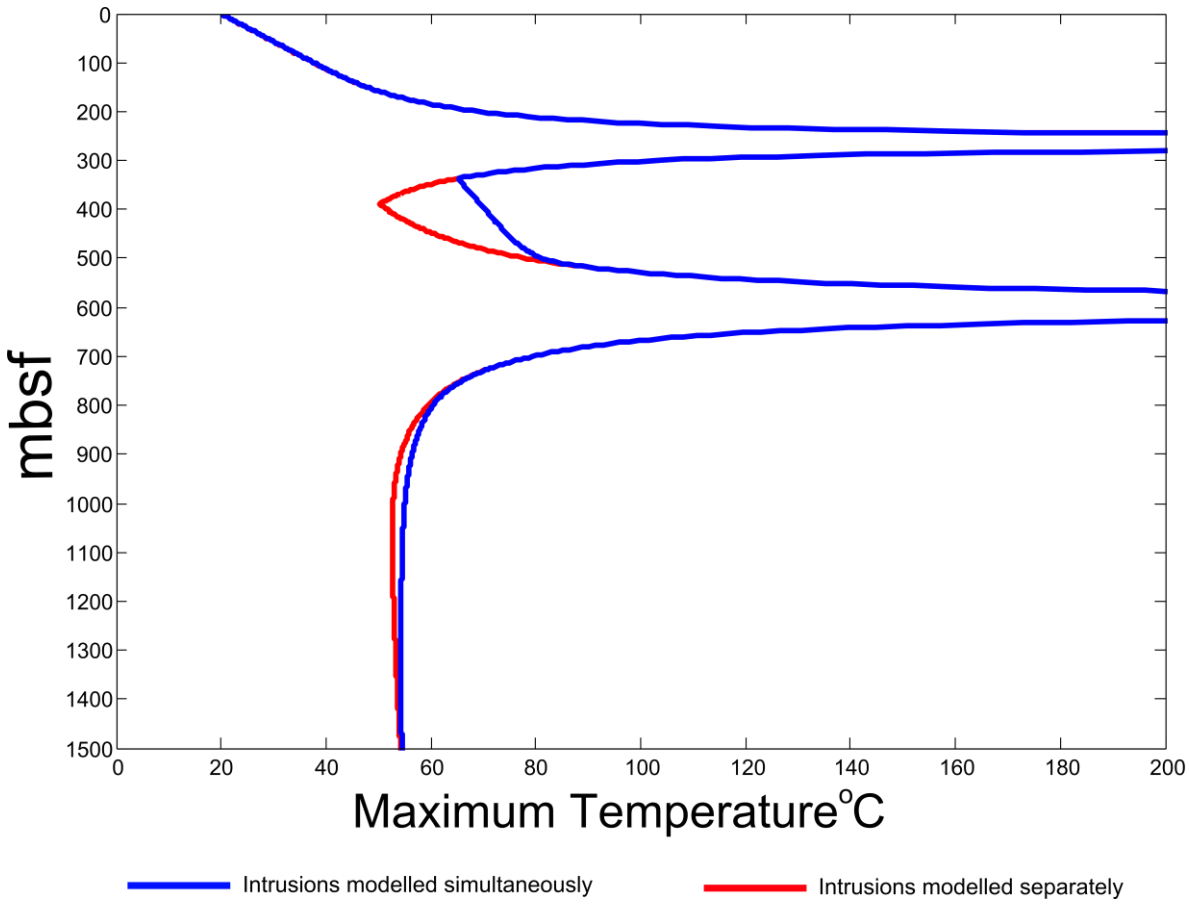

Figure 7.6

Maximum temperatures achieved when the sills are modelled separately and simultaneously. All other figures depict the results from either a singular sill or models where the sills cooled separately, and the results subsequently combined.

As $^{40}Ar/^{39}Ar$ ages of (Hart and Blusztajn, 2006), represent the time of cooling to closure temperature, they do not allow us to rule out if the sills acted as long-term conduits for magma. This is plausible in what appears on seismic reflection data to be a large, complex, intrusive system. If a sill acts for a large duration of time as a conduit for magmatism, then the thermal effect on the surrounding sediments will be increased when compared to an instantaneously intruded sill.

To provide a constraint on the duration in which a sill acted as a magmatic conduit we modelled systems in which the upper sill acted as a magma conduit for 10, 100 and 1000 years prior to cooling, quantifying the effects on theoretical vitrinite reflectance values produced using the EASY%R_o of Sweeney and Burnham, (1990). The modelled vitrinite reflectance values are then compared to the observed values of Pross et al. (2007), allowing estimations of the duration that the upper sill acted as a magmatic conduit to be constrained.

Emulating an open magmatic conduit is achieved by maintaining the sill at its starting temperature for the desired duration prior to cooling. In these models the sill has a starting temperature of 1000°C, with the additional 488°C contribution from the latent heat of crystallisation added when the sill is allowed to cool. The magmatic conduit is assumed to be receiving a constant supply of magma, until it is allowed to cool.

During each model run the temperature at the boundaries was fixed to the initial conditions. Our discretisation of the thermal diffusion equation (Equation 7.1 and 7.2) allows for spatial variation in thermal parameters. The model resolution (dx) is 2 m and the timestep (dt) is 0.1 years in all the models we ran. The values used for the parameters in equations 7.1, 7.2 and 7.3 are given in Table 7.2.

7.3.2 Vitrinite reflectance modelling

Vitrinite reflectance (%R_o) is one of the most widely used indicators of source rock maturity. It is measured optically (Bostick and Alpern, 1977), and is useful in maturation studies as the degree of reflectivity varies smoothly and predictably with temperature (Burnham and Sweeney, 1989). However, there are several known drawbacks with the use of vitrinite reflectance as an indicator of organic sediment maturity (Heroux et al., 1979).

These include but are not limited to, measurements being taken from similar known vitrinite minerals and the possible reworking of organic material.

This work utilises the EASY%R_o model of Sweeney and Burnham, (1990), to calculate theoretical vitrinite reflectance values. EASY%R_o calculates vitrinite reflection against time for a given stratigraphic level if the temperature-time history has been calculated, and can be used to produce a depth profile if multiple levels are calculated. It is a simplified version of the earlier VITRIMAT model of Burnham and Sweeney, (1989), which is based on experimentally derived kinetic responses in a wide range of organic matter to account for the elimination of water, carbon dioxide, methane and higher hydrocarbons from vitrinite. The model is applicable over a wide range of vitrinite reflectance values (%R_o), and heating rates.

EASY%R_o is based on an Arrhenius first-order parallel reaction approach with a distribution of activation energies (Table 7.3), thus the reaction can be described as:

$$\frac{\partial w}{\partial t} = -kw \qquad \textit{Equation 7.4}$$

where the reaction rate k is defined as:

$$k = Aexp(-E/RT) \qquad \textit{Equation 7.5}$$

where w = amount of unreacted component, A = frequency or pre-exponential factor, E = activation energy, R = universal gas constant and T = temperature. EASY $\%R_o$ requires the extent of the reaction F (transform ratio) to be computed using:

$$F = -\frac{w}{w_0} = 1 - \Sigma_i f_i \left[\frac{w_i}{w_{0i}}\right] \qquad \textit{Equation 7.6}$$

where w = amount of unreacted component, w_0 = the initial concentration of the total reactant, w0i = initial concentration for component i and f_i = weight for i_{th} reaction (stoichiometric factor – Table 7.3). The transform ratio F for virtinite reflectance (or the extent of the reaction) can then be used to calculate the EASY$\%R_o$ vitrinite reflectance value using:

$$EASY\%R_0 = exp\ (3.7F\text{-}1.6) \qquad \textit{Equation 7.7}$$

where 3.7 and -1.6 are scaling factors calculated in the original derivation of EASY$\%R_o$ Sweeney & Burnham (1990). A comprehensive description of the EASY$\%R_o$ model is given in Appendix I of Sweeney and Burnham, (1990), while a detailed explanation of the application of EASY$\%R_o$ to a similar subsurface setting as modelled in this analysis is provided by Fjeldskaar et al. (2008) in their Appendix B.

Stoichiometric Factor (f_i)	Activation Energy (E) (kcal/mole)
0.03	34
0.03	36
0.04	38
0.04	40
0.05	42
0.05	44
0.06	46
0.04	48
0.04	50
0.07	52
0.06	54
0.06	56
0.06	58
0.05	60
0.05	62
0.04	64
0.03	66
0.02	68
0.02	70
0.01	72

Table 7.3

Stoichiometric factors and activation energies used in the EASY%R_o model produced by Sweeney and Burnham, (1990).

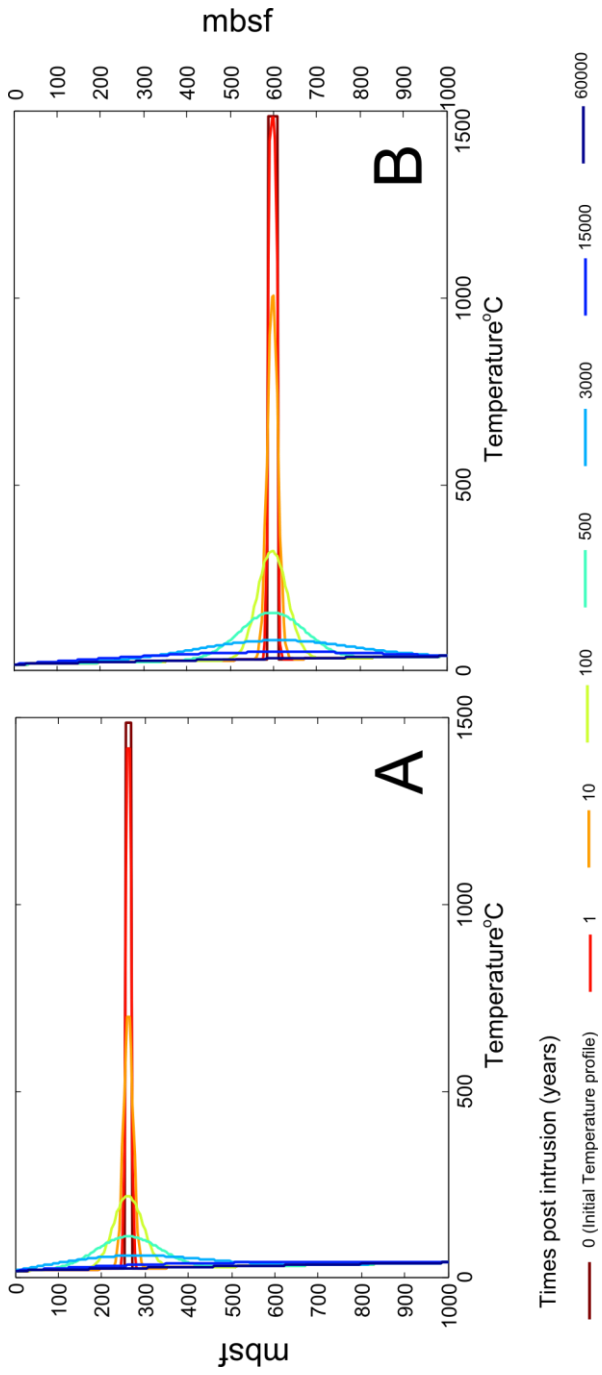

Figure 7.7

1D Thermal profiles for select times during the modelled cooling through from the upper (a) and lower sill (b) at ODP 210- 1276. Time 0 depicts the initial temperature profile in each case, including the addition of the latent heat of crystallisation. Modelling of the sills demonstrates that by 60,000 years the thermal anomaly created by the intrusion is virtually indistinguishable against the background geothermal gradient. The initial temperature conditions are shown as the time 0 years. Depth (m) is the depth at the time of intrusion according to the reconstruction by Tucholke et al. (2007).

The sills were modelled separately, recording the temperature of every node for every timestep for the entire 60,000 years of each model run (Fig. 7.7). This produces a temperature-time pathway for every node, which can be input into the EASY%R_o model of Sweeney and Burnham, (1990). This procedure, however, does not account for maturation as a result of burial (Fig. 7.8).

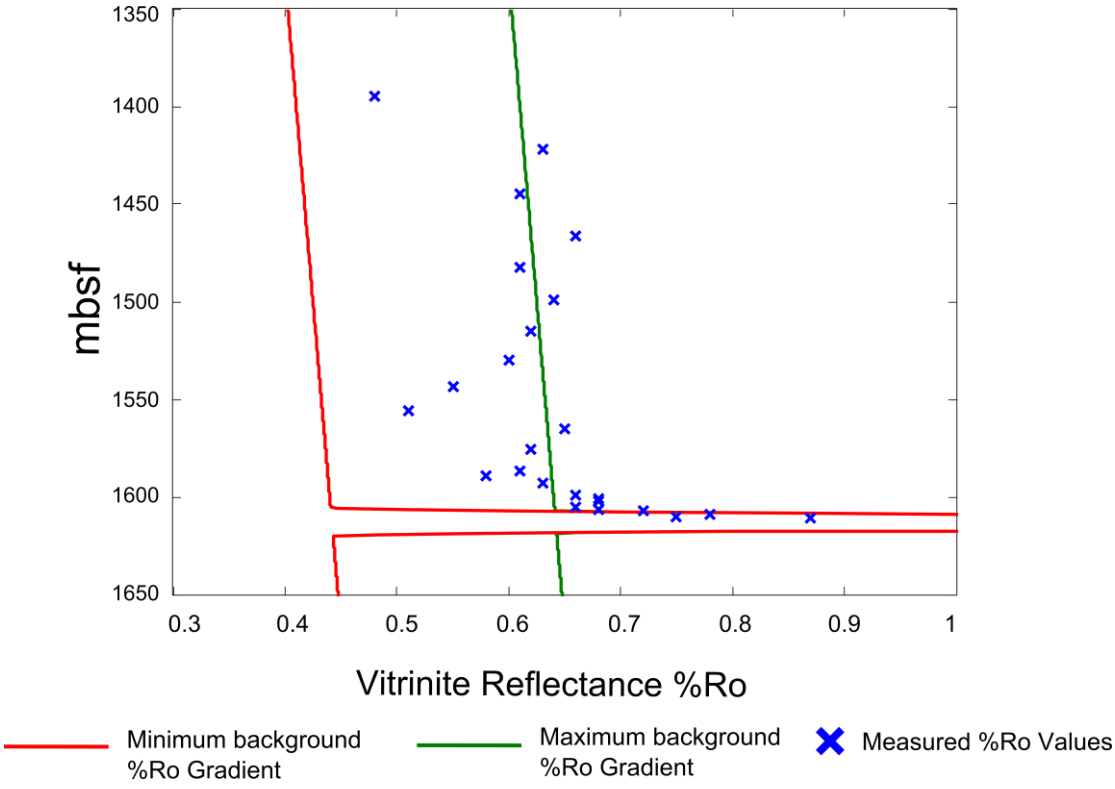

Figure 7.8

Measured %R_o values (Pross et al., 2007) alongside modelling results using both the minimum and maximum %R_o background values provided in Allen and Allen, (2005). The data used by Allen & Allen (2005) are a compilation of data from 28 extensional basins, where the range of surface intercept is between 0.2 and 0.4%R_o and with a gradient of 0.15 ± 0.09%R_o km^{-1} for depths <4 km. Both lines on this plot have a gradient of 0.15% R_o km^{-1}, with the 'mini- mum' using the surface intercept of 0.2% R_o and the 'maximum' using the surface intercept of 0.4%R_o.

As the sills were intruded and modelled at a shallow depth (260 and 590 m for the upper and lower sills respectively – Tucholke et al., 2004a), they are thus exposed to relatively

low background temperatures and therefore would not produce a representative background $\%R_o$ gradient irrespective of model run time. To account for 'Background' maturation, resulting from burial-related heating a vitrinite gradient is applied after calculation of the maturation due to the heat from the sills. The background, vitrinite reflectance gradient used is calculated by comparing the vitrinite reflectance data for ODP 210-1276 by Pross et al. (2007) with a compilation from 28 extensional basins (Allen and Allen, 2005) (Fig. 7.8). The data used by Allen and Allen, (2005) show a range of surface intercepts between 0.2 and 0.4 $\%R_o$ and with a gradient of $0.15 \pm 0.09\%$ R_o km^{-1} for depths <4 km. We have used a surface intercept of 0.4 and a gradient of 0.15% R_o km^{-1} in our models as the observed data for ODP 210-1276 of Pross et al. (2007) lie at the upper end of the values for its depth. This method has allowed us to apply a representative background $\%R_o$ gradient that has been calibrated using the (albeit limited) observed $\%R_o$ data of Pross et al. (2007) (Fig. 7.8).

Modelled $\%R_o$ is calculated as the maximum of the modelled vitrinite reflectance due to magmatic heating and the vitrinite reflectance due to burial-related heating at every depth node within the model. This procedure produces an estimate of vitrinite reflectance profile for the whole of ODP 210-1276, incorporating both the back- ground, burial-related maturation and the maturation effects of the sills.

7.3.3 Burial and Compaction

The sills were modelled at the estimated depths at the time of intrusion, as reconstructed from nano-fossil based age depth curves in Tucholke et al. (2004a). However, further burial and compaction of the sedimentary rocks occurred following intrusion. To allow accurate comparison between the modelled and the observed vitrinite reflectance profiles (Fig. 7.9), we have therefore corrected the models for post-intrusion burial and compaction

(Fig. 7.10). We assume that the sedimentary rocks underwent uniaxial compaction, but the thickness of the sills remains unchanged during burial. Post-intrusion compaction will have reduced the vertical extent of the thermal aureole.

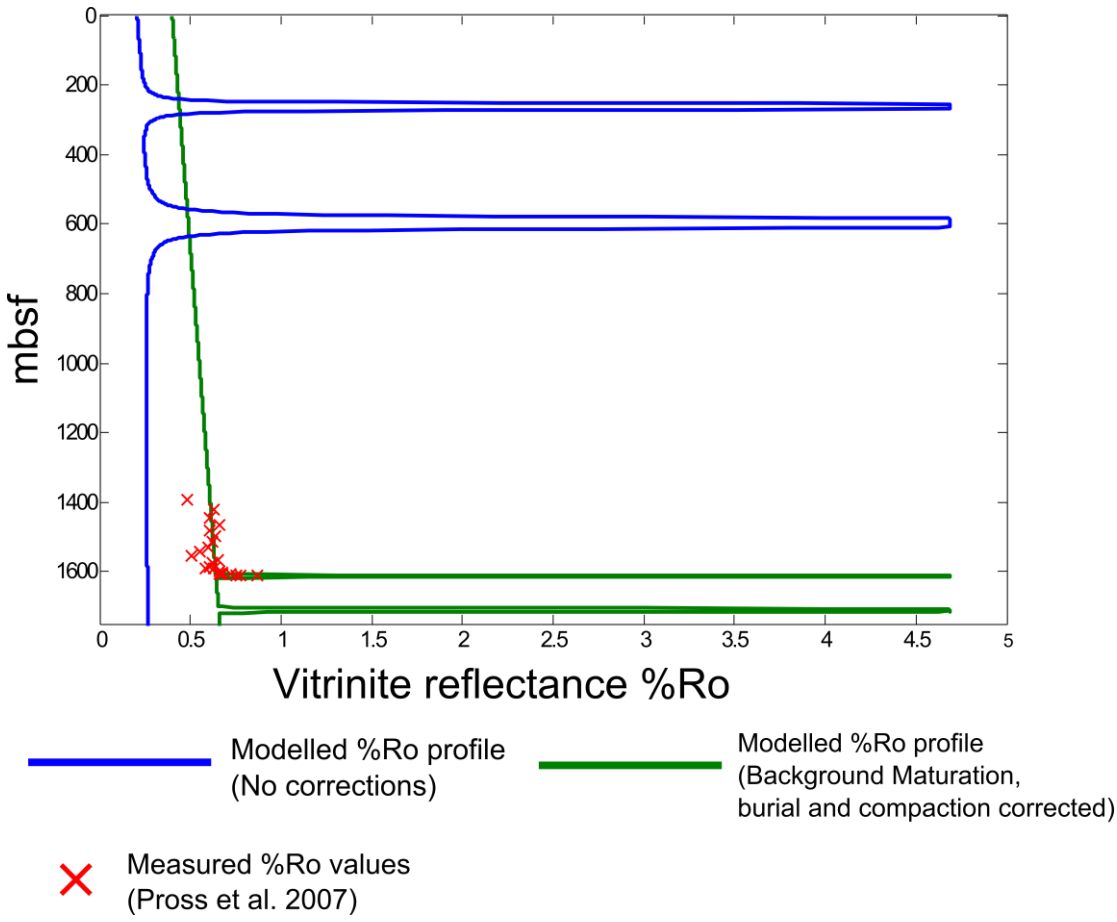

Figure 7.9

EASY%R_o vitrinite reflectance modelling (Sweeney and Burnham, 1990) results in proximity to both the upper and lower sills without any compensation for background maturation, compaction or burial (blue), alongside results corrected for background maturation, compaction and burial (green). This demonstrates the need to account for post-intrusion burial and compaction, and suggests that the spatial extent of the thermal influence upon maturation of these sills was much greater shortly after intrusion, but subsequent compaction has reduced the vertical extent of the aureole in the well.

Compaction is calculated by assuming uniform vertical shortening using the current vertical distance between the sills in the well by Tucholke et al. (2004a), and the

reconstructed depths at the time of intrusion from Tucholke et al. (2007). This compaction factor was then applied uniformly to all sedimentary rocks at ODP 210-1276. This is reasonable as the rocks found between the sills are lithologically comparable to the relevant parts of the well (sections thermally influenced by the sills).

The position of the sills was corrected to account for burial again using the reconstructed depths at the time of intrusion of Tucholke et al. (2007) and the current depth in the well provided by Tucholke et al. (2004a). The burial correction was calculated from the top of the upper sill (in the well and the modelled depths). Both the compaction and burial corrections are schematically depicted in Fig. 7.10.

Compartmentalisation of sedimentary basins by sill complexes is a well-known phenomenon (e.g. Holford et al., 2012). It should therefore be noted that this compartmentalisation will cause the degree of compaction sediments have undergone to be extremely variable. For this reason, our compaction correction is only applicable to the situation intersected at ODP 210-1276, and is unlikely to be representative of the entire area covered by the 'U-reflector'.

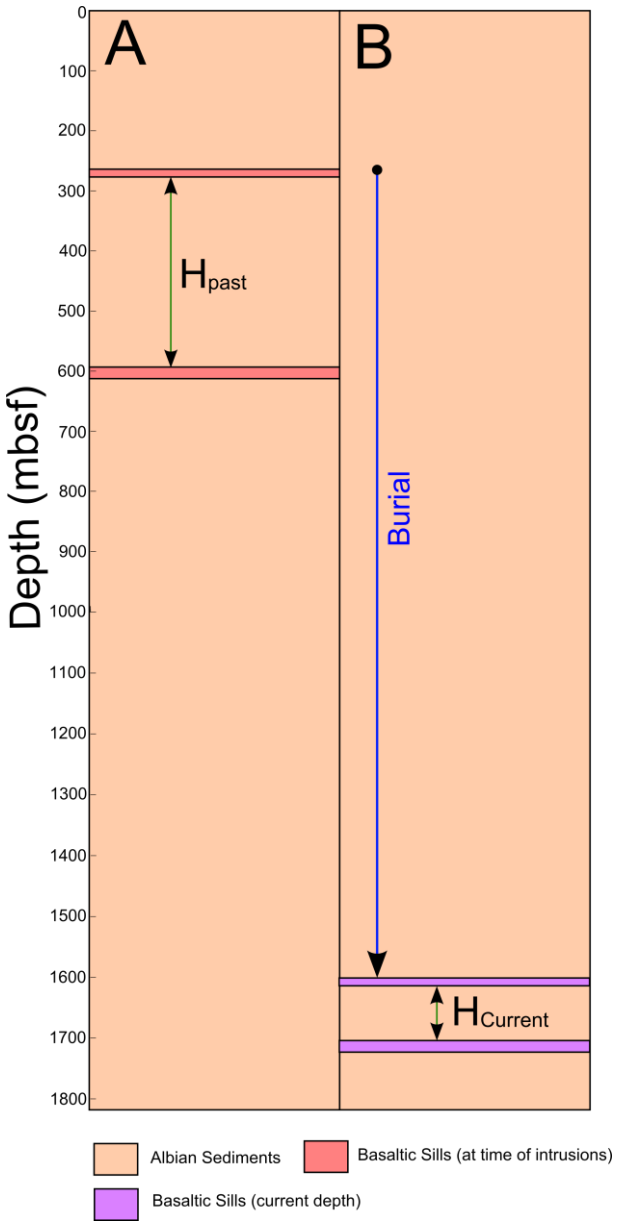

Figure 7.10

A schematic depiction of the methodology used to account for sediment compaction and burial where; (a) is the reconstructed depths at time of intrusion and (b) represents the current depths recorded at ODP-210-1276. Compaction of the profile is calculated using the % difference between the measured current distance between the sills in the well (Hcurrent) and the reconstructed separation at the time of the intrusion (Hpast). This value was then taken to be the sediment compaction % for the whole profile. The sills are assumed to have remained the same thickness. Burial is measured in reference to the top of the upper sill, using the reconstructed value of 260 m and the current position in the well of 1612.7 m.

It can be shown that heating due to burial during the period of intrusive activity is negligible. If we consider the minimum and maximum ages of the upper and lower sills, by taking the mean $^{40}Ar/^{39}Ar$ ages of Hart and Blusztajn, (2006) (Fig. 7.3 and Table 7.1) and the minimum and maximum 2σ uncertainties, it is likely that the shortest time between intrusion of the upper and lower sills was 1.5 Myrs and the longest time was 13.8 Myrs. Using the sedimentation rate of ca. 17.8 $mMyr^{-1}$ noted by Tucholke et al. (2004a) at ca. 100 Ma these durations translate to upper and lower limits on the amount of burial as 27 and 246 m respectively. Applying the upper limit scenario (i.e. 246 m of sedimentation) to the geothermal gradient used in the model would only translate to a temperature difference of 5.4 K (0.246 km x 22°Ckm^{-1}), and thus the effect of additional burial-related maturation on organic matter would be negligible. All plots showing the sills at their current depth have been corrected for compaction and burial. This is consistent with our approach of modelling intrusion of the upper and lower sills as distinct thermal events.

7.3.4 Hydrothermal activity

Although not the primary focus of this study, the effects of hydrothermal activity were estimated by increasing the thermal diffusivity for 10 and 20 m either side of the upper intrusion by one order of magnitude (Fig. 7.11). Previous work by Polyansky et al. (2003) on hydrothermalism induced by mafic intrusions emplaced at depths of 300–400 m, indicates that the effects can be observed above an intrusion at a distance of up to 1.5 times the diameter of the intrusion, while beneath an intrusion it can be observed up to a distance that is similar to the width of the intrusion. The upper sill at ODP 210-1276 is 10.3 m thick, thus in our model, enhanced diffusivity aureoles of 10 and 20 m (Fig. 7.11) are used, as a 20 m maximum extent of hydrothermalism either side of the sill is greater than the maximum estimates provided by Polyansky et al. (2003). As a result, a 20 m maximum

extent should overestimate the effects of hydrothermalism upon maturation, providing an end-member scenario.

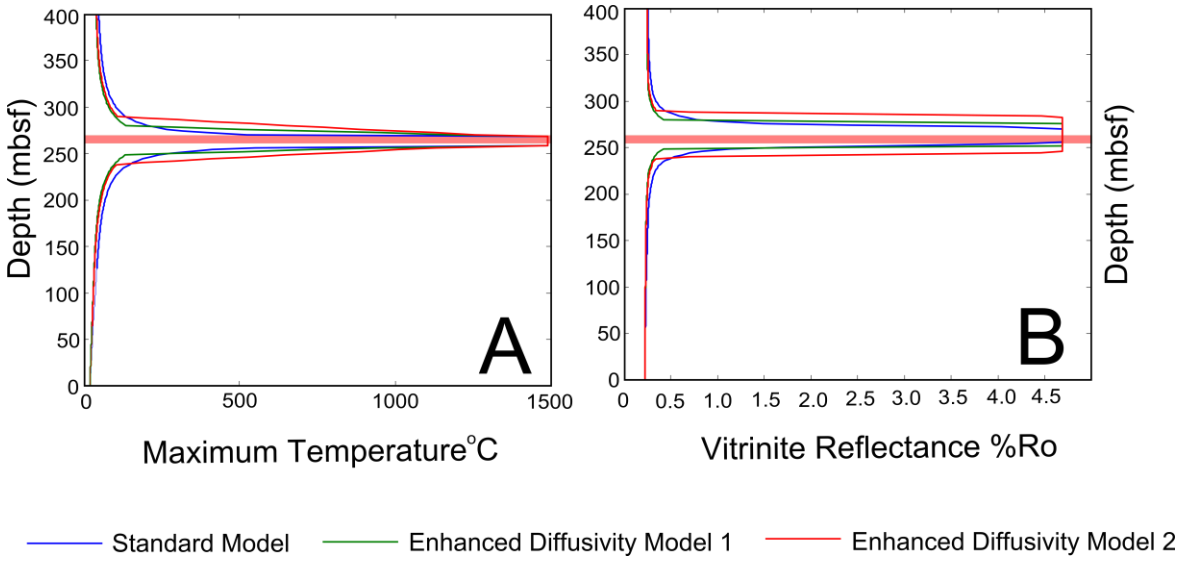

Figure 7.11

Maximum temperatures (A) and EASY%R_o vitrinite reflectance modelling results (B) in proximity to the upper sill using both the standard modelling parameters outlined in the methodology and two models for 'enhanced' diffusivity to emulate the effects of hydrothermalism as a heat transfer mechanism. Model 1 represents increasing the diffusivity by one order of magnitude for 10 m either side of the sill, while Model 2 represents increasing diffusivity by 1 order of magnitude for 20 m either side of the sill.

Omission of advection is an assumption made by most workers in this field (e.g. Fjeldskaar et al., 2008). This is probably the least reasonable of our assumptions as the effects of hydrothermal alteration have been observed in the well as subvertical calcite veins by Tucholke et al. (2004a) and potentially on seismic in the form of disturbed Albian sedimentary rocks above the U-reflector by Peron-Pinvidic et al. (2010) at ODP 210-1276.

7.4 Results

The final model outputs are shown in Figs 7.6, 7.7, 7.11, 7.12, 7.13 and 7.14. Figures 7.12, 7.13 and 7.14 are depth and compaction corrected, whereas Figs 7.6, 7.7 and 7.11 are presented as the depth at time of sill intrusion.

Figure 7.6 depicts the maximum temperatures achieved from the models when the sills are intruded simultaneously alongside the results from the standard model, in which the sills are modelled separately. These results demonstrate that if simultaneous intrusion of multiple igneous bodies is assumed higher temperatures are achieved in proximity to the sills, particularly in the interval between the sills.

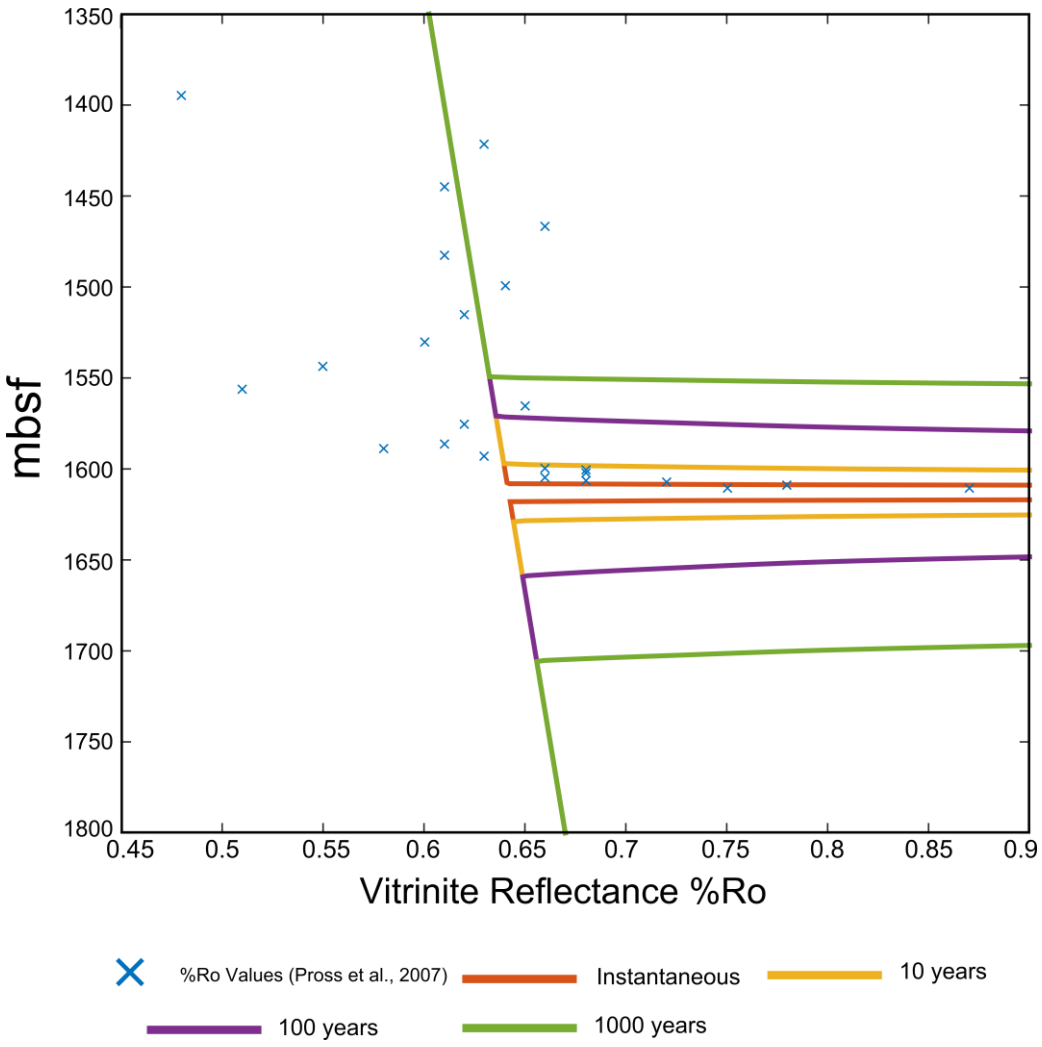

Figure 7.12

EASY%R_o vitrinite reflectance modelling results (Sweeney and Burnham, 1990) produced by maintaining the starting temperature of the upper sill for 10, 100 and 1,000 years. This emulates the heating effects which would be caused by the upper sill remaining a magmatic conduit prior to the magma cooling to the closing temperature as recorded by the $^{40}Ar/^{39}Ar$ ages.

The temperature profiles for select times for the upper and lower intrusions are shown in Fig. 7.7. It can be seen that after approximately 15,000 years the thermal perturbation caused by the intrusions are virtually indistinguishable from the background geothermal gradient. As expected the thicker, lower sill takes longer to cool. The results demonstrate

that the older sill had cooled to a value indistinguishable from the background geothermal gradient well before the second sill was intruded.

The results of the hydrothermal emulation models are presented in Fig. 7.11. It can be seen that even when the thermal diffusivity is increased by 1 order of magnitude for 20 m either side of the sill (Model 2 – the maximum hydrothermal influence modelled) the overall maximum temperature profile remains relatively unaffected and thus the influence upon maturation is also relatively insignificant as shown by the EASY%R_o modelling results (Fig. 7.11).

The EASY%R_o vitrinite reflectance results from the magmatic conduit duration experiments are provided in figure 7.12, along with the observed vitrinite reflectance values from Pross et al. (2007). These models show that in order to produce the observed vitrinite reflectance values above the upper sill, the duration in which the upper sill acted as a conduit probably was <10 years.

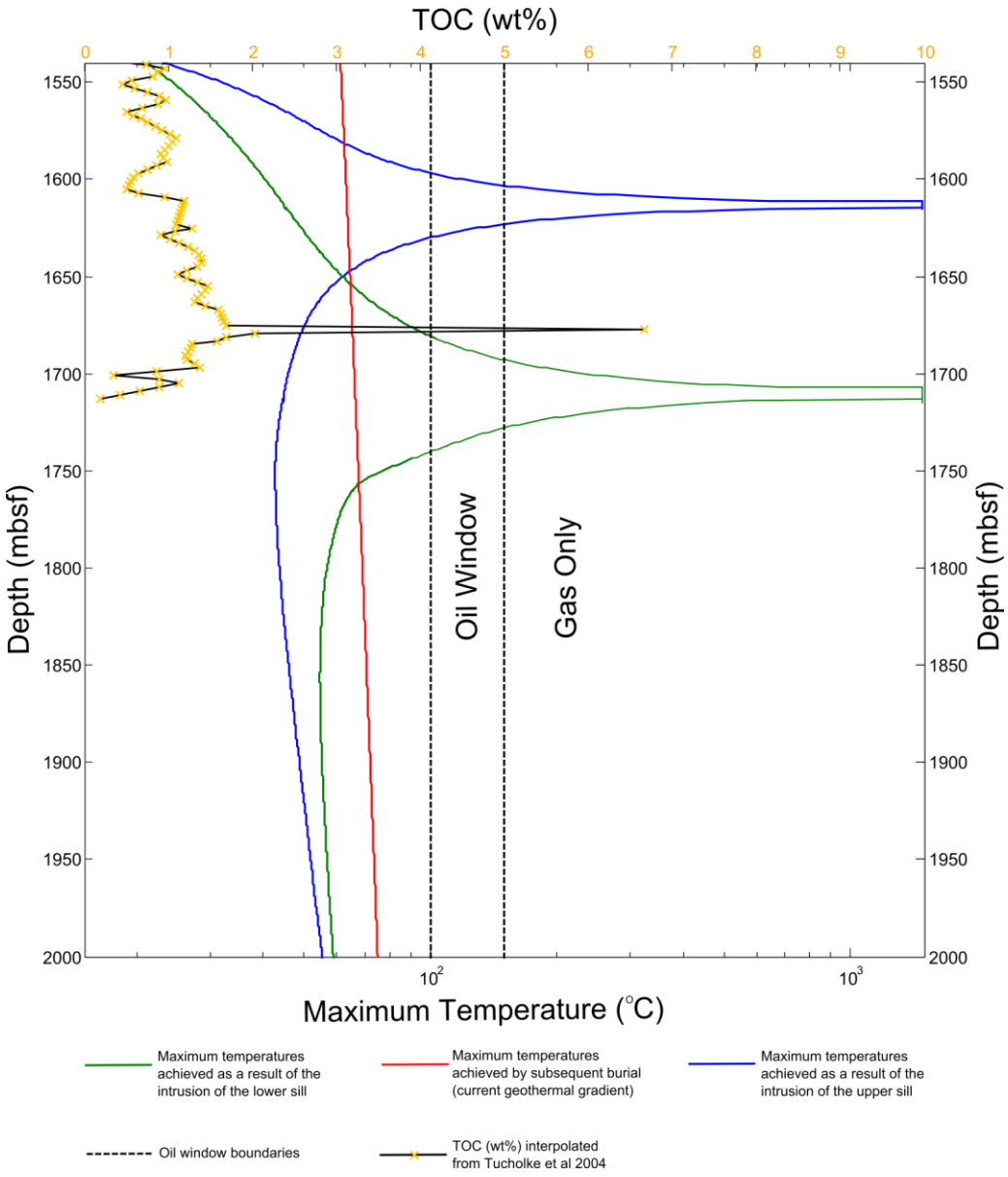

Figure 7.13

The maximum temperatures achieved (logarithmic scale) as a result of sill intrusions and subsequent burial (current geothermal gradient – Keen, 1979), TOC (wt%) interpolated from the data in Tucholke et al. (2004a). This demonstrates that for a considerable portion of the well, the highest temperature achieved was due to heating from the intrusions rather than subsequent burial. This is assuming that the current burial depth is the maximum and that no exhumation has occurred. Oil and Gas windows from England et al. (2002).

The maximum temperatures achieved from the intrusions, along with the current geothermal gradient (Keen, 1979) and TOC (wt%) (Tucholke et al., 2004a) are shown on Fig. 7.13. These modelling results show that for a considerable portion of ODP 210-1276 the highest temperature achieved was due to the sill intrusion rather than subsequent burial. It can also be seen that if the oil/gas windows of England et al. (2002) are used (Fig. 7.13) the sedimentary rocks at ODP 210-1276 would not have been sufficiently heated to enter either the oil or gas windows without the additional heat from the sills.

The modelled vitrinite reflectance profile for the entirety of ODP 210–1276 is presented in Fig. 7.14. These results demonstrate that the sills have probably caused a vertically limited, yet significant deviation from the background vitrinite reflectance gradient produced from the data in Allen and Allen, (2005).

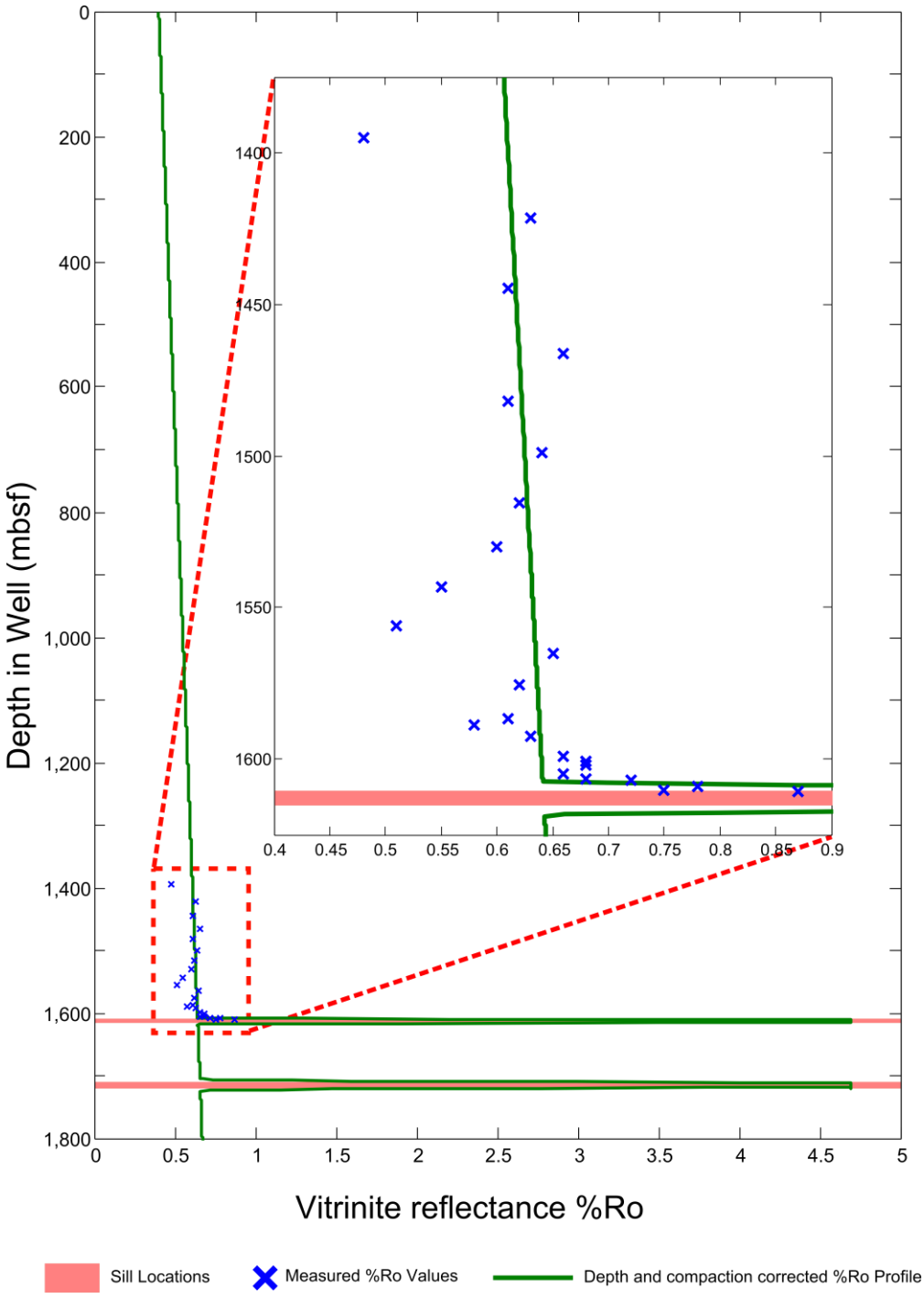

Figure 7.14

Vitrinite reflection profile for the entirety of ODP 210-1276 produced using the EASY%R_o model of Sweeney and Burnham, (1990) with the measured data provided by Pross et al. (2007) *plotted alongside for comparison. It can be seen that a vertically limited, yet significant spike in %R_o has been produced in proximity to the sills that needs to be taken into account in source rock maturation studies.*

7.5 Discussion

7.5.1 Timing and duration of magmatism

Demonstrating that the older sill had cooled to a temperature indistinguishable from the estimated background geothermal gradient well before the second sill was intruded is significant. It shows that an assumption of simultaneous emplacement of multiple intrusive bodies (e.g. Aarnes et al., 2010) could lead to an overestimation of the thermal perturbation. This has been demonstrated in Fig. 7.6 where it can be seen that if simultaneous intrusion of both sills is assumed, a higher maximum temperature is achieved in the region between the two sills. There is, however, no effect on the modelled vitrinite reflectance values, as the values generated for region between the sills (where there is greatest disparity in maximum temperature between the simultaneous and separate intrusion models – Fig. 7.6) are lower than the background vitrinite reflectance gradient from Allen and Allen, (2005).

Our results indicate that, where possible, future models should avoid assuming simultaneous intrusion of multiple bodies, particularly in areas unlike ours where intrusions are shallow enough for the maturation effects not to be masked by subsequent burial-related maturation. When absolute dates are unavailable, other, nondirect methods can be used to estimate the duration of emplacement. One such method is to use the timing of forced folds above sills, such as the work by Magee et al. (2014) on the Irish Rockall Basin which indicates that emplacement took place during an interval of 15 Myrs. Where age constraints are not available as in this study, an end-member approach to modelling would be best. Using this approach both a simultaneous intrusion model and a model whereby intrusions have cooled entirely before subsequent intrusions occur should be computed (Fig. 7.6).

Our models have demonstrated that the duration between the activation of the sill as a conduit and subsequent cooling to the closing temperature (as recorded by the $^{40}Ar/^{39}Ar$ ages of Hart and Blusztajn, (2006) was probably <10 years for the upper sill (Fig. 7.10). This implies that in order to produce such a widespread sill complex in a short duration of time, the system must have been fed from multiple points. It is also likely, that in addition, the sills intersected at ODP 210-1276 are not representative of the whole of the magmatic system imaged as the U-reflector. In order to achieve the magmatic flux required to produce such an apparently widespread sill complex, some parts of the system may have operated as conduits for longer prior to cooling than the sill modelled in this work.

Despite the upper sill not acting as a conduit for a prolonged period of time prior to cooling, the intrusion of these two compositionally similar upper and lower sills has occurred over a time span of ca. 10 Myrs (Hart and Blusztajn, 2006), thus a relatively long-lived, post-breakup mechanism is likely to have been required to produce the melt. Alternatively, the causal heat source may have diminished and been renewed on a timescale of ca. 107 years, although this seems less likely due to the similar composition of the two sills (Hart and Blusztajn, 2006).

The presence of a long-lived heat source could have influenced sediment maturation by introducing additional heat into the margin. This could explain the higher than average vitrinite reflectance gradient at this location on the margin (Fig. 7.8). Any elevated heat flow could have been caused by the same mechanism that generated the melts feeding the sills that are imaged on seismic data as the ‘U-reflector’ (Figs 7.1 and 7.2) and the two intrusions that are the subject of this modelling study.

7.5.2 Implications for maturation

The modelled vitrinite reflectance profile for the entirety of ODP 210-1276 presented in Fig. 7.14 demonstrates that the sills have caused a vertically limited, yet significant spike in $\%R_o$ that needs to be taken into account in source rock maturation studies. This is consistent with the vitrinite reflectance study by Pross et al. (2007), which notes thermal alteration associated with the upper sill is observable 20 m above the intrusion, with a significant increase at 4.23 m and the highest value recorded closest to the sill at 2.17 m. Although the sills intersected at ODP 210-1276 may not be representative of the situation across the area covered by the U-reflector, if this high amplitude anomaly does indeed represent a widespread sill complex (e.g. Deemer et al., 2010), then it is not unreasonable to suggest that a similar spike in maturation is likely to be exist elsewhere on the Newfoundland margin where similar sills are present.

7.5.3 Burial and compaction

Previous work proposes that the sills were intruded into relatively unconsolidated and not overpressured sedimentary rocks, particularly in the lower 30 m of the section (Tucholke et al., 2007). It has been claimed that this suggests that at the drill site considerable mechanical support probably provided by nearby dykes, protecting the sedimentary rocks between the sills from compression (Peron-Pinvidic et al., 2010).

However, we find that the EASY$\%R_o$ modelling results most closely resemble the observed vitrinite reflectance values when burial and compaction are accounted for (Fig. 7.8), perhaps suggesting that the sediments between the sills have been more compacted than previously suggested.

7.5.4 Hydrothermal activity

Enhancing the diffusivity increases rate at which the sill cools, as expected, but has little effect on the modelled vitrinite reflectance values (Fig. 7.11). While these results are interesting, they demonstrate that the role of hydrothermalism, in this particular instance, is trivial in the context of the other assumptions and uncertainties inherent in the model and the parameters used. This implies that advection may not be as important in influencing maturation as suggested by previous work e.g. Polyansky et al. (2003).

7.5.5 Source of the magmatism

The source of the magma producing the sills intersected at ODP210-1276, and probably of the U-reflector is still uncertain according to Peron-Pinvidic et al. (2010). It has been attributed to the migration of the Canary and Madeira plumes across the Newfoundland basin between 80 and 120 Ma (e.g. Karner and Shillington, 2005; Deemer et al., 2010), which is said to be supported by the geochemical signature observed by Hart and Blusztajn, (2006). Deemer et al. (2010) propose that volcanism was suppressed while the plumes travelled under the full thickness of the continental lithosphere, resulting in an accumulation of magma which was subsequently released when the hotspot approached the thinned lithosphere at the eastern edge of the Grand Banks.

However, given that the Newfoundland Margin is considered to be a typical NVPM (e.g. Melankholina, 2011) with the absence of any other plume related observations, other causal mechanisms should be considered. One such alternative theory is proposed by Peron-Pinvidic et al. (2010) stating that the melts were produced by asymmetric rift-drift related tectono-magmatic processes.

7.6 Conclusions

Collectively, the information acquired by the previous work at ODP 210-1276, and elsewhere on the Newfoundland Margin (e.g. Tucholke et al., 2004a; Hart and Blusztajn, 2006; Pross et al., 2007) has provided a unique opportunity to model the cooling of the sills and their thermal influence on the surrounding sedimentary rocks. This has allowed us to provide new insights into the relationship between intrusive magmatism, thermal evolution of passive margins and the influence on maturation on the Newfoundland margin, within a well constrained framework. The key findings of this study include:

1) The oldest sill at ODP 210-1276 had cooled to a temperature indistinguishable from the background geothermal gradient well before the younger, lower sill complex was intruded.

2) The temperatures achieved in the sedimentary rocks adjacent to the intrusions are higher than those achieved by post-depositional burial. This demonstrates the potential significance that regionally extensive intrusive magmatism could have on the thermal evolution of the Newfoundland margin, and suggests that the role of intrusive magmatism should be considered in thermal maturation studies in similar settings.

3) If the sills acted as magmatic conduits prior to cooling to the closing temperature (as recorded by the $^{40}Ar/^{39}Ar$ dates) it was for a short duration, probably <10 years.

4) The peak in vitrinite reflectance data observed at ODP 210-1276 can be completely attributed to rapid heating from the upper sill. We have also shown that the spatial extent of the thermal aureole of these sills was much greater shortly after intrusion, and that subsequent burial and compaction has reduced its current vertical extent at ODP 210-1276, which is probably representative of the situation across the Newfoundland margin.

5) The higher than average $\%R_o$ gradient for this part of the Newfoundland margin implies that at some point in the past the heat flow was elevated. This elevation of past heat flow could have been caused by the same mechanism that produced the sills which are imaged on seismic data as the ‘U-reflector’.

Finally, the EASY$\%R_o$ modelling results confirm that the sills at ODP 210-1276 have influenced the localised thermal evolution, and may be indicative of a broader, more regional thermal perturbation in the region covered by the ‘U-reflector’ on regional seismic data, and thus should be considered in source rock maturation studies.

Chapter 8

Discussion, future work and conclusions

8.0 Introduction

The analysis presented in this thesis has shed light on specific aspects of the West Greenland and Eastern Canadian margins. In this chapter the main findings of these individual studies presented in Chapters (4-7) are integrated to provide a synthesis of the roles of magmatism and structural inheritance for continental breakup between Eastern Canada and West Greenland and also for the wider North Atlantic region and other extensional regions globally. A preliminary discussion of the current northern Red Sea as a possible analogue for the North Atlantic region at c. 55 Ma is presented. The opportunities and challenges for hydrocarbon exploration in West Greenland and Eastern Canada and on other passive margins are also explored further in light of the results and implications previously described in this thesis. At the end of this chapter the main conclusions from the analysis presented in Chapters 4-7 are listed.

8.1 Magmatism in rifting and passive margin formation

The relationship between rifting, continental breakup and magmatism has been studied by many previous workers (e.g. White and McKenzie, 1989; Bowling and Harry, 2001) and thus, it is well established that magmatism invariably accompanies continental breakup (e.g. White, 1992). This thesis has built upon this previous work on the relationship between continental breakup and magmatism by showing that magmatism can be both a product of (Chapter 4) and a cause of (Chapter 7) passive margin processes depending on the phenomenon of interest and the scale of observation. This work has also demonstrated the importance of studying rift and passive margin magmatism at a complete range of scales from that of conjugate margin pairs down to individual intrusions (prospect scale) to enable its role within the rifting and continental breakup cycle to be fully understood.

At the largest scale considered in this study, it was demonstrated in Chapter 4 that the spatial distribution of magmatism is in part controlled by the rifting regime. Whereas at the smallest scale, results were presented detailing the thermal influence of individual intrusions (Chapter 7), demonstrating that the thermal regime required to generate the melt is potentially more important for source rock maturation than the more localised thermal effects of the actual intrusion. Understanding the magmatic processes that operate between the two scales considered in this study, and even beyond these scales should be the focus of future work into this topic. For example at the basin scale considerably more research is required, particularly as hydrocarbon exploration is continuing to move into previously overlooked, unexplored basins that often contain considerable volumes of igneous rocks (e.g. The Fareo-Shetland Basin - Schofield et al., 2015).

8.1.1 The mantle plume hypothesis in the North Atlantic

At an even larger scale than the analysis in this thesis remains the pertinent question of whether a thermal anomaly in the mantle is required to 1) to initiate rifting and 2) to produce widespread breakup related igneous rocks. This is a particularly challenging topic to address as the current models for both active and passive rifting (e.g. Geoffroy, 2005), as outlined in Chapter 1, do not predict observable phenomena that are unique.

The role of the mantle during continental breakup is a subject of continued controversial scientific debate (Campbell and Kerr, 2007; Lundin and Doré, 2005; Foulger and Anderson, 2005; Foulger, 2001), with many observations of continental breakup being claimed to only be explainable by the mantle plume hypothesis if ad hoc variants are invoked that are tailored to each particular case (Foulger and Anderson, 2005). This controversy demonstrates that further research into this topic should be undertaken to fully understand the largest scale controls on the nature of magmatism during rifting and

continental breakup in the North Atlantic as a thermal anomaly in the mantle is attributed to numerous phenomena across this region (e.g. White, 1988). However, many other aspects of the North Atlantic breakup do not appear to fit this causal explanation (e.g. Lundin and Doré, 2005). In this section the role of the mantle during breakup of the North Atlantic is explored. Observable phenomena in the North Atlantic that have been attributed to a mantle plume in the scientific literature include:

1. Lithospheric weakening facilitating breakup (White and McKenzie, 1989);
2. The widespread magmatism comprising the North Atlantic Igneous Province (NAIP) (White and McKenzie, 1989);
3. Ridge jump from Aegir to the Kolbeinsey ridge (Talwani and Eldholm, 1977);
4. Microcontinent (Jan Mayen) separation from East Greenland (Müller et al., 2001);
5. The positive North Atlantic Geoid (Marquart, 1991)
6. The onset of seafloor spreading in the Labrador Sea (Chalmers and Larsen, 1995; Gerlings et al., 2009);
7. Major volcanism in West Greenland and Baffin Island (Chalmers and Larsen, 1995; Storey et al., 1998);
8. Underplating of the Davis Strait by a high-velocity body (Gerlings et al., 2009);
9. High $^{3}He/^{4}He$ (Graham et al., 1998) and low $^{187}Os/^{188}Os$ ratios in picrites (Schaefer et al., 2000);
10. Uplift of onshore sedimentary successions (Dam et al., 1998);
11. High melting temperatures for picrites located West of Greenland (Gill et al., 1992) and;
12. Seismically observable volcanic rocks for 400 km east of Baffin Island (Funck et al., 2007).

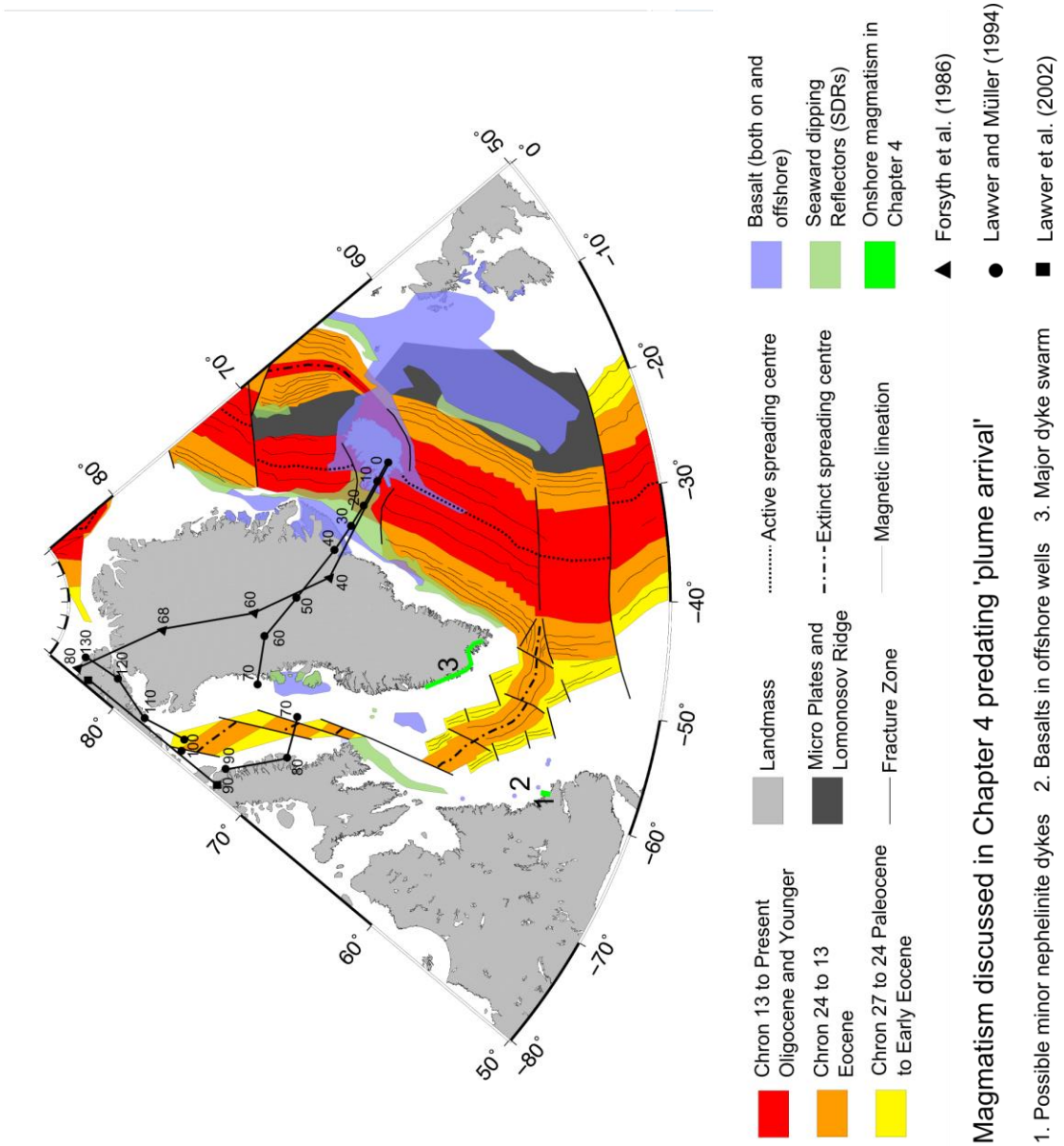

Figure 8.1

An overview of the North Atlantic oceanic spreading systems, including: the age of oceanic crust; major active and extinct spreading axes; major oceanic fracture zones; proposed microplates; and magnetic lineations (Oakey and Chalmers, 2012). The spatial distribution of on and offshore flood basalts and seaward dipping reflectors (SDRs) are overlain (Larsen and Saunders, 1998) in addition to the magmatism discussed in the previous chapters. The hotspot tracks of Lawver and Müller (1994), Lawver et al. (2002) and Forsyth et al. (1986) are also included.

However, observations suggesting that a mantle plume was not the primary driver in the in the breakup of the North Atlantic region include:

1) Seafloor spreading starting in the southern Labrador Sea before the north (Roest and Srivastava, 1989);

2) Delayed initiation of seafloor spreading in Baffin Bay (Suckro et al., 2012);

3) Absence of fully initiated seafloor spreading in the Davis Strait (Suckro et al., 2013);

4) Geochemistry of igneous rocks being claimed to be incompatible with a plume origin (Herzberg and O'Hara, 2002);

5) the presence of coast parallel dyke swarms predating the alleged plume arrival (Larsen et al., 2009) and;

6) the lack of a clear hot-spot track, particularly when the hot spot is assumed to be fixed within the mantle reference frame (Lundin and Doré, 2005).

The timing of seafloor spreading in Baffin Bay is contrary to what would be predicted by the plume hypothesis. The hotspot track reconstruction of (Lawver and Müller, 1994) places the proto-Icelandic plume in the Baffin Bay area at ca. 120 - 70 Ma, whereas seafloor spreading did not initiate until much later at Chron 27 - 25 (52 - 62 Ma), even though it is situated in close proximity to the alleged plume track for a much earlier prolonged period of time. However, it has been recognised that there would be a delay in the onset of seafloor spreading to account for the time it would take a cold lithosphere to conduct heat from a plume (Hill, 1993). Seafloor spreading has been proposed to postdate plume arrival by 10 – 40 Myrs (Hill, 1993). However, using even the uppermost limit proposed by Hill (1993) the delay in Baffin Bay is too great with a timespan of ca. 60 Myrs

between first plume arrival (in Northern Baffin Bay) and seafloor spreading initiation (Suckro et al., 2012). It is nevertheless possible that this delay could possibly be influenced by local factors such as crustal thickness, structure and composition.

Tectonic reconstructions of the movements of Greenland relative to Canada have suggested an ‘unzipping’ motion with progressive opening from south to north (e.g. Oakey and Chalmers, 2012). Although there is some debate regarding the precise age of seafloor spreading initiation it is accepted that it started in the southern Labrador Sea before the north (e.g. Roest and Srivastava, 1989). This does not fit a model whereby a plume producing voluminous magmatism initiated seafloor spreading (e.g. Gerlings et al., 2009). If rifting and subsequent seafloor spreading were driven by a mantle plume it would be expected to start nearest to the plume and to propagate away from it (Fig. 8.2).

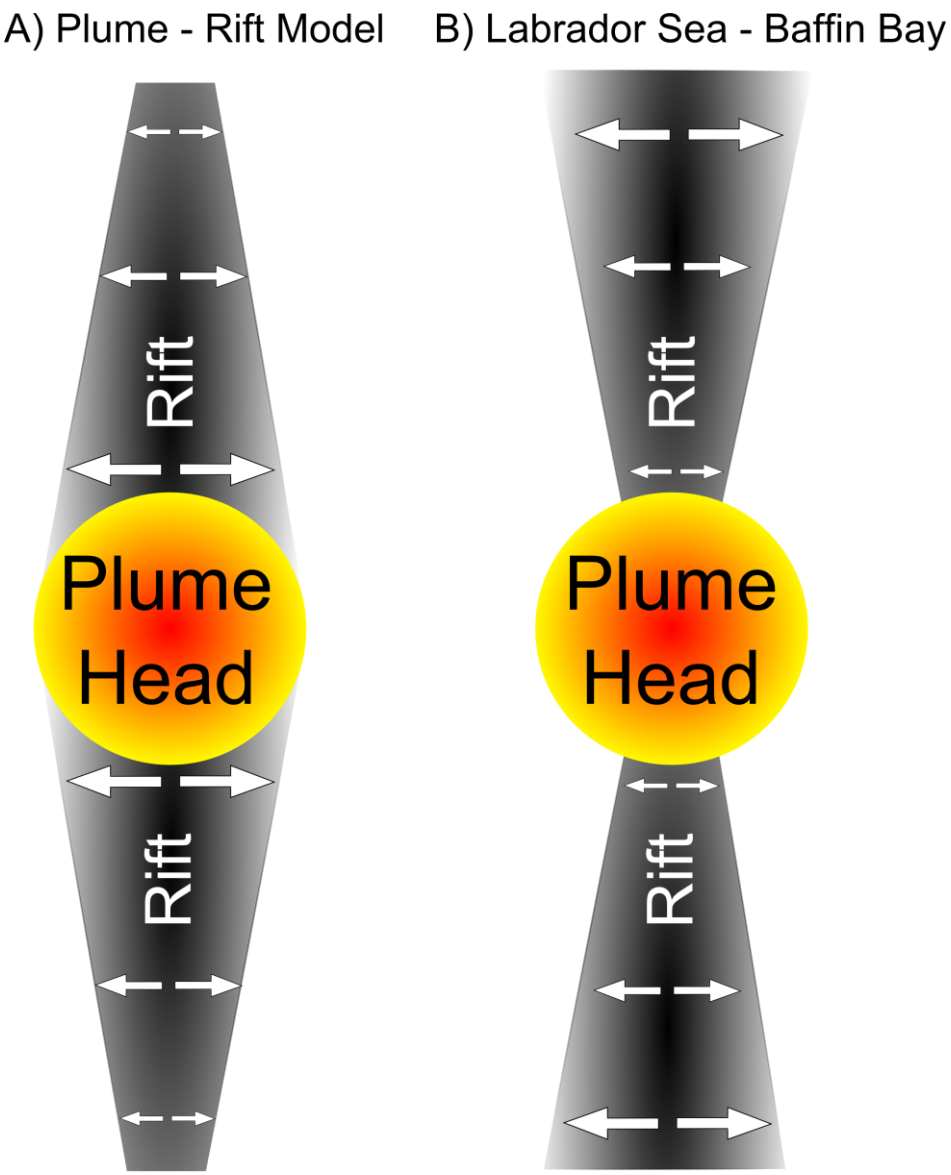

Figure 8.2

A) Predictions of rifting in response to a rising thermal anomaly in the mantle and B) observations in the Labrador Sea – Baffin Bay rift system. Modified from Franke (2013) whereby the original figure showed a similar example from the South Atlantic where observations of rifting and breakup again do not appear to fit the predictions of the mantle plume hypothesis.

It has however been suggested that the prolonged location of a plume could 'pin' the position of subsequent spreading (Hill, 1993), through thermal and mechanical weakening of the lithosphere, which a subsequent stress field could exploit. Onshore coast parallel dykes in southwest Greenland have however been geochemically dated as early as the

Jurassic and Triassic (Larsen et al., 2009; Larsen, 2006). This implies that the weakness exploited by subsequent continental breakup was already in place before the proposed plume was in the vicinity.

Finally, in the more volcanic Davis Strait region (Chapter 6) seafloor spreading was never fully initiated in contrast to the Labrador Sea (Srivastava, 1978) and Baffin Bay (Suckro et al., 2012). Instead a 'leaky transform' system has developed (Funck et al., 2007). It is not clear why a mantle plume should cause seafloor spreading in the distant Labrador Sea (Gerlings et al., 2009) but not at the Davis Strait which is situated much closer to the alleged plume, unless the pre-existing terrains adjacent to the Davis Strait proved particularly resistant to rift-propagation, a concept developed further in the following sections of this chapter.

If continental breakup between Canada and Greenland were caused by the arrival of a plume (e.g. Gerlings et al., 2009), now located under Iceland, it would be expected that the earliest and most extensive seafloor spreading would have occurred closest to the plume (Fig. 8.2). In fact, the opposite is observed. Since the observations do not match the model predictions, the plume hypothesis as applied here is unlikely to be correct in its current form. Non-plume mechanisms and variations on the current hypothesis should thus be considered to be the causal factor in the breakup of the North Atlantic region.

Several alternatives to the plume hypothesis have been previously proposed to explain the formation of VPMs including:

1) a direct effect of rifting (van Wijk et al., 2001; Armitage et al., 2010) and;

2) small-scale convection (e.g. Mutter et al 1988; Simon et al., 2009).

These mechanisms may provide a better explanation for continental breakup in the North Atlantic region, and in particular the formation of the West Greenland VPM. The reason that the aforementioned alternatives to the plume theory of breakup of the North Atlantic may provide better explanations of the observable phenomena is principally because they do not require a hot spot track.

8.2 Inherited structure in rifting and passive margin formation

In addition to magmatism the other major theme of this study is the rejuvenation of pre-existing structures through the process of tectonic inheritance (e.g. Holdsworth et al., 2001; Holdsworth et al., 1997). In the following sections the role of pre-existing structures in all of the studies described in this thesis are synthesised and a model for breakup of the North Atlantic region being primarily controlled by the large-scale location of orogenic belts is proposed. A comparison between the modern Red Sea and the North Atlantic at ca. 55 Ma is made to determine if the Red Sea represents an appropriate analogue for breakup of the North Atlantic region. The findings of this work suggest that the structures inherited from previous tectonic events played a key role in the breakup of West Greenland and Eastern Canada, as is the case with many other extensional tectonic settings (e.g. NW Australia - Wu et al., 2016), a relationship that is examined further in the subsequent sections of this chapter.

8.2.1 Observations of structural inheritance in this study: discrete structures and pervasive fabrics

As with magmatism, the results of this study have reaffirmed that the consequences of inherited structure occur at a range of scales from discrete individual structures (Chapter 6) to widespread, pervasive, metamorphic fabrics (Chapter 5).

As detailed in the Chapter 1, Peacock and Sanderson, (1992) recognise three types of directional heterogeneity (anisotropy) that may occur in rocks, these are: 1) layering-alternations of materials with differing mechanical properties (e.g. bedding); 2) continuous anisotropy from pervasive fabrics (e.g. foliation and shear zones); and 3) discrete planes of weakness with reduced cohesion and coefficients of sliding friction (e.g. faults and cleavage planes). This classification can however be simplified into pervasive and discrete structures (Peacock and Sanderson, 1992; Morley et al., 2004; Morley, 1999). In this study examples of the latter two types of anisotropy identified by Peacock and Sanderson, (1992) were observed, demonstrating that both pervasive and discrete structures may have played a role in the breakup between Greenland and Canada.

An example of the second type of anisotropy identified by Peacock and Sanderson, (1992) whereby a large-scale pervasive fabric appears to have influenced rift propagation is presented in Chapter 5. Here, the orientation of the basement metamorphic foliation was orientated such that it was likely to have been conducive to allowing rift propagation. However, this conclusion is based on preliminary results and further work is required to further establish the nature of this possible relationship, a proposal expanded upon in the future work section of this chapter. An example of the third type of reactivation described by Peacock and Sanderson, (1992), whereby discrete faults have provided the heterogeneity in which subsequent movement occurs was documented in Chapter 6. Here, the orientation of pre-existing structures was concluded to have controlled the orientation of faulting during rifting of the Davis Strait, through oblique reactivation. The role of oblique and orthogonal extension during rifting is examined in the next section.

8.2.2 Observations of structural inheritance in this study: orthogonal and oblique extension

When extension occurs orthogonal to the rift trend, the fault geometries produced are relatively simple and conform to Andersonian plane strain fault models (Anderson, 1951). However, in nature the likelihood of extension formaing orthogonal to any pre-existing structures is low (Fig. 8.3 - Wu et al., 2016). In oblique extension, the trend of the deformation zone is oblique to the regional extension direction (e.g. Morley et al., 2004; Brune et al., 2012; Bott, 1959; Autin et al., 2013). It has been shown that during rifting structures that lie oblique between 45 and 60° from the regional extension direction are commonly exploited (reviewed by Morley, 1995). Depending on the size of the pre-existing structure and its relative mechanical strength oblique trends can range in size from oblique localised fault zones to entire rift systems being oblique to the regional extension direction (e.g. Rukwa Rift, East Africa - Morley et al., 1992; Gulf of Aden - Autin et al., 2013). In this study the role of pre-existing structures occurring both approximately orthogonally (Chapter 5) and obliquely (Chapter 6) to the reconstructed extension direction (Abdelmalak et al., 2012) was observed and documented.

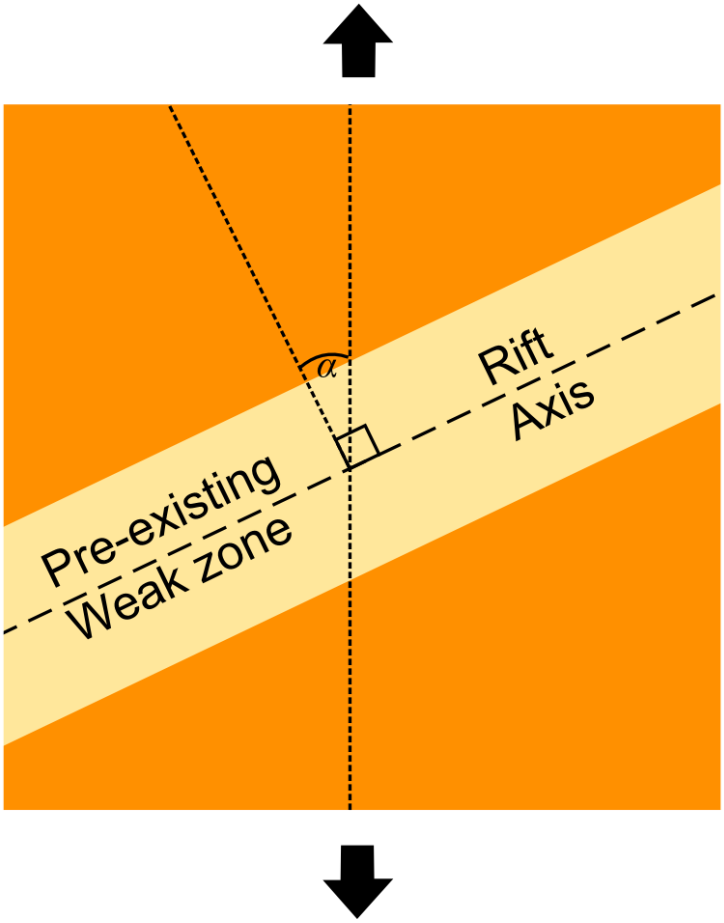

Figure 8.3

Schematic depiction of the relationship between a pre-existing structure and rifting direction. α = the extension obliquity, that is the angle between normal to the pre-existing structure and the extension direction. Reproduced from Wu et al. (2016).

In Chapter 5 it was concluded that the approximately N-S striking, dominant metamorphic mineral fabrics recorded during fieldwork in the Makkovik region were orientated such that a rift propagating from the south towards the north (Srivastava and Roest, 1999) was orientated approximately parallel to the dominant basement fabric. Such a geometric relationship is likely to have allowed rift propagation to have occurred relatively easily compared to in other less favourably orientated geological terrains in the region such as the Palaeoproterozoic Nagssugtoqidian and Torngat Orogenic belts that lie adjacent to the

study area in Chapter 6. However, the role of larger, crustal-scale features is possibly more likely to influence large-scale rift propagation, a concept discussed below. By contrast the work on the Davis Strait region presented in Chapter 6 represents a situation in which pre-existing structures occur much more obliquely to the reconstructed rifting directions (Abdelmalak et al., 2012).

8.2.3 Inherited structures in continental breakup across the North Atlantic region

The model for rifting in the Davis Strait presented in Chapter 6 is that pre-existing structures are likely to have exerted a considerable influence upon the nature and orientation of Mesozoic-Cenozoic rifting offshore West Greenland, an assertion that is supported by observations of fault reactivation in West Greenland in both offshore (this study) and onshore (e.g. Wilson et al., 2006) studies. Furthermore, the rejuvenation of pre-existing geological structures through reactivation and reworking (Holdsworth et al., 2001a) is also likely to have exerted a considerable influence on the timing, nature and geometry of breakup processes in many areas across the North Atlantic region (Wilson, 1966).

As previously described in Chapter 6, considerable variation exists in the nature, geometry and timing of the continental breakup process in the West Greenland – Eastern Canada region. Seafloor spreading was certainly initiated in the Labrador Sea (e.g. Srivastava and Roest, 1999) and probably in Baffin Bay (Suckro et al., 2012) but not in the Davis Strait where it is proposed that moderate crustal thinning (Welford and Hall, 2013) occurred along with the development of a transform fault system (e.g. Funck et al., 2012). Rifting and breakup of the Labrador Sea was successful through the Archean Nain Province and North Atlantic Craton terrains and the Palaeoproterozoic Makkovik and Ketilidian orogenic belts, but was unsuccessful in the Davis Strait (e.g. Funck et al., 2007), adjacent

to the Palaeoproterozoic Nagssugtoqidian and Torngat Orogenic belts (Fig. 8.4). All of the contacts and large-scale structures between the aforementioned basement terrains lie approximately perpendicular (Wilson et al., 2006; Japsen et al., 2006) to the interpreted rifting direction (e.g. Abdelmalak et al., 2012), and thus may have had an unfavourable orientation with respect to the reconstructed rifting direction. However, it is the Nagssugtoqidian and Torngat Orogenic belts that appear to have been least susceptible to rifting. There are a number of reasons why these orogenic belts could have been particularly resistant to rifting. Such reasons include; thicker crust and the orientation of the dominant basement fabric within these orogenic belts being at a high angle to the orientation of subsequent crustal extension.

'The Wilson Cycle' (Wilson, 1966) suggests that rifting and formation of new oceans often occurs along orogenic fronts formed during the closure of older oceans (e.g. Vauchez et al., 1997). However, the exact opposite was the case during rifting and incomplete breakup in the Labrador Sea – Baffin Bay system (Funck et al., 2007), particularly as the regional metamorphic fabric in the Nagssugtoqidian follows a ~NE-SW trend (Wilson et al., 2006). This 'non-Wilson cycle' type partial breakup between West Greenland and Eastern Canada may have been initially possible but as rifting propagated from south to north (e.g. Srivastava, 1978) it may have become progressively more difficult as the rift propagated further into the Nagssugtoqidian, intersecting more of the resistant terrains. Thus, structures to the east of Greenland that were originally not conducive to rifting at the onset of extension may have become the line of least resistance as the process progressed. This may have resulted in a slowing and subsequent cessation of seafloor spreading west of Greenland and the complementary opening of the North Atlantic to the east of Greenland as extension was transferred to less resistant crustal domains.

One such terrain to the east of Greenland that has been proposed to have provided structures that were exploited during rifting prior to the opening of the North Atlantic are the structures associated with the Caledonian Orogeny (e.g. Norwegian margin - Dore et al., 1997). These Caledonian age structures could have initially been relatively unfavourable to rejuvenation as the natural progression of a northward propagating rift would have been to the west of Greenland. However, if breakup of the Palaeoproterozoic Nagssugtoqidian-Torngat orogenic belt in proximity to the proto-Davis Strait proved problematic these terrains may have subsequently become favourable for the propagation of rifting following the change in extension direction (Abdelmalak et al., 2012). This would have resulted in a ridge jump from breakup to the west of Greenland to the east of Greenland (Fig. 8.4). This is not to say that rifting in the NE Atlantic was not occurring simultaneously with that West of Greenland, as rifting of the NE Atlantic is inferred to have started in the Jurassic and Triassic, with some possible production of oceanic crust in the Middle Cretaceous (Lundin, 2002) but that it was not as developed and thus breakup here was achieved after it occurred west of Greenland.

This model does not explain, however, why breakup was successful through the Archean North Atlantic Craton but not the Palaeoproterozoic Nagssugtoqidian given that previous work suggests that Archean lithosphere is thicker, cooler and thus stronger than the surrounding younger terrains (Krabbendam, 2001). This may imply that: 1) Archean lithosphere may not be as strong as previously suggested; 2) the North Atlantic Craton is atypical of Archean lithosphere; or 3) the pre-existing structures in the North Atlantic Craton were particularly susceptible to Mesozoic rifting.

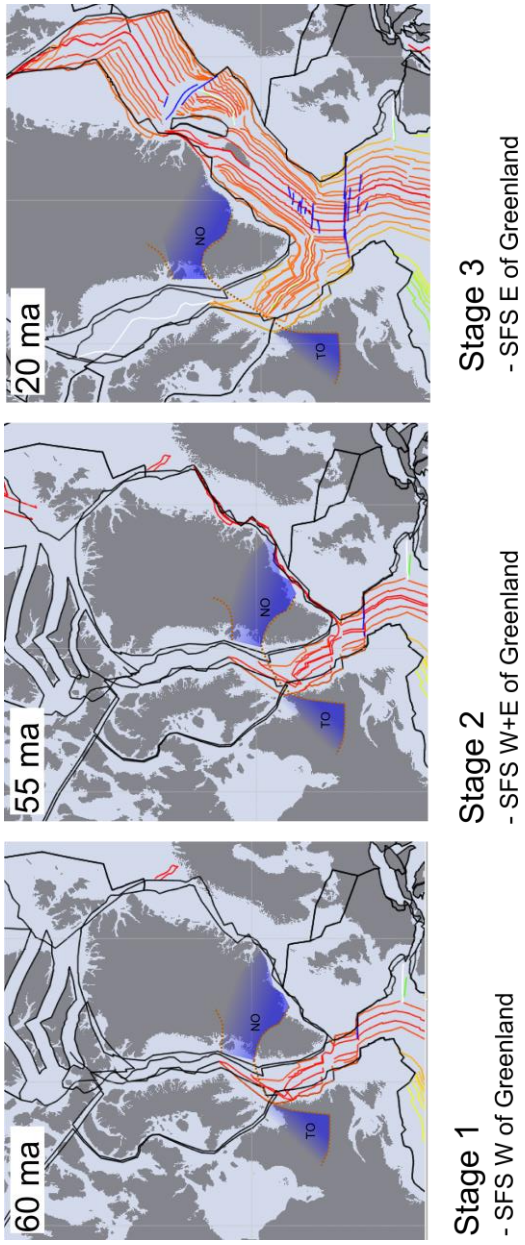

Figure 8.4

Extracts from the Seton et al. (2012) plate tectonic reconstructions for the North Atlantic plotting in a Mercator projection using GPlates for 60, 55 and 20 Ma, along with the approximate location of the Torngat-Nagssutoquidian orogenic belt (Van Gool et al., 2002).

Overall, a model in which pre-existing structures may have inhibited continental breakup of Greenland and Canada, resulting in the cessation of seafloor spreading to the west of Greenland and the ultimate opening of the Atlantic to the east of Greenland is proposed to explain the kinematics of the North Atlantic breakup (Fig. 8.4). However, it is also

possible that the changing rifting configuration as breakup progressed could have been also influenced by stress perturbation and/or interaction, as happens at a much smaller scale in fault systems (Cowie et al., 2006; Crider and Pollard, 1998). Such interactions between propagating rifts may have produced the phenomena described above including the apparent rift jump from the west to the east of Greenland.

8.2.4 The role of structural inheritance: Comparison between the North Atlantic and the northern Red Sea

This study has developed some new ideas concerning the role of structural inheritance during continental breakup by showing that structural inheritance not only controlled the small-scale manifestation of rifting and breakup geometries (Chapter 6) but also potentially the large-scale temporal evolution of the North Atlantic (Chapter 5 and this chapter). To test the proposed model for the role of pre-existing structures during breakup of the North Atlantic outlined in the previous section other global examples have been sought, that may offer comparable geological scenarios to further develop the proposed model. One such area that may offer an appropriate tectonic setting for comparison of the model proposed in the previous section is the northern Red Sea and in particular the geological evolution of the Gulfs of Aqaba (Barjous and Mikbel, 1990) and Suez (Steckler et al., 1988).

The Red Sea represents the northern continuation of the Gulf of Aden (Fig. 8.5 - Bosworth et al., 2005). The Gulf of Aden, the Red Sea and the East African Rift system meet at the Afar Triple Junction (ATJ) (McClusky et al., 2010). The Gulfs of Aqaba and Suez are located at the northern end of the Red Sea, representing attempts at rift propagation towards the Mediterranean Sea (e.g. Steckler and ten Brink, 1986). Rifting has been active in the Red Sea since the Oligocene whilst seafloor spreading has been taking place in the southern part for the last 5 myrs (Cochran et al., 1986). The northern Red Sea shows no

evidence of sea-floor spreading (Cochran et al., 1986), indicating that the northern Red Sea is still experiencing the late stages of continental rifting prior to the onset of seafloor spreading (Cochran, 1983).

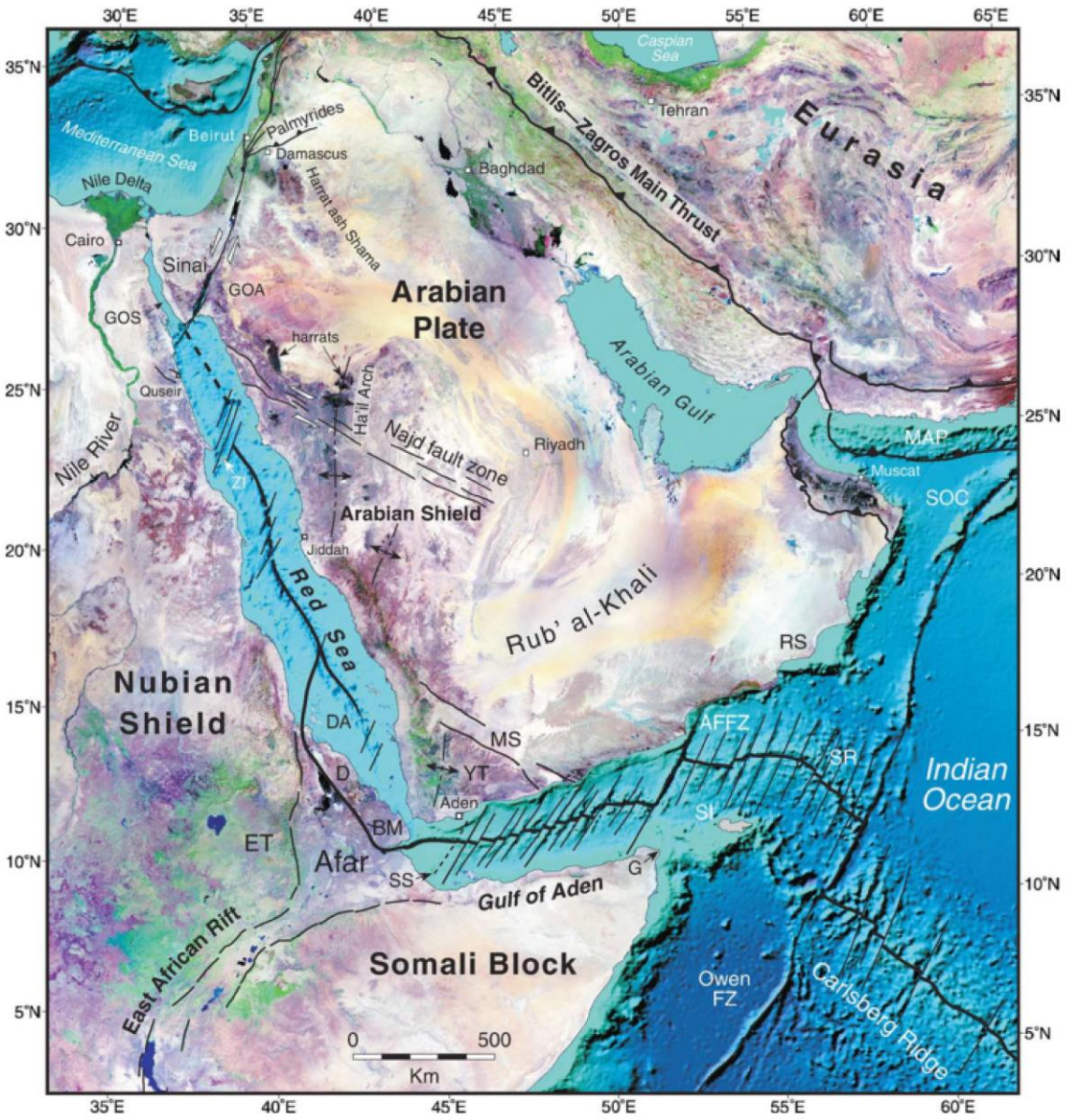

Figure 8.5

Landsat imagery (onshore) and Seasat-derived bathymetry (offshore) of the Red Sea–Gulf of Aden rift system reproduced from Bosworth et al. (2005). Abbreviations on map: AFFZ = Alula-Fartaq fracture zone; BM= Bab al Mandeb; D = Danakil horst; DA = Dahlak archipelago; ET = Ethiopian trap series; G = Cape Gwardafuy; GOA = Gulf of Aqaba; GOS = Gulf of Suez; MAP = Makran accretionary prism; MER= main Ethiopian rift; MS = Mesozoic Marib-Shabwa Basin; SI = Socotra Island; SOC = Semail oceanic crust; SR = Sheba Ridge; SS = Shukra al Sheik discontinuity; RS = Ras Sharbithat; YT = Yemen trap series; and ZI = Zabargad Island.

In this area previous work has linked the failure of the Red Sea to propagate NNW towards the Mediterranean Sea via the Gulf of Suez during early rifting to be as a direct result of the stronger lithosphere inhibiting the rift from reaching the Mediterranean (Fig. 8.6) (Steckler and ten Brink, 1986). Subsequent to failure of the rift to propagate along the Gulf of Suez structures which were initially unfavourable for rifting became more conducive and thus rifting, and in particular transform system development, moved to the Gulf of Aqaba and Dead Sea region (Steckler and ten Brink, 1986). The stronger lithosphere that inhibited rift propagation in the model of Steckler and ten Brink (1986) is attributed to be as a result of the Mediterranean hinge zone (Fig. 8.6), a term used to describe the region of a continental margin which marks the beginning of substantial extension (Watts and Steckler, 1978). At the hinge zone, there is a rapid increase in sediment thickness especially of Jurassic age, and decrease of crustal thickness which is claimed to provide the stronger crust in this region (Steckler and ten Brink, 1986).

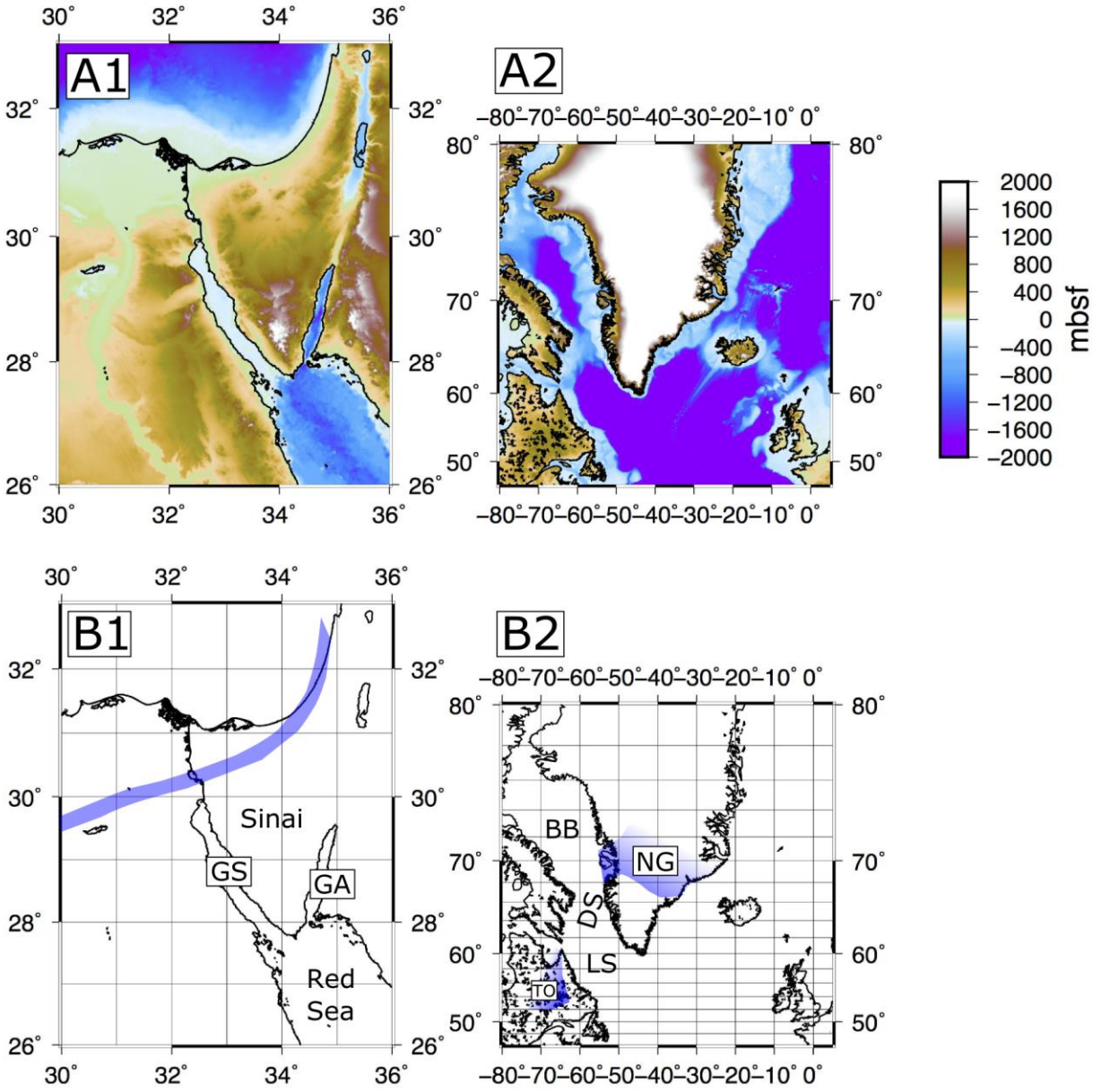

Figure 8.6

Topography and bathymetry (Smith and Sandwell, 1997) for A1) the northern Red Sea region and A2) the North Atlantic. B1) The proposed Mediterranean hinge zone of stronger lithosphere (Steckler and ten Brink, 1986) and B2) the Torngat-Nagssutoquidian orogenic belt (Van Gool et al., 2002). GS = Gulf of Suez; GA= Gulf of Aqaba; BB = Baffin Bay; DS = Davis Strait; LS = Labrador Sea; TO = Torngat orogeny; and NG = Nagssutoquidian Orogen. Plotted with a Mercator projection and the Globe colour pallet in the GMT package.

One potential problem with using the Neogene to recent rifting in the northern Red Sea region (Steckler and ten Brink, 1986) as an analogue for the Mesozoic to Cenozoic North Atlantic breakup is that rifting in these two areas occurred at very different scales, with the central block between the failed and the successful rifts in the North Atlantic (Greenland) being c. 1200 km wide whereas the comparable block between the Gulfs of Aqaba and Suez (Sinai) is only c. 300 km wide. However, the apparent similarities in rift propagation in these two regions possibly implies that the role of pre-existing structures in inhibiting rift propagation is scale invariant. To further test both the main model proposed for the North Atlantic breakup in the previous section and the comparison with the northern Red Sea described here other global examples of rift systems considered to have failed due to an inability to propagate through pre-existing structures should be investigated.

8.3 Interplay between magmatism and structural inheritance

The two major thoroughgoing themes of this thesis have been magmatism and inherited structure during the continental rifting and breakup cycle. Although these two themes have for the most part been considered separately to allow particular elements to be constrained certain interplays and overlaps can be identified between these topics. However, for the most part these potential relationships between magmatism and structural inheritance require further examination to fully establish the nature of any possible connections.

In Chapter 4, it was concluded that the Labrador Sea rifted under a simple shear dominated regime leading to the asymmetric magmatic distribution characterised herein. It is possible that pre-existing structures could have contributed to the observed asymmetry by providing conditions that were conducive to the establishment of a simple shear rifting regime (Corti and Manetti, 2006; Corti et al., 2007). Corti and Manetti, (2006) used analogue models to show that an initially asymmetric Moho is prone to producing asymmetric rifting and thus

asymmetric conjugate margins. Asymmetric atributes that were observed in the models of Corti and Manetti, (2006) include; amount of extension, patterns of lithopsheric thinning/asthenospheric upwelling and the amount of volcanism. The models of Corti and Manetti, (2006) demonstrated that an asymmetric Moho may control the mode of extension leading to a narrow strongly magmatic margin and a wider less volcanic margin, a situation that appears to be very similar to that observed in the analysis on the Labardor Sea margins detailed in Chapter 4.

Another possible interaction between magmatism and pre-existing structures is in the Davis Strait, where in Chapter 6 the reactivation of discrete pre-existing structures was shown to contribute significantly to the development of rifting. However, at the larger scale of the basement terrains containing the aforementioned structures it is intriguing that the foci of the magmatism to the west of Greenland occurred in the Davis Strait, which as outlined in Chapter 6 formed adjacent to the Palaeoproterozoic Nagssugtoqidian (e.g. Connelly and Mengel, 2000) and Torngat Orogenic (e.g. Funck and Louden, 1999) belts of West Greenland and Labrador respectively. More generally, Lundin and Doré (2005) postulated that VPM in the South, Central and North Atlantic are natural products of the Wilson Cycle, finding a broad correlation between VPM segments and reopened Late Neoproterozoic-Phanerozoic fold belts, although the Davis Strait was not one of the locations outlined in their study.

The crustal structure of the Davis Strait may have been conducive to melt generation due to the keel effects of the thicker crust depicted in this region by previous work (Fig. 8.4) whereby crust in the Davis Strait and Northern Labrador Sea may be up to 50 km thick (Keen et al., 2012). Regions of thick crust have been inferred to influence asthenospheric flow elsewhere for example in SE Brazil (Assumpção et al., 2006) and have even been proposed to be capable of deflecting mantle material (Sleep et al., 2002). It may be

possible that such effects could be conducive to the establishment of small-scale convection cells leading to adiabatic melting (Ballmer et al., 2010; Simon et al., 2009). Another potential effect of the thicker crust in the Davis Strait is that it could have had an insulating effect that could have enhanced the effects of other mechanisms (e.g. Hoggard et al., 2016), particularly as there was a prolonged presence of continental crust in the Davis Strait compared to in the Labrador Sea and Baffin Bay where seafloor spreading was initiated (Srivastava and Roest, 1999).

Interactions between magmatism and pre-existing structures at a range of scales have also been described in the previous work (e.g. Valentine and Krogh, 2006; Wilson and Guiraud, 1992). For example previous work has related the Icelandic magmas to remelted Iapetus crust that was subducted during the Caledonian Orogeny (Foulger et al., 2005a). In such a situation as that proposed by Foulger et al. (2005) voluminous melt generation may be produced at a lower temperature than in models without the preserved pre-existing Iapetus crust. It has also been proposed that a correlation exists between Neoproterozoic – Phanerozoic orogenic belts and the locations of VPMs in the Southern, Central and North Atlantic (Lundin and Doré, 2005). At a much smaller scale previous work has also shown that pre-existing structure controlled dyke emplacement. One such example of this phenomena includes the Paiute Ridge in southern Nevada, USA where pre-existing normal faults have been occupied by dykes (Valentine and Krogh, 2006) and normal faults have focused on dyke structures (Ashby, 2013).

Overall, this work has shown examples of how both magmatism and tectonic inheritance can contribute significantly to the continental rifting and breakup process. However, considerably more work is required to fully understand interactions between these two large and complex groups of mechanisms.

8.4 Implications for hydrocarbon exploration and production

This work has reaffirmed that margins containing significant volumes of igneous rocks offer distinct challenges but also considerable opportunities for hydrocarbon exploration and production. This section aims to evaluate the implications of the results detailed in the data chapters (4-7) for hydrocarbon exploration and production on the margins of West Greenland and Eastern Canada, but also for other passive margins generally, in particular margins containing significant volumes of igneous rocks.

8.4.1 Hydrocarbon exploration and production in West Greenland and Eastern Canada

There have been several significant developments with respect to hydrocarbon exploration and production in West Greenland and Eastern Canada since the start of this project. Some of the most notable successful developments have occurred towards the south of the study area (Chapter 1) on the Grand Banks, offshore Newfoundland (Chapter 7) but also towards the north with the discovery of new sedimentary basins on the Labrador Shelf and thus, the potential for further exploration and production opportunities in this more northern region is high. During the same time period exploration has been less successful in West Greenland where gas discoveries have been made but an economically viable oil discovery has yet to be made. The following sections highlight particular parts of the analysis presented in this thesis that have direct implications for hydrocarbon exploration and production in this region.

The conjugate margin asymmetry documented in Chapter 4 showed that despite the opportunities offered for hydrocarbon exploration on the Labrador margin, as recently confirmed through the demonstration of an active petroleum system (e.g. Haggart, 2014), the southwest Greenland margin may not contain a comparable resource for a number of reasons. Firstly, the magmatic asymmetry described in Chapter 4 will have significant

implications for the heat flow regime on each of the conjugate margins. As more magmatism occurs on the southwest Greenland margin the heat flow is likely to have been higher during rifting (Latin and White, 1990). This is particularly relevant when the results of Chapter 7 are considered as the thermal influence of individual intrusions was shown to be less important than the thermal regime leading to the production of melt. Thus, because source rock maturation has been achieved on the Labrador margin it does not imply that a comparably mature source rock should exist offshore southwest Greenland due to the different thermal regime implied by the model presented in Chapter 4. However, given that discoveries on the Labrador Shelf to date are gas rather than oil a less mature source rock offshore southwest Greenland could potentially have remained in the oil window due to lower burial depths and heat flow. Another implication of the asymmetry described in Chapter 4 for petroleum exploration on the margins of the Labrador Sea is that the distribution of sediments between these margins is also extremely asymmetric in favour of the Labrador margin having much thicker sedimentary cover (Chapter 4 - Fig. 4.12). The much thicker sedimentary infill on the Labrador margin has consequences for numerous components of the petroleum system including: 1) extent of source, reservoir and sealing units; and 2) burial depths and thus maturation. Overall, the recognition of conjugate margin asymmetry in the Labrador Sea, as described in Chapter 4, should be taken into account when conducting regional scale exploration in the study area, but also when conducting conjugate margin studies elsewhere.

The analysis presented in Chapter 6 has multiple implications for our understanding of petroleum systems in the Davis Strait region. Firstly, the small isolated basins depicted on the earlier isochrons (Chapter 6 - Fig. 6.10A-D) would potentially provide a suitable location for the accumulation of organic matter in a spatially restricted environment. Such a restricted environment could lead to anoxic conditions conducive to the preservation of

source rock material. However, the small basins could make potential source rocks spatially limited and laterally variable, resulting in source rocks being difficult to predict between basins. This is particularly paramount as the time interval where source material offshore West Greenland is believed to have been deposited, primarily within the Cretaceous successions but also in the Palaeocene (Schenk, 2011), corresponds to this interval. Opportunities to form trapping structures occur multiple times; including the major reorganisation at Chron 24 resulting in the strike slip tectonics forming the Ikermiut thrust and fold structures (Chapter 6 - Fig. 6.11D).

The thermal models presented in Chapter 7 also have implications for petroleum systems in the study area and further afield. In this chapter it was shown that without the additional heat pulse from the intrusive magmatism the organic rich sediments noted at ODP 210-1276 would have never reached the oil or gas windows (England et al., 2002). Thus, the thermal effects of igneous rocks should be considered when evaluating the prospectively of an area during exploration.

8.5 Future work

Although this work has provided new insights into the roles of magmatism and structural inheritance during continental breakup between West Greenland and Eastern Canada there still remains significant areas of ambiguity, both within the areas addressed in this thesis and new research directions that have become apparent as a result of the work described in this thesis. For this reason a number of possible research topics that will help to address some of the knowledge gaps that have become apparent as a result of this study are proposed below.

8.5.1 Magmatic asymmetry between other conjugate margin pairs

In Chapter 4 an analysis was presented of the degree of asymmetry displayed by numerous aspects of the conjugate margins of the Labrador Sea including the spatial distribution of rift-related igneous rocks. The Labrador Sea work allowed us to apply the passive margin formation by simple shear model of Lister et al. (1986) to the margins of the Labrador Sea. Applying this model to other conjugate margin pairs will allow the integrity and applicability of the model to be further tested to enquire if the observations made on the margins of the Labrador Sea represent an anomalous situation explainable by other mechanisms, or normal for a conjugate passive margin pair.

Another possible location in which an analysis of the degree of magmatic symmetry could be conducted is between the relatively magma-poor Orphan Basin NE (Dafoe et al., 2015) of Newfoundland and its conjugate the Rockall Trough NW of Ireland where significant occurrences of both intrusive and extrusive magmatism have been documented (Archer et al., 2005; Thomson, 2005; Upton, 1988). Such a pronounced asymmetric magmatic distribution between conjugate margin pairs may be an expression of the fundamental mechanisms leading to continental breakup, melt production and passive margin development. This conjugate pair is also an appealing target to test the asymmetry model developed in this study as the Canadian part of the conjugate pair (Orphan Basin) lies on the same NVPM and is not separated by any major structures such as transform zones as the Makkovik study described in Chapter 4. Thus, this location may offer the opportunity to conduct a study in which only the upper plate half of the conjugate pair (southwest Greenland and possibly the Rockall trough) would be changed during a comparison allowing the model to be tested further. Another attractive aspect of the Orphan Basin is that new geophysical data has recently been acquired here as a result of the interest in hydrocarbon the hydrocarbon potential, including several new 2D and 3D seismic

reflection surveys that would allow the Orphan Basin to be characterised in detail that has until now been unachievable.

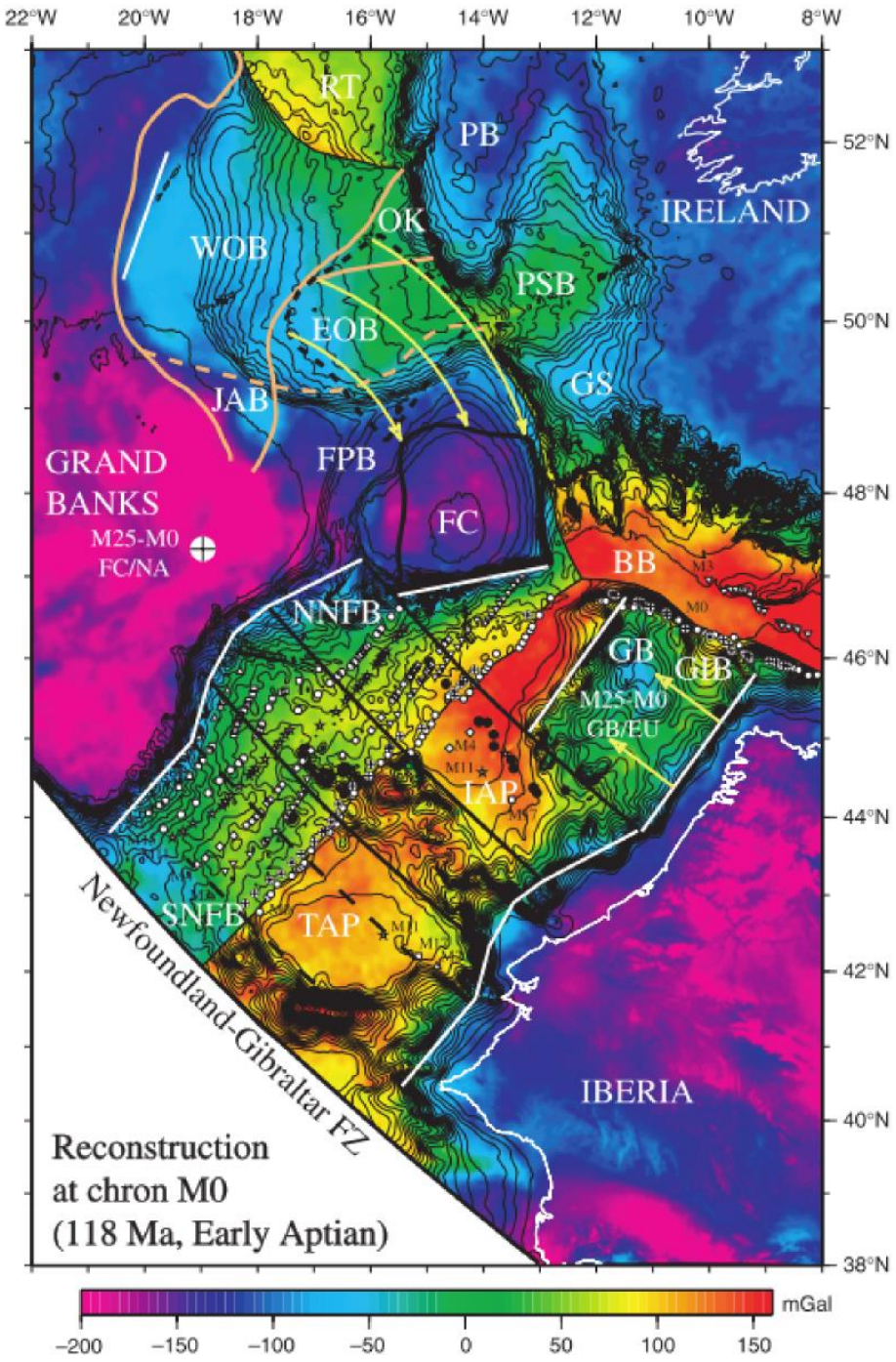

Figure 8.7

Reproduced from Sibuet et al. (2007) showing a reconstruction of the North Atlantic at 118 Ma with the West Orphan Basin (WOB) adjacent to the Rockall Trough (RT). Gravity anaomalies are shown in colour whilst the bathymetry is shown at 200 m intervals using contours. Other abbreviations on this figure include: FC = Flemish Cap; FPB = Flemish Pass Basin; GB = Galicia Bank; GS = Goban Spur; IAP = Iberian Abyssal Plain; and JAB = Jeanne d'Arc Basin.

In addition to further testing the simple shear model of passive margin formation (Lister et al., 1986) elsewhere further work should also be conducted on the conjugate margins of the Labrador Sea. One such area of ambiguity in our analysis includes the geographical distribution of rift-related igneous rocks in certain parts of both the on and offshore regions of the study area. This was particularly apparent offshore southwest Greenland where the lack of well coverage inhibited a complete comparison of the offshore extent of magmatism with the Labrador margin. The nature of rift-related magmatism underneath the Greenland Ice Sheet represents another unknown that future work should aim to address. This is particularly paramount as the Lister et al. (1986) simple shear model of passive margin formation predicts magmatic underplating to occur beneath the upper plate margin which in the application of the model in this work is represented by Greenland.

8.5.2 The chronology of deformation events in Labrador and Greenland

This study has also uncovered several significant unknowns in the current understanding of the sequence of deformation events that occurred prior to and during continental breakup in the North Atlantic region (Chapter 5 and 6). For example, it is problematic to fully understand the role of pre-existing structures during rifting as the early deformation features which comprise such pre-existing terrains are often poorly characterised. It is clear that the onshore expressions of the structures that either developed or were reactivated during the Mesozoic-Cenozoic breakup of the region require further study to allow their influence on the development of rifting in the area to be better characterised. These ambiguities have arisen as a result of lack of exposure for example due to glaciation in particular underneath the Greenland Ice Sheet but also due to difficulties in access to remote locations in both Greenland and Canada.

The preliminary structural study presented in Chapter 5 in the Aillik Domain of the Makkovik Province demonstrated that the region certainly has the potential for further studies of this kind. In particular, future studies should aim to increase the geographical distribution of structural data collection to elsewhere on the Labrador margin. Ideally this proposed work should be conducted across the multiple basement terrains that comprise the region (Chapter 4 – Figure 4.2) to test how rift-related deformation has manifest within these different units. In addition, geochronological work should be conducted where possible to provide a temporal constraint on the identified deformation events, this should include attempting to gain an absolute date for the deformation event which was used for the stress inversion in Chapter 5.

8.6 Conclusions

The conclusions of the analysis detailed in chapters 4-7 are summarised in this final section of the thesis. The order of these conclusions reflects the order in which the analysis they are based upon are presented.

My conclusions on the characteristics and extent of Early Cretaceous magmatism in proximity to the town of Makkovik as detailed in Chapter 4 are as follows:

- Early Cretaceous magmatism around Makkovik, Labrador, is volumetrically and spatially extremely minor compared to the numerous other phases of extensive, readily observable intrusive magmatism exposed in the area.
- Early Cretaceous magmatism is not sufficiently simple and consistent to consider this event as a single coherent intrusive suite of Early Cretaceous nephelinite dykes, as the outcrops are too sparse, variable, and unreliable. The most reliable evidence for Mesozoic magmatism around Makkovik is the diatreme in Ford's Bight.

The conclusions with respect to margin asymmetry, rifting mechanisms and the relationship between Mesozoic magmatism in West Greenland and Labrador as detailed in Chapter 4 are as follows:

- The magmatic distribution across the conjugate margins of the Labrador Sea is extremely asymmetric, with the Mesozoic magmatism exposed at surface in the area around Makkovik being minor compared to observations of rift-related dyking exposed at surface on the conjugate southwest Greenland margin.
- This asymmetric magmatic distribution complements other observations of asymmetry, including deeper sedimentary basins and a wider continental shelf on the Labrador margin compared to the southwest Greenland margin allowing us to propose a simple shear model for early rifting prior to the opening of the Labrador Sea, as opposed to a pure shear rifting model. In a simple shear rifting model the southwest Greenland margin would be the upper plate margin and the Labrador margin would be the lower plate margin.

The conclusions of the preliminary structural study in the Aillik Domain of the Makkovik Province as detailed in Chapter 5 are that:

- The deformation event characterised by abundant epidote mineralisation is likely to have been produced during an ENE-WSW extensional event. This ENE-WSW extensional event is younger than ~590 - 555 Ma based on the age of mafic dykes containing most of the deformation. It is possible that the post ~590 - 555 Ma extensional event is the cause of all brittle deformation analysed in the stress inversions in this section, with the epidote mineralisation representing a localised effect due to proximity to mafic dykes.

- Given the extension directions interpreted by previous work it is possible that the deformation event(s) analysed in this study represent an onshore expression deformation prior to the opening of the Labrador Sea, that is approximately ENE-WSW during the Cretaceous.
- The regional metamorphic mineral fabric within the studied part of the Aillik Domain of the Makkovik Province is orientated parallel to the rifting direction inferred by previous studies on the conjugate West Greenland margin and by the stress inversion performed by this work. Such an orientation of the basement fabric with respect to rifting would have potentially made this the Aillik Domain particularly susceptible to ~E-W Mesozoic rifting. Thus, the metamorphic basement fabric is likely to have exerted a considerable effect on rift development by allowing rifting to easily propagate through the proto-Labrador Sea region.

Our conclusions on the role of pre-existing structures during Mesozoic rifting between Greenland and Canada as detailed in Chapter 6 are as follows:

- Three fault systems were identified offshore in the Davis Strait study area. These are 1) NE-SW, 2) NW-SE and 3) N-S. All the fault sets identified offshore correlate with observed structural trends identified onshore by previous work in the North Atlantic Craton and the Nagssugtoqidian orogenic belt. During the first phase of rifting faulting is primarily controlled by pre-existing structures with fault set 1 (NE-SW) representing an oblique normal reactivation; fault set 2 (NW-SE) representing normal faults approximately orthogonal to the rifting direction possibly but not necessarily exploiting pre-existing structures and fault set 3 (N-S) representing oblique normal reactivation. In the second rifting stage, a sinistral transform system developed in the Davis Strait (Ungava Fault Zone) as a result of

deformation being accommodated on a transform fault system due to the lateral offset between the Labrador Sea and Baffin Bay. This lateral offset was established in the first rift stage probably due to the presence of the Nagssugtoqidian-Torngat orogenic belt being unsusceptible to rift propagation. Without the influence of pre-existing structures the manifestation of deformation cannot be easily explained under either the first or second rifting phase.

- The primary control on the location of rifting has changed through time with basement anisotropy providing the main control on the location and style of early offshore faulting and thus basin development. The dominance of faulting and thus basement anisotropy as the primary control diminishes throughout the synrift and into the postrift. However, despite the diminishing role of pre-existing structures in the rifting process through time some large structures may continue to remain important even into the postrift. The thermal profile and thus lithospheric strength through the rift cycle may provide an explanation for the diminishing basement influence in that initial rifting may weaken the lithosphere resulting in localised isostatic compensation compared to in the postrift whereas a stronger lithosphere may result in regional flexure type isostatic compensation.

- There is a distinct division between the north and south of the study area throughout the studied geological interval, with the synrift being dominated by deposition in the south, whereas the postrift is dominated by deposition in the north. This long-lived division could reflect a significant pre-existing structure that may represent the offshore continuation of the boundary between the Archean North Atlantic Craton and the Palaeoproterozoic Nagssugtoqidian.

The conclusions related to the thermal modelling of sills at ODP 210-1276 detailed in Chapter 7 are as follows:

- The older sill at ODP 210-1276 had cooled to a temperature indistinguishable from the background geothermal gradient well before the younger, lower sill complex was intruded.

- The temperatures achieved in the sedimentary rocks adjacent to the intrusions are higher than those achieved by post-depositional burial. This demonstrates the potential significance that regionally extensive intrusive magmatism could have on the thermal evolution of the Newfoundland margin, and suggests that the role of intrusive magmatism should be considered in thermal maturation studies in similar settings.

- If the sills acted as magmatic conduits prior to cooling to the closing temperature (as recorded by the $^{40}Ar/^{39}Ar$ dates) it was for a short duration, probably <10 years.

- The peak in vitrinite reflectance data observed at ODP 210-1276 can be completely attributed to rapid heating from the upper sill. We have also shown that the spatial extent of the thermal aureole of these sills was much greater shortly after intrusion, and that subsequent burial and compaction has reduced its current vertical extent at ODP 210-1276, which is probably representative of the situation across the Newfoundland margin.

- The higher than average $\%R_o$ gradient for this part of the Newfoundland margin implies that at some point in the past the heat flow was elevated. This elevation of past heat flow could have been caused by the same mechanism that produced the sills which are imaged on seismic data as the ‘U-reflector’.

- The EASY%R_o modelling results confirm that the sills at ODP 210-1276 have influenced the localised thermal evolution, and may be indicative of a broader, more regional thermal perturbation in the region covered by the ‘U-reflector’ on regional seismic data, and thus should be considered in source rock maturation studies.

References

Aarnes, I., Svensen, H., Connolly, J.A.D., and Podladchikov, Y.Y., 2010, How contact metamorphism can trigger global climate changes: Modeling gas generation around igneous sills in sedimentary basins: Geochimica et Cosmochimica Acta, v. 74, no. 24, p. 7179–7195, doi: 10.1016/j.gca.2010.09.011.

Aarnes, I., Svensen, H., Polteau, S., and Planke, S., 2011, Contact metamorphic devolatilization of shales in the Karoo Basin, South Africa, and the effects of multiple sill intrusions: Chemical Geology, v. 281, no. 3–4, p. 181–194, doi: 10.1016/j.chemgeo.2010.12.007.

Abdelmalak, M.M., Geoffroy, L., Angelier, J., Bonin, B., Callot, J.P., Gélard, J.P., and Aubourg, C., 2012, Stress fields acting during lithosphere breakup above a melting mantle: A case example in West Greenland: Tectonophysics, v. 581, p. 132–143, doi: 10.1016/j.tecto.2011.11.020.

Abdunaser, K.M., and McCaffrey, K.J.W., 2015, A new structural interpretation relating NW Libya to the Hun Graben , western Sirt Basin based on a new paleostress inversion: Journal of Earth Systems science, v. 124, no. 8, p. 1745–1763.

Ainsworth, N.R., Riley, L.A., Bailey, H.W., and Gueinn, J.J., 2014, Cretaceous - Tertiary Stratigraphy of the Labrador Shelf: Riley Geoscience Limited for Nalcor Energy,.

Ajay, K.K., Chaubey, A.K., Krishna, K.S., Rao, D.G., and Sar, D., 2010, Seaward dipping reflectors along the SW continental margin of India: Evidence for volcanic passive margin: Journal of Earth System Science, v. 119, no. 6, p. 803–813, doi: 10.1007/s12040-010-0061-2.

Allen, P., and Allen, J., 2005, Basin Analysis: Blackwell Publishing.

Alves, T.M., Bell, R.E., Jackson, C.A.L., and Minshull, T.A., 2014, Deep-water continental margins: Geological and economic frontiers: Basin Research, v. 26, no. 1, p. 3–9, doi: 10.1111/bre.12053.

Anderson, E.M., 1951, The Dynamics of Faulting: Oliver and Boyd, Edinburgh.

Angelier, J., 1990, Inversion of field data in fault tectonics to obtain the regional stress-III. A new rapid direct inversion method by analytical means: Geophysical Journal International, v. 103, no. 2, p. 363–376, doi: 10.1111/j.1365-246X.1990.tb01777.x.

Angelier, J., and Mechler, P., 1977, Sur une methode graphique de recherche des contraintes principales egalement utilisable en tectonique et en seismologie: la methode des diedres droits: Bulletin of the Geological Society of France,.

Archer, S.G., Bergman, S.C., Iliffe, J., Murphy, C.M., and Thornton, M., 2005, Palaeogene igneous rocks reveal new insights into the geodynamic evolution and petroleum potential of the Rockall Trough, NE Atlantic Margin: Basin Research, v. 17, no. 1, p. 171–201, doi: 10.1111/j.1365-2117.2005.00260.x.

Armitage, J.J., Collier, J.S., and Minshull, T. a, 2010, The importance of rift history for volcanic margin formation.: Nature, v. 465, no. 7300, p. 913–917, doi:

10.1038/nature09063.

Ashby, D., 2013, Influences on continental margin development: a case study from the Santos Basin, South-eastern Brazil: Durham University E-Theses,.

Aslanian, D., Moulin, M., Olivet, J.L., Unternehr, P., Matias, L., Bache, F., Rabineau, M., Nouzé, H., Klingelheofer, F., Contrucci, I., and Labails, C., 2009, Brazilian and African passive margins of the Central Segment of the South Atlantic Ocean: Kinematic constraints: Tectonophysics, v. 468, no. 1–4, p. 98–112, doi: 10.1016/j.tecto.2008.12.016.

Assumpção, M., Heintz, M., Vauchez, A., and Silva, M.E., 2006, Upper mantle anisotropy in SE and Central Brazil from SKS splitting: Evidence of asthenospheric flow around a cratonic keel: Earth and Planetary Science Letters, v. 250, no. 1–2, p. 224–240, doi: 10.1016/j.epsl.2006.07.038.

Audet, P., and Bürgmann, R., 2011, Dominant role of tectonic inheritance in supercontinent cycles: Nature Geoscience, v. 4, no. 3, p. 184–187, doi: 10.1038/ngeo1080.

Autin, J., Bellahsen, N., Leroy, S., Husson, L., Beslier, M.O., and d'Acremont, E., 2013, The role of structural inheritance in oblique rifting: Insights from analogue models and application to the Gulf of Aden: Tectonophysics, v. 607, p. 51–64, doi: 10.1016/j.tecto.2013.05.041.

Van Avendonk, H.J.A., Holbrook, W.S., Nunes, G.T., Shillington, D.J., Tucholke, B.E., Louden, K.E., Larsen, H.C., and Hopper, J.R., 2006, Seismic velocity structure of the rifted margin of the eastern Grand Banks of Newfoundland, Canada: Journal of Geophysical Research: Solid Earth, v. 111, no. 11, p. B11404, doi: 10.1029/2005JB004156.

Bacon, M., Simm, R., and Redshaw, T., 2003, 3-D sesimic interpretation: Cambridge University Press.

Balkwill, H.R., 1987, Labrador Basin: structural and stratigraphic style: Sedimentary Basins and Basin Forming Mechanisms, Canadian Society of Petroleum Geology Memoirs 12 (eds) Beaumont, C. and Tankard, A. J., v. 12, p. 17–43.

Ballmer, M.D., van Hunen, J., Ito, G., Tackley, P.J., and Bianco, T.A., 2007, Non-hotspot volcano chains originating from small-scale sublithospheric convection: Geophysical Research Letters, v. 34, no. 23, doi: 10.1029/2007GL031636.

Ballmer, M.D., Ito, G., van Hunen, J., and Tackley, P.J., 2010, Small-scale sublithospheric convection reconciles geochemistry and geochronology of "Superplume" volcanism in the western and south Pacific: Earth and Planetary Science Letters, v. 290, no. 1–2, p. 224–232, doi: 10.1016/j.epsl.2009.12.025.

Barckhausen, U., Engels, M., Franke, D., Ladage, S., and Pubellier, M., 2014, Evolution of the South China Sea: Revised ages for breakup and seafloor spreading: Marine and Petroleum Geology, v. 58, no. PB, p. 599–611, doi: 10.1016/j.marpetgeo.2014.02.022.

Barjous, M., and Mikbel, S., 1990, Tectonic evolution of the gulf of Aqaba-Dead Sea

transform fault system: Tectonophysics, v. 180, no. 1, p. 49–59, doi: 10.1016/0040-1951(90)90371-E.

Barker, C.E., Bone, Y., and Lewan, M.D., 1998, Fluid inclusion and vitrinite-reflectance geothermometry compared to heat-flow models of maximum paleotemperature next to dikes, western onshore Gippsland Basin, Australia: International Journal of Coal Geology, v. 37, no. 1–2, p. 73–111, doi: 10.1016/S0166-5162(98)00018-4.

Le Bas, M.J., 1989, Nephelinitic and basanitic rocks: Journal of Petrology, v. 30, no. 5, p. 1299–1312, doi: 10.1093/petrology/30.5.1299.

Le Bas, M.J., Le Maitre, R.W., Streckeisen, A., and Zanettin, B., 1986, A chemical classification of volcanic rocks based on the total alkali silica diagram: Journal of Petrology, v. 27, no. 3, p. 745–750, doi: 10.1093/petrology/27.3.745.

Becker, K., Tanner, D.C., Franke, D., and Krawczyk, C.M., 2016, Fault-controlled lithospheric detachment of the volcanic southern South Atlantic rift: Geochemistry, Geophysics, Geosystems, p. 1–8, doi: 10.1002/2015GC006081.

Beglinger, S.E., Doust, H., and Cloetingh, S., 2012, Relating petroleum system and play development to basin evolution: West African South Atlantic basins: Marine and Petroleum Geology, v. 30, no. 1, p. 1–25, doi: 10.1016/j.marpetgeo.2011.08.008.

Behn, M.D., and Lin, J., 2000, Segmentation in gravity and magnetic anomalies along the U.S. East Coast passive margin: Implications for incipient structure of the oceanic lithosphere: Journal of Geophysical Research, v. 105, no. B11, p. 25769, doi: 10.1029/2000JB900292.

Bellahsen, N., Fournier, M., d'Acremont, E., Leroy, S., and Daniel, J.M., 2006, Fault reactivation and rift localization: Northeastern Gulf of Aden margin: Tectonics, v. 25, no. 1, p. 1–14, doi: 10.1029/2004TC001626.

Berg, S.S., and Skar, T., 2005, Controls on damage zone asymmetry of a normal fault zone: Outcrop analyses of a segment of the Moab fault, SE Utah: Journal of Structural Geology, v. 27, no. 10, p. 1803–1822, doi: 10.1016/j.jsg.2005.04.012.

Boillot, G., and Froitzheim, N., 2001, Non-volcanic Rifted Margins, Continental Break-up and the Onset of Sea-floor Soreading: Some Outstanding Questions: Geological Society, London, Special Publications, v. 187, p. 9–30, doi: 10.1144/GSL.SP.2001.187.01.02.

Bostick, N.H., and Alpern, B., 1977, Principles of sampling, preparation and constituent selection for microphotometry in measurement of maturation of sedimentary organic matter: Journal of Microscopy, v. 109, no. 1, p. 41–47, doi: 10.1111/j.1365-2818.1977.tb01115.x.

Bosworth, W., 1987, Off-axis volcanism in the Gregory rift, east Africa: Implications for models of continental rifting: Geology, v. 15, no. 5, p. 397–400, doi: 10.1130/0091-7613(1987)15<397:OVITGR>2.0.CO;2.

Bosworth, W., Huchon, P., and McClay, K., 2005, The Red Sea and Gulf of Aden Basins: Journal of African Earth Sciences, v. 43, no. 1–3, p. 334–378, doi: 10.1016/j.jafrearsci.2005.07.020.

Bott, M.H.P., 1959, The Mechanics of Oblique Slip Faulting: Geological Magazine, v. 96, no. 2, p. 109, doi: 10.1017/S0016756800059987.

Bowling, J.C., and Harry, D.L., 2001, Geodynamic models of continental extension and the formation of non-volcanic rifted continental margins: Geological Society, London, Special Publications, v. 187, no. 1, p. 511–536, doi: 10.1144/GSL.SP.2001.187.01.25.

Bradley, D.C., 2008, Passive margins through earth history: Earth-Science Reviews, v. 91, no. 1–4, p. 1–26, doi: 10.1016/j.earscirev.2008.08.001.

Bridgwater, D., Watson, J., and Windley, B.F., 1973, The Archean Craton of the North Atlantic Region: Philosophical Transactions of the Royal Society, v. 273, p. 493–512.

Brooks, C.K., 2011, The East Greenland rifted volcanic margin, Geological Survey of Danmark and Greenland Bulletin 24: Geological Survey of Greenland and Denmark Bulletin, v. 24, p. 96.

Brown, A.R., 2011, Interpretation of Three-Dimensional Seismic Data: AAPG Memoir series, , no. 42, p. 1–528, doi: 10.1190/1.9781560802884.

Brune, S., Popov, A.A., and Sobolev, S. V., 2012, Modeling suggests that oblique extension facilitates rifting and continental break-up: Journal of Geophysical Research: Solid Earth, v. 117, no. 8, p. n/a-n/a, doi: 10.1029/2011JB008860.

Bujak, J., and Mudge, D., 1994, A high-resolution North Sea Eocene dinocyst zonation: Journal of the Geological Society, v. 151, no. 3, p. 449–462, doi: 10.1144/gsjgs.151.3.0449.

Bureau, D., Mourgues, R., Cartwright, J., Foschi, M., and Abdelmalak, M.M., 2013, Characterisation of interactions between a pre-existing polygonal fault system and sandstone intrusions and the determination of paleo-stresses in the Faroe-Shetland basin: Journal of Structural Geology, v. 46, p. 186–199, doi: 10.1016/j.jsg.2012.09.003.

Burnham, A.K., and Sweeney, J.J., 1989, A chemical kinetic model of vitrinite maturation and reflectance: Geochimica et Cosmochimica Acta, v. 53, no. 10, p. 2649–2657, doi: 10.1016/0016-7037(89)90136-1.

Butler, R.W.H., Holdsworth, R.E., and Lloyd, G.E., 1997, The role of basement reactivation in continental deformation: Journal of the Geological Society, v. 154, no. 1, p. 69–71, doi: 10.1144/gsjgs.154.1.0069.

Callot, J.P., Grigné, C., Geoffroy, L., and Brun, J.P., 2001, Development of volcanic passive margins: Two-dimensional laboratory models: Tectonics, v. 20, no. 1, p. 148–159, doi: 10.1029/2000TC900030.

Campbell, I.H., and Kerr, A.C., 2007, Testing the plume theory: Chemical Geology, v. 241, no. 3–4, p. 153–176, doi: 10.1016/j.chemgeo.2007.01.024.

Cardozo, N., and Allmendinger, R.W., 2013, Spherical projections with OSXStereonet: Computers and Geosciences, v. 51, p. 193–205, doi: 10.1016/j.cageo.2012.07.021.

Casu, F., and Manconi, A., 2016, Four-dimensional surface evolution of active rifting from spaceborne SAR data: Geosphere, v. 12, no. 3, p. 697–705, doi:

10.1130/GES01225.1.

Centreville, S., and Scott, D.J., 1998, An overview of the U-Pb geochronology of the Paleoproterozoic Torngat Orogen, Northeastern Canada David: Precambrian Research, v. 91, no. 1–2, p. 91–107, doi: 10.1016/S0301-9268(98)00040-0.

Chalmers, J. a., 1991, New evidence on the structure of the Labrador Sea/Greenland continental margin: Journal of the Geological Society, v. 148, no. 5, p. 899–908, doi: 10.1144/gsjgs.148.5.0899.

Chalmers, J.A., 1997, The continental margin off southern Greenland: along-strike transition from an amagmatic to a volcanic margin: Journal of the Geological Society, v. 154, no. 3, p. 571–576, doi: 10.1144/gsjgs.154.3.0571.

Chalmers, J.A., Larsen, L.M., and Pedersen, A.K., 1995, Widespread Palaeocene volcanism around the northern North Atlantic and Labrador Sea: evidence for a large, hot, early plume head: Journal of the Geological Society, v. 152, no. 6, p. 965–969, doi: 10.1144/GSL.JGS.1995.152.01.14.

Chalmers, J.A., and Laursen, K.H., 1995, Labrador Sea: the extent of continental and oceanic crust and the timing of the onset of seafloor spreading: Marine and Petroleum Geology, v. 12, no. 2, p. 205–217, doi: 10.1016/0264-8172(95)92840-S.

Chalmers, J.A., and Pulvertaft, T.C.R., 2001, Development of the continental margins of the Labrador Sea: a review: Geological Society, London, Special Publications, v. 187, no. 1, p. 77–105, doi: 10.1144/GSL.SP.2001.187.01.05.

Chattopadhyay, A., and Chakra, M., 2013, Influence of pre-existing pervasive fabrics on fault patterns during orthogonal and oblique rifting: An experimental approach: Marine and Petroleum Geology, v. 39, no. 1, p. 74–91, doi: 10.1016/j.marpetgeo.2012.09.009.

Chenin, P., Manatschal, G., Lavier, L.L., and Erratt, D., 2015, Assessing the impact of orogenic inheritance on the architecture, timing and magmatic budget of the North Atlantic rift system: a mapping approach: Journal of the Geological Society, v. 172, p. 711–720, doi: 10.1144/jgs2014-139.

Chian, D., Keen, C., Reid, I., and Louden, K.E., 1995a, Evolution of nonvolcanic rifted margins: new results from the conjugate margins of the Labrador Sea: Geology, v. 23, no. 7, p. 589–592, doi: 10.1130/0091-7613(1995)023<0589:EONRMN>2.3.CO;2.

Chian, D., and Louden, K.E., 1994, The continent-ocean crustal transition across the southwest Greenland margin: Journal of Geophysical Research, v. 99, no. B5, p. 9117–9135, doi: 10.1029/93JB03404.

Chian, D., Louden, K.E., and Reid, I., 1995b, Crustal structure of the Labrador Sea conjugate margin and implications for the formation of nonvolcanic continental margins: Journal of Geophysical Research, v. 100, no. B12, p. 24239, doi: 10.1029/95JB02162.

Christie, P.A.F., and White, R.S., 2008, Imaging through Altantic Margin basalts: An introduction to the sub-basalt mini-set: Geophysical Prospecting, v. 56, no. 1, p. 1–4, doi: 10.1111/j.1365-2478.2007.00676.x.

Cloetingh, S., Beekman, F., Ziegler, P.A., van Wees, J.-D., and Sokoutis, D., 2008, Post-rift compressional reactivation potential of passive margins and extensional basins: Geological Society, London, Special Publications, v. 306, no. 1, p. 27–70, doi: 10.1144/sp306.2.

Cloetingh, S., Vanwees, J.D., Vanderbeek, P.A., and Spadini, G., 1995, Role of Pre-Rift Rheology in Kinematics of Extensional Basin Formation - Constraints From Thermomechanical Models of Mediterranean and Intracratonic Basins: Marine and Petroleum Geology, v. 12, no. 8, p. 793–807, doi: 10.1016/0264-8172(95)98848-y.

Cochran, J.R., 1983, A Model for Development of Red Sea: AAPG Bulletin, v. 67, no. 1, p. 41–69, doi: 10.1306/03B5ACBE-16D1-11D7-8645000102C1865D.

Cochran, J.R., Martinez, F., Steckler, M.S., and Hobart, M.A., 1986, Conrad Deep: a new northern Red Sea deep. Origin and implications for continental rifting: Earth and Planetary Science Letters, v. 78, no. 1, p. 18–32, doi: 10.1016/0012-821X(86)90169-X.

Connelly, J.N., and Mengel, F.C., 2000, Evolution of Archean components in the Paleoproterozoic Nagssugtoqidian orogen, West Greenland: Bulletin of the Geological Society of America, v. 112, no. 5, p. 747–763, doi: 10.1130/0016-7606(2000)112<747:EOACIT>2.0.CO;2.

Contreras, J., Zühlke, R., Bowman, S., and Bechstädt, T., 2010, Seismic stratigraphy and subsidence analysis of the southern Brazilian margin (Campos, Santos and Pelotas basins): Marine and Petroleum Geology, v. 27, no. 9, p. 1952–1980, doi: 10.1016/j.marpetgeo.2010.06.007.

Contrucci, I., Matias, L., Moulin, M., Geli, L., Klingelhofer, F., Nouze, H., Aslanian, D., Olivet, J.L., Rehault, J.P., and Sibuet, J.C., 2004, Deep structure of the West African continental margin (Congo, Zaire, Angola), between 5◦S and 8◦S, from reflection/refraction seismics and gravity data: Geophysical Journal International, v. 158, no. 2, p. 529–553, doi: 10.1111/j.1365-246X.2004.02303.x.

Corti, G., 2009, Continental rift evolution: From rift initiation to incipient break-up in the Main Ethiopian Rift, East Africa: Earth-Science Reviews, v. 96, no. 1–2, p. 1–53, doi: 10.1016/j.earscirev.2009.06.005.

Corti, G., and Manetti, P., 2006, Asymmetric rifts due to asymmetric Mohos: An experimental approach: Earth and Planetary Science Letters, v. 245, no. 1–2, p. 315–329, doi: 10.1016/j.epsl.2006.02.004.

Corti, G., van Wijk, J., Cloetingh, S., and Morley, C.K., 2007, Tectonic inheritance and continental rift architecture: Numerical and analogue models of the East African Rift system: Tectonics, v. 26, no. 6, p. 1–13, doi: 10.1029/2006TC002086.

Cowie, P.A., Attal, M., Tucker, G.E., Whittaker, A.C., Naylor, M., Ganas, A., and Roberts, G.P., 2006, Investigating the surface process response to fault interaction and linkage using a numerical modelling approach: Basin Research, v. 18, no. 3, p. 231–266, doi: 10.1111/j.1365-2117.2006.00298.x.

Crider, J.G., and Pollard, D.D., 1998, Fault linkage: Three-dimensional mechanical interaction between echelon normal faults: Journal of Geophysical Research, v. 103,

no. B10, p. 24373, doi: 10.1029/98JB01353.

Culshaw, N., Brown, T., Reynolds, P.H., and Ketchum, J.W.F., 2000, Kanairiktok shear zone : the boundary between the Paleoproterozoic Makkovik Province and the Archean Nain Province, Labrador, Canada .: Canadian Journal of Earth Science, v. 37, no. 9, p. 1245–1257, doi: 10.1139/e00-035.

Dafoe, L.T., Keen, C.E., Dickie, K., and Williams, G.L., 2015, Regional stratigraphy and subsidence of Orphan Basin near the time of breakup and implications for rifting processes: Basin Research, p. 1–22, doi: 10.1111/bre.12147.

Dalhoff, F., Chalmers, J.A., Gregersen, U., Nøhr-Hansen, H., Rasmussen, J.A., and Sheldon, E., 2003, Mapping and facies analysis of Paleocene-Mid-Eocene seismic sequences, offshore southern West Greenland: Marine and Petroleum Geology, v. 20, no. 9, p. 935–986, doi: 10.1016/j.marpetgeo.2003.09.004.

Dalhoff, F., Larsen, L.M., Ineson, J.R., Stouge, S., Bojesen-Koefoed, J.A., Lassen, S., Kuijpers, A., Rasmussen, J.A., and Nøhr-Hansen, H., 2006, Continental crust in the Davis Strait: new evidence from seabed sampling: Geological Survey of Denmark and Greenland Bulletin, v. 10, p. 33–36.

Dam, G., Larsen, M., and Sønderholm, M., 1998, Sedimentary response to mantle plumes: Implications from Paleocene onshore successions, West and East Greenland: Geology, v. 26, no. 3, p. 207–210, doi: 10.1130/0091-7613(1998)026<0207:SRTMPI>2.3.CO;2.

Davison, I.A.N., 1997, Wide and narrow margins of the Brazilian South Atlantic: Journal of the Geological Society, v. 154, no. 3, p. 471–476, doi: 10.1144/gsjgs.154.3.0471.

Decarlis, A., Manatschal, G., Haupert, I., and Masini, E., 2015, The tectono-stratigraphic evolution of distal, hyper-extended magma-poor conjugate rifted margins: Examples from the Alpine Tethys and Newfoundland-Iberia: Marine and Petroleum Geology, v. 68, p. 54–72, doi: 10.1016/j.marpetgeo.2015.08.005.

Deckart, K., Bertrand, H., and Liégeois, J.P., 2005, Geochemistry and Sr, Nd, Pb isotopic composition of the Central Atlantic Magmatic Province (CAMP) in Guyana and Guinea: Lithos, v. 82, no. 3–4 SPEC. ISS., p. 289–314, doi: 10.1016/j.lithos.2004.09.023.

Deemer, S., Hurich, C., and Hall, J., 2010, Post-rift flood-basalt-like volcanism on the Newfoundland Basin nonvolcanic margin: The U event mapped with spectral decomposition: Tectonophysics, v. 494, no. 1–2, p. 1–16, doi: 10.1016/j.tecto.2010.07.019.

Delvaux, D., and Sperner, B., 2003, New aspects of tectonic stress inversion with reference to the TENSOR program: Geological Society, London, Special Publications, v. 212, no. 1, p. 75–100, doi: 10.1144/GSL.SP.2003.212.01.06.

Dempsey, E.D., Holdsworth, R.E., Imber, J., Bistacchi, A., and Di Toro, G., 2014, A geological explanation for intraplate earthquake clustering complexity: The zeolite-bearing fault/fracture networks in the Adamello Massif (Southern Italian Alps): Journal of Structural Geology, v. 66, p. 58–74, doi: 10.1016/j.jsg.2014.04.009.

DeSilva, N.R., 1999, Sedimentary basins and petroleum systems offshore Newfoundland and Labrador: Petroleum Geology of Northwest Europe: Proceedings of the 5th Conference on the Petroleum Geology of Northwest Europe, p. 501–516, doi: 10.1144/0050501.

Dewey, J.F., and Horsfield, B., 1970, Plate Tectonics, Orogeny and Continental Growth: Nature, v. 225, no. January, p. 451–453.

Dichiarante, A.M., Holdsworth, R.E., Dempsey, E.D., Selby, D., McCaffrey, K.J.W., Michie, U.M., Morgan, G., and Bonniface, J., 2016, New structural and Re–Os geochronological evidence constraining the age of faulting and associated mineralization in the Devonian Orcadian Basin, Scotland: Journal of the Geological Society, v. 173, no. 3, p. 457–473, doi: 10.1144/jgs2015-118.

Dietz, R.S., 1961, Continent and Ocean Basin Evolution by Spreading of the Sea Floor: Nature, v. 190, p. 854–857.

Divins, D.L., 2003, Total Sediment Thickness of the World's Oceans & Marginal Seas: NOAA National Geophysical Data Center, Boulder, CO,.

Dixon, T.H., Ivins, E.R., and Franklin, B.J., 1989, Topographic and volcanic asymmetry around the Red Sea: Constraints on rift models: Tectonics, v. 8, no. 6, p. 1193–1216, doi: 10.1029/TC008i006p01193.

Dore, A.G., Lundin, E.R., Fichler, C., and Olesen, O., 1997, Patterns of basement structure and reactivation along the NE Atlantic margin: Journal of the Geological Society, v. 154, no. 1, p. 85–92, doi: 10.1144/gsjgs.154.1.0085.

Døssing, A., 2011, Fylla Bank: Structure and evolution of a normal-to-shear rifted margin in the northern Labrador Sea: Geophysical Journal International, v. 187, no. 2, p. 655–676, doi: 10.1111/j.1365-246X.2011.05184.x.

Duncan, R.A., Larsen, H.C., and Allan, J.F., 1996, Ch1 . Introduction: Leg 163 Background and Objectives 1: Proceedings of the Ocean Drilling Program, Initial Reports, v. 163.

Duraiswami, R.A., and Shaikh, T.N., 2013, Geology of the saucer-shaped sill near Mahad, western Deccan Traps, India, and its significance to the Flood Basalt Model: Bulletin of Volcanology, v. 75, no. 7, p. 1–18, doi: 10.1007/s00445-013-0731-4.

Eagles, G., Pérez-Díaz, L., and Scarselli, N., 2015, Getting over continent ocean boundaries: Earth-Science Reviews, v. 151, p. 244–265, doi: 10.1016/j.earscirev.2015.10.009.

Eldholm, D., and Grue, K., 1994, North Atlantic volcanic margins: dimensions and production rates: Journal of Geophysical Research, v. 99, no. B2, p. 2955–2968, doi: 10.1029/93JB02879.

Eldholm, O., and Sundvor, E., 1979, Geological events during the early formation of a passive margin: Tectonophysics, v. 59, no. 1–4, p. 233–237, doi: 10.1016/0040-1951(79)90047-7.

Eldholm, O., Thiede, J., Taylor, E., Bjorklund, K., Bleil, U., Cielsielski, P., Despraries, A., Donnally, D., Froget, C., Goll, R., Henrich, R., Jansen, E., Krissek, L., Kvenvolden,

K., et al., 1986, Dipping reflectors in the Norwegian Sea--ODP Leg 104 drilling results: LEG 104 SCIENTIFIC PARTY: Journal of the Geological Society, v. 143, no. 6, p. 911–912, doi: 10.1144/gsjgs.143.6.0911.

England, G.L., Rasmussen, B., Krapez, B., and Groves, D.I., 2002, Archaean oil migration in the Witwatersrand Basin of South Africa: Journal of the Geological Society, v. 159, no. 2, p. 189–201, doi: 10.1144/0016-764900-197.

Esedo, R., Wijk, J. Van, Coblentz, D., and Meyer, R., 2012, Uplift prior to continental breakup: Indication for removal of mantle lithosphere? Geosphere, v. 8, no. 5, p. 1078–1085, doi: 10.1130/GES00748.1.

Etheridge, M.A., Symonds, P.A., and Lister, G.S., 1989, Application of the Detachment Model to Reconstruction of Conjugate Passive Margins: Chapter 3: Concepts, *in* Tankard, A.J. and Balkwill, H.R. eds., Extensional Tectonics and Stratigraphy of the North Atlantic Margins, AAPG, p. 23–40.

Farnetani, C.G., and Richards, M.A., 1994, Numerical Investigations of the Mantle Plume Initiation Model for Flood-Basalt Events: Journal of Geophysical Research-Solid Earth, v. 99, no. B7, p. 13,813-13,833, doi: 10.1029/94JB00649.

Fernandez, M., Ayala, C., Torne, M., Verges, J., Gomez, M., and Karpuz, R., 2005, Lithospheric structure of the Mid-Norwegian Margin: comparison between the More and Voring margins: Journal of the Geological Society, v. 162, no. 1994, p. 1005–1012, doi: 10.1144/0016-764904-116.

Fjeldskaar, W., Helset, H.M., Johansen, H., Grunnaleite, I., and Horstad, I., 2008, Thermal modelling of magmatic intrusions in the Gjallar Ridge, Norwegian Sea: Implications for vitrinite reflectance and hydrocarbon maturation: Basin Research, v. 20, no. 1, p. 143–159, doi: 10.1111/j.1365-2117.2007.00347.x.

Fjeldskaar, W., Johansen, H., Dodd, T.A., and Thompson, M., 2003, Temperature and Maturity Effects of Magmatic Underplating in the Gjallar Ridge, Norwegian Sea, *in* Duppenbecker, S. and Marzi, R. eds., Multidimensional Basin Modeling, p. 71–85.

Flament, N., Gurnis, M., Williams, S., Seton, M., Skogseid, J., Heine, C., and Dietmar Müller, R., 2014, Topographic asymmetry of the South Atlantic from global models of mantle flow and lithospheric stretching: Earth and Planetary Science Letters, v. 387, p. 107–119, doi: 10.1016/j.epsl.2013.11.017.

Foley, S.F., 1989, Emplacement Features of Lamprophyre and Carbonatitic Lamprophyre Dykes at Aillik Bay, Labrador: Geological Magazine, v. 126, no. 1, p. 29–42, doi: doi:10.1017/S0016756800006129.

Forsyth, D.A., Morel-A-L'Huissier, P., Asudeh, I., and Green, A.G., 1986, Alpha Ridge and Iceland - Products of the same plume? Journal of Geodynamics, v. 6, no. 30, p. 197–214, doi: 10.1016/0264-3707(86)90039-6.

Fossen, H., and Dunlap, W.J., 1998, Timing and Kinematics of Caledonian thrusting and extensional collapse, southern Norway: evidence from 40Ar/39Ar thermochronology: Journal of Structural Geology, v. 20, no. 6, p. 765–781.

Foulger, G., 2001, Plumes, or plate tectonic processes? Astronomy & Geophysics, v. 43, p.

19–23.

Foulger, G.R., and Anderson, D.L., 2005, A cool model for the Iceland hotspot: Journal of Volcanology and Geothermal Research, v. 141, no. 1–2, p. 1–22, doi: 10.1016/j.jvolgeores.2004.10.007.

Foulger, G.R., Natland, J.H., and Anderson, D.L., 2005a, A source for Icelandic magmas in remelted Iapetus crust: Journal of Volcanology and Geothermal Research, v. 141, no. 1–2, p. 23–44, doi: 10.1016/j.jvolgeores.2004.10.006.

Foulger, G.R., Natland, J.H., Presnell, D.C., and Anderson, D.L., 2005b, Plates, Plumes, And Paradigms: Boulder, Colorado.

Franke, D., 2013, Rifting, lithosphere breakup and volcanism: Comparison of magma-poor and volcanic rifted margins: Marine and Petroleum Geology, v. 43, no. 0, p. 63–87, doi: 10.1016/j.marpetgeo.2012.11.003.

Franke, D., Savva, D., Pubellier, M., Steuer, S., Mouly, B., Auxietre, J.L., Meresse, F., and Chamot-Rooke, N., 2014, The final rifting evolution in the South China Sea: Marine and Petroleum Geology, v. 58, no. PB, p. 704–720, doi: 10.1016/j.marpetgeo.2013.11.020.

Frey, Ø., Planke, S., Symonds, P.A., and Heeremans, M., 1998, Deep crustal structure and rheology of the Gascoyne volcanic margin, western Australia: Marine Geophysical Researches, v. 20, no. 4, p. 293–312, doi: 10.1023/A:1004791330763.

Funck, T., Gohl, K., Damm, V., and Heyde, I., 2012, Tectonic evolution of southern Baffin Bay and Davis Strait: Results from a seismic refraction transect between Canada and Greenland: Journal of Geophysical Research: Solid Earth, v. 117, no. 4, p. B04107, doi: 10.1029/2011JB009110.

Funck, T., Jackson, H.R., Louden, K.E., and Klingelh??fer, F., 2007, Seismic study of the transform-rifted margin in Davis Strait between Baffin Island (Canada) and Greenland: What happens when a plume meets a transform: Journal of Geophysical Research: Solid Earth, v. 112, no. 4, p. B04402, doi: 10.1029/2006JB004308.

Funck, T., and Louden, K.E., 1999, Wide-angle seismic transect across the Torngat Orogen, northern Labrador: Evidence for a Proterozoic crustal root: Journal of Geophysical Research, v. 104, no. B4, p. 7463, doi: 10.1029/1999JB900010.

Funck, T., Louden, K.E., and Reid, I.D., 2001, Crustal structure of the Grenville Province in southeastern Labrador from refraction seismic data: evidence for a high-velocity lower crustal wedge: Canadian Journal of Earth Sciences, v. 38, no. 10, p. 1463–1478, doi: 10.1139/e01-026.

Gaina, C., Gernigon, L., and Ball, P., 2009, Palaeocene-Recent plate boundaries in the NE Atlantic and the formation of the Jan Mayen microcontinent: Journal of the Geological Society, v. 166, no. 4, p. 601–616, doi: 10.1144/0016-76492008-112.

Gaina, C., Torsvik, T.H., van Hinsbergen, D.J.J., Medvedev, S., Werner, S.C., and Labails, C., 2013, The African plate: A history of oceanic crust accretion and subduction since the Jurassic: Tectonophysics, v. 604, p. 4–25, doi: 10.1016/j.tecto.2013.05.037.

Galerne, C.Y., Galland, O., Neumann, E.R., and Planke, S., 2011, 3D relationships

between sills and their feeders: Evidence from the Golden Valley Sill Complex (Karoo Basin) and experimental modelling: Journal of Volcanology and Geothermal Research, v. 202, no. 3–4, p. 189–199, doi: 10.1016/j.jvolgeores.2011.02.006.

Gallagher, J.W., and Dromgoole, P.W., 2007, Exploring below the basalt, offshore Faroes: a case history of sub-basalt imaging: Petroleum Geoscience, v. 13, no. 3, p. 213–225, doi: 10.1144/1354-079306-711.

Galushkin, Y.I., 1997, Thermal effects of igneous intrusions on maturity of organic matter: A possible mechanism of intrusion: Organic Geochemistry, v. 26, no. 11–12, p. 645–658, doi: 10.1016/S0146-6380(97)00030-2.

Garde, A.A., Hamilton, M.A., Chadwick, B., Grocott, J., and McCaffrey, K.J.W., 2002, The Ketilidian orogen of South Greenland : geochronology, tectonics, magmatism, and fore-arc accretion during Palaeoproterozoic oblique convergence: Canadian Journal of Earth Sciences, v. 39, no. 5, p. 765–793, doi: 10.1139/E02-026.

Garfunkel, Z., Zak, I., and Freund, R., 1981, Active faulting in the dead sea rift: Tectonophysics, v. 80, no. 1–4, p. 1–26, doi: 10.1016/0040-1951(81)90139-6.

Gawthorpe, R.L., Jackson, C.A.L., Young, M.J., Sharp, I.R., Moustafa, A.R., and Leppard, C.W., 2003, Normal fault growth, displacement localisation and the evolution of normal fault populations: The Hammam Faraun fault block, Suez rift, Egypt: Journal of Structural Geology, v. 25, no. 6, p. 883–895, doi: 10.1016/S0191-8141(02)00088-3.

Geoffroy, L., 2001, The structure of volcanic margins: Some problematics from the North-Atlantic/ Labrador-Baffin system: Marine and Petroleum Geology, v. 18, no. 4, p. 463–469, doi: 10.1016/S0264-8172(00)00073-8.

Geoffroy, L., 2005, Volcanic passive margins: Comptes Rendus - Geoscience, v. 337, no. 16, p. 1395–1408, doi: 10.1016/j.crte.2005.10.006.

Geoffroy, L., Burov, E.B., and Werner, P., 2015, Volcanic passive margins: another way to break up continents: Scientific Reports, v. 5, p. 14828, doi: 10.1038/srep14828.

Gerlings, J., Funck, T., Jackson, H.R., Louden, K.E., and Klingelhofer, F., 2009, Seismic evidence for plume-derived volcanism during formation of the continental margin in southern Davis Strait and northern Labrador Sea: Geophysical Journal International, v. 176, no. 3, p. 980–994, doi: 10.1111/j.1365-246X.2008.04021.x.

Gibson, G.M., Totterdell, J.M., White, L.T., Mitchell, C.H., Stacey, A.R., Morse, M.P., and Whitaker, A., 2013, Pre-existing basement structure and its influence on continental rifting and fracture zone development along Australia's southern rifted margin: Journal of the Geological Society, v. 170, no. 2, p. 365–377, doi: 10.1144/jgs2012-040.

Gill, R.C.O., Pedersen, A.K., and Larsen, J.G., 1992, Tertiary picrites in West Greenland: melting at the periphery of a plume? Geological Society, London, Special Publications, v. 68, no. 1, p. 335–348, doi: 10.1144/GSL.SP.1992.068.01.21.

Gillard, M., Manatschal, G., and Autin, J., 2015, How can asymmetric detachment faults generate symmetric Ocean Continent Transitions? Terra Nova, v. 28, no. 1, p. n/a-n/a,

doi: 10.1111/ter.12183.

Van Gool, J.A.M., Connelly, J.N., Marker, M., and Mengel, F.C., 2002, The Nagssugtoqidian Orogen of West Greenland: tectonic evolution and regional correlations from a West Greenland perspective: Canadian Journal of Earth Sciences, v. 39, no. 5, p. 665–686, doi: 10.1139/e02-027.

Gouiza, M., Hall, J., and Welford, J.K., 2016, Tectono-stratigraphic evolution and crustal architecture of the Orphan Basin during North Atlantic rifting: International Journal of Earth Sciences, doi: 10.1007/s00531-016-1341-0.

Goutorbe, B., Drab, L., Loubet, N., and Lucazeau, F., 2007, Heat flow of the eastern Canadian rifted continental margin revisited: Terra Nova, v. 19, no. 6, p. 381–386, doi: 10.1111/j.1365-3121.2007.00750.x.

Gradstein, F.M., and Ogg, J.G., 2012, The Geological Timescale., *in* Chapter 2 - the Chronostratigraphic Scale, p. 31–42.

Graham, D.W., Larsen, L.M., Hanan, B.B., Storey, M., Pedersen, A.K., and Lupton, J.E., 1998, Helium isotope composition of the early Iceland mantle plume inferred from the Tertiary picrites of West Greenland: Earth and Planetary Science Letters, v. 160, no. 3–4, p. 241–255, doi: 10.1016/S0012-821X(98)00083-1.

Gregersen, U., and Skaarup, N., 2007, A mid-Cretaceous prograding sedimentary complex in the Sisimiut Basin, offshore West Greenland-stratigraphy and hydrocarbon potential: Marine and Petroleum Geology, v. 24, no. 1, p. 15–28, doi: 10.1016/j.marpetgeo.2006.10.005.

Grove, C., 2013, Submarine hydrothermal vent complexes in the Paleocene of the Faroe-Shetland Basin: Insights from three-dimensional seismic and petrographical data: Geology, v. 41, no. 1, p. 71–74, doi: 10.1130/G33559.1.

Gunn, P.J., 1997, Quantitative methods for interpreting aeromagnetic data: a subjective review: AGSA Journal of Australian Geology and Geophysics, v. 17, p. 105–113.

Haggart, J.W., 2014, New contributions in Baffin Bay/Labrador Sea petroleum exploration and development geoscience: Bulletin of Canadian Petroleum Geology, v. 63, no. 2.

Hand, M., and Buick, I.S., 2001, Tectonic evolution of the Reynolds-Anmatjira Ranges: a case study in terrain reworking from the Arunta Inlier, central Australia: Geological Society, London, Special Publications, v. 184, no. 1, p. 237–260, doi: 10.1144/GSL.SP.2001.184.01.12.

Hansen, D.M., and Cartwright, J., 2007, Reply to comment by K. Thomson on "The three-dimensional geometry and growth of forced folds above saucer-shaped sills" by D. M. Hansen and J. Cartwright: Journal of Structural Geology, v. 29, no. 4, p. 741–744, doi: 10.1016/j.jsg.2006.10.008.

Hansen, D.M., and Cartwright, J., 2006, The three-dimensional geometry and growth of forced folds above saucer-shaped igneous sills: Journal of Structural Geology, v. 28, no. 8, p. 1520–1535, doi: 10.1016/j.jsg.2006.04.004.

Hansen, J., Jerram, D. a., McCaffrey, K., and Passey, S.R., 2009, The onset of the North Atlantic Igneous Province in a rifting perspective: Geological Magazine, v. 146, no. 3,

p. 309, doi: 10.1017/S0016756809006347.

Hart, S.R., and Blusztajn, J., 2006, Age and geochemistry of the mafic sills, ODP site 1276, Newfoundland margin: Chemical Geology, v. 235, no. 3–4, p. 222–237, doi: 10.1016/j.chemgeo.2006.07.001.

Hatcher, R.D., 2010, The Appalachian orogen: A brief summary: Geological Society of America Memoirs , v. 206, p. 1–19, doi: 10.1130/2010.1206(01).

Haworth, R.T., Hipkin, R., Jacobi, R.D., Kane, M., Lefort, J.P., Max, M.D., Miller, H.G., and Wolff, F., 1988, Geophysical framework and the Appalachian-Caledonide connection: Geological Society, London, Special Publications, v. 38, no. 38, p. 3–20, doi: 10.1144/GSL.SP.1988.038.01.01.

Heirtzler, J.R., Dickson, G.O., Herron, E.M., Pitman, W.C., and Le Pichon, X., 1968, Marine magnetic anomalies, geomagnetic field reversals, and motions of the ocean floor and continents: Journal of Geophysical Research, v. 73, no. 6.

Heirtzler, J.R., and Hayes, D.E., 1967, Magnetic Boundaries in the North Atlantic Ocean: Science, v. 157, no. 3785, p. 185–187, doi: 10.1126/science.157.3785.185.

Henriksen, E., Ryseth, A.E., Larssen, G.B., Heide, T., Ronning, K., Sollid, K., and Stoupakova, A. V., 2011, Chapter 10 Tectonostratigraphy of the greater Barents Sea: implications for petroleum systems: Geological Society, London, Memoirs, v. 35, no. 1, p. 163–195, doi: 10.1144/M35.10.

Heroux, Y., Chagnon, A., and Bertrand, R., 1979, Compilation and correlation of major thermal maturation indicators.: American Association of Petroleum Geologists Bulletin, v. 63, no. 12, p. 2128–2144, doi: 10.1306/2F9188F1-16CE-11D7-8645000102C1865D.

Herzberg, C., and O'Hara, M.J., 2002, Plume-Associated Ultramafic Magmas of Phanerozoic Age: Journal of Petrology, v. 43, no. 10, p. 1857–1883, doi: 10.1093/petrology/43.10.1857.

Hess, H.H., 1962, History of Ocean Basins: Petrologic Studies: a Volume To Honor a. F. Buddington, , no. November 1862, p. 500–620, doi: CRL_P2_D.

Hill, R.I., 1993, Mantle plumes and continental tectonics: Lithos, v. 30, no. 3–4, p. 193–206, doi: 10.1016/0024-4937(93)90035-B.

Hinchey, A.M., 2013, Geology of the Makkovik Area, Labrador (NTS 13O/03 and parts of NTS 13O/02). Scale 1:50000: Government of Newfoundland and Labrador, Department of Natural Resources, Geological Survey MAp 2013-07, Open file 013O/0138,.

Hippler, S.J., and Knipe, R.J., 1990, The evolution of cataclastic fault rocks from a pre-existing mylonite: Geological Society Special Publications, v. 54, no. 54, p. 71–79, doi: 10.1144/GSL.SP.1990.054.01.08.

Hirsch, K.K., Scheck-Wenderoth, M., van Wees, J.D., Kuhlmann, G., and Paton, D.A., 2010, Tectonic subsidence history and thermal evolution of the Orange Basin: Marine and Petroleum Geology, v. 27, no. 3, p. 565–584, doi: 10.1016/j.marpetgeo.2009.06.009.

Hoggard, M., Shorttle, O., and White, N., 2016, Testing Predictions of Continental Insulation using Oceanic Crustal Thicknesses: Geophysical Research Abstracts, v. 18, p. 16611.

Holbrook, W.S., Mooney, W.D., and Nicolas, I.C., 1992, The seismic velocity structure of the deep continental crust in Continental Lower Crust, Dev: Geotectonics, v. 23, no. 1987, p. 1–34.

Holdsworth, R.E., Butler, C.A., and Roberts, A.M., 1997, The recognition of reactivation during continental deformation: Journal of the Geological Society, v. 154, no. 1, p. 73–78, doi: 10.1144/gsjgs.154.1.0073.

Holdsworth, R.E., Handa, M., Miller, J.A., and Buick, I.S., 2001a, Continental reactivation and reworking: an introduction: Geological Society, London, Special Publications, v. 184, no. 1, p. 1–12, doi: 10.1144/gsl.sp.2001.184.01.01.

Holdsworth, R.E., Stewart, M., Imber, J., and Strachan, R.A., 2001b, The structure and rheological evolution of reactivated continental fault zones : a review and case study: Geological Society, London, Special Publications, v. 184, no. 1, p. 115–137.

Holford, S.P., Schofield, N., Jackson, C.A.L., Magee, C., Green, P.F., and Duddy, I.R., 2013, Impacts of Igneous Intrusions on Source and Reservoir Potential in Prospective Sedimentary Basins Along the Western Australian Continental Margin: West Australian Basins Symposium, , no. August, p. 18–21.

Holford, S.P., Schofield, N., MacDonald, J.D., Duddy, I.R., and Green, P.F., 2012, Seismic analysis of igneous systems in sedimentary basins and their impacts on hydrocarbon prospectivity: examples from the Southern Australian margin: APPEA Journal, v. 229, p. 229–252.

Holford, S.P., Tuitt, A.K., Hillis, R.R., Green, P.F., Stoker, M.S., Duddy, I.R., Sandiford, M., and Tassone, D.R., 2014, Cenozoic deformation in the Otway Basin, southern Australian margin: Implications for the origin and nature of post-breakup compression at rifted margins: Basin Research, v. 26, no. 1, p. 10–37, doi: 10.1111/bre.12035.

Holm, P.M., Gill, R.C.O., Pedersen, A.K., Larsen, J.G., Hald, N., Nielsen, T.F.D., and Thirlwall, M.F., 1993, The Tertiary picrites of West Greenland: contributions from “Icelandic” and other sources: Earth and Planetary Science Letters, v. 115, no. 1–4, p. 227–244, doi: 10.1016/0012-821X(93)90224-W.

Hopper, J.R., Funck, T., Tucholke, B.E., Larsen, H.C., Holbrook, W.S., Louden, K.E., Shillington, D., and Lau, H., 2004, Continental break-up and the onset of ultraslow seafloor spreading off Flemish Cap on the Newfoundland rifted margin: Geology, v. 32, no. 1, p. 93–96, doi: 10.1130/G19694.1.

Houseman, G., and England, P., 1993, Crustal thickening versus lateral expulsion in the Indian-Asian continental collision: Journal of Geophysical Research: Solid Earth, v. 98, no. B7, p. 12233–12249, doi: 10.1029/93JB00443.

Houseman, G., and Molnar, P., 2001, Mechanisms of lithospheric rejuvenation associated with continental orogeny: Geological Society, London, Special Publications, v. 184, p. 13–38, doi: 10.1144/GSL.SP.2001.184.01.02.

Huismans, R.S., and Beaumont, C., 2002, Asymmetric lithospheric extension: The role of frictional plastic strain softening inferred from numerical experiments: Geology, v. 30, no. 3, p. 211–214, doi: 10.1130/0091-7613(2002)030<0211:ALETRO>2.0.CO.

Huismans, R., and Beaumont, C., 2011, Depth-dependent extension, two-stage breakup and cratonic underplating at rifted margins.: Nature, v. 473, no. 7345, p. 74–78, doi: 10.1038/nature09988.

Huismans, R.S., Podladchikov, Y.Y., and Cloetingh, S., 2001, Transition from passive to active rifting: Relative importance of asthenospheric doming and passive extension of the lithosphere.: Journal of Geophysical Research, v. 106, no. B6, p. 11,271-11291.

van Hunen, J., and Čadek, O., 2009, Reduced oceanic seismic anisotropy by small-scale convection: Earth and Planetary Science Letters, v. 284, no. 3–4, p. 622–629, doi: 10.1016/j.epsl.2009.05.034.

Hurter, S.J., and Pollack, H.N., 1995, Effect of the Cretaceous Serra Geral igneous event on the temperatures and heat flow of the Paraná Basin, southern Brazil: Basin Research, v. 7, p. 215–220.

Hutton, D.H.W., 1988, Granite emplacement mechanisms and tectonic controls: inferences from deformation studies: Transactions of the Royal Society of Edinburgh: Earth Sciences, v. 79, no. 2–3, p. 245–255, doi: 10.1017/S0263593300014255.

Hutton, D.H.W., 2009, Insights into magmatism in volcanic margins: bridge structures and a new mechanism of basic sill emplacement - Theron Mountains, Antarctica: Petroleum Geoscience, v. 15, no. 3, p. 269–278, doi: 10.1144/1354-079309-841.

Jackson, J.A., 1980, Reactivation of basement faults and crustal shortening in orogenic belts: Nature, v. 283, no. 5745, p. 343–346, doi: doi:10.1038/283343a0.

Jakobsson, M., Cherkis, N., Woodward, J., Macnab, R., and Coakley, B., 2000, New grid of Arctic bathymetry aids scientists and mapmakers: Eos, Transactions American Geophysical Union, v. 81, no. 9, p. 89, doi: 10.1029/00EO00059.

Japsen, P., Bonow, J.M., Peulvast, J.-P., and Wilson, R.W., 2006, Uplift, erosion and fault reactivation in southern West Greenland.: GEUS Field Reports, v. 63.

Japsen, P., Green, P.F., Bonow, J.M., Rasmussen, E.S., and Chalmers, J. a, 2010, Episodic uplift and exhumation along North Atlantic passive margins : implications for hydrocarbon prospectivity Pre-Quaternary Geology: Petroleum Geology: From Mature Basins to New Frontiers - Proceedings of the 7th Petroleum Geology conference, v. 7, p. 979–1004, doi: 10.1144/0070979.

Jauer, C.D., and Budkewitsch, P., 2010, Old marine seismic and new satellite radar data: Petroleum exploration of north west Labrador Sea, Canada: Marine and Petroleum Geology, v. 27, no. 7, p. 1379–1394, doi: 10.1016/j.marpetgeo.2010.03.003.

Jauer, C.D., Oakey, G.N., Williams, G., and Wielens, J.B.W.H., 2014, Saglek Basin in the Labrador Sea, east coast Canada; stratigraphy, structure and petroleum systems: Bulletin of Canadian Petroleum Geology, v. 62, no. 4.

Jegen, M.D., Hobbs, R.W., Tarits, P., and Chave, A., 2009, Joint inversion of marine magnetotelluric and gravity data incorporating seismic constraints. Preliminary results

of sub-basalt imaging off the Faroe Shelf: Earth and Planetary Science Letters, v. 282, no. 1–4, p. 47–55, doi: 10.1016/j.epsl.2009.02.018.

Karner, G.D., and Shillington, D.J., 2005, Basalt sills of the U reflector, Newfoundland basin: A serendipitous dating technique: Geology, v. 33, no. 12, p. 985–988, doi: 10.1130/G21971.1.

Kearey, P., and Brooks, M., 1991, An introduction to Geophysical Exploration: Blackwell Science Ltd, Oxford.

Kearey, P., Klepeis, K., and Vine, F., 2009, Global Tctonics: Wiley-Blackwell.

Keen, C.E., 1979, Thermal history and subsidence of rifted continental margins — evidence from wells on the Nova Scotia and Labrador shelves: Canadian Journal of Earth Sciences, v. 16, no. 3, p. 505–522, doi: 10.1139/e79-046.

Keen, C.E., Dickie, K., and Dehler, S.A., 2012, The volcanic margins of the northern Labrador Sea: Insights to the rifting process: Tectonics, v. 31, no. 1, p. 1–13, doi: 10.1029/2011TC002985.

Keen, C.E., Potter, P., and Srivastava, S.P., 1994, Deep seismic reflection data across the conjugate margins of the Labrador Sea: Canadian Journal Earth Sciences, v. 31, no. 1, p. 192–205, doi: 10.1139/e94-016.

Kerr, J.W., 1967, A submerged continental remnant beneath the Labrador Sea: Earth and Planetary Science Letters, v. 2, no. 4, p. 283–289, doi: http://dx.doi.org/10.1016/0012-821X(67)90143-4.

Kerr, A., Hall, J., Wardle, R.J., Gower, C.F., and Ryan, B., 1997, New reflections on the structure and evolution of the Makkovikian - Ketilidian Orogen in Labrador and southern Greenland: Tectonics, v. 16, no. 6, p. 942–965, doi: 10.1029/97TC02286.

Kerr, A., Ryan, B., Gower, C.F., and Wardle, R.J., 1996, The Makkovik Province: extension of the Ketilidian Mobile Belt in mainland North America: Geological Society, London, Special Publications, v. 112, no. 1, p. 155–177, doi: 10.1144/GSL.SP.1996.112.01.09.

Ketchum, J.W.F., Culshaw, N.G., and Barr, S.M., 2002, Anatomy and orogenic history of a Paleoproterozoic accretionary belt: the Makkovik Province, Labrador, Canada: Canadian Journal of Earth Sciences, v. 39, no. 5, p. 711–730, doi: 10.1139/e01-099.

King, A.F., and McMillan, N.J., 1975, A Mid-Mesozoic Breccia from the Coast of Labrador: Canadian Journal of Earth Sciences, v. 12, no. 1, p. 44–51, doi: 10.1139/e75-005.

Kolb, J., 2014, Structure of the Palaeoproterozoic Nagssugtoqidian Orogen, South-East Greenland: Model for the tectonic evolution: Precambrian Research, v. 255, no. P3, p. 809–822, doi: 10.1016/j.precamres.2013.12.015.

Koning, T., 2003, Oil and gas production from basement reservoirs: examples from Indonesia, USA and Venezuela: Geological Society, London, Special Publications, v. 214, no. 1, p. 83–92, doi: 10.1144/GSL.SP.2003.214.01.05.

Korme, T., Acocella, V., and Abebe, B., 2004, The Role of Pre-existing Structures in the

Origin, Propagation and Architecture of Faults in the Main Ethiopian Rift: Gondwana Research, v. 7, no. 2, p. 467–479, doi: 10.1016/S1342-937X(05)70798-X.

Korstgård, J., Ryan, B., and Wardle, R., 1987, The boundary between Proterozoic and Archaean crustal blocks in central West Greenland and northern Labrador: Geological Society, London, Special Publications, v. 27, no. 1, p. 247–259, doi: 10.1144/gsl.sp.1987.027.01.21.

Krabbendam, M., 2001, When the Wilson Cycle breaks down: how orogens can produce strong lithosphere and inhibit their future reworking: Geological Society, London, Special Publications, v. 184, no. 1, p. 57–75, doi: 10.1144/GSL.SP.2001.184.01.04.

Kyrkjebø, R., Gabrielsen, R, H., and Faleide, J.I.I., 2004, Unconformities related to the Jurassic – Cretaceous synrift – post-rift transition of the northern North Sea: Journal of the Geological Society of London, v. 161, p. 1–17, doi: 10.1144/0016-764903-051.

LaFlamme, C., Sylvester, P.J., Hinchey, A.M., and Davis, W.J., 2013, U-Pb age and Hf-isotope geochemistry of zircon from felsic volcanic rocks of the Paleoproterozoic Aillik Group, Makkovik Province, Labrador: Precambrian Research, v. 224, p. 129–142, doi: 10.1016/j.precamres.2012.09.005.

Larsen, L.M., 2006, Mesozoic to Palaeogene dyke swarms in West Greenland and their significance for the formation of the Labrador Sea and the Davis Strait: Geological Survey of Denmark and Greenland, v. 34, p. 1–69.

Larsen, L.M., Heaman, L.M., Creaser, R. a., Duncan, R. a., Frei, R., and Hutchison, M., 2009, Tectonomagmatic events during stretching and basin formation in the Labrador Sea and the Davis Strait: evidence from age and composition of Mesozoic to Palaeogene dyke swarms in West Greenland: Journal of the Geological Society, v. 166, no. 6, p. 999–1012, doi: 10.1144/0016-76492009-038.

Larsen, L.M., Rex, D.C., Watt, W.S., and Guise, P.G., 1999, 40Ar–39Ar dating of alkali basaltic dykes along the south-west coast of Greenland: Cretaceous and Tertiary igneous activity along the eastern margin of the Labrador Sea.: Geology of Greenland Survey Bulletin, v. 184, p. 19–29.

Larsen, H.C., and Saunders, A.D., 1998, Tectonism and volcanism at the southest Greenland rifted margin: a record of plume impact and later continental rupture: Proceedings of the Ocean Drilling Program, Scientific Results, v. 152, doi: 10.2973/odp.proc.sr.152.1998.

Latin, D., and White, N., 1990, Generating melt during lithospheric extension: Pure shear vs. simple shear: Geology, v. 18, no. 4, p. 327–331, doi: 10.1130/0091-7613(1990)018<0327:GMDLEP>2.3.CO;2.

Lavier, L.L., and Manatschal, G., 2006, A mechanism to thin the continental lithosphere at magma-poor margins.: Nature, v. 440, no. 7082, p. 324–328, doi: 10.1038/nature04608.

Lawver, L.A., Grantz, A., and Gahagan, L.M., 2002, Plate kinematic evolution of the present Arctic region since the Ordovician: GSA Special Paper, v. 360, p. 333–358, doi: 10.1130/0-8137-2360-4.333.

Lawver, L.A., and Müller, R.D., 1994, Iceland hotspot track: Geology, v. 22, no. 4, p. 311–314, doi: 10.1130/0091-7613(1994)022<0311:IHT>2.3.CO;2.

Leat, P.T., Thompson, R.N., Morrison, M.A., Hendry, G.L., and Dickin, A.P., 1990, Geochemistry of mafic lavas in the early Rio Grande Rift, Yarmony Mountain, Colorado, U.S.A.: Chemical Geology, v. 81, no. 1–2, p. 23–43, doi: 10.1016/0009-2541(90)90037-8.

Lee, G.H., Kwon, Y.I., Yoon, C.S., Kim, H.J., and Yoo, H.S., 2006, Igneous complexes in the eastern Northern South Yellow Sea Basin and their implications for hydrocarbon systems: Marine and Petroleum Geology, v. 23, no. 6, p. 631–645, doi: 10.1016/j.marpetgeo.2006.06.001.

Li, L., Clift, P.D., Stephenson, R., and Nguyen, H.T., 2014, Non-uniform hyper-extension in advance of seafloor spreading on the vietnam continental margin and the SW South China Sea: Basin Research, v. 26, no. 1, p. 106–134, doi: 10.1111/bre.12045.

Lister, G.S., Etheridge, M.A., and Symonds, P.A., 1986, Detachment Faulting and the Evolution of Passive Continental Margins - Reply: Geology, v. 14, no. 10, p. 891–892.

Lister, G.S., Etheridge, M.A., and Symonds, P.A., 1991, Detachment models for the formation of passive continental margins: Tectonics, v. 10, no. 5, p. 1038–1064, doi: 10.1029/90TC01007.

Lister, G.S., Forster, M.A., and Rawling, T.J., 2001, Episodicity during orogenesis: Continental Reactivation and Reworking, v. 184, no. 1, p. 89–113, doi: 10.1144/GSL.SP.2001.184.01.06.

Lonergan, L., Jamin, N.H., Jackson, C.A.L., and Johnson, H.D., 2013, U-shaped slope gully systems and sediment waves on the passive margin of Gabon (west africa): Marine Geology, v. 337, no. August 2016, p. 80–97, doi: 10.1016/j.margeo.2013.02.001.

Lonergan, L., and White, N., 1999, Three-dimensional seismic imaging of a dymanic Earth: Philosophical Transactions of the Royal Society A: Mathematical, Physical and Engineering Sciences, v. 357, no. 1763, p. 3359–3375, doi: 10.1098/rsta.1999.0498.

Lundin, E., 2002, North Atlantic – Arctic : Overview of sea-floor spreading and rifting history, *in* Mid Norway plate reconstructions atlas with global and Atlantic perspectives, p. 41–75.

Lundin, E., and Doré, A., 2005, Fixity of the Iceland "hotspot" on the Mid-Atlantic Ridge: Observational evidence, mechanisms, and implications for Atlantic volcanic margins: Geological Society of America Special Papers, v. 2388, no. 36, p. 627–651, doi: 10.1130/2005.2388(36).

Macrae, E.J., Bond, C.E., Shipton, Z.K., and Lunn, R.J., 2016, Increasing the quality of seismic interpretation: Interpretation, v. 4, no. 3, p. T395–T402, doi: 10.1190/INT-2015-0218.1.

Magee, C., Jackson, C.A.-L., and Schofield, N., 2012, Characteristics and hydrocarbon trap potential of dome-shaped forced folds generated by igneous intrusions: PETEX,

London,.

Magee, C., Jackson, C.A.L., and Schofield, N., 2014, Diachronous sub-volcanic intrusion along deep-water margins: Insights from the Irish Rockall Basin: Basin Research, v. 26, no. 1, p. 85–105, doi: 10.1111/bre.12044.

Magee, C., Muirhead, J.D., Karvelas, A., Holford, S.P., Jackson, C.A.L., Bastow, I.D., Schofield, N., Stevenson, C.T.E., McLean, C., McCarthy, W., and Shtukert, O., 2016, Lateral magma flow in mafic sill complexes: Geosphere, v. 12, no. 3, p. GES01256.1, doi: 10.1130/GES01256.1.

Manatschal, G., 2004, New models for evolution of magma-poor rifted margins based on a review of data and concepts from West Iberia and the Alps: International Journal of Earth Sciences, v. 93, no. 3, p. 432–466, doi: 10.1007/s00531-004-0394-7.

Manatschal, G., Lavier, L., and Chenin, P., 2015, The role of inheritance in structuring hyperextended rift systems: Some considerations based on observations and numerical modeling: Gondwana Research, v. 27, no. 1, p. 140–164, doi: 10.1016/j.gr.2014.08.006.

Manatschal, G., Sauter, D., Karpoff, A.M., Masini, E., Mohn, G., and Lagabrielle, Y., 2011, The Chenaillet Ophiolite in the French/Italian Alps: An ancient analogue for an Oceanic Core Complex? Lithos, v. 124, no. 3–4, p. 169–184, doi: 10.1016/j.lithos.2010.10.017.

Manhica, A.D.S.T., Grantham, G.H., Armstrong, R.A., Guise, P.G., and Kruger, F.J., 2001, Polyphase deformation and metamorphism at the Kalahari Craton — Mozambique Belt boundary: Geological Society, London, Special Publications, v. 184, no. 1, p. 303–322, doi: 10.1144/GSL.SP.2001.184.01.15.

Mann, P., Gahagan, L., and Gordon, M.B., 2003, Tectonic Setting of the World's Giant Oil and Gas Fields: , no. January 2001, p. 15–28.

Maresh, J., White, R.S., Hobbs, R.W., and Smallwood, J.R., 2006, Seismic attenuation of Atlantic margin basalts: Observations and modeling: Geophysics, v. 71, no. 6, p. B211–B221, doi: 10.1190/1.2335875.

Marquart, G., 1991, Interpretations of geoid anomalies around the Iceland hotspot: Geophysical Journal International, v. 106, no. 1, p. 149–160, doi: 10.1111/j.1365-246X.1991.tb04608.x.

Martins, L.T., Madeira, J., Youbi, N., Munhá, J., Mata, J., and Kerrich, R., 2008, Rift-related magmatism of the Central Atlantic magmatic province in Algarve, Southern Portugal: Lithos, v. 101, no. 1–2, p. 102–124, doi: 10.1016/j.lithos.2007.07.010.

Mason, R.G., and Raff, A.D., 1961, Magnetic Survey Off the West Coast of North America, 32-Degrees-N, Latitude to 42-Degrees-N Latitude: Geological Society of America Bulletin, v. 72, no. 8, p. 1259–1265, doi: Doi 10.1130/0016-7606(1961)72[1259:Msotwc]2.0.Co;2.

Maus, S., Barckhausen, U., Berkenbosch, H., Bournas, N., Brozena, J., Childers, V., Dostaler, F., Fairhead, J.D., Finn, C., Von Frese, R.R.B., Gaina, C., Golynsky, S., Kucks, R., L??hr, H., et al., 2009, EMAG2: A 2-arc min resolution Earth Magnetic

Anomaly Grid compiled from satellite, airborne, and marine magnetic measurements: Geochemistry, Geophysics, Geosystems, v. 10, no. 8, doi: 10.1029/2009GC002471.

McCaffrey, K., 1997, Controls on reactivation of a major fault zone: the Fair Head-Clew Bay line in Ireland: Journal of the Geological Society, v. 154, no. 1, p. 129–133, doi: 10.1144/gsjgs.154.1.0129.

McClay, K.R., and White, M.J., 1995, Analogue modelling of orthogonal and oblique rifting: Marine and Petroleum Geology, v. 12, no. 2, p. 137–151, doi: 10.1016/0264-8172(95)92835-K.

McClusky, S., Reilinger, R., Ogubazghi, G., Amleson, A., Healeb, B., Vernant, P., Sholan, J., Fisseha, S., Asfaw, L., Bendick, R., and Kogan, L., 2010, Kinematics of the southern Red Sea-Afar Triple Junction and implications for plate dynamics: Geophysical Research Letters, v. 37, no. 5, p. 1–5, doi: 10.1029/2009GL041127.

McGregor, E.D., Nielsen, S.B., Stephenson, R.A., Clausen, O.R., Petersen, K.D., and Macdonald, D.I.M., 2012, Evolution of the west Greenland margin: offshore thermostratigraphic data and modelling: Journal of the Geological Society, v. 169, no. 5, p. 515–530, doi: 10.1144/0016-76492011-139.

McIntosh, K., Lavier, L., van Avendonk, H., Lester, R., Eakin, D., and Liu, C.S., 2014, Crustal structure and inferred rifting processes in the northeast South China Sea: Marine and Petroleum Geology, v. 58, no. PB, p. 612–626, doi: 10.1016/j.marpetgeo.2014.03.012.

McKenzie, D.P., 1970, Plate Tectonics of the Mediterranean Region: Nature, v. 226, no. 5242, p. 239–243, doi: 10.1038/226239a0.

McKenzie, D., 1978, Some remarks on the development of sedimentary basins: Earth and Planetary Science Letters, v. 40, no. 1, p. 25–32, doi: 10.1016/0012-821X(78)90071-7.

McKenzie, D.P., and Parker, R.L., 1967, The North Pacific: an Example of Tectonics on a Sphere: Nature, v. 216, no. 5122, p. 1276–1280, doi: 10.1038/2161276a0.

McKerrow, W.S., Mac Niocaill, C., and Dewey, J.F., 2000, The Caledonian Orogeny redefined: Journal of the Geological Society, v. 157, no. 6, p. 1149–1154, doi: 10.1144/jgs.157.6.1149.

McWhae, J.R.H., Elie, R., Laughton, K.C., and Gunther, P.R., 1980, Stratigraphy and Petroleum Prospects of the Labrador Shelf.: Bulletin of Canadian Petroleum Geology, v. 28, no. 4, p. 460–488.

Meeuws, F., Holford, S., Foden, J., and Schofield, N., 2016, Distribution, chronology and causes of Cretaceous – Cenozoic magmatism along the magma-poor rifted southern Australian margin: Links between mantle melting and basin formation: Marine and Petroleum Geology, v. 73, doi: 10.1016/j.marpetgeo.2016.03.003.

Melankholina, E.N., 2011, Passive margins of the North and Central Atlantic: A comparative study: Geotectonics, v. 45, no. 4, p. 291–301, doi: 10.1134/S0016852111040042.

Menzies, M.A., Klemperer, S.L., Ebinger, C.J., and Baker, J., 2002, Characteristics of

volcanic rifted margins: Geological Society of America Special Papers, v. 362, p. 1–14, doi: 10.1130/0-8137-2362-0.1.

Michael, A.J., 1984, Determination of stress from slip data: Faults and folds: Journal of Geophysical Research, v. 89, no. B13, p. 11517, doi: 10.1029/JB089iB13p11517.

Mjelde, R., Breivik, A.J., Raum, T., Mittelstaedt, E., Ito, G., and Faleide, J.I.I., 2008, Magmatic and tectonic evolution of the North Atlantic: Journal of the Geological Society, v. 165, no. Sigmundsson 2006, p. 31–42, doi: 10.1144/0016-76492007-018.

Mjelde, R., Kvarven, T., Faleide, J.I., and Thybo, H., 2015, Lower crustal high-velocity bodies along North Atlantic passive margins, and their link to Caledonian suture zone eclogites and Early Cenozoic magmatism: Tectonophysics, v. 670, p. 16–29, doi: 10.1016/j.tecto.2015.11.021.

Mora, C.A.S., and Huismans, R.S., 2016, Orogenic structural inheritance and rifted passive margin formation: Geophysical Research Abstracts, v. 18, p. 8908.

Morgan, W.J., 1971, Convection plumes in the lower mantle: Nature, v. 2310, p. 42–43.

Morley, C.K., 1995, Developments in the structural geology of rifts over the last decade and their impact on hydrocarbon exploration: Geological Society, London, Special Publications, v. 80, no. 1, p. 1–32, doi: 10.1144/GSL.SP.1995.080.01.01.

Morley, C.K., 1999, How successful are analogue models in addressing the influence of pre-existing fabrics on rift structure? Journal of Structural Geology, v. 21, no. 8–9, p. 1267–1274, doi: 10.1016/S0191-8141(99)00075-9.

Morley, C.K., Cunningham, S.M., Harper, R.M., and Wescott, W.A., 1992, Geology and Geophysics of the Rukwa Rift, East Africa: Tectonics, v. 11, no. 1, p. 69–81.

Morley, C.K., Haranya, C., Phoosongsee, W., Pongwapee, S., Kornsawan, A., and Wonganan, N., 2004, Activation of rift oblique and rift parallel pre-existing fabrics during extension and their effect on deformation style: Examples from the rifts of Thailand: Journal of Structural Geology, v. 26, no. 10, p. 1803–1829, doi: 10.1016/j.jsg.2004.02.014.

Müller, R.D., Gaina, C., Roest, W.R., and Hansen, D.L., 2001, A recipe for microcontinent formation: Geology, v. 29, no. 3, p. 203–206, doi: 10.1130/0091-7613(2001)029<0203:ARFMF>2.0.CO;2.

Müller, R.D., Sdrolias, M., Gaina, C., and Roest, W.R., 2008, Age, spreading rates, and spreading asymmetry of the world's ocean crust: Geochemistry, Geophysics, Geosystems, v. 9, no. 4, p. Q04006, doi: 10.1029/2007GC001743.

Mutter, J.C., 1985, Seaward dipping reflectors and the continent-ocean boundary at passive continental margins: Tectonophysics, v. 114, no. 1–4, p. 117–131, doi: 10.1016/0040-1951(85)90009-5.

Nielsen, S.B., Stephenson, R., and Thomsen, E., 2007, Dynamics of Mid-Palaeocene North Atlantic rifting linked with European intra-plate deformations.: Nature, v. 450, no. 7172, p. 1071–1074, doi: 10.1038/nature06379.

Nøhr-Hansen, H., 2003, Dinoflagellate cyst stratigraphy of the Palaeogene strata from the

Hellefisk-1, Ikermiut-1, Kangamiut-1, Nukik-1, Nukik-2 and Qulleq-1 wells, offshore West Greenland: Marine and Petroleum Geology, v. 20, no. 9, p. 987–1016, doi: 10.1016/S0264-8172(02)00116-2.

Nutman, A.P., and Collerson, K.D., 1991, Very early Archean crustal-accretion complexes preserved in the North Atlantic craton: Geology, v. 19, no. 8, p. 791–794, doi: 10.1130/0091-7613(1991)019<0791:VEACAC>2.3.CO;2.

Oakey, G.N., and Chalmers, J. a, 2012, A new model for the Paleogene motion of Greenland relative to North America : Plate reconstructions of the Davis Strait and Nares Strait regions between Canada and Greenland: Journal of Geophysical Research: Solid Earth, v. 117, no. B10, p. 1–28, doi: 10.1029/2011JB008942.

Ortelius, A., 1596, Thesaurus Geographicus.

Padovano, M., Piccardo, G.B., and Vissers, R.L.M., 2015, Tectonic and magmatic evolution of the mantle lithosphere during the rifting stages of a fossil slow – ultraslow spreading basin: insights from the Erro – Tobbio peridotite (Voltri Massif , NW Italy): Geological Society, London, Special Publications, v. 413, no. 2007, p. 205–238, doi: 10.1144/SP413.7.

Paech, H.J., 2001, Pervasive Pan-African reactivation of the Grenvillian crust and large igneous intrusions in central Dronning Maud Land, East Antarctica: Geological Society, London, Special Publications, v. 184, no. 1, p. 343–355, doi: 10.1144/GSL.SP.2001.184.01.17.

De Paola, N., Holdsworth, R.E., and McCaffrey, K.J.W., 2005, The influence of lithology and pre-existing structures on reservoir-scale faulting patterns in transtensional rift zones: Journal of the Geological Society, v. 162, p. 471–480, doi: 10.1144/0016-764904-043.

Parsons, E.C.M., Dolman, S.J., Jasny, M., Rose, N.A., Simmonds, M.P., and Wright, A.J., 2009, A critique of the UK's JNCC seismic survey guidelines for minimising acoustic disturbance to marine mammals: Best practise? Marine Pollution Bulletin, v. 58, no. 5, p. 643–651, doi: 10.1016/j.marpolbul.2009.02.024.

Parsons, E.C.M., Dolman, S.J., Wright, A.J., Rose, N.A., and Burns, W.C.G., 2008, Navy sonar and cetaceans: Just how much does the gun need to smoke before we act? Marine Pollution Bulletin, v. 56, no. 7, p. 1248–1257, doi: 10.1016/j.marpolbul.2008.04.025.

Peace, A., McCaffrey, K.J.W., Imber, J., Hobbs, R.W., van Hunen, J., Foulger, G., and Gerdes, K., 2014a, Formation of the West Greenland Volcanic Margin : Exploring alternatives to the plume hypothesis: 4th Atlantic Conjugate Margins Conference, , no. August 2014, p. 161–162, doi: 10.13140/RG.2.1.4727.1925.

Peace, A., McCaffrey, K., Imber, J., Hobbs, R., van Hunen, J., and Gerdes, K., 2014b, Formation of the Volcanic Margins of West Greenland and North-Eastern Canada: AAPG ACE Houston, doi: dx.doi.org/10.13140/RG.2.1.1545.1128.

Peace, A., McCaffrey, K., Imber, J., Hobbs, R., van Hunen, J., and Gerdes, K., 2015, Quantifying the influence of sill intrusion on the thermal evolution of organic-rich sedimentary rocks in nonvolcanic passive margins: An example from ODP 210-1276,

offshore Newfoundland, Canada: Basin Research, doi: 10.1111/bre.12131.

Peace, A., McCaffrey, K., Imber, J., Hunen, J. Van, and Hobbs, R., 2013, Modelling the role of magmatic intrusions in the post-breakup thermal evolution of Volcanic Passive Margins, *in* EGU General Assembly Conference Abstracts, p. 9439.

Peacock, D.C.P., and Sanderson, D.J., 1992, Effects of layering and anisotropy on fault geometry: Journal of the Geological Society, v. 149, no. 5, p. 793–802, doi: 10.1144/gsjgs.149.5.0793.

Peron-Pinvidic, G., 2016, What is actually "breakup"? Can we define a recipe of how to break the lithosphere? Arthur Holmes Meeting 2016: The Wilson cycle : Plate tectonics and structural inheritance during continental deformation,.

Peron-Pinvidic, G., Gernigon, L., Gaina, C., and Ball, P., 2012, Insights from the Jan Mayen system in the Norwegian-Greenland sea-I. Mapping of a microcontinent: Geophysical Journal International, v. 191, no. 2, p. 385–412, doi: 10.1111/j.1365-246X.2012.05639.x.

Peron-Pinvidic, G., Manatschal, G., Minshull, T.A., and Sawyer, D.S., 2007, Tectonosedimentary evolution of the deep Iberia-Newfoundland margins: Evidence for a complex breakup history: Tectonics, v. 26, no. 2, p. TC2011, doi: 10.1029/2006TC001970.

Peron-Pinvidic, G., Manatschal, G., and Osmundsen, P.T., 2013, Structural comparison of archetypal Atlantic rifted margins: A review of observations and concepts: Marine and Petroleum Geology, v. 43, p. 21–47, doi: dx.doi.org/10.1016/j.marpetgeo.2013.02.002.

Peron-Pinvidic, G., Shillington, D.J., and Tucholke, B.E., 2010, Characterization of sills associated with the U reflection on the Newfoundland margin: Evidence for widespread early post-rift magmatism on a magma-poor rifted margin: Geophysical Journal International, v. 182, no. 1, p. 113–136, doi: 10.1111/j.1365-246X.2010.04635.x.

Petford, N., and McCaffrey, K., 2003, Hydrocarbons in crystalline rocks: an introduction: Geological Society, London, Special Publications, v. 214, no. 1, p. NP-NP, doi: 10.1144/GSL.SP.2003.214.01.14.

Philippon, M., Willingshofer, E., Sokoutis, D., Corti, G., Sani, F., Bonini, M., and Cloetingh, S., 2015, Slip re-orientation in oblique rifts: Geology, v. 43, no. 2, p. 147–150, doi: 10.1130/G36208.1.

Piasecki, S., 2003, Neogene dinoflagellate cysts from Davis Strait, offshore West Greenland: Marine and Petroleum Geology, v. 20, no. 9, p. 1075–1088, doi: 10.1016/S0264-8172(02)00089-2.

Pichot, T., Delescluse, M., Chamot-Rooke, N., Pubellier, M., Qiu, Y., Meresse, F., Sun, G., Savva, D., Wong, K.P., Watremez, L., and Auxiètre, J.L., 2014, Deep crustal structure of the conjugate margins of the SW South China Sea from wide-angle refraction seismic data: Marine and Petroleum Geology, v. 58, no. PB, p. 627–643, doi: 10.1016/j.marpetgeo.2013.10.008.

Pierce, K.L., and Morgan, L.A., 2009, Is the track of the Yellowstone hotspot driven by a deep mantle plume? - Review of volcanism, faulting, and uplift in light of new data: Journal of Volcanology and Geothermal Research, v. 188, no. 1–3, p. 1–25, doi: 10.1016/j.jvolgeores.2009.07.009.

Polat, A., Wang, L., and Appel, P.W.U., 2014, A review of structural patterns and melting processes in the Archean craton of West Greenland: Evidence for crustal growth at convergent plate margins as opposed to non-uniformitarian models: Tectonophysics, v. 662, p. 67–94, doi: 10.1016/j.tecto.2015.04.006.

Polteau, S., Mazzini, A., Galland, O., Planke, S., and Malthe-Sørenssen, A., 2008, Saucer-shaped intrusions: Occurrences, emplacement and implications: Earth and Planetary Science Letters, v. 266, no. 1–2, p. 195–204, doi: 10.1016/j.epsl.2007.11.015.

Polyansky, O.P., Reverdatto, V. V., Khomenko, A. V., and Kuznetsova, E.N., 2003, Modeling of fluid flow and heat transfer induced by basaltic near-surface magmatism in the Lena-Tunguska petroleum basin (Eastern Siberia, Russia): Journal of Geochemical Exploration, v. 78–79, no. 0, p. 687–692, doi: 10.1016/S0375-6742(03)00079-7.

Pross, J., Pletsch, T., Shillington, D.J., Ligouis, B., Schellenberg, F., and Kus, J., 2007, Thermal alteration of terrestrial palynomorphs in mid-Cretaceous organic-rich mudstones intruded by an igneous sill (Newfoundland Margin, ODP Hole 1276A): International Journal of Coal Geology, v. 70, no. 4, p. 277–291, doi: 10.1016/j.coal.2006.06.005.

Pulvertaft, T.C.R., 1986, The development of thin thrust sheets and basement-cover sandwiches in the southern part of the Rinkian belt, Umanak district, West Greenland: Geological Survey of Greenland Report, v. 128, p. 75–87.

Ranero, C.R., and Pérez-Gussinyé, M., 2010, Sequential faulting explains the asymmetry and extension discrepancy of conjugate margins.: Nature, v. 468, no. 7321, p. 294–299, doi: 10.1038/nature09520.

Rasmussen, J.A., Nøhr-Hansen, H., and Sheldon, E., 2003, Palaeoecology and palaeoenvironments of the lower palaeogene succession, offshore West Greenland: Marine and Petroleum Geology, v. 20, no. 9, p. 1043–1073, doi: 10.1016/j.marpetgeo.2003.11.001.

Rateau, R., Schofield, N., and Smith, M., 2013, The potential role of igneous intrusions on hydrocarbon migration, West of Shetland: Petroleum Geoscience, v. 19, no. 3, p. 259–272, doi: 10.1144/petgeo2012-035.

Rattey, R.P., and Hayward, A.B., 1993, Sequence stratigraphy of a failed rift system: the Middle Jurassic to Early Cretaceous basin evolution of the Central and Northern North Sea: Petroleum Geology of Northwest Europe: Proceedings of the 4th Conference on Petroleum Geology of NW. Europe, at the Barbican Centre, London, v. 1, p. 215–249, doi: 10.1144/0040215.

Ravelo, A.C., Dekens, P.S., and McCarthy, M.D., 2006, Tectonic inheritance at a continental margin: GSA Today, v. 16, no. 3, p. 4–11, doi: 10.1130/1052-5173(2006)016<4.

Redmond, H.L., and King, S.D., 2004, A numerical study of a mantle plume beneath the Tharsis Rise: Reconciling dynamic uplift and lithospheric support models: Journal of Geophysical Research E: Planets, v. 109, no. 9, p. E09008, doi: 10.1029/2003JE002228.

Reid, I.D., and Keen, C.E., 1990, High seismic velocities associated with reflections from within the lower oceanic crust near the continental margin of eastern Canada: Earth and Planetary Science Letters, v. 99, no. 1–2, p. 118–126, doi: 10.1016/0012-821X(90)90075-9.

Rivers, T., 2008, Assembly and preservation of lower, mid, and upper orogenic crust in the Grenville Province-Implications for the evolution of large hot long-duration orogens: Precambrian Research, v. 167, no. 3–4, p. 237–259, doi: 10.1016/j.precamres.2008.08.005.

Rivers, T., 1997, Lithotectonic elements of the Grenville Province: review and tectonic implications: Precambrian Research, v. 86, no. 3–4, p. 117–154, doi: 10.1016/S0301-9268(97)00038-7.

Roberts, D., 2003, The Scandinavian Caledonides: Event chronology, palaeogeographic settings and likely modern analogues: Tectonophysics, v. 365, no. 1–4, p. 283–299, doi: 10.1016/S0040-1951(03)00026-X.

Roberts, D.G., Backman, J., Morton, A.C., Murray, J.W., and Keene, J.B., 1984, Evolution of volcanic rifted margins: synthesis of Leg 81 results on the west margin of Rockall Plateau: Initial reports of the deep sea drilling project, p. 883–923.

Roberts, E.A., and Houseman, G.A., 2001, Geodynamics of central Australia during the intraplate Alice Springs Orogeny: thin viscous sheet models: Geological Society, London, Special Publications, v. 184, no. 1, p. 139–164, doi: 10.1144/GSL.SP.2001.184.01.08.

Roberts, A.W., White, R.S., Lunnon, Z.C., Christie, P.A.F., Spitzer, R., and iSIMM Team, 2005, Imaging magmatic rocks on the Faroes margin: Petroleum Geology: North-West Europe and Global Perspectives—Proceedings of the 6th Petroleum Geology Conference, v. 6, p. 755–766, doi: 10.1144/0060755.

Rock, N.M.S., 1986, The nature and origin of ultramafic lamprophyres: Alnoites and allied rocks: Journal of Petrology, v. 27, no. 1, p. 155–196, doi: 10.1093/petrology/27.1.155.

Roest, W.R., and Srivastava, S.P., 1989, Sea-floor spreading in the Labrador Sea: a new reconstruction: Geology, v. 17, no. 11, p. 1000–1003, doi: 10.1130/0091-7613(1989)017<1000:SFSITL>2.3.CO;2.

Rogers, D.A., Marshall, J.E.A., and Astin, T.R., 1989, Short Paper: Devonian and later movements on the Great Glen fault system, Scotland: Journal of the Geological Society, v. 146, no. 3, p. 369–372, doi: 10.1144/gsjgs.146.3.0369.

Rohrman, M., 2007, Prospectivity of volcanic basins: Trap delineation and acreage de-risking: AAPG Bulletin, v. 91, no. 6, p. 915–939, doi: 10.1306/12150606017.

Rolle, F., 1985, Late Cretaceous – Tertiary sediments offshore central West Greenland: lithostratigraphy, sedimentary evolution, and petroleum potential: Canadian Journal

of Earth Sciences, v. 22, no. 7, p. 1001–1019, doi: 10.1139/e85-105.

Romm, J., 1994, A new forerunner for continental drift: Nature, v. 367, p. 407–408, doi: 10.1038/367407a0.

Rowan, M.G., 2014, Passive-margin salt basins: Hyperextension, evaporite deposition, and salt tectonics: Basin Research, v. 26, no. 1, p. 154–182, doi: 10.1111/bre.12043.

Ruppel, C., 1995, Extensional processes in continental lithosphere: Journal of Geophysical Research, v. 100, no. B12, p. 24187, doi: 10.1029/95JB02955.

Ryan, P.D., 2001, The role of deep basement during continent-continent collision: a review: Geological Society, London, Special Publications, v. 184, no. 1, p. 39–55, doi: 10.1144/GSL.SP.2001.184.01.03.

Sandwell, D., Anderson, D.L., and Wessel, P., 2005, Global tectonic maps: Geological Society of America Special Papers, v. 388, p. 1–10, doi: 10.1046/j.1365-246x.2001.00321.x.

Sandwell, D.T., Müller, R.D., Smith, W.H.F., Garcia, E., and Francis, R., 2014, New global marine gravity model from CryoSat-2 and Jason-1 reveals buried tectonic structure.: Science, v. 346, no. 6205, p. 65–7, doi: 10.1126/science.1258213.

Saunders, A.D., Storey, M., W., K.R., and Norry, M., 1992, Consequences of plume-lithosphere interactions: Geological Society, London, Special Publications, , no. 68, p. 41–60.

Sayers, J., Symonds, P. a., Direen, N.G., and Bernardel, G., 2001, Nature of the continent-ocean transition on the non-volcanic rifted margin of the central Great Australian Bight: Geological Society, London, Special Publications, v. 187, no. 1, p. 51–76, doi: 10.1144/GSL.SP.2001.187.01.04.

Schaefer, B.F., Parkinson, I.J., and Hawkesworth, C.J., 2000, Deep mantle plume osmium isotope signature from West Greenland Tertiary picrites: Earth and Planetary Science Letters, v. 175, no. 1–2, p. 105–118, doi: 10.1016/S0012-821X(99)00290-3.

Schenk, C.J., 2011, Chapter 41 Geology and petroleum potential of the West Greenland-East Canada Province: Arctic Petroleum Geology, v. 35, no. 1, p. 627–645, doi: 10.1144/M35.41.

Schiffer, C., Balling, N., Jacobsen, B.H., Stephenson, R.A., and Nielsen, S.B., 2014, Seismological evidence for a fossil subduction zone in the East Greenland Caledonides: Geology, v. 42, no. 4, p. 311–314, doi: 10.1130/G35244.1.

Schofield, N., Holford, S., Millett, J., Brown, D., Jolley, D., R. Passey, S., Muirhead, D., Grove, C., Magee, C., Murray, J., Hole, M., Jackson, C., and Stevenson, C., 2015, Regional magma plumbing and emplacement mechanisms of the Faroe-Shetland Sill Complex: Implications for magma transport and petroleum systems within sedimentary basins: Basin Research, p. 1–23, doi: 10.1111/bre.12164.

Schofield, N., and Jolley, D.W., 2013, Development of intra-basaltic lava-field drainage systems within the Faroe-Shetland Basin: Petroleum Geoscience, v. 19, no. 3, p. 273–288, doi: 10.1144/petgeo2012-061.

Schutter, S.R., 2003, Hydrocarbon occurrence and exploration in and around igneous rocks: Geological Society, London, Special Publications, v. 214, no. 1, p. 7–33, doi: 10.1144/gsl.sp.2003.214.01.02.

Sengör, A.M.C., and Burke, K., 1978, Relative timing of rifting and volcanism on Earth and its tectonic implications: Geophysical Research Letters, v. 5, no. 6, p. 419–421, doi: 10.1029/GL005i006p00419.

Seton, M., Müller, R.D., Zahirovic, S., Gaina, C., Torsvik, T., Shephard, G., Talsma, A., Gurnis, M., Turner, M., Maus, S., and Chandler, M., 2012, Global continental and ocean basin reconstructions since 200Ma: Earth-Science Reviews, v. 113, no. 3–4, p. 212–270, doi: 10.1016/j.earscirev.2012.03.002.

Shallaly, N.A., Beier, C., Haase, K.M., and Hammed, M.S., 2013, Petrology and geochemistry of the Tertiary Suez rift volcanism, Sinai, Egypt: Journal of Volcanology and Geothermal Research, v. 267, p. 119–137, doi: 10.1016/j.jvolgeores.2013.10.005.

Shillington, D.J., Holbrook, W.S., Tucholke, B.E., Hopper, J.R., Louden, K.E., Larsen, H.C., Van Avendonk, H.J.A., Deemer, S., and Hall, J., 2004, Data report: Marine geophysical data on the Newfoundland nonvolcanic rifted margin around SCREECH transect 2: Proceedings of the Ocean Drilling Program, Initial Reports Volume 210, v. 210, p. 1–36.

Shipboard Scientific Party, 1987, Site 646: Initial Reports., 105: College Station, TX (Ocean Drilling Program), doi: doi:10.2973/odp.proc.ir.105.104.1987.

Sibuet, J.-C., Srivastava, S.P., Enachescu, M., and Karner, G.D., 2007, Early Cretaceous motion of Flemish Cap with respect to North America: implications on the formation of Orphan Basin and SE Flemish Cap Galicia Bank conjugate margins: Geological Society, London, Special Publications, v. 282, no. 1, p. 63–76, doi: 10.1144/SP282.4.

Simon, K., Huismans, R.S., and Beaumont, C., 2009, Dynamical modelling of lithospheric extension and small-scale convection: Implications for magmatism during the formation of volcanic rifted margins: Geophysical Journal International, v. 176, no. 1, p. 327–350, doi: 10.1111/j.1365-246X.2008.03891.x.

Skogseid, J., 2001, Volcanic margins: Geodynamic and exploration aspects: Marine and Petroleum Geology, v. 18, no. 4, p. 457–461, doi: 10.1016/S0264-8172(00)00070-2.

Sleep, N.H., Ebinger, C.J., and Kendall, J.-M., 2002, Deflection of mantle plume material by cratonic keels: Geological Society, London, Special Publications, v. 199, no. 1, p. 135–150, doi: 10.1144/GSL.SP.2002.199.01.08.

Smith, W.H., and Sandwell, D., 1997, Global Sea Floor Topography from Satellite Altimetry and Ship Depth Soundings: Science, v. 277, no. 5334, p. 1956–1962, doi: 10.1126/science.277.5334.1956.

Sørensen, A.B., 2006, Stratigraphy, structure and petroleum potential of the Lady Franklin and Maniitsoq Basins, offshore southern West Greenland: Petroleum Geoscience, v. 12, no. 3, p. 221–234, doi: 10.1144/1354-079305-692.

Spear, F.S., and Peacock, S.M., 1989, Metamorphic Pressure Temperature Time Paths (F.

S. Spear & S. M. Peacock, Eds.): American Geophysical Union, Washington, DC.

Spencer, A.M., Embry, A.F., Gautier, D.L., Stoupakova, A. V., and Sorensen, K., 2011, Chapter 1 An overview of the petroleum geology of the Arctic: Geological Society, London, Memoirs, v. 35, no. 1, p. 1–15, doi: 10.1144/M35.1.

Srivastava, S.P., 1978, Evolution of the Labrador Sea and its bearing on the early evolution of the North Atlantic: Geophysical Journal International, v. 52, no. 2, p. 313–357, doi: 10.1111/j.1365-246X.1978.tb04235.x.

Srivastava, S.P., and Keen, C.E., 1995, A deep seismic reflection profile across the extinct Mid-Labrador Sea spreading center: Tectonics, v. 14, no. 2, p. 372–389, doi: 10.1029/94TC02453.

Srivastava, S.P., and Roest, W.R., 1999, Extent of oceanic crust in the Labrador Sea: Marine and Petroleum Geology, v. 16, no. 1, p. 65–84, doi: 10.1016/S0264-8172(98)00041-5.

Srivastava, S.P., and Tapscott, C.R., 1986, Plate Kinematics of the North Atlantic, *in* The Western North Atlantic Region: The Geology of North America, Geological Society of America, p. 379–404.

Stab, M., Bellahsen, N., Pik, R., Quidelleur, X., Ayalew, D., and Leroy, S., 2015, Modes of rifting in magma-rich settings: Tectono-magmatic evolution of Central Afar: Tectonics, p. 2–38, doi: 10.1002/2015TC003893.Received.

Starkey, N.A., Stuart, F.M., Ellam, R.M., Fitton, J.G., Basu, S., and Larsen, L.M., 2009, Helium isotopes in early Iceland plume picrites: Constraints on the composition of high 3He/4He mantle: Earth and Planetary Science Letters, v. 277, no. 1–2, p. 91–100, doi: 10.1016/j.epsl.2008.10.007.

Steckler, M.S., Berthelot, F., Lyberis, N., and Le Pichon, X., 1988, Subsidence in the gulf of suez: implications for rifting and plate kinematics: Tectonophysics, v. 153, no. 1–4, p. 249–270, doi: 10.1016/0040-1951(88)90019-4.

Steckler, M.S., and ten Brink, U.S., 1986, Lithospheric strength variations as a control on new plate boundaries: examples from the northern Red Sea region: Earth and Planetary Science Letters, v. 79, p. 120–132.

St-Onge, M.R., Van Gool, J.A.M., Garde, A.A., and Scott, D.J., 2009, Correlation of Archaean and Palaeoproterozoic units between northeastern Canada and western Greenland: constraining the pre-collisional upper plate accretionary history of the Trans-Hudson orogen: Geological Society, London, Special Publications, v. 318, no. 1, p. 193–235, doi: 10.1144/sp318.7.

Storey, M., Duncan, R.A., Pedersen, A.K., Larsen, L.M., and Larsen, H.C., 1998, 40Ar/39Ar geochronology of the West Greenland Tertiary volcanic province: Earth and Planetary Science Letters, v. 160, no. 3–4, p. 569–586, doi: 10.1016/S0012-821X(98)00112-5.

Suckro, S.K., Gohl, K., Funck, T., Heyde, I., Ehrhardt, A., Schreckenberger, B., Gerlings, J., Damm, V., and Jokat, W., 2012, The crustal structure of southern Baffin Bay: Implications from a seismic refraction experiment: Geophysical Journal International,

v. 190, no. 1, p. 37–58, doi: 10.1111/j.1365-246X.2012.05477.x.

Suckro, S.K., Gohl, K., Funck, T., Heyde, I., Schreckenberger, B., Gerlings, J., and Damm, V., 2013, The Davis Strait crust-a transform margin between two oceanic basins: Geophysical Journal International, v. 193, no. 1, p. 78–97, doi: 10.1093/gji/ggs126.

Sutton, J., and Watson, J. V, 1986, Architecture of the Continental Lithosphere Author: Philosphical transactions of the Royal Society of London, v. 317, p. 5–12.

Sweeney, J.J., and Burnham, A.K., 1990, Evaluation of a Simple Model of Vitrinite Reflectance Baced on Chemical Kinetics: American Association of Petroleum Geologists Bulletin, v. 74, no. 10, p. 1559–1570.

Talwani, M., and Eldholm, O., 1977, Evolution of the Norwegian-Greenland Sea: Bulletin of the Geological Society of America, v. 88, no. 7, p. 969–999, doi: 10.1130/0016-7606(1977)88<969:EOTNS>2.0.CO;2.

Tappe, S., Foley, S.F., Jenner, G.A., Heaman, L.M., Kjarsgaard, B.A., Romer, R.L., Stracke, A., Joyce, N., and Hoefs, J., 2006, Genesis of ultramafic lamprophyres and carbonatites at Aillik Bay, Labrador: A consequence of incipient lithospheric thinning beneath the North Atlantic Craton: Journal of Petrology, v. 47, no. 7, p. 1261–1315, doi: 10.1093/petrology/egl008.

Tappe, S., Foley, S.F., Stracke, A., Romer, R.L., Kjarsgaard, B.A., Heaman, L.M., and Joyce, N., 2007, Craton reactivation on the Labrador Sea margins: 40Ar/39Ar age and Sr-Nd-Hf-Pb isotope constraints from alkaline and carbonatite intrusives: Earth and Planetary Science Letters, v. 256, no. 3–4, p. 433–454, doi: 10.1016/j.epsl.2007.01.036.

Tate, M.P., 1993, Structural framework and tectono-stratigraphic evolution of the Porcupine Seabight Basin, offshore Western Ireland: Marine and Petroleum Geology, v. 10, no. 2, p. 95–123, doi: 10.1016/0264-8172(93)90016-L.

Taylor, F.B., 1910, Bearing of the tertiary mountain belt on the origin of the earth's plan: Bulletin of the Geological Society of America, v. 21, no. 4, p. 179–226.

Thomson, K., 2007, Comment on "The three-dimensional geometry and growth of forced folds above saucer-shaped igneous sills" by Hansen and Cartwright: Journal of Structural Geology, v. 29, no. 4, p. 736–740, doi: 10.1016/j.jsg.2006.10.009.

Thomson, K., 2005, Extrusive and intrusive magmatism in the North Rockall Trough: Petroleum Geology Conference series, v. 6, p. 1621–1630, doi: 10.1144/0061621.

Torske, T., and Prestvik, T., 1991, Mesozoic detachment faulting between Greenland and Norway: inferences from Jan Mayen fracture zone system and associated alkalic volcanic rocks: Geology, v. 19, no. 5, p. 481–484, doi: 10.1130/0091-7613(1991)019<0481:MDFBGA>2.3.CO;2.

Torsvik, T.H., Van Der Voo, R., Meert, J.G., Mosar, J., and Walderhaug, H.J., 2001, Reconstructions of the continents around the North Atlantic at about the 60th parallel: Earth and Planetary Science Letters, v. 187, no. 1–2, p. 55–69, doi: 10.1016/S0012-821X(01)00284-9.

Tucholke, B.E., Sawyer, D.S., and Sibuet, J.-C., 2007a, Breakup of the Newfoundland

Iberia rift: Geological Society, London, Special Publications, v. 282, no. 1, p. 9–46, doi: 10.1144/SP282.2.

Tucholke, B.E., Sibuet, J.-C., and Klaus, A., 2004a, Leg 210 summary: Proceedings of the Ocean Drilling Program, Initial reports, v. 210, p. 1–78, doi: 10.2973/odp.proc.ir.210.2004.

Tucholke, B.E., Sibuet, J., and Klaus, 2007b, Leg 210 synthesis: tectonic, magmatic, and sedimentary evolution of the Newfoundland-Iberia rift: Proceedings of the Ocean Drilling Program, Scientific Results Volume 210, v. 210, p. 1–56, doi: 10.2973/odp.proc.sr.210.101.2007.

Tucholke, B.E., Sibuet, J.-C., and Klaus, A., 2004b, Site 1276: Proceedings of the Ocean Drilling Program, Initial reports, v. 210, p. 1–358.

Umpleby, D.C., 1979, Geology of the Labrador Shelf: Geological Survey of Canada, v. 79–13.

Upton, B.G.J., 1988, History of Tertiary igneous activity in the N Atlantic borderlands: Geological Society, London, Special Publications, v. 39, no. 1, p. 429–453, doi: 10.1144/GSL.SP.1988.039.01.38.

Vail, P.R., and Mitchum, R.M., 1977, Seismic Stratigraphy and Global Changes of Sea Level , Part 1 : AAPG Memoir 26, v. 26, p. 51–52.

Valentine, G.A., and Krogh, K.E.C., 2006, Emplacement of shallow dikes and sills beneath a small basaltic volcanic center - The role of pre-existing structure (Paiute Ridge, southern Nevada, USA): Earth and Planetary Science Letters, v. 246, no. 3–4, p. 217–230, doi: 10.1016/j.epsl.2006.04.031.

Vauchez, A., Barruol, G., and Tommasi, A., 1997, Why do continents break-up parallel to ancient orogenic belts? Terra Nova, v. 9, no. 2, p. 62–66, doi: 10.1111/j.1365-3121.1997.tb00003.x.

Wallace, R.E., 1984, Patterns and Timing of Late Quaternary Faulting in the Great Basin Province and Relation to Some Regional Tectonic Feature: Journal of Geophysical Research, v. 89, no. B7, p. 5763–5769.

Wang, K., Lu, X., Chen, M., Ma, Y., Liu, K., Liu, L., Li, X., and Hu, W., 2012, Numerical modelling of the hydrocarbon generation of Tertiary source rocks intruded by doleritic sills in the Zhanhua depression, Bohai Bay Basin, China: Basin Research, v. 24, no. 2, p. 234–247, doi: 10.1111/j.1365-2117.2011.00518.x.

Wang, D., Lu, X., Song, Y., Shao, R., and Qi, T., 2010, Influence of the temperature dependence of thermal parameters of heat conduction models on the reconstruction of thermal history of igneous-intrusion-bearing basins: Computers and Geosciences, v. 36, no. 10, p. 1339–1344, doi: 10.1016/j.cageo.2010.03.014.

Wang, D., Lu, X., Zhang, X., Xu, S., Hu, W., and Wang, L., 2007, Heat-model analysis of wall rocks below a diabase sill in Huimin Sag, China compared with thermal alteration of mudstone to carbargilite and hornfels and with increase of vitrinite reflectance: Geophysical Research Letters, v. 34, no. 16, p. L16312, doi: 10.1029/2007GL030314.

Wardle, R.J., Gower, C.F., James, D.T., St-Onge, M.R., Scott, D.J., Garde, A. a, Culshaw, N.G., van Gool, J.A., Connelly, J.N., Perreault, S., and Hall, J., 2002, Correlation chart of the Proterozoic assembly of the northeastern Canadian - Greenland Shield: Canadian Journal of Earth Sciences, v. 39, no. 5, p. 895, doi: 10.1139/e01-088.

Watts, A.B., and Steckler, M.S., 1978, Subsidence and Eustacy at the continental margin of Eastern North America: American Geophysical Union, Maurice Ewing Series, v. 3, doi: DOI: 10.1029/ME003p0218.

Wegener, A., 1912, Die Entstehung der Kontinente: Geologische Rundschau, v. 3, no. 4, p. 276–292, doi: 10.1007/BF02202896.

Welford, J.K., and Hall, J., 2007, Crustal structure of the Newfoundland rifted continental margin from constrained 3-D gravity inversion: Geophysical Journal International, v. 171, no. 2, p. 890–908, doi: 10.1111/j.1365-246X.2007.03549.x.

Welford, J.K., and Hall, J., 2013, Lithospheric structure of the Labrador Sea from constrained 3-D gravity inversion: Geophysical Journal International, v. 195, no. 2, p. 767–784, doi: 10.1093/gji/ggt296.

Wernicke, B., 1981, Low-angle normal faults in the Basin and Range Province: nappe tectonics in an extending orogen: Nature, v. 291, no. 5817, p. 645–648, doi: 10.1038/291645a0.

Wernicke, B., 1985, Uniform-sense normal simple shear of the continental lithosphere: Canadian Journal of Earth Sciences, v. 22, no. 1, p. 108–125, doi: 10.1139/e85-009.

White, R.S., 1988, A hot-spot model for early Tertiary volcanism in the N Atlantic: Geological Society, London, Special Publications, v. 39, no. 1, p. 3–13, doi: 10.1144/GSL.SP.1988.039.01.02.

White, R.S., 1992, Magmatism during and after continental break-up: Geological Society, London, Special Publications, v. 68, no. 1, p. 1–16, doi: 10.1144/GSL.SP.1992.068.01.01.

White, R., and McKenzie, D., 1989, Magmatism at rift zones: The generation of volcanic continental margins and flood basalts: Journal of Geophysical Research, v. 94, no. B6, p. 7685, doi: 10.1029/JB094iB06p07685.

White, J.D.L., and Ross, P.S., 2011, Maar-diatreme volcanoes: A review: Journal of Volcanology and Geothermal Research, v. 201, no. 1–4, p. 1–29, doi: 10.1016/j.jvolgeores.2011.01.010.

White, N., Thompson, M., and Barwise, T., 2003, Understanding the thermal evolution of deep-water continental margins.: Nature, v. 426, no. 6964, p. 334–343, doi: 10.1038/nature02133.

Whitmarsh, R.B., Manatschal, G., and Minshull, T. a, 2001a, Evolution of magma-poor continental margins from rifting to seafloor spreading.: Nature, v. 413, no. 6852, p. 150–154, doi: 10.1038/35093085.

Whitmarsh, R.B., Minshull, T.A., Russell, S.M., Dean, S.M., Louden, K.E., and Chian, D., 2001b, The role of syn-rift magmatism in the rift-to-drift evolution of the West Iberia continental margin: geophysical observations: Geological Society, London, Special

Publications, v. 187, no. 1, p. 107–124, doi: 10.1144/GSL.SP.2001.187.01.06.

Whittaker, J.M., Goncharov, A., Williams, S.E., Müller, R.D., and Leitchenkov, G., 2013, Global sediment thickness data set updated for the Australian-Antarctic Southern Ocean: Geochemistry, Geophysics, Geosystems, v. 14, no. 8, p. 3297–3305, doi: 10.1002/ggge.20181.

Williams, G.D., 1993, Tectonics and seismic sequence stratigraphy: Journal of the Geological Society, v. 148, no. 5, p. 935–937, doi: 10.1144/gsjgs.148.5.0935.

Wilson, T., 1966, Did the Atlantic close and the re-open? Nature, v. 209, p. 1246–1248.

Wilson, M., and Guiraud, R., 1992, Magmatism and rifting in Western and Central Africa, from Late Jurassic to Recent times: Tectonophysics, v. 213, no. 1–2, p. 203–225, doi: 10.1016/0040-1951(92)90259-9.

Wilson, R.W., Klint, K.E.S., Van Gool, J. a M., McCaffrey, K.J.W., Holdsworth, R.E., and Chalmers, J.A., 2006, Faults and fractures in central West Greenland: onshore expression of continental break-up and sea-floor spreading in the Labrador–Baffin Bay Sea: Geological Survey Of Denmark And Greenland Bulletin, v. 11, p. 185–204.

Wilson, R.C.L., Manatschal, G., and Wise, S., 2001a, Rifting along non-volcanic passive margins: stratigraphic and seismic evidence from the Mesozoic successions of the Alps and western Iberia: Geological Society, London, Special Publications, v. 187, no. 1, p. 429–452, doi: 10.1144/GSL.SP.2001.187.01.21.

Wilson, R.C.L., Whitmarsh, R.B., Taylor, B., and Froitzheim, N., 2001b, Introduction: the land and sea approach: Geological Society, London, Special Publications, v. 187, no. 1, p. 1–8, doi: 10.1144/GSL.SP.2001.187.01.01.

Wilton, D.H.C., Taylor, R.C., Sylvester, P.J., and Penney, G.T., 2002, A Review of Kimberlitic and Ultramafic Lamprophyre Intrusives From Northern Labrador: Current Research Newfoundland Department of Mines and Energy Geological Survey, v. 2–1, p. 343–352.

Woodcock, N.H., and Mort, K.M., 2008, Classification of fault breccias and related fault rocks: Geological Magazine Rapid Comminication, v. 145, p. 435–440, doi: 10.1017/S0016756808004883.

Woodcock, N., and Strachen, R., 2000, Chapter 12 The Caledonian Orogeny: a multiple plate collision, *in* Geological History of Britain and Ireland, Blackwell Publishing, p. 185–205.

Woolley, A.R., Bergman, S.C., Edgar, A.D., Le Bas, M.J., Mitchell, R.H., Rock, N.M.S., and Scott Smith, B.H., 1996, Classification of lamprophyres, lamproites, kimberlites, and the kalsilitic, melilitic, and leucitic rocks: Canadian Mineralogist, v. 34, no. 2, p. 175–186.

Wu, L., Trudgill, B.D., and Kluth, C.F., 2016, Salt diapir reactivation and normal faulting in an oblique extensional system, Vulcan Sub-basin, NW Australia: Journal of the Geological Society, v. 173, p. jgs2016-008, doi: 10.1144/jgs2016-008.

Zamani, B., Angelier, J., and Zamani, A., 2008, State of stress induced by plate convergence and stress partitioning in northeastern Iran, as indicated by focal

mechanisms of earthquakes: Journal of Geodynamics, v. 45, no. 2–3, p. 120–132, doi: 10.1016/j.jog.2007.07.003.

Ziegler, P.A., 1992, Geodynamics of rifting and implications for hydrocarbon habitat: Tectonophysics, v. 215, no. 1–2, p. 221–253, doi: 10.1016/0040-1951(92)90083-I.

Ziolkowski, A., Hanssen, P., Gatliff, R., Jakubowicz, H., Dobson, A., Hampson, G., Li, X.Y., and Liu, E., 2003, Use of low frequencies for sub-basalt imaging: Geophysical Prospecting, v. 51, no. 3, p. 169–182, doi: 10.1046/j.1365-2478.2003.00363.x.

Appendices

Appendix 1 Table of Contents

Supplementary materials for Chapter 4

1. Fieldwork Basemaps:
    i. Southern part of study area
    ii. Northern part of study area
2. Supplementary materials as available in 2016 Geosphere paper:
    i. Sample description tables
    ii. Description of sample locations and coordinate systems
    iii. Google Earth (.kmz) file containing sample locations (digital version only)
    iv. XRF and other datasets
3. XRF raw data tables
    i. Main data table
    ii. Loss on ignition (LOI) data
    iii. Standards

Appendix 1.1.1 Basemap used for fieldwork in south of study area

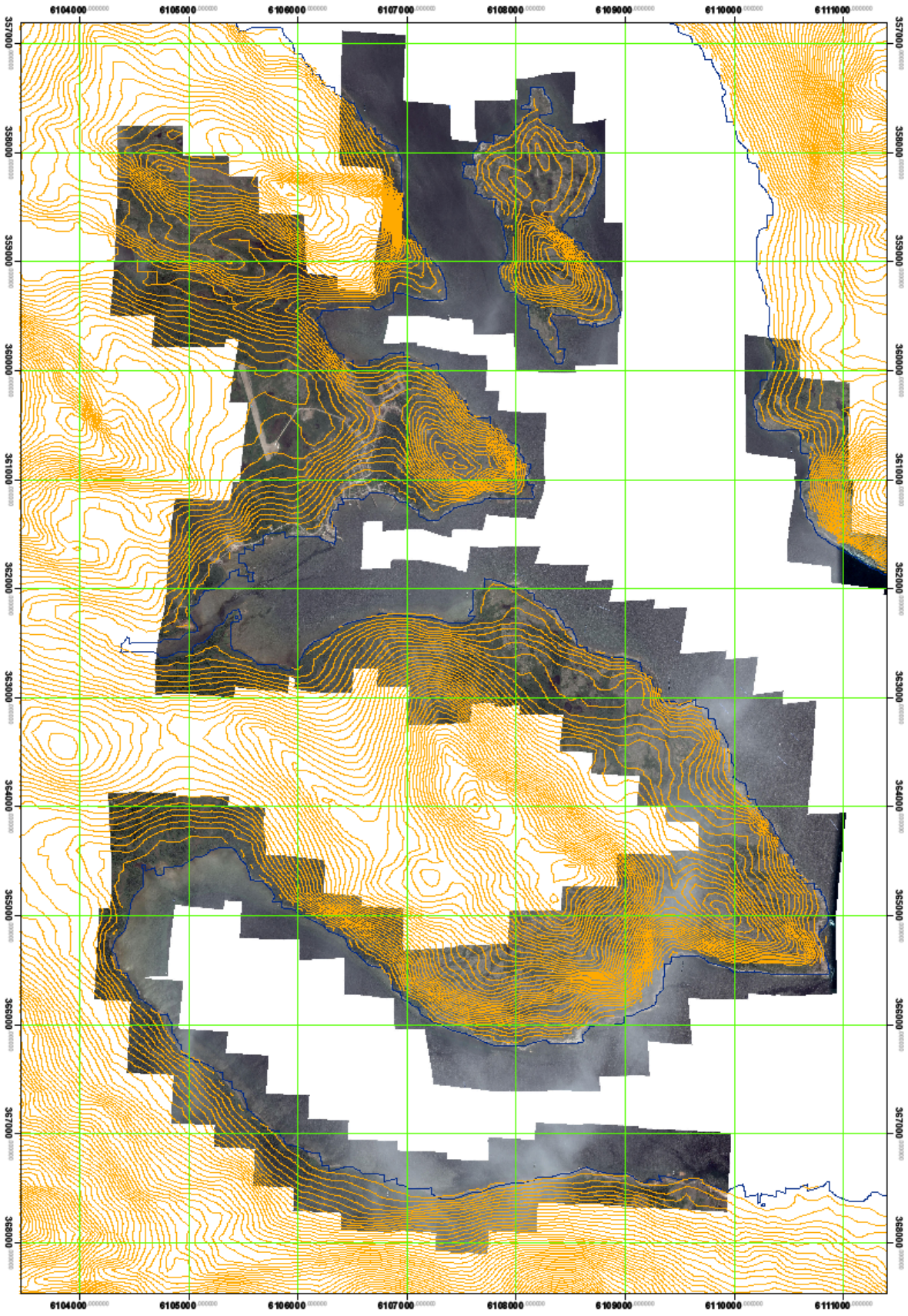

Appendix 1.1.2 Basemap used for fieldwork in north of study area

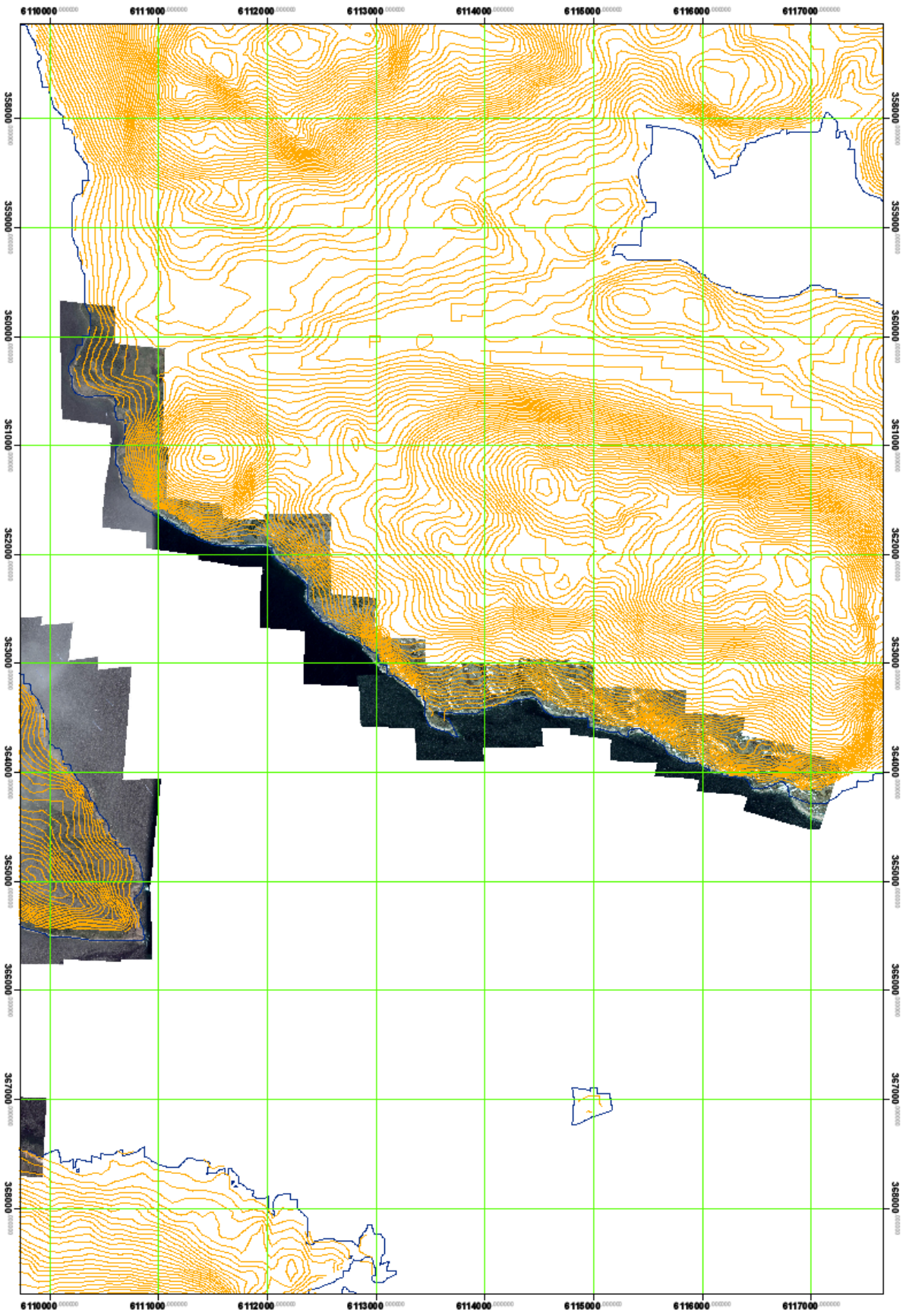

Appendix 1.2.1

Sample description tables (as in 2016 Geosphere Paper)

Sample Name	Location	Description of Outcrop/Sample	Mineralogy	Cross Polarised Light	Plane Polarised Light
AP1-S1 *(In proximity to Tappe et al., (2007) location ST241b)*	55.099270°N 59.183560°W *Dyke margin orientation* 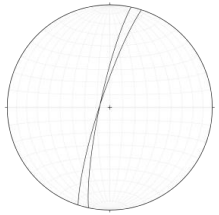	Good quality exposure on beach c.10 m from ST241b on the peninsula north of the town of Makkovik. Very fine grained groundmass. Abundant clinopyroxene, often arranged into star shaped clusters or two crystals which have intergrown. Highly altered olivine is present. Small apatite needles can be observed in the groundmass, along with small amphibole and biotite crystals. Opaque minerals are present in small quantities throughout the sample. Infilled vesicles up to 6mm wide (but usually around 2mm wide) containing predominantly calcite are abundant. Some vesicles are not entirely filled. There is no metamorphic mineral fabric.	Clinopyroxene – 60% Altered olivine – 15% Vesicles (calcite infill) – <5% Apatite – <5% Amphibole – <5% Biotite – <5% Opaque minerals – <5% *Interpretation and Rocktype* **Olivine Lamprophyre** - the intergrown clusters of clinopyroxene may indicate an early, rapid crystalisation phase. The infilled vesicles and altered olivines demonstrate that multiple post intrusion fluid phases have affected the dyke.	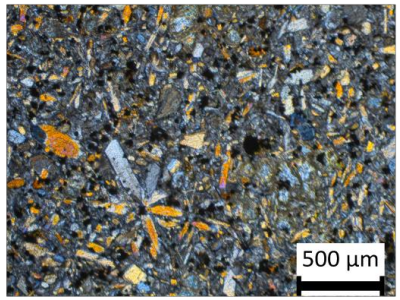	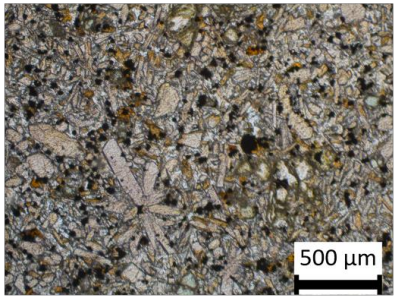
AP1-S2 *(In proximity to Tappe et al., (2007) location ST241b)*	55.099270°N 59.183560°W *Dyke margin orientation* 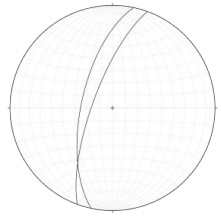	Good quality exposure on beach c.10 m from ST241b on the peninsula north of the town of Makkovik. Rock weathers to a dark green in outcrop. The largest crystal phase is ploagioclase. The plagioclase is always highly altered and often occurring as two intergrown crystals. The most abundant mineral is chlorite, occurring predominantly as large clusters of numerous crystals in the groundmass. The amphibole and apatite crystals are present in small quantities usually amongst the large clusters of chlorite. The small opaque minerals occur predominantly within the chlorite dominated groundmass but there are also some opaque minerals in the altered plagioclase. There is no metamorphic mineral fabric.	Chlorite – 50% Altered Plagioclase – 30% Amphibole – 10% Apatite – <2% Opaque minerals – <2% *Interpretation and Rocktype* **Basanite** - Plagioclase appears to be an early crystalisation phase with the other minerals often bisecting it. The rock has been heavily altered by subsequent fluidisation.	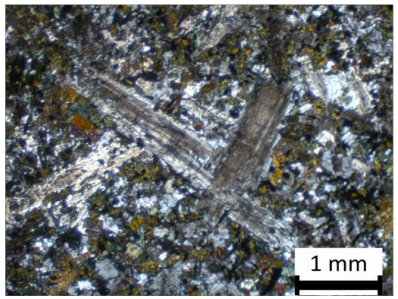	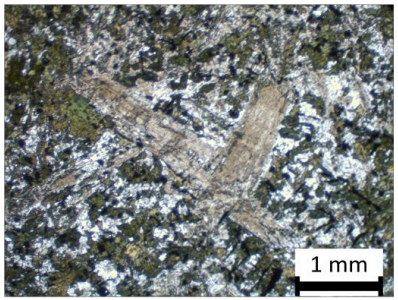
AP1-S3 *(In proximity to Tappe et al., (2007) location ST241b)*	55.099270°N 59.183560°W *Dyke margin orientation* 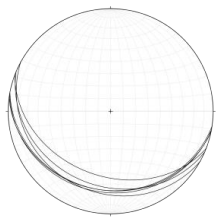	Good quality exposure on beach at the exact location of ST241b on the peninsula north of the town of Makkovik. The rock weathers to reddish brown in outcrop. In hand specimen the clean surface displays a very fine grained grey-blue groundmass with scarce occurrences of pyrite (<1 mm). The most abundant mineral in this sample is plagioclase, which occurs as highly altered interlocking crystals where it is often difficult to determine the boundary between individual crystals. Chlorite is the next most abundant mineral phase occurring as both clusters and individual crystals. Although not abundant, amphibole sometimes occurs amongst the chlorite crystals. Titanite and apatite also occur in very small quantities within the plagioclase and chlorite.	Altered Plagioclase – 60% Chlorite – 25% Amphibole – <5% Titanite – < 5% Apatite – <5% Pyrite – <5% *Interpretation and Rocktype* **Basaltic Trachyandesite** - The mineral assemblage of AP1-S3 is quite similar to AP1-S2 but with different mineral abundances and a more fine grained texture.	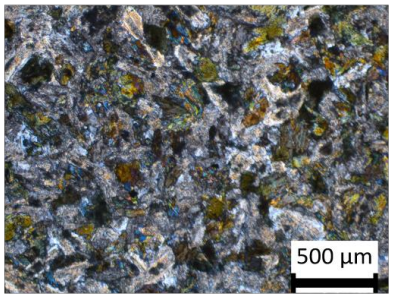	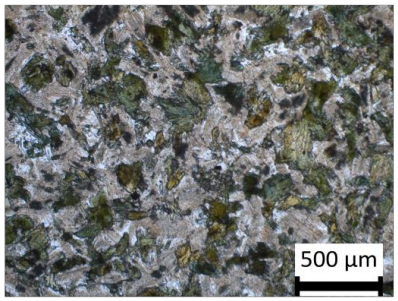

Sample Name	*Location*	*Description of Outcrop/Sample*	*Mineralogy*	*Cross Polarised Light*	*Plane Polarised Light*
AP2-S1 *(In proximity to Tappe et al., (2007) location ST103)*	55.073890°N 59.094330°W *Dyke margin orientation* 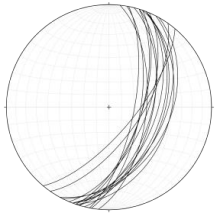	Dyke 1 of 2 at a poor quality outcrop in intertidal range which is partially covered by sand in Fords Bight. The contact between dyke and the surrounding breccia was observed. In outcrop both the dyke and breccia are moderately fractured. In hand specimen olivine phenocrysts can be observed as well as vesicles which have been infilled with calcite. The most abundant mineral phase is melinlinite which occurs in the groundmass as easily distinguishable crystals which possibly display a preferential orientation. The largest crystals in AP2-S1 are olivine. The opaque minerals are very small but occur throughout the sample. Very fine calcite veins can be observed in thin section.	Melilinite – 70% Olivine – 20% Opaque minerals – 10% Vesicles – calcite infill 5% *Interpretation and Rocktype* **Olivine Melilitite** - Dyke within the poorly exposed diatreme. Not part of a regional dyke swarm.	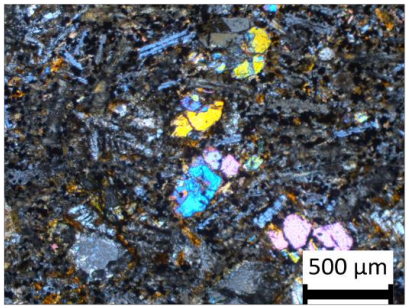	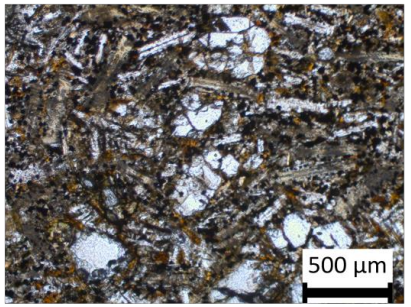
AP2-S2 *(In proximity to Tappe et al., (2007) location ST103)*	55.073890°N 59.094330°W *Dyke margin orientation* 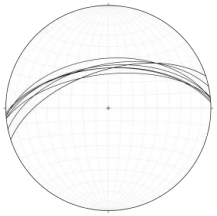	Dyke 2 of 2 at a poor quality outcrop in intertidal range which is partially covered by sand in Fords Bight. The contact between dyke and the surrounding breccia was observed along with the contact with the metamorphosed basement (quartzite). The mineral assemblage in AP2-S2 is indistinguishable from AP2-S1. AP2-S2 crosscuts AP2-S1 and is thus younger.	Melilinite – 70% Olivine – 20% Opaque minerals – 10% Vesicles – calcite infill 5% *Interpretation and Rocktype* **Olivine Melilitite** - Dyke within the poorly exposed diatreme. Not part of a regional dyke swarm.	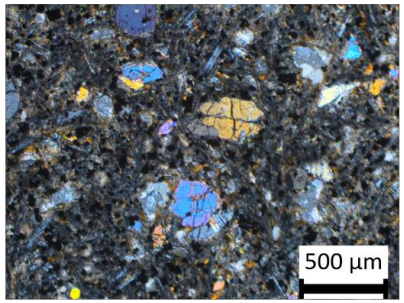	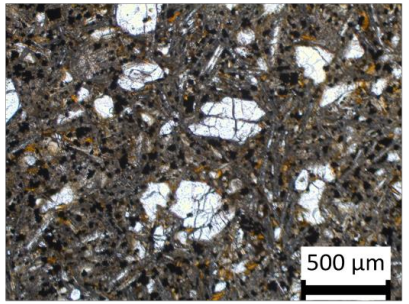
AP2-S3 *(In proximity to Tappe et al., (2007) location ST253)*	55.073890°N 59.094330°W *Contact Description* In contact with the quartzite basement (AP2-S4) and AP2-S2.	Part of the collection of poorly exposed outcrops in Fords Bight. Bluish grey in hand specimen and outcrop, with some weathered surfaces showing orange oxidation. This unit is best exposed at the back of the beach. Fine grained but with a distinct mineral fabric observable in outcrop, hand specimen and thin section. Amphibole is common in this sample, taking two forms a small euhedral type and a larger anhedral variety. The amphibole crystals form distinct bands in the rock. Plagioclase is a major mineral phase, occurring as highly altered indistinct crystals, although some less altered plagioclase can also be observed in the ground mass. Epidote occurs in AP2-S3 as large crystals between the other mineral phases, whilst small amounts of chlorite occasionally accompany the amphibole.	Amphibole – 45% Plagioclase (highly altered) – 35% Epidote – 10% Chlorite – 10% *Interpretation and Rocktype* **Amphibolite dyke** - Forming part of the metamorphosed basement,	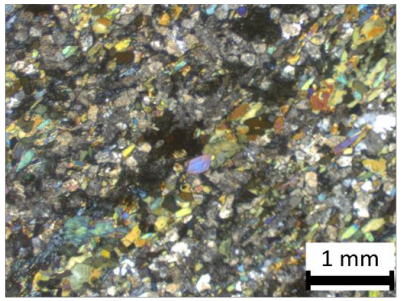	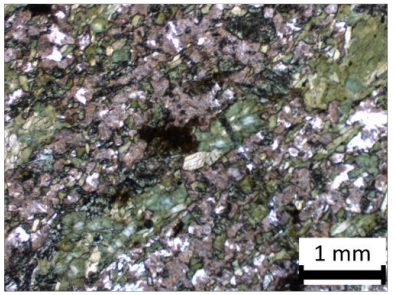

Sample Name	Location	Description of Outcrop/Sample	Mineralogy	Cross Polarised Light	Plane Polarised Light
AP2-S4 *(In proximity to Tappe et al., (2007) location ST103)*	55.073890°N 59.094330°W *Contact Description* In contact with the Diatreme Breccia (AP2-S5) and the melilitite dyke (AP2-S2).	A poorly exposed outcrop in Fords Bight of pale grey to white rock. The most abundant mineral in the sample is quartz at around 80%. The quartz is mostly anhedral with no pores or vesicles between crystals. Calcite is readily observable as much larger anhedral crystals amongst the quartz. Plagioclase is also found in the sample usually being larger than the quartz but smaller than the calcite crystals. Garnet is also present in the sample occurring as clusters of crystals. Opaque minerals are found in the sample being mostly anhedral and occurring as singular crystals. A mineral fabric is clearly observable in both hand sample and thin section with larger quartz crystals along with the calcite, garnet and plagioclase forming distinct bands of a regular orientation.	Quartz – 80% Garnet – 7% Calcite – 7% Plagioclase - 4% Opaque minerals - 2% *Interpretation and Rocktype* **Quartzite Basement** - Metamorphosed from a silica rich protolith.	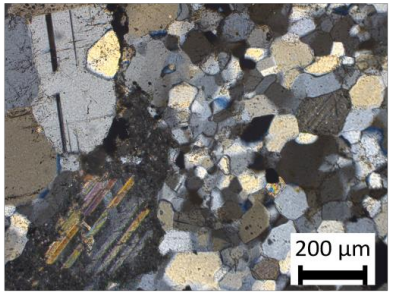	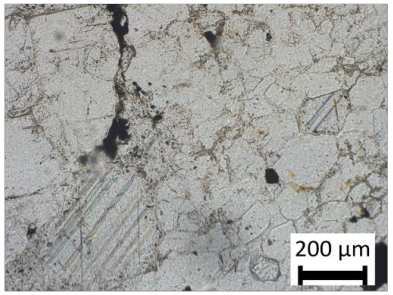
AP2-S5 *(In proximity to Tappe et al., (2007) location ST103)*	55.073890°N 59.094330°W *Contact Description* In contact with both Melilitite dykes (AP2-S1 and AP2-S2) along with the quartzite basement (AP2-S4).	Part of the poorly exposed outcrop in Fords Bight consisting of a dark green ground mass containing a variety of clasts. Clast size varies from >30cm to individual crystal fragments observable in thin section. The same clast types as AP2-S6 are found but with more of the melilite inclusions and less quartzite and amphibolite. Melilinite clasts are found down to a much smaller size in AP2-S5 than AP2-S6. The distribution of different clast types varies on an extremely localised scale. The clasts of the quartzite and amphibolite are very angular, whereas the melilinite are more rounded. There is no preferential orientation or imbrication clasts. Clasts constitute a considerably higher proportion of the rock than the matrix. The matrix of AP2-S5 is extremely fine grained containing predominantly carbonate.	Matrix - Calcite Clast type 1 – similar to AP2-S4 (Quartzite basement) Clast type 2 – similar to AP2-S3 (Amphibolite dyke) Clast type 3 - similar to AP2-S1 and AP2-S2 (Melilitite Dyke) Clast type 4 – individual crystals of quartz, olivine, microcline and plagioclase *Interpretation and Rocktype* **Diatreme Breccia** - more melilinite and less basment clasts may indicate that this sample represents the centre of the diatreme system.	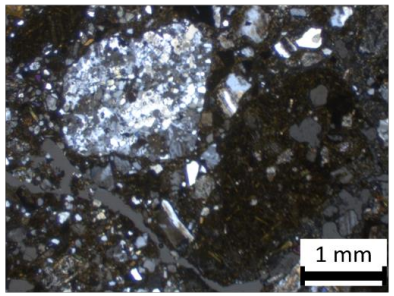	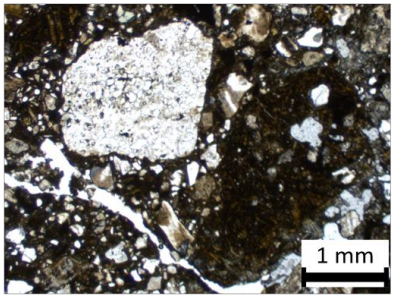
AP2-S6 *(In proximity to Tappe et al., (2007) location ST103)*	55.074259°N 59.094011°W *Contact Description* No insitu outcrop at location. Collected 45 m of AP2/ ST103 on a bearing of 025°.	Out of situ sample from 100 m NE of AP2. In outcrop and hand specimen consists of a dark yellow ground mass on the weathered surface, which is pale grey when clean, containing a variety of clasts. Clast size varies from >30cm down to individual crystal fragments observable in thin section. The major difference between AP2-S5 and AP2-S6 is the ratio of clasts to matrix where AP2-S6 is much more matrix dominated compared to AP2-S5. The matrix of AP2-S6 is extremely fine grained containing small fragments of quartz in a carbonate matrix. Individual crystals cannon be discerned within the carbonate matrix. The same clast types as AP2-S5 are found but with much more of the quartzite and amphibolite and less of the melilitite inclusions (melilite usually altered to calcite). The clasts of the quartzite and amphibolite are very angular, whereas the melilinite are again rounded.	Matrix - Calcite and quartz fragments. Clast type 1 – similar to AP2-S4 (Quartzite basement) Clast type 2 – similar to AP2-S3 (Amphibolite dyke) Clast type 3 - similar to AP2-S1 and AP2-S2 (Melilitite Dyke) Clast type 4 – individual crystals of quartz, olivine, microcline and plagioclase *Interpretation and Rocktype* **Diatreme Breccia** - more inclusions of basement may indicate that this sample represens a proximal part of the diatreme system.	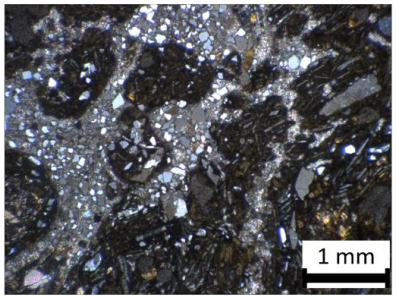	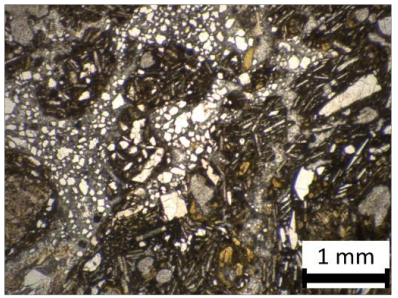

Sample Name	Location	Description of Outcrop/Sample	Mineralogy	Cross Polarised Light	Plane Polarised Light
AP3-S1 *(In proximity to Tappe et al., (2007) location ST253)*	55.149590°N 59.015420°W *Contact Description* No insitu dyke at location.	Out of situ boulder in gully c.70 m way from ST253 on Cape Strawberry. An in situ outcrop of this dyke is located c.120 m away from ST253. The weathered surface is reddish brown, whereas the clean surface is dark grey. In hand specimen olivine phenocrysts and calcite infilled vesicles (up to 7mm) are visible. The sample contains two types of olivine, serpentinised and unserpentinised. The serpentinised olivine crystals are typically smaller and euhedral, compared to the larger unserpentinised anhedral olivine crystals which also commonly contain opaque inclusions. Clinopyroxene occurs as both euhedral larger crystals and in the groundmass.	Clinopyroxene (groundmass) - 25% Olivine (unserpentinised) - 20% Olivine (serpentinised) - 15% Clinopyroxene (non-groundmass) - 15% Opaque minerals - 15% Vesicles – calcite infill 10% *Interpretation and Rocktype* **Olivine Lamprophyre** - based on the dominant mineral phases. The infilled vesicles and altered olivines demonstrate that multiple post intrusion fluid phases have affected the dyke.	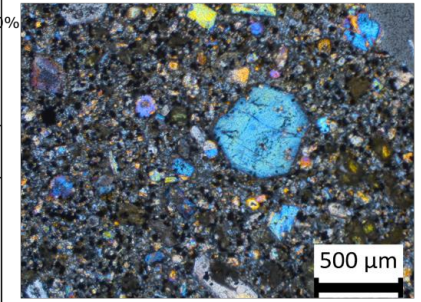	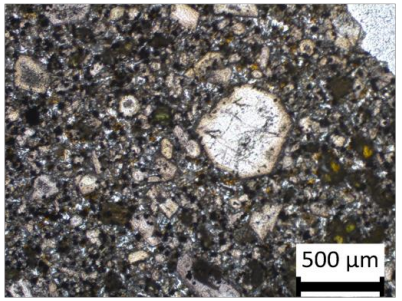
AP4-S1 *(In proximity to Tappe et al., (2007) location ST245)*	55.161383°N 59.143383°W *Dyke margin orientation* 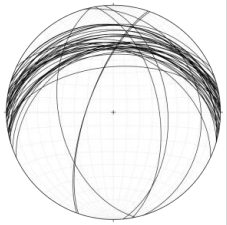	Reasonably good quality exposure of a small < 13 cm wide dyke 15 m away from ST245. In outcrop the weathered surface varies from dark grey through to reddish brown. No phenocrysts are identifyable in hand specimen. Clinopyroxene is abundant, often being arranged into star shaped clusters of two crystals which have intergrown, this texture is common as both a large crystal phase and within the ground mass. Calcite filled vesicles are present and are common in the sample but are not as large as those in the other samples. Olivine (both serpentinised and unaltered) is also common within the sample.	Clinopyroxene (groundmass) – 40% Clinopyroxene (phenocrysts) – 20% Vesicles – calcite infill – 15% Olivine serpentinised – 10% Olivine (unaltered) – 5% *Interpretation and Rocktype* **Basanite** - the intergrown clusters of clinopyroxene may indicate an early, rapid crystalisation phase. The infilled vesicles and altered olivines demonstrate that multiple post intrusion fluid phases have affected the dyke.	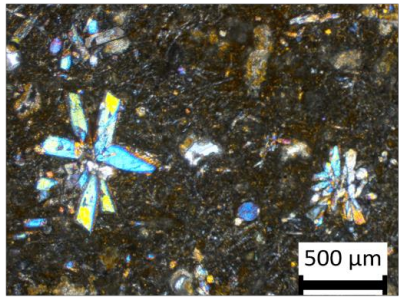	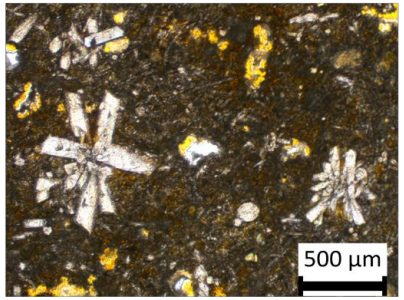
AP4-S2 *(In proximity to Tappe et al., (2007) location ST245)*	55.161383°N 59.143383°W *Dyke margin orientation* 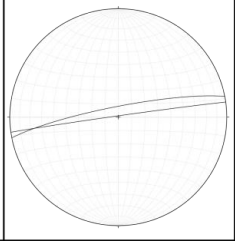	Reasonably good quality exposure of a small < 25 cm wide dyke 17 m away from ST245. In outcrop this dyke is highly fractured compared to AP4-1 with a brown weathered surface. The sample is extremely fine grained. Clinopyroxene is the most abundant mineral phase occurring in both the ground mass and as slightly larger crystals. Olivine occurs as small isolated crystals. Plagioclase occurs in the groundmass, with individual crystals hard to discern. Opaque minerals and small calcite filled vesicles are abundant in this sample.	Clinopyroxene – 50% Plagioclase – 20% Opaque minerals – 10% Olivine – 10% Vesicles – calcite infill – 10% *Interpretation and Rocktype* **Basanite** - Although this dyke is larger than AP4-S1 the very fine groundmass implies that it has still cooled exceptionally quickly and was unable to produce phenocrysts.	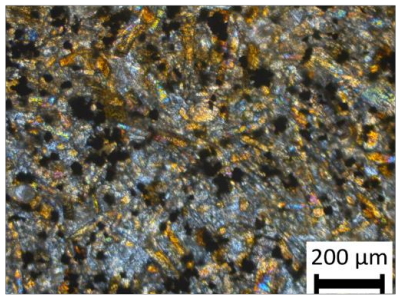	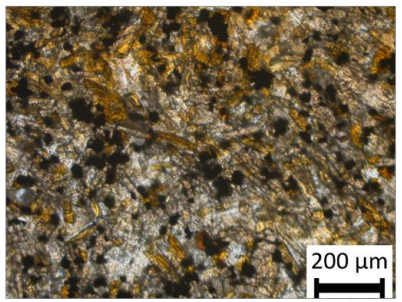

Appendix 1.2.2

Sample locations and coordinate systems (as in 2016 Geosphere Paper)

Tappe et al., (2007) quote North American Datum 1983 (NAD83) as the map datum in supplementary data file ‘mmc5.xls’, as opposed to North American Datum 1927 (NAD27). Using NAD83 however plots many of the sample locations offshore. Thus our study converted the location data twice; once using NAD27 and again using NAD83. Where possible (i.e. both onshore) both sites were visited to account for any map datum ambiguity associated with either the location data collection or our use of the location data. The difference between using NAD83 and NAD27 is around 63m for all locations, and in reality this is much smaller than the area around each location which was investigated. Comparison between locations plotted using NAD83 and the widely used WGS84 (World Geodetic System 1984) was found to be insignificant compared to the difference between NAD83 and NAD27, especially considering the large search radius at each sample location.

Appendix 1.2.3

XRF analysis and datasets (as in 2016 Geosphere Paper)

XRF (X-ray fluorescence) major element analysis was undertaken at the University of Leicester, UK to determine the weight percent of major elements as oxides. The XRF laboratory at the University of Leicester operates a PANalytical Axios Advanced X-Ray Fluoresence spectrometer which runs a 4Kw Rhodium (Rh) anode end window super sharp ceramic technology X-Ray tube. The major element analysis was performed on fused beads to eliminate mineralogical effects and reduce inter-element effects.

Other datasets used by this study include: the NOAA total sediment thickness data Version 2 (Whittaker et al., 2013); and Smith and Sandwell global topography and Bathymetry Version 18.1 (Smith and Sandwell, 1997). Our investigation into offshore sediment distribution utilises Version 2 of the NOAA total sediment thickness dataset despite the update of the original only applying to the Australia-Antarctic region as this was the latest version available at the time of this work. The NOAA total sediment thickness dataset has a grid resolution of five by five arc-minutes, with the data contributing to this dataset obtained from sources including; previously published isopach maps, ocean drilling results and seismic reflection profiles. Version 18.1 of the global topography and bathymetry data (Smith and Sandwell, 1997) dataset is primarily sourced from multibeam cruise data, supplemented by Version 23 (Sandwell et al., 2014) of the satellite derived free air gravity.

Appendix 1.3.1 - XRF Main Data Table

X.R.F. Results for Alex Peace Job 4788

Bead	Sample	SiO2	TiO2	Al2O3	Fe2O3	MnO	MgO	CaO	Na2O	K2O	P2O5	SO3	CrO3	NiO	LOI	Total
LF41063	**AP3-S1**	39.19	2.440	12.34	12.43	0.213	9.07	13.55	2.26	1.725	0.863	0.197	0.040	0.022	5.18	99.51
LF41064	**AP1-S1**	38.93	2.631	12.93	13.77	0.229	8.09	11.25	2.78	1.907	1.019	0.332	0.018	0.011	5.61	99.51
LF41065	**AP1-S2**	44.96	3.309	13.42	16.91	0.333	5.36	6.94	3.25	0.998	1.864	0.006	0.002	0.001	2.27	99.63
LF41066	**AP1-S3**	53.66	0.744	17.15	9.45	0.205	4.85	5.97	3.14	2.393	0.177	<0.002	<0.001	0.000	1.88	99.62
LF41067	**AP2-S1**	34.43	2.098	10.79	11.43	0.225	10.66	16.00	2.00	2.565	2.314	0.824	0.024	0.019	5.29	98.67
LF41068	**AP2-S2**	32.17	2.151	10.18	12.04	0.242	10.96	14.52	2.22	1.994	2.582	1.036	0.023	0.020	8.40	98.52
LF41069	**AP4-S1**	42.62	1.917	14.33	12.03	0.208	6.93	10.19	2.67	1.540	0.651	0.153	0.030	0.016	6.15	99.44
LF41070	**AP4-S2**	43.98	1.903	14.68	11.87	0.184	8.45	9.99	2.93	1.753	0.664	0.164	0.032	0.021	2.73	99.34

Notes;

i) Major elements determined on fused glass beads prepared from ignited powders
sample to flux ratio 1:5, 80% Li metaborate: 20% Li tetraborate flux
results quoted as component oxide weight percent, re-calculated to include LOI

ii) Samples analysed on University of Leicester, Department of Geology
PANalytical Axios Advanced XRF spectrometer

iii) Components with concentrations below the lower limit of detection reported

Appendix 1.3.2 - XRF Loss on Ignition Data

LOI data for Alex Peace, Durham University, Job 4788

Job	Bead	Sample	Crucible	Cruc.wt.	Cruc.+sam	Ignited	%LOI
APD4788	LF41063	**AP3-S1**	blank	15.0411	17.4851	17.3586	5.18
APD4788	LF41064	**AP1-S1**	5	13.4533	16.0767	15.9295	5.61
APD4788	LF41065	**AP1-S2**	F	15.2818	17.5906	17.5382	2.27
APD4788	LF41066	**AP1-S3**	11	13.2105	15.2357	15.1976	1.88
APD4788	LF41067	**AP2-S1**	6	15.7471	18.5503	18.4021	5.29
APD4788	LF41068	**AP2-S2**	D	13.1375	15.6389	15.4289	8.40
APD4788	LF41069	**AP4-S1**	1	13.287	16.0981	15.9252	6.15
APD4788	LF41070	**AP4-S2**	E	12.7516	15.4869	15.4122	2.73

Appendix 1.3 - XRF Standards

11/12/2015 09:13

PANalytical

Results quantitative - FusionUM

Selected arcl FusionUM

Number of results selected:

Seq.	Sample name (1-24)	Meas. date/time	Sum of conc. (%)	Result type	SiO2 Si1 (%)	TiO2 Ti1 (%)	Al2O3 Al1 (%)	Fe2O3 Fe1 (%)	MnO Mn1 (%)	MgO Mg1 (%)	CaO Ca1 (%)	Na2O Na1 (%)	K2O K1 (%)	P2O5 P1 (%)	SO3 S1 (%)	CrO3 Cr (%)	NiO Ni (%)
1	MAJMON	10/12/2015 17:45	322.30	Concentration	172.786	6.364	33.926	10.256	1.026	21.211	4.063	55.170	12.554	3.135	0.030	0.472	1.304
2	MAJMON	10/12/2015 17:53	324.86	Concentration	173.598	6.352	34.075	10.231	1.024	21.453	4.045	56.589	12.565	3.132	0.021	0.472	1.300
3	MAJMON	10/12/2015 18:00	331.47	Concentration	178.087	6.492	34.805	10.414	1.042	21.783	4.158	56.616	13.024	3.211	0.036	0.482	1.319
4	MAJMON	10/12/2015 18:07	331.36	Concentration	178.035	6.503	34.734	10.414	1.040	21.827	4.167	56.610	12.987	3.207	0.033	0.482	1.321
5	MAJMON	10/12/2015 18:15	331.32	Concentration	177.864	6.494	34.835	10.412	1.042	21.866	4.169	56.655	12.934	3.216	0.030	0.484	1.321
6	LF41063 APD 4788	10/12/2015 18:23	99.51	Concentration	41.337	2.573	13.015	13.115	0.224	9.568	14.291	2.380	1.819	0.911	0.208	0.042	0.024
7	LF41064 APD 4788	10/12/2015 18:32	99.51	Concentration	41.254	2.788	13.707	14.589	0.243	8.576	11.925	2.944	2.021	1.080	0.352	0.019	0.012
8	LF41065 APD 4788	10/12/2015 18:41	99.63	Concentration	46.003	3.386	13.737	17.307	0.341	5.489	7.101	3.328	1.021	1.907	0.006	0.003	0.001
9	LF41066 APD 4788	10/12/2015 18:50	99.56	Concentration	54.694	0.759	17.479	9.630	0.208	4.942	6.081	3.204	2.440	0.181	-0.060	-0.001	0.000
10	LF41067 APD 4788	10/12/2015 18:59	98.67	Concentration	36.384	2.216	11.403	12.078	0.238	11.264	16.905	2.111	2.710	2.445	0.870	0.026	0.020
11	LF41068 APD 4788	10/12/2015 19:08	98.52	Concentration	35.162	2.351	11.128	13.161	0.265	11.978	15.870	2.425	2.180	2.823	1.132	0.026	0.021
12	LF41069 APD 4788	10/12/2015 19:17	99.44	Concentration	45.435	2.043	15.274	12.826	0.222	7.386	10.863	2.845	1.641	0.694	0.163	0.032	0.017
13	LF41070 APD 4788	10/12/2015 19:26	99.34	Concentration	45.222	1.957	15.092	12.203	0.189	8.688	10.271	3.012	1.802	0.683	0.169	0.033	0.021
14	PCC-1	10/12/2015 19:35	100.79	Concentration	43.429	0.010	0.484	8.995	0.125	46.503	0.512	-0.029	-0.004	0.007	-0.042	0.413	0.385
15	DTS-1	10/12/2015 19:44	101.77	Concentration	40.084	0.007	-0.048	8.996	0.123	51.736	0.072	-0.074	-0.013	0.002	-0.060	0.583	0.363
16	NIM-PA	10/12/2015 19:53	99.28	Concentration	49.980	0.184	4.012	13.275	0.224	25.336	2.537	0.204	0.075	0.000	-0.063	3.432	0.083
17	NIM-P	10/12/2015 20:02	100.81	Concentration	50.717	0.182	4.042	13.228	0.224	26.128	2.550	0.215	0.075	-0.005	-0.063	3.431	0.083
18	UM-1	10/12/2015 20:11	101.77	Concentration	37.386	0.076	0.638	21.123	0.163	38.382	2.163	0.012	0.000	0.023	-0.087	0.428	1.469
19	UM-2	10/12/2015 20:20	101.92	Concentration	42.232	0.257	7.671	16.172	0.074	28.489	4.846	0.198	0.036	0.014	-0.105	1.447	0.592
20	UM-4	10/12/2015 20:29	100.22	Concentration	40.735	0.330	8.998	15.271	0.158	25.085	6.279	0.285	0.114	0.014	-0.027	2.588	0.394
21	SARM7	10/12/2015 20:38	100.54	Concentration	50.985	0.229	8.251	12.685	0.196	20.624	5.490	0.541	0.148	0.005	0.154	0.873	0.360

22	JP-1	10/12/2015 20:47	102.05	Concentration	43.256	0.006	0.421	8.822	0.123	48.317	0.497	-0.070	-0.011	0.005	-0.117	0.422	0.384
23	BH-1	10/12/2015 20:56	99.82	Concentration	68.639	0.400	14.643	5.926	0.135	2.771	3.531	2.956	0.824	0.047	-0.045	-0.003	-0.004
24	WS-1	10/12/2015 21:05	101.07	Concentration	51.778	2.436	14.600	13.976	0.181	5.592	8.607	2.244	1.305	0.273	0.072	0.005	0.002
25	BCS375	10/12/2015 21:14	97.11	Concentration	66.768	0.370	20.177	0.100	0.004	0.024	0.783	8.229	0.745	0.002	-0.084	-0.001	-0.005
26	BCS376	10/12/2015 21:23	98.69	Concentration	66.633	0.007	18.092	0.092	0.002	0.042	0.416	2.206	11.357	-0.011	-0.139	-0.004	-0.003
27	blank	10/12/2015 21:32	0.08	Concentration	-0.602	0.004	-0.106	0.515	0.002	0.139	-0.040	0.016	-0.015	-0.016	-0.093	-0.001	0.274
28	ARSiO2	10/12/2015 21:41	99.65	Concentration	100.169	0.004	-0.250	-0.009	0.000	0.005	-0.047	-0.047	-0.015	-0.016	-0.136	-0.006	-0.005
29	ARAl2O3	10/12/2015 21:50	101.41	Concentration	-0.628	0.004	102.201	0.087	0.001	-0.059	-0.040	-0.037	-0.011	-0.016	-0.111	-0.005	0.018
30	MRG-1	10/12/2015 21:59	100.99	Concentration	39.440	3.770	8.653	18.880	0.175	14.280	14.846	0.543	0.170	0.043	0.105	0.066	0.024
31	NIM-D	10/12/2015 22:08	102.94	Concentration	38.369	0.019	-0.005	17.841	0.222	45.819	0.216	-0.114	-0.011	-0.016	-0.126	0.405	0.319
32	BCS372/1	10/12/2015 22:17	102.40	Concentration	19.518	0.269	5.198	3.490	0.074	1.452	67.584	0.027	0.766	0.056	3.963	0.004	0.000

Appendix 2 Table of Contents

Supplementary materials for Chapter 5

Appendix 2.1 - Basement fabric Measurements

Orientation			Location		Notes
Strike	**Dip**	**Direction**	**Latitude**	**Longitude**	
50			55.09939	-59.18277	Site 4
41	88	S	55.09655	-59.1758	
35	60	S	55.09655	-59.1758	
36	70	S	55.09655	-59.1758	
31	64	S	55.09655	-59.1758	
10	70	E	55.07388	-59.09431	Site 11
5	51	E	55.07388	-59.09431	Site 11
13	56	E	55.07388	-59.09431	Site 11
175	70	E	55.07388	-59.09431	Site 11
16	59	E	55.07388	-59.09431	Site 11
10	73	E	55.07388	-59.09431	Site 11
9	55	E	55.07388	-59.09431	Site 11
19	56	E	55.07388	-59.09431	Site 11
24	72	E	55.07388	-59.09431	Site 11
14	67	E	55.07388	-59.09431	Site 11
19	69	E	55.07388	-59.09431	Site 11
1	68	W	55.10235	-59.19981	Site 29
171	62	W	55.10235	-59.19981	Site 29
1	62	W	55.10574	-59.2013	Site 33
3	82	W	55.10574	-59.2013	Site 33
8	90		55.10651	-59.20751	Site 36
11	90		55.10651	-59.20751	Site 36
19	85	S	55.10617	-59.2087	Site 37
22	82	W	55.16134	-59.14333	Site 41b
152	76	E	55.126	-59.11172	Site 45
177			55.126	-59.11172	Site 45
167	76	E	55.126	-59.11172	Site 45
178			55.126	-59.11172	Site 45
9			55.126	-59.11172	Site 45
174			55.126	-59.11172	Site 45
125	48	W	55.09566	-59.1877	
125	52	W	55.09566	-59.1877	
116	50	W	55.0962	-59.18736	
130	48	W	55.09663	-59.18725	
143	51	W	55.09663	-59.18725	
117	38	S	55.09717	-59.1864	
136	52	S	55.09792	-59.18531	
110	30	S	55.09903	-59.18335	
147	52	W	55.10025	-59.18056	
159	50	W	55.10025	-59.18056	
167	44	SW	55.09997	-59.1763	
157	55	W	55.09823	-59.1757	
115	60	SW	55.09673	-59.17589	
25	70	S	55.09657	-59.17576	
28	70	S	55.09657	-59.17576	
10	76	N	55.09526	-59.17553	
25	63	W	55.09618	-59.17542	
21	68	W	55.09483	-59.17476	
59	55	S	55.10438	-59.22638	
75	30	S	55.10438	-59.22638	
15	65	SW	55.1032	-59.2274	
30	48	SW	55.1032	-59.2274	
45	40	S	55.10295	-59.22705	Site 58
113	63	S	55.10223	-59.22842	Site 39
19	68	E	55.09874	-59.22981	
15	71	E	55.09535	-59.22564	
19	78	E	55.09512	-59.22468	
11	75	E	55.09623	-59.21925	

Appendix 2.2 - Epidote Surface Measurements

Slicken Line (Surfaces)			Slicken Lines (Lines)		Location		Sense	Notes
Strike	**Dip**	**Direction**	**Plunge**	**Azimuth**	**Latitude**	**Longitude**		
101	82	S			55.10000	-59.17635		Site 10
104	86	N	22	104	55.10000	-59.17635		Site 10
149	87	W	82	243	55.09518	-59.18885		Site 22
158	89	W	42	330	55.09518	-59.18885		Site 22
154	70	W	72	240	55.09518	-59.18885		Site 22
151	83	W	80	213	55.09518	-59.18885	REVERSE?	Site 22
60	25	S	18	104	55.09518	-59.18885	REVERSE?	Site 22
146	53	W	52	219	55.09518	-59.18885	REVERSE?	Site 22
142	82	W	62	319	55.09518	-59.18885	REVERSE?	Site 22
149	67	W	77	236	55.09518	-59.18885		Site 22
21	72	E			55.09518	-59.18885		Site 22
149	71	E	68	145	55.09518	-59.18885		Site 22
105	5	S	2	296	55.09518	-59.18885		Site 22
136	76	W	50	325	55.09518	-59.18885		Site 22
157	78	W	70	262	55.09518	-59.18885		Site 22
150	83	W	75	277	55.09518	-59.18885		Site 22
139	53	W	51	330	55.09518	-59.18885		Site 22
143	73	W	72	248	55.09518	-59.18885		Site 22
140	58	W	52	248	55.09518	-59.18885		Site 22
170	80	W	48	305	55.09518	-59.18885		Site 22
156	66	W	53	281	55.09518	-59.18885		Site 22
163	57	W	47	259	55.09518	-59.18885		Site 22
151	68	W	60	216	55.09518	-59.18885	NORMAL?	Site 22
148	75	W	75	232	55.09477	-59.18968		Site 24
97	75	N			55.09477	-59.18968		Site 24
157	75	W	60	276	55.09477	-59.18968		Site 24

144	84	W	63	261	55.09477	-59.18968		Site 24
154	84	W			55.09477	-59.18968		Site 24
107	70	S			55.09891	-59.18395		Site 25
151	50	W			55.09891	-59.18395		Site 25
148	53	W			55.09891	-59.18395		Site 25
159	80	W			55.09891	-59.18395		Site 25
133	76	W			55.09891	-59.18395		Site 25
75	45	S	36	120	55.09891	-59.18395	dextral	Site 25
87	57	S	37	120	55.09891	-59.18395	dextral	Site 25
142	73	W	24	287	55.09891	-59.18395		Site 25
154	67	W	65	260	55.09891	-59.18395		Site 25
149	69	W	63	243	55.09891	-59.18395		Site 25
149	70	W	63	225	55.09891	-59.18395		Site 25
175	52	W	51	244	55.09266	-59.177261		Site 27
1	60	W	43	210	55.09266	-59.177261		Site 27
94	77	S			55.09266	-59.177261		Site 27
136	25	E			55.09266	-59.177261		Site 27
39	62	N	40	246	55.09335	-59.17355		Site 28
13	58	W			55.090783	-59.077917		Site 5
3	87	W			55.090783	-59.077917		Site 5
164	70	E			55.090783	-59.077917		Site 5
169	71	E			55.090783	-59.077917		Site 5
87	87	N			55.090783	-59.077917		Site 5
7	62	W			55.090783	-59.077917		Site 5
65	82	N	8	166	55.090783	-59.077917		Site 5
162	53	E	50	95	55.090783	-59.077917		Site 5
169	83	E			55.090783	-59.077917		Site 5
158	65	E			55.090783	-59.077917		Site 5
154	62	E			55.090783	-59.077917		Site 5

165	72	E			55.090783	-59.077917	Site 5
89	81	N			55.090783	-59.077917	Site 5
179	70	N			55.090783	-59.077917	Site 5
6	90				55.090783	-59.077917	Site 5
52	85	S			55.10235	-59.19981	Site 29
60	83	N			55.10235	-59.19981	Site 29
67	89	N			55.10235	-59.19981	Site 29
59	84	N			55.10235	-59.19981	Site 29
57	87	N			55.10235	-59.19981	Site 29
61	86	S			55.10235	-59.19981	Site 29
56	82	N			55.10235	-59.19981	Site 29
60	82	N			55.10235	-59.19981	Site 29
52	81	N			55.10235	-59.19981	Site 29
65	86	N			55.10235	-59.19981	Site 29
87	30	S			55.10235	-59.19981	Site 29
90	20	S			55.10235	-59.19981	Site 29
104	18	S			55.10235	-59.19981	Site 29
89	17	S			55.10235	-59.19981	Site 29
136	20	S			55.10235	-59.19981	Site 29
80	22	S			55.10235	-59.19981	Site 29
105	18	S			55.10235	-59.19981	Site 29
118	21	S			55.10235	-59.19981	Site 29
106	19	S			55.10235	-59.19981	Site 29
84	25	S			55.10235	-59.19981	Site 29
154	82	E	38	132	55.10235	-59.19981	Site 29
180	70	E			55.10235	-59.19981	Site 29
150	80	N			55.10235	-59.19981	Site 29
155	74	E	60	95	55.10235	-59.19981	Site 29
168	82	E			55.10235	-59.19981	Site 29

170	43	W			55.10237	-59.20301	Site 30
129	40	E			55.10237	-59.20301	Site 30
127	40	N			55.10469	-59.2016	Site 32
140	46	N			55.10469	-59.2016	Site 32
111	83	N			55.10469	-59.2016	Site 32
101	79	N			55.10469	-59.2016	Site 32
115	82	N			55.10469	-59.2016	Site 32
75	65	S			55.10469	-59.2016	Site 32
53	7	S			55.10469	-59.2016	Site 32
99	80	N			55.10469	-59.2016	Site 32
100	78	N			55.10469	-59.2016	Site 32
103	38	S			55.10574	59.20137	Site 33
96	20	S			55.126	-59.11172	Site 45
161	16	W			55.126	-59.11172	Site 45
96	25	S			55.126	-59.11172	Site 45
159	78	E			55.12107	-59.13016	Site 52
4	90				55.12107	-59.13016	Site 52
170	79	E			55.12107	-59.13016	Site 52
170	71	W			55.12107	-59.13016	Site 52
6	54	E	50	93	55.12107	-59.13016	Site 52
79	81	W			55.12107	-59.13016	Site 52
1	79	E			55.12107	-59.13016	Site 52
163	69	W			55.12107	-59.13016	Site 52
87	61	W			55.12107	-59.13016	Site 52
165	80	E	66	114	55.12107	-59.13016	Site 52
161	75	W			55.12107	-59.13016	Site 52
7	90		10	12	55.12107	-59.13016	Site 52

Appendix 2.3 - All Slickenline Data

Plane			Slicken Lines (Lines)				
Dip	**Direction**	**Plunge**	**Plunge**	**Azimuth**	**Latitude**	**Longitude**	**Site**
152	78	E	6	142	55.09760	-59.18221	Site 2b
163	70	E	4	160	55.09760	-59.18221	Site 2b
160	79	E	18	164	55.09760	-59.18221	Site 2b
171	79	E	13	335	55.09760	-59.18221	Site 2b
65	82	N	8	166	55.09078	-59.07792	site 5
162	53	E	50	95	55.09078	-59.07792	site 5
86	66	N	16	281	55.09980	-59.17632	Site 8b
79	75	N	18	69	55.09980	-59.17632	Site 8b
88	54	N	13	91	55.09980	-59.17632	Site 8b
73	63	NE	18	87	55.09980	-59.17632	Site 8b
87	52	N	20	80	55.09980	-59.17632	Site 8b
84	76	N	10	82	55.09980	-59.17632	Site 8b
104	86	N	22	104	55.09980	-59.17632	Site 8b
158	20	E	10	30	55.09980	-59.17632	Site 8b
104	18	S	18	193	55.09980	-59.17632	Site 8b
175	45	W	37	225	55.10000	-59.17635	Site 10
149	58	W	57	248	55.09474	-59.17472	Site 14
149	59	W	55	247	55.09474	-59.17472	Site 14
63	88	S	3	60	55.09261	-59.19422	Site 21
41	82	S	8	44	55.09261	-59.19422	Site 21
67	72	N	5	251	55.09261	-59.19422	Site 21
87	64	N	12	262	55.09261	-59.19422	Site 21
81	63	N	16	267	55.09261	-59.19422	Site 21
49	89	N	80	182	55.09261	-59.19422	Site 21
8	56	W	59	263	55.09261	-59.19422	Site 21
133	85	S	42	171	55.09261	-59.19422	Site 21
1	90		22	165	55.09261	-59.19422	Site 21
149	87	W	82	243	55.09518	-59.18885	Site 22
158	89	W	42	330	55.09518	-59.18885	site 22
154	70	W	72	240	55.09518	-59.18885	Site 22
151	83	W	80	213	55.09518	-59.18885	Site 22
60	25	S	18	104	55.09518	-59.18885	Site 22
146	53	W	52	219	55.09518	-59.18885	Site 22
142	82	W	62	319	55.09518	-59.18885	Site 22
149	67	W	77	236	55.09518	-59.18885	Site 22
149	71	E	68	145	55.09518	-59.18885	Site 22
105	5	S	2	296	55.09518	-59.18885	Site 22
136	76	W	50	325	55.09518	-59.18885	Site 22
157	78	W	70	262	55.09518	-59.18885	Site 22
150	83	W	75	277	55.09518	-59.18885	Site 22
139	53	W	51	330	55.09518	-59.18885	Site 22
143	73	W	72	248	55.09518	-59.18885	Site 22
140	58	W	52	248	55.09518	-59.18885	Site 22
170	80	W	48	305	55.09518	-59.18885	Site 22
156	66	W	53	281	55.09518	-59.18885	Site 22
163	57	W	47	259	55.09518	-59.18885	Site 22
151	68	W	60	216	55.09518	-59.18885	Site 22

148	75	W	75	232	55.09477	-59.18968	Site 24
157	75	W	60	276	56.09477	-59.18968	Site 24
144	84	W	63	261	57.09477	-59.18968	Site 24
75	45	S	36	120	55.09891	-59.18395	site 25
87	57	S	37	120	55.09891	-59.18395	site 25
142	73	W	24	287	55.09891	-59.18395	site 25
154	67	W	65	260	55.09891	-59.18395	site 25
149	69	W	63	243	55.09891	-59.18395	site 25
149	70	W	63	225	55.09891	-59.18395	site 25
175	52	W	51	244	55.09266	-59.17726	site 27
1	60	W	43	210	55.09266	-59.17726	site 27
39	62	N	40	246	55.09335	-59.17355	site 28
154	82	E	38	132	55.10235	-59.19981	site 29
155	74	E	60	95	55.10235	-59.19981	site 29
96	48	N	13	286	55.10235	-59.19981	site 29
89	64	N	5	81	55.10235	-59.19981	site 29
91	54	N	4	96	55.10235	-59.19981	site 29
107	64	N	18	115	55.10235	-59.19981	site 29
107	62	N	10	118	55.10235	-59.19981	site 29
90	55	N	11	285	55.10235	-59.19981	site 29
86	22	N	11	280	55.10235	-59.19981	site 29
119	23	E	2	109	55.10235	-59.19981	site 29
101	36	S	22	112	55.10237	-59.20301	site 30
26	79	S	20	19	55.10237	59.20301	site 30
27	72	S	40	49	55.10237	59.20301	site 30
29	70	S	41	46	55.10237	59.20301	site 30
110	45	W	18	295	55.10237	59.20301	site 30
150	60	W	30	311	55.10237	59.20301	site 30
103	86	S	18	103	55.07546	59.16948	Site 42
92	86	N	13	94	55.07546	59.16948	Site 42
94	85	N	2	94	55.07546	59.16948	Site 42
109	78	S	23	112	55.07546	59.16948	Site 42
6	54	E	50	93	55.12107	-59.13016	Site 52
165	80	E	66	114	55.12107	-59.13016	Site 52
7	90		10	12	55.12107	-59.13016	Site 52
171	78	W	28	348	55.10223	59.22842	Site 59
178	73	W	20	3	55.10223	59.22842	Site 59
25	50	W	26	10	55.10223	59.22842	Site 59

Appendix 2.4 - Re-Os analysis

Name	Re (ppb)	±	Total Os (ppt)	±	192Os (ppt)	±	187Osr (ppt)	±	%187Osr	187Re/188Os	±	187Os/188Os	±	rho	Model age	±
RO715-1_pyrite	0.45	##	36.24	##	1.50	##	0.02	##	97.80	602.8	49.6	36.3	3.2	###	3438.8	145.2
RO749-7_Loc52_py	0.50	##	25.89	##	0.72	##	0.01	##	99.45	1364.9	###	54.6	##	###	2341.2	464.7

Appendix 3 Table of Contents

Supplementary materials for Chapter 6

Appendix 3.1 - Offshore fault orientations

Labrador	Labrador(split)	Davis Strait	Davis Strait (split)	Both	Both (split)
322	322	62	62	322	322
291	291	60	60	291	291
115	115	58	60	115	115
105	105	38	58	105	105
305	114	70	57	305	114
294	305	50	42	294	305
296	306	294	19	296	306
292	294	53	66	292	294
302	293	278	38	302	293
106	296	60	71	106	296
	296	68	70	62	296
	320	73	50	60	320
	293	100	294	58	293
	292	345	53	38	292
	288	11	278	70	288
	300	61	21	50	300
	289	6	60	294	289
	285	53	303	53	285
	302	355	311	278	302
	145	296	334	60	145
	114	136	5	68	114
	142	120	315	73	142
	113	294	68	100	113
	106	309	39	345	106
	149	305	12	11	149
	137	112	23	61	137
	142	128	15	6	142
	137	124	58	53	137
	137	329	63	355	137
		339	73	296	62
		298	41	136	60
		11	39	120	60
		35	17	294	58
		160	100	309	57
		321	345	305	42
		70	11	112	19
		351	61	128	66
		35	34	124	38
		41	6	329	71
		57	53	339	70
		311	355	298	50
		25	310	11	294
		352	327	35	53
		58	296	160	278
		293	283	321	21
		338	174	70	60
		321	136	351	303

359	119	35	311
39	120	41	334
41	294	57	5
1	309	311	315
58	299	25	68
291	4	352	39
315	305	58	12
284	282	293	23
61	314	338	15
	141	321	58
	112	359	63
	128	39	73
	124	41	41
	329	1	39
	358	58	17
	343	291	100
	339	315	345
	319	284	11
	325	61	61
	330		34
	64		6
	298		53
	328		355
	28		310
	303		327
	16		296
	11		283
	304		174
	35		136
	297		119
	160		120
	321		294
	70		309
	351		299
	35		4
	41		305
	57		282
	323		314
	353		141
	311		112
	25		128
	320		124
	348		329
	309		358
	352		343
	306		339
	300		319
	331		325
	314		330
	58		64

319
313
293
302
308
338
349
321
8
359
38
47
20
39
64
56
41
34
1
58
291
303
315
284
298
3
61

298
328
28
303
16
11
304
35
297
160
321
70
351
35
41
57
323
353
311
25
320
348
309
352
306
300
331
314
58
319
313
293
302
308
338
349
321
8
359
38
47
20
39
64
56
41
34
1
58
291

303

315

284

298

3

61

Appendix 3.2 - Processing parameters for Spectrum West Greenland 2D seismic data

Page numbers from original report not this thesis.

2012 Reprocessing

Offshore West Greenland

Spectrum Geo Limited
Dukes Court
Duke Street
Woking
Surrey, GU21 5BH
England

Contents

1. Acquisition Parameters

Survey name	Date Acquired	Acquired by	Data Supplied	Available Km	Process Km (TBC)	SP Interval (m)	Group Interval (m)	Cable Length (m)	Number channels	Nominal Fold	Record Length (s)	Sample Rate (ms)
BUR 1971	1971	Burmah Oil	**GEUS**	3247	1884	50	100	2400	24	24	6	4
FYLLA2001	2001	Statoil	**GEUS**	948	895	25	12.5	6000	480	120	8	2
GGU1990	1990	GGU	**GEUS**	3288	2114	25	25	3000	120	60	8	2
GGU1991	1991	GGU	**GEUS**	339	336	25	25	3000	120	60	8	2
GGU1992	1992	GGU	**GEUS**	3031	2636	25	25	3000	120	60	8	2
GGU1995	1995	GEUS	**GEUS**	3769	1060	25	12.5	3000	240	60	8	2
ST9708	1997	Statoil	**GEUS**	2293	212	25	12.5	3600	288	72	8	2
FYLLA1994	1994	Nunaoil	**NUNAOIL**	1708	1708	25	12.5	3000	240	60	8	2
NFE 1997	1997	Nunaoil	**NUNAOIL**	2115	2006	25	12.5	3000/3600	240/288	60/72	8	2
NSI 1998	1998	Nunaoil	**NUNAOIL**	709	710	25	12.5	4500	360	90	8	2

2. Processing Parameters

Reformat	Input SEG-Y
Source Designature	Convert to zero phase – wavelet extracted from data
Start of Data Delay	-51.2 ms for GGU90 -70.0 ms for GGU91 & GGU92 -50.0 ms for BUR71 & NU9401 & NU97-01 & ST9701 -94.0 ms for FY01 -31.0 ms for GGU95
Resample (Where necessary)	2 ms to 4 ms sample rate (anti-alias filter applied)
Geometry Assignment	
Low Cut Filter	5Hz, 12dB/oct
Amplitude Compensation	T^2 correction applied
Tau-P Noise Attenuation & Deconvolution	Applied in the shot domain. 320ms operator/ 24ms Gap.
SRME (Not Applied to BUR71 survey)	
Trace Drop (Where necessary)	Group 12.5m to 25m
Velocity Analysis	2km intervals
Radon Multiple Attenuation	-500ms to 1255ms, P=195 Multiple energy modelled in tau-p domain
Pre Migration Filter	Time-variant following digitized horizon WB 5(18) – 100(78) Hz Horizon-500ms 5(18) – 80(78) Hz Horizon 5(18) – 40(78) Hz 8000ms 5(18) – 40(78) Hz
Remove T^2 gain correction	
Pre-Stack Time Migration	Straight ray Kirchhoff algorithm 3000m aperture radius Smoothed 2 km velocity field
Velocity Analysis	1km intervals

Pre-Stack Time Migration	Straight ray Kirchhoff algorithm 3000m aperture radius Smoothed 1 km velocity field
Amplitude Compensation	V^2T correction applied
Radon Multiple Attenuation	-0ms to 2000ms, P 401 Multiple energy modelled in tau-p domain
Residual NMO Correction	Calculated for all CMPs, 12.5m interval Including 4th order correction calculation
NMO Correction	Using final residual / 4th order velocity field
Outer & Inner Trace Mutes	
Stack	
Method	Mean
Enhance Coherent Data	
Eigenvalue Filtering	
K-Filter	
Bandpass Filter	Time-variant following water depth & digitized

horizon	
WB + 300	12(24) – 70(78) Hz
Horizon 1	6(18) – 50(78) Hz
Horizon 2	6(18) – 40(78) Hz
8000ms	6(18) – 40(78) Hz

Equalisation	Expanding window alpha trimmed AGC

Tabelle 5

Vorläufige Ergebnisse der refraktionsseismischen Messungen

Sonoboje Nr.	Profil Nr.	Schußpunkt Nr.	Geschwindigkeit (km/sec) v_0	v_1	v_2	v_3	v_4	v_5	v_6	Mächtigkeit (km) h_0	h_1	h_2	h_3	h_4	h_5	Bemerkungen
1	1	500-994	1.50	2.31	3.08	4.35	5.75			3.52	0.62	0.91	1.18			Hydrophon 36 m
2	1	3700-4100	1.48	2.24	2.78	4.03	6.85			2.1	0.68	0.62	2.08			Hydrophon 36 m
3	2	3634-4200	1.48	1.94	3.25	4.50	6.41	7.35	9.26	3.36	0.79	1.34	0.90	2.10	4.56	Hydrophon 36 m
4	3	4209-4330														ausgefallen
5	3	4337-5319	1.48	1.97	2.54	4.38	7.69			3.50	1.44	1.17	2.02			Hydrophon 36 m
6	4	4921-5520	1.48	2.17	2.78	3.67	4.54			3.26	0.86	0.64	1.96			Hydrophon 36 m
7	5	3849-4431	1.48	1.98	2.27	2.63	5.55			2.85	0.09	0.17	0.80			Hydrophon 36 m
8	6	1685-2285	1.48	1.97	2.33	2.91	6.09	7.57		2.44	1.17	0.48	2.12	1.98		Hydrophon 36 m
9	6	5147-5747	1.40	1.99	3.49	4.54	7.63			2.39	0.39	1.31	1.85			Hydrophon 36 m
10	6	8082-8682	1.35	1.86	2.63	5.74				1.27	0.94	1.17				Hydrophon 36 m
11	8	1000-1600	1.42	2.85	4.63					0.19	3.15					Hydrophon 36 m
12	21	1004-1625	1.48	2.96	4.67	6.25				0.23	0.13	0.36				Hydrophon 36 m
13	11	25-673	1.45	3.87	5.88					0.28	1.05					Hydrophon 36 m
14	12	1901-2864	1.50	1.84	2.08	3.05	7.46			2.28	0.93	0.71	0.29			Hydrophon 36 m
15	12	4007-4707	1.45	2.05	2.78	3.49	5.49	(7.57)		2.70	0.89	1.56	0.25	(4.37)		Hydrophon 36 m
16	12	9201-10031	1.45	2.35	2.92	4.38	9.43			2.68	1.22	1.33	2.51			Hydrophon 36 m
17	13	435-1435	1.47	2.38	3.82	5.10				0.18	2.14	3.67				Hydrophon 36 m
18	16	14-40														ausgefallen

MARINE SURVEY

General Information

Survey vessel: 'EXPLORA' Line 8 - 21 Party chief: G. Repenning

1. Sketch of shotpoint-geometry

A. SEISMIC SURVEY DATA

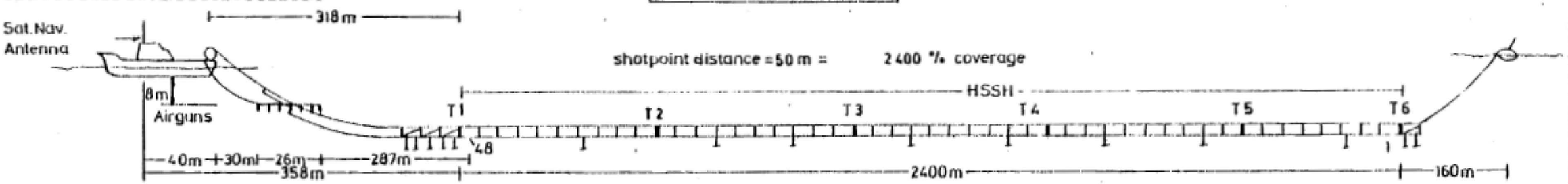

2. Seismic energy source

No. of airguns	1x0.16 ltr =0.16 ltr	4x1.20 ltr = 4.80 ltr
	3x0.25 ltr =0.75 ltr	3x1.60 ltr = 4.80 ltr
AIRGUN ARRAY	3x0.33 ltr =0.99 ltr	2x2.00 ltr = 4.00 ltr
„U"-TYPE	3x0.45 ltr = 1.35 ltr	1x2.30 ltr = 2.30 ltr
	3x0.60 ltr = 1.80 ltr	1x2.50 ltr = 2.50 ltr
		24 guns 23.45 ltr
Total - capacity		
Airgun-pressure	150 kp/cm^2	
Depth of airguns	8 m	

3. Streamer

Type of cable	HSSH
Towing cable length	168 m
Damping cable length	150 m
Cable length	2400 m
Group interval	50 m
Active group length	44 m
No of detectors each group	64
Depth of detectors	15 m

4. Seismic instruments

Type DFS V
Record time 5-12 sec, sample rate 4 ms
Filter 8 Hz 18 db - 64 Hz 70db down at 128 Hz
Monitor record on SDW 400 every 50 shots
Lineprofiler MR 101 trace No. 47 every 2 shots
Lineprofiler 'EDO trace No. 48 every shot

B CHANNEL ARRANGEMENT

DFS V SEG-B 800 BPI

Data channel	1 - 48	Active groups
Aux	1	timing word
	2	synchronisation puls
	3	
	4	sono buoy
	5	sono buoy

C. OTHER SURVEY METHODS

Gravity

Seagravimeter ASKANIA GSS 3
Girotable ANSCHÜTZ
Analogrecorder LINSEIS
Reference poits: BREMEN
LERWICK
GODTHAAB

Magnetic

Magnetometer GEOMETRICS
Analogrecorder HEWLETT - PACKARD
Distance between shipsposition and sensor 200 m

D. NAVIGATION

System: SAT NAV / SONAR DOPPLER
LORAN C SL 7

Digital data aquisition: KENNEDY every shot
Punch - Tape: 1 per 45p = 200 m
Echosounder: ATLAS EDIG / ELAC

Author: S V EXPLORA		Sc: ——	Encl ——
Drawn: GM	Date: 6.8.77		

BGR
Labrador See

77 20 25

Remarks: T = Depth - indicator ⊥ Depth - controller

Appendix 4 Table of Contents

Supplementary materials for Chapter 7

cooling.m

– Example of the application of the models detailed in Chapter 7

```
%Thermal profile of 1st sill at ODP site 210-1276a
%Dolerite sill
%Produce plot after sill has cooled to the geothermal
gradient
%Includes hydrothermalism
close all
clear all

dx = 2;    % discretization step in m
dt = 0.01; % timestep in yrs


h=1000;    % height of box in m
nx=ceil(h/dx)+1; %number of x


%length of model
model_length_years=5000;

%number of tsteps to reach end of model
nt=ceil(model_length_years/dt)+1;

% x array
x=0:dx:h;

%spatially variable thermal diffusivity (m/s-2)
kappa=zeros(1,nx-1); %create diffusivity array

%array for time
time=zeros(1,nt);
t=0;

T=20+0.02175.*x;  % initial Temp grad
T_grad=T;

Tnew = zeros(1,nx); %calculated new temperature


Tm=1488; %Temperature of dolerite intrusions

%define positions of intrusions

%Upper sill
sill_1_thickness=ceil(10/dx);
sill_1_top=ceil(260/dx);
sill_1_bottom=sill_1_top+sill_1_thickness;
T(sill_1_top:sill_1_bottom)=Tm;
```

```
%for intrusion
Cp_intrusion=820;
density_intrusion=2960;
conductivity_intrusion=2.5;
kappa_intrusion=conductivity_intrusion/(density_intrusion*Cp
_intrusion);

%for host
Cp_host=1090;
density_host=2400;
conductivity_host=2.1;
kappa_host=conductivity_host/(density_host*Cp_host);

%Appy calculated kappa values to array
kappa(1:sill_1_top-1)=kappa_host;
kappa(sill_1_top:sill_1_bottom)=kappa_intrusion;
kappa(sill_1_bottom+1:nx)=kappa_host;


%initial condition
T_initial=T;


% unit conversion to SI:
secinyr=24*3600*365;   % dt in sec
secinmyr=secinyr*1e6;
dt=dt*secinyr;

%model hydrothermalism
hydro=20/dx; %extent of hydrothrmalism (metres)
kappa(sill_1_top-hydro:sill_1_top)=kappa(1)*10;
kappa(sill_1_bottom:sill_1_bottom+hydro)=kappa(1)*10;

%plot kappa profile
figure(1)
plot(kappa,x)
set(gca,'YDir','reverse');%Reverse y axis

%Main calculation
for it=1:nt

    tyears=floor(t/secinyr);


    for i = 2:nx-1

        Tnew(i) = T(i) + (((kappa(i-1)*(T(i+1)-T(i))/dx)-
(kappa(i)*(T(i)-T(i-1))/dx))/dx^2)*dt;
    end
```

```
    Tnew(1) = T(1);
    Tnew(nx) = T(nx);


    time(it) = t;

    T = Tnew; %Set old Temp to = new temp for next loop


    %Times to plot

    plot_times_years = [1 10 100 500 1000 3500 5000]; %years
to plot

    plot_times = ceil(plot_times_years*dx); %convert years
to timesteps

    if it==plot_times(1);
        T_plot1=T;
    end
    if it==plot_times(2);
        T_plot2=T;
    end

    if it==plot_times(3);
        T_plot3=T;
    end

    if it==plot_times(4);
        T_plot4=T;
    end

    if it==plot_times(5);
        T_plot5=T;
    end
    if it==plot_times(6);
        T_plot6=T;
    end

    if it==plot_times(7);
        T_plot7=T;
    end


    t=t+dt;
end


figure(2), clf

%produce a colormap with a gradient
```

```
Colors = jet;
NoColors = length(Colors);
I = [8,7,6,5,4,3,2,1];
Ireduced = (I-min(I))/(max(I)-min(I))*(NoColors-1)+1;
RGB = interp1(1:NoColors,Colors,Ireduced);
set(gcf,'DefaultAxesColorOrder',RGB)

plot
(T_initial,x,T_plot1,x,T_plot2,x,T_plot3,x,T_plot4,x,T_plot5
,x,T_plot6,x,T_plot7,x,'LineWidth',1.5);set(gca,'FontSize',1
2)
xlabel('T [^oC]','FontSize',15)
ylabel('Depth [m]','FontSize',15)
title(' Temperature against Depth for selected times post
intrusion of the upper sill','FontSize',15)
axis([0 1500 0 1000])
set(gca,'YDir','reverse');%Reverse y axis
hleg1 = legend('initial
conditions',num2str(plot_times_years(1)),num2str(plot_times_
years(2)),num2str(plot_times_years(3)),num2str(plot_times_ye
ars(4)),num2str(plot_times_years(5)),num2str(plot_times_year
s(6)),num2str(plot_times_years(7)));
drawnow
```

EASY_Ro.m

– Example of the EASY_Ro function called in cooling.m and in elsewhere Chapter 7

```
%EASY%RO2

%A MATLAB function to calculate %Ro from a temperature/time
history

function [Max_Ro] = EASY_Ro(Time,Temperature_C)

%Strontiometric Factor
Weights=[0.03 0.03 0.04 0.04 0.05 0.05 0.06 0.04 0.04 0.07
0.06 0.06 0.06 0.05 0.05 0.04 0.03 0.02 0.02 0.01]; %Weights

%Activation energy
E=[34 36 38 40 42 44 46 48 50 52 54 56 58 60 62 64 66 68 70
72]; %E(Kcal/m)

nx=numel(E);


%Gas constant
R=1.987;

%E/R
E_div_R=(E*1000)/R;

%pre exponential factor
PEF = 1e13;

%Convert temperature input to kelvins
Temperature_K = Temperature_C(:)+273;

%Length of Arrays
nt=numel(Time);


%Prepare temperature arrays
for i=2:nt
    if Temperature_K(i)==Temperature_K(i-1);
        Temperature_K(i)=Temperature_K(i)+1E-5;
    end
end


%Heating rates(seconds)

yrs_to_Secs=31536000;

Heating_rate=zeros(1,nt-1);
```

```
for i=2:nt
    Heating_rate(i)=(Temperature_K(i)-Temperature_K(i-
1))/(Time(i)-Time(i-1))/yrs_to_Secs;
end

%E/RTs

E_div_RT = zeros(nt,nx); %create array

for i=1:nt
    for j=1:nx

        E_div_RT(i,j)= E_div_R(j)/Temperature_K(i);

    end
end


%I

I = zeros (nt,nx); %create array

for i=1:nt
    for j=1:nx

        I(i,j)= PEF*Temperature_K(i)*exp(E_div_RT(i,j)*-
1)*(1-
(E_div_RT(i,j)^2+2.334733*E_div_RT(i,j)+0.250621)/(E_div_RT(
i,j)^2+3.330657*E_div_RT(i,j)+1.681534));

    end
end


%Delta I's

Delta_I = zeros(nt,nx);

Delta_I(:,1)=0;

for i=2:nt
    for j=1:nx

        Delta_I(i,j)=Delta_I(i-1,j)+(I(i,j)-I(i-
1,j))/Heating_rate(i);

    end
end
```

```
%Calculation of cumulative reacted

Cumulative = zeros(nt,nx);

Cumulative(1,:)=zeros; %no reation yet

for i=1:nt
    for j=1:nx

          Cumulative(i,j)=Weights(j)*(1-(exp(Delta_I(i,j)*-
1)));

    end
end

%Cumulative Reaction Weights

Cum_reaction_weights = sum(Cumulative,2);

% %Ro

Ro=zeros(nt,1);


for i=1:nt

    Ro(i)=exp(-1.6+3.7*Cum_reaction_weights(i));

end

 Max_Ro=max(Ro);


end
```

Appendix 5 Table of Contents

List of software

Appendix 5.1

A complete list of softwhere used during this study and the preparation of this thesis.

- **ArcGIS** (10.3) including ArcMap, ArcScene, ArcCatalogue
- **GMT** (5.1.1)
- **MATLAB** (2011b and 2015a)
- **MyFault** (1.05)
- **GPlates** (1.4.0)
- **Petrel** (2014)
- **Google Earth Pro** (7.1.2.2041)
- **Garmin Basecamp** (4.4.5)
- **Stereonet** by R. W. Allmendinger (9.3.0)
- **Inkskape** (0.48)
- **Microsoft Excel** (2010 version 14.0.7172.5000 on pc and 2011 version 14.0.0 on Mac)
- **Microsoft Word** (2010 version 14.0.7172.5000 on pc and 2011 version 14.0.0 on Mac)

Appendix 6 Table of Contents

Publications and conference contributions

Research Paper

THEMED ISSUE: Anatomy of Rifting: Tectonics and Magmatism in Continental Rifts, Oceanic Spreading Centers, and Transforms

GEOSPHERE

GEOSPHERE; v. 12, no. 6

doi:10.1130/GES01341.1

16 figures; 5 tables; 3 supplemental files

CORRESPONDENCE: a.l.peace@durham.ac.uk

CITATION: Peace, A., McCaffrey, K., Imber, J., Phethean, J., Nowell, G., Gerdes, K., and Dempsey, E., 2016, An evaluation of Mesozoic rift-related magmatism on the margins of the Labrador Sea: Implications for rifting and passive margin asymmetry: Geosphere, v. 12, no. 6, doi:10.1130/GES01341.1.

Received 9 April 2016
Revision received 3 August 2016
Accepted 24 August 2016

An evaluation of Mesozoic rift-related magmatism on the margins of the Labrador Sea: Implications for rifting and passive margin asymmetry

Alexander Peace[1], Ken McCaffrey[1], Jonathan Imber[1], Jordan Phethean[1], Geoff Nowell[1], Keith Gerdes[2], and Edward Dempsey[1]

[1]Department of Earth Sciences, Science Labs, Durham University, Elvet Hill, Durham DH1 3LE, UK
[2]Shell International, 40 Bank Street, London E14 5NR, UK

ABSTRACT

The Labrador Sea is a small (~900 km wide) ocean basin separating southwest Greenland from Labrador, Canada. It opened following a series of rifting events that began as early as the Late Triassic or Jurassic, culminating in a brief period of seafloor spreading commencing by polarity chron 27 (C27; Danian) and ending by C13 (Eocene-Oligocene boundary). Rift-related magmatism has been documented on both conjugate margins of the Labrador Sea. In southwest Greenland this magmatism formed a major coast-parallel dike swarm as well as other smaller dikes and intrusions. Evidence for rift-related magmatism on the conjugate Labrador margin is limited to igneous lithologies found in deep offshore exploration wells, mostly belonging to the Alexis Formation, along with a postulated Early Cretaceous nephelinite dike swarm (ca. 142 Ma) that crops out onshore, near Makkovik, Labrador. Our field observations of this Early Cretaceous nephelinite suite lead us to conclude that the early rift-related magmatism exposed around Makkovik is volumetrically and spatially limited compared to the contemporaneous magmatism on the conjugate southwest Greenland margin. This asymmetry in the spatial extent of the exposed onshore magmatism is consistent with other observations of asymmetry between the conjugate margins of the Labrador Sea, including the total sediment thickness in offshore basins, the crustal structure, and the bathymetric profile of the shelf width. We propose that the magmatic and structural asymmetry observed between these two conjugate margins is consistent with an early rifting phase dominated by simple shear rather than pure shear deformation. In such a setting Labrador would be the lower plate margin to the southwest Greenland upper plate.

INTRODUCTION

Stretching of the continental lithosphere results in rifting and may lead to continental breakup accompanied by seafloor spreading (Eldholm and Sundvor, 1979). The production of pairs of conjugate continental passive margins is the inevitable result of the continental breakup process (Geoffroy, 2005). Although conjugate margins may inherit similar geological and structural components, many aspects of these conjugate pairs often display significant asymmetry.

The degree of symmetry displayed between conjugate passive margins has traditionally been linked to the mode by which the preceding rifting occurred (Lister et al., 1986), with models of continental rifting being described as either pure shear (McKenzie, 1978), simple shear (Wernicke, 1985), or combinations of these (Lister et al., 1986). Rifting under a pure shear–dominated regime occurs by symmetrical, brittle extension of an upper layer and ductile stretching of a lower layer. The simple shear model of rifting predicts that extension occurs along lithosphere-scale normal faults and/or ductile shear zones usually resulting in an asymmetric rift in cross section (e.g., Lister et al., 1986; Etheridge et al., 1989). The large detachment faults required by simple shear models are claimed to be mechanically problematic (Ranero and Pérez-Gussinyé, 2010); it has also been claimed that both conjugate margins often display characteristics of being the upper plate to the detachment fault (Lavier and Manatschal, 2006). It has also been argued that it is difficult to generate melt under simple shear rifting (Latin and White, 1990). Despite these problems, the simple shear model or derivatives of it are often used to explain various aspects of asymmetry on conjugate margin systems, for example, the South Atlantic margins (Becker et al., 2016). Testable predictions of the detachment model of passive margin formation (Lister et al., 1986) include a wide continental shelf, and deep sag basins overlying the sedimentary synrift fill on the lower plate margin. In contrast, the upper plate margin remains relatively unfaulted with an induced continental drainage divide caused by uplift due to magmatic underplating.

In this contribution we assess the degree of asymmetry displayed by the conjugate margins of the Labrador Sea (Fig. 1A) to determine if rifting prior to the formation of these margins is likely to have taken place under a pure or a simple shear–dominated regime. This assessment was achieved through observations made during four weeks of field work between June and July 2015 near the town of Makkovik, Labrador, Canada. The primary aim of the field work was to identify and characterize the spatial extent and field relationships of previously described Mesozoic igneous rocks, which Tappe et al. (2007)

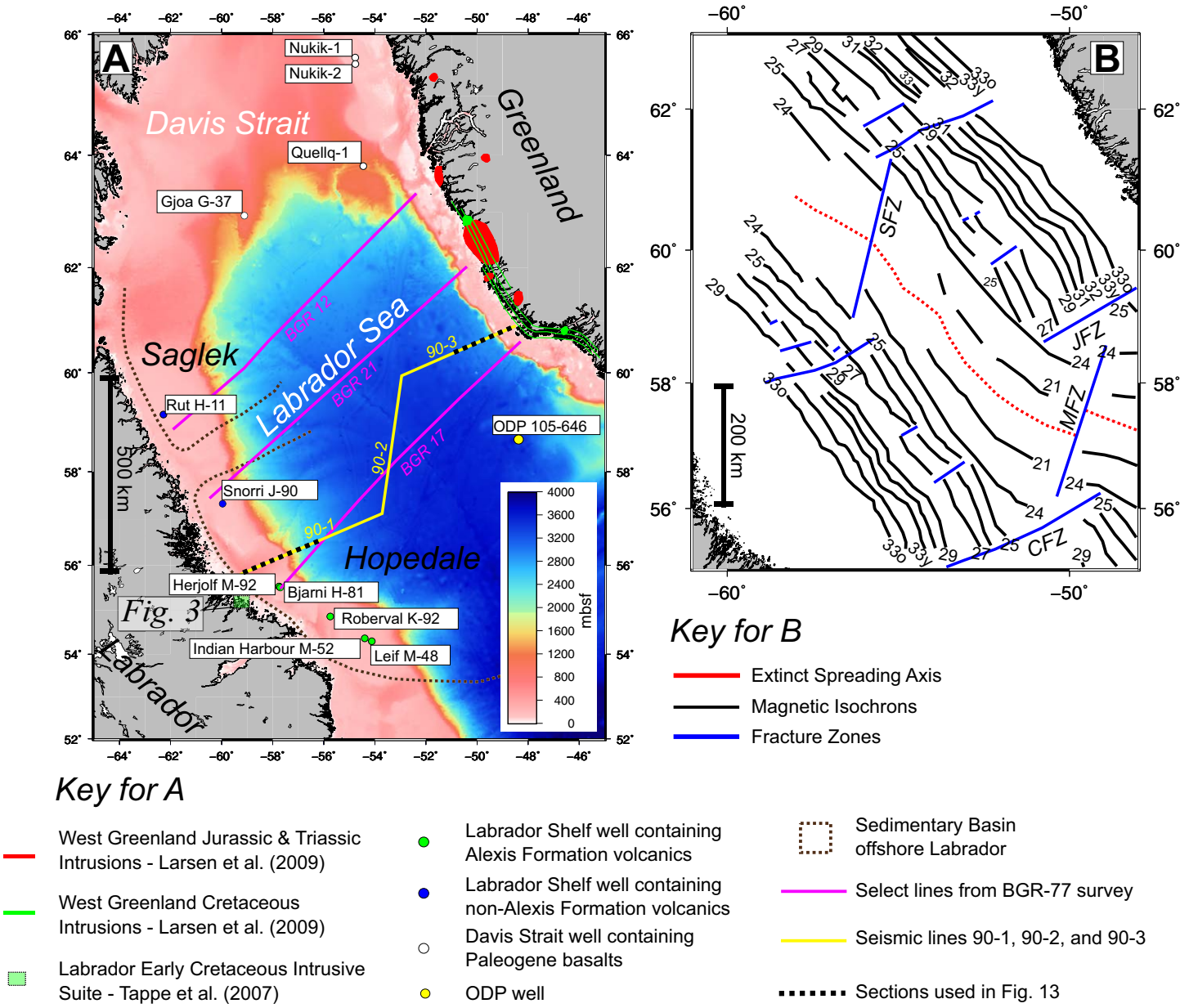

Figure 1. (A) Summary of documented occurrences of early rift-related (Triassic–Cretaceous) magmatism on the margins of the Labrador Sea, both onshore and in offshore wells. ODP—Ocean Drilling Program. (B) Interpretation of the age and structure of oceanic crust in the Labrador Sea (modified from Srivastava and Roest, 1999). Abbreviations: SFZ—Snorri fracture zone; CFZ—Cartwright fracture zone; JFZ—Julinhaab fracture zone; MFZ—Minna fracture zone. The bathymetry data are from Smith and Sandwell (1997; global topography and bathymetry).

related to rifting prior to the opening of the Labrador Sea. Field observations were supplemented by whole-rock geochemistry (X-ray fluorescence, XRF) of igneous rock samples. Our field data are then considered in the context of observations from elsewhere on the margins of the Labrador Sea. We integrate these observations with analysis of large-scale geophysical data sets including that of the National Oceanic and Atmospheric Administration (NOAA; Divins, 2003), seismic reflection profiles, and the Smith and Sandwell (1997) global topography data set to further test our interpretation of margin asymmetry.

GEOLOGICAL SETTING

The Labrador Sea separates Labrador in eastern Canada from southwest Greenland (Fig. 1A) and is floored by a small (~900 km wide) oceanic basin that provides an ideal place to study conjugate passive margin pairs where the production of oceanic crust was relatively limited (Chalmers and Laursen, 1995). Rifting of the Labrador Sea has previously been attributed to either a pure shear–type model, based on seismic and other geophysical data indicating that faulting is confined to the upper crust (Keen et al., 1994), or a simple shear–type model, based on observations of the asymmetry of the transition zones (Chian et al., 1995a).

Rifting prior to the opening of the Labrador Sea started as early as the Late Triassic to Jurassic, based on ages obtained from dike swarms in West Greenland that are interpreted to be related to early rifting (Larsen et al., 2009) (Fig. 1A). The early seafloor spreading history of the Labrador Sea is poorly constrained, with the oldest undisputed magnetic anomaly interpretation in the Labrador Sea being from polarity chron 27 (C27; Danian; Chalmers and Laursen, 1995). However, seafloor spreading may have initiated earlier, at C32 (Campanian) in the southern Labrador Sea and C28 (Maastrichtian) in the northern Labrador Sea (Srivastava, 1978). Seafloor spreading in the Labrador Sea underwent a major reorganization and change in spreading direction at C24–C25N (Thanetian–Ypresian) (Fig. 1B), coincident with the onset of North Atlantic spreading (Srivastava, 1978). After the reorganization of the North Atlantic and Labrador Sea between C24 and C25N there was a reduction in the rate of seafloor spreading before it eventually ceased at C13N (Eocene-Oligocene boundary) (Geoffroy, 2001).

The sedimentary basins offshore Labrador record the progressive opening of the Labrador Sea from south to north (DeSilva, 1999) during the Mesozoic. Two major sedimentary basins are present off the coast of Labrador (DeSilva, 1999): the Hopedale Basin in the south and the Saglek Basin to the north (Fig. 1A). Both the Saglek and Hopedale Basins contain synrift and postrift, clastic-dominated sequences of Cretaceous to Pleistocene age (Jauer et al., 2014). Exposures of Mesozoic and Cenozoic sediments onshore along the Labrador coast are extremely rare (Haggart, 2014).

From north to south the basement tectonic units exposed at surface on the coast of Labrador are the Archean Nain Province, the Paleoproterozoic Makkovik Province, and the Mesoproterozoic Grenville Province (LaFlamme et al., 2013; Fig. 2). The Makkovik Province is separated from the Nain Province by the Kanairiktok shear zone (Culshaw et al., 2000) and from the Grenville Province by the Grenville Front, which marks the northern limit of widespread Grenvillian deformation (Funck et al., 2001). The Makkovik Province is characterized as a Paleoproterozoic accretionary belt and is the smallest defined tectonic component of the Canadian shield (Ketchum et al., 2002). Prior to the opening of the Labrador Sea the Makkovik Province was adjacent to the Ketilidian mobile belt (KMB; Fig. 2), which currently forms part of southwest Greenland (e.g., Garde et al., 2002; Wardle et al., 2002; Kerr et al., 1997). The Makkovik Province can be separated into three distinct zones with distinctive geological characteristics (Kerr et al., 1996); from northwest to southeast, they are the Kaipokok, Aillik, and Cape Harrison domains (Fig. 2) (Kerr et al., 1997).

Onshore Rift-Related Magmatism on the Margins of the Labrador Sea

Our field work was carried out in the Aillik domain of the Makkovik Province. Here, the Early Cretaceous nephelinite suite (ca. 142 Ma) located near Makkovik (Fig. 3; Table 1) is the most recent of three magmatic events identified by Tappe et al. (2007). The older two magmatic events formed a Neoproterozoic ultramafic lamprophyre and carbonatite dike suite (ca. 590–555 Ma) and a Mesoproterozoic olivine lamproite dike suite (ca. 1374 Ma) (Tappe et al., 2006). These two older events are not considered to be directly related to the rifting that culminated in the Mesozoic opening of the Labrador Sea (Tappe et al., 2007).

The Tappe et al. (2007) nephelinite suite (Fig. 3; Table 1) comprises fine-grained olivine melilitite, nephelinite, and basanite dikes and sills as much as 2 m thick with a preferential east-west orientation, and has been characterized as a type of rift-related magmatism. This intrusive suite was claimed by Tappe et al. (2007) to be analogous to the coast-parallel alkaline basaltic dikes observed between 60° and 63°N in West Greenland (Larsen, 2006). The samples categorized by Tappe et al. (2007) as belonging to the nephelinite suite are summarized in Table 1, along with their relationship to the samples collected and our analyses (described herein). Here we use the definition of Le Bas (1989) of a nephelinite as containing >20% normative nepheline.

Magmatism in West Greenland has also been attributed to early rifting, prior to the opening of the Labrador Sea. According to Larsen et al. (2009) this magmatism is manifest as Mesozoic–Paleogene intrusive rocks that range in scale and abundance from large, coast-parallel dike swarms to small, poorly exposed dike swarms or single intrusions (Fig. 1; Table 2). The large coast-parallel dikes extend for 380 km along the southwest Greenland coast (Larsen et al., 1999). Chalmers et al. (1995) described the later Paleogene breakup-related flood basalts farther north in and around the Davis Strait, but these are beyond the geographical and temporal scope of this study. The igneous rocks observed onshore southwest Greenland (Table 2) demonstrate that multiple magmatic events occurred on this margin during and after the Mesozoic. Although many of these events are likely to be rift related, it is extremely unlikely that all these igneous rocks were produced due to the same event.

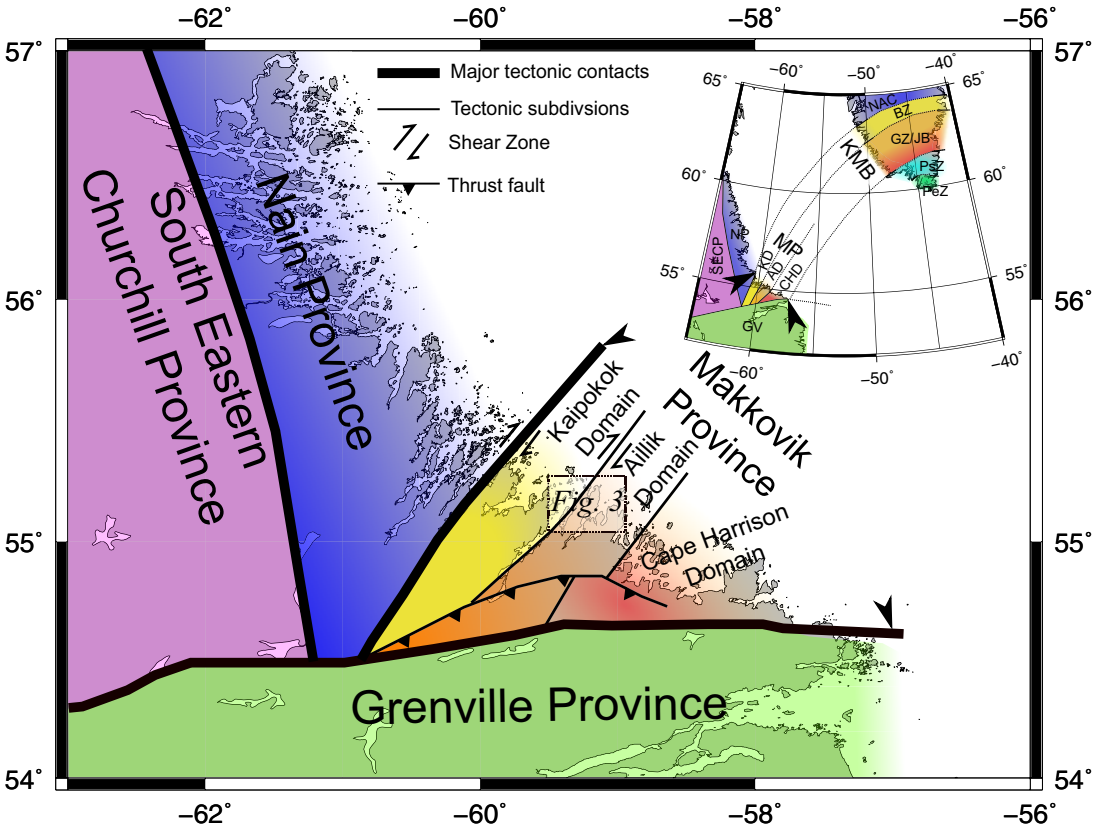

Figure 2. Simplified tectonic framework of central Labrador modified from LaFlamme et al. (2013), including the location of Figure 3 within the Makkovik Province. Abbreviations: NAC—North Atlantic Craton; BZ—Border Zone; GZ/JB—Granite Zone/Julianehåb Batholith; NP—Nain Province; MP—Makkovik Province; PsZ—Psammite Zone; PeZ—Peliet Zone; SECP—southeastern Churchill Province; KD—Kaipokok Domain; AD—Ailik Domain; GV—Grenville Province; KMB—Ketilidian Mobile Belt. Inset: The correlation of the Makkovik and Ketilidian orogenic belts modified from Kerr et al. (1997).

Offshore Rift-Related Magmatism on the Margins of the Labrador Sea

Mesozoic magmatism has also been observed and documented in exploration wells on the Labrador shelf (Fig. 1A; Table 3) (Umpleby, 1979). Volcanic rocks that are believed to have been erupted during the early stages of rifting are mostly assigned to the Alexis Formation; the type section is recorded in the Bjarni H-81 well (e.g., Ainsworth et al., 2014; Umpleby, 1979). Here a sequence of basalts interspersed with sandstones and silty clays was recorded, but no pyroclastic rocks were documented (Umpleby, 1979). Two cores from the Alexis Formation in Bjarni H-81 have been dated using K-Ar bulk-rock analysis. The lowermost core came from 2510 m and basaltic rocks have been dated as 139 ± 7 Ma (Valanginian), while those in the upper core at 2260 m were dated as 122 ± 6 Ma (Aptian). The age of the lower core is deemed to be less reliable due to alteration; Umpleby (1979) suggested that the inferred duration of ~17 m.y. for the magmatic event resulting in the eruption of the Alexis Formation is too long and that the lower core might be younger.

The total thickness and areal extent of the basalts of the Alexis Formation is not well constrained, beyond the occurrence of volcanic rocks in the Leif M-48, Robertval K-92, Bjarni H-81, Indian Harbour M-52, and Herjolf M-92 wells (Fig. 1A and Table 3). The Alexis Formation occurs in the Hopedale Basin (Hamilton and Harrison subbasins) and within the southern part of the Saglek Basin, but has not been recorded in the more northern Nain subbasin within the Hopedale Basin (Ainsworth et al., 2014). The thickest recorded occurrence of the Alexis Formation is 357 m in the Robertval K-92 well (Ainsworth et al., 2014). Note that some igneous rocks intersected by wells on the Labrador Shelf have not been assigned to a formation (Ainsworth et al., 2014). Occurrences of unclassified igneous rocks include the "Tuff" and "Diabase" intervals (Canada-Newfoundland and Labrador Offshore Petroleum Board, 2007) in Rut H-11 and the sediments derived from volcanic material in Snorri J-90 (McWhae et al., 1980).

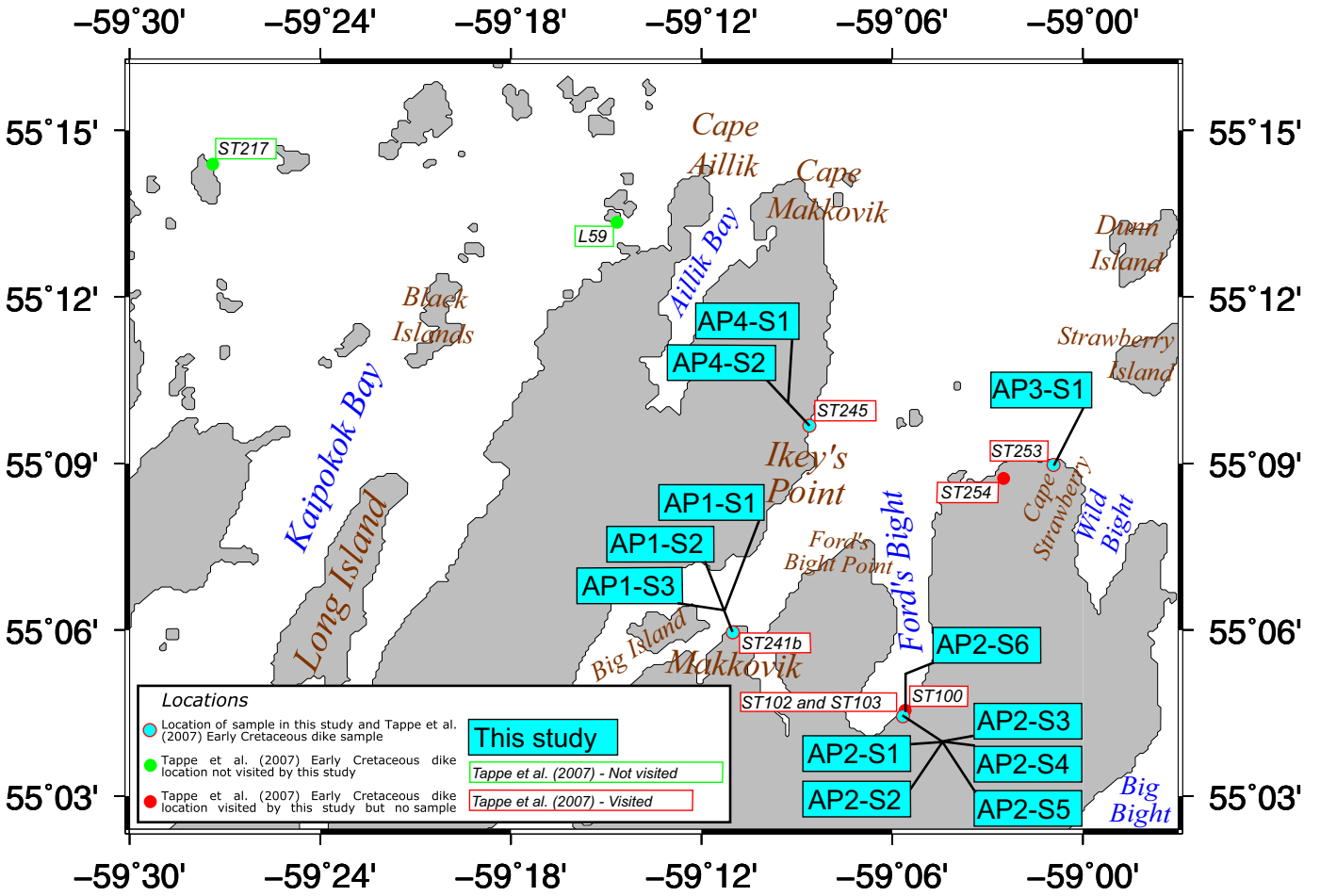

Figure 3. Map of the area surrounding Makkovik. Blue filled boxes depict the samples collected and analyzed in this study. The Tappe et al. (2007) samples are depicted as smaller red and green boxes, for sites visited and not visited by this study, respectively.

TABLE 1. SUMMARY OF RELATIONSHIP BETWEEN EARLY CRETACEOUS NEPHELINITE SUITE SAMPLES OF TAPPE ET AL. (2007) AND SAMPLES COLLECTED FOR THIS WORK

Tappe et al. (2007) sample number	ST100	ST102	ST241b	L59	ST217	ST103	ST253	ST245	ST254
Composition (Tappe et al., 2007)	Nephelinite	Basanite	Nephelinite	Nephelinite	Basanite	Melilitite	Nephelinite	Basanite	Nephelinite
Samples collected by this work (AP)	No in situ outcrop at location	No in situ outcrop at location	AP1-S1 AP1-S2 AP1-S3	Not visited in our study	Not visited in our study	AP2-S1 AP2-S2	AP3-S1	AP4-S1 AP4-S2	Area of basement exposure but no dikes of any age anywhere in proximity to location.
Coordinates of samples collected by this work (WGS84)	n/a	n/a	55.09927N 59.18356W	n/a	n/a	55.07389N 59.09430W	55.14959N 59.01542W	55.16138N 59.14338W	n/a

Note: WGS84—World Geodetic System 1984. n/a—not applicable as no equivalent sample was obtained by this work.

TABLE 2. DOCUMENTED OCCURANCES OF RIFT-RELATED MAGMATISM IN SOUTHWEST GREENLAND

Locality	Character	Rock type	Method	Age (Ma)	Reference
Uummannaq Fjord	Few small dikes	ailikite	Rb-Sr	186	Larsen et al. (2009)
Ubekendt Ejland	Small dike swarm	camptonite, monchiquite	$^{40}Ar/^{39}Ar$	34 ± 0.2	Storey et al. (1998)
Southeast Nuussuaq	Dikes and sill, some large	tholeiitic basalt	$^{40}Ar/^{39}Ar$	56.8 ± 0.2	Larsen et al. (2009)
West of Disko	Volcanic neck	alkali basalt	$^{40}Ar/^{39}Ar$	27.8 ± 0.6	Storey et al. (1998)
Western Disko	Regional dike swarm	tholeiitic basalt	$^{40}Ar/^{39}Ar$	54.3 ± 0.3	Storey et al. (1998)
Aasiaat district	Three large dikes , one sill	tholeiitic basalt	$^{40}Ar/^{39}Ar$	56, 61	Larsen et al. (2009)
Itilleq	One dike	tholeiitic basalt	$^{40}Ar/^{39}Ar$	64 ± 1.3	Larsen et al. (2009)
Qaqqarsuk	Central complex and dikes	carbonatite, aillikite	Rb-Sr U-Pb*	ca. 165	Secher et al. (2009)
Fossilik	One explosion breccia	ailikite	Rb-Sr	164.2 ± 1.8	Secher et al. (2009)
Søndre Isortoq	Small dike swarm	camptonite, one alkali basalt	$^{40}Ar/^{39}Ar$	56, 58	Larsen et al. (2009)
Godthåbsfjord	Scattered dikes	camptonite	$^{40}Ar/^{39}Ar$	51.8 ± 0.9	Larsen et al. (2009)
Tikiusaaq	Central complex and dikes	carbonatite and aillikite	Rb-Sr U-Pb*	165–155	Tappe et al. (2009)
Færingehavn	Few dikes	aillikite	Rb-Sr U-Pb	159 223	Larsen et al. (2009)
Frederikshåb Isblink	One large dike	phonolite	$^{40}Ar/^{39}Ar$	106.1 ± 1.5	Larsen et al. (2009)
Frederikshåb Isblink	Loose dike swarm	monchiquite, alnöite, carbonatite	Rb-Sr U-Pb*	152–149	Larsen et al. (2009)
Paamiut	Small dike swarm	aillikite	K-Ar	166 ± 5	Larsen and Møller (1968)
Pyramidefjeld	Small dikes and sills, including a thick sheet on Midternæs (16 km NNE)	aillikite	U-Pb	152–150	Frei et al. (2008) Larsen et al. (2009)
Southwest Greenland	Large regional dike swarm	mildly alkaline basalt	$^{40}Ar/^{39}Ar$	141–133	Larsen et al. (1999) Larsen et al. (2009)
Tuttutooq	One or a few sills	camptonite	$^{40}Ar/^{39}Ar$	115.4 ± 4.7	Larsen et al. (2009)

Note: A summary from north to south of documented intrusive rift-related magmatism in West Greenland as summarized by Larsen et al. (2009).
*Samples dated by Rb-Sr or U-Pb on phlogopite or perovskite.

[1]Supplemental Materials 1. Detailed descriptions of all samples mentioned in the manuscript. Please visit http://dx.doi.org/10.1130/GES01341.S1 or the full-text article on www.gsapubs.org to view Supplemental Materials 1.

[2]Supplemental Materials 2. Sample locations and coordinate systems. Please visit http://dx.doi.org/10.1130/GES01341.S2 or the full-text article on www.gsapubs.org to view Supplemental Materials 2.

Although no exploration wells have been drilled on the continental shelf offshore southwest Greenland, Site 646 (Leg 105 of the Ocean Drilling Program, ODP) was drilled on oceanic crust in the southern Labrador Sea (Fig. 1A). With the exception of the oceanic crust, Site 646 did not encounter igneous rocks; however, sediments containing clasts of mafic material were described (Shipboard Scientific Party, 1987).

FIELD OBSERVATIONS OF MESOZOIC MAGMATISM NEAR MAKKOVIK, LABRADOR

The aim of the field work was to characterize the nature and extent of Mesozoic magmatism near Makkovik to gain insights into rifting in the region prior to the opening of the Labrador Sea. Our field study of the Mesozoic magmatism near Makkovik was guided by the description of the Early Cretaceous magmatism in Tappe et al. (2007) (Fig. 3; Table 1). Of the nine locations where Tappe et al. (2007) documented Early Cretaceous magmatism, we visited seven sample locations (with exception of L59 and ST217). Eight samples of igneous material were obtained at four of the seven locations visited during this study. Where appropriate, samples collected adjacent to the dikes are also described to provide geological context and to emphasize the field relationships observed for the dikes.

At three of the Tappe et al. (2007) sample locations (ST100, ST102, and ST245; Fig. 3) we were unable to locate the in situ dikes reported by them. Descriptions including mineralogy, texture, and orientation of all the samples are available in the supplemental data (Supplemental Materials 1[1]). Details of the locations, coordinate systems, and the relationship between samples in this work and Tappe et al. (2007) are also available in the supplemental data (Supplemental Materials 2[2]).

Sample Locations, Field Relationships, and Structural Analysis

Makkovik Peninsula

The three samples with the prefix AP1 represent the three dikes found on the peninsula north of the town of Makkovik (Fig. 3), locally referred to as the Hill. The outcrops from which these samples were obtained are on the southern end

TABLE 3. OCCURRENCES OF VOLCANIC ROCKS IN OFFSHORE WELLS ON THE LABRADOR SHELF

Well name	Depths of igneous rocks	Dating method	Age	Description and Interpretation of igneous rocks
Bjarni H-81	2255 m–total depth	K-Ar	139 ± 7 Ma for the lower core (2510 m) 122 ± 6 Ma for the upper core (2260 m)	Basalts interspersed with sandstones and silty clays, with no pyroclastic rocks. Bjarni H-81 is the type section of the Alexis Formation.
Leif M-48	1839 m–total depth	K-Ar	104 ± 5 Ma to 131 ± 6 Ma	The Leif Basalts are deemed to be coeval and lithologically similar to those in Bjarni H-81, and thus can be considered part of the Alexis Formation.
Indian Harbour M-52	3250 m–3484 m	K-Ar	90 ± 4 Ma for rock fragments (exact stratigraphic position unknown)	The recovered rock samples are lapilli tuff deposits. The volcanic rocks in this well are noted as being lithologically very different from occurrences of the Alexis Formation elsewhere on the Labrador shelf. The lithological difference along with the younger age suggests that these rocks may not be part of the Alexis Formation.
Herjolf M-92	3751 m–4048 m	K-Ar	The top of the volcanic section has been dated as 122 ± 2 Ma, whereas the bottom is dated as 314 ± 12 Ma. This bottom section is severely altered and thus the age is likely to be unreliable.	Subaerial weathered basalt flows overlying Precambrian basement. Lithologically similar to the igneous rocks in Bjarni H-81, and thus can be considered part of the Alexis Formation.
Roberval K-92	3188 m–3544 m	n/a	undated	This is the thickest recorded section of the Alexis Formation (Ainsworth et al., 2014).
Rut H-11	Tuff top at 4432 m and “Diabase intrusive” 4451 m C-NLOPB (2007)	n/a	undated	Igneous rocks are noted twice in the Canada-Newfoundland and Labrador Offshore Petroleum Board (2007) report: Tuff top at 4432 m and “Diabase intrusive” at 4451 m.
*Snorri J-90	3150 m–3061 m (Umpleby, 1979)	palynology	Valanginian to Barremian	A series of graywackes, sands, silts, and coal beds interpreted to be derived from volcanic rocks that may be coeval with the Alexis Formation but should not be referred to as part of the Alexis Formation (McWhae et al., 1980).

Note: Summary of occurrences of volcanic rocks in offshore wells on the Labrador shelf well depths are from C-NLOPB (2007); all other data and information are from Umpleby (1979) and references therein, unless otherwise stated.
*Indicates the presence of sediments potentially derived from igneous rocks. n/a—not applicable as the sample has not been dated.

of a beach (Fig. 4) that marks the intersection between a large linear gully that extends 1 km inland on a bearing of 198°, and the western coast of the peninsula. The dikes that provided samples AP1-S1 and AP1-S2 are well exposed, but the dike from which AP1-S3 was collected is only fully exposed during low tide.

AP1-S1 and AP1-S2 were collected from two different parallel dikes in an approximately north-south orientation (Fig. 4), and are ~1 m and ~2 m thick, respectively. The dike that provided sample AP1-S3 is oriented approximately east-west and is much smaller than the north-south dikes, being only ~30 cm wide. The dike from which AP1-S3 was obtained is crosscut by the dike from which AP1-S2 was obtained. The age relationship between AP1-S1 and AP1-S2 could not be determined from field relationships.

Ford's Bight

Ford's Bight is the elongate bay between Ford's Bight Point and Cape Strawberry, where three of the nine occurrences of Early Cretaceous magmatism reported by Tappe et al. (2007) are located (Fig. 3). Samples in this study with the prefix AP2 were collected at the Tappe et al. (2007) location ST103 on the eastern side of Ford's Bight (Figs. 3 and 5A), with the exception of AP2-S6, which was collected 45 m away from AP2 on a bearing of 025° (Fig. 5B). At the location of AP2 (Fig. 5B), a poorly exposed outcrop within the intertidal range (Figs. 5C, 5D) contained two dikes (sites of samples AP2-S1 and AP2-S2), within a diatreme breccia (samples AP2-S5 and AP2-S6) in proximity to exposed metamorphosed basement (samples AP2-S3 and AP2-S4) (Fig. 5C). An overview of the spatial relationship between the lithologies at AP2 is provided in Figures 5B and 5C. Although we visited sites ST100, ST102, and ST103 (Fig. 5A) during our field study, no in situ outcrop was found at ST100 and ST102; however, small boulders, as wide as 1 m, of the breccia material similar to that observed in samples AP2-S5 and AP2-S6 were observed at these locations.

The dike from which sample AP2-S1 (Fig. 5) was collected (dike 1) is oriented approximately north-south, whereas the dike from which sample AP2-S2 was obtained (dike 2) is oriented approximately east-west. Both dikes vary in thickness along their observable length; dike 1 varies in thickness from 25 to 40 cm and dike 2 varies from 20 to 30 cm. At the AP2 location it was observed that dike 2 crosscuts dike 1, and thus the east-west–oriented dike 2 is younger.

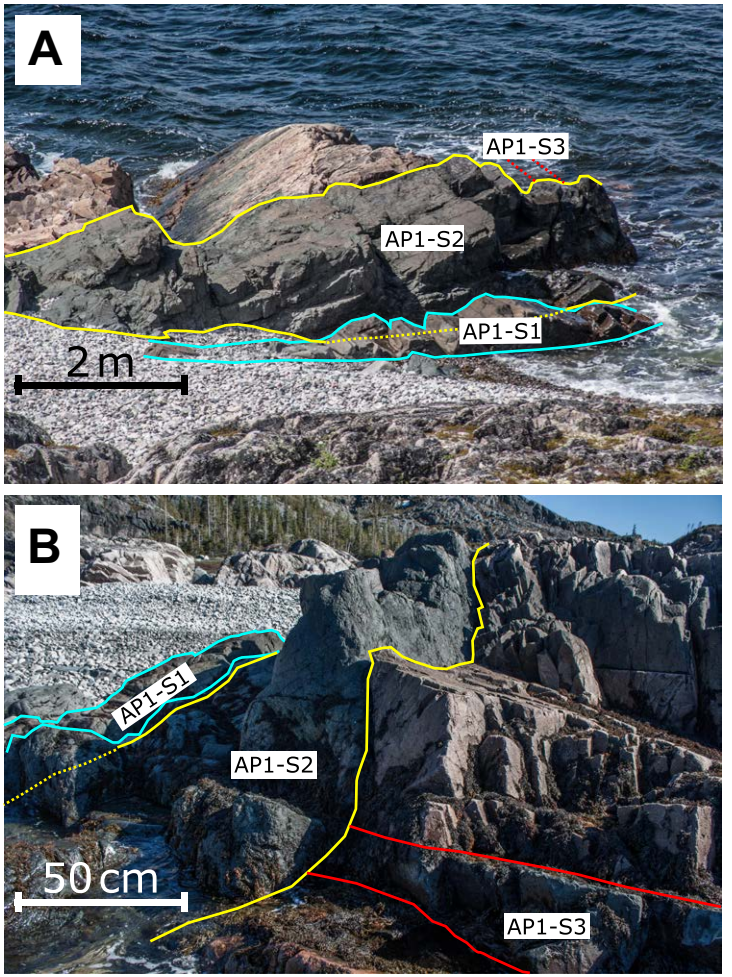

Figure 4. (A) Looking west onto the location AP1 in which three dike samples were analyzed during the study (AP1-S1, AP1-S2, AP1-S3). (B) Looking southeast.

Cape Strawberry

Cape Strawberry is a large headland between Ford's Bight and Big Bight to the northeast of Makkovik. Tappe et al. (2007) described Early Cretaceous magmatism on Cape Strawberry at two locations (ST254 and ST253; Fig. 3). We collected sample AP3-S1 in proximity to ST253 (Fig. 6). ST254 is the location of the only sample in the Early Cretaceous suite that was been dated by $^{40}Ar/^{39}Ar$ methods (141.6 ± 1.0 Ma) by Tappe et al. (2007), and it is also the only location situated inland (Fig. 3). While it is an area of relatively good exposure (Fig. 7) of the 1720 Ma Cape Strawberry Granite (Hinchey, 2013), no nephelinite dikes were observed at this location or anywhere in the vicinity. Thus we were unable to establish field relationships or acquire an equivalent sample for further analysis.

North of Ikey's Point

Ikey's Point is located on the southeastern side of the large peninsula north of Makkovik (Fig. 3). Two dike samples were collected from the area north of Ikey's Point, at the site of previously reported Mesozoic magmatism, and are denoted with the prefix AP4 (Fig. 8). Sample AP4-S1 was collected ~15 m south of ST245, and sample AP4-S2 was collected on a separate dike a further 5 m south of AP4-S1.

Samples AP4-S1 and AP4-S2 are both oriented approximately east-west and display multiple bridge structures (Fig. 8C). The dikes are <13 cm and 25 cm thick for AP4-S1 and AP4-S2, respectively. No crosscutting relationships were observed between AP4-S1 and AP4-S2, thus relative ages could not be determined for the AP4 dikes.

Structural Analysis

An overview of the orientations of the dikes sampled during this study is provided in Figure 9. AP3-S1 is not included in Figure 9 because this sample was obtained from a boulder (Fig. 6B). Figure 9A demonstrates that the dikes sampled by this study do not appear to be part of a singular, systematic dike swarm. Figure 9B demonstrates that none of the dikes analyzed during our study at locations where Mesozoic magmatism has been documented previously are margin parallel, i.e., striking 130°–150°. Margin-parallel orientations might be the predominant trend expected for dikes intruded during rifting, unless a stress reorientation occurred at the rift margin (e.g., Philippon et al., 2015).

Lithological Descriptions and XRF Analysis

In the following section lithologies are described and the results of XRF analysis (Supplemental Materials 3[3]) on the samples obtained by this study are presented. Thin sections in both plane and cross-polarized light are presented in Figure 10; full descriptions to complement those given in this section are provided in the Supplemental Materials 1 (see footnote 1).

Makkovik Peninsula

The gray dike from which sample AP1-S1 was obtained has an extremely fine-grained groundmass that surrounds a main phenocryst phase of clinopyroxene (60%), which is generally arranged into star-shaped clusters of two or more crystals. Highly altered olivine (15%) is also present, along with apatite (<5%), amphibole (<5%), and biotite (<5%). Some vesicles infilled with calcite were as much as 6 mm wide, but most were ~2 mm wide.

Supplementary information 3: XRF analysis and datasets

XRF (X-ray fluorescence) major element analysis was undertaken at the University of Leicester, UK to determine the weight percent of major elements as oxides. The XRF laboratory at the University of Leicester operates a PANalytical Axios Advanced X-Ray Fluoresence spectrometer which runs a 4Kw Rhodium (Rh) anode end window super sharp ceramic technology X-Ray tube. The major element analysis was performed on fused beads to eliminate mineralogical effects and reduce inter-element effects.

Other datasets used by this study include: the NOAA total sediment thickness data Version 2 (Whittaker et al., 2013); and Smith and Sandwell global topography and Bathymetry Version 18.1 (Smith and Sandwell, 1997). Our investigation into offshore sediment distribution utilises Version 2 of the NOAA total sediment thickness dataset despite the update of the original only applying to the Australia-Antarctic region as this was the latest version available at the time of this work. The NOAA total sediment thickness dataset has a grid resolution of five by five arc-minutes, with the data contributing to this dataset obtained from sources including; previously published isopach maps, ocean drilling results and seismic reflection profiles. Version 18.1 of the global topography and bathymetry data (Smith and Sandwell, 1997) dataset is primarily sourced from multibeam cruise data, supplemented by Version 23 (Sandwell et al., 2014) of the satellite derived free air gravity.

[3]Supplemental Materials 3. X-Ray Fluorescence analysis and other datasets. Please visit http://dx.doi.org/10.1130/GES01341.S3 or the full-text article on www.gsapubs.org to view Supplemental Materials 3.

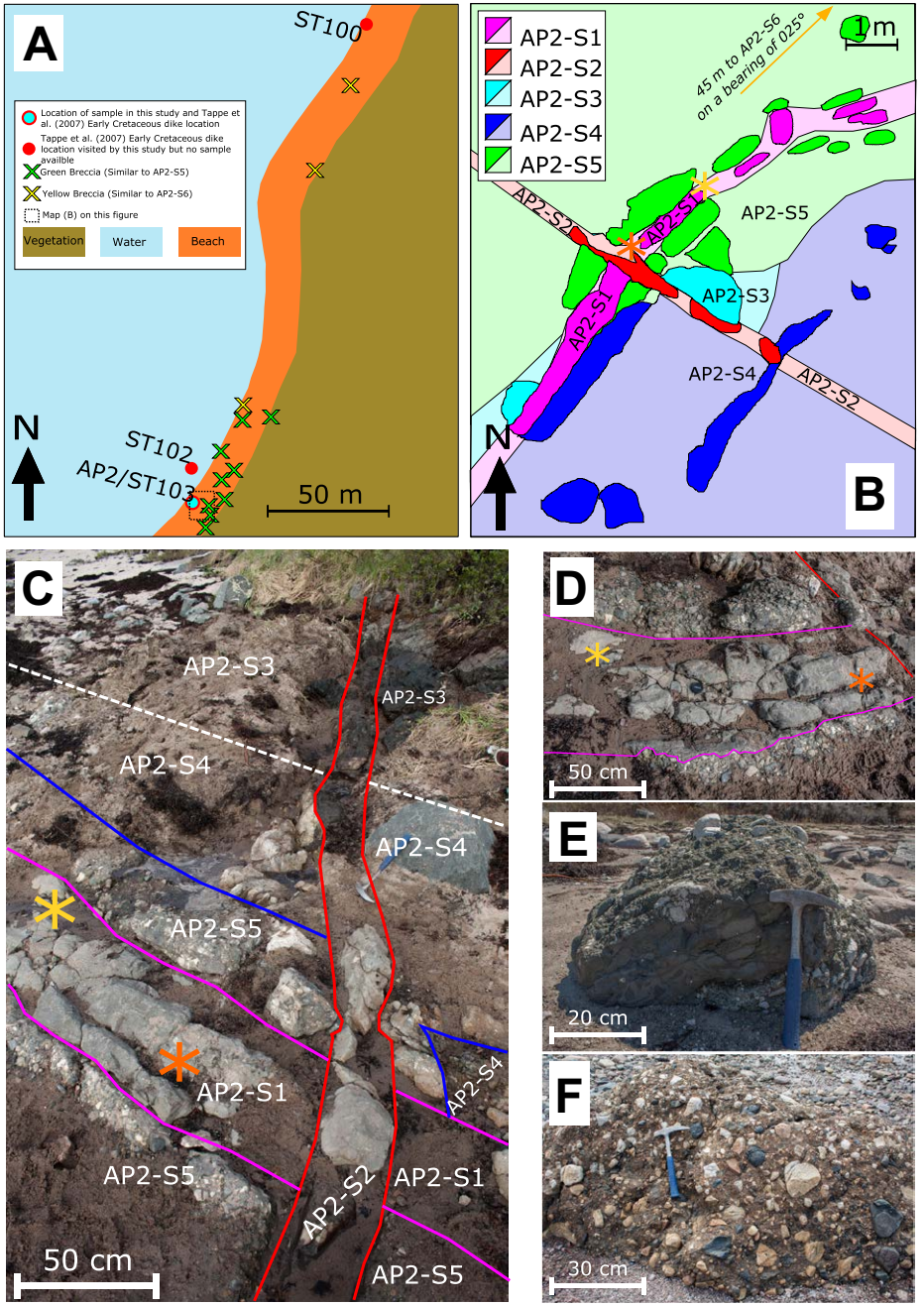

Figure 5. (A) An overview of occurrences of diatreme breccia in Ford's Bight along with the locations of samples collected during this study and Tappe et al. (2007). For the location of the samples on this inset within Ford's Bight, see Figure 3. Differentiation is made between a green diatreme breccia that resembles AP2-S5 (green cross) and one that is more yellow in color, similar to AP2-S6 (yellow cross). Many of the occurrences shown are not in situ. (B) The spatial relationship between the different lithologies described at AP2. (C) Looking southeast onto the two small (<50 cm) crosscutting melilitite dikes (samples AP2-S1 and AP2-S2) within the Ford's Bight diatreme. (D) The contact between dike 1 (sample AP1-S1) and the surrounding diatreme breccia (sample AP2-S5) looking toward the south. (E) Boulder on the beach in Ford's Bight looking west comprising green diatreme breccia (similar to AP2-S5) but with an exceptionally large inclusion of mafic igneous material. (F) Possible in situ outcrop similar to sample AP2-S6 in Ford's Bight looking west. In C and D, purple and red outlines are used to denote the contacts of the dikes from which the samples AP2-S1 and AP2-S2, respectively, were obtained with the breccia and the metamorphosed basement. The blue line in C and D is the contact between the breccia and the basement, whereas the dashed white line represents the boundary between the quartzite basement and an amphibolite dike also forming part of the basement. The orange and yellow stars in B, C, and D are located at the same point for reference between these subfigures.

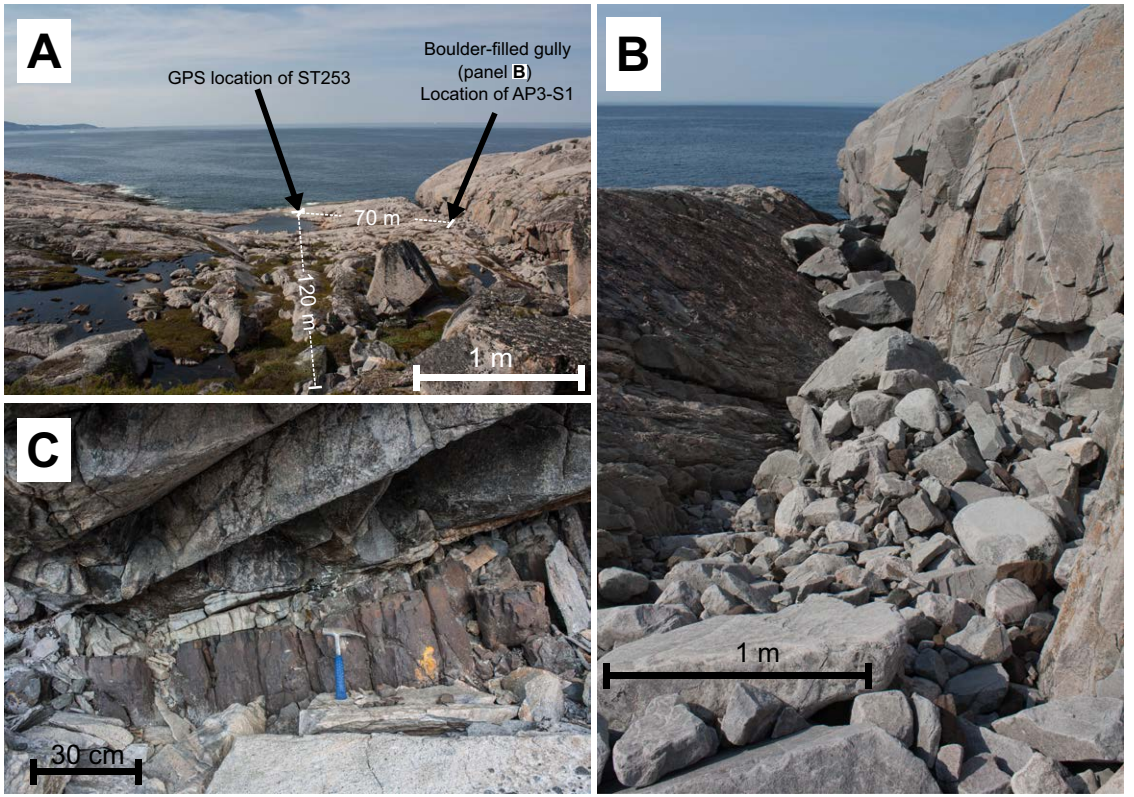

Figure 6. (A) An overview looking north of the area surrounding the global positioning system (GPS) location of ST253 in Tappe et al. (2007) taken from the location of the in situ dike shown in C. (B) Looking north onto out of situ boulders in the gully 70 m away from ST253. Two rock types of boulders were present in this gully: (1) granite and (2) olivine clinopyroxenite. Our sample AP3-S1 is olivine clinopyroxenite. (C) A relatively good exposure of in situ dike 120 m away on a bearing of 170° from AP2-ST253, which may have been part of the dike contributing to the boulders in the gully.

Figure 7. Looking northwest from the location of sample ST254. A good exposure of the Cape Strawberry Granite was observed at ST254, but no nephelinite dikes were observed at this location. This is the location of the only sample $^{40}Ar/^{39}Ar$ dated by Tappe et al. (2007), to which the rest of the Early Cretaceous nephelinite suite is tied.

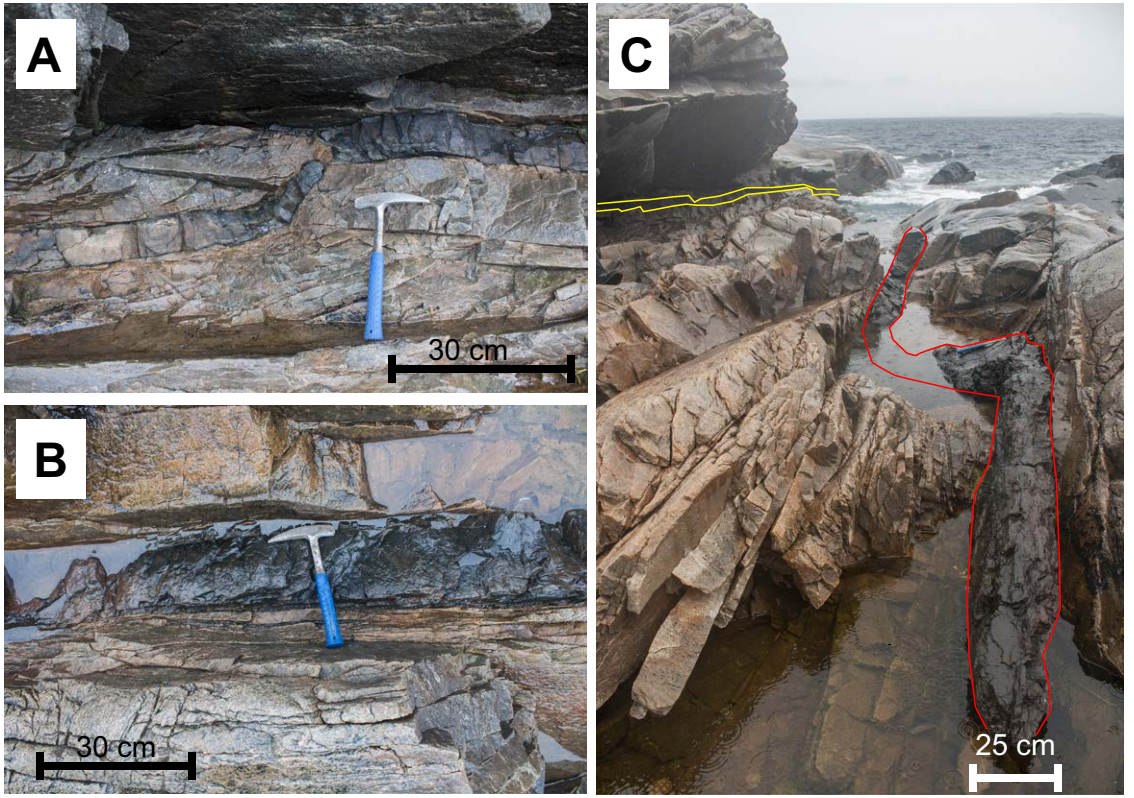

Figure 8. (A) Looking north toward a bridge structure in a small dike (sample AP4-S1) observed 15 m south of the global positioning system location of ST245. (B) 17 m away from ST245 looking down (north up) onto the other dike observed at this location (sample AP4-S2). (C) Looking east onto location AP4 depicting dikes from which samples AP4-S1 (yellow outline) and AP4-S2 (red outline) were obtained. The dike from which sample AP4-S2 was obtained also contains a bridge structure.

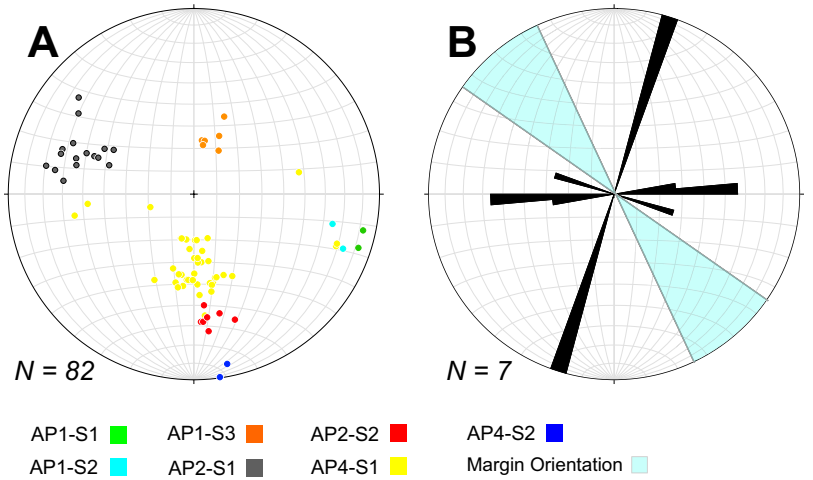

Figure 9. (A) Stereonet of poles to planes for the dike contacts at the sample localities. (B) Rose diagram using 5° bins of the dike contacts using the mean value of each dike contact data set plotted alongside the margin orientation (130° and 150°) derived using the modern coastline on satellite imagery.

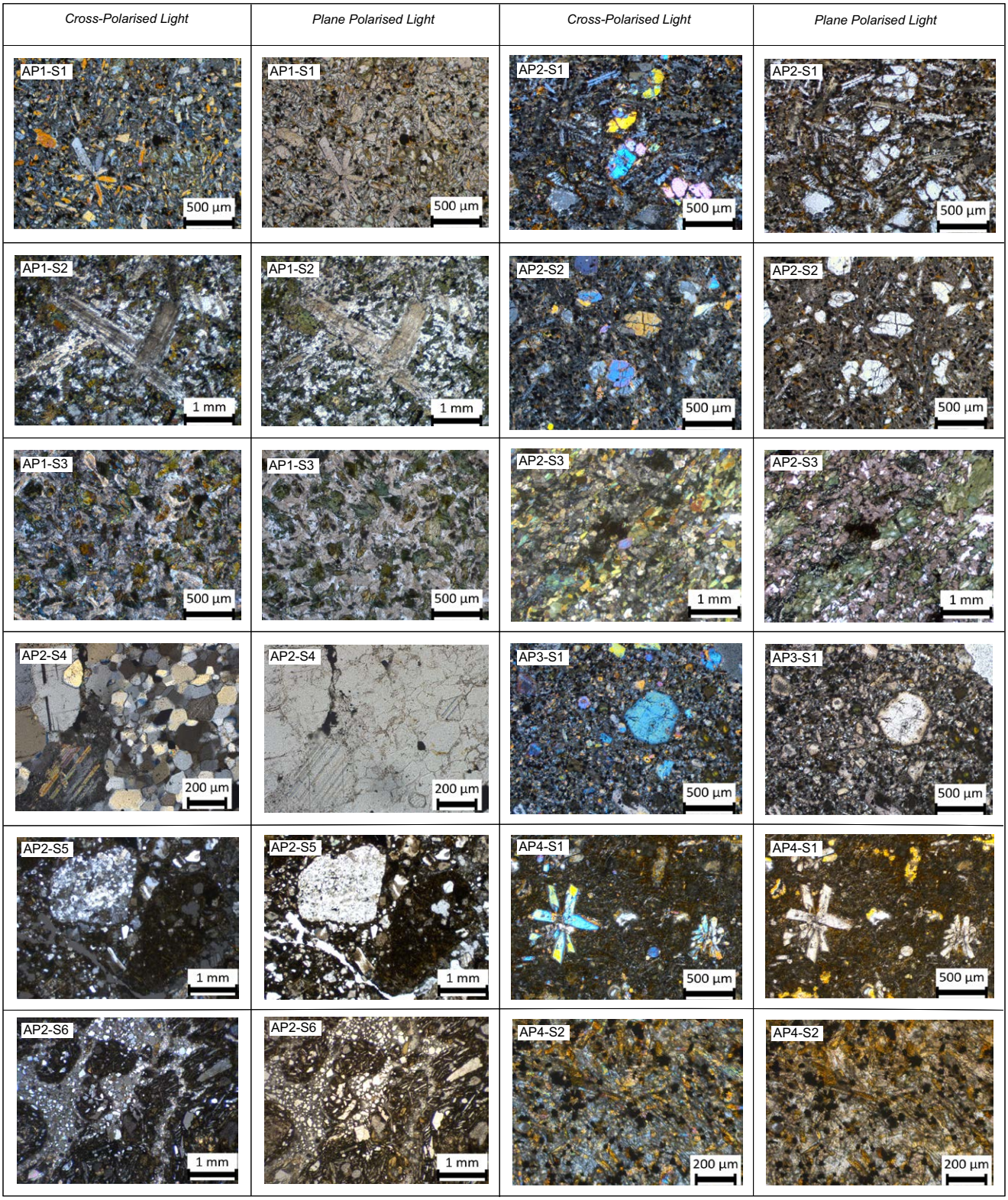

Figure 10. Thin section micrographs in both plane and cross-polarized light for all the samples described herein.

There is no observable metamorphic mineral fabric in AP1-S1. The SiO_2 content of sample AP1-S1 is too low to use the total alkalies versus silica (TAS) classification (Le Bas et al., 1986), but it can be classified as a lamprophyre (Woolley et al., 1996; Rock, 1986) due to the mineral assemblage and composition. Lamprophyre dikes are well studied and known to be extensive in the area (Foley, 1989).

Sample AP1-S2 was collected from a dark green dike. The most abundant mineral phase is chlorite (50%), which occurs as clusters of multiple crystals in the groundmass. This sample also contains altered plagioclase (30%), amphibole (10%), and apatite (<2%). No metamorphic mineral fabric was observed in sample AP1-S2. Sample AP1-S2 was classified as a basanite according to the TAS classification (Le Bas et al., 1986).

The dike from which sample AP1-S3 was obtained has a red-brown weathered surface and a blue-gray clean surface. The most abundant mineral phase in AP1-S3 is plagioclase (60%) occurring as highly altered interlocking crystals. Chlorite (25%) is the next most abundant mineral phase and occurs as both individual crystals and clusters. Other minerals present with abundances <5% in sample AP1-S3 include: amphibole, titanite, apatite, and pyrite. As with the other two samples collected at AP1, no mineral fabric is present in AP1-S3. Sample AP1-S3 was classified as a basaltic trachyandesite according to the TAS classification (Le Bas et al., 1986).

In addition to the different mineral assemblages, all the samples analyzed from the AP1 location have notably different compositions according to the XRF data (Table 4) with the alkali ($Na_2O + K_2O$) content of the AP1 samples not being as variable as the SiO_2 content (Fig. 11). The XRF data from the Makkovik Peninsula shows that SiO_2 content is lowest in AP1-S1 and highest in AP1-S3, which is the most felsic of all the samples analyzed. The sample with the composition most similar to the data collected by Tappe et al. (2007) is AP1-S1. In summary, the AP1 samples (AP1-S1, AP1-S2, and AP1-S3) have been classified as olivine lamprophyre, basanite, and basaltic trachyandesite, respectively. Of particular note, however, was the absence of the mineral phase nepheline in all the samples collected at this location.

Ford's Bight

Samples AP2-S1 and AP2-S2 were obtained from two separate dikes but are virtually indistinguishable from one another in thin section (Fig. 10), both texturally and mineralogically. The main mineral phases in both AP2-S1 and AP2-S2 are melilitite (70%) and olivine (20%), resulting in our classification of these dikes as olivine melilitite according to the classification of Woolley et al. (1996). Olivine melilitite is the expected composition at this location according to previous work by Tappe et al. (2007). No metamorphic mineral fabric was observed in either AP2-S1 or AP2-S2.

The XRF major element analysis of AP2-S1 and AP2-S2 demonstrates that these samples have very similar compositions (Fig. 11; Table 4). There are, however, several small, but notable compositional differences between these two dikes in that sample AP2-S1 has slightly higher SiO_2 and total alkali values than sample AP2-S2 (Fig. 11). Comparison of the major element XRF data obtained from our AP2 dike samples (AP2-S1 and AP2-S2) with the major element composition of sample ST103 (Fig. 11) obtained by Tappe et al. (2007) demonstrates that all three of these samples have very similar compositions and may represent samples collected from the same dike.

The two types of metamorphosed basement observed at the AP2 sample sites are an amphibolite (sample AP2-S3) and quartzite (sample AP2-S4) (Figs. 5B, 5C). Sample AP2-S3 contains amphibole (45%), highly altered plagioclase (35%), epidote (10%), and chlorite (10%). Sample AP2-S4 contains quartz (80%),

TABLE 4. X-RAY FLUORESCENCE DATA

	AP1-S1	AP1-S2	AP1-S3	AP2-S1	AP2-S2	AP3-S1	AP4-S1	AP4-S2
SiO_2	38.93	44.96	53.66	34.43	32.17	39.19	42.62	43.98
TiO_2	2.63	3.31	0.74	2.10	2.15	2.44	1.92	1.90
Al_2O_3	12.93	13.42	17.15	10.79	10.18	12.34	14.33	14.68
Fe_2O_3	13.77	16.91	9.45	11.43	12.04	12.43	12.03	11.87
MnO	0.23	0.33	0.21	0.23	0.24	0.21	0.21	0.18
MgO	8.09	5.36	4.85	10.66	10.96	9.07	6.93	8.45
CaO	11.25	6.94	5.97	16.00	14.52	13.55	10.19	9.99
Na_2O	2.78	3.25	3.14	2.00	2.22	2.26	2.67	2.93
K_2O	1.91	1.00	2.39	2.57	1.99	1.73	1.54	1.75
P_2O_5	1.02	1.86	0.18	2.31	2.58	0.86	0.65	0.66
SO_3	0.33	0.01	<0.002	0.82	1.04	0.20	0.15	0.16
CrO_3	0.02	0.00	<0.001	0.02	0.02	0.04	0.03	0.03
NiO	0.01	0.00	0.00	0.02	0.02	0.02	0.02	0.02
LOI	5.61	2.27	1.88	5.29	8.40	5.18	6.15	2.73
Total	99.51	99.63	99.62	98.67	98.52	99.51	99.44	99.34

Note: The results of X-ray fluorescence analyses for major element oxides in the dike samples (AP prefix) collected during this study. LOI—loss on ignition.

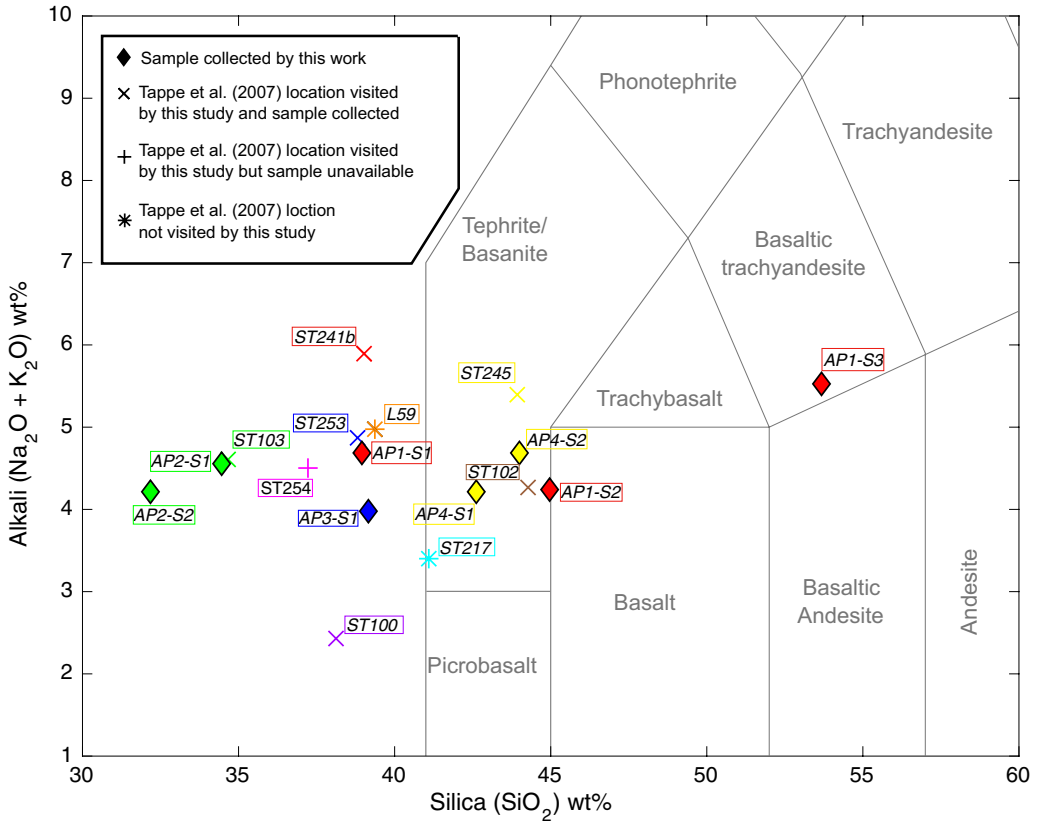

Figure 11. Total alkalies versus silica plot (Le Bas et al., 1986) depicting the dike samples collected and analyzed by this study along with the Early Cretaceous nephelinite suite of Tappe et al. (2007). Samples of the same color represent the same location.

garnet (7%), calcite (7%), plagioclase (4%), and opaque minerals (2%). Both samples AP2-S3 and AP2-S4 display a distinct metamorphic mineral fabric (Supplemental Materials 1; see footnote 1). The exposure of these lithologies is limited to a few square meters. However, both dikes (samples AP2-S1 and AP2-S2) were observed to continue into these metamorphosed units (Figs. 5B, 5C). The extent of the continuation of the younger dikes into the metamorphic basement could not be quantified due to lack of exposure.

The final lithology present at the AP2 sample site is a diatreme breccia that hosts the two dikes (samples AP2-S1 and AP2-S2). The diatreme breccia was observed as two distinct varieties, as characterized in samples AP2-S5 and AP2-S6. Sample AP2-S5 was taken from the breccia located at AP2 (Figs. 5C, 5D) but is also representative of the nearby boulders on the beach (Figs. 5A, 5E), whereas sample AP2-S6 was taken from a large boulder 45 m away from the rest of the AP2 samples on a bearing of 025° (Fig. 5E). AP2-S5 is green in outcrop, whereas AP2-S6 is dark yellow. This color variation is a reflection of AP2-S5 having a higher ratio of clasts to matrix compared to AP2-S6. The clast types found in both the breccia samples are very similar, mostly consisting of highly variable amounts of quartzite basement, amphibolite dike, olivine melilitite dike, and fragments of individual crystals primarily including but not limited to quartz, olivine, microcline feldspar, and plagioclase. Most clasts are angular, except the melilitite inclusions, which are typically rounded with an undulose texture at their perimeters. Clast size in both AP2-S5 and AP2-S6 is extremely variable, ranging from <0.1 mm to >10 cm. The matrix in both the AP2-S5 and AP2-S6 samples is predominantly carbonate.

Cape Strawberry

The eastern tip of Cape Strawberry (AP3, Fig. 3) is an area of exceptionally well exposed basement rocks (Fig. 6A) that were not observed to be intruded by dikes of any type. However, a distinct gully (Fig. 6B) filled with two types of boulders (granite and a mafic igneous material) was noted. The mafic igneous

material in this gully provided sample AP3-S1. The boulder from which AP3-S1 was obtained has a red-brown weathered surface and a dark gray clean surface. In hand specimen, calcite-infilled vesicles (to 7 mm) and olivine phenocrysts are visible. The dominant mineral phases in this sample are olivine, both fresh (20%) and serpentinized (15%), along with clinopyroxene in the groundmass (25%) and as a larger crystal phase (15%). The SiO_2 content of sample AP1-S1 is too low to use the TAS classification (Le Bas et al., 1986), but it can be classified as a lamprophyre (Woolley et al., 1996; Rock, 1986) due to the mineral assemblage and composition.

The XRF major element analysis of AP3-S1 (Fig. 11; Table 4) demonstrates that it is compositionally very similar to the igneous rocks sampled by Tappe et al. (2007) near this location, having a nearly identical SiO_2 value but slightly lower alkali content. However, given that AP3-S1 does not contain the mineral phase nepheline, as expected the dike from which AP3-S1 was collected does not belong to the nephelinite suite. The nearest in situ outcrop of the olivine lamprophyre composing the boulders in the gully was 120 m away from the location of ST253 (Fig. 6C).

North of Ikey's Point

In outcrop the weathered surface of the dike from which sample AP4-S1 was obtained varies from dark gray through to reddish-brown. The dominant mineral phase in sample AP4-S1 is clinopyroxene, occurring in both the groundmass (40%) and as larger crystals (20%). Olivine also occurs in AP4-S1 as a serpentinized (10%) and unaltered variety (5%). Vesicles with a calcite infill are common in AP4-S1. The XRF data obtained from AP4-S1 (Fig. 11; Table 4) indicate that this sample is a basanite according to the TAS classification of Le Bas et al. (1986).

Sample AP4-S2 was obtained from a separate dike 5 m south of the dike from which sample AP4-S1 was collected (Fig. 8). This second dike is slightly wider, 25 cm; in outcrop it is brown and more fractured and weathered than the previous dike. Sample AP4-S2 contains clinopyroxene (50%), plagioclase (20%), and olivine. Some minor opaque minerals are also present in AP4-S2 along with numerous calcite-infilled vesicles. AP4-S2 was classified as a basanite based on the major element composition derived using XRF and plotted on a TAS diagram (Fig. 11).

Although both AP4-S1 and AP4-S2 were classified as basanites, slight compositional differences between the two samples are apparent in the XRF major element data (Fig. 11; Table 4). These results show that AP4-S2 has a slightly higher SiO_2 and alkali content than AP4-S1. Given this slight compositional variation between these two dikes, it is very likely that these two dikes represent the same magmatic event, particularly given the similar orientations (Fig. 9). Overall our observations and analysis of the data collected at the AP4 location in the area north of Ikey's Point indicate that Early Cretaceous magmatism north of Ikey's Point may comprise two small (13 and 25 cm wide) basanite dikes.

BATHYMETRY, SEDIMENT THICKNESS, AND CRUSTAL STRUCTURE

An analysis of the degree of symmetry displayed in the bathymetry, sediment thickness, and crustal structure of the conjugate margins of the Labrador Sea is presented here to complement the asymmetry shown in the magmatic distribution in the preceding discussion (Fig. 12). To assess the margin symmetry displayed in the NOAA total sediment thickness (Whittaker et al., 2013) data and the global bathymetry data set (Smith and Sandwell, 1997), profiles approximating the traces of seismic lines BGR77–17, BGR77–21, and BGR77–12 (Fig. 1A) were created (Fig. 12). These profiles were then extended along the same trajectory as their corresponding seismic line until they reached the modern coastline, thus allowing us to study the full width of the continental shelf. Our observations of conjugate margin asymmetry are summarized in Table 5.

Figure 12A displays the Smith and Sandwell (1997) global bathymetry data set for the Labrador Sea. The Labrador Sea has a maximum depth of ~3500 m, with water depths mostly <200 m on both continental shelves (Fig. 12B). The continental shelf is ~150 km wide offshore Labrador compared to southwest Greenland, where it is mostly <50 km wide. The profiles (Fig. 12B) show that the continental shelf remains relatively consistent in width along the southwest Greenland margin, whereas on the Labrador margin it increases to the north.

The distribution of sediments between the margins of the Labrador Sea is highly asymmetric (Welford and Hall, 2013). The Labrador margin displays considerably thicker and more extensive synrift and postrift sedimentary sequences compared to the southwest Greenland margin (Figs. 12C, 12D, and 13). The Labrador margin is dominated by a large margin-parallel basin containing in excess of ~8000 m of sediments for much of its length (Fig. 12C). This basin is particularly prominent in the central and northern segments of the margin, where isolated areas contain more than ~11,000 m of sediment infill. Even outside this main basin it can be seen that for a large region extending from ~50 km to ~300 km offshore, a more diffuse area containing ~3000–6000 m of sediment infill is present. This region is much wider at the northern end of the margin compared to the south. In contrast, sediment infill on the southwest Greenland margin is significantly thinner and less spatially extensive than its Labrador conjugate. On the southwest Greenland margin sedimentary basins with thicknesses in excess of 4000 m are absent, with most areas containing <2000 m of sedimentary infill. Thus, comparison of sediment thickness along profiles 1, 2, and 3 (Fig. 12D) supports the observation of significantly more sediment deposition on the Labrador margin consistently along the length of the margin. It is interesting that the distance between the start of the profile (modern coastline) and the point of greatest sedimentary thickness appears to decrease from profile 1 in the south to profile 3 in the north. Profiles 1–3 in Figure 12D also demonstrate the differing basin geometry between these conjugate margins. On the Labrador margin the main margin-parallel basin appears to represent a distinct feature compared to the southwest Greenland

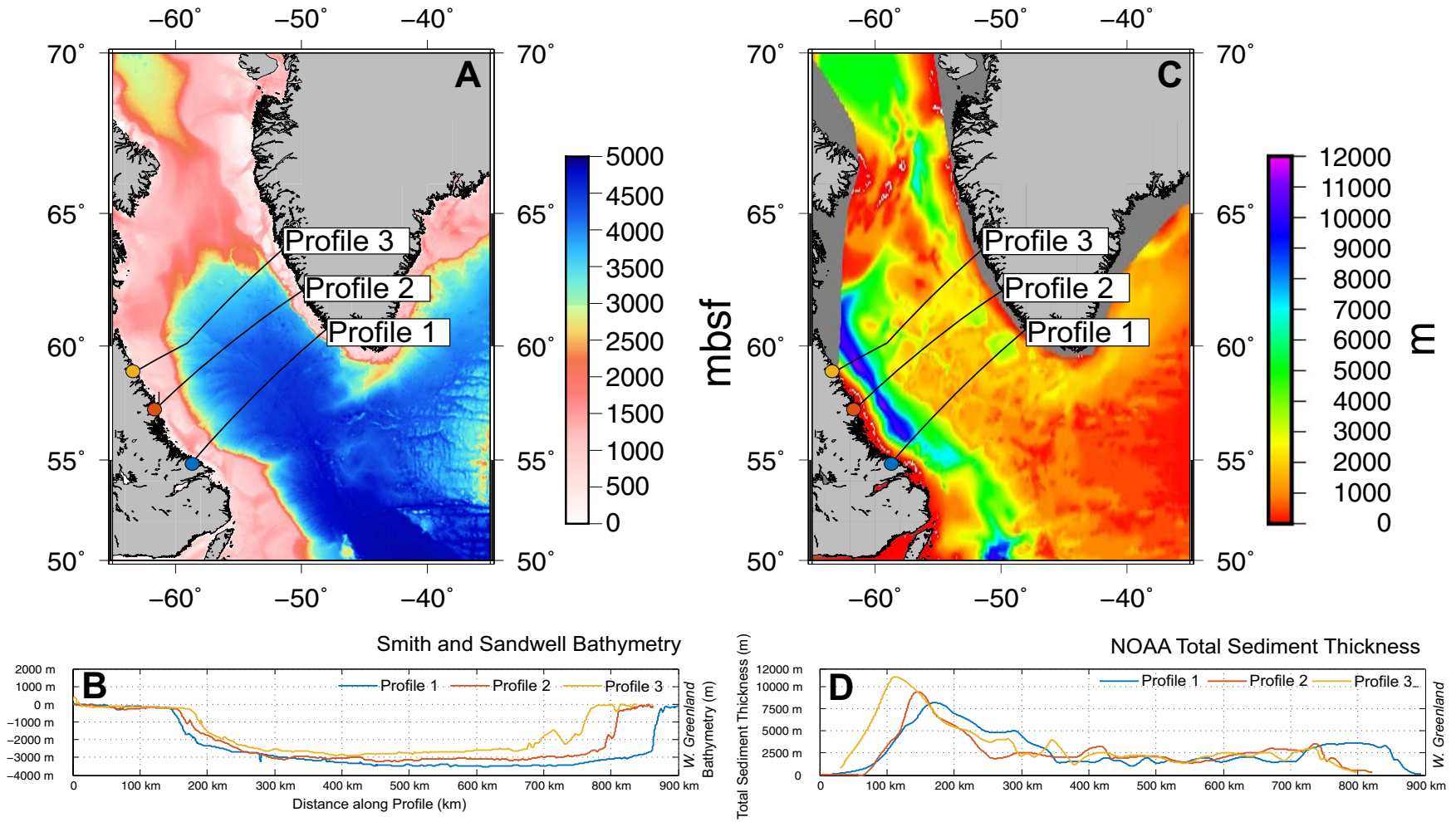

Figure 12. (A) Bathymetry of the Labrador Sea from Smith and Sandwell (1997) data; mbsf—meters below seafloor. (B) Bathymetric transects along profiles 1, 2, and 3. (C) Total sedimentary thickness in the Labrador Sea from the National Oceanic and Atmospheric Administration world's oceans and marginal seas total sedimentary thickness (version 2; Whittaker et al., 2013). (D) Total sedimentary thickness transects along profiles 1, 2, and 3. For C and D, the Labrador end of the transect is at the left (0 km) and the West Greenland end is on the right. Profiles 1, 2, and 3 approximately correspond to the seismic reflection lines BGR77–17, BGR77–21, and BGR77–12, respectively. The profiles used in this study have been extended along the same trajectory as their corresponding seismic line to the present coastline, thus allowing us to study the full width of the continental shelf.

margin where the sedimentary basins, if present, appear to have a less well defined, more diffuse appearance.

The crustal velocity model depicted in Chian et al. (1995b) that incorporates the data from Chian and Louden (1994) was used to assess asymmetry displayed in the crustal structure between the Labrador and southwest Greenland margins (Fig. 14). Previously workers (Keen et al., 1994; Chian and Louden, 1994; Chian et al., 1995a) considered the velocity structure of both the southwest Greenland and Labrador margins to be divided into three distinct zones (Fig. 14).

Zone 1 is characterized as a region that has a typical continental crustal velocity structure. On the Labrador margin zone 1 is ~140 km wide and is characterized by highly extended continental crust that has undergone consider-

TABLE 5. MAJOR STRUCTURAL AND MAGMATIC COMPONENTS OF THE LABRADOR AND SOUTHWEST GREENLAND MARGINS

	Labrador	Southwest Greenland
Continental shelf width (Figs. 4A, 4B)	Wide (~150 km)	Narrow (~50 km)
Maximum offshore sedimentary cover (synrift and postrift) (Figs. 12C, 12D, and Fig. 13)	~12,000 m	~3700 m
Onshore intrusive magmatism	Minor nephelinite suite proposed by Tappe et al. (2007) but disputed in this study	Summarized in Table 2
Offshore magmatism	Alexis formation and other volcanics in offshore wells (Table 3)	Unknown due to absence of offshore wells
Crustal-scale detachment faults	Possibly; inferred by the presence of distinct basin (Welford and Hall, 2013)	No

able subsidence. However, on the southwest Greenland margin zone 1 is only ~70 km wide and has undergone considerably less subsidence (Chian, et al., 1995a). Zone 2 represents a region of transitional crust located oceanward of zone 1 on both margins (Chian et al., 1995a). Compared to zone 1, zone 2 displays similar velocity characteristics, and is ~70–80 km wide on both margins. Zone 2 is characterized by a 5-km-thick region with a high velocity (6.4–7.7 km/s) overlain by a thin (<2 km) low-velocity region (4–5 km km/s). Zone 3 is characterized by typical oceanic crustal velocities and is oceanward of zone 2 on both margins.

DISCUSSION

Comparison of the Composition of the Makkovik Magmatism with Other Rift-Related Magmatism

The XRF results obtained during this study have been compared to other selected occurrences of rift-related magmatism globally (Fig. 15). The Yarmony Mountain lavas of the Rio Grande Rift (Leat et al., 1990) were selected for comparison because they are interpreted to represent small-volume, early rift-

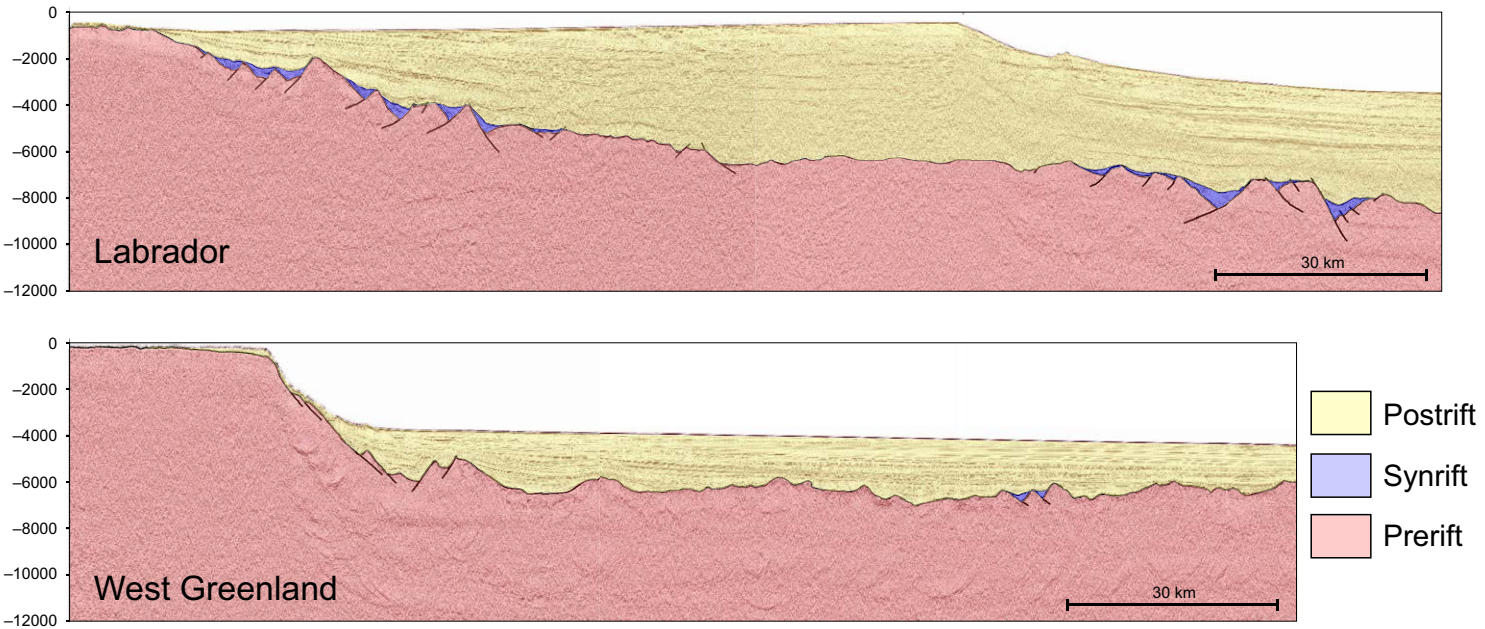

Figure 13. Segments of the two-dimensional seismic reflection profiles 90-3 and 90-1 (Keen et al., 1994) for the Labrador and southwest Greenland margins, respectively, with interpretations of the base postrift and base synrift. The location of these segments is depicted in Figure 1.

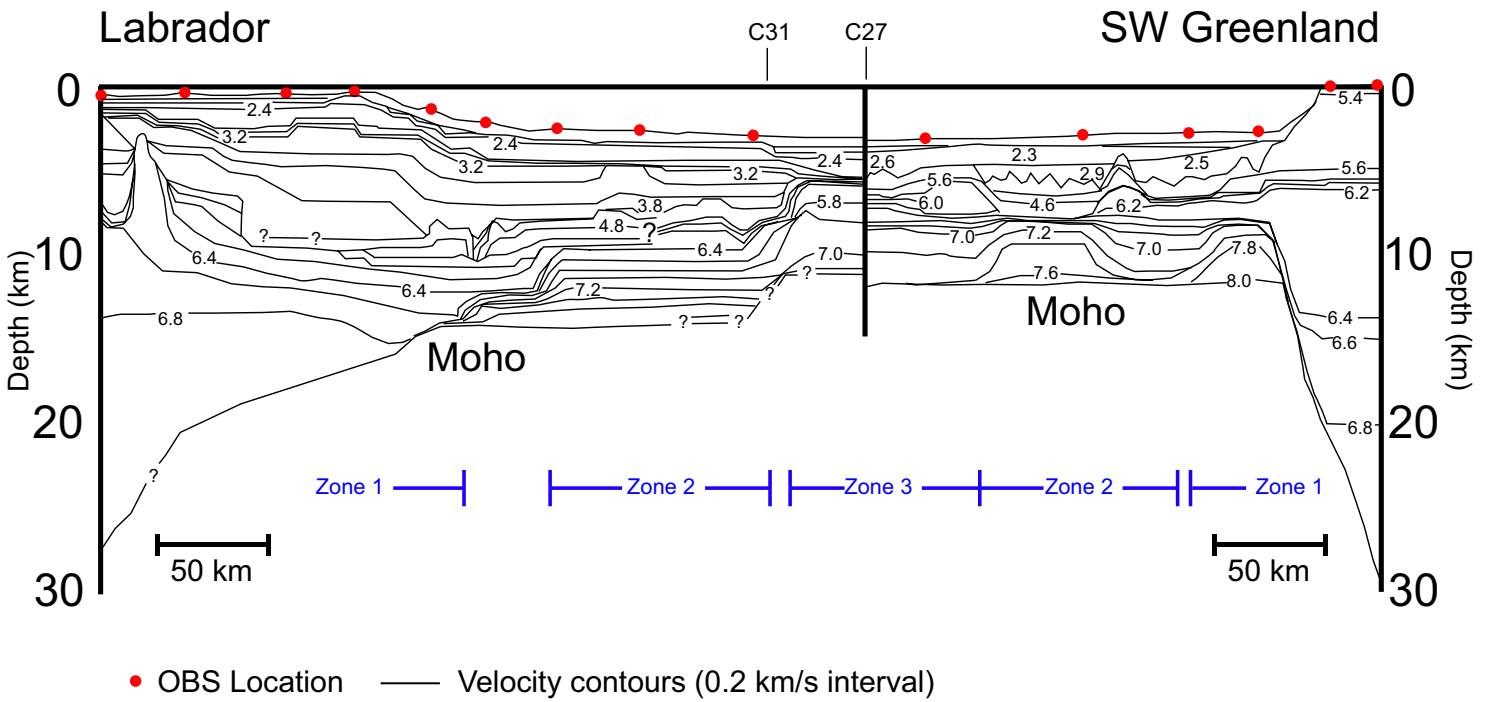

Figure 14. Velocity structure of the margins of the Labrador Sea reconstructed to polarity chron C27 (Danian) reproduced from Chian et al. (1995b). OBS—ocean bottom seismograph.

related melts, and therefore may have been produced in a geological setting similar to that of the proposed Early Cretaceous magmatism near Makkovik (Tappe et al., 2007). The Suez Rift magmatism (Shallaly et al., 2013) was selected because it contains a wide array of rift-related manifestations of magmatism, including sills, dikes, and extrusives. Two magmatic suites attributed to the Central Atlantic Magmatic Province (CAMP) are also included for comparison: Algarve in southern Portugal (Martins et al., 2008) along with the magmatism in Guyana and Guinea (Deckart et al., 2005). The CAMP magmatism was selected because it enables comparison with a widespread rift-related magmatic event that resulted in continental breakup.

Comparing the composition of the Makkovik Early Cretaceous nephelinite suite (Tappe et al., 2007) with other selected occurrences of rift-related magmatism shows that it is compositionally more diverse than any of the other magmatic suites considered (Fig. 15), displaying greater variation in both the alkali and silica values than any of these systems. Although it is extremely unlikely that all of the AP samples belong to the Early Cretaceous nephelinite suite (particularly sample AP1-S3), the more mafic AP samples depict a similar range of silica values to the Early Cretaceous nephelinite suite. The Tappe et al. (2007) samples show considerably higher variation in total alkali values than the AP samples or any of the other data sets included for comparison. The wide range of compositions found in the Early Cretaceous nephelinite suite (Tappe et al., 2007) may imply that not all of the dikes analyzed by the previous work are part of the same event.

Extent of Mesozoic Magmatism around Makkovik

Given the relatively close proximity of Makkovik to observations of Early Cretaceous magmatism in offshore wells (Fig. 1; Table 3), it would not be unreasonable to observe evidence of contemporaneous early rift-related magmatism cropping out onshore. Our field observations, however, indicate that the Early Cretaceous magmatism around Makkovik is volumetrically and spatially extremely minor compared to the numerous stages of extensive, readily observable intrusive magmatism that preceded it (e.g., Foley, 1989) and the well-documented magmatism on the conjugate southwest Greenland margin (Larsen et al., 2009). Although the field study area around Makkovik (Fig. 3) is significantly smaller than the extent of the dikes observed in southwest Greenland, no other evidence for Mesozoic magmatism has been recorded elsewhere onshore Labrador.

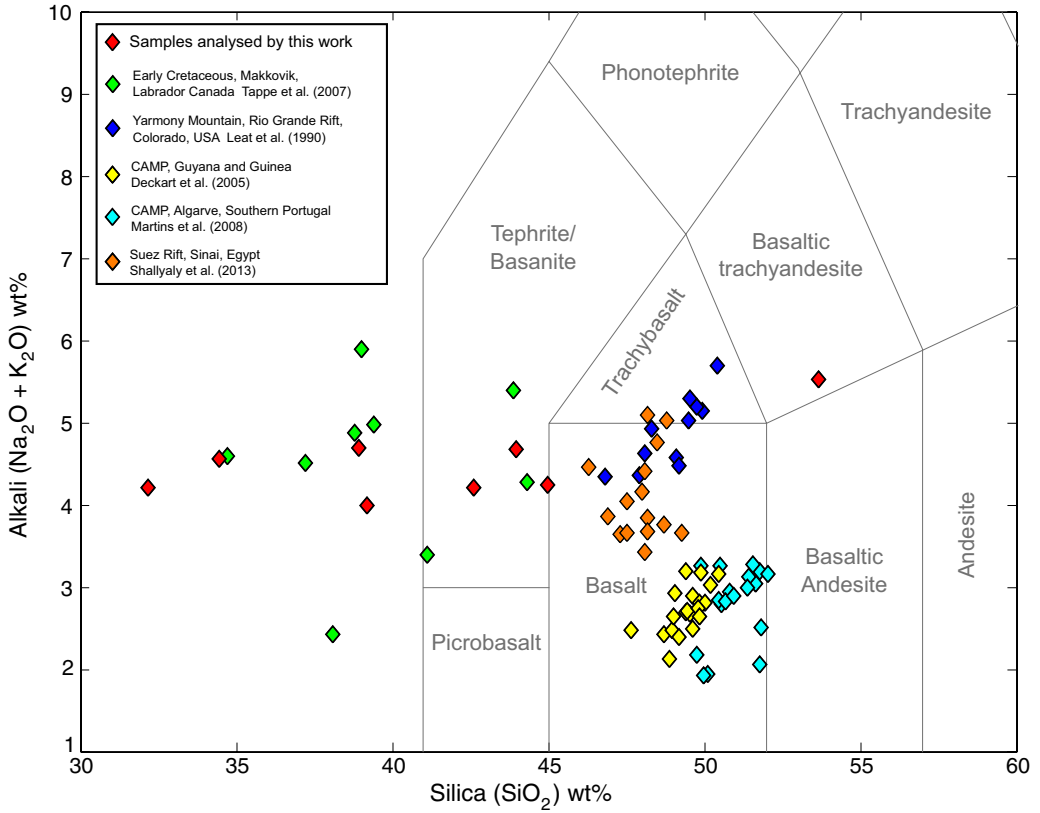

Figure 15. Total alkalies versus silica plot (Le Bas et al., 1986) depicting the dike samples collected and analyzed by this study along with the Early Cretaceous magmatic suite near Makkovik (Tappe et al., 2007), the Rio Grande Rift, Yarmony Mountain lavas (Leat et al., 1990), the Suez Rift (Shallaly et al., 2013), and the Central Atlantic Magmatic Province (CAMP) in Algarve, southern Portugal (Martins et al., 2008) along with Guyana and Guinea (Deckart et al., 2005).

Of the seven sample locations in Tappe et al. (2007) visited during this study none provided clear, undisputable evidence for belonging to a contiguous Early Cretaceous magmatic event. We think it is also exceptionally unlikely that the outcrops were removed by subsequent erosion between this study and the work of Tappe et al. (2007). Our observations on the peninsula north of the town of Makkovik (AP1) and on Cape Strawberry (AP3) did not provide sufficient evidence for the Early Cretaceous magmatism previously described at these locations. The most reliable evidence confirmed by this study for the magmatism characterized by Tappe et al. (2007) as Early Cretaceous was found in Ford's Bight (AP2, Fig. 5) and north of Ikey's Point (AP4, Fig. 8).

Our AP2 sample location in Ford's Bight is in very close proximity to the diatreme originally described as a sedimentary breccia by King and McMillan (1975) and later as a diatreme by Wilton et al. (2002). Our field observations concur with that of Wilton et al. (2002) that the AP2 sample location is part of the previously documented Ford's Bight diatreme. This confirms that of the nine samples stated as belonging to the Mesozoic dike suite in Tappe et al. (2007) (Table 1), three are part of a diatreme, not a dike swarm as previously claimed, with two of the Ford's Bight samples locations not containing in situ outcrop. Within the diatreme there are dikes present, but it is misleading to imply that they are part of a singular geographically widespread intrusive event that can be described as the nephelinite suite. The diatreme was mentioned in Tappe et al. (2007, p. 438) as "poorly described mafic dikes cutting a breccia bed"; however, it is not made clear that this area is either (1) the location of three of their samples or (2) a diatreme rather than a dike swarm. Furthermore, confirming that ST103 is, as expected, an olivine melilitite demonstrates that there is unlikely to be a problem associated with the original acquisition or our use of the coordinates provided by Tappe et al. (2007) and the original characterization of the mineralogy at ST103. The geological context of the dikes needs clarifying, because the observed dikes in Ford's Bight are intrinsically associated with the diatreme (Wilton et al., 2002)

and do not appear to be associated with a regional-scale intrusive event such as that described in Tappe et al. (2007). However, if the biostratigraphic age provided by King and McMillan (1975) of 197–145 Ma is correct, then this is currently the most reliable evidence in the area for Mesozoic magmatism, with the fossils possibly being derived from the maar above the diatreme (White and Ross, 2011).

Our analysis also indicates that one of the dikes north of Ikey's Point at AP4 is likely to be that described and sampled by Tappe et al. (2007), the other basanite dike at this location being part of the same event. However, even if one or both of the dikes at AP4 is the dike analyzed by Tappe et al. (2007), they are extremely small (13 cm and 25 cm wide) and localized.

Comparison of the XRF data with other suites of rift-related magmatism globally has demonstrated that the nephelinite suite (Tappe et al., 2007) is compositionally much more diverse than the other events considered (Fig. 15). This observation provides further evidence that the samples collected by Tappe et al. (2007) might not form part of the same magmatic event.

Overall, our comparison of the field relationships, orientation, mineralogy, and composition of the samples collected at the locations of the samples prefixed with AP2 and AP4, where some evidence for the Early Cretaceous magmatism described by Tappe et al. (2007) was found, suggests that there is no reason to attribute the exceptionally different style of magmatism in Ford's Bight (AP2) and north of Ikey's Point (AP4) to the same event.

Furthermore, given that the one location in this dike suite that was dated by $^{40}Ar/^{39}Ar$ methods by Tappe et al. (2007) (sample ST254) was found to not contain any exposed comparable dikes, the coherence of the proposed Early Cretaceous nephelinite suite as being as a result of a singular magmatic event should be reconsidered. In terms of the age of the nephelinite suite characterized by Tappe et al. (2007), the plateau age from the $^{40}Ar/^{39}Ar$ dating is not defined by a continuous outgassing plateau and the two segments used in each are considerably less than the 50% gas release generally accepted as the hallmark of a reliable step-heating age. Even when the two segments in Tappe et al. (2007) are combined, it seems that the total gas fraction plateau used is only 52%, i.e., only just above 50%. In addition, another problem with the $^{40}Ar/^{39}Ar$ date of Tappe et al. (2007) is the fact that the inverse isochron age is well outside of error and the plateau age is far from the atmospheric value. Thus the $^{40}Ar/^{39}Ar$ age of 142 Ma for sample ST254 is of marginal reliability.

Another aspect of the Early Cretaceous magmatism on the Labrador margin that remains unclear is why the orientations of the dikes observed by Tappe et al. (2007) are described as predominantly east-west. If these dikes are rift related, then they would be expected to have been intruded under the influence of the extensional stress field parallel to the rift axis i.e., coast parallel as they are in southwest Greenland (Larsen et al., 2009). Although the only compositionally appropriate east-west dikes observed by this study were at Ikey's Point (AP4), should a larger suite exist with this orientation it would not be compatible with simple northeast-southwest–trending Mesozoic rifting, culminating in the opening of the Labrador Sea (Abdelmalak et al., 2012).

Implications for Early Rifting of the Labrador Sea Region

The results of this study have demonstrated that considerable asymmetry exists in many aspects of the conjugate margins of the Labrador Sea, including the distribution of rift-related magmatic rocks, the bathymetric expression, the sediment distribution, and the crustal structure. These observations of asymmetry may support a simple shear mode of rifting (Fig. 16). Here we systematically evaluate our observations of asymmetry against the predictions of the Lister et al. (1986) simple shear model of passive margin formation that has been previously applied to explain the observed asymmetry in many conjugate margin pairs and rift systems including the Greenland-Norway conjugate margins (Torske and Prestvik, 1991) and the south Atlantic (Becker et al., 2016). Of particular importance when evaluating the simple shear model (Lister et al., 1986) is whether the polarity of the different aspects of asymmetry all agree with the predictions of the model.

A full comparison of the extent of rift-related magmatism on the margins of the Labrador Sea is inhibited by the absence of well data offshore southwest Greenland (Fig. 1A). The nearest offshore well on the Greenland side of the Labrador Sea is Qulleq-1, which is much farther north in the Davis Strait (Fig. 1A), and is influenced more by transform margin tectonics rather than the rifted margin regime in the Labrador Sea (Wilson et al., 2006).

Although the absence of well data offshore southwest Greenland prevents us from making a full comparison of the volume of rift-related magmatism, this study has shown that the Early Cretaceous magmatism identified onshore in Labrador by Tappe et al. (2007) is considerably less extensive than that observed on the coast parallel dikes onshore in southwest Greenland (Larsen et al., 2009). This allows us to state that there is an asymmetric distribution in the extent of the exposed onshore Mesozoic magmatism between the Labrador margin and the southwest Greenland margin. This asymmetric distribution of rift-related magmatism supports the predictions of the simple shear model of passive margin formation, whereby the center of the melt generation may have been offset from the central rift axis (Fig. 16A), resulting in a greater amount of melt on the upper plate southwest Greenland margin (Fig. 16A). That is, the greater extent of coast-parallel dikes in southwest Greenland suggests that the southwest Greenland margin may represent the upper plate margin in a simple shear system.

Magmatic underplating on the upper plate margin is another prediction of the Lister et al. (1986) simple shear model. High-velocity zones have been observed in seismic studies on these conjugate margins, but whether they represent serpentinized peridotite (Reid and Keen, 1990) or magmatic underplating (Keen et al., 1994) is debatable (Chian et al., 1995b). Chian et al. (1995b) determined that serpentinized peridotite is more consistent with the observations than magmatic underplating. Due to the inconclusive nature of these observations, we have chosen not to use them as evidence in our analysis of the applicability of the simple shear model (Lister et al., 1986) to the margins of the Labrador Sea. However, magmatic underplating might help to explain the absence of significant postrift sedimentary basins offshore southwest Green-

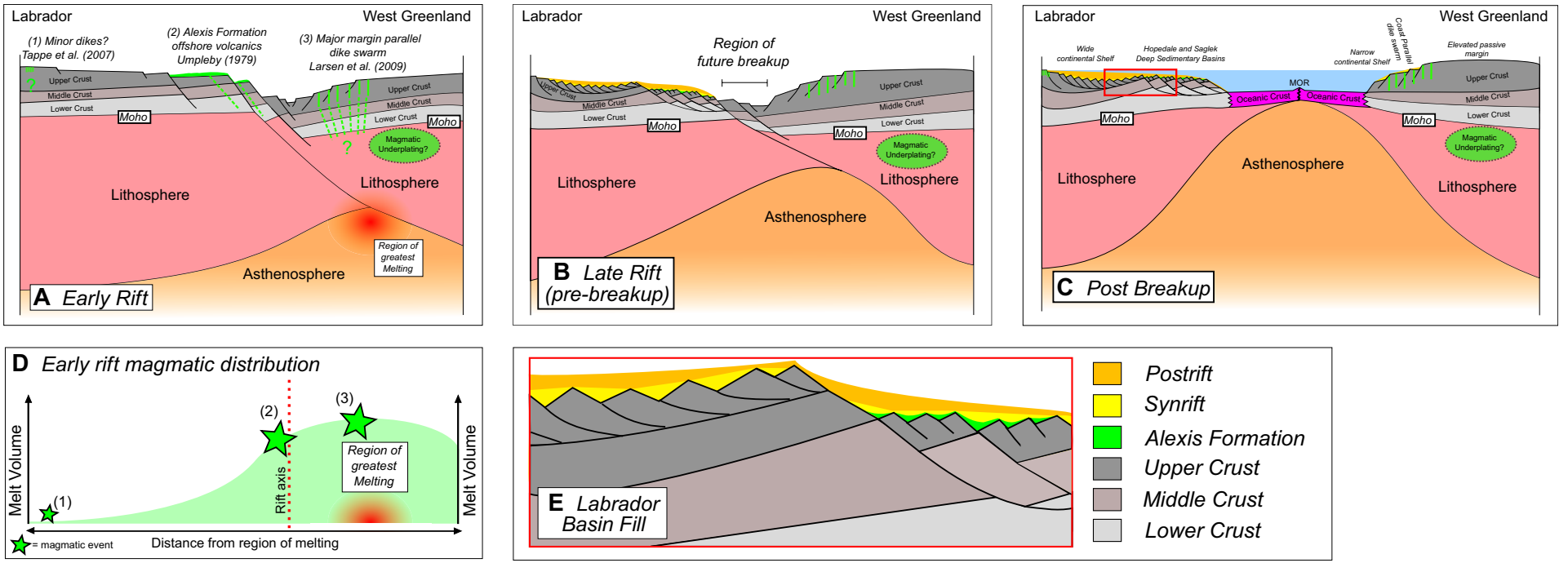

Figure 16. (A) Conceptual model of early continental rifting prior to the opening of the Labrador Sea under a simple shear rifting regime. (B) Conceptual model of late continental rifting. (C) Schematic depiction of the post-breakup (present) architecture of the conjugate passive margins of the Labrador Sea showing the preserved architecture from the early simple shear rifting modified from Lister et al. (1986), including the wide and narrow continental shelves for the Labrador and Greenland margins, respectively, the deep sedimentary basins offshore Labrador, and the minimal offshore sedimentary cover and elevated passive margin on the Greenland side of the rift. (D) The theoretical distribution of melt volumes against proximity to the rift axis where the region of melting is offset from the rift axis due to the simple shear–type early rifting. The three documented rift-related magmatic events included in green in A and D are (1) Early Cretaceous nephelinite dikes near Makkovik (Tappe et al., 2007); (2) the offshore Labrador volcanics (Umpleby, 1979); and (3) the coast-parallel dikes onshore southwest Greenland (Larsen et al., 2009). (E) Enlarged section off inset C in this figure showing the theoretical basin geometries on the upper plate Labrador margin.

land (Figs. 12C, 12D), as magmatic underplating could provide the additional buoyancy required to prevent significant postrift subsidence from occurring. Alternatively, the lack of postrift sedimentation offshore southwest Greenland could be due to a deficiency of sediment supply to the offshore basins; however, if this was the case we would still expect to observe deeper water depths.

Despite the obvious disparity in the extent of onshore rift-related intrusive magmatism between southwest Greenland and that near Makkovik, quantifying the melt volumes associated with rifting on each margin even approximately is problematic for a number of reasons. First, offshore magmatism cannot be accurately quantified on both margins given the sparse seismic and well data coverage. Second, it is difficult to estimate the contributions of magmatic underplating and other intrusives in the lower crust; these contributions were estimated by White (1992) to potentially represent three times the volumes of other intrusive and extrusive magmatic rocks on passive margins. However, it seems more likely that significant magmatic underplating is present in southwest Greenland due to the potential additional support this margin has received.

A wider continental shelf on the lower plate margin is another prediction of the simple shear model of passive margin formation (Lister et al., 1986). The asymmetric nature of the bathymetric profiles across the Labrador Sea depicted in this study (Figs. 12A, 12B) using the Smith and Sandwell (1997) bathymetric data is consistent with a model in which the Labrador margin would be the lower plate margin.

An asymmetric distribution of sedimentation as described in this study is also a prediction of the simple shear model of passive margin formation (Lister et al., 1986), the greater amount of sedimentary deposition occurring on the lower plate margin. The NOAA total sediment thickness data show that the Labrador margin has considerably deeper sedimentary basins (Figs. 12C, 12D), and thus would represent the lower plate margin in a simple shear system.

Another aspect of the sediment distribution on the margins of the Labrador Sea that supports the simple shear model is the geometry of the marginal basins. In the marginal basin on the Labrador margin the total sediment

thickness data profile depicts an abrupt increase in sediment thickness, as opposed to the southwest Greenland margin, where a much less apparent peak in sediment thickness is present. This abrupt increase in sediment thickness may imply a fault-controlled basin as opposed to the marginal basins offshore southwest Greenland, in which the NOAA data record more diffuse sedimentation.

The simple shear model implies a much greater degree of synrift structuring on the lower plate margin. Our analysis has demonstrated that the Labrador margin displays considerably greater synrift deformation and sedimentation than the southwest Greenland margin. The more significant synrift deformation and sedimentation on the Labrador margin supports a simple shear–dominated mode of early rifting with Labrador being the lower plate margin.

Welford and Hall (2013) calculated sediment difference (excess and deficiency), also using the NOAA sediment thickness data for the Labrador Sea. The work of Welford and Hall (2013) showed that most of the Labrador Sea appears from isostatic calculations to be deficient in sediments, whereas the Hopedale Basin is near balanced and the Saglek Basin has an excess of sediments. Welford and Hall (2007) showed that high gradients in the sediment excess and deficiency could indicate the presence of steep listric faults, a key component of a simple shear–dominated rifting regime, supporting a simple shear model of margin formation in the Labrador Sea.

The velocity structure of the margins of the Labrador Sea (Fig. 14; Chian et al., 1995b) also displays asymmetry consistent with a simple shear–dominated phase of early rifting. This is evident in zone 1 (stretched continental crust, Fig. 14), where this region is ~140 km wide on the Labrador margin compared to the southwest Greenland margin, where this zone occupies ~70 km. In the simple shear model of passive margin formation the greater amount of stretching, faulting, and subsequent subsidence occurs on the lower plate margin, which, as with the other observations made by this study, would be the Labrador margin. Using their velocity structure, Chian et al. (1995a) proposed a model of continental breakup whereby breakup occurred closer to the southwest Greenland margin. Breakup occurring closer to the southwest Greenland margin is consistent with the other observations implying that southwest Greenland may have constituted the upper plate margin.

Overall, the high degree of magmatic, sedimentary, and structural asymmetry observed between these two conjugate margins allows us to suggest a simple shear mechanism of early rifting, as opposed to rifting under a pure shear–dominated regime. Under a simple shear rifting regime the upper plate margin would be southwest Greenland and the lower plate margin would be Labrador, according to the distinction between the margin types in the original model by Lister et al. (1986). The asymmetry documented between these margins may have implications for petroleum exploration in the Labrador Sea (e.g., Jauer et al., 2014; Jauer and Budkewitsch, 2010). Such implications include the deeper, potentially more prospective basins on the Labrador margin and the inevitable asymmetry in the heat flow due to the asymmetric magmatic distribution, which may potentially influence the maturation of source material (Peace et al., 2015).

CONCLUSIONS

This study used the previous descriptions of Mesozoic rift-related magmatism (Tappe et al., 2007) to guide field work with the aim of understanding the controls on rifting in the region prior to the opening of the Labrador Sea. Through the field work and subsequent analysis of the data we have further characterized this event, demonstrating that certain aspects differ from the descriptions provided in the previous work. Our conclusions on the characteristics and extent of Early Cretaceous magmatism in proximity to the town of Makkovik are as follows.

1. Early Cretaceous magmatism around Makkovik, Labrador, is volumetrically and spatially extremely minor compared to the numerous other phases of extensive, readily observable intrusive magmatism exposed in the area.

2. Of the nine Early Cretaceous magmatism sample locations described by Tappe et al. (2007), we visited seven for this study. Only two of these seven localities provided any evidence for the magmatism described in the previous work.

3. Mesozoic magmatism is not sufficiently simple and consistent to consider this event as a single coherent intrusive suite of Early Cretaceous nephelinite dikes, as the outcrops are too sparse, variable, and unreliable. At least three of the Tappe et al. (2007) samples are actually from a diatreme, and the rest are either unobservable or ambiguous in nature.

4. The most reliable evidence for Mesozoic magmatism around Makkovik is the diatreme in Ford's Bight dated using fossil evidence by King and McMillan (1975). The diatreme was not observed to be part of a dike swarm as implied by the sample locations in Tappe et al. (2007).

Our conclusions on margin asymmetry, rifting mechanisms, and the relationship between Mesozoic magmatism in West Greenland and Labrador are the following.

1. The magmatic distribution across these two conjugate margins is extremely asymmetric, with the Mesozoic magmatism exposed at surface in the area around Makkovik being minor compared to observations of rift-related diking exposed at surface on the conjugate southwest Greenland margin.

2. This asymmetric magmatic distribution complements other observations of asymmetry, including deeper sedimentary basins and a wider continental shelf on the Labrador margin compared to southwest Greenland allowing us to propose a simple shear model for early rifting prior to the opening of the Labrador Sea, as opposed to a pure shear rifting model.

3. In a simple shear rifting model the southwest Greenland margin would be the upper plate margin and the Labrador margin would be the lower plate margin.

ACKNOWLEDGMENTS

Funding for this research was primarily provided by Royal Dutch Shell in the form of a CeREES (Centre for Research into Earth Energy Systems) studentship at Durham University. We thank the Durham University Center for Doctoral Training in Energy and the Durham Energy Institute for their contribution toward the costs of this research. This research would not have been possible

without the advice of Alana Hinchey of the Geological Survey of Newfoundland and Labrador; Henry Emeleus of the Department of Earth Sciences, Durham University; and the hospitality of the people of Makkovik. We also thank BGR (Bundesanstalt für Geowissenschaften und Rohstoffe, Hannover, Germany) and Schlumberger Limited for providing access to the seismic data and the Petrel seismic interpretation software, respectively. We acknowledge the contribution of the two anonymous reviewers.

REFERENCES CITED

Abdelmalak, M.M., Geoffroy, L., Angelier, J., Bonin, B., Callot, J.P., Gélard, J.P., and Aubourg, C., 2012, Stress fields acting during lithosphere breakup above a melting mantle: A case example in West Greenland: Tectonophysics, v. 581, p. 132–143, doi:10.1016/j.tecto.2011.11.020.

Ainsworth, N.R., Riley, L.A., Bailey, H.W., and Gueinn, J.J., 2014, Cretaceous–Tertiary Stratigraphy of the Labrador Shelf: St. John's, Riley Geoscience Limited for Nalcor Energy, 56 p.

Becker, K., Tanner, D.C., Franke, D., and Krawczyk, C.M., 2016, Fault-controlled lithospheric detachment of the volcanic southern South Atlantic rift: Geochemistry, Geophysics, Geosystems, v. 17, p. 887–894, doi:10.1002/2015GC006081.

Chalmers, J.A., and Laursen, K.H., 1995, Labrador Sea: The extent of continental and oceanic crust and the timing of the onset of seafloor spreading: Marine and Petroleum Geology, v. 12, p. 205–217, doi:10.1016/0264-8172(95)92840-S.

Chalmers, J.A., Larsen, L.M., and Pedersen, A.K., 1995, Widespread Palaeocene volcanism around the northern North Atlantic and Labrador Sea: Evidence for a large, hot, early plume head: Journal of the Geological Society [London], v. 152, p. 965–969, doi:10.1144/GSL.JGS.1995.152.01.14.

Chian, D., and Louden, K.E., 1994, The continent-ocean crustal transition across the southwest Greenland margin: Journal of Geophysical Research, v. 99, p. 9117–9135, doi:10.1029/93JB03404.

Chian, D., Keen, C., Reid, I., and Louden, K.E., 1995a, Evolution of nonvolcanic rifted margins: New results from the conjugate margins of the Labrador Sea: Geology, v. 23, p. 589–592, doi:10.1130/0091-7613(1995)023<0589:EONRMN>2.3.CO;2.

Chian, D., Louden, K.E., and Reid, I., 1995b, Crustal structure of the Labrador Sea conjugate margin and implications for the formation of nonvolcanic continental margins: Journal of Geophysical Research, v. 100, 24239, doi:10.1029/95JB02162.

Canada-Newfoundland and Labrador Offshore Petroleum Board, 2007, C-NLOPB Wells: St. John's, Newfoundland, Canada-Newfoundland and Labrador Offshore Petroleum Board: Schedule of Wells, http://www.cnlopb.ca/wells/.

Culshaw, N., Brown, T., Reynolds, P.H., and Ketchum, J.W.F., 2000, Kanairiktok shear zone: The boundary between the Paleoproterozoic Makkovik Province and the Archean Nain Province, Labrador, Canada: Canadian Journal of Earth Sciences, v. 37, p. 1245–1257, doi:10.1139/e00-035.

Deckart, K., Bertrand, H., and Liégeois, J.P., 2005, Geochemistry and Sr, Nd, Pb isotopic composition of the Central Atlantic Magmatic Province (CAMP) in Guyana and Guinea: Lithos, v. 82, p. 289–314, doi:10.1016/j.lithos.2004.09.023.

DeSilva, N.R., 1999, Sedimentary basins and petroleum systems offshore Newfoundland and Labrador, *in* Fleet, A.J., and Boldy, S.A.R., eds., Petroleum Geology of Northwest Europe: Proceedings of the 5th Conference on the Petroleum Geology of Northwest Europe: Geological Society of London Petroleum Geology Conference Series, v. 1, p. 501–516, doi:10.1144/0050501.

Divins, D., 2003, Total Sediment Thickness of the World's Oceans and Marginal Seas: Boulder, Colorado, National Oceanic and Atmospheric Administration National Geophysical Data Center, https://www.ngdc.noaa.gov/mgg/sedthick/sedthick.html.

Eldholm, O., and Sundvor, E., 1979, Geological events during the early formation of a passive margin: Tectonophysics, v. 59, p. 233–237, doi:10.1016/0040-1951(79)90047-7.

Etheridge, M.A., Symonds, P.A., and Lister, G.S., 1989, Application of the detachment model to reconstruction of conjugate passive margins, *in* Tankard, A.J., and Balkwill, H.R., eds., Extensional Tectonics and Stratigraphy of the North Atlantic Margins: American Association of Petroleum Geologists Memoir 46, p. 23–40, doi:10.1306/M46497C3.

Foley, S.F., 1989, Emplacement features of lamprophyre and carbonatitic lamprophyre dykes at Aillik Bay, Labrador: Geological Magazine, v. 126, p. 29–42, doi:10.1017/S0016756800006129.

Frei, D., Hutchison, M.T., Gerdes, A., and Heaman, L.M., 2008, Common-lead corrected U-Pb age dating of perovskite by laser ablation – magnetic sectorfield ICP-MS: 9th International Kimberlite Conference Extended Abstract, v. No. 9IKC-A, p. 1–3.

Funck, T., Louden, K.E., and Reid, I.D., 2001, Crustal structure of the Grenville Province in southeastern Labrador from refraction seismic data: Evidence for a high-velocity lower crustal wedge: Canadian Journal of Earth Sciences, v. 38, p. 1463–1478, doi:10.1139/e01-026.

Garde, A.A., Hamilton, M.A., Chadwick, B., Grocott, J., and McCaffrey, K.J.W., 2002, The Ketilidian orogen of South Greenland: Geochronology, tectonics, magmatism, and fore-arc accretion during Palaeoproterozoic oblique convergence: Canadian Journal of Earth Sciences, v. 39, p. 765–793, doi:10.1139/e02-026.

Geoffroy, L., 2001, The structure of volcanic margins: Some problematics from the North-Atlantic/Labrador-Baffin system: Marine and Petroleum Geology, v. 18, p. 463–469, doi:10.1016/S0264-8172(00)00073-8.

Geoffroy, L., 2005, Volcanic passive margins: Comptes Rendus Geoscience, v. 337, p. 1395–1408, doi:10.1016/j.crte.2005.10.006.

Haggart, J.W., 2014, New contributions in Baffin Bay/Labrador Sea petroleum exploration and development geoscience: Bulletin of Canadian Petroleum Geology, v. 62, p. 213–216, doi:10.2113/gscpgbull.62.4.213.

Hinchey, A.M., 2013, Geology of the Makkovik Area, Labrador (NTS 13O/03 and Parts of NTS 13O/02): Government of Newfoundland and Labrador, Department of Natural Resources Geological Survey Map 2013–07, Open File 013O/0138, scale 1:50000.

Holgate, N.E., Jackson, C.A.-L., Hampson, G.J., and Dreyer, T., 2015, Seismic stratigraphic analysis of the Middle Jurassic Krossfjord and Fensfjord formations, Troll oil and gas field, northern North Sea: Marine and Petroleum Geology, v. 68, p. 352–380, doi:10.1016/j.marpetgeo.2015.08.036.

Jauer, C.D., and Budkewitsch, P., 2010, Old marine seismic and new satellite radar data: Petroleum exploration of northwest Labrador Sea, Canada: Marine and Petroleum Geology, v. 27, p. 1379–1394, doi:10.1016/j.marpetgeo.2010.03.003.

Jauer, C.D., Oakey, G.N., Williams, G., Hans Wielens, J.B.W., and Haggart, J.W., 2014, Saglek Basin in the Labrador Sea, east coast Canada; stratigraphy, structure and petroleum systems: Bulletin of Canadian Petroleum Geology, v. 62, p. 232–260, doi:10.2113/gscpgbull.62.4.232.

Keen, C.E., Potter, P., and Srivastava, S.P., 1994, Deep seismic reflection data across the conjugate margins of the Labrador Sea: Canadian Journal of Earth Sciences, v. 31, p. 192–205, doi:10.1139/e94-016.

Kerr, A., Ryan, B., Gower, C.F., and Wardle, R.J., 1996, The Makkovik Province: Extension of the Ketilidian mobile belt in mainland North America, *in* Brewer, T.S., ed., Precambrian Crustal Evolution in the North Atlantic Region: Geological Society of London Special Publications 112, p. 155–177, doi:10.1144/GSL.SP.1996.112.01.09.

Kerr, A., Hall, J., Wardle, R.J., Gower, C.F., and Ryan, B., 1997, New reflections on the structure and evolution of the Makkovikian-Ketilidian orogen in Labrador and southern Greenland: Tectonics, v. 16, p. 942–965, doi:10.1029/97TC02286.

Ketchum, J.W., Culshaw, N.G., and Barr, S.M., 2002, Anatomy and orogenic history of a Paleoproterozoic accretionary belt: The Makkovik Province, Labrador, Canada: Canadian Journal of Earth Sciences, v. 39, p. 711–730, doi:10.1139/e01-099.

King, A.F., and McMillan, N.J., 1975, A Mid-Mesozoic breccia from the coast of Labrador: Canadian Journal of Earth Sciences, v. 12, p. 44–51, doi:10.1139/e75-005.

LaFlamme, C., Sylvester, P.J., Hinchey, A.M., and Davis, W.J., 2013, U-Pb age and Hf-isotope geochemistry of zircon from felsic volcanic rocks of the Paleoproterozoic Aillik Group, Makkovik Province, Labrador: Precambrian Research, v. 224, p. 129–142, doi:10.1016/j.precamres.2012.09.005.

Larsen, L.M., 2006, Mesozoic to Palaeogene Dyke Swarms in West Greenland and Their Significance for the Formation of the Labrador Sea and the Davis Strait: Geological Survey of Denmark and Greenland Report, 69 p.

Larsen, L.M., Rex, D.C., Watt, W.S., and Guise, P.G., 1999, ^{40}Ar-^{39}Ar dating of alkali basaltic dykes along the south-west coast of Greenland: Cretaceous and Tertiary igneous activity along the eastern margin of the Labrador Sea: Geology of Greenland Survey Bulletin, v. 184, p. 19–29.

Larsen, L.M., Heaman, L.M., Creaser, R.A., Duncan, R.A., Frei, R., and Hutchison, M., 2009, Tectonomagmatic events during stretching and basin formation in the Labrador Sea and the Davis Strait: Evidence from age and composition of Mesozoic to Palaeogene dyke swarms in West Greenland: Journal of the Geological Society [London], v. 166, p. 999–1012, doi:10.1144/0016-76492009-038.

Larsen, O., and Møller, J., 1968, K/Ar age determinations from western Greenlandl. Reconnaissance programme: Rapport Grønlands Geologiske Undersøgelse, v. 15, p. 82–86.

Latin, D., and White, N., 1990, Generating melt during lithospheric extension: Pure shear vs. simple shear: Geology, v. 18, p. 327–331, doi:10.1130/0091-7613(1990)018<0327:GMDLEP>2.3.CO;2.
Lavier, L.L., and Manatschal, G., 2006, A mechanism to thin the continental lithosphere at magma-poor margins: Nature, v. 440, p. 324–328, doi:10.1038/nature04608.
Leat, P.T., Thompson, R.N., Morrison, M.A., Hendry, G.L., and Dickin, A.P., 1990, Geochemistry of mafic lavas in the early Rio Grande Rift, Yarmony Mountain, Colorado, U.S.A.: Chemical Geology, v. 81, p. 23–43, doi:10.1016/0009-2541(90)90037-8.
Le Bas, M.J., 1989, Nephelinitic and basanitic rocks: Journal of Petrology, v. 30, p. 1299–1312, doi:10.1093/petrology/30.5.1299.
Le Bas, M.J., Le Maitre, R.W., Streckeisen, A., and Zanettin, B., 1986, A chemical classification of volcanic rocks based on the total alkali silica diagram: Journal of Petrology, v. 27, p. 745–750, doi:10.1093/petrology/27.3.745.
Lister, G.S., Etheridge, M.A., and Symonds, P.A., 1986, Detachment faulting and the evolution of passive continental margins: Reply: Geology, v. 14, p. 891–892, doi:10.1130/0091-7613(1986)14<891:CARODF>2.0.CO;2.
Martins, L.T., Madeira, J., Youbi, N., Munhá, J., Mata, J., and Kerrich, R., 2008, Rift-related magmatism of the Central Atlantic magmatic province in Algarve, southern Portugal: Lithos, v. 101, p. 102–124, doi:10.1016/j.lithos.2007.07.010.
McKenzie, D., 1978, Some remarks on the development of sedimentary basins: Earth and Planetary Science Letters, v. 40, p. 25–32, doi:10.1016/0012-821X(78)90071-7.
McWhae, J.R.H., Elie, R., Laughton, K.C., and Gunther, P.R., 1980, Stratigraphy and petroleum prospects of the Labrador Shelf: Bulletin of Canadian Petroleum Geology, v. 28, p. 460–488.
Peace, A., McCaffrey, K., Imber, J., Hobbs, R., van Hunen, J., and Gerdes, K., 2015, Quantifying the influence of sill intrusion on the thermal evolution of organic-rich sedimentary rocks in nonvolcanic passive margins: An example from ODP 210–1276, offshore Newfoundland, Canada: Basin Research, doi:10.1111/bre.12131.
Philippon, M., Willingshofer, E., Sokoutis, D., Corti, G., Sani, F., Bonini, M., and Cloetingh, S., 2015, Slip re-orientation in oblique rifts: Geology, v. 43, p. 147–150, doi:10.1130/G36208.1.
Ranero, C.R., and Pérez-Gussinyé, M., 2010, Sequential faulting explains the asymmetry and extension discrepancy of conjugate margins: Nature, v. 468, p. 294–299, doi:10.1038/nature09520.
Reid, I.D., and Keen, C.E., 1990, High seismic velocities associated with reflections from within the lower oceanic crust near the continental margin of eastern Canada: Earth and Planetary Science Letters, v. 99, p. 118–126, doi:10.1016/0012-821X(90)90075-9.
Rock, N.M.S., 1986, The nature and origin of ultramafic lamprophyres: Alnoites and allied rocks: Journal of Petrology, v. 27, p. 155–196, doi:10.1093/petrology/27.1.155.
Shallaly, N.A., Beier, C., Haase, K.M., and Hammed, M.S., 2013, Petrology and geochemistry of the Tertiary Suez rift volcanism, Sinai, Egypt: Journal of Volcanology and Geothermal Research, v. 267, p. 119–137, doi:10.1016/j.jvolgeores.2013.10.005.
Smith, W.H., and Sandwell, D., 1997, Global sea floor topography from satellite altimetry and ship depth soundings: Science, v. 277, p. 1956–1962, doi:10.1126/science.277.5334.1956.
Srivastava, S.P., 1978, Evolution of the Labrador Sea and its bearing on the early evolution of the North Atlantic: Geophysical Journal International, v. 52, p. 313–357, doi:10.1111/j.1365-246X.1978.tb04235.x.
Srivastava, S.P., and Roest, W.R., 1999, Extent of oceanic crust in the Labrador Sea: Marine and Petroleum Geology, v. 16, p. 65–84, doi:10.1016/S0264-8172(98)00041-5.
Shipboard Scientific Party, 1987, Site 646, *in* Srivastava, S.P., et al., Proceedings of the Ocean Drilling Program, Initial reports, Volume 105: College Station, Texas, Ocean Drilling Program, p. 419–674, doi:10.2973/odp.proc.ir.105.104.1987.
Storey, M., Duncan, R.A., Pedersen, A.K., Larsen, L.M., and Larsen, H.C., 1998, $^{40}Ar/^{39}Ar$ geochronology of the West Greenland Tertiary volcanic province: Earth and Planetary Science Letters, v. 160, p. 569–586, doi:10.1016/S0012-821X(98)00112-5.
Tappe, S., Foley, S.F., Jenner, G.A., Heaman, L.M., Kjarsgaard, B.A., Romer, R.L., Stracke, A., Joyce, N., and Hoefs, J., 2006, Genesis of ultramafic lamprophyres and carbonatites at Aillik Bay, Labrador: A consequence of incipient lithospheric thinning beneath the North Atlantic Craton: Journal of Petrology, v. 47, p. 1261–1315, doi:10.1093/petrology/egl008.
Tappe, S., Foley, S.F., Stracke, A., Romer, R.L., Kjarsgaard, B.A., Heaman, L.M., and Joyce, N., 2007, Craton reactivation on the Labrador Sea margins: $^{40}Ar/^{39}Ar$ age and Sr-Nd-Hf-Pb isotope constraints from alkaline and carbonatite intrusives: Earth and Planetary Science Letters, v. 256, p. 433–454, doi:10.1016/j.epsl.2007.01.036.
Tappe, S., Steenfelt, A., Heaman, L.M., and Simonetti, A., 2009, The newly discovered Jurassic Tikiusaaq carbonatite-aillikite occurrence, West Greenland, and some remarks on carbonatite-kimberlite relationships: Lithos, v. 112, p. 385–399, doi:10.1016/j.lithos.2009.03.002.
Torske, T., and Prestvik, T., 1991, Mesozoic detachment faulting between Greenland and Norway: Inferences from Jan Mayen fracture zone system and associated alkalic volcanic rocks: Geology, v. 19, p. 481–484, doi:10.1130/0091-7613(1991)019<0481:MDFBGA>2.3.CO;2.
Umpleby, D., 1979, Geology of the Labrador Shelf: Geological Survey of Canada Paper 79-13, 34 p.
Wardle, R.J., et al., 2002, Correlation chart of the Proterozoic assembly of the northeastern Canadian-Greenland Shield: Canadian Journal of Earth Sciences, v. 39, 895, doi:10.1139/e01-088.
Welford, J.K., and Hall, J., 2007, Crustal structure of the Newfoundland rifted continental margin from constrained 3-D gravity inversion: Geophysical Journal International, v. 171, p. 890–908, doi:10.1111/j.1365-246X.2007.03549.x.
Welford, J.K., and Hall, J., 2013, Lithospheric structure of the Labrador Sea from constrained 3-D gravity inversion: Geophysical Journal International, v. 195, p. 767–784, doi:10.1093/gji/ggt296.
Wernicke, B., 1985, Uniform-sense normal simple shear of the continental lithosphere: Canadian Journal of Earth Sciences, v. 22, p. 108–125, doi:10.1139/e85-009.
White, J.D.L., and Ross, P.S., 2011, Maar-diatreme volcanoes: A review: Journal of Volcanology and Geothermal Research, v. 201, p. 1–29, doi:10.1016/j.jvolgeores.2011.01.010.
White, R.S., 1992, Magmatism during and after continental break-up, *in* Storey, B.C., et al., eds., Magmatism and the Causes of Continental Break-up: Geological Society of London Special Publications 68, p. 1–16, doi:10.1144/GSL.SP.1992.068.01.01.
Whittaker, J.M., Goncharov, A., Williams, S.E., Müller, R.D., and Leitchenkov, G., 2013, Global sediment thickness data set updated for the Australian-Antarctic Southern Ocean: Geochemistry, Geophysics, Geosystems, v. 14, p. 3297–3305, doi:10.1002/ggge.20181.
Wilson, R.W., Klint, K.E.S., Van Gool, J.A.M., McCaffrey, K.J.W., Holdsworth, R.E., and Chalmers, J.A., 2006, Faults and fractures in central West Greenland: Onshore expression of continental break-up and sea-floor spreading in the Labrador–Baffin Bay Sea: Geological Survey of Denmark and Greenland Bulletin 11, p. 185–204, http://www.geus.dk/DK/publications/geol-survey-dk-gl-bull/11/Documents/nr11_p185-204.pdf.
Wilton, D.H.C., Taylor, R.C., Sylvester, P.J., and Penney, G.T., 2002, A review of kimberlitic and ultramafic lamprophyre intrusives from northern Labrador, *in* Current Research: Newfoundland Department of Mines and Energy Geological Survey Report 02-1, p. 343–352.
Woolley, A.R., Bergman, S.C., Edgar, A.D., Le Bas, M.J., Mitchell, R.H., Rock, N.M.S., and Scott Smith, B.H., 1996, Classification of lamprophyres, lamproites, kimberlites, and the kalsilitic, melilitic, and leucitic rocks: Canadian Mineralogist, v. 34, p. 175–186.

Basin Research

IAS EAGE

Basin Research (2015) 1–17, doi: 10.1111/bre.12131

Quantifying the influence of sill intrusion on the thermal evolution of organic-rich sedimentary rocks in nonvolcanic passive margins: an example from ODP 210-1276, offshore Newfoundland, Canada

Alexander Peace,* Ken McCaffrey,* Jonathan Imber,* Richard Hobbs,* Jeroen van Hunen* and Keith Gerdes†

**Department of Earth Sciences, Durham University, Durham, UK*

†*Shell International Exploration and Production, Den Haag, The Netherlands*

ABSTRACT

Intrusive magmatism is an integral and understudied component in both volcanic and nonvolcanic passive margins. Here, we investigate the thermal effects of widespread (*ca.* 20 000 km^2) intrusive magmatism on the thermal evolution of organic-rich sedimentary rocks on the nonvolcanic Newfoundland passive margin. ODP 210-1276 (45.41°N, 44.79°W) intersects two sills: an older, upper sill and a younger, lower sill that are believed to correspond to the high amplitude 'U-reflector' observed across the Newfoundland Basin. A compilation of previous work collectively provides; (1) emplacement depth constraints, (2) vitrinite reflectance data and (3) $^{40}Ar/^{39}Ar$ dates. Collectively, these data sets provide a unique opportunity to model the conductive cooling of the sills and how they affect thermal maturity of the sedimentary sequence. A finite differences method was used to model the cooling of the sills, with the model outputs then being entered into the EASY%R_o vitrinite reflectance model. The modelled maturation profile for ODP 210-1276 shows a significant but localized effect on sediment maturity as a result of the intrusions. Our results suggest that even on nonvolcanic margins, intrusive magmatism can significantly influence the thermal evolution in the vicinity of igneous intrusions. In addition, the presence of widespread sills on nonvolcanic passive margins such as offshore Newfoundland may be indicative of regional-scale thermal perturbations that should be considered in source rock maturation studies.

INTRODUCTION

Continental extension causes rifting and thinning of the lithosphere that may result in continental breakup and eventually the initiation of seafloor spreading (Eldholm & Sundvor, 1979). Passive continental margins are a product of this continental breakup and subsequent seafloor spreading (Geoffroy, 2005). Passive margins are traditionally classified as one of two end-member types: (1) volcanic (VPM) or (2) nonvolcanic (NVPM), in reference to the relative abundance or scarcity of igneous rocks produced during rifting and breakup (e.g. Franke, 2013).

Passive margins globally represent a significant host for both current (e.g. offshore Newfoundland; DeSilva, 1999) and future hydrocarbon exploration targets (e.g. offshore West Africa; Beglinger *et al.*, 2012). Source rock quality, and in particular maturity, is of paramount concern when exploring new areas in deep water passive margins where operating costs may be high. To reduce the exploration risk in these settings, it is thus important to understand and quantify the thermal evolution of NVPMs, and their source rock maturation characteristics. Syn and post-rift magmatism is a common feature on passive margins, with spatially extensive igneous sill complexes being a common feature on both volcanic (e.g. the Western Australian margin; Holford *et al.*, 2013) and nonvolcanic passive margins (e.g. the South Australian Margin; Holford *et al.*, 2012). The heat from these intrusions may contribute to the thermal evolution of a margin, and thus the maturation of potential source rock material. It is for this reason that the additional heat introduced by igneous intrusions into prospective sedimentary basins on passive margins needs to be quantified.

ODP 210-1276 intersects two sills which provide an opportunity to model potential changes in the maturity of the encasing organic-rich sedimentary host rocks instigated by post-rift magmatism in a NVPM. Here, we report the results of 1D conductive modelling of the influence of sill intrusion and compare the model predictions with the measured vitrinite reflectance data of Pross *et al.* (2007) to estimate the maturation state of the encasing sedimentary rocks. Experiments were also undertaken to understand the roles of timing, hydrothermalism

Correspondence: Alexander Peace, Department of Earth Sciences, Durham University, Durham DH1 3LE, UK.
E-mail: a.l.peace@durham.ac.uk.

and the duration in which sills acted as magmatic conduits.

The aim of this work was to show that despite all the variables present in a complex intrusive system such as this, a simple model can be used to account for the majority of thermal effects. This allows us to discount less important processes, resulting in insights into the major controls on the thermal maturation of organic-rich sedimentary rocks in proximity to igneous intrusions. We conclude that the sills intersected at ODP 210-1276 have influenced the localized thermal evolution of the sedimentary rocks, which may be indicative of a broader, more regional thermal perturbation in the region covered by the 'U-reflector'. Although, given that ODP 210-1276 essentially represents a 1D profile through a spatially extensive, complex, igneous system, it is likely that the results presented herein are not representative of the situation in other parts of the Newfoundland Basin.

GEOLOGICAL SETTING

The Newfoundland margin was formed during the opening of the North Atlantic and in conjunction with its conjugate, the Iberian margin, it is considered to be a typical NVPM (e.g. Melankholina, 2011; Peron-Pinvidic *et al.*, 2013). ODP site 210-1276 (45.41°N, 44.79°W) was drilled into transitional crust offshore Newfoundland, Canada (Fig. 1). The aim of this ODP

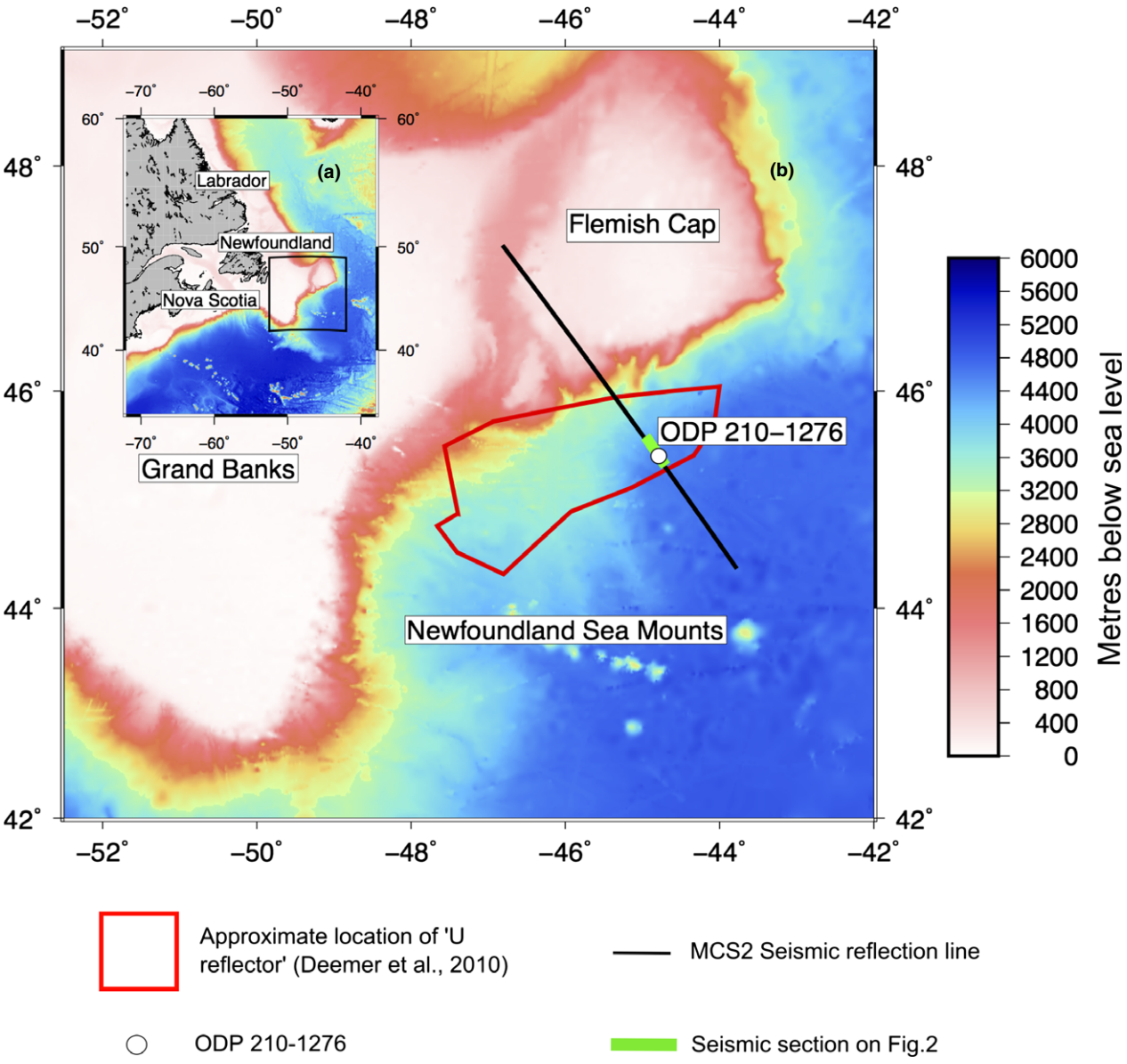

Fig. 1. (a) An overview of the Eastern Canadian continental margin. (b) The study area showing the location of ODP site 210-1276, along with seismic line MCS2 (section shown in Fig. 2 in green) and the approximate location of the 'U-reflector' (Deemer *et al.*, 2010). Bathymetry data produced from satellite altimetry by Smith & Sandwell (1997).

Table 1. Intrusion parameters of the sills at ODP 210-1276. Current positions in well (Tucholke *et al.*, 2004a), depth when intruded (Tucholke *et al.*, 2007) and $^{40}Ar/^{39}Ar$ ages (Hart & Blusztajn, 2006)

Name	Current top of unit (mbsf)	Current bottom (mbsf)	Thickness (m)	Depth when intruded (mbsf)	Youngest $^{40}Ar/^{39}$ Ar age (ma)	Oldest $^{40}Ar/^{39}$ Ar age (ma)
Upper sill	1612.7	1623	10.30	*ca.* 260	104.7 ± 1.7	105.9 ± 1.8
Lower sill	1719	>1736.9	17.90	*ca.* 590	95.9 ± 2	99.7 ± 1.8

leg was to provide a greater understanding of the syn and post-rift stratigraphy and magmatic history of the conjugate Newfoundland-Iberia nonvolcanic passive margins (Tucholke *et al.*, 2004a), with the specific aim of targeting what was believed from seismic reflection data to be the breakup unconformity, which ultimately turned out to be igneous intrusions. The drill site is located near the edge of the thinned continental crust (Van Avendonk *et al.*, 2006), with the well encountering two intervals of igneous rocks which are modelled herein. These two intervals; are the only igneous rocks recorded at ODP 210-1276, consisting of an upper, singular sill which is 10.3 m thick and a lower sill complex where the main body is at least 17.9 m thick (Table 1). Drilling ceased 17.9 m after penetrating the main body of the lower sill, thus modelling a sill of this thickness represents a minimum and the thermal influence is likely to be greater. The first sill was emplaced after the onset of seafloor spreading (Peron-Pinvidic *et al.*, 2010), which was initiated by Barremian to Aptian time (anomaly M3 to M0, or 127–112 Ma) Hopper *et al.* (2004).

Previous work has associated the sills at this site with the widespread 'U-reflector' observed in 2D seismic reflection profiles (e.g. Fig. 2) across the Newfoundland basin (e.g. Shillington *et al.*, 2004; Deemer *et al.*, 2010). The U-reflector is considered to represent a suite of post-breakup magmatic intrusions covering an area of *ca.* 20 000 km^2 Deemer *et al.* (2010) in an otherwise nonvolcanic margin. It is observable on seismic reflection data as one or two high amplitude reflectors, at a depth corresponding to the igneous intrusions at ODP 210-1276. Within the resolution of the seismic reflection profile it is not possible to determine if the high amplitude reflectors correspond to singular or multiple igneous intrusions, but given the observed situation intersected by ODP 210-1276 it is likely that the high amplitude reflectors at this depth across the Newfoundland Basin represent at least one igneous intrusion.

The widespread nature of the sills on the Newfoundland margin (Deemer *et al.*, 2010) implies that this igneous activity represents a significant margin-scale event. In contrast, no significant post-rift intrusive activity is known on the conjugate Iberian margin, implying an asymmetric post-breakup magmatic history (Peron-Pinvidic *et al.*, 2010). The sills of the U-reflector are of interest due to their close proximity to the offshore Newfoundland petroleum systems. Karner & Shillington (2005) qualitatively suggested that these sills could have implications for the thermal history of the region.

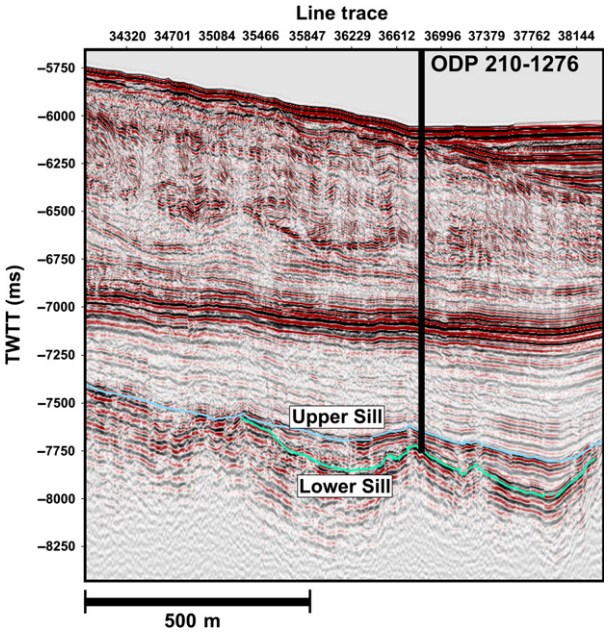

Fig. 2. Segment of MCS (multichannel seismic) reflection profile SCREECH 2 (Studies of Continental Rifting and Extension on the Eastern Canadian Shelf) by Shillington *et al.* (2004) where it intersects ODP site 210-1276. The location of this seismic line segment is shown on the study area overview map (Fig. 1b). Interpretation of the U-reflector (green/blue lines) from Peron-Pinvidic *et al.* (2010).

Chronological analysis by Hart & Blusztajn (2006) of the sills at ODP 210-1276 provided $^{40}Ar/^{39}Ar$ dates of 104.7 ± 1.7 Ma and 105.9 ± 1.8 Ma for the upper sill, and 95.9 ± 2 Ma and 99.7 ± 1.8 Ma for the lower sill (Table 1 and Fig. 3). The $^{40}Ar/^{39}Ar$ dates demonstrate that there was a time interval of *ca.* 5–10 Myrs between the intrusions cooling to their closing temperatures. Compositionally, both sills are classified as alkali basalt – hawaiite (Hart & Blusztajn, 2006).

The sills are located within uppermost Aptian to lowermost Albian syn-rift sequences at *ca.* 90–160 m and *ca.* 200–270 m above basement for the upper and lower sills respectively. This is based on the interpretation of seismic reflection profiles, including the SCREECH MCS2 line which crosses ODP 210-1276 (Fig. 2), and calculated vertical seismic velocities which are;

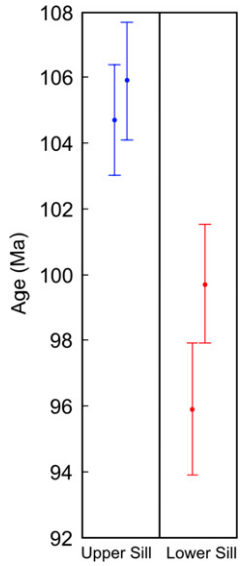

Fig. 3. $^{40}Ar/^{39}Ar$ dates, and associated 2σ errors for the upper and lower sills from Hart & Blusztajn (2006).

4738–5030 ms^{-1}, 5527–6193 ms^{-1} and 1650–3200 ms^{-1} for the upper sill, lower sill and sediments between the sills, respectively, according to Tucholke *et al.* (2004b).

The sills were intruded at shallow depths of *ca.* 260 m and *ca.* 590 m into relatively unconsolidated, and not overpressured sedimentary rocks, particularly in the lower 30 m of the section (Tucholke *et al.*, 2007). This suggests that at the drill site the upper sill had considerable mechanical support probably provided by nearby dykes, protecting the underlying sedimentary rocks from compaction due to the load of the later sedimentary overburden (Peron-Pinvidic *et al.*, 2010). The emplacement depths were calculated by consideration of the $^{40}Ar/^{39}Ar$ dates in the context of the nano-fossil based age vs depth curve provided by Tucholke *et al.* (2004a). This age depth relationship was established using zonal boundary ages of microfossils at ODP 210-1276. Karner & Shillington (2005) used a reconstruction of porosity–depth relationships to estimate an intrusion depth of 0–556 m below sea floor. These two independent estimates do not account for any subsequent burial and compaction (Tucholke *et al.*, 2007).

The sedimentary rocks present at ODP 210-1276 include siltstones, sandstones, carbonates and shale-clast conglomerates (Fig. 4). Of most interest to this study are the organic-rich rocks found in several intervals in ODP 210-1276 (Fig. 4), as these could provide potential source material. Total Organic Carbon (TOC wt% – the amount of carbon bound in an organic compound) was collected between 801 and 1713 m below seafloor by Tucholke *et al.* (2004a). TOC values are recorded between 0 and 9.7 wt% at ODP 210-1276, with values in proximity to the intrusions <2 wt%. Pross *et al.* (2007) conducted a maturation study on the rocks in proximity to the upper sill describing them as predominantly dark grey mudrocks, with minor sand to silt-based turbidites and black shales (Fig. 4).

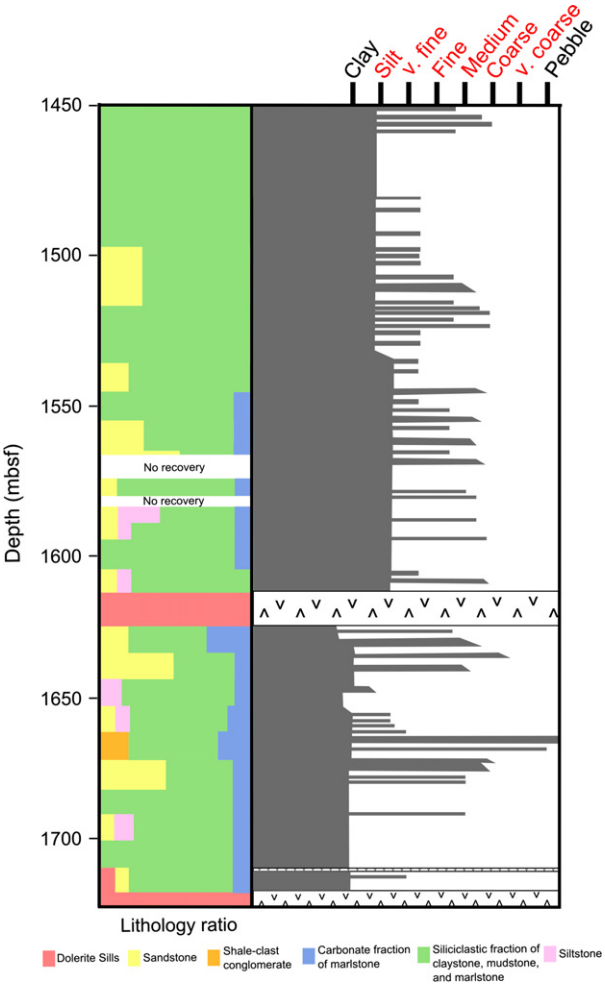

Fig. 4. Lithostratigraphic column and grain size reproduced from Tucholke *et al.* (2004a) for the interval of ODP 210-1276 in proximity to the sills, with depth in mbsf (metres below seafloor). The organic-rich sedimentary rocks of interest to this study can be found in several intervals and are depicted in pink.

METHODOLOGY

Model setup

We performed numerical calculations to investigate the thermal influence of the igneous intrusions intersected at ODP 210-1276 on the surrounding sedimentary rocks. The temperatures obtained from one-dimensional finite difference MATLAB models were entered into the EASY%R_o model of Sweeney & Burnham (1990) to produce theoretical vitrinite reflectance values.

Thermal heat diffusion was considered to be the dominant process affecting thermal evolution, and is described in the models by:

$$\frac{\partial T}{\partial t} = D\frac{\partial^2 T}{\partial x^2}, \quad (1)$$

where T is the Temperature, t is time, x is distance and D = the thermal diffusion coefficient:

$$D = \frac{k}{\rho C_p}, \quad (2)$$

where k = thermal conductivity, ρ = density and C_p = specific heat capacity.

The simplifications and assumptions made in our model include: (1) the only form of heat transfer is considered to be conduction; (2) latent heat released from crystallization of the sills is accounted for by the inclusion of a calculated higher starting temperature equivalent to an extra 488°C; (3) emplacement of the sills was instantaneous; (4) thermal parameters are not temperature dependent; (5) stratigraphical units are considered to be internally homogeneous; and (6) the regional geothermal gradient (Table 2) remained constant during margin evolution. The validity of these assumptions is discussed below.

(1) Our models assume that heat transfer was by conduction only (e.g. Fjeldskaar *et al.*, 2008; Aarnes *et al.*, 2010; Wang *et al.*, 2010, 2007). Advective heat transport by hydrothermal activity is negligible in low permeability materials such as shales (Aarnes *et al.* (2010), although the stratigraphic sequence encountered in ODP 210-1276 (Fig. 4) is dominated by sandstones (Tucholke *et al.*, 2004a) with a higher permeability than shale. Therefore, additional heat advection due to heating and circulation of pore waters may lead to more rapid cooling than conduction alone, and our results may represent a minimum estimate of the cooling rate.

(2) We approximate the latent heat effect of magma crystallization in our model by applying a starting temperature of the sill that is increased with the released heat during magma crystallization: (3)

$$\Delta T_{\text{latent}} = \frac{L_{\text{intrusion}}}{C_{p\,\text{intrusion}}}, \quad (3)$$

where ΔT_{latent} is the additional heat from latent heat of crystallization, $L_{\text{intrusion}}$ is the latent heat of crystallization (Spear & Peacock, 1989) and $C_{p\ \text{intrusion}}$ is the specific heat capacity of mafic intrusions (Barker *et al.*, 1998).

The sills are compositionally alkali basalt-hawaiite according to Hart & Blusztajn (2006). The initial temperature of the intrusion is therefore taken to be 1000°C; the same temperature as previous work modelling intrusions of similar composition (e.g. Barker *et al.*, 1998). Inclusion of latent heat of crystallization gives a modelled starting temperature of 1488°C, this includes 488°C additional heat from the latent heat of crystallization, on top of the initial temperature value of 1000°C for the sills as in Barker *et al.* (1998).

Latent heat has been omitted by some previous workers in this area of study (e.g. Barker *et al.*, 1998; Fjeldskaar *et al.*, 2008), whereas in others it has been included (e.g. Wang *et al.*, 2012). We choose to include latent heat in our models as it is a physical phenomenon, which could have a significant effect on the results. Although it has been noted by Galushkin (1997) that models accounting for latent heat could potentially over estimate its effects, as all the additional heat is added instantaneously rather than over the duration in which cooling occurs.

(3) The main models presented herein assume instantaneous intrusion. This is a reasonable assumption

Table 2. Parameters utilized in the thermal modelling and symbols used in equations, excluding the EASY%R_o parameters which are defined alongside the equations and in Table 3

Parameter	Symbol	Value	Units	Reference
Density of country rock	ρ_{host}	2400	kg m^{-3}	Wang *et al.* (2012)
Density of intrusion	$\rho_{\text{intrusion}}$	2960	kg m^{-3}	Wang *et al.* (2007)
Specific heat capacity of host	C_{p_host}	1090	J kg^{-1} °C^{-1}	Wang *et al.* (2012)
Specific heat capacity of intrusion	$C_{p\_\text{intrusion}}$	820	J kg^{-1} °C^{-1}	Barker *et al.* (1998)
Conductivity of organic-rich host	K_{host}	2.1	W m^{-1} °C^{-1}	Wang *et al.* (2012)
Conductivity of intrusion	$K_{\text{intrusion}}$	2.5	W m^{-1} °C^{-1}	Wang *et al.* (2012)
Heat release from latent heat of crystallization	ΔT_{latent}	488	°C	Calculated from $L_{\text{intrusion and}}$ $C_{p\_\text{intrusion}}$ Equation 3
Diffusion coefficient	D	Varies spatially	m s^{-2}	This work using Equation 2
Latent heat of crystallization	$L_{\text{intrusion}}$	400	kJ kg^{-1}	Spear & Peacock (1989)
Geothermal gradient	G	21.75	°C km^{-1}	Keen (1979)
Starting temperature of intrusion	T_{initial}	1000	°C	Barker *et al.* (1998)
Temperature at surface	T_{surf}	20	°C	This work
Spatial discretization step	dx	2	m	This work
Timestep	dt	0.1	years	This work
Distance between sills at time of intrusion	H_{past}	330	m	Tucholke *et al.* (2004a)
Current distance between sills	H_{current}	96	m	Tucholke *et al.* (2004a)
Current depth of upper sill top	S_{current}	260	m (below sea floor)	Tucholke *et al.* (2004a)
Upper sill top at time of intrusion	S_{past}	1612.7	m (below sea floor)	Tucholke *et al.* (2004a)
Compaction factor	C	29.09%	%	Calculated from H_{current} and H_{past}
Burial	B	1353	m	Calculated from S_{current} and S_{past}

because the periods of emplacement were probably very short, as multiple samples from the sills gave statistically similar $^{40}Ar/^{39}Ar$ ages (Hart & Blusztajn, 2006). Noninstantaneous intrusion will reduce the thermal effects of the intrusion as multiple smaller bodies will cool faster, than a singular large body. Previous authors modelling the influence of sills on organic matter have also assumed intrusion to be instantaneous (e.g. Aarnes *et al.*, 2010). Considering emplacement to be instantaneous increases the thermal effects of the intrusions in the modelling, and thus may lead to an overestimate of the maturation of organic-rich sedimentary rocks.

(4) Keeping the thermal parameters (specific heat capacity and thermal conductivity – Table 2) constant over a temperature range, simplifies the modelling and is an assumption made by most previous work (e.g. Fjeldskaar *et al.*, 2008). It should also be considered that reducing the variables allows us to study the main controls on maturation, particularly as this study has observed vitrinite reflectance data available to provide a constraint.

(5) Our model incorporates spatial variability in the thermal parameters between the units, but the units are internally assumed to be homogeneous, with the host having the thermal properties of dry organic-rich shale. It is assumed to be dry so that heat transfer occurs through conduction only. Two units are recognized in our model; (1) 'host rock' and (2) 'sills' (Table 2, Fig. 5). This is a simplification also made by previous work (e.g. Wang *et al.*, 2012) which utilized separate values of thermal conductivity, density and specific heat capacity for 'wall rock' and 'magma').

(6) The background geothermal gradient used in the model is based upon calculations by Keen (1979) for the current geothermal gradient on other parts of the Eastern Canadian Margin (17.5°C km^{-1} for the Scotian Margin and 26°C km^{-1} for the Labrador Shelf). Our model utilizes an average of these values of 21.75°C km^{-1} (Table 2) as the study area is located between the Scotian Margin and the Labrador Shelf. Goutorbe *et al.* (2007) produced a detailed analysis of heat flow along the Eastern Canadian margin from offshore Labrador to Nova Scotia finding, there was no significant variation between the different subareas on the margin and that the nature of the continental basement and the age of the ocean floor had little influence. The geothermal gradient can justifiably remain constant for the modelled period as it only represents 60, 000 years, and these sills were both emplaced post margin breakup.

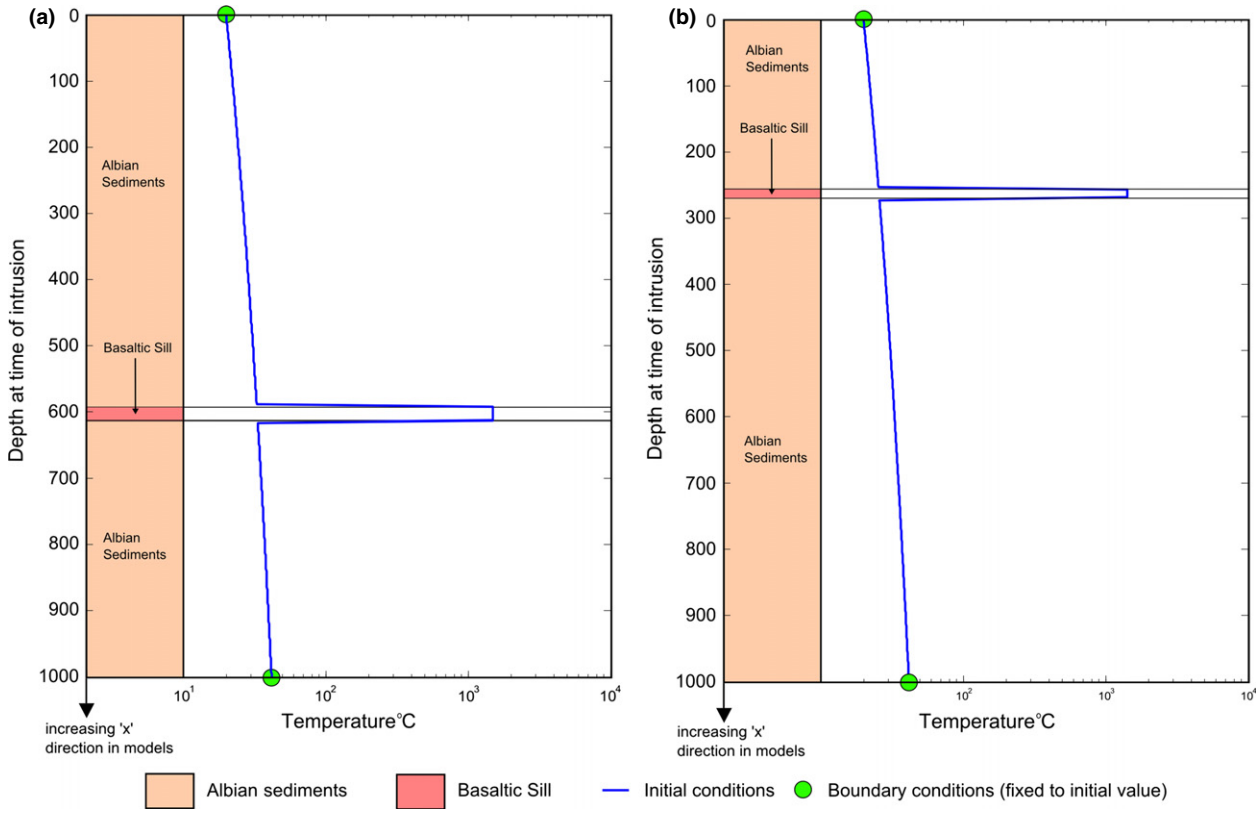

Fig. 5. Schematic depiction of the model setup for (a) the lower sill and (b) the upper sill. The initial temperature profile is depicted in blue for both (a) and (b). The boundaries are fixed and are shown in green. The relative positions of the two lithologies in (a) and (b) are shown. The parameters applicable to these lithologies can be found in Table 2. Model resolution (dx) is 2 m and the time step (dt) is 0.1 years. The X direction in the model is down hole.

The heat diffusion equation is solved in MATLAB with a finite differences method. Initial temperature conditions are shown in Fig. 5, and prescribed temperature boundary conditions equal the initial conditions. We model sills of 10 and 18 m thickness for which a vertical resolution of 2 m proved sufficient. Our discretization allows for spatial variation in thermal parameters.

The $^{40}Ar/^{39}Ar$ ages provided by the previous work of Hart & Blusztajn (2006) record the closing temperatures, implying that these two cooling events were at least 1.5 Myrs apart (Fig. 3 and Table 1), a timescale that will be shown below to be much larger than the thermal equilibrium timescales of the sills. In our primary models we therefore consider the sills as individual thermal events rather than having occurred simultaneously. This is an improvement over previous models that consider multiple intrusions occur simultaneously (e.g. Fjeldskaar *et al.*, 2008), potentially overestimating the total heating event. The $^{40}Ar/^{39}Ar$ dates provided by Hart & Blusztajn (2006) are highly statistically significant, with a *ca.* 7.5 Myrs difference using 2σ uncertainties in measured age between the two sills. Comparison between the maximum temperatures achieved (and resulting maturation effects) when simultaneous intrusion is assumed was also modelled, and compared to the results of modelling the sills separately (Fig. 6).

As $^{40}Ar/^{39}Ar$ ages of Hart & Blusztajn (2006), represent the time of cooling to closure temperature, they do not allow us to rule out if the sills acted as long-term conduits for magma. This is plausible in what appears on seismic reflection data to be a large, complex, intrusive system. If a sill acts for a large duration of time as a conduit for magmatism, then the thermal effect on the surrounding sediments will be increased when compared to an instantaneously intruded sill.

To provide a constraint on the duration in which a sill acted as a magmatic conduit we modelled systems in which the upper sill acted as a magma conduit for 10, 100 and 1000 years prior to cooling, quantifying the effects on theoretical vitrinite reflectance values produced using the EASY%R_o of Sweeney & Burnham (1990). The modelled vitrinite reflectance values are then compared to the observed values of Pross *et al.* (2007), allowing estimations of the duration that the upper sill acted as a magmatic conduit to be constrained.

Emulating an open magmatic conduit is achieved by maintaining the sill at its starting temperature for the desired duration prior to cooling. In these models the sill has a starting temperature of 1000°C, with the additional 488°C contribution from the latent heat of crystallization added when the sill is allowed to cool. The magmatic conduit is assumed to be receiving a constant supply of magma, until it is allowed to cool.

During each model run the temperature at the boundaries was fixed to the initial conditions. Our discretization of the thermal diffusion equation (*Equation 1* and *2*) allows for spatial variation in thermal parameters. The model resolution (dx) is 2 m and the timestep (dt) is 0.1 years in all the models we ran. The values used for the parameters in *equations 1, 2 and 3* are given in Table 2.

Vitrinite reflectance modelling

Vitrinite reflectance (%R_o) is one of the most widely used indicators of source rock maturity. It is measured optically (Bostick & Alpern, 1977), and is useful in maturation studies as the degree of reflectivity varies smoothly and predictably with temperature (Burnham & Sweeney, 1989). However, there are several known drawbacks with the use of vitrinite reflectance as an indicator of organic sediment maturity (Heroux *et al.* (1979). These include

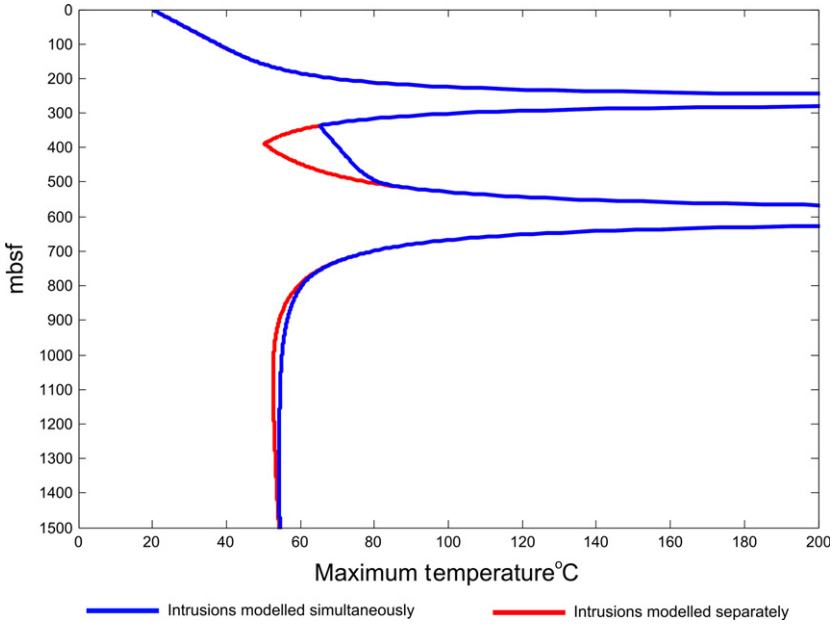

Fig. 6. Maximum temperatures achieved when the sills are modelled separately and simultaneously. All other figures depict the results from either a singular sill or models where the sills cooled separately, and the results subsequently combined.

but are not limited to, measurements being taken from similar known vitrinite minerals and the possible reworking of organic material.

This work utilizes the EASY%R_o model of Sweeney & Burnham (1990), to calculate theoretical vitrinite reflectance values. EASY%R_o calculates vitrinite reflection against time for a given stratigraphic level if the temperature-time history has been calculated, and can be used to produce a depth profile if multiple levels are calculated. It is a simplified version of the earlier VITRIMAT model of Burnham & Sweeney (1989), which is based on experimentally derived kinetic responses in a wide range of organic matter to account for the elimination of water, carbon dioxide, methane and higher hydrocarbons from vitrinite. The model is applicable over a wide range of vitrinite reflectance values (%R_o), and heating rates.

EASY%R_o is based on an Arrhenius first-order parallel reaction approach with a distribution of activation energies (Table 3), thus the reaction can be described as:

$$\frac{dw}{dt} = -kw, \tag{4}$$

where the reaction rate k is defined as:

$$k = A\exp(-E/RT), \tag{5}$$

w = amount of unreacted component, A = frequency or pre-exponential factor, E = activation energy, R = universal gas constant and T = temperature. EASY %R_o requires the extent of the reaction F (transform ratio) to be computed using:

$$F = -\frac{w}{w_0} = 1 - \Sigma_i f_i \left[\frac{w_i}{w_{0i}}\right], \tag{6}$$

Table 3. Stoichiometric factors and activation energies used in the EASY%R_o model produced by Sweeney & Burnham (1990)

Stoichiometric factor (f_i)	Activation energy (E) (kcal mole^{-1})
0.03	34
0.03	36
0.04	38
0.04	40
0.05	42
0.05	44
0.06	46
0.04	48
0.04	50
0.07	52
0.06	54
0.06	56
0.06	58
0.05	60
0.05	62
0.04	64
0.03	66
0.02	68
0.02	70
0.01	72

where w = amount of unreacted component, w_0 = the initial concentration of the total reactant, w_{0i} = initial concentration for component i and f_i = weight for i_{th} reaction (stoichiometric factor – Table 3). The transform ratio F for virtinite reflectance (or the extent of the reaction) can then be used to calculate the EASY%R_o vitrinite reflectance value using:

$$\text{EASY\%R}_0 = \exp(3.7F - 1.6), \tag{7}$$

where 3.7 and −1.6 are scaling factors calculated in the original derivation of EASY%R_o Sweeney & Burnham (1990). A comprehensive description of the EASY%R_o model is given in Appendix I of Sweeney & Burnham (1990), while a detailed explanation of the application of EASY%R_o to a similar subsurface setting as modelled in this analysis is provided by Fjeldskaar *et al.* (2008) in their Appendix B.

The sills were modelled separately, recording the temperature of every node for every timestep for the entire 60, 000 years of each model run (Fig. 7). This produces a temperature-time pathway for every node, which can be input into the EASY%R_o model of Sweeney & Burnham (1990). This procedure, however, does not account for maturation as a result of burial (Fig. 8).

As the sills were intruded and modelled at a shallow depth (260 and 590 m for the upper and lower sills respectively – Tucholke *et al.*, 2004a), they are thus exposed to relatively low background temperatures and therefore would not produce a representative background %R_o gradient irrespective of model run time. To account for 'Background' maturation, resulting from burial-related heating a vitrinite gradient is applied after calculation of the maturation due to the heat from the sills. The background, vitrinite reflectance gradient used is calculated by comparing the vitrinite reflectance data for ODP 210-1276 by Pross *et al.* (2007) with a compilation from 28 extensional basins (Allen & Allen, 2005) (Fig. 8). The data used by Allen & Allen (2005) show a range of surface intercepts between 0.2 and 0.4%R_o and with a gradient of $0.15 \pm 0.09\%$ R_o km^{-1} for depths <4 km. We have used a surface intercept of 0.4 and a gradient of 0.15% R_o km^{-1} in our models as the observed data for ODP 210-1276 of Pross *et al.* (2007) lie at the upper end of the values for its depth. This method has allowed us to apply a representative background %R_o gradient that has been calibrated using the (albeit limited) observed %R_o data of Pross *et al.* (2007) (Fig. 8).

Modelled %R_o is calculated as the maximum of the modelled vitrinite reflectance due to magmatic heating and the vitrinite reflectance due to burial-related heating at every depth node within the model. This procedure produces an estimate of vitrinite reflectance profile for the whole of ODP 210-1276, incorporating both the background, burial-related maturation and the maturation effects of the sills.

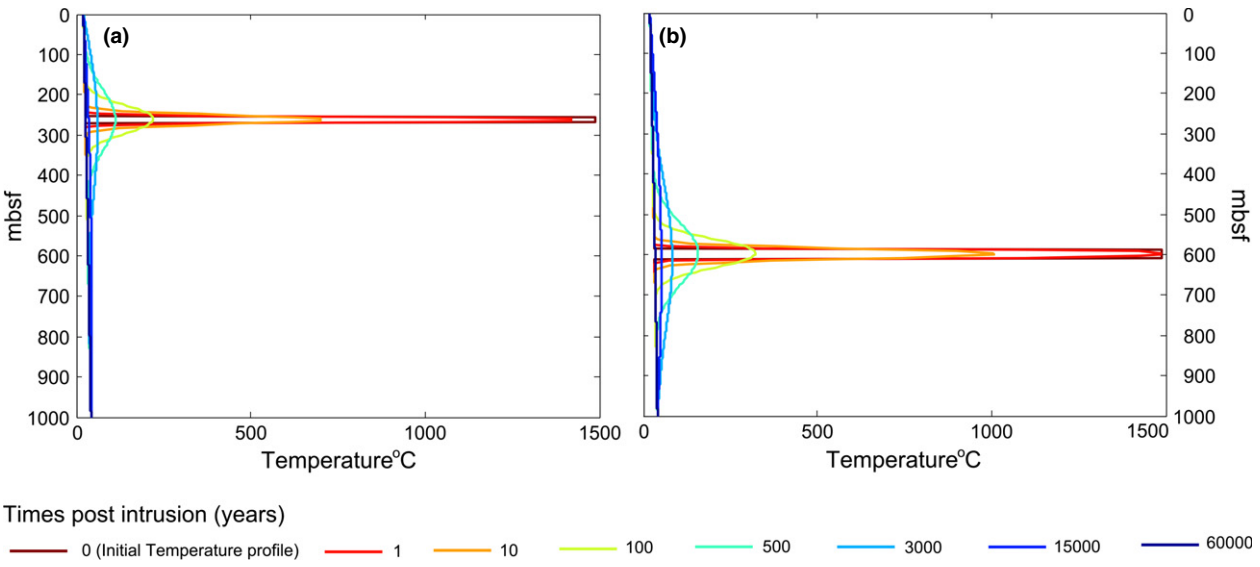

Fig. 7. 1D Thermal profiles for select times during the modelled cooling through from the upper (a) and lower sill (b) at ODP 210-1276. Time 0 depicts the initial temperature profile in each case, including the addition of the latent heat of crystallization. Modelling of the sills demonstrates that by 60, 000 years the thermal anomaly created by the intrusion is virtually indistinguishable against the background geothermal gradient. The initial temperature conditions are shown as the time 0 years. Depth (m) is the depth at the time of intrusion according to the reconstruction by Tucholke *et al.* (2007).

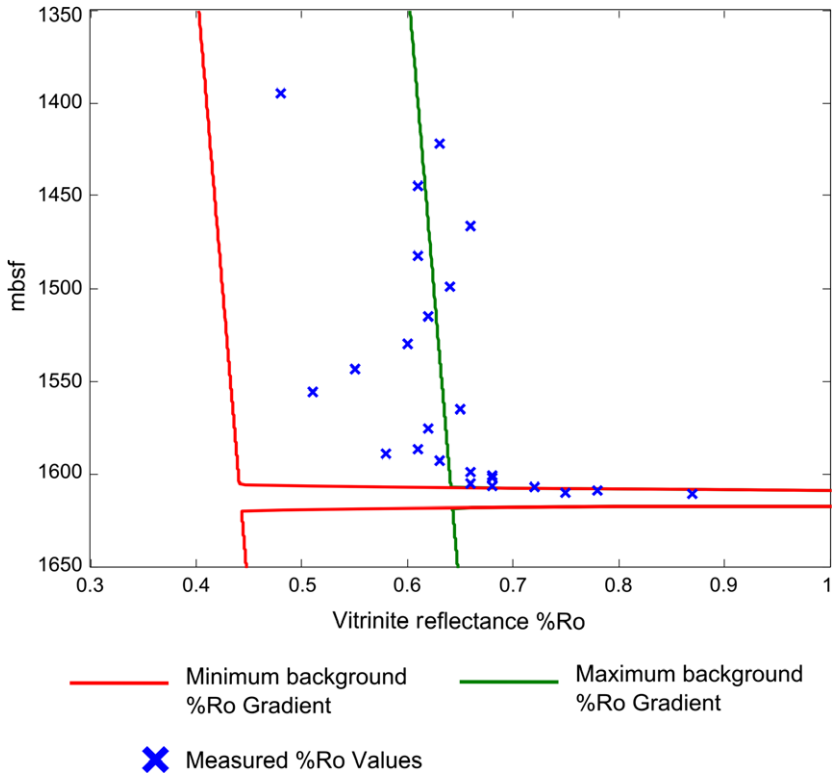

Fig. 8. Measured %Ro values (Pross *et al.*, 2007) alongside modelling results using both the minimum and maximum %Ro background values provided in Allen & Allen (2005). The data used by Allen & Allen (2005) are a compilation of data from 28 extensional basins, where the range of surface intercept is between 0.2 and 0.4%Ro and with a gradient of 0.15 ± 0.09%Ro km^{-1} for depths <4 km. Both lines on this plot have a gradient of 0.15% Ro km^{-1}, with the 'minimum' using the surface intercept of 0.2% Ro and the 'maximum' using the surface intercept of 0.4%Ro.

Burial and compaction

The sills were modelled at the estimated depths at the time of intrusion, as reconstructed from nano-fossil based age depth curves in Tucholke *et al.* (2004a). However, further burial and compaction of the sedimentary rocks occurred following intrusion. To allow accurate comparison between the modelled and the observed vitrinite reflectance profiles (Fig. 9), we have therefore corrected the models for post-intrusion burial and compaction (Fig. 10). We assume that the sedimentary rocks underwent uniaxial compaction, but the thickness of the sills remains unchanged during burial. Post-intrusion compaction will have reduced the vertical extent of the thermal aureole.

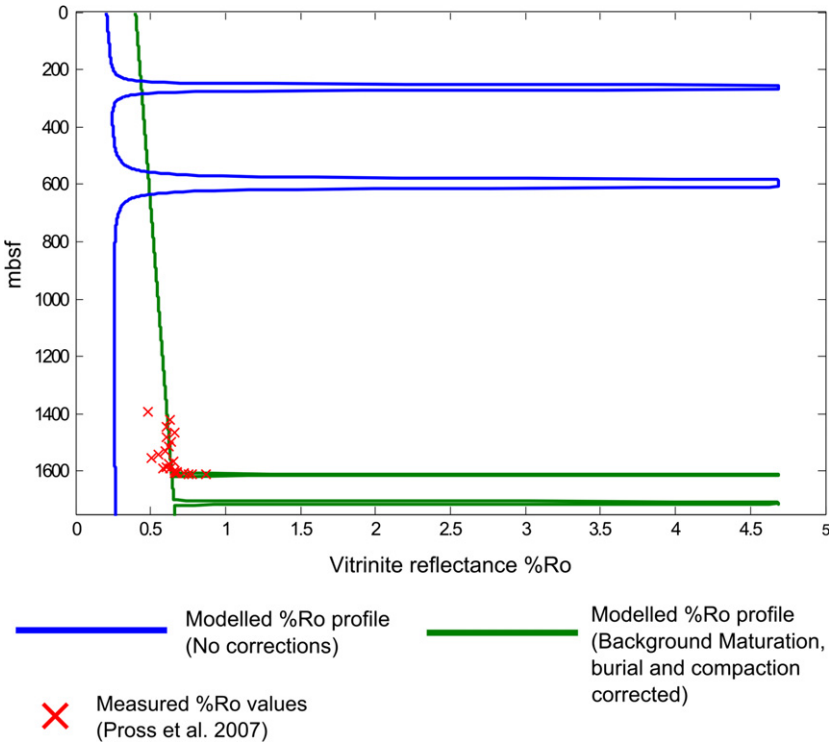

Fig. 9. EASY%Ro vitrinite reflectance modelling (Sweeney & Burnham, 1990) results in proximity to both the upper and lower sills without any compensation for background maturation, compaction or burial (blue), alongside results corrected for background maturation, compaction and burial (green). This demonstrates the need to account for post-intrusion burial and compaction, and suggests that the spatial extent of the thermal influence upon maturation of these sills was much greater shortly after intrusion, but subsequent compaction has reduced the vertical extent of the aureole in the well.

Compaction is calculated by assuming uniform vertical shortening using the current vertical distance between the sills in the well by Tucholke *et al.* (2004a), and the reconstructed depths at the time of intrusion from Tucholke *et al.* (2007). This compaction factor was then applied uniformly to all sedimentary rocks at ODP 210-1276. This is reasonable as the rocks found between the sills are lithologically comparable to the relevant parts of the well (sections thermally influenced by the sills).

The position of the sills was corrected to account for burial again using the reconstructed depths at the time of intrusion of Tucholke *et al.* (2007) and the current depth in the well provided by Tucholke *et al.* (2004a). The burial correction was calculated from the top of the upper sill (in the well and the modelled depths). Both the compaction and burial corrections are schematically depicted in Fig. 10.

Compartmentalization of sedimentary basins by sill complexes is a well-known phenomenon (e.g. Holford *et al.*, 2012). It should therefore be noted that this compartmentalization will cause the degree of compaction sediments have undergone to be extremely variable. For this reason, our compaction correction is only applicable to the situation intersected at ODP 210-1276, and is unlikely to be representative of the entire area covered by the 'U-reflector'.

It can be shown that heating due to burial during the period of intrusive activity is negligible. If we consider the minimum and maximum ages of the upper and lower sills, by taking the mean $^{40}Ar/^{39}Ar$ ages of Hart & Blusztajn (2006) (Fig. 3 and Table 1) and the minimum and maximum 2σ uncertainties, it is likely that the shortest time between intrusion of the upper and lower sills was 1.5 Myrs and the longest time was 13.8 Myrs. Using the sedimentation rate of *ca.* 17.8 $mMyr^{-1}$ noted by Tucholke *et al.* (2004a) at *ca.* 100 Ma these durations translate to upper and lower limits on the amount of burial as 27 and 246 m respectively. Applying the upper limit scenario (i.e. 246 m of sedimentation) to the geothermal gradient used in the model would only translate to a temperature difference of 5.4 K (0.246 km × 22°C km^{-1}), and thus the effect of additional burial-related maturation on organic matter would be negligible. All plots showing the sills at their current depth have been corrected for compaction and burial. This is consistent with our approach of modelling intrusion of the upper and lower sills as distinct thermal events.

Hydrothermal activity

Although not the primary focus of this study, the effects of hydrothermal activity were estimated by increasing the thermal diffusivity for 10 and 20 m either side of the upper intrusion by one order of magnitude (Fig. 11). Previous work by Polyansky *et al.* (2003) on hydrothermalism induced by mafic intrusions emplaced at depths of 300–400 m, indicates that the effects can be observed above an intrusion at a distance of up to 1.5 times the diameter of the intrusion, while beneath an intrusion it can be observed up to a distance that is similar to the width of the intrusion. The upper sill at ODP 210-1276 is 10.3 m thick, thus in our model, enhanced diffusivity aureoles of 10 and 20 m (Fig. 11) are used, as a 20 m maximum extent of hydrothermalism either side of the sill is greater than the maximum estimates provided by Polyansky *et al.* (2003). As a result, a 20 m maximum extent

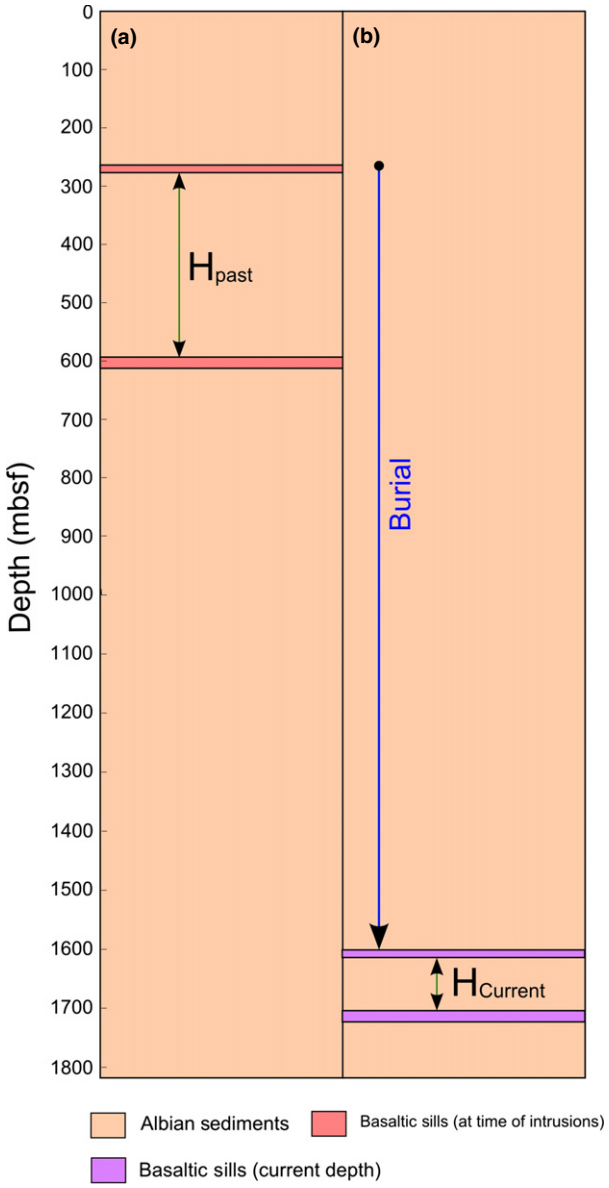

Fig. 10. A schematic depiction of the methodology used to account for sediment compaction and burial where; (a) is the reconstructed depths at time of intrusion and (b) represents the current depths recorded at ODP-210-1276. Compaction of the profile is calculated using the % difference between the measured current distance between the sills in the well ($H_{current}$) and the reconstructed separation at the time of the intrusion (H_{past}). This value was then taken to be the sediment compaction % for the whole profile. The sills are assumed to have remained the same thickness. Burial is measured in reference to the top of the upper sill, using the reconstructed value of 260 m and the current position in the well of 1612.7 m.

should overestimate the effects of hydrothermalism upon maturation, providing an end-member scenario.

Omission of advection is an assumption made by most workers in this field (e.g. Fjeldskaar *et al.*, 2008). This is probably the least reasonable of our assumptions as the effects of hydrothermal alteration have been observed in the well as subvertical calcite veins by Tucholke *et al.* (2004a) and potentially on seismic in the form of disturbed Albian sedimentary rocks above the U-reflector by Peron-Pinvidic *et al.* (2010) at ODP 210-1276.

RESULTS

The final model outputs are shown in Figs 6, 7, 11, 12, 13 and 14. Figures 12, 13 and 14 are depth and compaction corrected, whereas Figs 6, 7 and 11 are presented as the depth at time of sill intrusion.

Figure 6 depicts the maximum temperatures achieved from the models when the sills are intruded simultaneously alongside the results from the standard model, in which the sills are modelled separately. These results demonstrate that if simultaneous intrusion of multiple igneous bodies is assumed higher temperatures are achieved in proximity to the sills, particularly in the interval between the sills.

The temperature profiles for select times for the upper and lower intrusions are shown in Fig. 7. It can be seen that after approximately 15 000 years the thermal perturbation caused by the intrusions are virtually indistinguishable from the background geothermal gradient. As expected the thicker, lower sill takes longer to cool. The results demonstrate that the older sill had cooled to a value indistinguishable from the background geothermal gradient well before the second sill was intruded.

The results of the hydrothermal emulation models are presented in Fig. 11. It can be seen that even when the thermal diffusivity is increased by 1 order of magnitude for 20 m either side of the sill (Model 2 – the maximum hydrothermal influence modelled) the overall maximum temperature profile remains relatively unaffected and thus the influence upon maturation is also relatively insignificant as shown by the EASY%R_o modelling results (Fig. 11).

The EASY%R_o vitrinite reflectance results from the magmatic conduit duration experiments are provided in figure 12, along with the observed vitrinite reflectance values from Pross *et al.* (2007). These models show that in order to produce the observed vitrinite reflectance values above the upper sill, the duration in which the upper sill acted as a conduit probably was <10 years.

The maximum temperatures achieved from the intrusions, along with the current geothermal gradient (Keen, 1979) and TOC (wt%) (Tucholke *et al.*, 2004a) are shown on Fig. 13. These modelling results show that for a considerable portion of ODP 210-1276 the highest temperature achieved was due to the sill intrusion rather than subsequent burial. It can also be seen that if the oil/gas windows of England *et al.* (2002) are used (Fig. 13) the sedimentary rocks at ODP 210-1276 would not have been sufficiently heated to enter either the oil or gas windows without the additional heat from the sills.

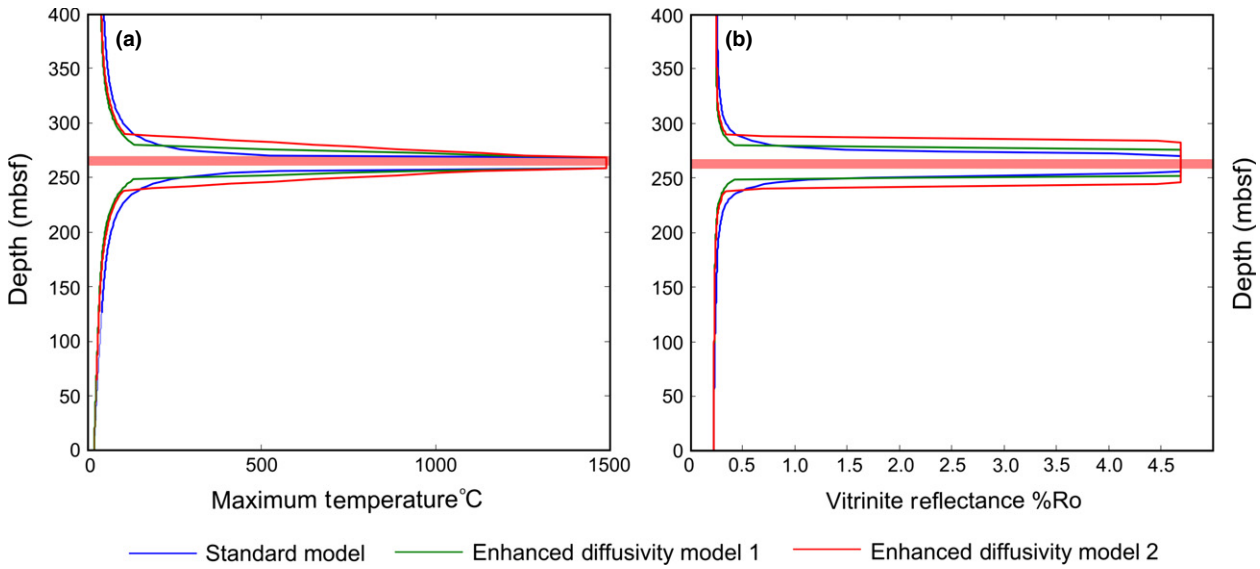

Fig. 11. Maximum temperatures (A) and EASY%Ro vitrinite reflectance modelling results (B) in proximity to the upper sill using both the standard modelling parameters outlined in the methodology and two models for 'enhanced' diffusivity to emulate the effects of hydrothermalism as a heat transfer mechanism. Model 1 represents increasing the diffusivity by one order of magnitude for 10 m either side of the sill, while Model 2 represents increasing diffusivity by 1 order of magnitude for 20 m either side of the sill.

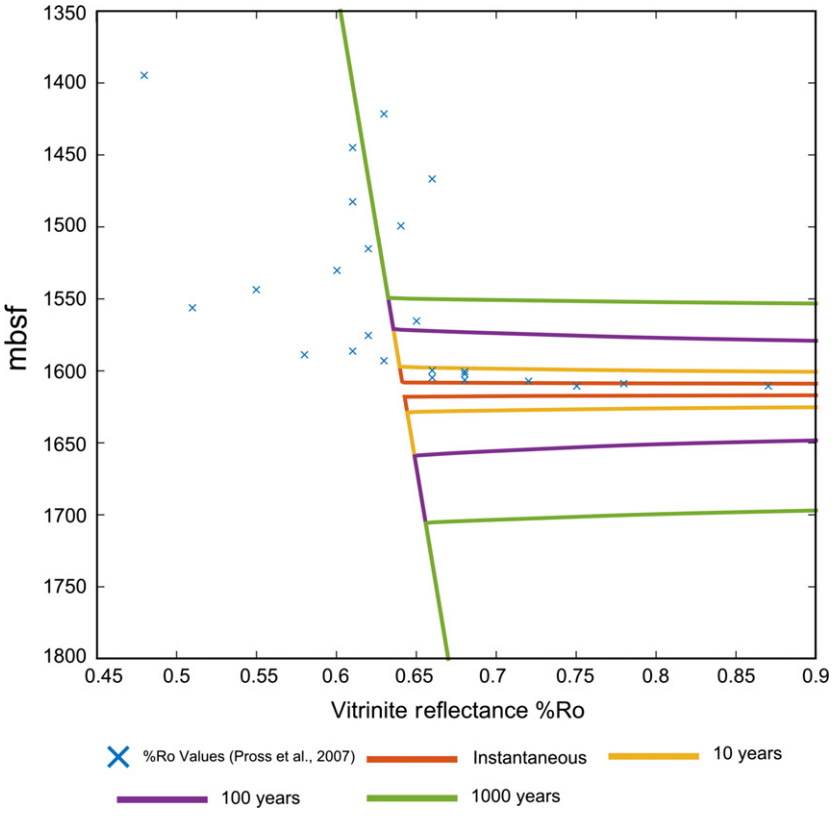

Fig. 12. EASY%Ro vitrinite reflectance modelling results (Sweeney & Burnham, 1990) produced by maintaining the starting temperature of the upper sill for 10, 100 and 1,000 years. This emulates the heating effects which would be caused by the upper sill remaining a magmatic conduit prior to the magma cooling to the closing temperature as recorded by the 40Ar/39Ar ages.

The modelled vitrinite reflectance profile for the entirety of ODP 210–1276 is presented in Fig. 14. These results demonstrate that the sills have probably caused a vertically limited, yet significant deviation from the background vitrinite reflectance gradient produced from the data in Allen & Allen (2005).

DISCUSSION

Timing and duration of magmatism

Demonstrating that the older sill had cooled to a temperature indistinguishable from the estimated background

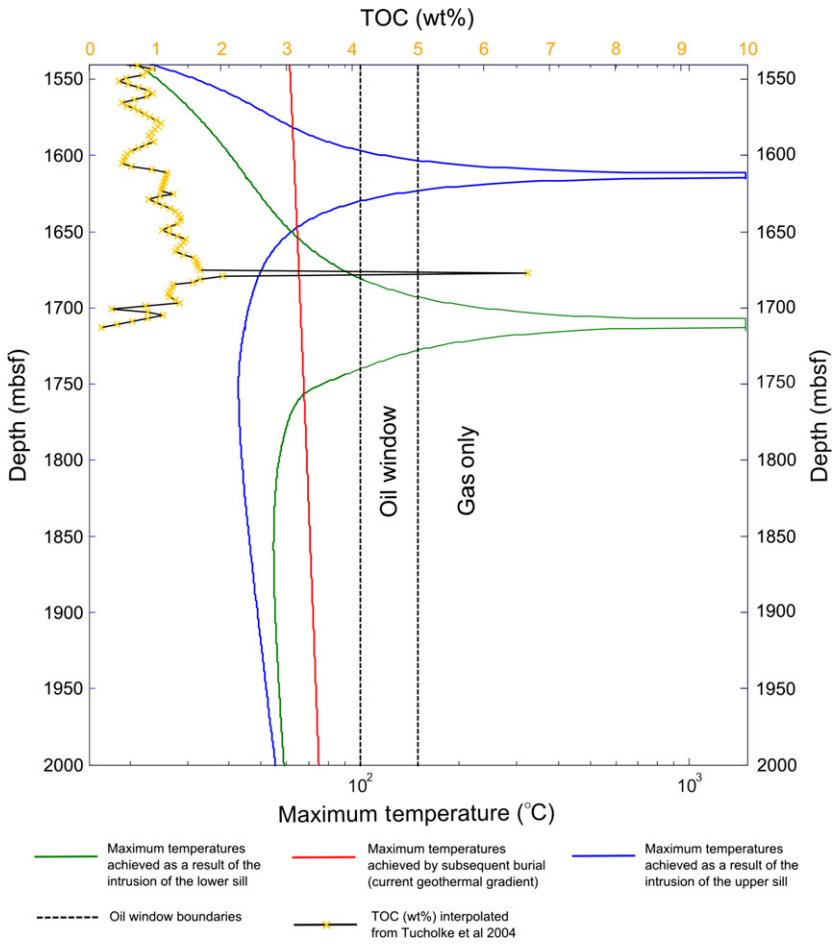

Fig. 13. The maximum temperatures achieved (logarithmic scale) as a result of sill intrusions and subsequent burial (current geothermal gradient – Keen, 1979), TOC (wt%) interpolated from the data in Tucholke *et al.* (2004a). This demonstrates that for a considerable portion of the well, the highest temperature achieved was due to heating from the intrusions rather than subsequent burial. This is assuming that the current burial depth is the maximum and that no exhumation has occurred. Oil and Gas windows from England *et al.* (2002).

geothermal gradient well before the second sill was intruded is significant. It shows that an assumption of simultaneous emplacement of multiple intrusive bodies (e.g. Aarnes *et al.*, 2010) could lead to an overestimation of the thermal perturbation. This has been demonstrated in Fig. 6 where it can be seen that if simultaneous intrusion of both sills is assumed, a higher maximum temperature is achieved in the region between the two sills. There is, however, no effect on the modelled vitrinite reflectance values, as the values generated for region between the sills (where there is greatest disparity in maximum temperature between the simultaneous and separate intrusion models – Fig. 6) are lower than the background vitrinite reflectance gradient from Allen & Allen (2005).

Our results indicate that, where possible, future models should avoid assuming simultaneous intrusion of multiple bodies, particularly in areas unlike ours where intrusions are shallow enough for the maturation effects not to be masked by subsequent burial-related maturation. When absolute dates are unavailable, other, nondirect methods can be used to estimate the duration of emplacement. One such method is to use the timing of forced folds above sills, such as the work by Magee *et al.* (2014) on the Irish Rockall Basin which indicates that emplacement took place during an interval of 15 Myrs. Where age constraints are not available as in this study, an end-member approach to modelling would be best. Using this approach both a simultaneous intrusion model and a model whereby intrusions have cooled entirely before subsequent intrusions occur should be computed (Fig. 6).

Our models have demonstrated that the duration between the activation of the sill as a conduit and subsequent cooling to the closing temperature (as recorded by the $^{40}Ar/^{39}Ar$ ages of Hart & Blusztajn, 2006) was probably <10 years for the upper sill (Fig. 10). This implies that in order to produce such a widespread sill complex in a short duration of time, the system must have been fed from multiple points. It is also likely, that in addition, the sills intersected at ODP 210-1276 are not representative of the whole of the magmatic system imaged as the U-reflector. In order to achieve the magmatic flux required to produce such an apparently widespread sill complex, some parts of the system may have operated as conduits for longer prior to cooling than the sill modelled in this work.

Despite the upper sill not acting as a conduit for a prolonged period of time prior to cooling, the intrusion of these two compositionally similar upper and lower sills has occurred over a time span of *ca.* 10 Myrs (Hart & Blusztajn, 2006), thus a relatively long-lived, post-breakup mechanism is likely to have been required to produce the melt. Alternatively, the causal heat source may have diminished and been renewed on a timescale of *ca.* 10^7 years, although this seems less likely due to the similar composition of the two sills (Hart & Blusztajn, 2006).

The presence of a long-lived heat source could have influenced sediment maturation by introducing additional heat into the margin. This could explain the higher than average vitrinite reflectance gradient at this location on the margin (Fig. 8). Any elevated heat flow could have been caused by the same mechanism that generated the melts feeding the sills that are imaged on seismic data as the 'U-reflector' (Figs 1 and 2) and the two intrusions that are the subject of this modelling study.

Implications for maturation

The modelled vitrinite reflectance profile for the entirety of ODP 210-1276 presented in Fig. 14 demonstrates that the sills have caused a vertically limited, yet significant spike in $\%R_o$ that needs to be taken into account in source rock maturation studies. This is consistent with the vitrinite reflectance study by Pross *et al.* (2007), which notes thermal alteration associated with the upper sill is observable 20 m above the intrusion, with a significant increase at 4.23 m and the highest value recorded closest to the sill at 2.17 m. Although the sills intersected at ODP 210-1276 may not be representative of the situation across the area covered by the U-reflector, if this high amplitude anomaly does indeed represent a widespread sill complex (e.g. Deemer *et al.*, 2010), then it is not unreasonable to suggest that a similar spike in maturation is likely to be exist elsewhere on the Newfoundland margin where similar sills are present.

Burial and compaction

Previous work proposes that the sills were intruded into relatively unconsolidated and not overpressured sedimentary rocks, particularly in the lower 30 m of the section (Tucholke *et al.*, 2007). It has been claimed that this suggests that at the drill site considerable mechanical support probably provided by nearby dykes, protecting the sedimentary rocks between the sills from compression (Peron-Pinvidic *et al.*, 2010).

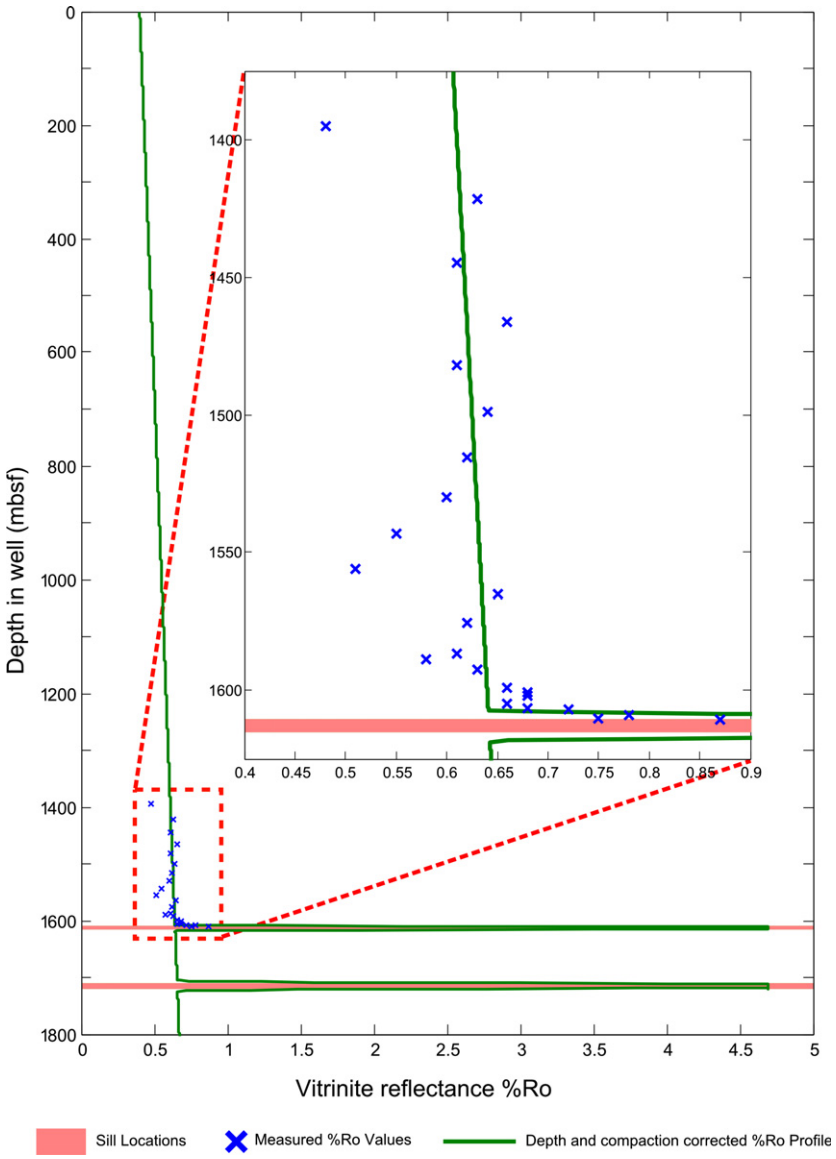

Fig. 14. Vitrinite reflection profile for the entirety of ODP 210-1276 produced using the EASY%Ro model of Sweeney & Burnham (1990) with the measured data provided by Pross *et al.* (2007) plotted alongside for comparison. It can be seen that a vertically limited, yet significant spike in %Ro has been produced in proximity to the sills that needs to be taken into account in source rock maturation studies.

However, we find that the EASY%R_o modelling results most closely resemble the observed vitrinite reflectance values when burial and compaction are accounted for (Fig. 8), perhaps suggesting that the sediments between the sills have been more compacted than previously suggested.

Hydrothermal activity

Enhancing the diffusivity increases rate at which the sill cools, as expected, but has little effect on the modelled vitrinite reflectance values (Fig. 11). While these results are interesting, they demonstrate that the role of hydrothermalism, in this particular instance, is trivial in the context of the other assumptions and uncertainties inherent in the model and the parameters used. This implies that advection may not be as important in influencing maturation as suggested by previous work e.g. Polyansky *et al.* (2003).

Source of the magmatism

The source of the magma producing the sills intersected at ODP210-1276, and probably of the U-reflector is still uncertain according to Peron-Pinvidic *et al.* (2010). It has been attributed to the migration of the Canary and Madeira plumes across the Newfoundland basin between 80 and 120 Ma (e.g. Karner & Shillington, 2005; Deemer *et al.*, 2010), which is said to be supported by the geochemical signature observed by Hart & Blusztajn (2006). Deemer *et al.* (2010) propose that volcanism was suppressed while the plumes travelled under the full thickness of the continental lithosphere, resulting in an accumulation of magma which was subsequently released when the hotspot approached the thinned lithosphere at the Eastern edge of the Grand Banks.

However, given that the Newfoundland Margin is considered to be a typical NVPM (e.g. Melankholina, 2011) with the absence of any other plume related observations, other causal mechanisms should be considered. One such alternative theory is proposed by Peron-Pinvidic *et al.* (2010) stating that the melts were produced by asymmetric rift-drift related tectono-magmatic processes.

CONCLUSIONS

Collectively, the information acquired by the previous work at ODP 210-1276, and elsewhere on the Newfoundland Margin (e.g. Tucholke *et al.*, 2004a; Hart & Blusztajn, 2006; Pross *et al.*, 2007) has provided a unique opportunity to model the cooling of the sills and their thermal influence on the surrounding sedimentary rocks. This has allowed us to provide new insights into the relationship between intrusive magmatism, thermal evolution of passive margins and the influence on maturation on the Newfoundland margin, within a well constrained framework. The key findings of this study include:

(1) The oldest sill at ODP 210-1276 had cooled to a temperature indistinguishable from the background geothermal gradient well before the younger, lower sill complex was intruded.
(2) The temperatures achieved in the sedimentary rocks adjacent to the intrusions are higher than those achieved by post-depositional burial. The sedimentary rocks at ODP 210-1276 would not have entered the oil or gas windows in the absence of this thermal pulse. This demonstrates the potential significance that regionally extensive intrusive magmatism could have on the thermal evolution of the Newfoundland margin, and suggests that the role of intrusive magmatism should be considered in thermal maturation studies in similar settings.
(3) If the sills acted as magmatic conduits prior to cooling to the closing temperature (as recorded by the $^{40}Ar/^{39}Ar$ dates) it was for a short duration, probably <10 years.
(4) The peak in vitrinite reflectance data observed at ODP 210-1276 can be completely attributed to rapid heating from the upper sill. We have also shown that the spatial extent of the thermal aureole of these sills was much greater shortly after intrusion, and that subsequent burial and compaction has reduced its current vertical extent at ODP 210-1276, which is probably representative of the situation across the Newfoundland margin.
(5) The higher than average %R_o gradient for this part of the Newfoundland margin implies that at some point in the past the heat flow was elevated. This elevation of past heat flow could have been caused by the same mechanism that produced the sills which are imaged on seismic data as the 'U-reflector'.

Finally, the EASY%R_o modelling results confirm that the sills at ODP 210-1276 have influenced the localized thermal evolution, and may be indicative of a broader, more regional thermal perturbation in the region covered by the 'U-reflector' on regional seismic data, and thus should be considered in source rock maturation studies.

ACKNOWLEDGEMENTS

Funding for this research was provided by Royal Dutch Shell in the form of a CeREES studentship at Durham University. We also thank Jerry Sweeney and Alan Burnham for providing the EASY%R_o model and guiding its application to our study. This research was made possible by data collected during leg 210 of the Ocean Drilling Program along with that collected during the SCREECH geophysical surveys. We thank Craig Magee and Nick Schofield for their constructive reviews which contributed significantly to this manuscript.

REFERENCES

Aarnes, I., Svensen, H., Connolly, J.A.D. & Podladchikov, Y.Y. (2010) How contact metamorphism can trigger global climate changes: modeling gas generation around igneous sills in sedimentary basins. *Geochim. Cosmochim. Acta*, **74**, 7179–7195.

Allen, P.A. & Allen, J.R. (2005) *Basin Analysis*. Blackwell Publishing, Malden, MA, USA.

Barker, C.E., Bone, Y. & Lewan, M.D. (1998) Fluid inclusion and vitrinite-reflectance geothermometry compared to heat-flow models of maximum paleotemperature next to dikes, western onshore Gippsland Basin, Australia. *Int. J. Coal Geol.*, **37**, 73–111.

Beglinger, S.E., Doust, H. & Cloetingh, S. (2012) Relating petroleum system and play development to basin evolution: West African South Atlantic Basins. *Mar. Pet. Geol.*, **30**, 1–25.

Bostick, N.H. & Alpern, B. (1977) Principles of sampling, preparation and constituent selection for microphotometry in measurement of maturation of sedimentary organic matter. *J. Microsc.*, **109**, 41–47.

Burnham, A.K. & Sweeney, J.J. (1989) A chemical kinetic model of vitrinite maturation and reflectance. *Geochim. Cosmochim. Acta*, **53**, 2649–2657.

Deemer, S., Hurich, C. & Hall, J. (2010) Post-rift flood-basalt-like volcanism on the Newfoundland Basin nonvolcanic margin: the U event mapped with spectral decomposition. *Tectonophysics*, **494**, 1–16.

DeSilva, N.R. (1999) Sedimentary basins and petroleum systems offshore Newfoundland and Labrador. *Geol. Soc. Lond. Petrol. Geol. Conf. Ser.*, **5**, 501–515.

Eldholm, O. & Sundvor, E. (1979) Geological events during the early formation of a passive margin. *Tectonophysics*, **59**, 233–237.

England, G.L., Rasmussen, B., Krapez, B. & Groves, D.I. (2002) Archaean oil migration in the Witwatersrand Basin of South Africa. *J. Geol. Soc.*, **159**, 189–201.

Fjeldskaar, W., Helset, H.M., Johansen, H., Grunnaleite, I. & Horstad, I. (2008) Thermal modelling of magmatic intrusions in the Gjallar Ridge, Norwegian Sea: implications for vitrinite reflectance and hydrocarbon maturation. *Basin Res.*, **20**, 143–159.

Franke, D. (2013) Rifting, lithosphere breakup and volcanism: comparison of magma-poor and volcanic rifted margins. *Mar. Pet. Geol.*, **43**, 63–87.

Galushkin, Y.I. (1997) Thermal effects of igneous intrusions on maturity of organic matter: a possible mechanism of intrusion. *Org Geochem.*, **26**, 645–658.

Geoffroy, L. (2005) Volcanic passive margins. *C.R. Geosci.*, **337**, 1395–1408.

Goutorbe, B., Drab, L., Loubet, N. & Lucazeau, F. (2007) Heat flow of the Eastern Canadian rifted continental margin revisited. *Terra Nova*, **19**, 381–386.

Hart, S.R. & Blusztajn, J. (2006) Age and geochemistry of the mafic sills, Odp Site 1276, Newfoundland margin. *Chem. Geol.*, **235**, 222–237.

Heroux, Y., Chagnon, A. & Bertrand, R. (1979) Compilation and correlation of major thermal maturation indicators. *AAPG Bull.*, **63**, 2128–2144.

Holford, S.P., Schofield, N., MacDonald, J.D., Duddy, I.R. & Green, P.F. (2012) Seismic analysis of igneous systems in sedimentary basins and their impacts on hydrocarbon prospectivity: examples from the Southern Australian margin. *APPEA J.*, **52**, 229–252.

Holford, S.P., Schofield, N., Jackson, C.A.-L., Magee, C., Green, P.F. & Duddy, I.R. (2013) Impacts of Igneous Intrusions on Source and Reservoir Potential in Prospective Sedimentary Basins Along the Western Australian Continental Margin. *West Australian Basins Symposium 18–21 August 2013*.

Hopper, J.R., Funck, T., Tucholke, B.E., Larsen, H.C., Holbrook, W.S., Louden, K.E., Shillington, D. & Lau, H. (2004) Continental breakup and the onset of ultra-slow spreading off flemish cap on the Newfoundland rifted margin. *Geology*, **32**, 93–96.

Karner, G.D. & Shillington, D.J. (2005) Basalt sills of the U reflector, Newfoundland basin: a serendipitous dating technique. *Geology*, **33**, 985–988.

Keen, C.E. (1979) Thermal history and subsidence of rifted continental margins—evidence from wells on the Nova Scotian and Labrador Shelves. *Can. J. Earth Sci.*, **16**, 505–522.

Magee, C., Jackson, C.A.L. & Schofield, N. (2014) Diachronous sub-volcanic intrusion along deep-water margins: insights from the Irish Rockall Basin. *Basin Res.*, **26**, 85–105.

Melankholina, E.N. (2011) Passive margins of the North and Central Atlantic: a comparative study. *Geotectonics*, **45**, 291–301.

Peron-Pinvidic, G., Shillington, D.J. & Tucholke, B.E. (2010) Characterization of sills associated with the U reflection on the Newfoundland margin: evidence for widespread early post-rift magmatism on a magma-poor rifted margin. *Geophys. J. Int.*, **182**, 113–136.

Peron-Pinvidic, G., Manatschal, G. & Osmundsen, P.T. (2013) Structural comparison of archetypal Atlantic rifted margins: a review of observations and concepts. *Mar. Pet. Geol.*, **43**, 21–47.

Polyansky, O.P., Reverdatto, V.V., Khomenko, A.V. & Kuznetsova, E.N. (2003) Modeling of fluid flow and heat transfer induced by basaltic near-surface magmatism in the Lena-Tunguska Petroleum Basin (Eastern Siberia, Russia). *J. Geochem. Explor.*, **78–79**, 687–692.

Pross, J., Pletsch, T., Shillington, D.J., Ligouis, B., Schellenberg, F. & Kus, J. (2007) Thermal alteration of terrestrial palynomorphs in mid-cretaceous organic-rich mudstones intruded by an igneous sill (Newfoundland Margin, Odp Hole 1276a). *Int. J. Coal Geol.*, **70**, 277–291.

Shillington, D.J., Holbrook, W.S., Tucholke, B.E., Hopper, J.R., Louden, K.E., Larsen, H.C., Van Avendonk, H.J.A., Deemer, S. & Hall, J. (2004) 5. Data Report: Marine Geophysical Data on the Newfoundland Nonvolcanic Rifted Margin around Screech Transect 2. *Proceedings of the Ocean Drilling Program, Initial Reports*, **210**, 1–36.

Smith, W.H.F. & Sandwell, D.T. (1997) Global seafloor topography from satellite altimetry and ship depth soundings. *Science*, **277**, 1957–1962.

Spear, F.S. & Peacock, S.M. (1989) *Metamorphic Pressure-Temperature-Time Paths*. American Geophysical Union, Washington, DC.

Sweeney, J.J. & Burnham, A.K. (1990) Evaluation of a simple model of vitrinite reflectance based on chemical kinetics. *AAPG Bull.*, **74**, 1559–1570.

Tucholke, B.E., Sibuet, J.-C. & Klaus, A. (2004a) 1. Leg 210 Summary. *Proc. Ocean Drill. Program, Initial Rep.*, **210**, 1–78.

Tucholke, B.E., Sibuet, J.-C. & Klaus, A. (2004b) 3. Site 1276. *Proc. Ocean Drill. Program, Initial Rep.*, **210**, 1–358.

Tucholke, B.E., Sibuet, J.-C. & Klaus, A. (2007) 1. Leg 210 synthesis: tectonic, magmatic, and sedimentary evolution of the Newfoundland-Iberia rift. *Proc. ODP Sci. Results*, **210**, 1–56.

Van Avendonk, H.J.A., Holbrook, W.S., Nunes, G.T., Shillington, D.J., Tucholke, B.E., Louden, K.E., Larsen, H.C. & Hopper, J.R. (2006) Seismic velocity structure of the rifted margin of the Eastern Grand Banks of Newfoundland, Canada. *J. Geophys. Res. Solid Earth*, **111**, B11404.

Wang, D., Lu, X., Zhang, X., Xu, S., Hu, W. & Wang, L. (2007) Heat-model analysis of wall rocks below a diabase sill in Huimin Sag, China Compared with thermal alteration of mudstone to carbargilite and hornfels and with increase of vitrinite reflectance. *Geophys. Res. Lett.*, **34**, L16312.

Wang, D., Lu, X., Song, Y., Shao, R. & Qi, T. (2010) Influence of the temperature dependence of thermal parameters of heat conduction models on the reconstruction of thermal history of igneous-intrusion-bearing basins. *Comput. Geosci.*, **36**, 1339–1344.

Wang, K., Lu, X., Chen, M., Ma, Y., Liu, K., Liu, L., Li, X. & Hu, W. (2012) Numerical modelling of the hydrocarbon generation of tertiary source rocks intruded by doleritic sills in the Zhanhua depression, Bohai Bay Basin, China. *Basin Res.*, **24**, 234–247.

Manuscript received 1 October 2014; In revised form 5 March 2015; Manuscript accepted 31 March 2015.

Formation of the West Greenland Volcanic Margin: Exploring alternatives to the plume hypothesis

Alex Peace[1], Ken McCaffrey[1], Jonny Imber[1], Richard Hobbs[1], Jeroen van Hunen[1], Gillian Foulger[1], Keith Gerdes[2],
[1]*Dept. Earth Sciences, Durham University, Durham, UK. DH1 3LE; (a.l.peace@durham.ac.uk)*
[2]*Shell International Exploration and Production, Den Haag, The Netherlands*

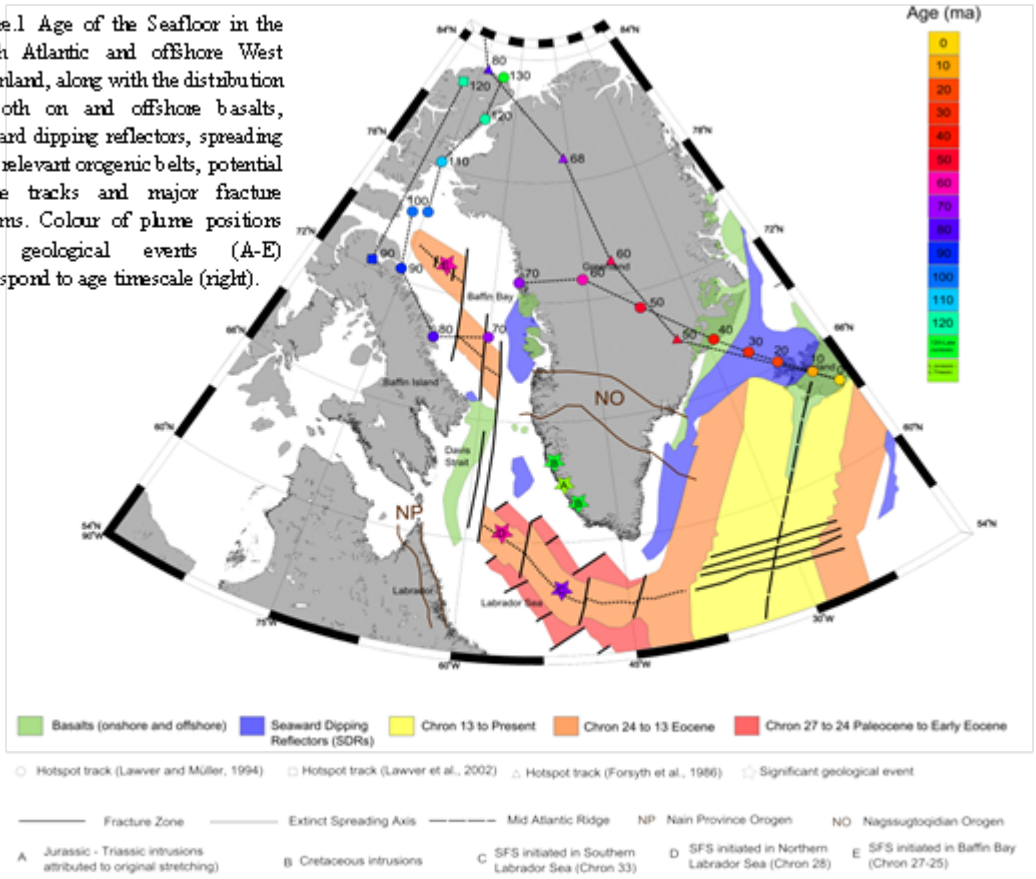

Figure.1 Age of the Seafloor in the North Atlantic and offshore West Greenland, along with the distribution of both on and offshore basalts, seaward dipping reflectors, spreading axis, relevant orogenic belts, potential plume tracks and major fracture systems. Colour of plume positions and geological events (A-E) correspond to age timescale (right).

Introduction

The abundance of igneous rocks on the West Greenland volcanic passive margin (VPM – Figure 1) has generally been attributed to a mantle plume elevating mantle temperatures resulting in the excess volcanism. Similar hypotheses have been proposed for many other VPMs worldwide.

The mantle plume hypothesis in West Greenland

Observations on the West Greenland margin that have been attributed to the passage of a hypothesised mantle plume beneath the region at 120 - 60Ma (Figure 1) include; 1) the onset of seafloor spreading in the Labrador Sea, 2) major volcanism in West Greenland and Baffin Island, 3) underplating of the Davis Strait by a high-velocity body, 4) uplift of onshore sedimentary successions, 5) seismically observable volcanics for 400km east of Baffin Island 6) high $^{3}He/^{4}He$ and low $^{187}Os/^{188}Os$ ratios in Picrites.

The presence and role of mantle plumes during the formation of VPMs nevertheless remains equivocal. On the West Greenland and North-Eastern Canadian margins, it is at odds with several large-scale features. These include; 1) timing of seafloor spreading in Baffin Bay, 2) the progressive, fan-shaped opening of the Labrador Sea from south to north, 3) the age of onshore margin-parallel dyke swarms and 4) the nature of the crust in the Davis Strait.

1. The timing of seafloor spreading in Baffin Bay is contrary to what would be predicted by the plume hypothesis. The hotspot track reconstruction of Lawver and Müller (1994) places the proto-Icelandic plume in the Baffin Bay area at ca. 120 – 70 Ma, whereas seafloor spreading did not initiate until much later at Chron 27-25 (52 – 62 Ma). This is despite the fact that it lay in close proximity to the alleged plume track for a prolonged period of time at a much earlier time. It has been recognised that there should be a delay to account for the time it would take a cold lithosphere to heat up,

on the arrival of a plume, with spreading proposed to postdate plume arrival by 10 – 40 Myrs (Hill, 1993). However, using even the uppermost limit proposed by Hill (1993), the delay in Baffin Bay is too great with a timespan of approximately 60 Myrs between first plume arrival (in Northern Baffin Bay) and seafloor spreading initiation is too great.

2. Tectonic reconstructions of the movements of Greenland relative to Canada suggest an 'unzipping' motion with progressive opening from south to north. Although there is some debate regarding the precise onset date of seafloor spreading it is accepted that it started in the southern Labrador Sea before the north. This does not fit a model whereby a plume producing voluminous magmatism initiated seafloor spreading (Gerlings et al., 2009). If a plume were present, then rifting, and subsequent seafloor spreading would be expected to start nearest to the plume and to propagate away from it.
3. It has been suggested that the prolonged location of a plume could "pin" the position of subsequent spreading, through thermal and mechanical weakening of the lithosphere, which a subsequent stress field could exploit (Hill, 1993). Onshore coast-parallel dykes have however been geochemically dated as early as the Jurassic (Figure 1). This implies that the weakness exploited by subsequent continental breakup was already in place before the proposed plume was in the vicinity.
4. In the more volcanic Davis Strait seafloor spreading was never fully initiated as it did in the Labrador Sea and Baffin Bay. Instead a 'leaky transform' system developed (Funck et al., 2007). It is not clear why a mantle plume should cause seafloor spreading in the distant Labrador Sea but not at the Davis Strait which is much closer to the alleged plume.

Reliability of 'Hotspot Tracks'

This work has primarily considers the hotspot track of Lawver and Müller (1994) (Figure 1). It is of course possible that this hotspot track is erroneous and the plume hypothesis could still provide an explanation for the formation of the West Greenland margin. This hotspot track is however based on relatively well-constrained plate tectonic reconstructions, and even significant unreliability would still be insufficient to account for the observations made on the West Greenland margin.

It should also be pointed out that the hotspot tracks considered herein are not based on observations; they were produced from absolute plate motion reconstructions. Some subsequent work has however misused them, assuming they were based on an observable hotspot track. This has led to the problems discussed herein.

Alternatives to the Mantle Plume Hypothesis

If continental breakup between Canada and Greenland occured in response to the arrival of a mantle plume, now located under Iceland, it would be expected that the earliest and most extensive seafloor spreading would have occurred closest to the plume. In fact the opposite is observed. Since the *observations* do not match the model predictions, the plume hypothesis as applied here is unlikely to be correct in its current form. Non-plume mechanisms should thus be considered to be the causal factor in the formation of the West Greenland margin. We cannot however entirely rule out that although not the causal factor behind initial rifting and seafloor spreading initiation a mantle plume may have contributed to the later volcanic evolution of the area.

Several mechanisms have been previously proposed to explain the formation of VPMs including; 1) a direct effect of rifting and 2) small scale convection. These margin formation mechanisms (along with the plume hypothesis) produce different predictions for the sedimentary and tectonic evolution of the margin which should be detectable through appropriate seismic interpretation, and subsequent reconstructions. This should allow us to contribute to understanding the likely causal mechanism(s) reasonable for the formation of this VPM.

Methodology

Access to industry well and seismic data has enabled us to elucidate the tectono-stratigraphic evolution of the various segments of this margin, in particular at the syn-rift to post-rift transition. Integration of the well and seismic reflection data has allowed us to produce isochron thickness maps of defined sediment ages, enabling us to reconstruct the syn-to-post-rift evolution of the West Greenland margin in detail and to critically test the predictions of contrasting models of margin development. Our results demonstrate that the widely-cited plume model cannot explain key observations on the West Greenland margin. A mantle plume may have contributed to the later development of the margin but is unlikely to have influenced the early stages of margin development as proposed by some previous workers.

Key References

Funck, T., Jackson, H.R., Louden, K.E., Klingelhöfer, F., 2007. Seismic study of the transform-rifted margin in Davis Strait between Baffin Island (Canada) and Greenland: What happens when a plume meets a transform. Journal of Geophysical Research: Solid Earth 112, B04402.

Gerlings, J., Funck, T., Jackson, H.R., Louden, K.E., Klingelhöfer, F., 2009. Seismic evidence for plume-derived volcanism during formation of the continental margin in southern Davis Strait and northern Labrador Sea. Geophysical Journal International 176, 980-994.

Hill, R.I., 1993. Mantle plumes and continental tectonics. Lithos 30, 193-206.

Lawver, L.A., Müller, R.D., 1994. Iceland Hotspot track. Geology 22, 311-314.

To what extent does sill intrusion affect the thermal evolution of non-volcanic passive margins? An example from ODP 210-1276, offshore Newfoundland, Canada

ALEXANDER L. PEACE[1], KEN J W. MCCAFFREY[1], JONNY IMBER[1], RICHARD W. HOBBS[1], JEROEN VAN HUNEN[1], KEITH GERDES[2]

[1]Dept. Earth Sciences, Durham University, Durham, UK. DH1 3LE; (a.l.peace@durham.ac.uk)
[2]Shell International Exploration and Production, Den Haag, The Netherlands

Dolerite sills are imaged on seismic data throughout the Newfoundland Basin as the high amplitude "U-reflector", covering an area of ca. 20,000km^2 and providing evidence for a major post-rift magmatic event on an otherwise non-volcanic margin.

At ODP site 210-1276 (45.41N, –44.79W), an older (^{39}Ar/^{40}Ar date: 104.7±1.7 - 105.9±1.8 Ma), singular sill intrudes organic rich sediments between 1612 – 1623 mbsf, whilst the largest sill in a younger (^{39}Ar/^{40}Ar date: 95.9±2 - 99.7±1.8 Ma) sill complex has a top contact at 1719 mbsf and is present till the base of the well at 1736.9 mbsf. This lower sill complex consists of multiple small intrusions (3-30cm), above the larger sill which is not sampled in its entirety.

Previous work has provided depth at time of intrusion (from nano-fossil based age depth curves) as ~260 mbsf and ~575 mbsf, for the upper and lower sills respectively. Vitrinite reflectance data is also available from above the upper sill. The availability of these constraints provides a unique opportunity to model sill intrusion and its influence on margin thermal evolution.

Conductive cooling of the sills was modelled using a finite differences code, incorporating the EASY%Ro model to calculate theoretical vitrinite reflectance values and thus quantify the thermal influence of the sills on the maturation state of the host sediments.

Results show that the 1st intrusion had cooled to a value indistinguishable from the background geothermal gradient before the 2nd intrusion event occurred, and that temperatures achieved in proximity to the intrusions are higher than the temperature achieved by subsequent burial.

The vitrinite reflectance modelling has allowed us to produce a theoretical maturation profile for ODP 210-1276, demonstrating a significant but localised effect on sediment maturity as a result of the intrusions. This profile indicates that the organic rich sediments may have been overmatured in proximity to the sills.

The model shows that even on non-volcanic margins intrusive magmatism can significantly influence localised thermal evolution, and may be indicative of broader, more regional thermal perturbations that should be considered in source rock maturation studies.

Geophysical Research Abstracts
Vol. 15, EGU2013-9439, 2013
EGU General Assembly 2013

Modelling the role of magmatic intrusions in the post-breakup thermal evolution of Volcanic Passive Margins

Alexander Peace (1), Ken McCaffrey (1), Jonny Imber (1), Jeroen van Hunen (1), Richard Hobbs (1), and Keith Gerdes (2)

(1) Durham, Earth Sciences, Durham, United Kingdom (a.l.peace@durham.ac.uk), (2) Shell International Exploration and Production B.V, Carel van Bylandtlaan 5, 2596 HP Den Haag, The Netherlands

Passive margins are produced by continental breakup and subsequent seafloor spreading, leaving a transition from continental to oceanic crust. Magmatism is associated with many passive margins and produces diagnostic criteria that include 1) abundant breakup related magmatism resulting in a thick igneous crust, 2) a high velocity zone in the lower crust and 3) seaward dipping reflectors (SDRs) in seismic studies. These Volcanic Passive Margins (VPMs) represent around 75% of the Atlantic passive margins, but beyond this high level description, these magma-rich settings remain poorly understood and present numerous challenges to petroleum exploration.

In VPMs the extent to which the volume, timing, location and emplacement history of magma has played a role in controlling heat flow and thermal evolution during margin development remains poorly constrained. Reasons for this include; 1) paucity of direct heat flow and thermal gradient measurements at adequate depth ranges across the margins, 2) poor onshore exposure 3) highly eroded flood basalts and 4) poor seismic imaging beneath thick offshore basalt sequences. As a result, accurately modelling the thermal history of the basins located on VPMs is challenging, despite the obvious importance for determining the maturation history of potential source rocks in these settings.

Magmatism appears to have affected the thermal history of the Vøring Basin on the Norwegian VPM, in contrast the effects on the Faeroe-Shetland Basin was minimal. The more localised effects in the Faeroe-Shetland Basin compared to Vøring Basin may be explained by the fact that the main reservoir sandstones appear to be synchronous with thermal uplift along the basin margin and pulsed volcanism, indicating that the bulk of the magmatism occurred at the basin extremities in the Faeroe-Shetland Basin, where its effect on source maturation was lessened. Our hypothesis is that source maturation occurs as a result of regional temperature and pressure increases, and the effects of even a large singular magmatic event are small beyond the immediate vicinity, therefore quantifying cumulative regional heat flow is of utmost importance.

The apparently complex relationships between source rock maturation and magmatism are not limited to the north-east Atlantic margins. Other VPMs of interest include the regions between West Greenland and Eastern Canada (Labrador Sea, Davis Strait and Baffin Bay), East Greenland, NW Australia, Western India and segments of the Western African and Eastern South American margins.

This project utilises 1D numerical modelling of magmatic intrusions into a sedimentary column to gain an understanding into the thermal influence of post-breakup magmatic activity on source rock maturation in representative VPMs. Considerations include the timing, periodicity of intrusions, thickness, spacing and background heat in the basin.